

**Phytochemical investigation and bioactivity screening
of promising medicinal plants of the families
Combretaceae and Zingiberaceae**

Dissertation

zur Erlangung des Doktorgrades der Naturwissenschaften
(Dr. rer. nat.)

der

Naturwissenschaftlichen Fakultät II
Chemie, Physik und Mathematik

der Martin-Luther-Universität
Halle-Wittenberg

vorgelegt von

Herr Dipl.-LMChem. Jonas Kappen

This dissertation has been created under the supervision of Prof. Dr. Ludger A. Wessjohann and mentorship of Dr. Katrin Franke at Leibniz Institute of Plant Biochemistry (IPB) Halle (Saale) in cooperation with the Martin-Luther University Halle-Wittenberg.

1st Reviewer: Prof. Dr. Ludger A. Wessjohann

2nd Reviewer: Prof. Dr. Ricardo M. Kuster

Date of public defense: 13.10.2025

Phytochemical investigation and bioactivity screening of promising medicinal plant of the families Combretaceae and Zingiberaceae

Table of Contents

Table of Contents	I
Acknowledgements	II
List of Abbreviations.....	IV
Summary	1
Zusammenfassung.....	3
1 General Introduction.....	5
2 Analysis of Unusual Sulfated Constituents and Anti-infective Properties of Two Indonesian Mangroves, <i>Lumnitzera littorea</i> and <i>Lumnitzera racemosa</i> (Combretaceae)	29
3 Challenging Structure Elucidation of Lumnitzerallactone, an Ellagic Acid Derivative from the Mangrove <i>Lumnitzera racemosa</i>	51
4 Phytochemical profiling of the Omani medicinal plant <i>Terminalia dhofarica</i>	71
5 Exploring <i>Hornstedtia scyphifera</i> : An extensive multimethod phytochemical investigation reveals the chemical composition and bioactive potential	89
6 Discussion and conclusion	117
7 Appendix	129
Declaration on author contributions	239
Curriculum vitae.....	241
Publications	242
Eidesstattliche Erklärung.....	244

Acknowledgements

An erster Stelle möchte ich Herrn Prof. Dr. Ludger A. Wessjohann danken für die Möglichkeit an diesem interessanten und vielseitigen Thema am Leibniz-Institut für Pflanzenbiochemie arbeiten zu können. Sein stetiges Interesse und seine Ideen haben maßgeblich den Fortschritt dieser Arbeit beeinflusst. Des Weiteren danke ich für die stetige Diskussionsbereitschaft, die Unterstützung bei der Durchsetzung von Autorenrechten sowie für die Ermöglichung der Teilnahme an zahlreichen Workshops und Konferenzen, die mich in meiner persönlichen Entwicklung weitergebracht haben.

Ein ganz besonderer Dank gilt meiner Mentorin Dr. Katrin Franke. Dein steter Support, dein zugängliches Wesen und deine inspirierende Leidenschaft für deine Forschung haben maßgeblich zum Erfolg dieser Arbeit beigetragen. Bei den diversen Problemen, die sich im Laufe dieser Arbeit gestellt haben, hat mir deine hilfsbereite Art und deine immense Kompetenz stets weitergeholfen. Auch für die Freiheit bei der Gestaltung meiner Vorträge, das unermüdliche Korrekturlesen und das Hinweisen auf mögliche Fehler oder etwas zu ausschweifigen Passagen meiner Arbeit bin ich sehr dankbar. Vielen herzlichen Dank liebe Katrin! Dr. Norbert Arnold möchte ich ebenfalls für seine stete Hilfsbereitschaft und sein inspirierendes Wesen danken. Das ein oder andere Experiment wäre ohne deine erfahrungsgeleiteten Ideen sicher gescheitert. Vielen Dank Norbert!

Ich möchte mich auch bei meinen fleißigen Diplomanden Klara Pieplow (Batch 1) und Annika Wujtschik (Batch 2) bedanken, die ebenfalls einen bedeutenden Beitrag zu dieser Arbeit geleistet haben. Ohne euch hätte ich nicht nur viel mehr Arbeit sondern auch deutlich weniger Spaß gehabt.

Ein ganz ähnlicher Dank geht an Dr. Lea Schmitz, Dr. Pauline Stark und Dr. Annegret Laub für die herzliche Aufnahme und die Unterstützung besonders in den ersten Zeit am IPB. Eure Ratschläge, die geteilten Erfahrungen und die gemeinsam verbrachte Zeit waren für mich unschätzbar bereichernd, vielen lieben Dank dafür!

Ich möchte noch einen besonderen Dank an Prof. Dr. Christian Griesinger sowie Dr. S. Phani B. Vemulapalli vom Max-Planck-Institut in Göttingen aussprechen für ihre bereitwillige Kooperation, die vielen hilfreichen Gespräche und die unschätzbar wertvolle Unterstützung bei der Klärung der Struktur von Lumnitzerlacton. In diesem Zusammenhang gilt mein großer Dank ebenfalls Dr. Andrea Porzel, Dr. Pauline Stark, Dr. Lea Schmitz, Dr. Katrin Franke und Dr. Tristan Fuchs.

Dr. Pauline Stark, Gudrun Hahn und Nicole Hünecke danke ich für die Messung unzählige NMR-Proben sowie die Durchführung von UV-Vis-, CD- und Drehwert-Messungen. Dr. Annegret Laub, Elana Kysil, Marvin Hempel, Dr. André Frolov und Dr. Alena Soboleva gilt mein Dank für die Messung der ebenso zahlreichen LC-HRMS Proben. Die wissenschaftliche Arbeit am IPB läuft unter anderem nur so reibungslos ab, weil die Funktionsfähigkeit der Geräte sowie diverse Serviceleistungen durch das stets freundliche und hilfsbereite technische Personal sichergestellt wird. Darum geht ein großer Dank an alle (ehemaligen) technischen Angestellten aus der NWC sowie an die Handwerkliche Abteilung. Mein besonderer Dank gilt dabei Luisa Kratzmann, Martina Lerbs, Martina Brode, Ymy Thi Ngo, Marie Richter, Felix Ölke und Eberhard Warkus. Ich danke den Gärtnern des IPBs, die sich um Anzucht und Pflege der Exemplare von *H. scyphifera* gekümmert haben. Dipendu Dhar und Dr. Mehdi Davari danke ich für die Kalkulationen der CD-Spektren, sowie Dr. Christoph Wagner (MLU Halle) für die Durchführung der Röntgenkristallanalyse.

Den Ombudspersonen Prof. Dr. Bettina Hause und Prof. Dr. Holger Kohlmann möchte ich für ihr offenes Ohr, das entgegengebrachte Verständnis und ihre Unterstützung danken.

Mein großer Dank gilt nicht zuletzt auch der gesamten Abteilung der Natur- und Wirkstoffchemie vor allem

aber dem Team aus Haus R2. Vielen herzlichen Dank für die gute und angenehme Arbeitsatmosphäre, für die Kollegialität, für die funktionierende Kaffeeversorgung, für die vielen kleinen und großen Hilfestellungen im Alltag, für zahlreiche teils auch fachliche Gespräche aber besonders auch für die schönen Ausflüge, die Abendessen und gemeinsam verbrachten Abende jenseits der Arbeit.

Ein ganz besonderer Dank geht an dieser Stelle an meine Freundin Claudia. Deine Unterstützung hat mir immer wieder den Rücken freigehalten! Vielen lieben Dank für deine unendliche Geduld, dein offenes Ohr und deine Rücksicht in den letzten Jahren.

List of Abbreviations

Å	Ångström
[α]	specific roation
AChE	acetylcholinesterase
ACD	advanced chemistry developement
ACD-SE	ACD-structure elucidator
ADEQUATE	adequate sensitivity double-quantum spectroscopy
calcd.	calculated
CASE	computer-assisted structure elucidation
CD	circular dichroism
CID	collision induced dissociation
COSY	correlation spectroscopy
<i>d</i>	doublet
<i>dd</i>	doublet of doublet
Da	Dalton
DAD	diode array detector
DFT	density functional theory
DMSO	dimethylsulfoxide
ESI	electrospray ionization
FA	formic acid
GC	gas chromatography
HMBC	heteronuclear multiple bond correlation
HRMS	high resolution mass spectrometry
HSQC	heteronuclear single quantum correlation
Hz	Hertz
INADEQUATE	incredible natural abundance double quantum transfer experiment
ITS	internal transcribed spacer
<i>J</i>	coupling constant
LC-MS	liquid chromatography-mass spectrometry
LSD	logic for structure determination
<i>m</i>	multiplet
<i>m/z</i>	mass-to-charge-ratio
MCD	molecular connectivity diagram
MeOH	methanol
min	minute(s)
MS	mass spectrometry
MS ²	tandem mass spectrometry
MS ⁿ	multistage mass spectrometry
NMR	nuclear magnetic resonance
NOESY	nuclear overhauser enhancement spectroscopy
NP	natural product
P	peak number
ppm	parts per million
<i>q</i>	quartett
RDB	ring double bond equivalent
rel. Int.	relative intensity
R _f	retention factor
ROESY	rotating-frame overhauser effect spectroscopy
RP	reversed phase
R _t	retention time
<i>s</i>	singlet
<i>t</i>	triplet
TIC	total ion chromatogram
TLC	thin layer chromatography
TMS	tetramethylsilane
TOCSY	total correlation spectroscopy
TOF	time of flight
(U)HPLC	(ultra) high performance liquid chromatography
UV/vis	ultraviolet/visible

Summary

History has shown that plants have always been one of the most important sources for medicinal applications for humankind. Even today, plants remain one of the most promising sources for the discovery of new (bioactive) compounds, thanks to an immense reservoir of yet unknown natural products. However, this resource is at risk due to species extinction driven by climate change and the global decline in biodiversity. The focus of the present thesis was the explorative investigation of secondary metabolites from three yet briefly studied medicinal plants from the Combretaceae and Zingiberaceae families, native to the Middle East and Southeast Asia. The aim was to connect potential bioactivity with the medicinal applications described in the literature, as well as to perform a most complete characterization of the secondary metabolites, including isolation and structure elucidation, with a particular emphasis on the identification of new compounds.

Roots of the mangrove species *Lumnitzera littorea* and *Lumnitzera racemosa* from 31 various Indonesian regions were investigated to discover new anti-infective compounds. Phytochemical analysis revealed a unique diversity of sulfated ellagic acid derivatives, with 3,3',4'-tri-*O*-methyl-ellagic acid-4-sulfate (**2-15**) being the most abundant one. Targeted isolation yielded six pure compounds, of which five were described for the first time within the species and three contained a sulfate moiety. Phylogenetic data corroborated samples with specific phytochemical patterns to form well-supported clades in the ITS tree, showing evolutionary insights. Antibacterial activity was observed for both species but not all sampled specimen. Instead, activity was connected to certain locations, hinting to environmental influence.

Further, the discovery, isolation and characterization of the novel natural product, lumnitzeralactone (**3-1**), derived from *L. racemosa* was achieved (Chapter 3). Its structure was elucidated by using advanced NMR experiments (1,1-ADEQUATE, 1-n-ADEQUATE), partly deuterated solvents (MeOH-*d*₃), computational methods (CASE, DFT), and eventually confirmed by a total synthesis. However, lumnitzeralactone was exclusively found in extracts with antibacterial effects, but did not show activity when tested as pure compound, suggesting that the observed activity may be due to synergistic effects. Additionally, a biosynthetic pathway involving associated microorganisms was suggested.

The phytochemical investigation of *Terminalia dhofarica* (Chapter 4) revealed simple phenolics and polyphenols, such as flavonoids and tannins, particularly galloyl and chebulic acid derivatives, as the major secondary metabolites. An isolation approach yielded 20 compounds. Eight compounds were described for the first time within the species. Additionally, 1-*O*-galloyl-6-*O*-coumaroyl- β -D-glucose (**4-1**) was isolated for the first time and unequivocally characterized by a complete NMR dataset. Noteworthy, seven isolated compounds contained methylations and therefore led to critical examination of the dataset for possible artefact generation. Antimicrobial effects of the crude extract were attributed to the combined effects of various compounds with nonspecific activity.

Moreover, the first comprehensive phytochemical analysis of the leaves of *Hornstedtia scyphifera* was conducted (Chapter 5). Major compound classes are terpenoids, flavonoids, and phenolics. Isolation yielded two new sesquiterpenoids, mustak-14-oic acid (**5-1**) and 6-hydroxy-anhuienosol (**5-2**), along with 24 known compounds of which 21 were reported for the first time from this species. Moreover, the crystal structure of the flavonoid kumatakenin (**5-13**) was described for the first time, and its fragmentation pathway was established by MSⁿ analysis. Reported bioactivities for isolated compounds were collected from literature and explain the observed antimicrobial effect of *H. scyphifera* crude extract.

In conclusion, this work has significantly expanded the knowledge of the chemical diversity of the three plant species studied and provided new insights into their secondary metabolite profile. The findings have been published in three peer-reviewed journals, with a fourth publication under preparation. A total of 53 substances were isolated and characterized using various methods (HRMS, MS^{2/n}, 1D and 2D NMR, CD, X-ray), leading to the structural identification of these compounds, three of which were previously unknown to science.

Zusammenfassung

Die Geschichte hat gezeigt, dass Pflanzen seit jeher eine der wichtigsten Quellen für medizinische Anwendungen waren. Auch heute noch gelten Pflanzen als eine der vielversprechendsten Quellen zur Entdeckung neuer (bioaktiver) Verbindungen, da sie über ein enormes Reservoir bisher unbekannter Naturstoffe verfügen. Diese Ressource ist jedoch durch Artensterben und den durch den klimawandelbedingten globalen Rückgang der Biodiversität, gefährdet. Im Fokus der vorliegenden Dissertation stand die explorative Untersuchung der Sekundärmetaboliten von drei bisher kaum erforschten Heilpflanzen aus den Familien Combretaceae und Zingiberaceae, die im Nahen Osten und Südostasien beheimatet sind. Ziel war es, eine mögliche Bioaktivität mit den in der Literatur beschriebenen medizinischen Anwendungen zu verknüpfen sowie eine möglichst vollständige Charakterisierung der Sekundärmetaboliten, einschließlich Isolierung und Strukturaufklärung, mit besonderem Schwerpunkt auf der Identifizierung neuer Verbindungen durchzuführen.

Kapitel 2 befasst sich mit der Untersuchung der Mangrovenarten *Lumnitzera littorea* und *Lumnitzera racemosa*. Aus den Wurzeln dieser beiden Spezies, welche an 31 verschiedenen indonesischen Standorten gesammelt wurden, sollten neue antimikrobielle Verbindungen identifiziert werden. Die phytochemische Analyse zeigte eine einzigartige Vielfalt sulfatierter Ellagsäurederivate, wobei 3,3',4'-Tri-*O*-methyellagsäure-4-sulfat (**2-15**) das mengenmäßig bedeutsamste Derivat darstellt. Die gezielte Isolierung aus *L. racemosa* lieferte sechs Reinsubstanzen, von denen fünf erstmals für diese Art beschrieben wurden, darunter drei sulfatierte Verbindungen. Phylogenetische Daten zeigten das Clustern von Proben mit ähnlichem phytochemischen Profil im, ITS-Baum, was evolutionäre Einblicke ermöglichte. Die antibakterielle Aktivität wurde für beide Arten nachgewiesen, jedoch nicht für alle Individuen. Stattdessen war die Aktivität standortspezifisch, was auf einen Umwelteinfluss hinweist.

Kapitel 3 umfasst die Identifizierung, Isolierung und Charakterisierung des neuartigen Naturstoffes Lumnitzeralacton (**3-1**) aus *L. racemosa*. Die Struktur konnte durch eine Kombination aus speziellen 2D NMR-Experimenten (1,1-ADEQUATE, 1-n-ADEQUATE), Nutzung teildeuterierter Lösungsmittel (MeOH-*d*₃), computergestützten Methoden (CASE, DFT) und der Entwicklung einer Totalsynthese aufgeklärt werden. Interessanterweise wurde Lumnitzeralacton ausschließlich in Extrakten mit antibakterieller Wirkung gefunden, zeigte jedoch als reine Verbindung keine derartige Aktivität. Dies deutet auf synergistische Effekte hin. Darüber hinaus wurde eine mögliche Biosynthese unter Einbeziehung assoziierter Mikroorganismen vorgeschlagen.

Die phytochemische Untersuchung von *Terminalia dhofarica* in Kapitel 4 offenbarte als Hauptverbindungsklassen einfache Phenole und Polyphenole wie Flavonoide und Tannine, insbesondere Galloyl- und Chebulinsäurederivate. Insgesamt konnten 20 Verbindungen isoliert und ihre Struktur aufgeklärt werden. Acht Verbindungen wurden erstmals innerhalb der Art beschrieben. Zudem konnte erstmalig die Verbindung 1-*O*-Galloyl-6-*O*-cumaryl- β -D-glucose (**4-1**) isoliert und mittels NMR charakterisiert werden. Sieben der isolierten Verbindungen zeigten Methylierungen auf, was eine kritische Prüfung der Datensätze auf mögliche Artefaktbildung erforderlich machte. Die antimikrobielle Wirkung des Rohextrakts wurde den kombinierten Effekten verschiedener Verbindungen mit unspezifischer Aktivität zugeschrieben.

Die erste umfassende phytochemische Analyse der Blätter von *Hornstedtia scyphifera* wird in Kapitel 5 beschrieben. Die Hauptverbindungsklassen sind Terpenoide, Flavonoide und Phenole. Es konnten

insgesamt 26 Substanzen isoliert werden, darunter zwei neue Sesquiterpenoide, Mustak-14-oinsäure (**5-1**) und 6-Hydroxy-Anhuienosol (**5-2**). 21 Verbindungen wurden erstmals für diese Art beschrieben. Zudem wurde die Kristallstruktur des Flavonoids Kumatakenin (**5-13**) erstmals beschrieben, und dessen Fragmentierungsmuster durch MSⁿ-Analyse geklärt. Die in der Literatur beschriebenen Aktivitäten der isolierten Verbindungen erklären die beobachtete antimikrobielle Wirkung des Rohextrakts von *H. scyphifera* hinreichend.

Zusammenfassend hat diese Dissertation das Wissen über die chemische Vielfalt der drei untersuchten Pflanzenarten erheblich erweitert und neue Einblicke in ihr sekundäres Metabolitenprofil geliefert. Die Ergebnisse wurden in drei Peer-Review-Zeitschriften veröffentlicht, und eine vierte Publikation befindet sich in Vorbereitung. Insgesamt wurden 53 Substanzen isoliert und mittels verschiedener Methoden (HRMS, MS^{2/n}, 1D- und 2D-NMR, CD, Röntgenstrukturanalyse) charakterisiert, was zur strukturellen Identifizierung dieser Verbindungen führte, von denen drei der Wissenschaft bisher unbekannt waren.

1 General Introduction

1.1 Natural products – origin, structure, activities

Plants are an essential part of life on Earth. They not only serve as producers of oxygen and sequester carbon dioxide but also provide a primary source of food for both animals and humans. Additionally, they have played a pivotal role in traditional medicine. From treating infections and digestive issues to functioning as pain relievers, ancient plant formulations such as powders, tinctures, teas, inhalations, and other herbal preparations form the foundation of modern medicine [1,2]. However, knowledge of traditional medicinal uses is disappearing along with plant biodiversity, largely due to climate change and the current pace of globalization. This puts much valuable information at risk of being lost forever [3]. A rough estimate suggests that less than 10% of the world's biodiversity has been evaluated for potential biological activity [4]. Moreover, according to previous estimates, only 6% of the described plant species have been systematically investigated pharmacologically, and only around 15% have been examined phytochemically [1,5]. The remaining potential for the vast number of yet unexplored species is therefore immense! Each year, new species are described. In 2020 over 8600 plant species were added to the list that counts now approximately 377,000 accepted species [6]. But there are estimated around 100,000 species of vascular plants still to be described as new to science [7].

All plant-derived substances are broadly classified into primary and secondary natural products (NPs). Primary NPs, such as amino acids, lipids, and carbohydrates, primarily serve the essential life-sustaining functions of the organism. In contrast, secondary NPs have a more specialized definition and serve specific functions that enhance a plant's survival. For instance, fragrances and pigments attract pollinators, bitter compounds such as alkaloids and terpenes protect the plant from herbivores, while antibiotic compound shield from microbial infection [8,9]. All of these substances are a result of constant evolutionary adaptation pressure [10]. This wide range of functions is achieved through a vast chemical diversity, which gives rise to the broad spectrum of biological activities, including antimicrobial [11,12], antioxidative [13], anti-inflammatory [13,14], anthelmintic [15], antifungal [16], anticancer [17,18], analgesic [14], and neuro-protective activity [19], just to mention some. These examples demonstrate the immense pharmacological potential of secondary metabolites.

The review by Newman and Cragg [20] on natural products as sources of new drugs provides a comprehensive statistical overview of drugs entering the global market from January 1981 to September 2019. Throughout this period, 1394 new drugs were approved, of which 1188 were small molecules. Among these small molecules, 53% were identified as natural products, natural product derivatives, or synthetics with a natural product pharmacophore. This statistic clearly underlines the significant impact of natural products on pharmaceutical innovation, resulting from the potential mentioned above. However, it is noteworthy that there are therapeutic classes with synthetic drugs only, such as antihistamines, diuretics, and hypnotics [20].

The beginning of rational drug discovery using pure compounds, as opposed to crude materials, occurred over 200 years ago with the work of the German pharmacist's apprentice Friedrich Sertürner, who isolated morphine, the active compound of the narcotic plant *Papaver somniferum*, commonly known as the opium poppy, in the form of a water-insoluble crystal [1,21]. A notable example of a modern medication derived from plant-based natural products is metformin, an antidiabetic drug whose origins can be traced back to

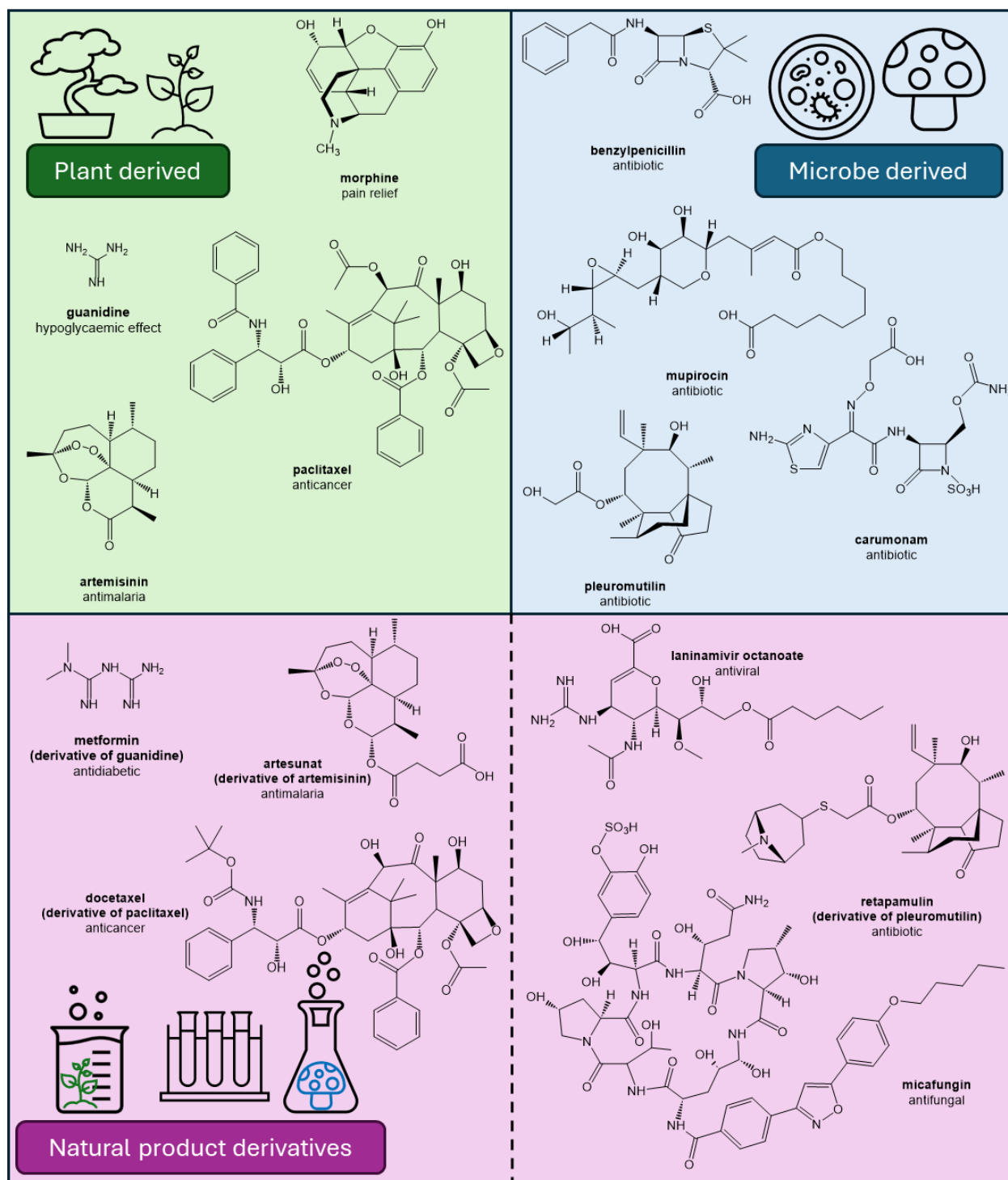


Fig 1-1 Representative bioactive natural products from plant origin, microbial origin, and natural product derivatives [20]

the medieval use of the herbal remedy Goat's Rue (*Galega officinalis*) [22]. Traditionally, this plant species was employed to treat various ailments, including plague, worms, snakebites, miasma, and dysuria, as well as symptoms now associated with type 2 diabetes [23]. Subsequent investigations revealed that Goat's Rue contains high levels of guanidines, which were found to exhibit hypoglycemic effects in the early 20th century [24]. However, their significant toxicity necessitated further chemical modification. This resulted in the development of biguanides, including dimethylbiguanide (metformin) in 1929 [25,26]. While other biguanides displayed undesirable side effects, such as hypoglycemia and weight gain, metformin effectively lowers blood sugar without inducing these adverse effects [27]. Furthermore, metformin offers unique benefits, particularly in addressing insulin resistance, reducing cardiovascular mortality, and improving

survival rates in overweight and obese patients with type 2 diabetes when administered in the early stages of the disease [28,29].

While plants are, as mentioned above, a highly valuable source of bioactive compounds, they are not always the true producers of these compounds. Ecosystems are characterized by interactions among various organisms. For the benefit of both parties, plants often engage in synergistic relationships with associated microorganisms such as fungi, algae, and bacteria. These microorganisms possess a different enzymatic range and can facilitate reactions that plants cannot perform on their own. The microorganisms contribute to plant growth, health, and stress resistance through various mechanisms, including improved nutrient uptake, enhanced resistance to diseases, and the production of beneficial compounds that promote plant growth and protect against pathogens [30–35]. Since microorganisms have received considerable attention, it has become clear that a significant number of natural product drugs are, in fact, produced by microbes or through microbial interactions with the host plant species from which the compounds were isolated [20]. A similar phenomenon is discussed in chapter 3. Moreover, microorganisms themselves represent a valuable source of bioactive natural products. With advancements in microbiology, their applications have expanded to include enzymes, biological control agents, antibiotics, and other pharmacologically active products. Undoubtedly, one of the most famous natural product discoveries derived from a microorganism is the antibiotic penicillin, which was isolated from the fungus *Penicillium notatum* by Alexander Fleming in 1928 [4].

However, natural product-based drug discovery is associated with several intrinsic challenges pushing the pharmaceutical industry to shift its primary focus toward synthetic compound libraries. The results obtained from this approach, however, have not always met expectations. The declining number of new drugs reaching the market, due to rising admission costs and requirements, has revitalized interest in natural product-based drug discovery. Despite their often inherent complexity and high costs, natural products still represent one of the best options for identifying novel agents [20]. When developed in cooperation with specialists from synthetic chemistry and biology, these natural products offer the potential to discover innovative structures and new modes of action that can lead to effective treatments for a variety of human diseases [1,20].

1.2 Objectives

The general objective of the present thesis was thus the explorative investigation of secondary metabolites of promising medical plants for the identification of new bioactive compounds. In particular, the thesis covered the following aspects:

- Investigation of the medicinal plant families Combretaceae and Zingiberaceae as sources for new bioactives
- Isolation, characterization, and structure elucidation of secondary metabolites from the species *Lumnitzera racemosa*, *Terminalia dhofarica* and *Hornstedtia scyphifera*
- Application of sophisticated methods including ADEQUATE NMR experiments and modern Computer-Assisted Structure Elucidation (CASE) systems for structure elucidation of proton deficient natural products
- Bioactivity screening of extracts and of isolated compounds to evaluate their potential as new bioactive natural product templates.

1.3 The Combretaceae family

The family Combretaceae belongs to the flowering plants (Angiosperms) and is first described in 1810 by botanist Robert Brown in *Prodromus Florae Novae Hollandiae et Insulae Van Diemen*, with focus on the Australian flora [36]. Today, the family comprises approximately 12-23 genera, due to a matter of controversy, with over 500 species [37–40] and is classified into two subfamilies, *Combretoidae*, and *Strephonematoideae*. The latter consists of a single genus, *Strephonema*, which includes only three species of trees native to western tropical Africa. *Strephonematoideae* are distinguished from *Combretoidae* by having a semi-inferior ovary, while all members of *Combretoidae* possess an inferior ovary [39,40].



Fig 1-2 Worldwide distribution of Combretaceae family [41]

The family predominantly inhabits tropical and subtropical regions, with a broad distribution across Africa, Central and South America, Southern Asia, and Northern Australia [39,40]. These species exhibit remarkable ecological adaptability, occupying a wide range of habitats, including forests, woodlands, and savannahs [39,40]. Members of the family include a variety of growth forms, like lianas, shrubs, trees, mangroves, and rarely creepers [39,40]. Notably, mangrove species from the genus *Laguncularia* and *Conocarpus* are found along the coasts of the Americas, Australia, and Africa, whereas species from *Lumnitzera*, alongside with *Terminalia*, is distributed across Asia and Africa [39,40].

Leaves of the Combretaceae family are simple, entire, and often exhibit stalked glands or glandular scales [37,39,40]. They are generally opposite, verticillate, spiral, or alternate, and are petiolate (rarely sessile) [39,40]. The flowers are typically small. The ovary is inferior or semi-inferior, and the hypanthium (floral cup) is divided into a lower part that surrounds the ovary and an upper part that forms a tube, terminating in calyx lobes [37,39,40].

Members of the family are useful crops for humanity by producing partially edible fruits and kernels, serving as important commercial sources of gum, and are recognized as valuable timber trees in Europe, America, and Africa. Additionally, various parts of these plants, including the tannin-rich bark, but also fruit, leaves, and timber, have been utilized in traditional medicine in Asia and Africa for approximately over 90 medical indications, many of them related to treating infections [37,40,42].

1.3.1 Genus *Lumnitzera*

The genus *Lumnitzera* consists of two species of true mangroves distributed from eastern tropical Africa to Australia, including India and some islands in the Indian and Pacific Oceans, namely *Lumnitzera littorea* and *Lumnitzera racemosa* [39]. The genus was named in honor of the Hungarian botanist, István Lumnitzer (1750-1806), a pioneer in systematic description of European plants, who worked also in the German cities Jena and Halle. [43–46]. Usually, the distribution areas of the two species do not overlap, but are adjacent to each other, so that isolated exchanges of individuals can still take place. Rarely, this results in an apparently sterile hybrid of mixed characteristics, *Lumnitzera x rosea* [44,47–49].

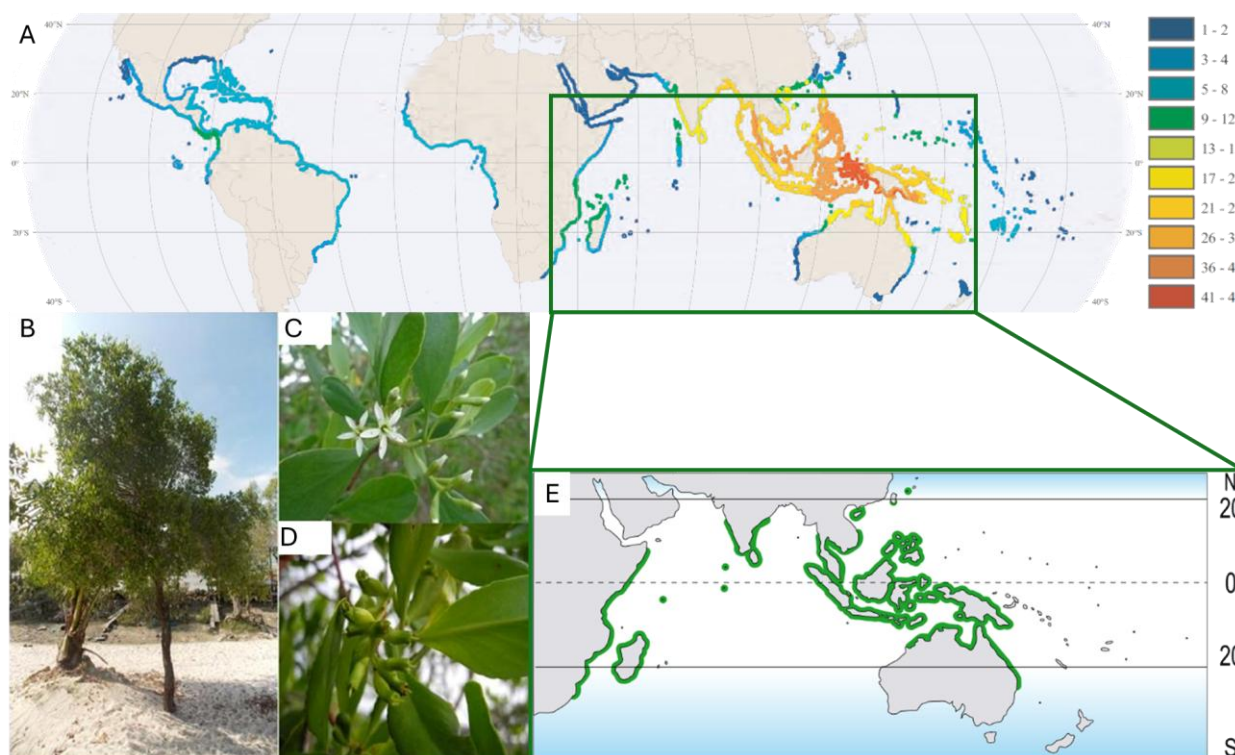


Fig 1-3 **A** Diversity of mangrove species worldwide, Colors indicate the potential number of species, adapted from Spalding et al. [50]; **B** Tree, **C** Flower; **D** Fruit , and leaf (B, C, D) of *L. racemosa*, adapted from Manurung [51]; **E** Worldwide distribution of *L. racemosa*, adapted from Duke et al.[44]

1.3.2 Species *Lumnitzera racemosa*

Lumnitzera racemosa appears as scattered sparse shrubs or as slender trees in small forests, depending on the growing conditions. Shrubs predominantly appear in arid landward upland margins of mangrove forests, bordering to exposed salt pans with high salinity levels and nearly dry sediments. In wetter habitats, *L. racemosa* grows in its tree form, typically in association with other mangroves, like *Avicennia marina* (grey mangrove), *Excoecaria agallocha* (blind-your-eye mangrove), or *Ceriops australis* (yellow mangrove) [44]. *L. racemosa* is an evergreen plant, exhibiting in both growing forms often multiple stems. The white self-compatible flowers attract a variety of day-active pollinators, like wasps, bees, butterflies, or moths and is the easiest feature to distinguish between *L. racemosa* and its close relative, the red flowered *L. littorea*. After successful fertilization, the resulting fruits are 1-1.5 cm long, 1-seeded hard drupes that have an elliptic shape, a fibrous epicarp, and the useful ability to float [44,49,51].

Due to its widespread distribution (Figure 2 E), *L. racemosa* is used in traditional medicine in many countries to treat health conditions. The sap from old bark, juice from young twigs, and fruits have been found particularly effective in treating skin disorders, herpes, scabies, itching (pruritus), wounds, and thrush caused by fungal infections in countries such as India, Sri Lanka, China, Malaysia, Singapore, Thailand, Taiwan, the Maldives, and the Philippines [49,52–55]. In parts of India, local tribes use this plant to treat snakebites and as a blood purifier. Preparations from *L. racemosa* have also been employed to treat sores, asthma, leprosy, and as an antifertility agent to prevent pregnancy [49,56,57]. In China, the trunk's juice is used to treat mouth or tongue ulcers (aphtha), while the bark is utilized for managing diabetes and treating kidney stones [49,58–60].

L. racemosa was already subject of many studies to report the phytochemical classes present. Nevertheless, many of them focused on qualitative test for compound classes [61–65] or analysis of volatile compounds

via GC-MS [63,65], instead of isolating pure compounds, followed by full characterization and structure elucidation. However, the major compound classes of secondary metabolites reported from extracts of *L. racemosa* are tannins [66–68], flavonoids [66,67,69–71], alkaloids [72], terpenes [66,67,72], and phenols [66,67,70,72].

1.3.3 Genus *Anogeissus* (syn. *Terminalia*)

The genus *Anogeissus* (Combretaceae) consists of eight species: *A. acuminata*, *A. bentii*, *A. dhofarica*, *A. latifolia*, *A. leiocarpus*, *A. pendula*, *A. rivularis*, and *A. sericea* [73]. These species are primarily native in Southern Asia, the Arabian Peninsula and West Africa. [40,73].

Most species of *Anogeissus* are growing either as trees or shrubs, characterized by their distinct foliage and notable flowers. The leaves are alternate or opposite, and they are typically short-petiolate with entire margins. When young, the leaves are often pubescent, giving them a fine, soft texture due to small hairs on their surface. The flowers of *Anogeissus* species are notable for their dense, globose heads, which are borne on short, axillary or terminal peduncles. These flower heads can be either solitary or arranged in racemes, contributing to the plant's unique floral architecture [73,74]. The fruits of *Anogeissus* are particularly distinctive. They are small, numerous, and typically either two-winged or four-ribbed, which aids in wind dispersal. These fruits are tightly packed into dense, cone-like clusters, further enhancing the plant's reproductive efficiency. This compact arrangement of fruits and the winged or ribbed structures are morphological traits shared with the genus *Terminalia*, reflecting their evolutionary relationship [73,74]. Connection between these genera became even more apparent as recent research reported convincing molecular reconstructions and phylogenetic analysis that led to the transfer of the genus *Anogeissus* into the genus *Terminalia*, including formal taxonomic name changes for certain species [39,75,76].

Commonly referred to by names such as ghatti tree, button tree, axlewood tree, and chewing stick tree, these plants hold significant ethnomedicinal value among indigenous communities [77–80]. Various parts of former *Anogeissus* species are used to treat ailments ranging from gastric disorders, skin diseases, and diabetes to wound healing and coughs [77,78,80,81]. For instance, *Terminalia phillyreifolia* (Basionym: *Anogeissus acuminata* [76]) is known for its antidiabetic properties in Thailand [81], while *Terminalia dhofarica* (Basionym: *Anogeissus dhofarica* [76,82]) is used in Oman for wound healing and as an antiseptic [78].

The phytochemistry of *Anogeissus* reveals a wealth of bioactive compounds, including alkaloids, flavonoids, terpenoids, generally polyphenols and tannins, which underpin the pharmacological activities of these species [83,84]. Most of the so far isolated compounds are phenolics. Especially gallic acid and derivatives were abundant, such as ellagic acid, glycosides of ellagic and flavellagic acid such as 3,3'-di-*O*-methyl ellagic acid-4'- β -D-xyloside and 3,4,3'-tri-*O*-methylflavellagic acid-4'- β -D-glucoside. But also flavonoids like quercetin, rutin, castalagin, and other compounds such as anolignan A, B, C, anogeissinin are well described [74,85–89].

Modern pharmacological evaluations were carried out of crude extracts and of isolated compounds. Screenings revealed that extracts from species such as *T. phillyreifolia*, *T. anogeissiana* (Basionym: *A. latifolia* [76]), and *T. schimperi* (Basionym: *A. leiocarpus* [76]) have antioxidant, antimicrobial, antiparasitic, wound healing, and antidiabetic properties [74,78,83,90–93]. Despite the rich medicinal and pharmacological applications of former *Anogeissus* species, certain species such as *T. schimperi* (Basionym: *A. bentii* [76]) and *T. dhofarica* are threatened due to overexploitation as wood, habitat loss, and climate change, with the latter being classified as vulnerable by the IUCN [74,94]. This calls for

increased conservation efforts and further research into the phytochemistry and therapeutic potential of these underexplored species.

1.3.4 Species *Terminalia dhofarica*

Terminalia dhofarica (A.J. Scott) (Basionym: *Anogeissus dhofarica*) is a member of the Combretaceae family, and former member of the genus *Anogeissus* [75,76]. The species is a significant endemic tree found along a coastal strip approximately 300 km long in southeastern Yemen and the Dhofar region of southwestern Oman, representing the largest forested areas in both countries [95]. It is commonly referred to as "Gahtti," and is the only representative of its genus in these regions, thriving in the unique monsoon fog oasis ecosystems. It is capable of growing up to 12 meters in height, although often reduced to a shrub by browsing and chopping [96]. The leaves of *T. dhofarica* are initially bright green, often shifting to a bluish-green hue, and they fall off at the onset of the dry season in November and December. New leaves emerge 7 to 8 months later, just before the arrival of the monsoon season (kareef), and are commonly utilized as fodder for dromedary herds in Oman. The small, yellowish flowers are grouped into globose clusters, attracting bees and subsequently developing into cone-shaped fruit heads [95].

Historically, *T. dhofarica* has been integral to local communities, where its useful properties have been exploited since millennia. The foliage is widely used as fodder and believed to boost milk production in livestock. Bark is used to color the coarse, unbleached cotton cloth [74,97]. Dhofari women use water infused with dried leaves for personal hygiene and antibacterial purposes [95]. Additionally, leaves are applied as a paste around infected wounds to treat sores and prevent infection [78,98]. Despite its extensive use in traditional medicine as a wound healer and an antiseptic, the phytochemical and pharmacological profile of *T. dhofarica* has been largely overlooked, especially when compared to other members of its genus, such as *T. anogeissiana* (Basionym: *A. latifolia*) and *T. schimperi* (Basionym: *A. leiocarpus*), which have been studied extensively [74,99].

Previous research has demonstrated that aqueous and alcoholic extracts of *T. dhofarica* exert significant antioxidant activity in a DPPH radical scavenging assay, [78]. together with a high phenolic content of 551 mg/g in gallic acid equivalents [78]. In terms of antibacterial effects, *T. dhofarica* exhibited inhibitory activity against *Staphylococcus aureus* (Gram-positive) at a concentration of 250 µg/ml and against *Pseudomonas aeruginosa* (Gram-negative) at 500 µg/ml [78,100]. Furthermore, the plant has antifungal properties, showing inhibition against *Candida albicans* at concentrations of 500 µg/ml [78].

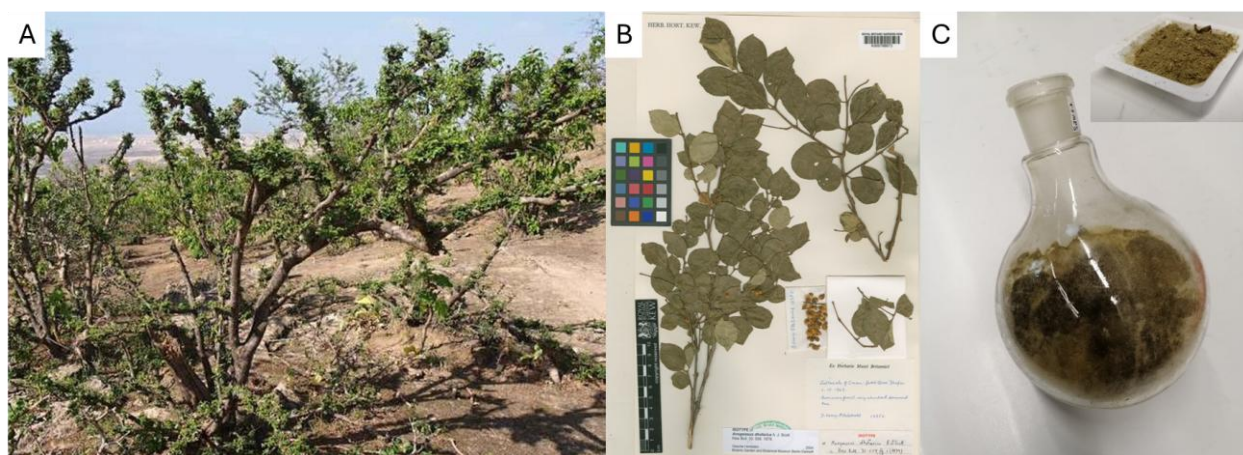


Fig 1-4 A *T. dhofarica* tree [101]; B Dried leaves [102]; C Leaf powder and dried crude extract

This indicates, that *T. dhofarica* must contain bioactive compounds, most certainly of the same major classes found in other species of the genus, which means tannins, phenolics, flavonoids, and terpenes [74].

Recent studies of Maqsood et al., and Abuarqoub et al. [97,103] show, that the plant's potential goes beyond antioxidant, antifungal and antimicrobial activity and underline activities for the first time assigning chemical structures from LC-MS analysis of diverse extracts. Both verified the high phenolic content and could show a high content of flavonoids which is strongly connected to the observed anti-oxidative and radical scavenging effects. Additionally, they annotated preliminarily 28 compounds, most of them flavonoids and phenolic acids, all known to the genus. Testing of diverse extracts suggested that *T. dhofarica* may also have anticancer and antidiabetic properties, making it a promising candidate for the development of novel therapeutic agents [97,103]. Further, Abuarqoub et al revealed significant anti-inflammatory properties. The extracts notably increased the secretion of pro-inflammatory cytokines such as IL-1, IL-6, and TNF- α , which are crucial for macrophage activation and differentiation into the M1 subtype. This subtype is involved in pathogen defense and tissue repair [97]. Additionally, IL-12p70 secretion was upregulated indicating the promotion of an immune response. Next to that, the wound healing capabilities already described in traditional medicine were verified in a standard scratch test assay, showing enhanced fibroblast migration and wound healing promotion. The findings of both tests suggest that *T. dhofarica* could play a valuable role in managing inflammation and aiding tissue regeneration. Although *T. dhofarica* has been extensively used in traditional medicine, its phytochemical and pharmacological properties remain largely unexplored. Current research indicates that this species holds significant promise as a source of a broad range of agents, and further studies are needed to fully understand its therapeutic potential.

1.4 The Zingiberaceae family

The Zingiberaceae family, better known as the ginger family, is the largest within the eight families of Zingiberales order, consisting of 53 genera and more than 1,200 species. The still accepted classification categorizes the Zingiberaceae into four main tribes: Alpinieae, Globbeae, Hedychieae, and Zingibereae. While several morphological features, such as ovary structure, leaf distichy, and staminode presence have been employed to differentiate the four tribes, the defining characteristics are often neither unique to a specific tribe nor consistently present across all taxa within [104]. Therefore, a new classification through DNA sequencing of nuclear internal transcribed spacer (ITS) and plastid *matK* regions might change the old order. Generally, plants of the family are perennial and have an aromatic fleshy, sometimes tuberous rhizome. The stem is usually short and sometimes replaced by pseudostems formed from leaves. The inflorescence is usually terminal on the pseudostems or on short shoots arising from the rhizomes. They

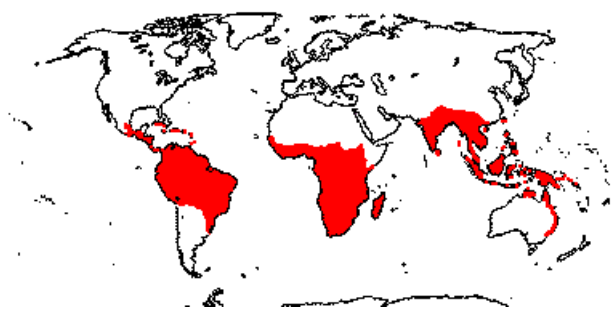


Fig 1-5 Worldwide distribution of Zingiberaceae family [105]

can have many or just a few bisexual flowers but often with conspicuous colored bracts [106]. The fruit is a capsule, which may be either fleshy or dry, and can be dehiscent or indehiscent, occasionally resembling a berry [106]. However, members of the family are distributed in tropical regions, including India, SE Asia, Africa, and Australia [104–106]. The most well-known species of the family is the common ginger, *Zingiber officinale*, famous for the typical thick fleshy rhizome full of aromatic and flavor compounds like mono- and sesquiterpenoids, and especially for the pungent gingerols and shogaols. Many other species of this family are traditionally used as spices, perfumes or ornamental plants, but also cultivated for their showy flowers and much more for their medicinal properties due to the presence of abundant bioactive compounds [107–109]. Extracts and isolates from various Zingiberaceae species have demonstrated antioxidative [110–113], antimicrobial [112], anti-inflammatory [111,113], or anticancer [112,113] properties, as well as neuroprotective effects [114]. In our days, they gained more attention due to their anti-aging, anticancer, anti-Alzheimer effects as well as a variety of other medicinal applications [110,115].

1.4.1 Genus *Hornstedtia*

The genus *Hornstedtia* contains approximately 43 species that are distributed across tropical Southeast Asia, from the Malay Peninsula to the Himalayas [116,117]. It features radical inflorescences that are encased in a rigid involucre made up of sterile bracts. These inflorescences are typically elevated above the ground on stilt roots. The flowers usually emerge gradually, with only their tips visible at a time [118]. Species of the genus are known to be used in traditional medicine for the treatment of various ailments, such as stomach issues, diarrhea, fever, and chills [115,119,120]. Surprisingly, although a relevant potential for medical uses of the plants is unquestionable, much less research was performed on the phytochemical composition of the genus, except the analysis of essential oils and volatile fraction of diverse organs (table 1-1).

1.4.2 Species *Hornstedtia scyphifera*

One yet briefly researched member of this genus is *Hornstedtia scyphifera*, which is also known under the synonyms *Amomum scyphiferum*, *Cardamomum scyphiferum*, *Greenwaya scyphifer*, or *Greenwaya scyphiferus* [121].

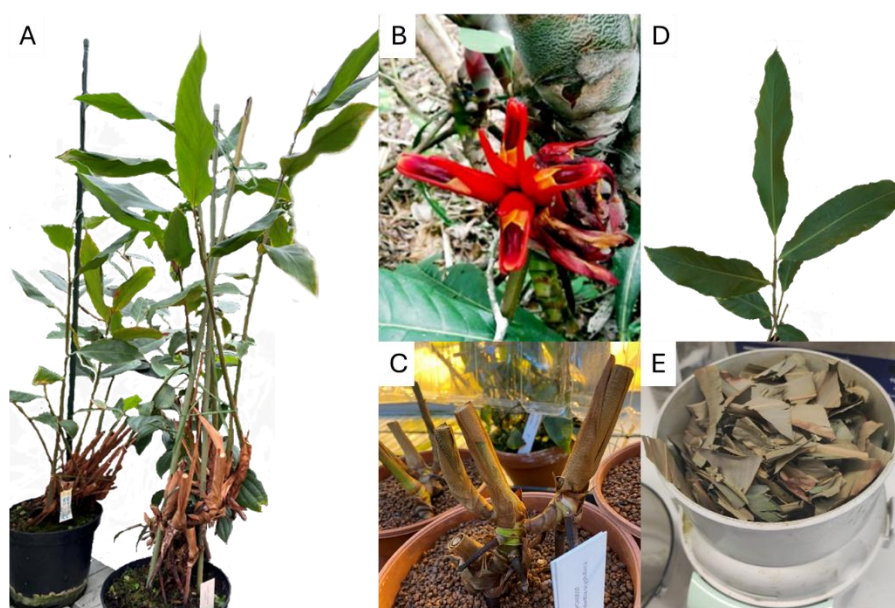


Fig 1-6 *Hornstedtia scyphifera* **A** Plant growing in Greenhouse of IPB; **B** Flower [122] **C** Fresh planted rhizome ; **D** Fresh leaf; **E** Dried leaves

Table 1-1 Volatiles of different species of the genus *Hornstedtia*, adapted from the diploma thesis of Klara Pieplow [126]

	Compound	Formula	Exact mass [g/mol]	Plant organ*				Bioactivity
				Rhizome	Flower	Leaf	Stem	
Monoterpenoids	1,8-Cineol	C ₁₀ H ₁₈ O	154.1358	<i>H.scy.</i> [123] <i>H.bel.</i> [127]	<i>H.scy.</i> [123] <i>H.hav.</i> [128]	<i>H.scy.</i> [123] <i>H.bel.</i> [127]	<i>H.scy.</i> [123] <i>H.leo.</i> [129]	anti-inflammatory[130,131], antidepressive [130], antioxidative [130,132], antimicrobial[132,133], antifungal[133], AChE inhibitor[134]
	Isoborneol	C ₁₀ H ₁₈ O	154.1358		<i>H.hav.</i> [128]		<i>H.scy.</i> [123]	antibacterial[135], antiviral[136], antioxidative[137], neuroprotektive[137]
	Borneol	C ₁₀ H ₁₈ O	154.1358	<i>H.scy.</i> [123] <i>H.hav.</i> [128] <i>H.bel.</i> [127]	<i>H.scy.</i> [123] <i>H.hav.</i> [128]	<i>H.scy.</i> [123]	<i>H.scy.</i> [123]	antibacterial[138]
	Terpineol	C ₁₀ H ₁₈ O	154.1358	<i>H.san.</i> [139] <i>H.scy.</i> [123] <i>H.hav.</i> [128] <i>H.bel.</i> [127]	<i>H.scy.</i> [123] <i>H.hav.</i> [128]	<i>H.san.</i> [139] <i>H.scy.</i> [123] <i>H.bel.</i> [127]	<i>H.san.</i> [139] <i>H.scy.</i> [123]	antibacterial[140], antifungal[141]
	Camphor	C ₁₀ H ₁₆ O	152.237	<i>H.san.</i> [139] <i>H.hav.</i> [128] <i>H.scy.</i> [123] <i>H.bel.</i> [127]	<i>H.hav.</i> [128] <i>H.scy.</i> [123]	<i>H.san.</i> [139] <i>H.scy.</i> [123]		insecticide[142], antibacterial[143], AChE inhibitor[134]
	Myrtenal	C ₁₀ H ₁₄ O	150.1045		<i>H.scy.</i> [123]	<i>H.scy.</i> [123]		AChE inhibitor [134], anticancer[144], antioxidative[144]
Sesquiterpenes	β -Cubeben	C ₁₅ H ₂₄	204.1878	<i>H.hav.</i> [128]	<i>H.hav.</i> [128]			antioxidative[145]
	α -Copaen	C ₁₅ H ₂₄	204.1878	<i>H.bel.</i> [127]		<i>H.scy.</i> [123] <i>H.bel.</i> [127]	<i>H.scy.</i> [123]	antioxidative[146]
	β -Elemen	C ₁₅ H ₂₄	204.1878	<i>H.san.</i> [139] <i>H.hav.</i> [128] <i>H.bel.</i> [127]	<i>H.hav.</i> [128]	<i>H.scy.</i> [123] <i>H.bel.</i> [127]	<i>H.san.</i> [139] <i>H.scy.</i> [123]	anticancer[147,148], antifungal[149]
	α -Humulen	C ₁₅ H ₂₄	204.1878	<i>H.san.</i> [139] <i>H.scy.</i> [123] <i>H.hav.</i> [128] <i>H.bel.</i> [127]	<i>H.hav.</i> [128]	<i>H.san.</i> [139] <i>H.bel.</i> [127]	<i>H.san.</i> [139] <i>H.scy.</i> [123]	anti-inflammatory[150], anticancer[151]
	β -Caryophyllen	C ₁₅ H ₂₄	204.1878	<i>H.san.</i> [139] <i>H.scy.</i> [123] <i>H.hav.</i> [128] <i>H.bel.</i> [127]	<i>H.scy.</i> [123] <i>H.hav.</i> [128]	<i>H.san.</i> [139] <i>H.scy.</i> [123] <i>H.bel.</i> [127]	<i>H.san.</i> [139] <i>H.scy.</i> [123]	antioxidative[112,152], antibacterial[112], anti-inflammatory[151]
	Germacren D	C ₁₅ H ₂₄	204.1878	<i>H.scy.</i> [123] <i>H.hav.</i> [128] <i>H.bel.</i> [127]	<i>H.scy.</i> [123] <i>H.hav.</i> [128]	<i>H.san.</i> [139] <i>H.scy.</i> [123] <i>H.bel.</i> [127]	<i>H.san.</i> [139] <i>H.scy.</i> [123]	insecticide[153], antibacterial[154]
	β -Bisabolen	C ₁₅ H ₂₄	204.1878	<i>H.hav.</i> [128]	<i>H.hav.</i> [128]	<i>H.san.</i> [139]		anticancer[155]
Sesqui- terpenes	β -Selinen	C ₁₅ H ₂₄	204.1878	<i>H.scy.</i> [123] <i>H.hav.</i> [128] <i>H.bel.</i> [127]	<i>H.scy.</i> [123]	<i>H.scy.</i> [123]	<i>H.scy.</i> [123]	AChE inhibitor [156], insecticide[156]
	γ -Cadinen	C ₁₅ H ₂₄	204.1878	<i>H.san.</i> [139] <i>H.hav.</i> [128] <i>H.leo.</i> [129]	<i>H.scy.</i> [123] <i>H.hav.</i> [128]	<i>H.san.</i> [139] <i>H.scy.</i> [123] <i>H.bel.</i> [127]	<i>H.san.</i> [139] <i>H.scy.</i> [123]	antioxidative[157]
Sesqui- terpenoids	α -Cadinol	C ₁₅ H ₂₆ O	222.1984	<i>H.scy.</i> [123] <i>H.hav.</i> [128] <i>H.leo.</i> [129] <i>H.bel.</i> [127]	<i>H.hav.</i> [128]	<i>H.san.</i> [139] <i>H.scy.</i> [123] <i>H.bel.</i> [127]	<i>H.san.</i> [139] <i>H.scy.</i> [123] <i>H.leo.</i> [129]	antifungal[158], antibacterial[158], insecticide[159]
	Humulen-Epoxide	C ₁₅ H ₂₄ O	220.1827	<i>H.scy.</i> [123] <i>H.bel.</i> [127]	<i>H.scy.</i> [123]	<i>H.bel.</i> [127]		-
	α -Bisabolol	C ₁₅ H ₂₆ O	222.1984	<i>H.scy.</i> [123] <i>H.hav.</i> [128]		<i>H.scy.</i> [123]	<i>H.scy.</i> [123]	antioxidative[160], anti-inflammatory[161], antibacterial[162], anticancer[163]
Phenyl- propanoids	Eugenol	C ₁₀ H ₁₂ O ₂	164.0837	<i>H.leo.</i> [129]		<i>H.leo.</i> [129]	<i>H.leo.</i> [129]	antioxidative[164,165], antibacterial[164], anti-inflammatory [164,166]
	Methyleugenol	C ₁₁ H ₁₄ O ₂	178.0994	<i>H.leo.</i> [129]		<i>H.leo.</i> [129]	<i>H.leo.</i> [129]	antioxidative[167], anti-inflammatory[167], anesthetic[168]
	Methylchavicol	C ₁₀ H ₁₂ O	148.0888	<i>H.san.</i> [139] <i>H.leo.</i> [129]		<i>H.san.</i> [139]	<i>H.san.</i> [139]	antioxidative[169], antifungal[170]
*Abbreviations of Hornstedtia species								
<i>Hornstedtia scyphifera</i>		<i>H. scy.</i>	<i>Hornstedtia leonurus</i>		<i>H.leo</i>	<i>Hornstedtia bella</i>		<i>H. bel.</i>
<i>Hornstedtia havilandii</i>		<i>H. hav.</i>	<i>Hornstedtia sanhan</i>		<i>H.san</i>			

Morphologically, *H. scyphifera* is characterized by a robust rhizome located just below or at the soil surface and large leaf shoots that can reach heights of 2 to 5 meters, featuring green leaves that are sheathed at the base (fig 1-6). This species produces short inflorescences, which are surrounded by a series of scales encasing the floral bracts. The red flowers bloom individually for one day and give rise to smooth, elongated fruits. Notably, *H. scyphifera* is the most prevalent species of its genus in Malaysia [117], where it has been traditionally employed as a spice and insect repellent [117,123]. The essential oils extracted from various plant parts have been well studied and predominantly consist of mono- and sesquiterpenes, as well as terpenoids, including camphor, germacrene D, borneol, and β -selinene (table 1-1). However, research on non-volatile compounds is limited, with only two brief reports documenting the isolation of four flavonoids, two phytosterols, and a fatty acid from the leaves of *H. scyphifera* [122,124]. In the same studies, extracts derived from the leaves exhibit promising antibacterial and antioxidative activities [122], but also anti-inflammatory and neuroprotective effects [125]. These properties may be attributed to a high concentration of sesquiterpenes, which have been associated with antidepressant and neuroprotective activities [114].

1.5 Identification and isolation of bioactive natural products

When starting a bioactivity driven isolation attempt, the first step comprises the screening of crude plant extracts for various bioactivities [171]. To ensure reproducibility, it is important to ensure documentation of the plant material's identity and processing. The choice of extraction method and solvent significantly impacts the chemical composition and biological activity of the extract. If the bioactive compounds are unknown, broad-spectrum extraction with solvents like 80% aqueous methanol for dried material or pure methanol for fresh material is commonly employed. Alternatively, sequential extraction with solvents of increasing polarity following the eluotropic series (e.g., *n*-hexane, dichloromethane, methanol) may be used to produce multiple crude extracts [172]. After successful detection of biological activity, bioactivity-guided fractionation is used to isolate the pure active compounds. This process involves iterative fractionation, testing, and further separation, employing techniques such as liquid–liquid extraction and several chromatographic techniques [1]. With each cycle, the concentration of active constituents increases until pure compounds are obtained, which are then identified using spectroscopic methods such as nuclear magnetic resonance spectroscopy (NMR) and high-resolution mass spectrometry (HRMS) [172]. Although traditional bioactivity-guided isolation is effective in identifying novel bioactive compounds, it is time-consuming, and costly [173]. Additionally, this method might lead to the reisolation of already known compounds instead of new bioactives (replication) [1,174].

Since plant extracts are complex mixtures containing a variety of active, partially active, and inactive components, interactions between these constituents might occur. High activity in crude extracts may result from the additive or synergistic effects of multiple weakly active compounds [175]. However, fractionation can disrupt these interactions and by this potentially reduces the extract's overall activity. Additionally, bioactive compounds might be present in low concentrations within crude extracts, leading to overlooked bioactivity, or they may be masked by more abundant substances. For example, compounds like chlorophyll and polyphenols (e.g., tannins) can interfere with assays. Chlorophyll has been shown to interact with fatty acids and exhibits antioxidant activity [176], while tannins form complexes with polysaccharides, proteins, and metals, influencing cell-based assays and also showing antioxidant properties [177,178]. From the mentioned issues, especially synergism is highly challenging for bioactivity-guided isolation. When synergism exists between multiple compounds in the crude extract, isolating individual components reduces or eliminates the overall activity. To address this issue, a synergy-directed fractionation strategy has been developed [175]. This approach combines bioactivity testing of the generated fractions for synergistic

interactions with MS profiling and natural product isolation, aiming to identify interactions that would otherwise be missed using traditional fractionation techniques. Next to synergism, another problem while isolating pure compounds is substance stability. If bioactive compounds degrade when in pure form but are more stable within the extract or have better bioavailability, crude extracts might offer greater therapeutic efficacy compared to isolated pure compounds [1,172]. Nevertheless, for unambiguous characterization, the isolation of the compound is usually necessary.

1.6 Structure elucidation

Until around 50 years ago, elucidating the structures of natural products was a challenging and time-consuming process that involved numerous synthetic and degradation reactions. These reactions provided essential pieces of information that, when put together, enabled the determination of a compound's structure. However, advancements in spectroscopic instrumentation have significantly transformed the field of natural product structure elucidation over time [179]. Today, after a successful isolation, the full characterization of natural products is classically performed by a combination of analytical techniques, including high-resolution mass spectrometry (HRMS), nuclear magnetic resonance spectroscopy (NMR), and chiroptical methods such as circular dichroism (CD), to determine both their relative structure and absolute configuration. A newly discovered structure of a natural product often requires verification. This is traditionally achieved by chemical synthesis [180,181]. However, computational methods, such as computer-assisted structure elucidation (CASE) systems, are gaining increasing attention for this purpose.

1.6.1 High-resolution mass spectrometry (HRMS)

High-resolution mass spectrometry (HRMS) has become a fundamental pillar in structure elucidation, particularly for small molecules. Its high sensitivity and speed have made it the method of choice for the rapid determination of natural products, even in complex mixtures and at low concentrations [182]. Instruments with mass analyzers like quadrupole-time-of-flight (QTOF) and Orbitrap are commonly used and favored for their ease of use compared to earlier Fourier transform ion cyclotron resonance spectrometers [183]. Modern HRMS systems offer exceptional resolving power and highly accurate elemental formula determination, with typical accuracies in the sub-ppm range, corresponding to mass deviations as low as sub-millidaltons (mDa). Despite this precision, high mass accuracy alone may not always be sufficient to guarantee the correctness of the elemental composition, especially if the elemental composition is complex [184]. Therefore, other parameters, such as isotope cluster ratios, the number of rings and double bonds (RDB), double bond equivalents (DBE), and the nitrogen rule, must also be considered [184]. While exact mass measurements are essential, they are only part of the full identification process for unknown compounds. Advances in fragmentation techniques and MS/MS data acquisition are equally important. Modern spectrometers enable next to classical targeted MS² analysis diverse untargeted MS² strategies. One example is the data-dependent acquisition (DDA), where a product ion scan is automatically triggered when a precursor ion reaches a specific intensity during an initial LC-MS run [185]. Such automatic MS² operation modes are useful for extract screening during bioactivity- or synergism-guided isolation. For follow-up structural identification, measured fragmentation spectra are compared with MS² reference spectra from libraries such as MassBank [186], and GNPS [187] or with spectra from computational fragmentation tools such as MetFrag [188] and MSFinder [189]. Another experiment is the multistage fragmentation (MSⁿ) analysis. This experiment provides insights into the structural origin of ions by reconstructing fragmentation pathways and can reveal clues about precursors and (sub)structures [183]. The interested reader will find an example for this technique in chapters 3 and 5. One of the major

drawbacks of MS remains the differential ionization propensity of the analytes as well as matrix effects and other effects that can efficiently reduce or hinder ionization.

1.6.2 Nuclear Magnetic Resonance (NMR)

Over the past 28 years there have been several thousand publications describing the use of 2D NMR to identify and characterize natural products. During this time period, the amount of sample needed for this purpose has decreased from the 20–50 mg range to under 1 mg [179]. Next to the 1D experiments for ^1H proton and ^{13}C carbon NMR, the introduction of two-dimensional (2D) NMR [190] was a crucial step to establish NMR as the powerful tool, we know today. Although NMR will probably never hit the sensitivity of mass spectrometers, even low concentrated compounds might be detectable by increasing the number of scans, applying a longer measurement time, and by employing higher magnetic fields [179,191]. Compared to a moderate 600 MHz machine, the state of the art 1,2 GHz machines increase sensitivity by a factor of 2.8 [191]. Other hardware improvements can increase the sensitivity as well. A cryogenically cooled probe head can provide a signal to noise ratio (SNR) improvement by a factor of 3 to 4 [191]. A major advantage of NMR compared to HRMS is its non-destructive character which allows to perform several experiments on the very same sample and to recover the whole sample afterwards. The typical 2D experiments used in natural product structure elucidation includes COSY (Correlation Spectroscopy) for ^1H - ^1H interactions, and HSQC (Heteronuclear Single Quantum Correlation) and HMBC (Heteronuclear Multiple Bond Correlation) for ^1H - ^{13}C interactions. COSY identifies correlations between protons in the same spin system typically through scalar J_{HH} couplings, typically over two or three bonds. The experiment is homonuclear, focusing on ^1H - ^1H couplings, and provides a simple yet effective method for small molecule structure elucidation. To explore wider coupling ranges, the related TOCSY (Total Correlation Spectroscopy) experiment can be performed. Unlike COSY, TOCSY propagates magnetization across an entire proton network, detecting both direct and long-range couplings, thus offering insights into more complex spin systems. HSQC is heteronuclear and correlates ^1H - ^{13}C couplings over one bond. With the ^{13}C - and ^1H -spectra displayed on separate axes, the cross peaks mark corresponding proton/carbon signals. HMBC detects long-range ^1H - ^{13}C couplings over two or three bonds, crucial for mapping connections between non-adjacent carbon atoms and providing detailed structural information [179,191]. Beside these basic experiments, NMR offers tools like 2D NOESY (Nuclear Overhauser Enhancement Spectroscopy) and ROESY (Rotating-Frame Overhauser Effect Spectroscopy) for stereochemical determination. Both measure spatial proximity between protons, even if separated by many bonds. NOESY is typically used for small molecules (up to ~700 Da), while ROESY is also suitable for larger molecules (700–1500 Da). These spectra can provide qualitative molecular geometry information in a single experiment [179]. For ^{13}C - ^{13}C correlations, the INADEQUATE (Incredible Natural Abundance Double Quantum Transfer Experiment) experiment is a powerful tool, revealing carbon skeletons through correlations between neighboring carbons by $^1J_{\text{CC}}$ coupling. Despite sensitivity challenges due to the low natural abundance of ^{13}C , recent advancements like cryogenic probes have improved its utility. However, INADEQUATE still requires significant sample amounts and long acquisition times. An alternative, the 1,1-ADEQUATE (Adequate Sensitivity Double-Quantum Spectroscopy) and 1,n-ADEQUATE experiment, combines a HSQC like $^1J_{\text{CH}}$ coupling with a $^{1/n}J_{\text{CC}}$ coupling, which increases the intensity of the measured correlation by a factor of 64 and therefore enables faster and more efficient structure determination with smaller sample sizes [192,193]. This additional information, in turn, facilitates quicker analysis through Computer-Assisted Structure Elucidation (CASE) software [179].

1.6.3 CASE (Computer-Assisted Structure Elucidation) systems

The beginning of Computer-Assisted Structure Elucidation (CASE) started 55 years ago [194]. Since then, substantial advancements have been made. Today, several commercial CASE systems are available, including NMRSAMS (Spectrum Research), CMCse (Bruker), and Mestrelab (MNovo). In addition, various research groups have developed alternative CASE programs, often available online and free-to-use, such as COCON [195], LSD (Logic for Structure Determination) [196], and SENECA [197]. These systems have been widely employed in recent studies for the structural confirmation of new natural products [198–200] and have proven useful in challenging cases, such as the proton-deficient chlorodepsidones [201]. Each system utilizes distinct mathematical algorithms and interfaces, characterized by varying levels of service and user-friendliness. The ability of a CASE program to efficiently determine the minimum number of possible structures depends significantly on the type of input data. However, all programs are designed to handle at least ^1H , ^{13}C , COSY, ^1HQC , HMBC spectra [194]. Of special interest are data from 1,1-ADEQUATE spectra [179]. These spectra typically display only $^2\text{J}_{\text{CH}}$ correlations [193]. By clarifying which HMBC correlations are due to 2-bond interactions and which arise from longer-range correlations, 1,1-ADEQUATE data can significantly reduce the time required for CASE structure generation and decrease the number of consistent structures [202]. One widely used system that has been validated in peer-reviewed literature and was utilized for the elucidation of lumnitzeralacton in chapter 3 is the ACD-Structure Elucidator (ACD-SE) [194,202,203]. Established in 2002, it has been regularly updated, and since 2011, its website features a “Structure of the Month,” primarily highlighting natural products elucidated with ACD-SE [202]. The minimum required data includes the molecular formula from HRMS, a list of ^{13}C signals, preferably alongside the number of attached protons from HSQC, and HMBC spectra data. The program provides a replication option that checks ^{13}C shifts against the ACD Labs database for exact matches. COSY is optional but recommended. Other 2D NMR data, as well as ^{15}N , ^{19}F , and ^{31}P spectra can also be included. 2D correlations can be manually entered in tabular form or by peak picking in the processed 1D and 2D raw data, which turns out to be much more user friendly. ACD-SE can process data from Bruker, JEOL, and Agilent NMR machines. If wanted, functional groups or molecular fragments can be added or excluded for the following process of finding structure matches. During the structure elucidation process, the program typically provides a list of possible structures consistent with the given correlations in the data set, ranking them according to the best agreement between calculated and observed chemical shifts. If long-range correlations are present, the ACD-SE first presents a Molecular Connectivity Diagram (MCD), flagging non-standard correlations for better clarity. The maximal correlation range may need to be extended from the usual three bonds to four or more if deemed appropriate. If the program fails to generate sensible structures, this may indicate that detected correlations are longer-range than anticipated. In such cases, the “Fuzzy Structure Generator” can be employed to extend all correlations to six bonds. The probability of suggested structures is evaluated using the ACD/NMR Predictor program, which is integrated into the ACD-SE. This program offers three methods for calculating chemical shifts: incremental, by a neural network, and by hierarchical organization of spherical environments (HOSE) code [194,202]. The most reliable, but time-consuming, method is the HOSE code [202]. Although the ACD database is extensive, errors may be more pronounced for compounds with unusual structures that lack close analogues in the database. Consequently, there are plans to incorporate DFT (Density functional theory) chemical shift calculations [204]. It is important to recognize that a single, conclusive answer may not be attainable in every instance, as the identified structure might align with the data without being definitively accurate [194]. Therefore, critical validation of structure suggestions from CASE systems by an experienced analytical chemist is still needed.

1.7 References

- [1] Atanasov, A.G.; Waltenberger, B.; Pferschy-Wenzig, E.-M.; Linder, T.; Wawrosch, C.; Uhrin, P.; Temml, V.; Wang, L.; Schwaiger, S.; Heiss, E.H., Discovery and resupply of pharmacologically active plant-derived natural products: A review, *Biotechnol. Adv.* **2015**, *33*, 1582–1614, doi:10.1016/j.biotechadv.2015.08.001.
- [2] Chaachouay, N.; Zidane, L., Plant-derived natural products: A source for drug discovery and development, *Drugs Drug Candidates*, **2024**, *3*, 184–207, doi:10.3390/ddc3010011.
- [3] Appendino, G.; Fontana, G.; Pollastro, F., Natural products drug discovery, in *Natural Products Structural Diversity-I, Secondary Metabolites: Organization and Biosynthesis*, 1st ed.; Townsend, C.A., Ebizuka, Y., Eds.; Elsevier: Boston, **2010**; pp 205–236, ISBN 9780080453828.
- [4] Dias, D.A.; Urban, S.; Roessner, U., A historical overview of natural products in drug discovery, *Metabolites* **2012**, *2*, 303–336, doi:10.3390/metabo2020303.
- [5] Seidel, V., Plant-derived chemicals: A source of inspiration for new drugs, *Plants (Basel)*, **2020**, *9*, doi:10.3390/plants9111562.
- [6] The World Flora Online. Available online: <https://www.worldfloraonline.org/> (accessed on 28 October 2024).
- [7] Antonelli, A.; Fry, C.; Smith, R.J.; Eden, J.; Govaerts, R.H.A.; Kersey, P.; Nic Lughadha, E.; Onstein, R.E.; Simmonds, M.S.J.; Zizka, A.; Ackerman, J.D.; Adams, V.M.; Ainsworth, A.M.; Albouy, C.; Allen, A.P.; Allen, S.P.; Allio, R.; Auld, T.D.; Bachman, S.P.; Zuntini, A.R., State of the world's plants and fungi, 2023: Tackling the nature emergency: Evidence, gaps and priorities, Royal Botanic Gardens, Kew, **2023**, doi:10.34885/WNWN-6S63.
- [8] Wink, M., Plant Breeding: Importance of plant secondary metabolites for protection against pathogens and herbivores, *Theoret. Appl. Genetics* **1988**, *75*, 225–233, doi:10.1007/BF00303957.
- [9] Gurib-Fakim, A., Medicinal plants: Traditions of yesterday and drugs of tomorrow, *Mol. Aspects Med.* **2006**, *27*, 1–93, doi:10.1016/j.mam.2005.07.008.
- [10] Berenbaum, M.R.; Zangerl, A.R., Phytochemical diversity, in *Phytochemical Diversity and Redundancy in Ecological Interactions*; Springer US: Boston, MA, **1996**; pp 1–24, ISBN 978-1-4899-1754-6.
- [11] Breitenbach Barroso Coelho, L.C., Antimicrobial activity of secondary metabolites and lectins from plants, in *Current Research, Technology and Education Topics in Applied Microbiology and Microbial Biotechnology*; Méndez-Vilas, A., Ed.; Formatex Research Center: Badajoz, Spain, **2010**; pp 396–406, ISBN 9788461461943.
- [12] Nussbaum, F. von; Brands, M.; Hinzen, B.; Weigand, S.; Häbich, D., Antibacterial natural products in medicinal chemistry - exodus or revival?, *Angew. Chem. Int. Ed Engl.* **2006**, *45*, 5072–5129, doi:10.1002/anie.200600350.
- [13] Dugasani, S.; Pichika, M.R.; Nadarajah, V.D.; Balijepalli, M.K.; Tandra, S.; Korlakunta, J.N., Comparative antioxidant and anti-inflammatory effects of 6-gingerol, 8-gingerol, 10-gingerol, and 6-shogaol, *J. Ethnopharmacol.* **2010**, *127*, 515–520, doi:10.1016/j.jep.2009.10.004.
- [14] Soares-Bezerra, R.J.; Calheiros, A.S.; da Silva Ferreira, N.C.; da Silva Frutuoso, V.; Alves, L.A., Natural products as a source for new anti-inflammatory and analgesic compounds through the inhibition of purinergic P2X receptors, *Pharmaceuticals (Basel)* **2013**, *6*, 650–658, doi:10.3390/ph6050650.
- [15] Liu, M.; Panda, S.K.; Luyten, W., Plant-based natural products for the discovery and development of novel anthelmintics against nematodes, *Biomolecules* **2020**, *10*, doi:10.3390/biom10030426.
- [16] El-Badry, A.S.; Abd El-Zaher, E.H.; Saad-Allah, K.M.; El-Sarnagaway, W.A.; Shaltout, K.H., Evaluation of antifungal activity of some plant extracts against causing agents of water-related fungal keratitis, *Egypt. J. Bot.*, *56*, *3*, **2016**, pp 837–861.
- [17] Reddy, L.; Odhav, B.; Bhoola, K.D., Natural products for cancer prevention: A global perspective, *Pharmacol. Ther.* **2003**, *99*, 1–13, doi:10.1016/s0163-7258(03)00042-1.
- [18] Kinghorn, A.D.; Chin, Y.-W.; Swanson, S.M., Discovery of natural product anticancer agents from biodiverse organisms, *Curr. Opin. Drug Discov. Devel.* **2009**, *12*, 189–196.
- [19] Rahman, M.H.; Bajgai, J.; Fadriquela, A.; Sharma, S.; Trinh, T.T.; Akter, R.; Jeong, Y.J.; Goh, S.H.; Kim, C.-S.; Lee, K.-J., Therapeutic potential of natural products in treating neurodegenerative disorders and their future prospects and challenges, *Molecules* **2021**, *26*, doi:10.3390/molecules26175327.
- [20] Newman, D.J.; Cragg, G.M., Natural products as sources of new drugs over the nearly four decades from 01/1981 to 09/2019, *J. Nat. Prod.* **2020**, *83*, 770–803, doi:10.1021/acs.jnatprod.9b01285.
- [21] Hamilton, G.R.; Baskett, T.F., In the arms of morpheus: The development of morphine for postoperative pain relief, *Can. J. Anaesth.* **2000**, *47*, 367–374, doi:10.1007/BF03020955.
- [22] Newman, D.J., Natural products and drug discovery, *Natl Sci Rev* **2022**, *9*, doi:10.1093/nsr/nwac206.
- [23] Culpeper, N.; Potterton, D., Culpeper's colour herbal; Foulsham: London, **2007**, ISBN 057203282X.

- [24] Watanabe, C.K., Studies in the metabolism changes induced by administration of guanidine bases, *J. Biol. Chem.* **1918**, 33, 253–265, doi:10.1016/S0021-9258(18)86579-6.
- [25] Hesse, E.; Taubmann, G., Die Wirkung des Biguanids und seiner Derivate auf den Zuckerstoffwechsel, *Arch. Exp. Pathol. Pharmacol.* **1929**, 142, 290–308, doi:10.1007/BF02000097.
- [26] Slotta, K.H.; Tschesche, R., Über Biguanide, II.: Die blutzucker-senkende Wirkung der Biguanide, *Ber. Dtsch. Chem. Ges. A/B* **1929**, 62, 1398–1405, doi:10.1002/cber.19290620605.
- [27] Campbell, I.W.; Howlett, H.C.S., Worldwide experience of metformin as an effective glucose-lowering agent: A meta-analysis, *Diabetes Metab. Rev.* **1995**, 11, S57–S62, doi:10.1002/dmr.5610110509.
- [28] Bailey, C.J.; Day, C., Metformin: Its botanical background, *Pract. Diab. Int.* **2004**, 21, 115–117, doi:10.1002/pdi.606.
- [29] Bailey, C.J., Biguanides and NIDDM, *Diabetes Care* **1992**, 15, 755–772, doi:10.2337/diacare.15.6.755.
- [30] Hori, Y.; Fujita, H.; Hiruma, K.; Narisawa, K.; Toju, H., Synergistic and offset effects of fungal species combinations on plant performance, *Front. Microbiol.* **2021**, 12, 713180, doi:10.3389/fmicb.2021.713180.
- [31] Santoyo, G.; Guzmán-Guzmán, P.; Parra-Cota, F.I.; Santos-Villalobos, S.d.l.; Del Orozco-Mosqueda, M.C.; Glick, B.R., Plant growth stimulation by microbial consortia, *Agronomy* **2021**, 11, 219, doi:10.3390/agronomy11020219.
- [32] Kang, Y.; Kim, M.; Shim, C.; Bae, S.; Jang, S., Potential of algae-bacteria synergistic effects on vegetable production, *Front. Plant Sci.* **2021**, 12, 656662, doi:10.3389/fpls.2021.656662.
- [33] Lee, S.-M.; Ryu, C.-M., Algae as new kids in the beneficial plant microbiome, *Front. Plant Sci.* **2021**, 12, 599742, doi:10.3389/fpls.2021.599742.
- [34] Chaeprasert, S.; Piapukiew, J.; Whalley, A.J.; Sihanonth, P., Endophytic fungi from mangrove plant species of Thailand: Their antimicrobial and anticancer potentials, *Bot. Mar.* **2010**, 53, doi:10.1515/bot.2010.074.
- [35] Arnold, A.E., Understanding the diversity of foliar endophytic fungi: Progress, challenges, and frontiers, *Fungal Biol. Rev.* **2007**, 21, 51–66, doi:10.1016/j.fbr.2007.05.003.
- [36] Brown, R., *Prodromus floræ Novæ Hollandiæ et Insulæ Van-Diemen: Exhibens Characteres Plantarum Quas Annis 1802–1805, typis R. Taylor et socii: Londini*, **1810**.
- [37] Rahate, S.; Hemke, A.; Umekar, M., Review on Combretaceae family, *Int. J. Pharm. Sci. Rev. Res.* **2019**, 4, 22–29.
- [38] Gere, J.; Yessoufou, K.; Daru, B.; Maurin, O.; Bank, M., African continent a likely origin of family Combretaceae (Myrtales): A biogeographical view, *Annu. Res. Rev. Biol.* **2015**, 8, 1–20, doi:10.9734/ARRB/2015/17476.
- [39] Maurin, O.; Chase, M.W.; Jordaan, M.; van der Bank, M., Phylogenetic relationships of Combretaceae inferred from nuclear and plastid DNA sequence data: Implications for generic classification, *Bot. J. Linn. Soc.*, **2010**, 162, 453–476, doi:10.1111/j.1095-8339.2010.01027.x.
- [40] Gere, J., *Combretaceae: DNA barcoding, phylogeny and biogeography*, Dissertation, University of Johannesburg, Johannesburg, **2014**.
- [41] Angiosperm Phylogeny Website - Myrtales. Available online: <http://www.mobot.org/MOBOT/research/APweb/orders/myrtalesweb2.htm#Combretaceae> (accessed on 7 October 2024).
- [42] Eloff, J.N.; Katerere, D.R.; McGaw, L.J., The biological activity and chemistry of the southern African Combretaceae, *J. Ethnopharmacol.* **2008**, 119, 686–699, doi:10.1016/j.jep.2008.07.051.
- [43] Stafleu, F.A.; Cowan, R.S.; Mennega, E.A.; Dorr, L.J., *Taxonomic literature: A selective guide to botanical publications and collections with dates, commentaries and types*, 2nd ed.; Bohn/Scheltama and Holkema; W. Junk; Koeltz Scientific Books; A.R.G. Gantner: Utrecht [etc.], The Hague [etc.], [sp.] Königstein, [sp.] Ruggell, **1976–2009**, ISBN 9031302244.
- [44] Duke, N.C., *Australia's mangroves: The authoritative guide to Australia's mangrove plants*, University of Queensland: St. Lucia, Qld., **2006**, ISBN 0646461966.
- [45] International Plant Names Index: István Lumnitzer. Available online: <https://www.ipni.org/?q=author%20std%3ALumn.> (accessed on 10 October 2024).
- [46] Magyar Életrajzi Lexikon 1000-1990. Available online: <http://mek.oszk.hu/00300/00355/html/ABC09006/09716.htm> (accessed on 10 October 2024).
- [47] Tomlinson, P.B.; Bunt, J.S.; Primack, R.B.; Duke, N.C., *Lumnitzera Rosea* (Combretaceae) — Its status and floral morphology, *J. Arnold Arboretum*, **1978**, 59, 342–351.
- [48] Guo, M.; Zhou, R.; Huang, Y.; Ouyang, J.; Shi, S., Molecular confirmation of natural hybridization between *Lumnitzera racemosa* and *Lumnitzera littorea*, *Aquatic Bot.* **2011**, 95, 59–64, doi:10.1016/j.aquabot.2011.03.001.
- [49] Manohar, S.M., A review of the botany, phytochemistry and pharmacology of mangrove *Lumnitzera racemosa* Willd., *Pharmacogn Rev.* **2021**, 15, 107–116, doi:10.5530/phrev.2021.15.13.
- [50] Spalding, M.; Kainuma, M.; Collins, L., *World atlas of mangroves*, Earthscan: London, U.K., **2010**, ISBN 9781136530951.

- [51] Manurung, J., Evolutionary ecology and discovery of new bioactive compounds from *Lumnitzera* mangroves across the Indonesian archipelago; Dissertation, University of Leipzig, Leipzig, **2023**.
- [52] Bandaranayake, W.M., Traditional and medicinal uses of mangroves, *Mangroves Salt Marshes* **1998**, 2, 133–148, doi:10.1023/A:1009988607044.
- [53] Neamsuvan, O., A survey of medicinal plants in mangrove and beach forests from sating phra peninsula, Songkhla Province, Thailand, *J. Med. Plants Res.* **2012**, 6, doi:10.5897/JMPR11.1395.
- [54] Ray, T., Customary use of mangrove tree as a folk medicine among the Sundarban resource collectors, *Int. J. Res. Hum. Arts Lit.* **2014**, 2, 43–48.
- [55] Chong, K.Y.; Hugh T.W.T.; Corlett, R.T., A Checklist of the total vascular plant flora of Singapore: Native, naturalized and cultivated species, Singapore, Republic of Singapore, **2009**, ISBN 978-981-08-4030-3.
- [56] Pattanaik, C.; Reddy, C.S.; Dhal, N.K.; Das, R., Utilisation of mangrove forests in Bhitarkanika wildlife sanctuary, Orissa, *Indian J. Tradit. Knowl.* **2008**, 7, 598–603.
- [57] Bandaranayake, W.M., Bioactivities, bioactive compounds and chemical constituents of mangrove plants, *Wetl. Ecol. Manag.* **2002**, 10, 421–452, doi:10.1023/A:1021397624349.
- [58] Lin, P., Mangrove ecosystem in China, Science Press: Beijing, China, **1999**, ISBN 7030070526.
- [59] Lin, P.; Fu, Q., Environmental ecology and economic utilization of mangroves in China, *China Higher Education Press; Springer*: Beijing, Berlin, **2000**, ISBN 7040091607.
- [60] Tam, N., Chapter 11 - Conservation and uses of mangroves in Hong Kong and mainland China, in *Wetlands Ecosystems in Asia: Developments in Ecosystems*, Wong, M.H., Ed.; Elsevier: Amsterdam, **2004**, pp 161–182, ISBN 15727785.
- [61] Poompozil, S.; Kumarasamy, D., Studies on phytochemical constituents of some selected mangroves, *J. Acad. Ind. Res.* **2014**, 590–592.
- [62] Ranjana, B.L.; Jadhav, P.P.; Dhavan, P.P.; Patel, P., *In vitro* antidiabetic activity and phytochemical analysis of *Lumnitzera racemosa* leaves, *Int. Res. J. Pharm.* **2019**, 10, 1–8.
- [63] Eswaraiah, G.; Peele, K.A.; Krupanidhi, S.; Indira, M.; Kumar, R.B.; Venkateswarulu, T.C., GC–MS analysis for compound identification in leaf extract of *Lumnitzera racemosa* and evaluation of its *in vitro* anticancer effect against MCF7 and HeLa Cell lines, *J. King Saud Univ. Sci.* **2020**, 32, 780–783, doi:10.1016/j.jksus.2019.01.014.
- [64] Malik, H.; Mohd Zin, Z.; Kasawani, I.; Abd Razak, S.B.; Zainol, K., Antioxidative activities and flavonoid contents in leaves of selected mangrove species in Setiu wetlands extracted using different solvents, *J. Sustain. Sci. Manag.* **2017**, 24, 24–34.
- [65] Eswaraiah, G.; Peele, K.A.; Krupanidhi, S.; Kumar, R.B.; Venkateswarulu, T.C., Studies on phytochemical, antioxidant, antimicrobial analysis and separation of bioactive leads of leaf extract from the selected mangroves, *J. King Saud Univ. Sci.* **2020**, 32, 842–847, doi:10.1016/j.jksus.2019.03.002.
- [66] Paul, T.; Ramasubbu, S., The antioxidant, anticancer and anticoagulant activities of *Acanthus ilicifolius* L. roots and *Lumnitzera racemosa* Willd. leaves, from southeast coast of India, *J. Appl. Pharm. Sci.* **2017**, 7, 81–87, doi:10.7324/JAPS.2017.70313.
- [67] Nguyen, P.T.; Bui, T.T.L.; Chau, N.D.; Bui, H.T.; Kim, E.J.; Kang, H.K.; Lee, S.H.; Jang, H.D.; Nguyen, T.C.; Van Nguyen, T.; et al., *In vitro* evaluation of the antioxidant and cytotoxic activities of constituents of the mangrove *Lumnitzera racemosa* Willd, *Arch. Pharm. Res.* **2015**, 38, 446–455, doi:10.1007/s12272-014-0429-y.
- [68] Lin, T.-C.; Hsu, F.-L.; Cheng, J.-T., Antihypertensive activity of corilagin and chebulinic acid, tannins from *Lumnitzera racemosa*, *J. Nat. Prod.* **1993**, 56, 629–632, doi:10.1021/np50094a030.
- [69] Glasenapp, Y.; Korth, I.; Nguyen, X.; Papenbrock, J., Sustainable use of mangroves as sources of valuable medicinal compounds: Species identification, propagation and secondary metabolite composition, *S. Afr. J. Bot.* **2019**, 317–328.
- [70] Yu, S.-Y.; Wang, S.-W.; Hwang, T.-L.; Wei, B.-L.; Su, C.-J.; Chang, F.-R.; Cheng, Y.-B., Components from the leaves and twigs of mangrove *Lumnitzera racemosa* with anti-angiogenic and anti-inflammatory effects, *Mar. Drugs* **2018**, 16, doi:10.3390/md16110404.
- [71] Darwish, A.G.G.; Samy, M.N.; Sugimoto, S.; Otsuka, H.; Abdel-Salam, H.; Matsunami, K., Effects of hepatoprotective compounds from the leaves of *Lumnitzera racemosa* on acetaminophen-induced liver damage in vitro, *Chem. Pharm. Bull.* **2016**, 64, 360–365, doi:10.1248/cpb.c15-00830.
- [72] Ravikumar, S.; Gnanadesigan, M., Hepatoprotective and antioxidant activity of a mangrove plant *Lumnitzera racemosa*, *Asian Pac. J. Trop. Biomed.* **2011**, 1, 348–352, doi:10.1016/S2221-1691(11)60078-6.
- [73] Scott, A.J., A revision of *Anogeissus* (Combretaceae), *Kew Bulletin* **1979**, 33, 555, doi:10.2307/4109799.
- [74] Singh, D.; Baghel, U.S.; Gautam, A.; Baghel, D.S.; Yadav, D.; Malik, J.; Yadav, R., The genus *Anogeissus*: A review on ethnopharmacology, phytochemistry and pharmacology, *J. Ethnopharmacol.* **2016**, 194, 30–56, doi:10.1016/j.jep.2016.08.025.

- [75] IPNI. *Terminalia dhofarica*, International Plant Names Index. Available online: <https://www.ipni.org/n/77164562-1> (accessed on 8 November 2024).
- [76] Maurin, O.; Gere, J.; van der Bank, M.; Boatwright, J.S., The inclusion of *Anogeissus*, *Buchenavia* and *Pteleopsis* in *Terminalia* (Combretaceae: Terminaliinae), *Bot. J. Linn.* **2017**, *184*, 312–325, doi:10.1093/botlinnean/box029.
- [77] Jain, A.; Katewa, S.S.; Galav, P.K.; Sharma, P., Medicinal plant diversity of Sitamata wildlife sanctuary, Rajasthan, India. *J. Ethnopharmacol.* **2005**, *102*, 143–157, doi:10.1016/j.jep.2005.05.047.
- [78] Marwah, R.G.; Fatope, M.O.; Mahrooqi, R.A.; Varma, G.B.; Abadi, H.A.; Al-Burtamani, S.K.S., Antioxidant capacity of some edible and wound healing plants in Oman, *Food Chem.* **2007**, *101*, 465–470, doi:10.1016/j.foodchem.2006.02.001.
- [79] Ezuruike, U.F.; Prieto, J.M., The use of plants in the traditional management of diabetes in Nigeria: Pharmacological and toxicological considerations, *J. Ethnopharmacol.* **2014**, *155*, 857–924, doi:10.1016/j.jep.2014.05.055.
- [80] Meena, K.L.; Yadav, B.L., Studies on ethnomedicinal plants conserved by Garasia tribes of Sirohi district, Rajasthan, India, *Indian J. Nat. Prod. Resour.* **2010**, *1*, 500–506.
- [81] Manosroi, J.; Moses, Z.Z.; Manosroi, W.; Manosroi, A. Hypoglycemic activity of Thai medicinal plants selected from the Thai/Lanna medicinal recipe database MANOSROI II, *J. Ethnopharmacol.* **2011**, *138*, 92–98, doi:10.1016/j.jep.2011.08.049.
- [82] IPNI. *Anogeissus dhofarica*, International Plant Names Index. Available online: <https://www.ipni.org/n/169727-1> (accessed on 8 November 2024).
- [83] Victor, B.Y.A.; Grace, A., Phytochemical studies, *in vitro* antibacterial activities and antioxidant properties of the methanolic and ethyl acetate extracts of the leaves of *Anogeissus leiocarpus*, *Int. J. Biochem. Res. Rev.* **2013**, *3*, 137–145, doi:10.9734/IJBCRR/2013/3349.
- [84] Hungund, B.L.; Pathak, C.H., A survey of plants in Gujarat, India, for alkaloids, saponins, and tannins. *Res. Pap. NE-201*, U.S. Department of Agriculture, Forest Service, Northeastern forest experiment Station. **1971**, 201.
- [85] Attioua, B.; Lagnika, L.; Yeo, D.; Antheaume, C.; Vonthron-Sénécheau, C., *In vitro* antiplasmodial and antileishmanial activities of flavonoids from *Anogeissus leiocarpus* (Combretaceae), *Int. J. Pharm. Sci. Rev. Res.* **2011**, *11*.
- [86] Nduji, A.A.; Okwute, S.K., Co-occurrence of 3,3',-tri-*O*-methylflavellagic acid and 3,3'-di-*O*-methyllellagic acid in the bark of *Anogeissus schimperi*, *Phytochemistry* **1988**, *27*, 1548–1550, doi:10.1016/0031-9422(88)80240-1.
- [87] Lin, T.-C.; Tanaka, T.; Nonaka, G.; Nishioka, I.; Young, T.-J., Tannins and related compounds. CVIII. Isolation and characterization of novel complex tannins (flavono-ellagitannins), anogeissinin and anogeissusins A and B, from *Anogeissus acuminata* (ROXB ex DC.) GUILL. et PERR. var lanceolata WALL. ex CLARKE, *Chem. Pharm. Bull.* **1991**, *39*, 1144–1147, doi:10.1248/cpb.39.1144.
- [88] Reddy, K.K.; Rajadurai, S.; Nayudamma, Y.; Reddy, K., Studies on dhava (*Anogeissus latifolia*) tannins: Part III-polyphenols of bark, sapwood and heartwood of dhava, *Indian J. Chem* **1965**, *3*, 308–310.
- [89] Reddy, K.K.; Rajadurai, S.; Nayudamma, Y.; Reddy, K., Studies on dhava tannins. II. Isolation of gallic, chebulagic and trigallic acids from dhava leaves, *Indian J. Chem* **1965**, *3*, 129–131.
- [90] Govindarajan, R.; Vijayakumar, M.; Singh, M.; Rao, C.V.; Shirwaikar, A.; Rawat, A.K.S.; Pushpangadan, P., Antiulcer and antimicrobial activity of *Anogeissus latifolia*, *J. Ethnopharmacol.* **2006**, *106*, 57–61, doi:10.1016/j.jep.2005.12.002.
- [91] Govindarajan, R.; Vijayakumar, M.; Rao, C.V.; Shirwaikar, A.; Mehrotra, S.; Pushpangadan, P., Healing potential of *Anogeissus latifolia* for dermal wounds in rats, *Acta Pharm.* **2004**, *54*, 331–338.
- [92] Kudi, A.C.; Myint, S.H., Antiviral activity of some Nigerian medicinal plant extracts, *J. Ethnopharmacol.* **1999**, *68*, 289–294, doi:10.1016/S0378-8741(99)00049-5.
- [93] Mishra, M.P.; Padhy, R.N., *In vitro* antibacterial efficacy of 21 Indian timber-yielding plants against multidrug-resistant bacteria causing urinary tract infection, *Osong Public Health Res. Perspect.* **2013**, *4*, 347–357, doi:10.1016/j.phrp.2013.10.007.
- [94] Patzelt, A., Oman plant: Red data book, First published.; Oman botanic garden: [Al Koud old], **2015**, ISBN 9789996950100.
- [95] Kürschner, H.; Hein, P.; Kilian, N.; Hubaishan, M.A., The *Hybantho durae*-*Anogeissetum dhofaricae* ass. nova - phytosociology, structure and ecology of an endemic south Arabian forest community, *Phyto* **2004**, *34*, 569–612, doi:10.1127/0340-269X/2004/0034-0569.
- [96] Oberprieler, C.; Meister, J.; Schneider, C.; Kilian, N., Genetic structure of *Anogeissus dhofarica* (Combretaceae) populations endemic to the monsoonal fog oases of the southern Arabian peninsula, *Biol. J. Linn. Soc.* **2009**, *97*, 40–51, doi:10.1111/j.1095-8312.2008.01173.x.
- [97] Abuarqoub, D.; Aburayyan, W.; Rashan, L.; Dayyih, W.A.; Al-Matubsi, H.Y., Phytochemical analysis and *in vitro* investigation of wound healing, cytotoxicity, and inflammatory response in potentially active extracts of *Anogeissus dhofarica*, *J. Appl. Pharm. Sci.* **2024**, doi:10.7324/JAPS.2024.174429.

- [98] Miller, A.G.; Morris, M., Plants of Dhofar: The southern region of Oman; traditional, economic and medicinal uses, First published.; The office of the adviser for conservation of the environment: Oman, **1988**, ISBN 0715708082.
- [99] Adekunle, Y.A.; Samuel, B.B.; Nahar, L.; Fatokun, A.A.; Sarker, S.D., *Anogeissus leiocarpus* (DC.) Guill. & Perr. (Combretaceae): A review of the traditional uses, phytochemistry and pharmacology of African birch, *Fitoterapia* **2024**, *176*, 105979, doi:10.1016/j.fitote.2024.105979.
- [100] Al-Noumani, A.J.; Al-Qasbi, M.Z.J.; Al-Shabibi, A.S.A.; Al-Mashani, S.A.I.; Said, S.A., Antimicrobial, antioxidant and cytotoxic activities of *Anogeissus dhofarica* from Oman, *Int. J. Recent. Adv. Pharm. Res.* **2013**, *3*(3), 35-38, ISSN: 2230-9306
- [101] Grulich, V.; Vydrová, A.; Reiter, A., *Anogeissus dhofarica* A. J. Scott. Botany.cz [Online], October 27, 2015. Available online: <https://botany.cz/cs/anogeissus-dhofarica/> (accessed on 6 November 2024).
- [102] Plants of the World Online. *Terminalia dhofarica* (A.J.Scott) Gere & Boatwr. | Plants of the World Online, Kew Science. Available online: <https://powo.science.kew.org/taxon/urn:lsid:ipni.org:names:77164562-1#publications> (accessed on 6 November 2024).
- [103] Maqsood, R.; Khan, F.; Ullah, S.; Khan, A.; Al-Jahdhami, H.; Hussain, J.; Weli, M.; Maqsood, D.; Rahman, S.M.; Hussain, A.; et al., Evaluation of antiproliferative, antimicrobial, antioxidant, antidiabetic and phytochemical analysis of *Anogeissus dhofarica* A. J. Scott, *Antibiotics* **2023**, *12*, 354, doi:10.3390/antibiotics12020354.
- [104] Kress, W.J.; Prince, L.M.; Williams, K.J., The phylogeny and a new classification of the gingers (Zingiberaceae): Evidence from molecular data, *Am. J. Bot.* **2002**, *89*, 1682–1696, doi:10.3732/ajb.89.10.1682.
- [105] Angiosperm Phylogeny Website - Zingiberales. Available online: <http://www.mobot.org/MOBOT/research/APweb/orders/zingiberalesweb.htm#Zingiberaceae> (accessed on 7 October 2024).
- [106] Wu, D.; Larsen, K., *Zingiberaceae*; Science-Press, Missouri botanical garden press: Beijing, St. Louis, **2000**, ISBN 0915279835
- [107] Pancharoen, O.; Prawat, U.; Tuntiwachwuttikul, P. Phytochemistry of the *Zingiberaceae*. in Studies in Natural products chemistry: Bioactive natural products (Part D); Atta-ur-Rahman, Ed.; Elsevier, **2000**; pp 797–865, ISBN 1572-5995.
- [108] Braga, M.C.; Vieira, E.C.S.; Oliveira, T.F., *Curcuma longa* L. leaves: Characterization (bioactive and antinutritional compounds) for use in human food in Brazil, *Food Chem.* **2018**, *265*, 308–315, doi:10.1016/j.foodchem.2018.05.096.
- [109] Alogla, R.N.; Wang, F.; Zhang, X.; Li, J.; Tran, L.P.; Yin, X., Bioactive compounds from the *Zingiberaceae* family with known antioxidant activities for possible therapeutic uses, *Antioxidants* **2022**, *11*, 1282, doi:10.3390/antiox11071281.
- [110] Ghasemzadeh, A.; Jaafar, H.Z.E.; Rahmat, A., Antioxidant activities, total phenolics and flavonoids content in two varieties of Malaysia young ginger (*Zingiber officinale* Roscoe), *Molecules* **2010**, *15*, 4324–4333, doi:10.3390/molecules15064324.
- [111] Souissi, M.; Azelmat, J.; Chaieb, K.; Grenier, D., Antibacterial and anti-inflammatory activities of *Elettaria cardamomum* extracts: Potential therapeutic benefits for periodontal infections, *Anaerobe* **2020**, *61*, 102089, doi:10.1016/j.anaerobe.2019.102089.
- [112] Dahham, S.S.; Tabana, Y.M.; Iqbal, M.A.; Ahamed, M.B.K.; Ezzat, M.O.; Majid, A.S.A.; Majid, A.M.S.A., The anticancer, antioxidant and antimicrobial properties of the sesquiterpene β -caryophyllene from the essential oil of *Aquilaria crassna*, *Molecules* **2015**, *20*, 11808–11829, doi:10.3390/molecules200711808.
- [113] Menon, V.P.; Sudheer, A.R., Antioxidant and anti-inflammatory properties of curcumin, *Adv. Exp. Med. Biol.* **2007**, *595*, 105–125, doi:10.1007/978-0-387-46401-5_3.
- [114] Ge, W.; Li, H.; Zhao, Y.; Cai, E.; Zhu, H.; Gao, Y.; Liu, S.; Yang, H.; Zhang, L., Study on antidepressant activity of sesquiterpenoids from ginseng root, *J. Funct. Foods* **2017**, *33*, 261–267, doi:10.1016/j.jff.2017.03.057.
- [115] Barbosa, G.B.; Nueva, M.C.Y., Antioxidant activity and phenolic content of *Hornstedtia conoidea* (Zingiberaceae), *Asian J. Biol. Sci.* **2019**, *8*, 1–7, doi:10.5530/ajbbs.2019.8.1.
- [116] Newman, M.; Lhuillier, A.; Poulsen, A.D., *Checklist of the Zingiberaceae of Malesia*; Nat. Herbar. Nederland, Uni. Leiden: Leiden, **2004**, ISBN 9071236560.
- [117] Holttum, R.E., The Zingiberaceae of the Malay peninsula, *The Gardens Bulletin*, Singapore **1950**, *13* (4), 1–249.
- [118] Julius, A.; Takano, A.; Suleiman, M.; Tukin, W.F., Zingiberaceae of Maliau basin, Sabah, Malaysia, *J. Trop. Biol. Conserv.* **2010**, *6*, 1-20.
- [119] Acma, F.M.; Mendez, N., Pollen morphology and pollen elemental composition of selected Philippine native gingers in tribe Alpinieae (Alpinioideae: Zingiberaceae), *Biol. Forum Int. J.* **2018**, *10*, 1–10.
- [120] Mendez, N.; Acma, F.M., *In vitro* studies on pollen viability, pollen germination and pollen tube growth of *Hornstedtia conoidea* Ridl. – a Philippine endemic ginger species, *J. Trop. Life Sci.* **2018**, *8*, 303–310, doi:10.11594/jtls.08.03.13.

- [121] Govaerts, R., The world checklist of vascular plants (WCVP); *The Royal Botanic Gardens, Kew* **2024**, doi:10.15468/6h8ucr.
- [122] John, U.I.; Hauwa, A.U.; Ojochenemi, Y.; Isaac, U.K., Isolation and characterization of chemical constituents, cytotoxicity, antibacterial and antioxidant activity of the isolates, crude extract from *Hornstedtia scyphifera* var. leaf, *GSC Biol. Pharm. Sci.* **2020**, *10*, 70–98, doi:10.30574/gscbps.2020.10.2.0027.
- [123] Hashim, S.E.; Sirat, H.M., Chemical composition, antioxidant, antimicrobial, and α -glucosidase activities of essential oils of *Hornstedtia scyphifera* (Zingiberaceae), *Nat. Prod. Commun.* **2018**, *13*, 1934578X1801300, doi:10.1177/1934578X1801300228.
- [124] Hashim, S.E.; Sirat, H.M.; Yen, K.H.; Ismail, I.S.; Matsuki, S.N., Antioxidant and α -glucosidase inhibitory constituents from *Hornstedtia* species of Malaysia, *Nat. Prod. Commun.* **2015**, *10*, 1934578X1501000, doi:10.1177/1934578X1501000919.
- [125] Zipp, F.; Ullrich, O., Extracts from the plant *Hornstedtia scyphifera* and immunosuppressive effects, *EP2163253A1*, **2008**.
- [126] Pieplow, K., Neuroaktive Inhaltsstoffe aus Pflanzen, Diplomarbeit; Martin-Luther-Universität Halle-Wittenberg, Halle (Saale), **2022**.
- [127] Donadu, M.G.; Le, N.T.; Ho, D.V.; Doan, T.Q.; Le, A.T.; Raal, A.; Usai, M.; Marchetti, M.; Sanna, G.; Madeddu, S.; et al., Phytochemical compositions and biological activities of essential oils from the leaves, rhizomes and whole plant of *Hornstedtia bella* Škorničk, *Antibiotics (Basel)* **2020**, *9*, doi:10.3390/antibiotics9060334.
- [128] Hashim, S.E.; Sirat, H.M.; Yen, K.H., Chemical compositions and antimicrobial activity of the essential oils of *Hornstedtia havilandii* (Zingiberaceae), *Nat. Prod. Commun.* **2014**, *9*, 119–120.
- [129] Jani, N.A.; Sirat, M.H.; Ali, N.M.; Aziz, A., Chemical compositions of the rhizome, leaf and stem oils from Malaysian *Hornstedtia leonurus*, *Nat. Prod. Commun.* **2013**, *8*, 513–514.
- [130] Borges, R.S.; Ortiz, B.L.S.; Pereira, A.C.M.; Keita, H.; Carvalho, J.C.T., *Rosmarinus officinalis* essential oil: A review of its phytochemistry, anti-inflammatory activity, and mechanisms of action involved, *J. Ethnopharmacol.* **2019**, *229*, 29–45, doi:10.1016/j.jep.2018.09.038.
- [131] Juhás, Š.; Bukovská, A.; Čikoš, Š.; Czikková, S.; Fabian, D.; Koppel, J., Anti-inflammatory effects of *Rosmarinus officinalis* essential oil in mice, *Acta Vet. Brno* **2009**, *78*, 121–127, doi:10.2754/avb200978010121.
- [132] Bajalan, I.; Rouzbahani, R.; Pirbalouti, A.G.; Maggi, F., Antioxidant and antibacterial activities of the essential oils obtained from seven Iranian populations of *Rosmarinus officinalis*, *Ind. Crops Prod.* **2017**, *107*, 305–311, doi:10.1016/j.indcrop.2017.05.063.
- [133] Mekonnen, A.; Yitayew, B.; Tesema, A.; Taddese, S., *In vitro* antimicrobial activity of essential oil of *Thymus schimperi*, *Matricaria chamomilla*, *Eucalyptus globulus*, and *Rosmarinus officinalis*, *Int. J. Microbiol.* **2016**, *2016*, 9545693, doi:10.1155/2016/9545693.
- [134] Kaufmann, D.; Dogra, A.K.; Wink, M., Myrtenal inhibits acetylcholinesterase, a known alzheimer target, *J. Pharm. Pharmacol.* **2011**, *63*, 1368–1371, doi:10.1111/j.2042-7158.2011.01344.x.
- [135] Katayama, T.; Nagai, I., Chemical significance of the volatile components of spices in the food preservative viewpoint I, *Nippon Suisan Gakkaishi* **1958**, *24*, 511–514, doi:10.2331/suisan.24.511.
- [136] Orhan, İ.E.; Özçelik, B.; Kartal, M.; Kan, Y., Antimicrobial and antiviral effects of essential oils from selected Umbelliferae and Labiatae plants and individual essential oil components, *Turk. J. Biol.* **2012**, doi:10.3906/biy-0912-30.
- [137] Tian, L.-L.; Zhou, Z.; Zhang, Q.; Sun, Y.-N.; Li, C.-R.; Cheng, C.-H.; Zhong, Z.-Y.; Wang, S.-Q., Protective effect of (+/-) isoborneol against 6-OHDA-induced apoptosis in SH-SY5Y cells, *Cell. Physiol. Biochem.* **2007**, *20*, 1019–1032, doi:10.1159/000110682.
- [138] Tabanca, N.; Kirimer, N.; Demirci, B.; Demirci, F.; Başer, K.H., Composition and antimicrobial activity of the essential oils of *Micromeria cristata* subsp. *phrygia* and the enantiomeric distribution of borneol, *J. Agric. Food Chem.* **2001**, *49*, 4300–4303, doi:10.1021/jf0105034.
- [139] Chau, D.T.M.; Dai, D.N.; Hoi, T.M.; Thai, T.H.; Thang, T.D.; Ogunwande, I.A., Essential oil constituents of *Etlingera yunnanensis* and *Hornstedtia sanhan* grown in Vietnam, *Nat. Prod. Commun.* **2015**, *10*, 365–366.
- [140] Li, L.; Shi, C.; Yin, Z.; Jia, R.; Peng, L.; Kang, S.; Li, Z., Antibacterial activity of α -terpineol may induce morphostructural alterations in *Escherichia coli*, *Braz. J. Microbiol.* **2014**, *45*, 1409–1413, doi:10.1590/s1517-83822014000400035.
- [141] Zhou, H.; Tao, N.; Jia, L., Antifungal activity of citral, octanal and α -terpineol against *Geotrichum citri-aurantii*, *Food Control* **2014**, *37*, 277–283, doi:10.1016/j.foodcont.2013.09.057.
- [142] Zhang, W.-J.; Yang, K.; You, C.-X.; Wang, Y.; Wang, C.-F.; Wu, Y.; Geng, Z.-F.; Su, Y.; Du, S.-S.; Deng, Z.-W., Bioactivity of essential oil from *Artemisia stolonifera* (Maxim.) Komar. and its main compounds against two stored-product insects, *J. Oleo Sci.* **2015**, *64*, 299–307, doi:10.5650/jos.ess14187.

- [143] Zhao, J.; Zheng, X.; Newman, R.A.; Zhong, Y.; Liu, Z.; Nan, P., Chemical composition and bioactivity of the essential oil of *Artemisia anomala* from China, *J. Essent. Oil Res.* **2013**, *25*, 520–525, doi:10.1080/10412905.2013.820670.
- [144] Babu, L.H.; Perumal, S.; Balasubramanian, M.P., Myrtenal, a natural monoterpene, down-regulates TNF- α expression and suppresses carcinogen-induced hepatocellular carcinoma in rats, *Mol. Cell. Biochem.* **2012**, *369*, 183–193, doi:10.1007/s11010-012-1381-0.
- [145] Lin, K.; Yeh, S.; Lin, M.; Shih, M.; Yang, K.; Hwang, S., Major chemotypes and antioxidative activity of the leaf essential oils of *Cinnamomum osmophloeum* Kaneh. from a clonal orchard, *Food Chem.* **2007**, *105*, 133–139, doi:10.1016/j.foodchem.2007.03.051.
- [146] Türkez, H.; Celik, K.; Toğar, B., Effects of copaene, a tricyclic sesquiterpene, on human lymphocytes cells in vitro, *Cytotechnology* **2014**, *66*, 597–603, doi:10.1007/s10616-013-9611-1.
- [147] Wang, G.; Li, X.; Huang, F.; Zhao, J.; Ding, H.; Cunningham, C.; Coad, J.E.; Flynn, D.C.; Reed, E.; Li, Q.Q., Antitumor effect of β -elemene in non-small-cell lung cancer cells is mediated via induction of cell cycle arrest and apoptotic cell death, *Cell. Mol. Life Sci.* **2005**, *62*, 881–893, doi:10.1007/s00018-005-5017-3.
- [148] Li, Q.Q.; Wang, G.; Huang, F.; Banda, M.; Reed, E., Antineoplastic effect of β -elemene on prostate cancer cells and other types of solid tumour cells, *J. Pharm. Pharmacol.* **2010**, *62*, 1018–1027, doi:10.1111/j.2042-7158.2010.01135.x.
- [149] Taniguchi, S.; Miyoshi, S.; Tamaoki, D.; Yamada, S.; Tanaka, K.; Uji, Y.; Tanaka, S.; Akimitsu, K.; Gomi, K., Isolation of jasmonate-induced sesquiterpene synthase of rice: product of which has an antifungal activity against *Magnaporthe oryzae*, *J. Plant Physiol.* **2014**, *171*, 625–632, doi:10.1016/j.jplph.2014.01.007.
- [150] Fernandes, E.S.; Passos, G.F.; Medeiros, R.; da Cunha, F.M.; Ferreira, J.; Campos, M.M.; Pianowski, L.F.; Calixto, J.B., Anti-inflammatory effects of compounds α -humulene and (-)-*trans*-caryophyllene isolated from the essential oil of *Cordia verbenacea*, *Eur. J. Pharmacol.* **2007**, *569*, 228–236, doi:10.1016/j.ejphar.2007.04.059.
- [151] Legault, J.; Pichette, A., Potentiating effect of beta-caryophyllene on anticancer activity of α -humulene, isocaryophyllene and paclitaxel, *J. Pharm. Pharmacol.* **2007**, *59*, 1643–1647, doi:10.1211/jpp.59.12.0005.
- [152] Al-Motwaa, S.M.; Al-Otaibi, W.A., Determination of the chemical composition and antioxidant, anticancer, and antibacterial properties of essential oil of *Pulicaria crispa* from Saudi Arabia, *J. Indian Chem. Soc.* **2022**, *99*, 100341, doi:10.1016/j.jics.2022.100341.
- [153] Kiran, S.R.; Devi, P.S., Evaluation of mosquitocidal activity of essential oil and sesquiterpenes from leaves of *Chloroxylon swietenia* DC., *Parasitol. Res.* **2007**, *101*, 413–418, doi:10.1007/s00436-007-0485-z.
- [154] Setzer, W.N.; Schmidt, J.M.; Noletto, J.A.; Vogler, B., Leaf oil compositions and bioactivities of Abaco bush medicines, *Pharmacologyonline* **2006**, *3*, 794–802.
- [155] Yeo, S.K.; Ali, A.Y.; Hayward, O.A.; Turnham, D.; Jackson, T.; Bowen, I.D.; Clarkson, R., β -Bisabolene, a sesquiterpene from the essential oil extract of *Opoponax* (*Commiphora guidottii*), exhibits cytotoxicity in breast cancer cell lines, *Phytother. Res.* **2016**, *30*, 418–425, doi:10.1002/ptr.5543.
- [156] Liu, J.; Hua, J.; Qu, B.; Guo, X.; Wang, Y.; Shao, M.; Luo, S., Insecticidal terpenes from the essential oils of *Artemisia nakaii* and their inhibitory effects on acetylcholinesterase, *Front. Plant Sci.* **2021**, *12*, 720816, doi:10.3389/fpls.2021.720816.
- [157] Kundu, A.; Saha, S.; Walia, S.; Ahluwalia, V.; Kaur, C., Antioxidant potential of essential oil and cadinene sesquiterpenes of *Eupatorium adenophorum*, *Toxicol. Environ. Chem.* **2013**, *95*, 127–137, doi:10.1080/02772248.2012.759577.
- [158] Chang, S.-T.; Wang, S.-Y.; Kuo, Y.-H., Resources and bioactive substances from *Taiwania* (*Taiwania cryptomerioides*), *J. Wood Sci.* **2003**, *49*, 1–4, doi:10.1007/s100860300000.
- [159] Chang, S.-T.; Chen, P.-F.; Wang, S.-Y.; Wu, H.-H., Antimite activity of essential oils and their constituents from *Taiwania cryptomerioides*, *J. Med. Entomol.* **2001**, *38*, 455–457, doi:10.1603/0022-2585-38.3.455.
- [160] Ruberto, G.; Baratta, M.T., Antioxidant activity of selected essential oil components in two lipid model systems, *Food Chem.* **2000**, *69*, 167–174, doi:10.1016/S0308-8146(99)00247-2.
- [161] Barreto, R.S.S.; Quintans, J.S.S.; Amarante, R.K.L.; Nascimento, T.S.; Amarante, R.S.; Barreto, A.S.; Pereira, E.W.M.; Duarte, M.C.; Coutinho, H.D.M.; Menezes, I.R.A.; et al., Evidence for the involvement of TNF- α and IL-1 β in the antinociceptive and anti-inflammatory activity of *Stachys lavandulifolia* Vahl. (*Lamiaceae*) essential oil and (-)- α -bisabolol, its main compound, in mice, *J. Ethnopharmacol.* **2016**, *191*, 9–18, doi:10.1016/j.jep.2016.06.022.
- [162] van Zyl, R.L.; Seatlholo, S.T.; Van Vuuren, S.F.; Viljoen, A.M., The biological activities of 20 nature identical essential oil constituents, *J. Essent. Oil Res.* **2006**, *18*, 129–133, doi:10.1080/10412905.2006.12067134.

- [163] Seki, T., Kokuryo, T., Yokoyama, Y., Suzuki, H., Itatsu, K., Mizutani, T., Miyake, T., Uno, M., Yamauchi, K., et al., Antitumor effects of α -bisabolol against pancreatic cancer, *Cancer Sci.* **2011**, *102*, 2199–2205, doi:10.1111/j.1349-7006.2011.02082.x.
- [164] Pramod, K., Ansari, S.H., Ali, J., Eugenol: a natural compound with versatile pharmacological actions, *Nat. Prod. Commun.* **2010**, *5*, 1999–2006.
- [165] Nagababu, E., Lakshmaiah, N., Inhibition of microsomal lipid peroxidation and monooxygenase activities by eugenol, *Free Radic. Res.* **1994**, *20*, 253–266, doi:10.3109/10715769409147521.
- [166] Thompson, D., Eling, T., Mechanism of inhibition of prostaglandin H synthase by eugenol and other phenolic peroxidase substrates, *Mol. Pharmacol.* **1989**, *36*, 809–817.
- [167] Choi, Y.K., Cho, G.-S., Hwang, S., Kim, B.W., Lim, J.H., Lee, J.-C., Kim, H.C., Kim, W.-K., Kim, Y.S., Methyl eugenol reduces cerebral ischemic injury by suppression of oxidative injury and inflammation, *Free Radic. Res.* **2010**, *44*, 925–935, doi:10.3109/10715762.2010.490837.
- [168] Sell, A.B., Carlini, E.A., Anesthetic action of methyleugenol and other eugenol derivatives, *Pharmacology* **1976**, *14*, 367–377, doi:10.1159/000136617.
- [169] Santos, B.C.S., Pires, A.S., Yamamoto, C.H., Couri, M.R.C., Taranto, A.G., Alves, M.S., Araújo, A.L.D.S.d.M., Sousa, O.V. de., Methyl chavicol and its synthetic analogue as possible antioxidant and antilipase agents based on the *in vitro* and *in silico* assays, *Oxid. Med. Cell. Longev.* **2018**, *2018*, 2189348, doi:10.1155/2018/2189348.
- [170] Donati, M., Mondin, A., Chen, Z., Miranda, F.M., do Nascimento, B.B., Schirato, G., Pastore, P., Frolidi, G., Radical scavenging and antimicrobial activities of *Croton zehntneri*, *Pterodon emarginatus* and *Schinopsis brasiliensis* essential oils and their major constituents: estragole, *trans*-anethole, β -caryophyllene and myrcene, *Nat. Prod. Res.* **2015**, *29*, 939–946, doi:10.1080/14786419.2014.964709.
- [171] Koehn, F.E., Carter, G.T., The evolving role of natural products in drug discovery, *Nat. Rev. Drug Discov.* **2005**, *4*, 206–220, doi:10.1038/nrd1657.
- [172] Liu, Z., Preparation of botanical samples for biomedical research, *Endocr. Metab. Immune Disord. Drug Targets* **2008**, *8*, 112–121, doi:10.2174/187153008784534358.
- [173] Baumgartner, R.R.; Steinmann, D.; Heiss, E.H.; Atanasov, A.G.; Ganzera, M.; Stuppner, H.; Dirsch, V.M., Bioactivity-guided isolation of 1,2,3,4,6-penta-*O*-galloyl-D-glucopyranose from *Paeonia lactiflora* roots as a PTP1B inhibitor, *J. Nat. Prod.* **2010**, *73*, 1578–1581, doi:10.1021/np100258e.
- [174] Vogl, S.; Atanasov, A.G.; Binder, M.; Bulusu, M.; Zehl, M.; Fakhrudin, N.; Heiss, E.H.; Picker, P.; Wawrosch, C.; Saukel, J.; et al., The herbal drug *Melampyrum pratense* L. (Koch): Isolation and identification of its bioactive compounds targeting mediators of inflammation, *Evid. Based Complement. Alternat. Med.* **2013**, *2013*, 395316, doi:10.1155/2013/395316.
- [175] Junio, H.A.; Sy-Cordero, A.A.; Etefagh, K.A.; Burns, J.T.; Micko, K.T.; Graf, T.N.; Richter, S.J.; Cannon, R.E.; Oberlies, N.H.; Cech, N.B., Synergy-directed fractionation of botanical medicines: A case study with goldenseal (*Hydrastis canadensis*), *J. Nat. Prod.* **2011**, *74*, 1621–1629, doi:10.1021/np200336g.
- [176] Cho, K.J.; Han, S.H.; Kim, B.Y.; Hwang, S.G.; Park, K.K.; Yang, K.H.; Chung, A.S., Chlorophyllin suppression of lipopolysaccharide-induced nitric oxide production in RAW 264.7 cells, *Toxicol. Appl. Pharmacol.* **2000**, *166*, 120–127, doi:10.1006/taap.2000.8958.
- [177] Cos, P.; Vlietinck, A.J.; Berghe, D.V.; Maes, L., Anti-infective potential of natural products: How to develop a stronger *in vitro* 'proof-of-concept', *J. Ethnopharmacol.* **2006**, *106*, 290–302, doi:10.1016/j.jep.2006.04.003.
- [178] Wei, S.-D.; Chen, R.-Y.; Liao, M.-M.; Tu, N.-W.; Lin, Y.-M., Antioxidant condensed tannins from *Machilus pauhoi* leaves, *J. Med. Plants Res.* **2011**, *5*.
- [179] Breton, R.C.; Reynolds, W.F., Using NMR to identify and characterize natural products, *Nat. Prod. Rep.* **2013**, *30*, 501–524, doi:10.1039/c2np20104f.
- [180] Paul, D.; Kundu, A.; Saha, S.; Goswami, R.K., Total synthesis: The structural confirmation of natural products, *Chem. Commun.* **2021**, *57*, 3307–3322, doi:10.1039/D1CC00241D.
- [181] Cheng, M.-J.; Yang, X.-Y.; Cao, J.-Q.; Liu, C.; Zhong, L.-P.; Wang, Y.; You, X.-F.; Li, C.-C.; Wang, L.; Ye, W.-C., Isolation, structure elucidation, and total synthesis of myrtuspirone A from *Myrtus communis*, *Org. Lett.* **2019**, *21*, 1583–1587, doi:10.1021/acs.orglett.9b00108.
- [182] Alvarez-Rivera, G.; Ballesteros-Vivas, D.; Parada-Alfonso, F.; Ibañez, E.; Cifuentes, A., Recent applications of high-resolution mass spectrometry for the characterization of plant natural products, *TrAC Trends Anal. Chem.* **2019**, *112*, 87–101, doi:10.1016/j.trac.2019.01.002.
- [183] Liu, Y.; Romijn, E.P.; Verniest, G.; Laukens, K.; Vijlder, T. de, Mass spectrometry-based structure elucidation of small molecule impurities and degradation products in pharmaceutical development, *TrAC Trends Anal. Chem.* **2019**, *121*, 115686, doi:10.1016/j.trac.2019.115686.
- [184] Kind, T.; Fiehn, O., Metabolomic database annotations via query of elemental compositions: mass accuracy is insufficient even at less than 1 ppm, *BMC Bioinform.* **2006**, *7*, 234, doi:10.1186/1471-2105-7-234.

- [185] Davies, V.; Wandy, J.; Weidt, S.; van der Hooft, J.J.J.; Miller, A.; Daly, R.; Rogers, S., Rapid Development of improved data-dependent acquisition strategies, *Anal. Chem.* **2021**, *93*, 5676–5683, doi:10.1021/acs.analchem.0c03895.
- [186] MassBank consortium and its contributors, MassBank/MassBank-data: Release version 2024.06; Zenodo.
- [187] Wang, M.; Carver, J.J.; Phelan, V.V.; Sanchez, L.M.; Garg, N.; Peng, Y.; Nguyen, D.D.; Watrous, J.; Kapon, C.A.; Luzzatto-Knaan, T.; et al., Sharing and community curation of mass spectrometry data with global natural products social molecular networking, *Nat. Biotechnol.* **2016**, *34*, 828–837, doi:10.1038/nbt.3597
- [188] Wolf, S.; Schmidt, S.; Müller-Hannemann, M.; Neumann, S., *In silico* fragmentation for computer-assisted identification of metabolite mass spectra, *BMC Bioinform.* **2010**, *11*, 148, doi:10.1186/1471-2105-11-148.
- [189] Tsugawa, H.; Kind, T.; Nakabayashi, R.; Yukihiro, D.; Tanaka, W.; Cajka, T.; Saito, K.; Fiehn, O.; Arita, M., Hydrogen rearrangement rules: Computational MS/MS fragmentation and structure elucidation using MS-Finder software, *Anal. Chem.* **2016**, *88*, 7946–7958, doi:10.1021/acs.analchem.6b00770.
- [190] Aue, W.P.; Bartholdi, E.; Ernst, R.R., Two-dimensional spectroscopy. Application to nuclear magnetic resonance, *J. Chem. Phys.* **1976**, *64*, 2229–2246, doi:10.1063/1.432450.
- [191] Letertre, M.P.M.; Giraudeau, P.; Tullio, P. de, Nuclear magnetic resonance spectroscopy in clinical metabolomics and personalized medicine: Current challenges and perspectives, *Front. Mol. Biosci.* **2021**, *8*, 698337, doi:10.3389/fmolb.2021.698337.
- [192] Köck, M.; Reif, B.; Gerlach, M.; Reggelin, M., Application of the 1,n-ADEQUATE experiment in the assignment of highly substituted aromatic compounds, *Molecules* **1996**, *1*, 41–45, doi:10.1007/s007830050007.
- [193] Köck, M.; Kerssebaum, R.; Bermel, W., A broadband ADEQUATE pulse sequence using chirp pulses, *Magn. Reson. Chem.* **2003**, *41*, 65–69, doi:10.1002/mrc.1097.
- [194] Elyashberg, M.; Argyropoulos, D., Computer assisted structure elucidation (CASE): Current and future perspectives, *Magn. Reson. Chem.* **2021**, *59*, 669–690, doi:10.1002/mrc.5115.
- [195] WebCocon, Available online: <https://cocon.nmr.de/> (accessed on 20 October 2024).
- [196] Nuzillard, J.-M.; Georges, M., Logic for structure determination, *Tetrahedron* **1991**, *47*, 3655–3664, doi:10.1016/S0040-4020(01)80878-4.
- [197] Steinbeck, C., SENECA: A platform-independent, distributed, and parallel system for computer-assisted structure elucidation in organic chemistry, *J. Chem. Inf. Comput. Sci.* **2001**, *41*, 1500–1507, doi:10.1021/ci000407n.
- [198] Liu, X.; Dong, S.-H.; Hao, J.-L.; Lin, B.; Bai, M.; Huang, X.-X.; Song, S.-J., (±) Camptothecin, a pair of ditetrahydrofuran lignans enantiomers from the fruit of *Camptotheca acuminata* and structure revision of biphenylneolignan, *J. Mol. Struct.* **2024**, *1295*, 136600, doi:10.1016/j.molstruc.2023.136600.
- [199] Tan, Y.-Z.; Yan, H.-L.; Liu, Y.-Y.; Yan, Y.-M.; Wang, L.; Qiao, J.-X.; Wu, J.; Tian, Y.; Peng, C., Structurally diverse phthalides from fibrous roots of *Ligusticum chuanxiong* Hort. and their biological activities, *Fitoterapia* **2024**, *175*, 105882, doi:10.1016/j.fitote.2024.105882.
- [200] Wang, D.-D.; Zhang, R.; Tang, L.-Y.; Long, G.-Q.; Yan, H.; Yang, Y.-C.; Guo, Z.-F.; Zheng, Y.-Y.; Wang, Y.; Jia, J.-M.; et al., (±)-Salvicatone A: A pair of C27-meroterpenoid enantiomers with skeletons from the roots and rhizomes of *Salvia castanea* Diels f. *tomentosa* Stib., *J. Org. Chem.* **2024**, *89*, 12894–12901, doi:10.1021/acs.joc.3c01664.
- [201] Ferron, S.; Ismed, F.; Elyashberg, M.E.; Buevich, A.V.; Arifa, N.; Boustie, J.; Uriac, P.; Le Pogam, P.; Le Dévéhat, F., CASE-DFT structure elucidation of proton-deficient chlorodepsidones from the Indonesian lichen *Teloschistes flavicans* and structure revision of flavicansone, *J. Nat. Prod.* **2024**, *87*, 2148–2159, doi:10.1021/acs.jnatprod.4c00277.
- [202] Cheatham, S.F.; Kline, M.; Sasaki, R.R.; Blinov, K.A.; Elyashberg, M.E.; Molodtsov, S.G., Enhanced automated structure elucidation by inclusion of two-bond specific data, *Magn. Reson. Chem.* **2010**, *48*, 571–574, doi:10.1002/mrc.2622.
- [203] Elyashberg, M.; Williams, A., ACD/Structure Elucidator: 20 years in the history of development, *Molecules* **2021**, *26*, doi:10.3390/molecules26216623.
- [204] Buevich, A.V.; Elyashberg, M.E., Synergistic combination of CASE algorithms and DFT chemical shift predictions: A powerful approach for structure elucidation, verification, and revision, *J. Nat. Prod.* **2016**, *79*, 3105–3116, doi:10.1021/acs.jnatprod.6b00799.

2 Analysis of Unusual Sulfated Constituents and Anti-infective Properties of Two Indonesian Mangroves, *Lumnitzera littorea* and *Lumnitzera racemosa* (Combretaceae)

Jeprianto Manurung*, Jonas Kappen*, Jan Schnitzler, Andrej Frolov, Ludger A. Wessjohann, Andria Augusta, Alexandra N. Muellner-Riehl, and Katrin Franke

* shared first authorship

Separations 2021, 8, 82; <https://doi.org/10.3390/separations8060082>

Abstract

Lumnitzera littorea and *Lumnitzera racemosa* are mangrove species distributed widely along the Indonesian coasts. Besides their ecological importance, both are of interest owing to their wealth of natural products, some of which constitute potential sources for medicinal applications. We aimed to discover and characterize new anti-infective compounds, based on population-level sampling of both species from across the Indonesian Archipelago. Root metabolites were investigated by TLC, hyphenated LC-MS/MS and isolation, the internal transcribed spacer (ITS) region of rDNA was used for genetic characterization. Phytochemical characterization of both species revealed an unusual diversity in sulfated constituents with 3,3',4'-tri-*O*-methyl-ellagic acid 4-sulfate representing the major compound in most samples. None of these compounds was previously reported for mangroves. Chemophenetic comparison of *L. racemosa* populations from different localities provided evolutionary information, as supported by molecular phylogenetic evidence. Samples of both species from particular locations exhibited anti-bacterial potential (Southern Nias Island and East Java against Gram-negative bacteria, Halmahera and Ternate Island against Gram-positive bacteria). In conclusion, *Lumnitzera* roots from natural mangrove stands represent a promising source for sulfated ellagic acid derivatives and further sulfur containing plant metabolites with potential human health benefits.

Keywords

sulfated natural products; ellagic acid; lumnitzera; combretaceae; mangrove; anti-infectives; phylogenetic analysis; metabolite profiling

MDPI statement concerning permissions

No special permission is required to reuse all or part of an article published by MDPI, including figures and tables. For articles published under an open access Creative Common CC BY license, any part of the article may be reused without permission provided that the original article is clearly cited. Reuse of an article does not imply endorsement by the authors or MDPI. Furthermore, no special permission is required for authors to submit their work to external repositories. This policy extends to all versions of a paper: submitted, accepted, and published.

Article

Analysis of Unusual Sulfated Constituents and Anti-infective Properties of Two Indonesian Mangroves, *Lumnitzera littorea* and *Lumnitzera racemosa* (Combretaceae)

Jeprianto Manurung ^{1,2,3,†} , Jonas Kappen ^{3,†} , Jan Schnitzler ^{1,2} , Andrej Frolov ^{3,4} , Ludger A. Wessjohann ^{2,3} , Andria Agusta ⁵ , Alexandra N. Muellner-Riehl ^{1,2,*}  and Katrin Franke ^{3,*} 

- ¹ Department of Molecular Evolution and Plant Systematics & Herbarium (LZ), Institute of Biology, Leipzig University, 04109 Leipzig, Germany; jeprianto_m@apps.ipb.ac.id (J.M.); j.schnitzler06@alumni.imperial.ac.uk (J.S.)
- ² German Centre for Integrative Biodiversity Research (iDiv) Halle-Jena-Leipzig, 04103 Leipzig, Germany; ludger.wessjohann@ipb-halle.de
- ³ Department of Bioorganic Chemistry, Leibniz Institute of Plant Biochemistry (IPB), 06120 Halle (Saale), Germany; jkappen@ipb-halle.de (J.K.); andrej.frolov@ipb-halle.de (A.F.)
- ⁴ Department of Biochemistry, St. Petersburg State University, 199034 St. Petersburg, Russia
- ⁵ Research Center for Chemistry, Indonesian Institute of Sciences (LIPI), Jl. Jend. Gatot Subroto 10, Jakarta 12710, Indonesia; andr002@lipi.go.id
- * Correspondence: muellner-riehl@uni-leipzig.de (A.N.M.-R.); katrin.franke@ipb-halle.de (K.F.); Tel.: +49-341-97-38581 (A.N.M.-R.); +49-345-5582-1380 (K.F.)
- † J.M. and J.K. contributed equally to this work.



Citation: Manurung, J.; Kappen, J.; Schnitzler, J.; Frolov, A.; Wessjohann, L.A.; Agusta, A.; Muellner-Riehl, A.N.; Franke, K. Analysis of Unusual Sulfated Constituents and Anti-infective Properties of Two Indonesian Mangroves, *Lumnitzera littorea* and *Lumnitzera racemosa* (Combretaceae). *Separations* **2021**, *8*, 82. <https://doi.org/10.3390/separations8060082>

Academic Editors: Alena Kubatova and Gavino Sanna

Received: 15 April 2021

Accepted: 6 June 2021

Published: 10 June 2021

Publisher's Note: MDPI stays neutral with regard to jurisdictional claims in published maps and institutional affiliations.



Copyright: © 2021 by the authors. Licensee MDPI, Basel, Switzerland. This article is an open access article distributed under the terms and conditions of the Creative Commons Attribution (CC BY) license (<https://creativecommons.org/licenses/by/4.0/>).

Abstract: *Lumnitzera littorea* and *Lumnitzera racemosa* are mangrove species distributed widely along the Indonesian coasts. Besides their ecological importance, both are of interest owing to their wealth of natural products, some of which constitute potential sources for medicinal applications. We aimed to discover and characterize new anti-infective compounds, based on population-level sampling of both species from across the Indonesian Archipelago. Root metabolites were investigated by TLC, hyphenated LC-MS/MS and isolation, the internal transcribed spacer (ITS) region of rDNA was used for genetic characterization. Phytochemical characterization of both species revealed an unusual diversity in sulfated constituents with 3,3',4'-tri-*O*-methyl-ellagic acid 4-sulfate representing the major compound in most samples. None of these compounds was previously reported for mangroves. Chemophenetic comparison of *L. racemosa* populations from different localities provided evolutionary information, as supported by molecular phylogenetic evidence. Samples of both species from particular locations exhibited anti-bacterial potential (Southern Nias Island and East Java against Gram-negative bacteria, Halmahera and Ternate Island against Gram-positive bacteria). In conclusion, *Lumnitzera* roots from natural mangrove stands represent a promising source for sulfated ellagic acid derivatives and further sulfur containing plant metabolites with potential human health benefits.

Keywords: sulfated natural products; ellagic acid; *Lumnitzera*; Combretaceae; mangrove; anti-infectives; phylogenetic analysis; metabolite profiling

1. Introduction

Mangrove forests represent a unique habitat that comprises salt-tolerant plant species (mostly trees), predominantly bordering tropical and subtropical coastlines [1]. Besides their ecological significance, mangrove plant species have a wide variety of economic uses, such as construction material, fodder or textiles [2,3]. In addition, many mangrove plant species possess medicinal value and have been used traditionally in several regions of the world [4–7]. Due to the tidal influence, mangrove soils contain high levels of sulfate which is connected to the occurrence of sulfate-reducing microbial communities [8]. Nevertheless, the investigation of bioactive natural sulfur compounds in mangrove species was so far completely neglected.

The most diverse mangrove systems on earth can be found in Southeast Asian seas [9]. Comprising five main and more than 17,500 smaller islands, Indonesian mangroves cover around 30% of the total mangrove area of the world [10]. *Lumnitzera littorea* (Jack) Voigt and *L. racemosa* Willd., two true mangrove species belonging to the plant family Combretaceae (Myrtales), are distributed widely across the Indonesian coastline. In Africa, where *L. racemosa* also naturally occurs at the eastern coast, other members of Combretaceae (*Combretum*, *Terminalia*) are widely used for medicinal purposes due to their anti-microbial [11–16], anti-fungal [17,18], antioxidant and anti-inflammatory activities [16]. In Asia, *L. racemosa* from Taiwan was reported to contain antihypertensive tannins [19]. Furthermore, hepatoprotective, antioxidant [20–23], antibacterial [24,25], anti-angiogenic, anti-inflammatory [26], anti-cancer [23,27], and anti-coagulant effects [23] were described in *L. racemosa* from different parts of Asia. In leaves and twigs of *L. racemosa* mainly flavonoids and triterpenes [22,28] as well as phenolic acids and their derivatives, such as gallic acid and related compounds—galloyl sugars, ellagic acid, 3,3',4-tri-*O*-methylellagic acid, neolignans and tannic acid—were found [22,26]. The extract of *L. littorea* leaves from Malaysia was reported to possess anti-microbial potential [29]. The leaf *n*-hexane extract of this species yielded triterpenes and sterols [30] whereas the twigs of *L. littorea* were described to contain macrocyclic lactones (represented by corniculatolide derivatives) and 6,7-dimethoxycoumarin [31].

Medicinally active compounds from mangroves are not always produced by the plant itself, but often by associated microorganisms such as endophytic fungi [32–34]. For example, the extracts of endophytic fungi isolated from leaves of ten mangrove species from Thailand, including *L. littorea*, showed some cytotoxic activity against cancer cell lines [35]. In line with the agenda of discovering new anti-infective and neuroactive constituents while at the same time promoting the protection and sustainable development of mangrove ecosystems, our work was focused on two mangrove species, namely *Lumnitzera littorea* and *L. racemosa*. Our aim was to (1) investigate the diversity of natural products present in the roots of *L. littorea* and *L. racemosa* from Indonesia, (2) evaluate selected biological effects, and (3) investigate the phylogenetic relationships of the two species as well as the chemophenetic patterns of their natural products across Indonesia. Therefore, we combined a molecular phylogeny of *Lumnitzera* based on the internal transcribed spacer (ITS) region with phytochemical analyses by hyphenated chromatographic and tandem mass spectrometric techniques. Chromatographic separation using reversed phase HPLC connected to high resolution ESI-MS that allow the determination of accurate mass and elemental composition represents a suitable technique to identify sulfur containing metabolites [36]. For the calculation of the molecular composition of sulfur-containing compounds, the small negative mass defect of sulfur isotopes and the isotopic pattern of sulfur distinct from that of carbon, nitrogen and hydrogen can be applied [36]. Since sulfur in addition to the most abundant isotope ^{32}S (95%) possesses a ^{34}S isotope (4.2%), also the larger as usual $\text{M}+2$ peak contributes to the determination of sulfur in compounds or fragments. Nevertheless, for complete structure elucidation, compounds have to be isolated and characterized by NMR. Phylogenetic approaches can be useful for identifying plant lineages with potential medicinal properties [37,38], the interpretation of chemical profiles [39], and might be a powerful tool for discovering novel compounds or novel compound variants [40–42], including antibiotic sources [43,44].

2. Materials and Methods

2.1. Plant Material

Leaf and root material of *Lumnitzera littorea* (Jack) Voigt and *Lumnitzera racemosa* Willd. was collected from 27 locations across the Indonesian archipelago (Table 1). Voucher specimens of the plants are deposited at *Herbarium Bogoriense* (BO), Indonesian Institute of Sciences (LIPI). Root samples for phytochemical analyses were cleaned and air-shadow-dried in the field, then kept in resealable zipper storage bags until being used for further treatment. For phylogenetic analyses, fresh leaves from the same plants were collected and dried in silica gel in resealable zipper storage bags.

Table 1. Samples from *L. littorea* (no. 1–12) and *L. racemosa* (no. 13–31) used for phytochemical and DNA analyses. Abbreviations: JM = Jeprianto Manurung, Fr = Fine root, Rb = Root bark, NS = North Sumatra, EK = East Kalimantan, SS = Southeast Sulawesi, NS = North Sulawesi, CS = Central Sulawesi, ENT = East Nusa Tenggara.

No.	Code	Collector's No.	Voucher No.	Collection Date	GenBank Accession (ITS)	Location	Coordinates Lat. (S/Long. E)	Tissue	Extract Amount (mg)	Growth Form
1	LI.1	J.M. 02L-02	BO1959909	20-04-2018	MT251443	Ladang Village, Aceh	5.61/95.49	Rb	11	tree
2	LI.2	J.M. 03L-7	BO1959384	25-04-2018	MT251447	Northern Nias Island	1.51/97.37	Fr	6	tree
3	LI.3	J.M. 03L-10	BO1959383	26-04-2018	MT251438	Southern Nias Island	0.56/97.78	Fr	8	tree
4	LI.4	J.M. 04L-3	BO1959378	30-04-2018	MT251446	Batam Island	0.91/104.15	Fr	7	tree
5	LI.5	J.M. 05L-10	BO1959420	09-05-2018	MT251437	Balikpapan, EK	-1.20/116.84	Fr	2	tree
6	LI.6	J.M. 07L-8	BO1959417	16-05-2018	MT251442	Kendari, SS	-4.48/122.13	Rb	13	tree
7	LI.7	J.M. 08L-10	BO1959415	19-05-2018	MT251444	Manado, NS	1.60/124.85	Rb	10	tree
8	LI.8	J.M. 09L-15	BO1959410	23-05-2018	MT251439	Halmahera Island, Maluku	1.04/127.50	Rb	4	tree
9	LI.9	J.M. 13L-12	BO1959404	31-05-2018	MT251440	Peling Island, CS	-1.23/123.40	Fr	7	tree
10	LI.10	J.M. 14L-11		05-06-2018	MT251436	Luwuk, CS	0.74/122.96	Fr	6	tree
11	LI.11	J.M. 16L-3	BO1959651	29-06-2018	MT251445	Banten, West Java	-6.83/105.45	Rb	21	tree
12	LI.12	J.M. 24L-4	BO1959653	27-07-2018	MT251441	Banyuwangi, East Java	-8.39/114.27	Rb	14	tree
13	LR1.1 LR1.2 LR1.3	J.M. 01L-13	BO1959913	18-04-2018	MT251462 MT251463 MT251464	Batu Bara, North Sumatra	3.22/99.57	Fr	7	tree
14	LR2	J.M. 02R-01a	BO1959908	21-04-2018	MT251467	Ladang Village, Aceh	5.65/95.45	Fr	8	shrub
15	LR3.1 LR3.2 LR3.3	J.M. 02R-02L	BO1959380	21-04-2018	MT251461 MT251470 MT251469	Durung Village, Aceh	5.61/95.49	Rb	22	shrub
16	LR4.1 LR4.2 LR4.3	J.M. 5R-11	BO1959421	08-05-2018	MT251473 MT251471 MT251468	Kartanegara, EK	-1.05/117.10	Fr	4	tree
17	LR5	J.M. 06R-3	BO1959416	11-05-2018	MT251454	Makassar, South Sulawesi	5.49/119.32	Fr	10	shrub
18	LR6	J.M. 07R-3	BO1959413	16-05-2018	MT250980	Kendari, SS	-4.51/122.10	Fr	6	shrub
19	LR7	J.M. 10R-2	BO1959402	24-05-2018	MT251456	Ternate Island, Maluku	0.84/127.31	Fr	3	shrub
20	LR8.1 LR8.2 LR8.3	J.M. 11R-8	BO1959776	29-05-2018	MT251472 MT251466 MT251465	Seram Island, Maluku	3.55/128.36	Fr	2	shrub
21	LR9	J.M. 13R-12	BO1959649	04-06-2018	MT251458	Peling Island, Central Sulawesi	-1.23/123.40	Fr	9	shrub
22	LR10	J.M. 16R-1	BO1959655	29-06-2018	MT251457	Banten, West Java	-6.83/105.45	Rb	10	tree
23	LR11	J.M. 18R-14	BO1959641	05-07-2018	MT251451	East Sumba, ENT	9.67/120.33	Fr	14	shrub
24	LR12	J.M. 18R-15	BO1959646	05-07-2018	MT251450	East Sumba, ENT	-9.64/120.24	Fr	19	shrub
25	LR13	J.M. 17R-13	BO1959642	04-07-2018	MT251449	Kupang, ENT	-10.15/123.64	Fr	3	shrub

Table 1. *Cont.*

No.	Code	Collector's No.	Voucher No.	Collection Date	GenBank Accession (ITS)	Location	Coordinates Lat. (S)/ Long. (E)	Tissue	Extract Amount (mg)	Growth Form
26	LR14	J.M. 19R-15	BO1939644	09-07-2018	M1251459	Labuan Bajo, ENI	−8.46/119.88	Fr	37	tree
27	LR15	J.M. 20R-3	BO1939423	11-07-2018	MT251453	Komodo Island, ENT	−8.51/119.55	Rb	32	tree
28	LR16	J.M. 21R-9	BO1939591	13-07-2018	MT251455	Padar Island, ENT	8.64/119.58	Rb	19	tree
29	LR17	J.M. 22R-15	BO1939588	13-07-2018	M1251448	Rinca Island, ENI	−8.65/119.72	Fr	21	tree
30	LR18	J.M. 23R-3	BO1939386	20-07-2018	MT251460	Bali Island	−8.73/115.20	Fr	9	tree
31	LR19	J.M. 24R-15	BO1939640	27-07-2018	MT251452	Banyuwangi, East Java	−8.59/114.27	Fr	17	tree

2.2. Root Sample Extraction

Air-dried samples (root bark and fine roots) were ground using a ball mill (Retsch, MM400) for two minutes. In extraction experiments with *n*-hexane, ethyl acetate and methanol, the highest extract amount could be obtained with methanol. Therefore, 100 mg of each sample were vortexed with 5 mL methanol in Eppendorf tubes before sonication for an hour. All samples were centrifuged for fifteen minutes using a Megafuge 1.0R (Unity Lab Services) to gain pure solutions. The extracts were aliquoted for analytical investigations and bioassay screening. The crude extracts were directly used for TLC and low-resolution ESI-MS analyses. For LCMS measurements, 250 μ L of each extract were purified by an SPE cartridge (RP18, Chromabond, Macherey-Nagel, Düren, Germany), using methanol as eluent, and the concentration was afterwards adjusted to 1 mg/mL.

2.3. General Experimental Procedures

Thin layer chromatography (TLC) analyses were done with silica gel 60 F₂₅₄ (Merck, Darmstadt, Germany) using the solvent system CHCl₃:MeOH 6:4. Compound spots were visualized using long-wavelength UV light (366 nm), short-wavelength UV light (254 nm) and spraying with vanillin-H₂SO₄ reagent, followed by heating. As sample LR15 in TLC displayed stronger spots compared to the others, preparative TLC (thickness 0.5 mm) was performed using the same conditions. The major bands were scraped off and extracted to verify the compound identity by MS investigations.

Low-resolution ESI-MS spectra were obtained from a Sciex API-3200 instrument (Applied Biosystems, Concord, ON, Canada) combined with an HTC-XT autosampler (CTC Analytics, Zwingen, Switzerland).

¹H and ¹³C NMR spectra were recorded on an Agilent DD2 400 NMR spectrometer at 399.917 and 100.570 MHz, respectively. Chemical shifts are reported relative to TMS (¹H NMR) or peaks of solvent (¹³C, CD₃OD 49.0 ppm and DMSO-*d*₆ 39.5 ppm). For samples with low concentration, ¹H and ¹³C NMR spectra were recorded on a Bruker Avance Neo 500 NMR spectrometer at 500.234 and 125.797 MHz, respectively, using a 5 mm prodigy probe with the TopSpin 4.0.7 spectrometer software. 2D NMR spectra were recorded on an Agilent VNMRS 600 MHz NMR spectrometer using standard CHEMPACK 8.1 pulse sequences (¹H, ¹³C gHSQCAD and ¹H, ¹³C gHMBCAD) implemented in Varian VNMRJ 4.2 spectrometer software.

Preparative HPLC was performed using an Agilent 1260/1290 system equipped with a quaternary pump and a diode array (DAD) detector (Agilent, VL+). Chromatographic separation was performed using a Macherey-Nagel Chromcart C18ec column (ID 4.6 mm, length 150 mm, particle size 5 μ m) using bidest. water (TKA ultrapure water system) and methanol (Roth, Rotisolv HPLC Gradient Grade) as eluents.

2.4. UHPLC-ESI-QqTOF-MS and MS/MS

Samples (2 μ L) were loaded on an EC 150/2 Nucleoshell RP 18 column (C₁₈-phase, ID 2 mm, length 150 mm, particle size 2.7 μ m, Macherey Nagel, Düren, Germany) under isocratic conditions (5% eluent B, 2 min), and separated using a linear gradient from 5% to 95% eluent B in 17 min. Separation was performed on an ACQUITY UPLC I-Class UHPLC System (Waters GmbH, Eschborn, Germany) with a flow rate of 0.4 mL/min and 40 °C column temperature. Eluents A and B were 0.3 mmol/L aq. ammonium formate and acetonitrile, respectively. The column effluent was introduced on-line into a TripleTOF 6600 QqTOF mass spectrometer equipped with a DuoSpray ESI/APCI ion source, operating in negative ion SWATH (Sequential Windowed Acquisition of All Theoretical Fragment Ion Mass Spectra) mode and controlled by the Analyst TF 1.7.1 software (AB Sciex GmbH, Darmstadt, Germany). The TOF scans (MS experiments) were acquired in the *m/z* range of 65 to 1250 (accumulation time 100 ms) with an ion spray voltage of −4.5 kV and 450 °C source temperature. For precursor selection, totally 38 SWATH windows (total *m/z* range of 65–1250) of 26 *m/z* were used. Nebulizer and drying gases were set to 60 and 70 psi, respectively, whereas the curtain gas was set to 55 psi. Declustering (DP) and collision (CE)

potentials were -35 and -10 V, respectively. The product ion spectra (tandem mass spectra, MS/MS) were acquired in the high sensitivity mode (accumulation time 20 ms) in the m/z range of 65–1250 using unit Q1 resolution with mass resolution above 30,000. Collision potential (CE) was set to -35 V, whereas collision energy spread (CES) was 15 V. The data were evaluated by Peak View 1.2.0.3 software (AB Sciex GmbH, Darmstadt, Germany).

2.5. RP-UHPLC-ESI-LIT-Orbitrap-MS

Samples (2 μ L) were loaded on an ACQUITY UPLC reversed-phase BEH column (C_{18} -phase, ID 1 mm, length 50 mm, particle size 1.7 μ m, Waters GmbH, Eschborn, Germany) under isocratic conditions (95% A + 5% eluent B, 2 min), and separated using a linear gradient from 5% to 95% eluent B in 10 min using water and acetonitrile (both containing 0.1% v/v formic acid) as eluents A and B, respectively. The separations were performed with a Dionex Ultimate 3000 UHPLC System (Thermo Fisher Scientific, Bremen, Germany) at the flow rate of 400 μ L/min and column temperature of 40 $^{\circ}$ C. The column effluents were transferred on-line into a hybrid LTQ-Orbitrap Elite mass spectrometer (Thermo Fisher Scientific, Bremen, Germany), equipped with a heated electrospray ionization (HESI) source at 300 $^{\circ}$ C and operated in the negative ion mode. The analysis was performed under ion spray (IS) voltage of 3.8 kV, with nebulizer and auxiliary gases set to 10 and 5 psig, respectively. The capillary temperature was set to 325 $^{\circ}$ C. The spectra were acquired at the mass to charge ratio (m/z) range of 120–2000 and resolution of 30,000. Tandem mass spectra were acquired with isolation width of 0.5–2 m/z and collision induced dissociation mode (30–35% normalized intensity), activation time 10 ms and activation frequency 250. Spectra evaluation was performed in Xcalibur 2.2 software (Thermo Fisher Scientific).

2.6. Extraction and Isolation

62.58 g roots of LR7 were exhaustively extracted with methanol to give 3.86 g of crude extract after evaporation of the solvent.

1.5 g crude extract was separated on a silica gel column with an increasing polar gradient, started with pure chloroform, followed by 2.5%, 5%, 10% and 50% methanolic chloroform and a final elution with pure methanol (volume of each step: 250 mL). Based on the TLC profiles, the fractions were combined into 21 main fractions. Fraction 5, eluted with 2.5% MeOH, could be identified as 3,3',4'-tri-*O*-methylellagic acid (**16**) (12 mg, $R_f = 0.92$ in $CHCl_3$ /MeOH (3:1, v/v) on SG60). Fraction 18 (252.6 mg) eluted with 50% MeOH was further separated on a Sephadex LH20 column eluted with MeOH followed by repeated CC on a reverse phase column (C_{18}) using H_2O :MeOH (60:40, v/v) as eluents to give 3,3',4'-tri-*O*-methylellagic acid 4-sulfate (**15**) (3.9 mg, $R_f = 0.33$ in MeOH/ H_2O (2:3, v/v) on RP18) and mixtures of compounds **2**, **3** and **4**. Final purification was performed by preparative HPLC. Compound **2** (0.6 mg, $R_f = 0.70$ in MeOH/ H_2O (2:3, v/v) on RP18) was purified using a water (A)/methanol (B) gradient system (0–1.5 min, 20% B; 1.5–14 min, 20–50% B, 14–16 min 50–100% B (isocratic for 8 min)) and a flow rate of 0.8 mL/min at 25 $^{\circ}$ C, absorbance detection at 210 to 254 nm ($R_t = 6.605$ min). Compound **3** (3.2 mg, $R_f = 0.15$ in MeOH/ H_2O (2:3, v/v) on RP18) was obtained using the following gradient: 0–18 min, 40% B; 18–20 min, 40–100% B (isocratic for 10 min), and a flow rate of 0.6 mL/min at 15 $^{\circ}$ C, absorbance detection at 210 to 254 nm ($R_t = 15.41$ min).

1.35 g crude extract were partitioned by liquid-liquid-extraction between water and ethyl acetate. The ethyl acetate phase (419.8 mg) was further separated using a Sephadex LH20 column eluting with MeOH (h: 37.5 cm, d: 2.5 cm). Based on TLC profiles seven main fractions were combined. Fraction 6 could be identified as ellagic acid (**6**) (7.5 mg, $R_f = 0.08$ in H_2O /MeOH (3:2, v/v + 1% formic acid) on RP18). Rechromatography of fraction 5 (16.2 mg) on Sephadex LH20 with MeOH (h: 76 cm, d: 2.5 cm) resulted in the isolation of 3,4-di-*O*-methylellagic acid (**13**) (4.7 mg, $R_f = 0.02$ in H_2O /MeOH (3:2, v/v + 1% formic acid) on RP18).

4-(4-Hydroxyphenyl)-2-butanol 2-sulfate (**2**): white amorphous compound; 1H NMR (400 MHz, methanol- d_4) δ 7.03 (d-like, $J = 8.4$ Hz, 2H, H-2'/6'), 6.67 (d-like, $J = 8.4$ Hz,

2H, H-3'/5'), 4.46 (m, 1H, H-2), 2.55–2.70 (m, 2H, H-4), 1.89 (m, 1H, H-3a), 1.75 (m, 1H, H-3b), 1.33 (d, $J = 6.3$ Hz, 3H, H-1). ^{13}C NMR (δ determined from cross peaks in HSQC and $^*\text{HMBC}$ experiments, methanol- d_4) δ 156.4* (C-4'), 134.6* (C-1'), 130.3 (C-2'/6'), 116.1 (C-3'/5'), 76.8 (C-2), 40.5 (C-3), 31.8 (C-4), 21.2 (C-1). 2D-NMR see Table S2.; HRESIMS m/z 245.0484 $[\text{M}-\text{H}]^-$ (calcd for $\text{C}_{10}\text{H}_{13}\text{SO}_5$, 245.0489).

4-(4-Sulfoxy-3-methoxyphenyl)-butan-2-one (3): yellow oily compound; ^1H NMR (400 MHz, methanol- d_4) δ 6.77 (d, $J = 2.0$ Hz, 1H, H-2'), 6.68 (d, $J = 8.0$ Hz, 1H, H-5'), 6.61 (dd, $J = 8.0, 2.0$ Hz, 1H, H-6'), 3.82 (s, 3H, 3'-OMe), 2.76 (s, 4H, H-3'/4'), 2.11 (s, 3H, H-1). ^{13}C NMR (126 MHz, methanol- d_4) δ 211.5 (C-2), 149.0 (3'), 145.8 (C-4'), 134.0 (C-1'), 121.7 (C-6'), 116.2 (C-5'), 113.1 (C-2'), 56.4 (3'-OMe), 46.3 (C-3), 30.5 (C-4), 30.1 (C-1). 2D-NMR see Table S3.; HRESIMS m/z 273.0435 $[\text{M}-\text{H}]^-$ (calcd for $\text{C}_{11}\text{H}_{13}\text{SO}_6$, 273.0438).

Ellagic acid (6): ^1H NMR (400 MHz, DMSO- d_6) δ 7.46 (s, 2H, H5/H5'), HRESIMS m/z 300.9996 $[\text{M}-\text{H}]^-$ (calcd for $\text{C}_{14}\text{H}_6\text{O}_8$, 300.9990).

3,4-*O*-Dimethylellagic acid (13): yellowish amorphous compound, ^1H NMR (600 MHz, DMSO- d_6) δ 7.53 (s, 1H, H5), 7.09 (s, 1H, H5'), 3.99 (s, 4H, 3-OMe), 3.96 (s, 3H, 4-OMe). ^{13}C NMR from HMBC (600/150 MHz, DMSO- d_6) δ 160.22 (C-7), 159.15 (C-7'), 156.46 (C-4'), 152.73 (C-4), 151.92 (C-3'), 141.79 (C-2), 140.04 (C-3), 134.51 (C-2'), 115.00 (C-1), 114.97 (C-1'), 113.09 (C-6'), 112.95 (C-6), 105.83 (C-5), 104.63 (C-5'), 60.83 (3-OMe), 56.32 (4-OMe). 2D-NMR see Table S4. HRESIMS m/z 329.0370 $[\text{M}-\text{H}]^-$ (calcd for $\text{C}_{16}\text{H}_{10}\text{O}_8$, 329.0303).

3,3',4'-Tri-*O*-methylellagic acid 4-sulfate (15): white yellowish amorphous compound; ^1H NMR (400 MHz, DMSO- d_6) δ 8.24 (s, 1H, H-5), 7.66 (s, 1H, H-5'), 4.12 (s, 3H, 3-OMe), 4.06 (s, 3H, 3'-OMe), 4.02 (s, 3H, 4'-OMe). ^{13}C NMR (126 MHz, DMSO- d_6) δ 158.46 (C-7'), 158.31 (C-7), 154.37 (C-4'), 147.64 (C-4), 143.32 (C-3), 141.34 (C-3'), 140.89 (C-2'), 140.86 (C-2), 117.61 (C-5), 114.13 (C-1'), 112.96 (C-1), 112.83 (C-6'), 111.52 (C-6), 107.50 (C-5'), 61.47 (3-OMe), 61.32 (3'-OMe), 56.75 (4'-OMe). 2D-NMR see Table S5; HRESIMS m/z 423.0024 $[\text{M}-\text{H}]^-$ (calcd for $\text{C}_{17}\text{H}_{11}\text{SO}_{11}$, 423.0028).

3,3',4'-Tri-*O*-methylellagic acid (16): white yellowish amorphous compound. ^1H NMR (400 MHz, DMSO- d_6) δ 7.61 (s, 1H, H-5'), 7.52 (s, 1H, H-5), 4.06 (s, 3H, 3-OMe), 4.04 (s, 3H, 3'-OMe), 4.00 (s, 3H, 4'-OMe); ^{13}C NMR (126 MHz, DMSO- d_6) δ 158.44 (C-7'), 158.24 (C-7), 153.62 (C-4'), 152.96 (C-4), 141.37 (C-2'), 140.85 (C-3'), 140.67 (C-2), 140.18 (C-3), 113.33 (C-6'), 112.39 (C-6), 111.74 (C-1'), 111.67 (C-5), 110.80 (C-1), 107.33 (C-5'), 61.19 (3'-OMe), 60.83 (3-OMe), 56.60 (C-4'). 2D NMR see Table S6; ESI-HRMS m/z 343.0423 $[\text{M}-\text{H}]^-$ (calcd for $\text{C}_{17}\text{H}_{11}\text{O}_8$, 343.0459).

2.7. DNA Extraction, Polymerase Chain Reaction, and Sequencing

Genomic DNA was isolated from leaf samples using the Nucleo Spin Plant II Kit (Macherey-Nagel GmbH & Co. KG, Dueren, Germany), with minor modifications, using buffer PL2 and adding 20 μL RNase, 30 μL mercaptoethanol and PVP (2%). The yield of DNA extraction was measured using a Qubit[®] 3.0 Fluorometer (Thermo Fischer Scientific, Waltham, MA, USA) and DNA bands were visualized with SYBR[®] Safe DNA gel stain (Thermo Fisher Scientific) on 1% agarose gels ($1 \times$ TAE buffer solution) using a GenoPlex VWR[®] gel documentation system with GenoCapture version 7.12.07.0 (Synoptics Ltd., Cambridge, UK). We performed polymerase chain reaction (PCR) of the ITS region, which comprises the ITS1 spacer, 5.8S rRNA gene, and ITS2 spacer using primers 17SE_m (5'-CGGTGAAGTGTTCCGATCG-3') and 26SE_m (5'-CGCTCGCCGTACTAGGG-3') [45], with reaction volumes of 25 μL , including 2 μL of genomic DNA, 0.3 μL of each primer, 0.5 μL BSA, 1 μL DMSO and 20.9 μL , and $1 \times$ Dream TaqGreen Master Mix, on a Labcycler Gradient PCR machine (SensoQuest GmbH, Germany). The initial denaturation step was set at 95 $^\circ\text{C}$ for 2 min, followed by 35 cycles of denaturation at 95 $^\circ\text{C}$ for 1 min, primer annealing at 53 $^\circ\text{C}$ for 1 min, extension at 72 $^\circ\text{C}$ for 2 min, followed by final extension at 72 $^\circ\text{C}$ for 10 min. PCR products were purified using a Nucleo Spin Gel and PCR clean-up kit (Macherey-Nagel GmbH & Co. KG, Dueren, Germany). The purified DNA samples were then measured using an Eppendorf Biophotometer to adjust the DNA concentration

before Sanger sequencing at LGC Genomics GmbH, Berlin, Germany, using the same primers as mentioned above.

2.8. Phylogenetic Analyses

All sequences were aligned using the MUSCLE algorithm as implemented in Geneious 6.1.8 [46] and corrected by hand. Phylogenetic analyses were done using Maximum Likelihood (ML) with RAxML [47,48], and Bayesian inference with MrBayes v3.2.7 [49]. We used the GTR + Γ substitution model in all analyses to ensure comparability between the Maximum Likelihood and Bayesian analyses. In RAxML, we inferred the maximum likelihood tree with 100 non-parametric bootstrap replicates. In MrBayes, we ran the inference for 5 million generations (sampling every 5000 generations) with four runs and four chains each. The appropriateness of sampling (all Effective Sample Sizes (ESS) >200) was checked in Tracer v1.7.1 [50], before building a majority-rule consensus tree (with 2 million generations excluded as burn-in). In both analyses, *Laguncularia racemosa* (L.) C.F.Gaertn. was set as outgroup.

2.9. Anti-infective Bioassays

Crude extracts (50 and 500 $\mu\text{g/mL}$) were tested in triplicate for antibacterial activity against the Gram-negative *Aliivibrio fischeri* and the Gram-positive *Bacillus subtilis* following the procedure described by dos Santos et al. [51]. Chloramphenicol (100 μM) was used as positive control and induced the complete inhibition of bacterial growth. The results are presented as relative values (% inhibition) in comparison to the negative control (bacterial growth in medium containing 1% DMSO without test compound = 0% inhibition). Negative values indicate an increase of bacterial growth, which is common with testing extracts containing further nutrients by nature.

The anthelmintic bioassay for all extracts (500 $\mu\text{g/mL}$) was performed in triplicate according to the method developed by Thomson and coworkers [52] using the model organism *Caenorhabditis elegans* (Bristol N2 wild-type strain) that previously was shown to correlate with anthelmintic activity against parasitic trematodes. The solvent DMSO (2%) and the standard anthelmintic drug ivermectin (10 $\mu\text{g/mL}$, 100% dead worms after 30 min incubation) were used as negative and positive controls, respectively. The number of dead and living nematodes in each sample was counted using the microscope Olympus CKX41. Results are given as percentage of dead worms.

The cytotoxic activity of selected samples (LL3, LL11, LR5, LR15) was evaluated at the concentrations of 0.05 and 50 mg/mL against the human prostate cancer cell line PC3 and the colon adenocarcinoma cell line HT-29 by determining cell viability in MTT and CV assays as described previously [51]. Digitonin (125 g/mL) was used as positive control. The results are given as percentage of control values without treatment (=100%).

3. Results and Discussion

3.1. Phytochemical Analyses

The metabolite profiles of roots from 12 accessions of *Lumnitzera littorea* and 19 accessions of *L. racemosa* collected across Indonesia were investigated by TLC (Figure 1) and liquid chromatography, coupled on-line to mass spectrometry (LC-MS) or tandem mass spectrometry (LC-MS/MS). For structure verification, selected compounds were isolated and investigated by nuclear magnetic resonance spectroscopy (NMR).

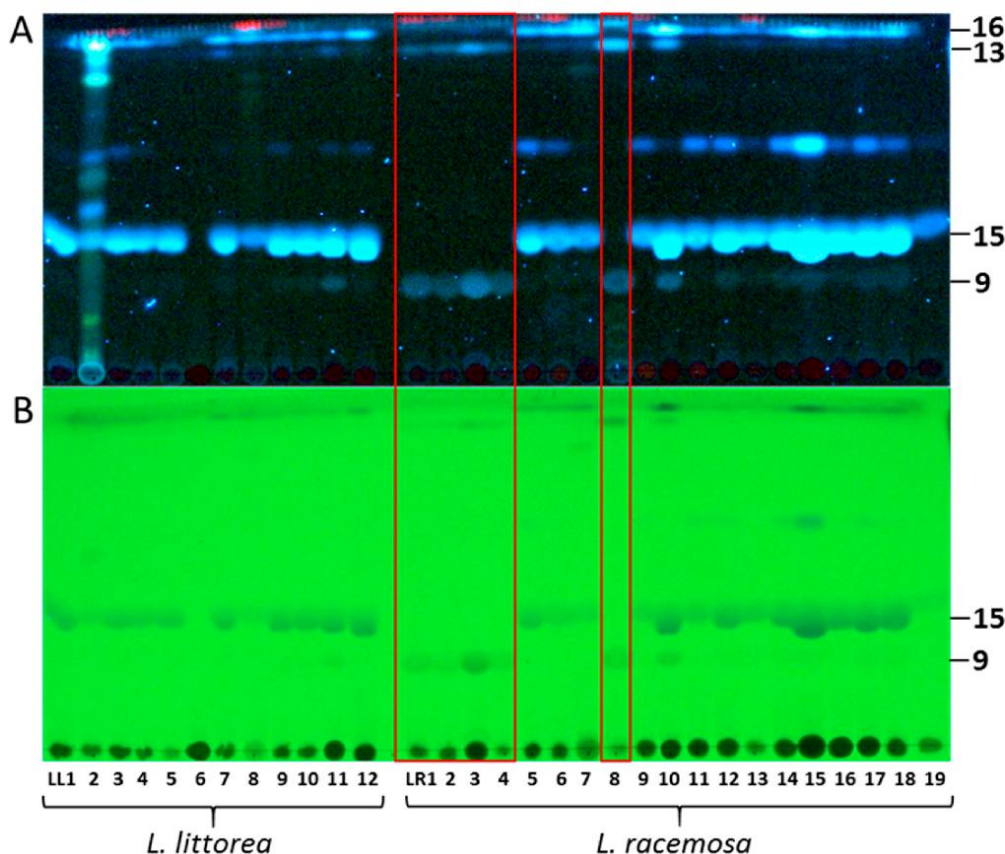


Figure 1. TLC profiles of root extracts from *Lumnitzera littorea* and *L. racemosa* showing the occurrence of dimethylellagic acid sulfate (9), 3,4-dimethylellagic acid (13), 3,3',4'-trimethylellagic acid 4-sulfate (15) and 3,3',4'-trimethylellagic acid (16): (A) Detection of bands at 366 nm (fluorescence), (B) Detection of bands at 254 nm (fluorescence quench). The red box highlights the samples LR1, LR2, LR3, LR4 and LR8 forming “Clade 2” in the phylogenetic analysis (Figure 4).

Quadrupole-time of flight mass spectrometry (QqTOF-MS) allowed annotation of 21 individual metabolites in the total ion current chromatograms (TICs) of *L. littorea* (LL11) and *L. racemosa* (LR15) root extracts (Table 2, Figure 2). The majority of the analytes could be detected in both species, while compound 17 could only be found in *L. littorea*, and constituents 7 and 10 are predominantly occurring in *L. racemosa* (Figure 2). These compounds were successfully cross-annotated in the root extracts obtained from other accessions by ultra-high-performance liquid chromatography – quadrupole mass spectrometry (RP-UHPLC-Q-MS) with detection in UV and visible (UV-VIS) spectra (Table S1, Figure S2).

Table 2. Metabolites annotated in roots of *Lumnitzera littorea* and *L. racemosa* by reversed phase ultra-high-performance chromatography-tandem mass spectrometry (RP-UHPLC-MS/MS). The annotated metabolites are numbered according to peak numbers in Figure 2. Individual tandem mass spectra are shown in Figure S1.

No	t _R (min)	m/z [M - H] ⁻ Observed	m/z [M - H] ⁻ Calculated	Elemental Composition	Fragmentation Patterns	RDB	Error (ppm)	Assignment
1	3.5	305.0702	305.0700	C ₁₂ H ₁₈ SO ₇	96.9596 (54) 79.9566 (22), 96.9592 (53), 130.9649 (9), 165.0506 (100), 168.9878 (77), 201.8320 (8), 219.8438 (8), 243.0313 (7), 245.0478 (53)	4	0.7	unknown
2	3.8	245.0488	245.0489	C ₁₀ H ₁₄ SO ₅		4	-0.4	4-(4-hydroxyphenyl)-2-butanol 2-sulfate
3	3.9	273.0436	273.0438	C ₁₁ H ₁₄ SO ₆	193.0867 (100), 258.0201 (4), 273.0434 (6) ^c	5	0.7	4-(4-sulfoxy-3-methoxy phenyl)-2-butanone (zingeron sulfate)
4	3.9	275.0591	275.0595	C ₁₁ H ₁₆ SO ₈	79.9567 (30), 121.0274 (16), 135.0441 (6), 178.0625 (15), 180.0786 (100), 193.0859 (35), 195.1019 (63), 273.0418 (19), 275.0583 (47), 180.0791 (6), 195.1025 (100), 260.0357 (5), 275.0592 (6) ^c	4	-1.5	unknown(e.g. zingerol sulfate)
5	4.4	499.1267	499.1280	C ₂₂ H ₂₈ SO ₁₁	96.9594 (5), 499.1267	9	-2.6	unknown
6 ^a	4.4	300.9989	300.9990	C ₁₄ H ₆ O ₈	173.0237 (4), 201.0188 (5), 229.0121 (5), 283.9959 (6), 299.9890 (6), 300.9992 (100)	12	0.3	ellagic acid
7 ^b	5.3	394.9707	394.9715	C ₁₅ H ₆ SO ₁₁	299.9906 (41), 315.0141 (100), 394.9662 (4)	12	-2.0	methyl ellagic acid sulfate
8	5.5	487.0179	487.0188	C ₁₈ H ₁₆ SO ₁₄	300.9981 (15), 316.0218 (17), 331.0445 (37), 375.0351 (100)	11	-1.8	unknown ellagic acid derivative
9	5.7	408.9898	408.9871	C ₁₆ H ₁₀ SO ₁₁	298.9820 (11), 314.0063 (40), 329.0256 (100)	12	-6.6	dimethyl ellagic acid sulfate, isomer I
10 ^b	6.0	551.1027	551.1026	C ₂₄ H ₂₄ O ₁₅	312.9971 (4), 328.0211 (14), 343.0452 (100), 491.0806 (2)	13	0.2	unknown trimethyl ellagic acid derivative
11	6.1	369.1221	369.1225	C ₁₄ H ₂₆ SO ₉	96.9593 (17), 177.0397 (18), 256.9953 (14), 369.1211 (100)	2	-1.1	unknown
12	6.3	449.2027	449.2028	C ₂₀ H ₁₄ O ₁₁	81.0338 (8), 83.0500 (57), 127.0395 (23), 233.1026 (100), 343.1388 (9), 361.1494 (6), 449.2016 (64)	4	-0.2	unknown
13	6.4	329.0301	329.0303	C ₂₀ H ₁₀ O ₈	242.9944 (5), 270.9875 (35), 298.9824 (60), 314.0052 (100), 329.0290 (29)	12	-0.6	3,4-O-dimethyl ellagic acid
14	6.5	408.9867	408.9871	C ₁₆ H ₁₀ SO ₁₁	298.9813 (6), 314.0049 (15), 329.0292 (100)	12	1.0	dimethyl ellagic acid sulfate, isomer II
15	6.9	423.0035	423.0028	C ₁₇ H ₁₂ SO ₁₁	297.9752 (5), 312.9987 (42), 328.0223 (100), 343.0480 (100), 423.0026 (5)	12	1.7	3,3',4'-trimethyl ellagic acid 4-sulfate

Table 2. Cont.

No	t_R (min)	m/z [M ⁺ H] Observed	m/z [M ⁺ H] Calculated	Elemental Composition	Fragmentation Patterns	RDB	Error (ppm)	Assignment
16	7.7	343.0455	343.0459	C ₁₇ H ₁₂ O ₈	269.9798 (9), 285.0031 (6), 297.9744 (28), 312.9981 (69), 328.0217 (100), 343.0443 (18)	12	−1.2	3,3',4'-trimethyl ellagic acid
17 ^a	9.8	487.3425	487.3429	C ₃₀ H ₄₈ O ₅	379.3010 (12), 391.3011 (11), 393.3163 (8), 409.3113 (100), 421.3114 (26), 441.3372 (8)	7	−0.8	unknown triterpene acid
18	12.2	265.1476	265.1479	C ₁₂ H ₂₀ SO ₄	79.9562 (12), 96.9596 (100), 98.9556 (9), 134.8930 (5), 166.8646 (4), 185.8829 (5), 201.8339 (6), 203.8311 (4), 265.1468 (95)	0	−1.1	unknown aliphatic sulfate
19	13.4	309.1733	309.1741	C ₁₄ H ₃₀ SO ₅	96.9604 (45), 122.9761 (5), 309.1744 (100) ^c	0	2.6	unknown aliphatic sulfate
20	13.4	311.1685	311.1686	C ₁₇ H ₂₈ SO ₃	183.0113 (28), 311.1677 (100)	4	−0.3	unknown
21	14.6	325.1833	325.1843	C ₁₈ H ₃₀ SO ₃	183.0111 (23), 325.1833 (100)	4	−3.1	unknown

The metabolites were annotated by the exact m/z values and tandem mass spectra (MS/MS) of corresponding [M−H][−] ions in both species or exclusively in *L. littorea*^a (LL11) or *L. racemosa*^b (LR12) by RP-UHPLC, coupled on-line to a quadrupole-time of flight (QqTOF) or hybrid linear ion trap-orbital trap (LIT-Orbitrap)^c mass spectrometer. Elemental compositions and RDB values refer to the non-ionized compounds.

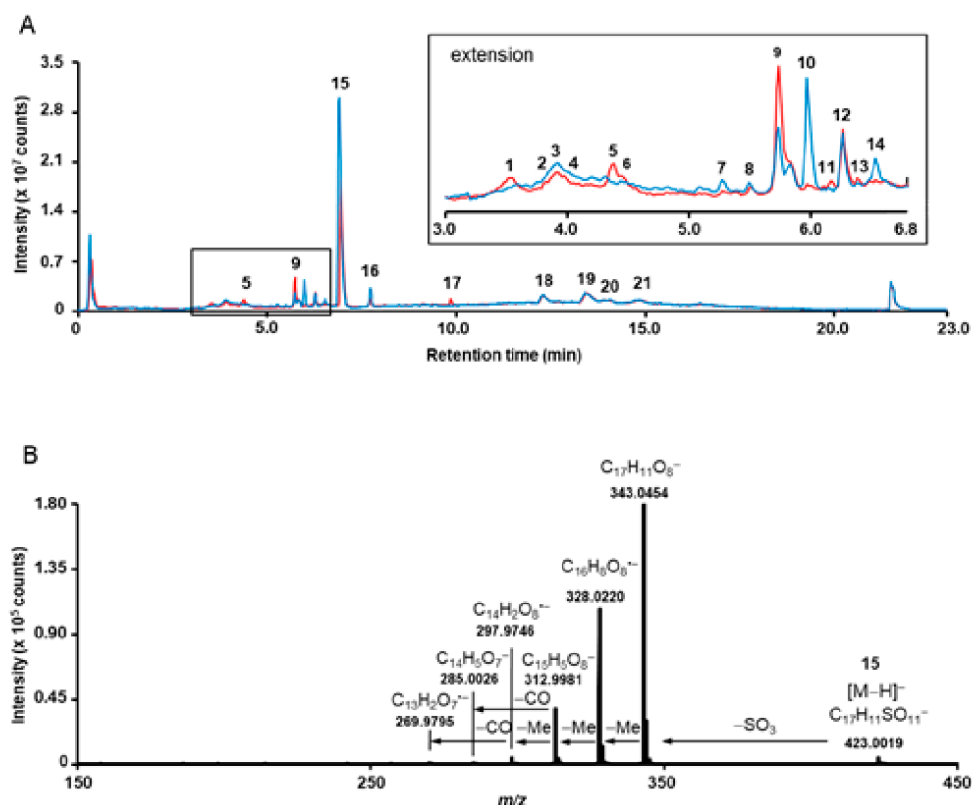


Figure 2. Overlay of the total ion chromatograms (TICs), acquired for the methanolic extracts obtained from *Lumnitzera littorea* (red, LL11) and *L. racemosa* (blue, LR15) roots (A) and tandem mass spectrum, acquired for the m/z 423.0 corresponding to 3,3',4'-tri-*O*-methylellagic acid 4-sulfate (15) (B). The insert in A represent the chromatogram section in the t_R range 3.0–6.8 min. The individual annotated metabolites are numbered with rising retention time according to Table 2.

The major metabolites detected in samples from both species were ellagic acid derivatives (Figures 1–3, Table 2), mostly *O*-methylated at different positions. Commonly, ellagic acid derivatives, including ellagitannins, are widespread in Combretaceae: Ellagic acid and several methylated derivatives were previously detected in leaves and twigs of *L. racemosa* [26,30] and in related species such as, e.g., in *Terminalia* species which are widely used in traditional medicine [53], in *Pteleopsis hylodendron* Mildbr. [54] and in *Combretum alfredii* Hance [55]. In our samples, the broad bands in TLCs along with multiple signals in specific extracted ion chromatograms (XICs) acquired in RP-UHPLC-QqTOF-MS experiments, indicate the presence of several positional isomers, i.e., compounds characterized by the same molecular weight, but featured with different substitution patterns. Such *O*-methylated species can be assigned by characteristic losses of 15 u, accompanying formation of an odd $[M-H-15]^-$ ion [53]. The corresponding signals are characteristic for methyl substitution both in cyclic [56] and aromatic (often in combination with a carbonyl loss) systems [57]. High intensities of such signals in tandem mass spectra of phenolic compounds typically indicate methylation as part of a methoxy group (OCH_3) [58].

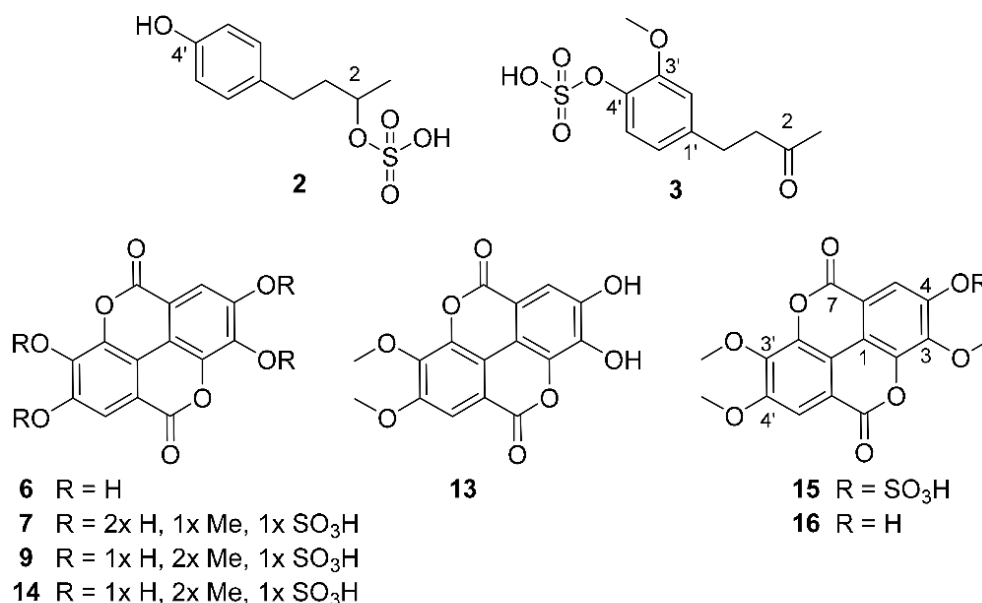


Figure 3. Ellagic acid derivatives and phenylbutanoides detected in root samples from *Lumnitzera littorea* and *L. racemosa*. The location of methyl and sulfate residues in compounds **7**, **9** and **14** is not determined. Compound numbers refer to peak numbers shown in Figure 2/Table 1.

Surprisingly, most of the *O*-methylated ellagic acid derivatives contain a sulfate moiety (Figure 3). This moiety can be easily identified by a characteristic loss of 80 u from the deprotonated ions, corresponding to the cleavage of sulfur trioxide (SO₃) under CID conditions resulting in the formation of characteristic [M–H–SO₃][−] fragments (for example m/z 315.0140 and 329.0296 for **7** and **9**, respectively, Table 2, Supplementary Figure S1). This neutral loss is well-known for sulfated phenolic compounds [59] which not only occur naturally in plants (reviewed by Correia de Silva and co-workers [60]), and marine organism [61,62] but are also quite typical as an important group of polyphenol metabolites dedicated for kidney-clearance from human plasma [63]. In addition to the characteristic loss of 80 u, the tandem mass spectra of sulfated compounds feature diagnostic signals in the low m/z range, which can be attributed to SO₃[−] (m/z 79.9567) and HSO₄[−] (m/z 96.9594) (Table 2 and Supplementary Figure S1). However, to the best of our knowledge, sulfated ellagic acid derivatives were not reported in mangrove species before.

Remarkably, further sulfur containing compounds could be detected (compounds **1–5**, **8**, **11**, **18–21**, Table 1, Figure S1). In compounds **20** and **21** the sulfur appears to be integrated in another form than as sulfate, based on the molecular formula and the MS/MS spectra. However, the exact structures of these compounds could not be assigned based on the acquired SWATH tandem mass spectra. Compounds **8** (m/z 487.0179) and **10** (m/z 551.1027) share common fragments with ellagic acid (**6**) and trimethylellagic acid (**16**), respectively, suggesting a structural relationship. Indeed, the mass difference of 208 u between **10** and **16** is, most likely, due to moieties localized outside the aromatic core. Its elemental composition (C₇H₁₂O₇) might indicate a probable presence of a sugar acid (hexahydroxyheptanoic acid) or a substituted sugar in the structure (Supplementary Figure S1–11).

The most prominent compound **15** present in both species was isolated and identified as 3,3',4'-tri-*O*-methylellagic acid 4-sulfate by 1D and 2D NMR measurements (Table S5) and comparison to published data [64]. Compound **16** (Table S6) was verified as the corresponding 3,3',4'-tri-*O*-methylellagic acid without sulfation [65]. During separation, the sulfation of this compound is reflected in a clear enhancement of polarity visible by lower R_f value on normal phase TLC (Figure 1) and reduced retention time on reversed phase column (Figure 2). 1D and 2D NMR allowed the elucidation of compound **13** as

3,4-di-O-methylellagic acid (Table S4). The substitution pattern was established by HMBC correlations and a ROESY correlation between 4-OMe and H-5. According to its chromatographic behavior compound **9** can be assigned as the derived sulfate. Compound **6** was verified as ellagic acid by ^1H NMR and comparison of MS data to a reference standard. Furthermore, we could obtain several sulfated phenylbutane derivatives including 4-(4-hydroxyphenyl)-2-butanol 2-sulfate (**2**, Table S2) previously isolated from roots of *Rheum maximowiczii* [66]. The downfield shift of H-2 and C-2 compared to the aglycon indicates sulfation at this position. However, due to the low amount of isolated compound we could not determine the configuration at C-2. Compound **3** was identified as the previously undescribed 4-(4-sulfoxy-3-methoxy phenyl)-butan-2-one (zingerone sulfate). NMR data (Table S3) are in good agreement with data published for the basic skeleton 4-(4-hydroxy-3-methoxyphenyl)-butan-2-one [67]. Compound **4** represents according to the MS fragmentation pattern most likely the corresponding zingerol sulfate.

Sulfated phenolics are rare natural products in plants and were not described before for Combretaceae. There are only a few reports about the occurrence of sulfated ellagic acid derivatives in plants, e.g., 3-O-methylellagic acid 4-sulfate and 3,3'-di-O-methylellagic acid 4-sulfate were detected previously in Jaboticaba wood from *Myrciaria cauliflora* (Mart.) O. Berg (Myrtaceae) [68]. The first compound was found to exhibit antioxidant and anti-inflammatory activities in cigarette smoke extract-exposed small airway epithelial cells and may be useful for the treatment of COPD [68]. The major metabolite 3,3',4'-tri-O-methylellagic acid 4-sulfate (**15**) found in this study in most of the *Lumnitzera* samples was reported to occur in rhizomes of *Geum rivale* L. [64] and roots of *Potentilla candidans* Humb. & Bonpl. Ex Nestl. [69], both members of the Rosaceae family.

So far, the biological function of sulfated secondary phenolics in plants is unknown. The presence of a sulfate moiety enhances the water solubility of compounds and increases ion strength in the containing tissue. The accumulation of sulfates may be organ-specific. In case of the investigated *Lumnitzera* species, they are found in the roots, which normally are in contact with sea water, while they were not reported from studies on leaves and twigs [26,29–31]. In this study, both species showed similar patterns of sulfated metabolites despite *L. littorea* is predominantly occurring at well-drained sites with less salinity, and typically growing as a tree, while *L. racemosa* is more resistant to saline conditions and occurs at the margin of bare salt pans [70] often growing as a shrub. It was postulated before that the occurrence of sulfated flavonoids in plants is an ecological trait rather than a systematic feature [64,71] and that these compounds might play a role in adaptation to water-stress in salty soils. Furthermore, natural products with a sulfated scaffold have emerged as antifouling agents with low or nontoxic effects to the environment [72]. Thus, a similar function can be assumed for the detected sulfated compounds in *Lumnitzera* roots.

In general, marine organisms contain a significant number of phenolic metabolites which occur in sulfated form [61,62,73]. Given the high concentration of sulfate in sea water, mangrove soils contain high levels of sulfate and thus, sulfate is easily available for plants. Sulfate-reducing bacteria influence iron, phosphorus and sulfur availability in anoxic mangrove sediments and mangrove species zonation across the intertidal zone [74]. Anaerobic sulfate reducing microbial communities are involved in sulfur cycling in these soils and in the decomposition of mangrove-derived soil organic matter [8,75].

3.2. Phylogenetic Analyses

The variation of the metabolite pattern across different populations could be supported by molecular phylogenetic evidence. As Bayesian and ML analyses yielded topologically identical trees, we here only show the results from the Bayesian analysis (with support values from both; Figure 4).

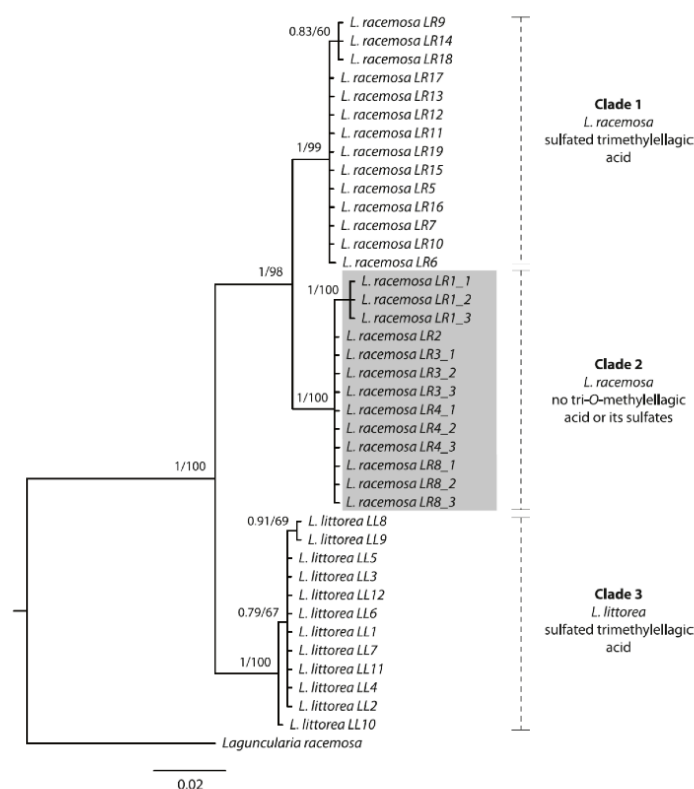


Figure 4. Bayesian majority-rule consensus tree based on the ITS rDNA region of *Lumnitzera littorea* and *L. racemosa* samples collected from various locations in Indonesia. Numbers above branches show Bayesian posterior probability values and corresponding bootstrap support values from the maximum likelihood analysis. Grey: highly supported clade, forming a different chemotype.

Both species form well-supported monophyletic groups. Notably, within *L. racemosa*, samples from populations LR1, LR2, LR3, LR4 and LR8 form a well-supported clade (Clade 2, Figure 4), which is characterized by sharing the same TLC and mass spectrometry metabolic profile, thus suggesting a different chemotype. These samples completely lacked sulfated and nonsulfated trimethylellagic acids, but were dominated by dimethylellagic acid and its sulfate. In contrast, the phylogenetic tree does not show a geographical pattern, at least not on the level where we have appropriate resolution. In order to confirm these results, we sequenced a second individual from each of these specific populations, except for LR2 (for which only one plant had been found at the location). On the one hand, the infraspecific, interpopulational variation in metabolic profiles calls for caution when selecting cultivated mangrove plants for the purpose of metabolic profiling for medicinal purposes (compare to [76]). On the other hand, the nuclear ITS region seems to constitute a useful guide for selecting individuals for cultivation, at least for *Lumnitzera* and some other mangrove plant species (this study, and [76]).

3.3. Evaluation of Anti-Infective Properties

To evaluate the anti-infective potential of the *Lumnitzera* root extracts, the antibacterial and anthelmintic activities were determined using nonpathogenic model organism as test systems. The samples from different locations varied significantly in their antibacterial activities (Figure 5).

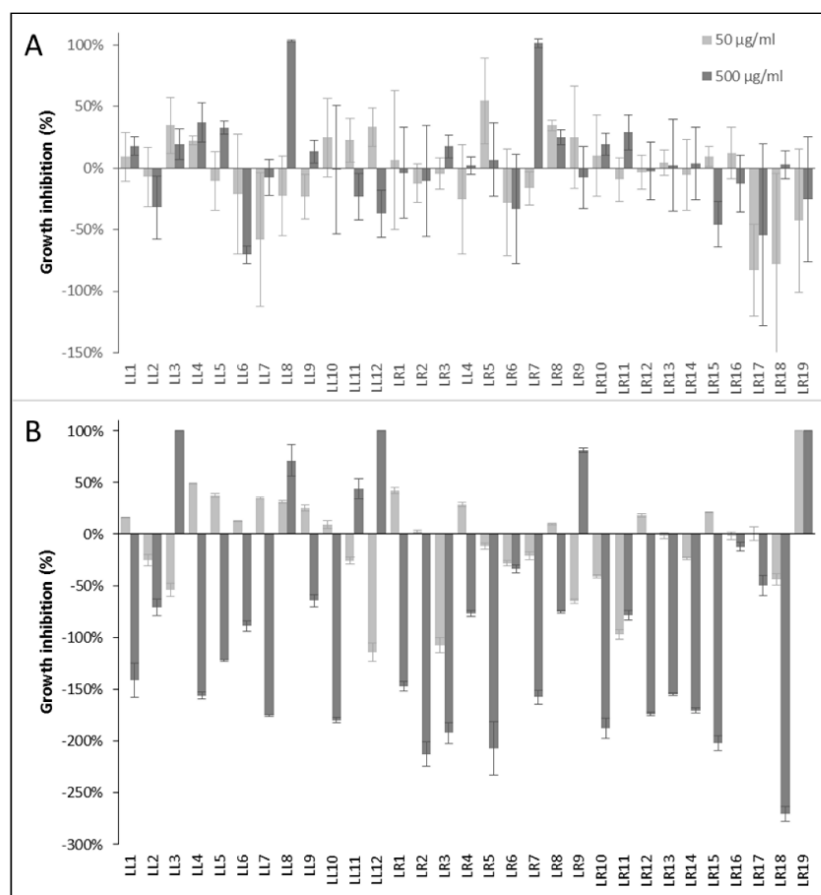


Figure 5. Antibacterial activity of *Lumnitzera littorea* and *L. racemosa* extracts against (A) Gram-positive *Bacillus subtilis* and (B) Gram-negative *Aliivibrio fischeri*. Chloramphenicol (100 µM) was used as positive control and induced the complete inhibition of bacterial growth. Negative values indicate growth enhancement.

Only two extracts (LL8 and LR7) completely inhibited the growth of the Gram-positive *Bacillus subtilis* at 500 µg/mL after 16 h (Figure 5A). The activity against Gram-negative bacteria showed a different pattern (Figure 5B). Here, samples LL3, LL12 and LR19 completely inhibited the growth of the test organism *Aliivibrio fischeri* at a concentration of 500 µg/mL after 24 h, LL8 and LR9 induced 71% and 81% inhibition, respectively. Especially the extract LR19 exhibited a noteworthy antibacterial potential against the Gram-negative test organism since it induced 100% growth inhibition already at the lower test concentration of 50 µg/mL. At this point, the assignment of the antibacterial properties to a certain (group of) constituents is not possible. The selective antibacterial activity of different accessions of only a few samples of the same plant species suggests, however, that the effects might be connected to associated microorganisms rather than intrinsic plant-produced metabolites.

None of the *Lumnitzera* crude extracts showed anthelmintic activity against the nematode *Caenorhabditis elegans* (Figure S3). This is in contrast to studies on mangrove plant species from other families. For example, anthelmintic activity was found for leaf and stem extracts of *Acanthus ilicifolius* L. (Acanthaceae) [77,78].

Two samples from each species (LL3, LL11, LR5, LR15) were exemplarily tested for their cytotoxic activity against the human prostate cancer cell line PC3 and the colon adenocarcinoma cell line HT-29. The investigated samples did not influence the viability of the cancer cell lines at a concentration of 0.05 µg/mL, however, completely inhibited

the cell growth at a concentration of 50 µg/mL indicating a moderate cytotoxic potential (Figure S4).

Ellagic acid is known to possess a wide range of biological activities based on its antioxidant and chemopreventive potential including antimicrobial, anti-inflammatory, neuroprotective, antihepatotoxic, anticholestatic, antifibrogenic, anticarcinogenic, cytotoxic, and antiviral effects [79,80]. Several of these multiple activities may, however, be related to general tanning properties of polyphenolics, rather than being specific effects [81,82]. Furthermore, ellagic acid and related compounds are potent Aldose reductase inhibitors that could play an important role in the management of diabetic complications [69]. Methylation often reduces these effects whereas the introduction of a sulfate group increases the inhibitory activity [69], but reduces membran permeability. In contrast, the only moderate cytotoxicity of ellagic acid against cancer cell lines is further decreased by the presence of a sulfate moiety [64]. The potassium salts of 3,3'-dimethylellagic acid 4-sulfate and 3,3',4'-trimethylellagic acid 4-sulfate were also found to exhibit moderate antimicrobial potential against Gram-positive *Bacillus subtilis* and *Staphylococcus aureus* with MIC values in the range of 22.5–50.8 µg/mL [83]. These compounds were, however, not effective against Gram-negative *Escherichia coli*. [83].

In our investigations the antibacterial activity is likely not directly connected to the sulfated ellagic acid derivatives or the other sulfated metabolites. These metabolites occur across all samples, but the antibacterial effects are limited to samples from particular locations (Figure 5). Nevertheless, *Lumnitzera* roots are a promising source for pharmacologically interesting sulfated ellagic acid derivatives and further sulfated plant metabolites.

4. Conclusions

In our study, a series of unusual sulfated constituents was characterized in root samples from the mangrove species *Lumnitzera littorea* and *L. racemosa* (Combretaceae). Thus, most of the methylated ellagic acid derivatives isolated from both species possess a sulfate moiety. However, *L. racemosa* samples from North Sumatra (LR1), Aceh (LR2, LR3), East Kalimantan (LR4), and Maluku (LR8), completely lack sulfated and non-sulfated trimethylellagic acid, but instead are dominated by dimethylellagic acid and its sulfate. This phytochemical pattern is corroborated by phylogenetic data, where these specific samples form a well-supported clade in the ITS tree. Interestingly, the occurrence of antimicrobial activity and sulfated ellagic acid derivatives are not connected. Although the ellagic acid derivatives are present within all samples, the antibacterial effects are limited to samples from particular locations in Indonesia, suggesting that other compounds from the plant or root-associated microorganisms might be responsible. The moderate cytotoxic effect, in contrast, can be attributed to the occurrence of the ellagic acid derivatives. In summary, *Lumnitzera* roots represent a potentially promising source for sulfated ellagic acid derivatives and further sulfur containing plant metabolites.

Supplementary Materials: The following are available online at <https://www.mdpi.com/article/10.3390/separations8060082/s1>, Figure S1: MS/MS spectra of compounds 1–21, Figure S2: PDA chromatograms of root extracts from *L. littorea* (LL1–LL12) and *L. racemosa* (LR1–LR19), Figure S3: Anthelmintic activity of root extracts from *Lumnitzera littorea* (LL1–LL12) and *L. racemosa* (LR1–LR19), Figure S4: Cytotoxic activity of root extracts from *L. littorea* (LL3, LL11) and *L. racemosa* (LR5, LR15) against PC3 and HT29 cells, Figure S5: NMR and MS spectra of compound 2, Figure S6: NMR and MS spectra of compound 3, Figure S7: NMR and MS spectra of compound 6, Figure S8: NMR and MS spectra of compound 13, Figure S9: NMR and MS spectra of compound 15, Figure S10: NMR and MS spectra of compound 16, Table S1: Peak areas (TIC) of main compounds detected in root extracts of *L. littorea* (LL1–LL12) and *L. racemosa* (LR1–LR19), Table S2: 2D NMR data of compound 2, Table S3: 2D NMR data of compound 3, Table S4: 2D NMR data of compound 13, Table S5: 2D NMR data of compound 15, Table S6: 2D NMR data of compound 16.

Author Contributions: Conceptualization, J.M., A.N.M.-R. and L.A.W.; methodology, K.F., A.F., A.N.M.-R. and J.S.; validation, K.F., A.F., A.N.M.-R. and J.S.; formal analysis, J.M., K.F., J.K. and J.S.; investigation, J.M. and J.K.; resources, A.N.M.-R.; data curation, K.F., A.N.M.-R. and J.S.; writing—original draft preparation, J.M. and K.F.; writing—review and editing, A.N.M.-R., J.M., J.K., J.S., K.F., A.F., L.A.W. and A.A.; visualization, J.M., K.F., J.K., A.F. and J.S.; supervision, A.N.M.-R., L.A.W., J.S., K.F. and A.A.; project administration, A.N.M.-R. and L.A.W.; funding acquisition, J.M., A.N.M.-R. and L.A.W. All authors have read and agreed to the published version of the manuscript.

Funding: This research was funded by BMBF (grants no. 16GW0120K and 16GW0123 to Alexandra Muellner-Riehl and Ludger Wessjohann) within the frame of the project “Indonesian Plant Biodiversity and Human Health – BIOHEALTH”. Jeprianto Manurung is funded by a PhD grant from the German Academic Exchange Service (DAAD project no. 91653688), hosted by Alexandra Muellner-Riehl. Jan Schnitzler was supported by the German Centre for Integrative Biodiversity Research (iDiv) Halle-Jena-Leipzig funded by the German Research Foundation (DFG—FZT 118). Jonas Kappen and Katrin Franke also received funds within the frame of the project ProCognito by EFRE and the state Saxony-Anhalt (ZS/2018/11/95581).

Institutional Review Board Statement: This work contains no human or animal studies.

Informed Consent Statement: This work contains no human studies. The plant studies were done according to Prior Informed Consent with LIPI as Indonesian representative.

Data Availability Statement: Plant material: Plant material is deposited at LIPI, Bogor, Indonesia. Chemical data: All primary data and reference compounds are stored at the IPB primary data storage for 10+ years, and in the compound depository to the extent available or stable. Pending availability, detailed data can be shared upon request. DNA data: All newly generated ITS sequences for this study have been deposited in GenBank (<https://www.ncbi.nlm.nih.gov/genbank/>) and are available from there.

Acknowledgments: The authors would like to thank Lina Juswara, Hetty I.P. Normakristagaluh, Ruliyana Susanti, and Witjaksono (all Research Center for Biology, Indonesian Institute of Sciences, LIPI) for administrative support regarding material collection; Fajria Novari (Ministry of Environment and Forestry Republic of Indonesia) for help with plant material export permits; and all local forestry officers at the different sampling locations for logistic support. We are grateful to Anke Dettmer, Mthandazo Dube, and Martina Lerbs (all IPB Halle) for the performance of antibacterial, anthelmintic and cytotoxic bioassays, respectively. Thanks to Andrea Porzel and Gudrun Hahn (IPB Halle) for NMR measurements. We acknowledge support from Leipzig University for Open Access Publishing.

Conflicts of Interest: The authors declare no conflict of interest. The funders had no role in the design of the study; in the collection, analyses, or interpretation of data; in the writing of the manuscript, or in the decision to publish the results.

References

1. Kathiresan, K.; Bingham, B.L. Biology of mangroves and mangrove ecosystems. *Adv. Mar. Biol.* **2001**, *40*, 81–251.
2. Noor, Y.R.; Khazali, M.; Suryadiputra, I.N.N. *Panduan Pengenalan Mangrove di Indonesia*; Ditjen PHKA; Wetlands International Indonesia Programme: Bogor, India, 2006; ISBN 9799589908.
3. Giesen, W.; Wulffraat, S.; Zieren, M.; Scholten, L. *Mangrove Guidebook for Southeast Asia*; FAO Regional Office for Asia and the Pacific, Wetlands International: Bangkok, Thailand, 2007; ISBN 974-7946-85-8.
4. Bandaranayake, W.M. Traditional and medicinal uses of mangroves. *Mangroves Salt Marshes* **1998**, *2*, 133–148. [[CrossRef](#)]
5. Kovacs, J.M. Assessing mangrove use at the local scale. *Landsc. Urban Plan.* **1999**, *43*, 201–208. [[CrossRef](#)]
6. Pattanaik, C.; Reddy, C.S.; Dhal, N.K.; Das, R. Utilisation of mangrove forests in Bhitarkanika wildlife sanctuary, Orissa. *Indian J. Tradit. Knowl.* **2008**, *7*, 598–603.
7. Govindasamy, C.; Kannan, R. Pharmacognosy of mangrove plants in the system of unani medicine. *Asian Pac. J. Trop. Dis.* **2012**, *2*, S38–S41. [[CrossRef](#)]
8. Balk, M.; Keuskamp, J.A.; Laanbroek, H.J. Potential for sulfate reduction in mangrove forest soils: Comparison between two dominant species of the Americas. *Front. Microbiol.* **2016**, *7*, 1855. [[CrossRef](#)]
9. Spalding, M.; Blasco, F.; Field, C.D. *World Mangrove Atlas*; International Society for Mangrove Ecosystems: Okinawa, Japan; World Conservation Monitoring Centre: Cambridge, UK; International Tropical Timber Organization: Yokohama, Japan, 1997; ISBN 4906584039.
10. Giri, C.; Ochieng, E.; Tieszen, L.L.; Zhu, Z.; Singh, A.; Loveland, T.; Masek, J.; Duke, N. Status and distribution of mangrove forests of the world using earth observation satellite data. *Glob. Ecol. Biogeogr.* **2011**, *20*, 154–159. [[CrossRef](#)]

11. Fyhrquist, P.; Mwasumbi, L.; Hæggström, C.-A.; Vuorela, H.; Hiltunen, R.; Vuorela, P. Ethnobotanical and antimicrobial investigation on some species of *Terminalia* and *Combretum* (Combretaceae) growing in Tanzania. *J. Ethnopharmacol.* **2002**, *79*, 169–177. [\[CrossRef\]](#)
12. Martini, N.D.; Katerere, D.R.P.; Eloff, J.N. Biological activity of five antibacterial flavonoids from *Combretum erythrophyllum* (Combretaceae). *J. Ethnopharmacol.* **2004**, *93*, 207–212. [\[CrossRef\]](#) [\[PubMed\]](#)
13. Eloff, J.N.; Famakin, J.O.; Katerere, D.R.P. Isolation of an antibacterial stilbene from *Combretum woodii* (Combretaceae) leaves. *Afr. J. Biotechnol.* **2005**, *4*, 1167–1171.
14. Eloff, J.N.; Famakin, J.O.; Katerere, D.R.P. *Combretum woodii* (Combretaceae) leaf extracts have high activity against Gram-negative and Gram-positive bacteria. *Afr. J. Biotechnol.* **2005**, *4*, 1161–1166.
15. Eloff, J.N.; Katerere, D.R.; McGaw, L.J. The biological activity and chemistry of the southern African Combretaceae. *J. Ethnopharmacol.* **2008**, *119*, 686–699. [\[CrossRef\]](#)
16. Aderogba, M.A.; Kgate, D.T.; McGaw, L.J.; Eloff, J.N. Isolation of antioxidant constituents from *Combretum apiculatum* subsp. *apiculatum*. *S. Afr. J. Bot.* **2012**, *79*, 125–131. [\[CrossRef\]](#)
17. Masoko, P.; Eloff, J.N. The diversity of antifungal compounds of six South African *Terminalia* species (Combretaceae) determined by bioautography. *Afr. J. Biotechnol.* **2005**, *4*, 1425–1431.
18. Masoko, P.; Picard, J.; Eloff, J.N. The antifungal activity of twenty-four southern African *Combretum* species (Combretaceae). *S. Afr. J. Bot.* **2007**, *73*, 173–183. [\[CrossRef\]](#)
19. Lin, T.-C.; Hsu, F.-L.; Cheng, J.-T. Antihypertensive Activity of Corilagin and Chebulinic Acid, Tannins from *Lumnitzera racemosa*. *J. Nat. Prod.* **1993**, *56*, 629–632. [\[CrossRef\]](#)
20. Ravikumar, S.; Gnanadesigan, M. Hepatoprotective and antioxidant activity of a mangrove plant *Lumnitzera racemosa*. *Asian Pac. J. Trop. Biomed.* **2011**, *1*, 348–352. [\[CrossRef\]](#)
21. Thao, N.P.; Bui, T.T.L.; Chau, N.D.; Bui, H.T.; Kim, E.J.; Kang, H.K.; Lee, S.H.; Jang, H.D.; Nguyen, T.C.; van Nguyen, T.; et al. In vitro evaluation of the antioxidant and cytotoxic activities of constituents of the mangrove *Lumnitzera racemosa* Willd. *Arch. Pharm. Res.* **2015**, *38*, 446–455. [\[CrossRef\]](#)
22. Darwish, A.G.G.; Samy, M.N.; Sugimoto, S.; Abdel-Salam, H.; Matsunami, K. Effects of Hepatoprotective compounds from the leaves of *Lumnitzera racemosa* on acetaminophen-induced liver damage in vitro. *Chem. Pharm. Bull.* **2016**, *64*, 360–365. [\[CrossRef\]](#) [\[PubMed\]](#)
23. Paul, T.; Ramasubbu, S. The antioxidant, anticancer and anticoagulant activities of *Acanthus ilicifolius* L. roots and *Lumnitzera racemosa* Willd. leaves, from southeast coast of India. *J. Appl. Pharm. Sci.* **2017**, *7*, 081–087. [\[CrossRef\]](#)
24. D'Souza, L.; Wahidulla, S.; Devi, P. Antibacterial phenolics from the mangrove *Lumnitzera racemosa*. *Indian J. Mar. Sci.* **2010**, *39*, 294–298.
25. Abeysinghe, P.D. Antibacterial activity of aqueous and ethanol extracts of mangrove species collected from Southern Sri Lanka. *Asian J. Pharm. Biol. Res.* **2012**, *2*, 79–83.
26. Yu, S.-Y.; Wang, S.-W.; Hwang, T.-L.; Wei, B.-L.; Su, C.-J.; Chang, F.-R.; Cheng, Y.-B. Components from the leaves and twigs of mangrove *Lumnitzera racemosa* with anti-angiogenic and anti-inflammatory effects. *Mar. Drugs* **2018**, *16*, 404. [\[CrossRef\]](#)
27. Eswaraiah, G.; Peele, K.A.; Krupanidhi, S.; Indira, M.; Kumar, R.B.; Venkateswarulu, T.C. GC–MS analysis for compound identification in leaf extract of *Lumnitzera racemosa* and evaluation of its in vitro anticancer effect against MCF7 and HeLa cell lines. *J. King Saud Univ. Sci.* **2020**, *32*, 780–783. [\[CrossRef\]](#)
28. Gosh, M.S.; Gouri, P. Chemical investigation of some mangrove species: Part VIII. *Lumnitzera racemosa*. *J. Indian Chem. Soc.* **1980**, *57*, 568–570.
29. Saad, S.; Taher, M.; Susanti, D.; Qaralleh, H.; Rahim, N.A.B.A. Antimicrobial activity of mangrove plant (*Lumnitzera littorea*). *Asian Pac. J. Trop. Biomed.* **2011**, *4*, 523–525. [\[CrossRef\]](#)
30. Le Nguyen, T.T.; Pham, T.T.; Hansen, P.E.; Nguyen, P.K.P. In vitro α -glucosidase inhibitory activity of compounds isolated from mangrove *Lumnitzera littorea* leaves. *Sci. Technol. Dev. J.* **2019**, *22*. [\[CrossRef\]](#)
31. Wongsomboon, P.; Maneerat, W.; Pyne, S.G.; Vittaya, L.; Limtharakul, T.R. 12-Hydroxycorniculatolide a from the mangrove tree, *Lumnitzera littorea*. *Nat. Prod. Commun.* **2018**, *13*, 1327–1328. [\[CrossRef\]](#)
32. Debbab, A.; Aly, A.H.; Proksch, P. Mangrove derived fungal endophytes—A chemical and biological perception. *Fungal Divers.* **2013**, *61*, 1–27. [\[CrossRef\]](#)
33. Ancheeva, E.; Daletos, G.; Proksch, P. Lead compounds from mangrove-associated microorganisms. *Mar. Drugs* **2018**, *16*, 319. [\[CrossRef\]](#)
34. Deng, Q.; Li, G.; Sun, M.; Yang, X.; Xu, J. A new antimicrobial sesquiterpene isolated from endophytic fungus *Cytospora* sp. from the Chinese mangrove plant *Ceriops tagal*. *Nat. Prod. Res.* **2018**, 555–564. [\[CrossRef\]](#) [\[PubMed\]](#)
35. Chaeprasert, S.; Piapukiew, J.; Whalley, A.J.; Sihanonth, P. Endophytic fungi from mangrove plant species of Thailand: Their antimicrobial and anticancer potentials. *Bot. Mar.* **2010**, *53*, 9. [\[CrossRef\]](#)
36. Raab, A.; Feldmann, J. Biological sulphur-containing compounds—Analytical challenges. *Anal. Chim. Acta* **2019**, *1079*, 20–29. [\[CrossRef\]](#)
37. Saslis-Lagoudakis, C.H.; Savolainen, V.; Williamson, E.M.; Forest, F.; Wagstaff, S.J.; Baral, S.R.; Watson, M.F.; Pendry, C.A.; Hawkins, J.A. Phylogenies reveal predictive power of traditional medicine in bioprospecting. *Proc. Natl. Acad. Sci. USA* **2012**, *109*, 15835–15840. [\[CrossRef\]](#)

38. Holzmeyer, L.; Hartig, A.-K.; Franke, K.; Brandt, W.; Muellner-Riehl, A.N.; Wessjohann, L.A.; Schnitzler, J. Evaluation of plant sources for anti-infective lead compound discovery by correlating phylogenetic, spatial, and bioactivity data. *Proc. Natl. Acad. Sci. USA* **2020**, *117*, 12444–12451. [\[CrossRef\]](#)
39. Leonhardt, S.D.; Rasmussen, C.; Schmitt, T. Genes versus environment: Geography and phylogenetic relationships shape the chemical profiles of stingless bees on a global scale. *Proc. Biol. Sci.* **2013**, *280*, 20130680. [\[CrossRef\]](#)
40. Schmitt, I.; Barker, F.K. Phylogenetic methods in natural product research. *Nat. Prod. Rep.* **2009**, *26*, 1585–1602. [\[CrossRef\]](#)
41. Adamek, M.; Alanjary, M.; Ziemert, N. Applied evolution: Phylogeny-based approaches in natural products research. *Nat. Prod. Rep.* **2019**, *36*, 1295–1312. [\[CrossRef\]](#)
42. Mawalagedera, S.M.U.P.; Callahan, D.L.; Gaskett, A.C.; Rønsted, N.; Symonds, M.R.E. Combining evolutionary inference and metabolomics to identify plants with medicinal potential. *Front. Ecol. Evol.* **2019**, *7*, 471. [\[CrossRef\]](#)
43. Abdelmohsen, U.R.; Pimentel-Elardo, S.M.; Hanora, A.; Radwan, M.; Abou-El-Ela, S.H.; Ahmed, S.; Hentschel, U. Isolation, phylogenetic analysis and anti-infective activity screening of marine sponge-associated actinomycetes. *Mar. Drugs* **2010**, *8*, 399–412. [\[CrossRef\]](#)
44. Prasad, M.A.; Zolnik, C.P.; Molina, J. Leveraging phytochemicals: The plant phylogeny predicts sources of novel antibacterial compounds. *Future Sci. OA* **2019**, *5*, FSO407. [\[CrossRef\]](#)
45. Grudinski, M.; Pannell, C.M.; Chase, M.W.; Ahmad, J.A.; Muellner-Riehl, A.N. An evaluation of taxonomic concepts of the widespread plant genus *Aglaia* and its allies across Wallace's Line (tribe Aglaieae, Meliaceae). *Mol. Phylogenet. Evol.* **2014**, *73*, 65–76. [\[CrossRef\]](#) [\[PubMed\]](#)
46. Kearse, M.; Moir, R.; Wilson, A.; Stones-Havas, S.; Cheung, M.; Sturrock, S.; Buxton, S.; Cooper, A.; Markowitz, S.; Duran, C.; et al. Geneious Basic: An integrated and extendable desktop software platform for the organization and analysis of sequence data. *Bioinformatics* **2012**, *28*, 1647–1649. [\[CrossRef\]](#)
47. Silvestro, D.; Michalak, I. raxmlGUI: A graphical front-end for RAxML. *Org. Divers. Evol.* **2012**, *12*, 335–337. [\[CrossRef\]](#)
48. Stamatakis, A. RAxML version 8: A tool for phylogenetic analysis and post-analysis of large phylogenies. *Bioinformatics* **2014**, *30*, 1312–1313. [\[CrossRef\]](#) [\[PubMed\]](#)
49. Ronquist, F.; Teslenko, M.; van der Mark, P.; Ayres, D.L.; Darling, A.; Höhna, S.; Larget, B.; Liu, L.; Suchard, M.A.; Huelsenbeck, J.P. MrBayes 3.2: Efficient Bayesian phylogenetic inference and model choice across a large model space. *Syst. Biol.* **2012**, *61*, 539–542. [\[CrossRef\]](#)
50. Rambaut, A.; Drummond, A.J.; Xie, D.; Baele, G.; Suchard, M.A. Posterior summarization in Bayesian phylogenetics using tracer 1.7. *Syst. Biol.* **2018**, *67*, 901–904. [\[CrossRef\]](#)
51. Dos Santos, C.H.C.; de Carvalho, M.G.; Franke, K.; Wessjohann, L. Dammarane-type triterpenoids from the stem of *Ziziphus glaziovii* Warm. (Rhamnaceae). *Phytochemistry* **2019**, *162*, 250–259. [\[CrossRef\]](#) [\[PubMed\]](#)
52. Thomsen, H.; Reider, K.; Franke, K.; Wessjohann, L.A.; Keiser, J.; Dagne, E.; Arnold, N. Characterization of constituents and anthelmintic properties of *Hagenia abyssinica*. *Sci. Pharm.* **2012**, *80*, 433–446. [\[CrossRef\]](#)
53. Singh, A.; Bajpai, V.; Kumar, K.; Sharma, K.; Kumar, B. Profiling of gallic and ellagic acid derivatives in different plant parts of *Terminalia Arjuna* by HPLC-ESI-QTOF-MS/MS. *Nat. Prod. Comm.* **2016**, *11*, 239–244. [\[CrossRef\]](#)
54. Atta-Ur-Rahman; Ngounou, F.N.; Choudhary, M.I.; Malik, S.; Makhmoor, T.; Nur-E-Alam, M.; Zareen, S.; Lontsi, D.; Ayafor, J.F.; Sondengam, B.L. New antioxidant and antimicrobial ellagic acid derivatives from *Pteleopsis hylocladron*. *Planta Med.* **2001**, *67*, 335–339. [\[CrossRef\]](#)
55. Bai, M.; Wu, L.-J.; Cai, Y.; Wu, S.-Y.; Song, X.-P.; Chen, G.-Y.; Zheng, C.-J.; Han, C.-R. One new lignan derivative from the *Combretum alfredii* Hance. *Nat. Prod. Res.* **2017**, *31*, 1022–1027. [\[CrossRef\]](#) [\[PubMed\]](#)
56. Bathe, U.; Frolov, A.; Porzel, A.; Tissier, A. CYP76 oxidation network of abietane diterpenes in Lamiaceae reconstituted in yeast. *J. Agric. Food Chem.* **2019**, *67*, 13437–13450. [\[CrossRef\]](#)
57. Song, R.; Lin, H.; Zhang, Z.; Li, Z.; Xu, L.; Dong, H.; Tian, Y. Profiling the metabolic differences of anthraquinone derivatives using liquid chromatography/tandem mass spectrometry with data-dependent acquisition. *Rapid Commun. Mass Spectrom.* **2009**, *23*, 537–547. [\[CrossRef\]](#) [\[PubMed\]](#)
58. Frolov, A.; Henning, A.; Böttcher, C.; Tissier, A.; Strack, D. An UPLC-MS/MS method for the simultaneous identification and quantitation of cell wall phenolics in *Brassica napus* seeds. *J. Agric. Food Chem.* **2013**, *61*, 1219–1227. [\[CrossRef\]](#)
59. Geng, C.-A.; Chen, H.; Chen, X.-L.; Zhang, X.-M.; Lei, L.-G.; Chen, J.-J. Rapid characterization of chemical constituents in *Saniculiphyllum guangxiense* by ultra fast liquid chromatography with diode array detection and electrospray ionization tandem mass spectrometry. *Int. J. Mass Spectrom.* **2014**, *361*, 9–22. [\[CrossRef\]](#)
60. Correia-da-Silva, M.; Sousa, E.; Pinto, M.M.M. Emerging sulfated flavonoids and other polyphenols as drugs: Nature as an inspiration. *Med. Res. Rev.* **2014**, *34*, 223–279. [\[CrossRef\]](#)
61. Subhashini, P.; Dilipan, E.; Thangaradjou, T.; Papenbrock, J. Bioactive natural products from marine angiosperms: Abundance and functions. *Nat. Prod. Bioprospect.* **2013**, *3*, 129–136. [\[CrossRef\]](#)
62. Kurth, C.; Welling, M.; Pohnert, G. Sulfated phenolic acids from *Dasycladales* siphonous green algae. *Phytochemistry* **2015**, *117*, 417–423. [\[CrossRef\]](#) [\[PubMed\]](#)
63. Mullen, W.; Borges, G.; Lean, M.E.J.; Roberts, S.A.; Crozier, A. Identification of metabolites in human plasma and urine after consumption of a polyphenol-rich juice drink. *J. Agric. Food Chem.* **2010**, *58*, 2586–2595. [\[CrossRef\]](#)

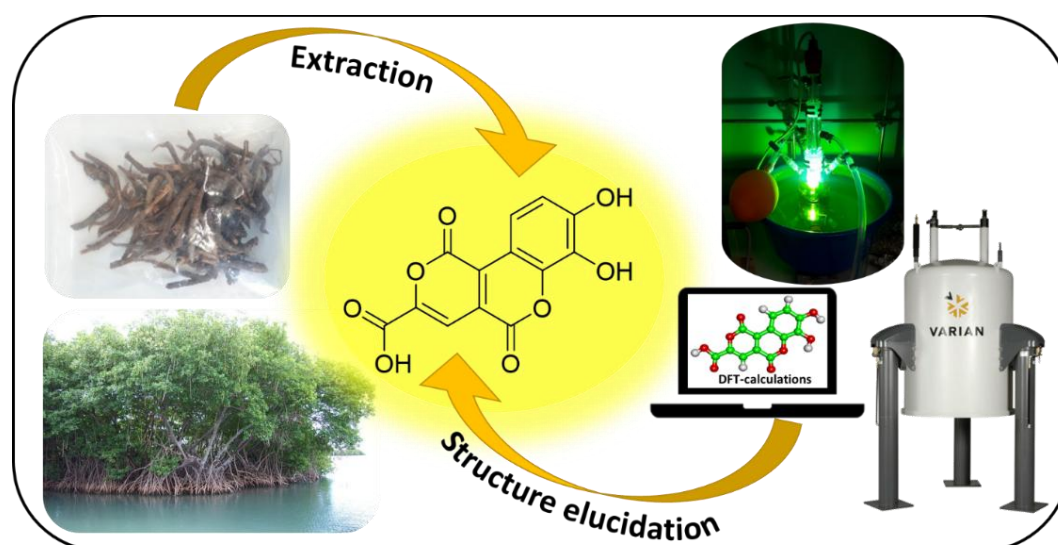
64. Owczarek, A.; Róžalski, M.; Krajewska, U.; Olszewska, M. Rare ellagic acid sulphate derivatives from the rhizome of *Geum rivale* L.—Structure, cytotoxicity, and validated HPLC-PDA Assay. *Appl. Sci.* **2017**, *7*, 400. [\[CrossRef\]](#)
65. Khac, D.D.; Tran-Van, S.; Campos, A.M.; Jean-Yves Lallemand, J.Y.; Fetizon, M. Ellagic compounds from *Diplopanax stachyathus*. *Phytochemistry* **1990**, *29*, 251–256. [\[CrossRef\]](#)
66. Shikishima, Y.; Takaishi, Y.; Honda, G.; Ito, M. Phenylbutanoids and stilbene derivatives of *Rheum maximowiczii*. *Phytochemistry* **2001**, *56*, 377–381. [\[CrossRef\]](#)
67. Pabst, A.; Barron, D.; Adda, J.; Schreier, P. Phenylbutan-2-one β -d-glucosides from raspberry fruit. *Phytochemistry* **1990**, *29*, 3853–3858. [\[CrossRef\]](#)
68. Zhao, D.-K.; Shi, Y.-N.; Petrova, V.; Yue, G.G.L.; Negrin, A.; Wu, S.-B.; D'Armiento, J.M.; Lau, C.B.S.; Kennelly, E.J. Jaboticabin and related polyphenols from Jaboticaba (*Myrciaria cauliflora*) with anti-inflammatory activity for Chronic Obstructive Pulmonary Disease. *J. Agric. Food Chem.* **2019**, *67*, 1513–1520. [\[CrossRef\]](#) [\[PubMed\]](#)
69. Terashima, S.; Shimizu, M.; Nakayama, H.; Ishikura, M.; Ueda, Y.; Imai, K.; Suzui, A.; Morita, N. Terashima et al 1990: Studies on aldose reductase Inhibitors from Medicinal plant of "Sinfito" *Potentilla candicans*, and further synthesis of their related compounds. *Chem. Pharm. Bull.* **1990**, *38*, 2733–2736. [\[CrossRef\]](#)
70. Tomlinson, P.B.; Bunt, J.S.; Primack, R.B.; Duke, N.C. *Lumnitzera rosea* (Combretaceae)—Its status and floral morphology. *J. Arnold Arbor.* **1978**, *59*, 342–351.
71. Harborne, J.B. Flavonoid sulphates: A new class of sulphur compounds in higher plants. *Phytochemistry* **1975**, *14*, 1147–1155. [\[CrossRef\]](#)
72. Almeida, J.R.; Correia-da-Silva, M.; Sousa, E.; Antunes, J.; Pinto, M.; Vasconcelos, V.; Cunha, I. Antifouling potential of nature-inspired sulfated compounds. *Sci. Rep.* **2017**, *7*, 42424. [\[CrossRef\]](#)
73. Filho, L.C.K.; Picão, B.W.; Silva, M.L.A.; Cunha, W.R.; Pauletti, P.M.; Dias, G.M.; Copp, B.R.; Bertanha, C.S.; Januario, A.H. Bioactive aliphatic sulfates from marine invertebrates. *Mar. Drugs* **2019**, *17*, 527. [\[CrossRef\]](#)
74. Sherman, R.E.; Fahey, T.J.; Howarth, R.W. Soil-plant interactions in a neotropical mangrove forest: Iron, phosphorus and sulfur dynamics. *Oecologia* **1998**, *115*, 553–563. [\[CrossRef\]](#) [\[PubMed\]](#)
75. Kristensen, E.; Holmer, M.; Bussarawit, N. Benthic metabolism and sulfate reduction in a Southeast Asian mangrove swamp. *Mar. Ecol. Prog. Ser.* **1991**, *73*, 93–103. [\[CrossRef\]](#)
76. Glasenapp, Y.; Korth, I.; Nguyen, X.-V.; Papenbrock, J. Sustainable use of mangroves as sources of valuable medicinal compounds: Species identification, propagation and secondary metabolite composition. *S. Afr. J. Bot.* **2019**, *121*, 317–328. [\[CrossRef\]](#)
77. Husori, D.I.; Sumardi, H.T.; Gemasih, S.; Ningsih, S.R. In vitro anthelmintic activity of *Acanthus ilicifolius* leaves extracts on *Ascaridia galli* and *Pheretima posthuma*. *J. Appl. Pharm. Sci.* **2018**, *8*, 164–167. [\[CrossRef\]](#)
78. Sardar, P.K.; Dev, S.; Al Bari, M.A.; Paul, S.; Yeasmin, M.S.; Das, A.K.; Biswas, N.N. Antiallergic, anthelmintic and cytotoxic potentials of dried aerial parts of *Acanthus ilicifolius* L. *Clin. Phytosci.* **2018**, *4*, 894. [\[CrossRef\]](#)
79. Vattem, D.A.; Shetty, K. Biological functionality of ellagic acid: A review. *J. Food Biochem.* **2005**, *29*, 234–266. [\[CrossRef\]](#)
80. García-Niño, W.R.; Zazueta, C. Ellagic acid: Pharmacological activities and molecular mechanisms involved in liver protection. *Pharmacol. Res.* **2015**, *97*, 84–103. [\[CrossRef\]](#)
81. Zhu, M.; Phillipson, J.D.; Greengrass, P.M.; Bowery, N.E.; Cai, Y. Plant Polyphenols: Biologically active compounds or non-selective binder protein? *Phytochemistry* **1997**, *44*, 441–447. [\[CrossRef\]](#)
82. Michels, K.; Heinke, R.; Schöne, P.; Kuipers, O.P.; Arnold, N.; Wessjohann, L.A. A fluorescence-based bioassay for antibacterials and its application in screening natural product extracts. *J. Antibiot.* **2015**, *68*, 734–740. [\[CrossRef\]](#) [\[PubMed\]](#)
83. Zhang, W.-K.; Xu, J.-K.; Zhang, X.-Q.; Yao, X.-S.; Ye, W.-C. Chemical constituents with antibacterial activity from *Euphorbia sororia*. *Nat. Prod. Res.* **2008**, *22*, 353–359. [\[CrossRef\]](#)

3 Challenging Structure Elucidation of Lumnitzerallactone, an Ellagic Acid Derivative from the Mangrove *Lumnitzera racemosa*

Jonas Kappen, Jeprianto Manurung, Tristan Fuchs, Sahithya Phani Babu Vemulapalli, Lea M. Schmitz, Andrej Frolov, Andria Agusta, Alexandra N. Muellner-Riehl, Christian Griesinger, Katrin Franke, and Ludger A. Wessjohann

Marine Drugs **2023**, *21*, 242; <https://doi.org/10.3390/md21040242>

Graphical abstract



Abstract

The previously undescribed natural product lumnitzerallactone (**1**), which represents a derivative of ellagic acid, was isolated from the anti-bacterial extract of the Indonesian mangrove species *Lumnitzera racemosa* Willd. The structure of lumnitzerallactone (**1**), a proton-deficient and highly challenging condensed aromatic ring system, was unambiguously elucidated by extensive spectroscopic analyses involving high-resolution mass spectrometry (HRMS), 1D ^1H and ^{13}C nuclear magnetic resonance spectroscopy (NMR), and 2D NMR (including 1,1-ADEQUATE and 1,n-ADEQUATE). Determination of the structure was supported by computer-assisted structure elucidation (CASE system applying ACD-SE), density functional theory (DFT) calculations, and a two-step chemical synthesis. Possible biosynthetic pathways involving mangrove-associated fungi have been suggested.

Keywords








Lumnitzera racemosa; lumnitzerallactone; isolation; synthesis; structure elucidation; ellagic acid; anti-bacterial; NMR; ^{13}C - ^1H ADEQUATE

MDPI statement concerning permissions

No special permission is required to reuse all or part of an article published by MDPI, including figures and tables. For articles published under an open access Creative Common CC BY license, any part of the article may be reused without permission provided that the original article is clearly cited. Reuse of an article does not imply endorsement by the authors or MDPI. Furthermore, no special permission is required for authors to submit their work to external repositories. This policy extends to all versions of a paper: submitted, accepted, and published.

Article

Challenging Structure Elucidation of Lumnitzerallactone, an Ellagic Acid Derivative from the Mangrove *Lumnitzera racemosa*

Jonas Kappen ¹, Jeprianto Manurung ^{1,2,3} , Tristan Fuchs ¹, Sahithya Phani Babu Vemulapalli ^{4,5}, Lea M. Schmitz ¹ , Andrej Frolov ¹, Andria Augusta ⁶ , Alexandra N. Muellner-Riehl ^{2,3} , Christian Griesinger ^{4,*} , Katrin Franke ^{1,3,7,*}  and Ludger A. Wessjohann ^{1,3,*} 

- ¹ Department of Bioorganic Chemistry, Leibniz Institute of Plant Biochemistry (IPB), Weinberg 3, 06120 Halle (Saale), Germany; jkappen@ipb-halle.de (J.K.); jeprianto_m@apps.ipb.ac.id (J.M.); tfuchs@ipb-halle.de (T.F.); lschmitz@ipb-halle.de (L.M.S.); andrej.frolov@ipb-halle.de (A.F.)
- ² Department of Molecular Evolution and Plant Systematics & Herbarium (LZ), Institute of Biology, Leipzig University, Johannisallee 21-23, 04103 Leipzig, Germany; muellner-riehl@uni-leipzig.de
- ³ German Centre for Integrative Biodiversity Research (iDiv) Halle-Jena-Leipzig, Puschstraße 4, 04103 Leipzig, Germany
- ⁴ Department of NMR-Based Structural Biology, Max Planck Institute for Multidisciplinary Sciences, Am Fassberg 11, 37077 Göttingen, Germany; save@mpinat.mpg.de
- ⁵ Research Group for Marine Geochemistry, Institute for Chemistry and Biology of the Marine Environment (ICBM), Carl von Ossietzky Universität Oldenburg, Carl-von-Ossietzky-Str. 9-11, 26129 Oldenburg, Germany
- ⁶ Research Center for Pharmaceutical Ingredients and Traditional Medicine, National Research and Innovation Agency (BRIN), Jl. M.H. Thamrin No. 8, Jakarta 10340, Indonesia; andr005@brin.go.id
- ⁷ Institute of Biology/Geobotany and Botanical Garden, Martin Luther University Halle-Wittenberg, 06108 Halle (Saale), Germany
- * Correspondence: cigr@mpinat.mpg.de (C.G.); kfranke@ipb-halle.de (K.F.); wessjohann@ipb-halle.de (L.A.W.); Tel.: +49-551-201-2201 (C.G.); +49-345-5582-1313 (K.F.); +49-345-5582-1300 (L.A.W.)



Citation: Kappen, J.; Manurung, J.; Fuchs, T.; Vemulapalli, S.P.B.; Schmitz, L.M.; Frolov, A.; Augusta, A.; Muellner-Riehl, A.N.; Griesinger, C.; Franke, K.; et al. Challenging Structure Elucidation of Lumnitzerallactone, an Ellagic Acid Derivative from the Mangrove *Lumnitzera racemosa*. *Mar. Drugs* 2023, 21, 242. <https://doi.org/10.3390/md21040242>

Academic Editor: Anake Kijjoa

Received: 16 March 2023

Revised: 11 April 2023

Accepted: 12 April 2023

Published: 14 April 2023



Copyright: © 2023 by the authors. Licensee MDPI, Basel, Switzerland. This article is an open access article distributed under the terms and conditions of the Creative Commons Attribution (CC BY) license (<https://creativecommons.org/licenses/by/4.0/>).

Abstract: The previously undescribed natural product lumnitzerallactone (**1**), which represents a derivative of ellagic acid, was isolated from the anti-bacterial extract of the Indonesian mangrove species *Lumnitzera racemosa* Willd. The structure of lumnitzerallactone (**1**), a proton-deficient and highly challenging condensed aromatic ring system, was unambiguously elucidated by extensive spectroscopic analyses involving high-resolution mass spectrometry (HRMS), 1D ¹H and ¹³C nuclear magnetic resonance spectroscopy (NMR), and 2D NMR (including 1,1-ADEQUATE and 1,n-ADEQUATE). Determination of the structure was supported by computer-assisted structure elucidation (CASE system applying ACD-SE), density functional theory (DFT) calculations, and a two-step chemical synthesis. Possible biosynthetic pathways involving mangrove-associated fungi have been suggested.

Keywords: *Lumnitzera racemosa*; lumnitzerallactone; isolation; synthesis; structure elucidation; ellagic acid; anti-bacterial; NMR; ¹³C-¹H ADEQUATE

1. Introduction

Mangroves are salt-tolerant plants, growing as shrubs or trees along coastlines at tropical and subtropical latitudes [1,2]. Together with associated microbes, fungi, other plants, and animals, they form a mangrove forest community also called mangal [2]. Altogether, about 75 true mangrove species from 11 families are recognized [3–5]. *Lumnitzera racemosa* Willd. belongs to the mostly (sub)tropical family Combretaceae. The species is widely distributed from the shores of East Africa to the Indo-West Pacific [6], as well as in the Malay Archipelago [2]. Its extracts are well known in traditional medicine, being used, among other applications, for the treatment of snake bites, rheumatism, skin allergies, asthma, and diabetes mellitus and as a blood purifier [2,7–10]. The fruits

and juice of young twigs, as well as sap of older bark, are used for treating skin disorders, herpes, pruritus, and thrush arising from fungal infections [6,11–13]. Biological activities of *L. racemosa* extracts and constituents were intensively studied. Antibacterial [6,14–16], anti-coagulant [17], anti-inflammatory [18], anti-cancer [17,19,20], anti-angiogenic [18], anti-oxidative [17,20], hepatoprotective [21,22], anti-hypertensive [23], anti-hyperglycemic [24], and anti-viral effects [16,25–27] have been described so far. The reported major classes of secondary metabolites present in *L. racemosa* extracts comprise tannins [17,20,23], flavonoids [10,17,18,20,22], phenols [17,18,20,21], alkaloids [21], and terpenes [6,17,20,21]. Gallic acid and its derivatives—soluble tannins and related compounds such as ellagic acid (EA) or 3,3',4-tri-*O*-methylellagic acid (TMEA)—were found as one of the possible biologically active classes of compounds [1,6,8,18,22]. These compounds are common for the Combretaceae family in general and for *L. racemosa* in particular. Recently, triterpene acids were identified as anti-bacterial compounds in Combretaceae [28], and their effect against *Staphylococcus aureus* was proposed to be a result of synergism with epicatechin [28]. However, not all bioactive compounds of mangroves originate from the plant itself, with many produced by associated microorganisms [6,29–31], including various fungal endophytes. While the same fungal species have been found on different host plant species, multiple samples of the same mangrove species do not necessarily bear the same microorganisms [32,33]. It is likely that differences in the diversity of associated microorganisms are due to species composition and environmental conditions, such as precipitation, frequency of tidal flooding, salinity, freshwater flow, soil types, and hours of radiation at the place of occurrence, as cases of no strict host specificity are known [32].

Recently, in our comprehensive metabolomics survey, we characterized the patterns of ellagic acid derivatives in the root extracts of *L. racemosa* [8]. In the present study, we report the isolation, structure elucidation, and chemical synthesis of the previously undescribed ellagic acid derivative lumnizeralactone (**1**) from *L. racemosa*. In addition, anti-bacterial activity was studied and putative biosynthetic pathways involving fungal participation are discussed.

2. Results and Discussion

2.1. Isolation and Identification of Compound **1**

During our previous LC-MS investigation of 31 extracts from air-dried root samples of the Indonesian mangroves *L. racemosa* and *L. littorea*, a series of interesting new sulfated natural products as well as unusual EA derivatives were identified and subsequently isolated [8]. The extracts from mangroves from different locations varied significantly in their anti-bacterial activity. Remarkably, only two extracts obtained from locations close to each other (the Maluku islands Ternate and Halmahera) completely inhibited the growth of the Gram-positive bacterium *Bacillus subtilis* when applied at 500 µg/mL [8,34], which could indicate a connection between the locations of the plants and their anti-bacterial activity. This activity correlated with the occurrence of a signal at m/z 289 $[M - H]^-$ (peak 1 in the chromatogram in Figure 1A) in the LC-MS profiles, which could be exclusively observed in the two active extracts. High-resolution mass spectrometry (HRMS) indicated the molecular formula $C_{13}H_6O_8$ for **1**, based on the $[M - H]^-$ ion at m/z 289.0002 calculated for $C_{13}H_5O_8^-$ to be 288.9990 with a mass tolerance of 4.2 ppm (Figure S5). Thus, as can be seen from the mass difference of 12 amu, **1** has one carbon atom less than EA (**2**). This elemental composition corresponds to only one known natural product, phelligridin J (**4**) (3-carboxyl-8,9-dihydroxypyrano[4,3-*c*]isochromen-4-one) (Figure 2), isolated from the Chinese medicinal fungus *Phellinus igniarius* [35]. However, the MS² investigations of **1** revealed a fragmentation behavior similar to **2**, suggesting a close structural relationship between these two compounds (Figure 1B). Indeed, the fragmentation of **1** and **2** followed the pathways characteristic for phenolic compounds, as was recently described by Schmidt [36]. These pathways, accompanied with multiple losses of CO and CO₂ and the formation of odd-electron *O*-centered radical ion intermediates, provide a good explanation for the observed patterns.

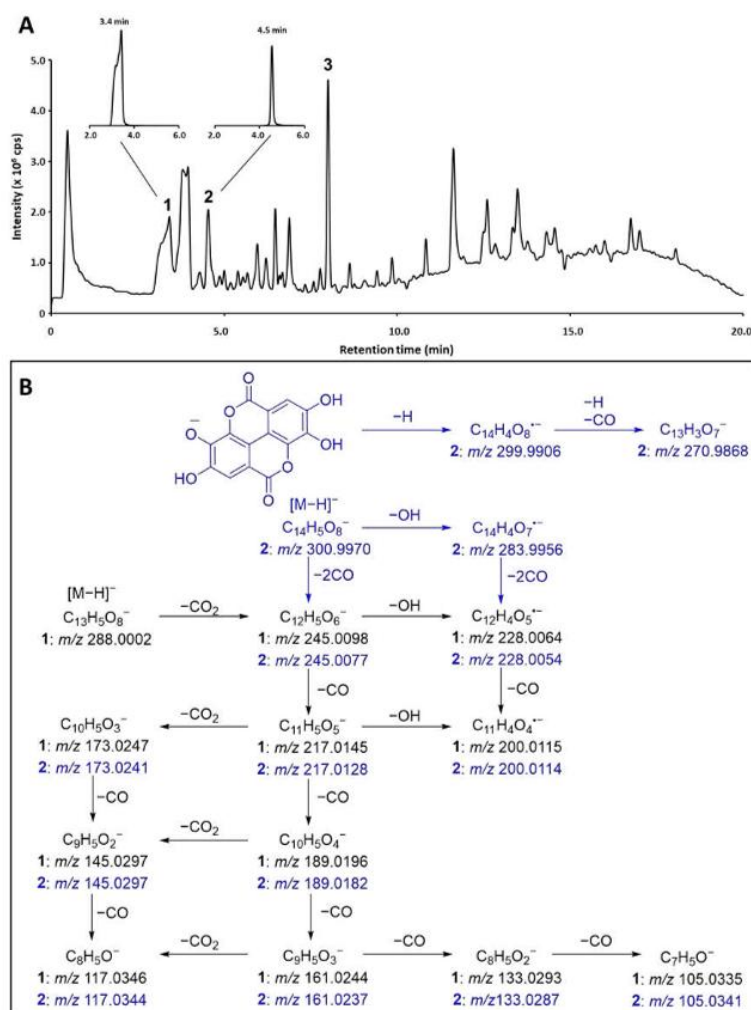


Figure 1. (A) Total ion chromatogram (TIC) acquired for the anti-bacterial *L. racemosa* sample LR7 along with the corresponding extracted ion chromatograms of m/z 289.0 \pm 0.5 (1) and 301.0 \pm 0.5 (2). Peak 3 represents 3,3',4'-tri-*O*-methylellagic acid (3). (B) Suggested tandem mass spectrometric fragmentation (MS/MS) patterns of 1 and 2. Fragments specific for EA are marked blue and fragments common for both compounds are in black.

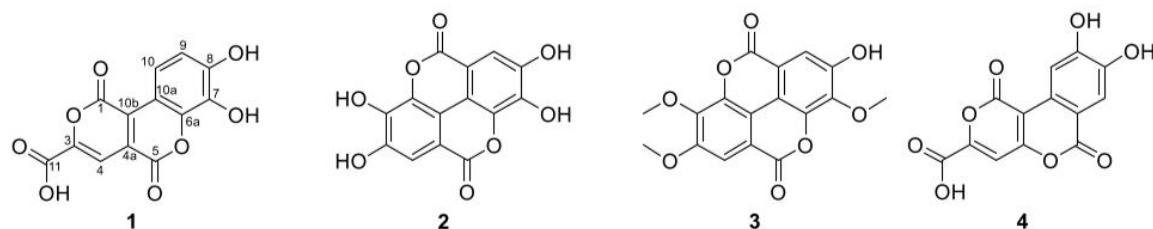


Figure 2. Structures of lumnitzeralactone (1), ellagic acid (EA, 2), 3,3',4'-tri-*O*-methylellagic acid (TMEA, 3), and phelligridin J (4).

EA (2) is a ubiquitous secondary metabolite in plants particularly found in the Combrretaceae family and quite characteristic of the genus *Lumnitzera*. The difference of

12 amu, observed between **1** and **2**, implies the potential occurrence of either a five-membered ring in **1**, instead of a six-membered ring in **2**, or a rearranged structure with the formal elimination of a (quarternary) carbon atom. To allow for unequivocal structure elucidation by NMR data, the compound had to be isolated.

An initial isolation approach under non-acidic conditions yielded 2.5 mg of **1**, which was only slightly soluble in methanol. Although initial preliminary NMR data could be obtained (Table S1), the amount was insufficient for further structure elucidation by 2D NMR. From the small amount of the remaining dried roots (15.06 g), an additional 14.6 mg of **1** was obtained. Acidification of the aqueous phase during liquid–liquid extraction of the crude extract with ethyl acetate allowed for extraction of the yellow-colored compound into the organic phase. Subsequently, **1** was purified by repeated column chromatography on Sephadex LH20 and reversed-phase 2 material (RP2), followed by semi-preparative RP-HPLC.

2.2. Structure Elucidation

Compound **1** was obtained as a yellow amorphous solid. Over time and through repeated dissolving and drying, the substance turned red and became less soluble in methanol. The bathochromic shift was reversible, and the color change could be repeated on a TLC plate (Figure S1). Under NH_3 vapor, the color of the yellow spot of **1** immediately changed to red and then back to bright yellow when treated with HCl vapor. By spraying the plate with a solution of magnesium acetate in methanol, the red color could be fixed due to the formation of the corresponding phenolate ions (Mechanism: Scheme S1) [37]. This effect is known as the Bornträger reaction. The decreased solubility in methanol, also observed during the first extraction under neutral conditions, might result from stable salts formed by the phenolate ions, which strongly enhances the polarity of the molecule. The observed halochromism, namely the color change through salt formation by charge change of a molecule, is a result of an extensive electron delocalization due to the participation of the free electrons of the negative-charged oxygen of the phenolate. This is a strong hint for the presence of phenolic hydroxyl groups in **1**, which was not unexpected for an EA derivative. In agreement with data from the literature [37–39], the presence of a benzene ring, conjugated carbonyl groups, and phenolic hydroxyl groups can be assumed based on the presence of the maxima at 232 (4.10), 290 (3.95), and 407 (3.96) nm in the UV-Vis absorption spectra of **1** (Figure S9-1).

The ^1H NMR spectrum of **1**, recorded in CD_3OD , revealed three proton signals at δ_{H} 6.87 (d, 9 Hz), 7.59 (s), and 8.46 (d, 9 Hz) (Figure S2-1, Table S1-1), two of which (δ_{H} 6.87 and 8.46) are *ortho*-coupled, which was supported by the correlation observed in the COSY and TOCSY spectra (Figures S2-2 and S2-3). This is not compatible with a structure similar to **2**, which would show only two aromatic singlets. Usually, the coupling constant for protons of the benzene ring in the *ortho* position is in the range of 7.6–8.5 Hz [40,41]. Nevertheless, larger coupling constants are known. For example, urolithin M5, a degradation product of **2** detected in extracts from *Elaeocarpus tonkinensis* and also formed in humans after ingestion of **2** [42], showed a coupling constant of 9 Hz, which was the same as what was observed in **1**.

The ^1H NMR spectrum of **1**, recorded in $\text{DMSO}-d_6$ (Table 1, Figure S2-7), shows two additional signals attributable to phenolic hydroxyl protons (δ_{H} 9.56, brs, 10.62, brs). The ^{13}C NMR spectrum of **1**, recorded in $\text{DMSO}-d_6$ (Table 1, Figure S2-8), revealed 13 carbon signals, which is in agreement with the molecular formula. Three carboxyl or lactone carbon signals at δ_{C} 160.0, 158.3, and 158.2 were visible, as well as ten more carbons, seven of which were non-protonated, including two oxygen-bearing carbons at δ_{C} 132.7 and 150.8. The three protonated sp^2 carbons were assigned by HSQC for δ_{C} 113.2, 117.9, and 107.3. Surprisingly, the ^{13}C NMR (CD_3OD) of **1**, isolated under non-acidic conditions, showed only 11 of the expected 13 carbon signals (Figure S2-4, Table S1-2). Nevertheless, the two missing signals (C-3 and C-11) could be determined by HMBC correlations (Figure S2-6).

The higher chemical shift values of these signals indicated the presence of a salt instead of the free acid.

Table 1. ^{13}C (100 MHz) and ^1H NMR (400 MHz) data of **1** and synthesized **1b** and **5**.

Position	Lumnitzeralactone (1)		Synthetic Lumnitzeralactone (1b)		Synthetic Intermediate (5)	
	δ_{C} , Type DMSO- <i>d</i> 6	δ_{H} , m (J in Hz) DMSO- <i>d</i> 6	δ_{C} , Type DMSO- <i>d</i> 6	δ_{H} , m (J in Hz) DMSO- <i>d</i> 6	δ_{C} , Type ^a THF- <i>d</i> 8	δ_{H} , m (J in Hz) ^a THF- <i>d</i> 8
1	158.2, C		158.3, C		158.8, C	
3	145.8, C		146.2, C		147.6, C	
4	107.3, CH	7.49, s	107.2, CH	7.48, s	107.4, CH	7.54, s
4a	125.1, C		125.1, C		124.9, C	
5	158.3, C		158.3, C		158.4, C	
6a	142.8, C		142.8, C		144.2, C	
7	132.7, C		132.7, C		135.2, C	
8	150.8, C		150.7, C		149.5, C	
9	113.2, CH	6.95, d (9.0)	113.2, CH	6.94, d (9.0)	115.9, CH	7.21, s
10	117.9, CH	8.33, d (9.0)	117.8, CH	8.33, d (9.0)	127.4, C	
10a	108.1, C		108.1, C		107.2, C	
10b	127.9, C		127.8, C		130.8, C	
11	160.0, C		160.1, C		160.4, C	
12					167.8, C	
7-OH		9.56, brs		9.56, brs		9.48, brs
8-OH		10.62, brs		10.59, brs		9.34, brs

^a NMR data in accordance with the study conducted by Tokutomi et al. [40].

Based on the acquired data set, it seemed highly probable that the structure of **1** contains three protonated sp² carbons (two of which are *ortho*-coupled aromatic protons), one carboxyl group, and two phenolic hydroxyl groups. Thus, a condensed system of three rings, including two lactones, was most likely, i.e., a structure representing a regioisomer of phelligrudin J (**4**) [35]. Since **1** contains only few protons, COSY and HMBC correlations were not sufficient to elucidate its complete structure.

Derivatization of the molecule to incorporate additional protons (e.g., by methylation of the hydroxyl groups and formation of a methyl ester of the carboxyl group) was not performed to avoid wasting the compound without obtaining decisive information. Consequently, non-destructive methods were preferred. All attempts for crystallization, as described for molecules with related structural elements [40,42,43], did not lead to crystals suitable for X-ray analysis. Thus, further elucidation strategies relied on more unusual 2D NMR experiments, such as ^{13}C - ^{13}C -INADEQUATE, 1,1-ADEQUATE, and 1,n-ADEQUATE, that require very high-field NMR instruments. ^{13}C - ^{13}C -INADEQUATE provides correlations for each carbon atom with the adjacent carbon atoms through $^1\text{J}_{\text{CC}}$ coupling. For molecules with a natural ^{13}C abundance, the sensitivity of this 2D NMR experiment is very low due to the ^{13}C - ^{13}C spin coupling ratio of just 0.012%. Therefore, a high sample concentration or ^{13}C enrichment is recommended [44]. Because these requirements could not be met, ^{13}C - ^{13}C -INADEQUATE experiments with a measurement time of 3 days did not provide a spectrum that showed visible correlations. Therefore, the 1,1-ADEQUATE experiment was performed, which shows pseudo $^2\text{J}_{\text{CH}}$ correlations which can be used to assign the neighboring carbon atoms of proton-bearing carbons in the carbon skeleton [45]. The 1,1-ADEQUATE correlations from H-9 to C-8 and C-10 and from H-10 to C-9 and C-10a allowed for the assignment of C-8 at δ_{C} 150.8 and the aromatic carbon C-10a (δ_{C} 108.1) (Figure S2-12). Correlations from H-4 lead to the assignment of the neighboring carbons C-4a (δ_{C} 125.1) and C-3 (δ_{C} 145.8) (Figure 3).

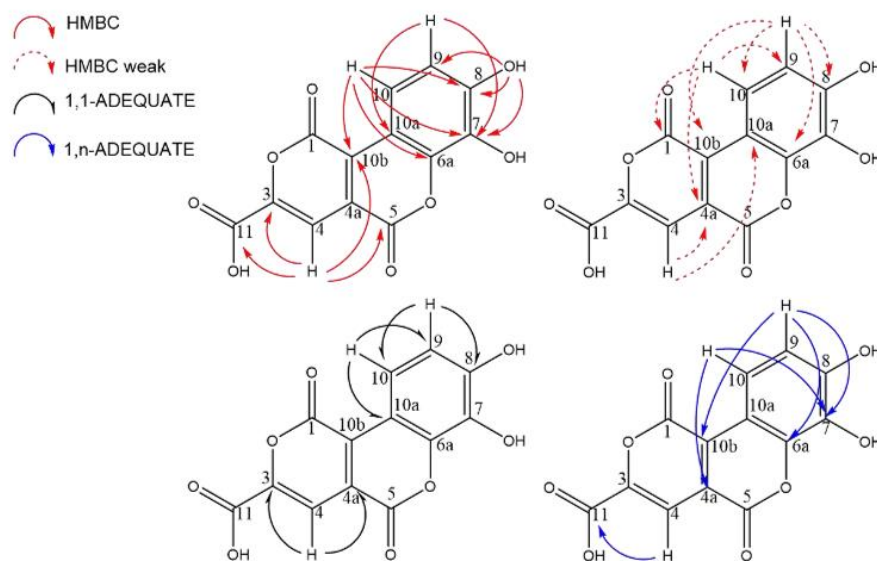


Figure 3. Crucial 2D HMBC (red: due to a large number of correlations, they are shown on two formulae), 1,1 ADEQUATE (black), and 1,n-ADEQUATE (blue) NMR correlations for lumnizeralactone (1).

The 1,n-ADEQUATE experiment provides information about the long-range carbon–carbon connectivity under natural abundance conditions [46], primarily via pseudo $^4J_{CH}$ ($^1J_{CH} + ^3J_{CC}$) correlations and occasional observations of $^3J_{CH}$ ($^1J_{CH} + ^2J_{CC}$) correlations [47,48]. Compared to the usual INADEQUATE experiment, sensitivity can be increased up to a factor of 64, making this approach applicable to smaller amounts of sample material [49]. In addition to the most common $^3J_{CC}$ and occasional $^2J_{CC}$ correlations, 2D 1,n-ADEQUATE also displays $^1J_{CC}$ correlations [48,50] similar to those observed in the 1,1-ADEQUATE spectrum. The inversion of $^1J_{CC}$ correlations [48,50] that leak into the 1,n-ADEQUATE spectrum would facilitate unambiguous discrimination between $^1J_{CC}$ correlations (blue contours, Figure S2-11) and $^nJ_{CC}$ correlations (red contours, Figure S2-11). Thus, 1,n-ADEQUATE can be used to obtain both $^1J_{CC}$ and $^nJ_{CC}$ correlations in a single experiment. However, it should be noted that 1,n-ADEQUATE is less sensitive compared to 1,1-ADEQUATE.

The combined evaluation of HMBC $^3J_{CH}$ and long-range 1,n-ADEQUATE $^4J_{CH}$ correlations from H-9 and H-10 to C-6a (δ_C 142.8) and C-7 (δ_C 132.7) leads to their assignment (Figures 3 and S2-11). C-10b is a special case because this carbon exhibited HMBC correlations to all three protons (H-4, H-9, and H-10). H-10 and H-4 both show strong HMBC correlations to C-10b, indicating $^3J_{CH}$ correlations. Although H-9 only shows a weak HMBC correlation to C-10b, the observed 1,n-ADEQUATE correlation suggested its $^4J_{CH}$ coupling. The assignment of the three COOR carbons was more complicated. The correlation observed in 1,n-ADEQUATE from H-4 to the carbon at δ_C 160.0 (C-11) is a $^3J_{CH}$ correlation, which was further supported by a strong HMBC correlation. The ^{13}C spectrum of **1**, obtained in DMSO- d_6 , displayed two unresolved carbonyl carbons at δ_C 158.2 and 158.3. Thus, the correlation from H-4 to the two carbons at δ_C ~158 in 1,n-ADEQUATE could either be a 3J (H4-C5) or 4J (H4-C1) correlation, yet it is impossible to distinguish them. While the carbon signals at δ_C 158.2 and 158.3 could belong to C-1 or C-5 under the discussed conditions, both signals were better resolved in CD_3OD (Tables S1-2 and S1-3). Here, the strong HMBC correlations of H-4 were interpreted as $^3J_{CH}$, which allowed for the assignment of C5.

To localize the hydroxyl groups, a low-temperature HMBC experiment was accomplished in CD_3OH at $-20^\circ C$ (Figure S2-13) analogous to the strategy used by Vemulapalli et al., which was successfully applied to elucidate the structure of phenanthroperylene quinone pig-

ments [51]. In this special NMR solvent and condition, the hydroxyl group of methanol is not deuterated. Consequently, the hydroxyl protons of the compound cannot be exchanged with a deuterium and remain visible as sharp signals. The hydroxyl proton at δ_{H} 10.62 (brs) shows correlations to C-7, C-8, and C-9, locating its position at C-8; another hydroxyl proton (δ_{H} 9.56, brs) did not show any correlations. This could be caused by low signal-to-noise ratios observed in the 2D NMR spectra, low sample concentration, or hardware limitations such as low observation frequencies or poorly performing probe technologies [52]. However, the location of the second hydroxyl group could be indirectly assigned to C-7 by HMBC correlations from H-9 and H-10 to C-7. An overview of all recorded HMBC spectra is shown in Table S1-3 and Figure S2. By combining all the obtained data, the structure of **1** was identified as 7,8-dihydroxy-1,5-dioxo-1,5-dihydropyrano[4,3-c]chromene-3-carboxylic acid (Figure 3). In reference to the source genus *Lumnitzera*, **1** was given the trivial name lumnitzeralactone.

2.3. Computer-Assisted Structure Elucidation (CASE)

To verify the structure of **1**, a CASE system was applied: the structure elucidator of Advanced Chemistry Development software (ACD-SE). All available NMR data and the molecular formula, though no predefined structural elements, were used to build the information set used as a basis for the calculation. Although it is possible to generate a “Found Fragments” (FF) library, especially for proton-deficient molecules, the calculations were performed in *common mode* to obtain unbiased results. After a long calculation time of more than eighteen hours, ACD-SE delivered the surprisingly low number of 44 structural proposals. Usually, more than 90% of the test sets could be calculated in less than thirty minutes, although there are cases with calculating times of more than 48 h and an output of more than 500 proposals [53]. However, even expert-challenging molecules often take just minutes to calculate when a good spectra information set (2D, 1,1-ADEQUATE) is provided, as was done here as well [53,54]. Remarkably, in the calculation results, the proposed structure for **1** was mentioned eight times, with slightly different ^{13}C annotations for the COOR carbons (C-1, C-5, C-11) and for two aromatic carbons with a single oxygen bond (C-6a, C-7). The ranking of most probable structure proposals is based on $d_{\text{N}}(^{13}\text{C}+^1\text{H})$, the average differences between predicted and experimental chemical shifts. This ranking confirmed our structure annotation for lumnitzeralactone (**1**). The proposal with the correct carbon annotation was listed as the first ranked hit with a d_{N} of 3.888. Furthermore, the correct structure appeared at positions 2 to 4, as well as at positions 7, 8, 11, and 12 (for the whole ranking, see Figure S8).

2.4. Density Functional Theory (DFT) Calculations

In addition, the structure of **1** was verified by DFT calculations. Five potential structural isomers of **1** (lumnitzeralactone and isomers II-V) were considered for this computational quantum mechanical modelling (Figure 4 and Table S2-1). For each structure, only one dominant conformer was obtained (Table S2-2). For these, the experimental and calculated chemical shifts were compared. The anticipated structure of lumnitzeralactone (**1**) is assigned a very high probability by ^1H -DP4+ (99.89%), ^{13}C -DP4+ (100%), and ($^1\text{H} + ^{13}\text{C}$)-DP4+ (100%), while the alternative structures (isomers II-V) are assigned a probability of almost 0%. Thus, the proposed structure for lumnitzeralactone (**1**) could be unambiguously identified as the correct structure.

2.5. Synthesis

A further proof of the structure of **1** was obtained by chemical synthesis, something which was required for final structural proof for many natural products [55,56]. The synthesis of **1** was achieved in a two-step reaction starting from **2**, as shown in Scheme 1. The first step is the photo-oxidation of **2**, which produces intermediate **5** that has a similar structure to the natural product **1**. Following the protocol of Tokutomi et al. [43] who first described this reaction, we could obtain a good yield of the desired intermediate **5** under

adapted conditions. To improve conversion, the reaction was conducted under oxygen atmosphere in an ice bath to avoid overheating from the lamp. All recorded NMR (Figure S3, Table 1) and HRMS data (Table 2, Figure S7) of **5** are in accordance with data reported in the literature [43]. For the second step, Cu-catalyzed and Ag-catalyzed protodecarboxylation was first attempted for a selective decarboxylation of aromatic carbonic acids [57,58], though no product could be observed. However, thermal decarboxylation of **5** in toluene at 180 °C yielded the desired singly decarboxylated product **1b**, as well as side products. NMR data (Table 1, Figure S4) and HRMS data (Table 2, Figure S6) of the synthesized lumnizeralactone (**1b**) are in full accordance with data from the natural lumnizeralactone (**1**).

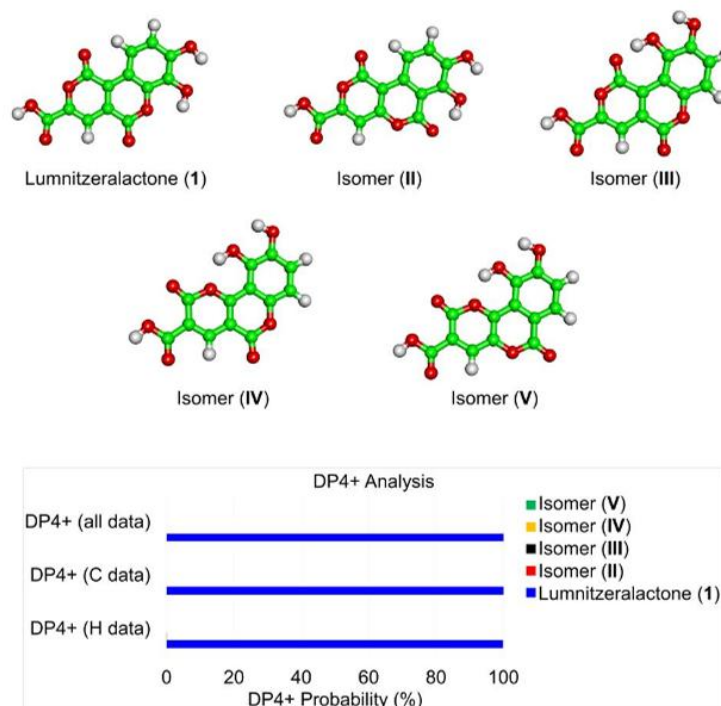
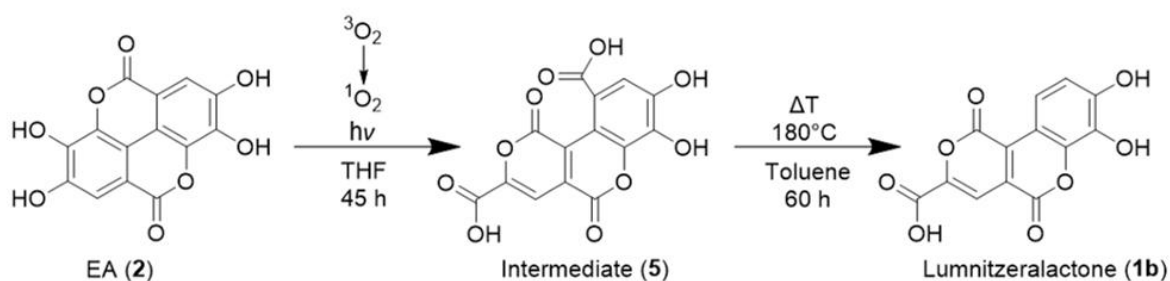


Figure 4. The proposed molecular structures of lumnizeralactone (**1**), its alternative isomeric structures, and their computed DP4+ probabilities using ¹H and ¹³C NMR data. The DP4+ probabilities were obtained by correlating the experimental ¹H and ¹³C NMR data with the calculated (PCM/mPW1PW91/6-311+G(d,p) // B3LYP/6-31+G(d,p)) nuclear shielding tensors. Compound **1** is unambiguously confirmed as the correct structure of the isolated compound through DP4+ probability (blue bars) for ¹H (99.89%), ¹³C (100%), and all data (100%). Isomeric structures (II–V) show a probability of 0%.



Scheme 1. Two-step chemical synthesis of lumnizeralactone (**1b**) from EA (**2**) via formation of a stable intermediate (**5**).

Table 2. Characterization of the natural lumnizeralactone (**1**) and synthesized compounds (**1b** and **5**) through reversed-phase ultra-high-performance liquid chromatography–quadrupole time-of-flight tandem mass spectrometry (RP-UHPLC–QqTOF MS/MS).

No	t_R (min)	m/z [M – H] [–] Observed	m/z [M – H] [–] Calculated	Δ ppm	Elemental Composition	RDB	Fragmentation Patterns
1	2.5	289.0002	288.9990	4.2	C ₁₃ H ₆ O ₈	11.5	65.0033 (C ₄ HO, 8), 117.0346 (C ₈ H ₅ O, 25), 133.0293 (C ₈ H ₅ O ₂ , 14), 145.0297 (C ₉ H ₅ O ₂ , 100), 151.0035 (C ₇ H ₃ O ₄ , 9), 161.0244 (C ₉ H ₅ O ₃ , 49), 173.0247 (C ₁₀ H ₅ O ₃ , 28), 189.0196 (C ₁₀ H ₅ O ₄ , 42), 200.0115 (C ₁₁ H ₄ O ₄ , 11), 217.0145 (C ₁₁ H ₅ O ₅ , 26) 228.0064 (C ₁₂ H ₄ O ₅ , 14) 245.0098 (C ₁₂ H ₅ O ₆ , 21)
1b	2.5	288.9990	288.9990	0	C ₁₃ H ₆ O ₈	11.5	65.0026 (C ₄ HO, 7), 117.0326 (C ₈ H ₅ O, 30), 133.0288 (C ₈ H ₅ O ₂ , 13), 145.0292 (C ₉ H ₅ O ₂ , 100), 151.0032 (C ₇ H ₃ O ₄ , 8), 161.0240 (C ₉ H ₅ O ₃ , 50), 173.0239 (C ₁₀ H ₅ O ₃ , 26), 189.0191 (C ₁₀ H ₅ O ₄ , 40), 200.0109 (C ₁₁ H ₄ O ₄ , 10), 217.0138 (C ₁₁ H ₅ O ₅ , 29), 228.0025 (C ₁₂ H ₄ O ₅ , 15), 245.0089 (C ₁₂ H ₅ O ₆ , 24)
5	1.9	332.9887	332.8889	–0.4	C ₁₄ H ₆ O ₁₀	12.5	77.0386 (C ₆ H ₅ , 5), 105.0333 (C ₇ H ₅ O, 19), 117.0332 (C ₈ H ₅ O, 9), 133.0284 (C ₈ H ₅ O ₂ , 38), 145.0282 (C ₉ H ₅ O ₂ , 10), 161.0233 (C ₉ H ₅ O ₃ , 100), 189.0186 (C ₁₀ H ₅ O ₄ , 57), 202.9975 (C ₁₀ H ₃ O ₅ , 3), 217.0134 (C ₁₁ H ₅ O ₅ , 12), 233.0086 (C ₁₁ H ₅ O ₆ , 13), 261.0039 (C ₁₂ H ₅ O ₇ , 22)

2.6. Biosynthetic Considerations

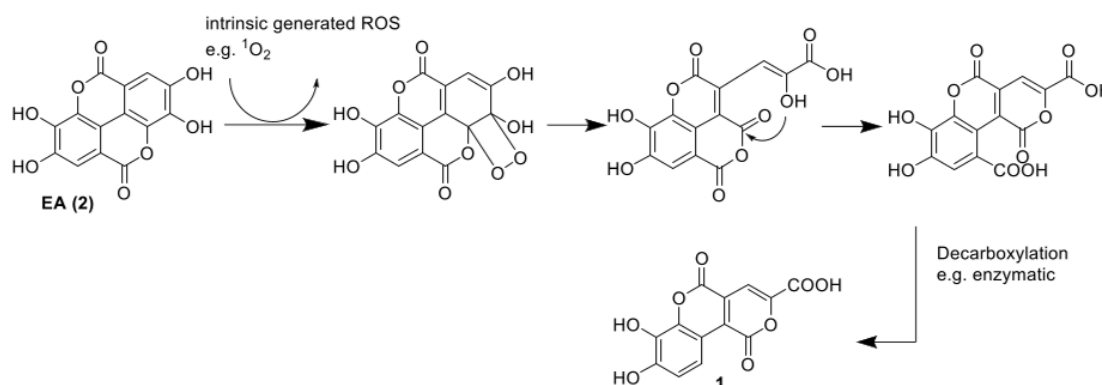
Compound **1** was found in only two of the 31 investigated *Lumnitzera* samples [8,34]. Therefore, it is likely that biosynthesis of the natural product is not (exclusively) dependent on the plant host, which shows low levels of genetic variation at a population level [59]. Instead, biosynthesis is the result of interactions with associated microorganisms that can highly depend on local environmental conditions. We suggest fungal participation in the transformation of **2** to **1** through an enzymatic process. In a fungal fermentation experiment by Aguilar-Zárate et al., an unknown EA degradation product with the same m/z as **1** was detected [60]. One possible biosynthetic pathway could begin with radical-triggered (oxidative) decarboxylation, performed by an oxidative enzyme originating from associated fungi. Subsequent steps include further oxidation and cyclization (Scheme S2-1). Several oxidizing enzymes are known from fungi, many of which exhibit extracellular activity and act on polyphenols [61–66]. Decarboxylating enzymes of fungal origin are involved in the degradation of lignin [67–69] and gallo- and ellagitannins [70].

Therefore, we suggest an alternative pathway analogous to chemical synthesis [43] via the intermediate **5**. The endoperoxide intermediate might be formed by cycloaddition of ROS [43] or enzymatically by an oxygen incorporating enzyme such as dioxygenase. This is followed by enzymatic decarboxylation (Scheme 2). However, **1** is found in the root bark, and we have no evidence at this point as to whether it is formed only superficially or by root penetrating or endophytic fungi and how the transport of EA (**2**), EA derivatives, or lumnizeralactone (**1**) occurs between species.

2.7. Biological Activity

Since **1** was detected exclusively in the two anti-bacterial crude extracts [8,34], the contribution of **1** to this activity was hypothesized. Thus, the anti-bacterial activity of **1** was checked. However, in contrast to expectations, **1** did not inhibit bacterial growth (Table 3). Interestingly, fractions resulting from the purification process and containing mainly **1** showed anti-bacterial effects (95% inhibition at a concentration of 500 µg/mL,

Table 3). Analysis of the metabolites in this active fraction revealed, besides **1**, the presence of **3** (Figure S10). In accordance with reports in the literature [71], **3** exhibited a clear anti-bacterial effect in the assay with an inhibition rate of nearly 100% at a concentration of 100 μ M (Table 3). However, **3** does not seem to be responsible for the observed anti-bacterial activity profile of the mangrove extracts, as this compound was detected in the majority of the 31 *Lumnitzera* crude extracts addressed in our previous comprehensive profiling study and its occurrence did not correlate with the effects [8]. At this moment, we can only speculate that a synergistic effect might contribute to the observed anti-bacterial effects, or that the other extracts had matrix effects countered by compound **1**.



Scheme 2. A suggested pathway for the biosynthesis of lumnitzeralactone (**1**), including ROS (analogous to Tokutomi et al. [43], cf. Scheme 1).

Table 3. Anti-bacterial activity against Gram-positive *Bacillus subtilis* of the crude extract, a fraction (both 500 μ g/mL), and pure compounds (100 μ M) derived from *L. racemosa* and its synthetic analog.

Sample	Growth Inhibition [%]
1	11.9 \pm 26.2
1b	21.7 \pm 11.4
5	28.9 \pm 10.6
3	99.9 \pm 3.0
Fraction containing 1 and 3	94.6 \pm 7.1
Crude extract	90.1 \pm 20.6
Pos. control (Chloramphenicol)	98.9 \pm 0.1

As mentioned above, mangroves often live in symbiosis with associated microorganisms, including fungi. An intensive investigation of endophytic fungi from mangroves, including *Lumnitzera*, revealed significant anti-microbial potential for 71 representative endophytic fungal species tested. Their extracts were applied against a set of two Gram-positive bacteria (*B. subtilis* and *S. aureus*) and two Gram-negative bacteria (*Pseudomonas aeruginosa* and *Escherichia coli*) [32]. Consistent with this study, our results imply that EA-metabolizing fungi might contribute to the anti-bacterial effects of selected *Lumnitzera* samples.

3. Material and Methods

3.1. General Experimental Procedures and Reagents

Thin layer chromatography (TLC) analyses were performed on silica gel 60 reversed-phase 18 F₂₅₄ (Merck, Darmstadt, Germany) using the solvent system H₂O:MeOH 3:2 or silica gel 60 reversed-phase 2 UV₂₅₄ (Macherey-Nagel, Düren, Germany) using the solvent system H₂O:MeOH 3:2. To visualize the compound spots, long-wavelength UV light

(366 nm), short-wavelength UV light (254 nm), and spraying with vanillin-H₂SO₄ reagent were used, followed by heating or spraying with a natural product spray reagent.

Low-resolution ESI-MS spectra were obtained using a Sciex API-3200 instrument (Applied Biosystems, Concord, ON, Canada) combined with an HTC-XT autosampler (CTC Analytics, Zwingen, Switzerland).

The UV spectra were recorded on a Jasco V-770 UV-Vis/NIR spectrophotometer (Jasco, Pfungstadt, Germany) using a 10 mm quartz glass cuvette.

Analytical and semi-preparative RP-HPLC were performed on a Shimadzu prominence system consisting of an SPD-M20A diode array detector, a FRC-10A fraction collector, a CBM-20A communications bus module, a DGU-20A5R degassing unit, an LC-20AT liquid chromatograph, and an SIL-20A HT auto sampler. Chromatographic separation was performed using an analytical YMC Pack Pro C18 column (ID 4.6 mm, length 150 mm, particle size 5 µm) and a semi-preparative YMC Pack Pro C18 column (ID 10.0 mm, length 150 mm, particle size 5 µm) using ultrapure water (TKA ultrapure water system) and methanol (Merck, LiChrosolv HPLC Gradient Grade) as eluents.

Ellagic acid was purchased from TCI Chemicals (Tokyo, Japan) and was used without further purification. All solvents were purchased from Merck Chemicals GmbH (Darmstadt, Germany) and were distilled prior to use. Deuterated solvents for NMR spectroscopy were purchased from Deutero GmbH (Kastellaun, Germany). TMEA (**3**) was obtained by earlier isolation [8].

3.2. Plant Material

The root material of *Lumnitzera racemosa* Willd. was collected from the Indonesian archipelago as described in Manurung et al. [8] in Table 1, No. 19. The material corresponding to sample LR7 comes from Ternate Island, Maluku (DD coordinates 0.84 / 127.31). The voucher specimen (BO1959402) is deposited at Herbarium Bogoriense (BO, Bogor, Indonesia), National Research and Innovation Agency (BRIN). The samples were cleaned, air-shadow-dried, and then kept in resealable zipper storage bags until use for further treatment.

3.3. Extraction and Isolation

An aliquot (1.35 g) of the crude extract used in previous work [8] was diluted in 200 mL water and extracted five times with 100 mL of ethyl acetate. Each ethyl acetate fraction was centrifuged. The combined supernatant of fractions 2–5 was dried (49.2 mg) and submitted to an RP18 column eluted with a mixture of water and methanol (30:20, *v/v*) followed by final purification by preparative HPLC (water (A)/methanol (B) gradient: 0–17.5 min, 5–31.5% B; 17.5–19.5 min, 31.5–100% B, isocratic for 8 min and a flow rate of 0.8 mL/min) to yield lumnizeralactone (**1**) (2.5 mg, *R*_f = 0.71 in MeOH/H₂O (2:3, *v/v*) on RP18).

For repeated isolation, 15.06 g of dried roots from *L. racemosa* was ground to fine powder in a ball mill, followed by an exhaustive extraction with methanol to provide 1.33 g of dried crude extract. The extract was partitioned by liquid–liquid extraction between water and ethyl acetate, first pure, then by adding some drops of 2M HCl to the water phase, resulting in three fractions: water (697.2 mg), ethyl acetate (pure) (312.8 mg), and acidic ethyl acetate (75.5 mg).

The last fraction was separated using a Sephadex LH20 column (h: 76 cm, d: 2.5 cm) eluted with pure methanol. Based on TLC profiles, six main fractions were combined. Fraction 3 (*R*_f = 0.72) was further purified on an RP2 cartridge (h: 5.5 cm, d: 1.6 cm) and eluted with a mixture of 40% methanolic water followed by 10% methanolic chloroform solution. Final purification of the water–methanol fraction was performed by preparative HPLC. Compound **1** (14.6 mg, *R*_f = 0.72 in MeOH/H₂O (2:3, *v/v*) on RP18) was purified using a water (A)/methanol (B) gradient system (0–17.5 min, 5–31.3% B; 17.5–19.5 min, 100% B (isocratic for 8 min)) and a flow rate of 7.089 mL/min at 25 °C with absorbance detection at 210 to 800 nm (*R*_t = 9.038 min, λ_{max}: 411 nm, 288 nm, 210 nm).

The pure ethyl acetate fraction resulting from the liquid–liquid extraction was separated in the same way using an LH20 column and an RP2 cartridge to obtain a fraction containing **1** and TMEA (**3**) (54.0 mg). This fraction was used in the anti-bacterial assay.

Lumnitzeralactone (7,8-dihydroxy-1,5-dioxo-1,5-dihydropyrano[4,3-*c*]chromene-3-carboxylic acid, **1**): yellow amorphous solid; UV (THF) λ_{max} (log ϵ) 232 (4.10), 290 (3.95), 407 (3.96) nm; ^1H and ^{13}C NMR, see Table 1; HR ESI-MS and MS² fragmentation, see Table 2.

3.4. Synthesis

3.4.1. Photoreaction

A solution of ellagic acid dihydrate (0.82 g, 2.4 mmol) in dry THF (800 mL) was irradiated using a mercury xenon lamp for 45 h inside a photoreactor. The reaction vessel was placed in an ice bath for additional cooling and a balloon filled with oxygen was attached to it. Reaction progress was monitored through measurement of UV spectra to detect the decreases in absorption intensity at 367 nm and increases in intensity at 400 nm, as performed by Tokutomi et al. [43]. After completion of the reaction, the solvent was distilled off and the residue was freeze-dried. The crude product was suspended in DCM and then stored overnight in the refrigerator. Subsequently, the supernatant was removed, and the precipitation step was repeated, yielding 0.79 g of an orange amorphous solid (**5**) which was used without further chromatographic purification.

Synthesized intermediate of lumnitzeralactone (7,8-dihydroxy-1,5-dioxo-1,5-dihydropyrano[4,3-*c*]chromene-3,10-dicarboxylic acid, **5**): orange amorphous solid; UV (THF) λ_{max} (log ϵ) 232 (4.13), 290 (3.77), 407 (3.63) nm; ^1H and ^{13}C NMR, see Table 1; HR ESI-MS and MS² fragmentation, see Table 2.

3.4.2. Decarboxylation

A solution of intermediate **5** (100 mg) in dry toluene (2 mL) was heated to 180 °C in a capped microwave vial for 60 h. After distilling off the solvent, the reaction product was dissolved in methanol and centrifuged to separate insoluble residues. The supernatant was purified using an RP18 column (h: 36 cm, d: 3.5 cm) and eluted with a water–methanol mixture (3:2, *v/v*) to obtain synthetic lumnitzeralactone (**1b**) (6.7 mg, 0.023 mmol, 7.5% yield over two steps).

Synthetic lumnitzeralactone (**1b**): yellow amorphous solid; UV (THF) λ_{max} (log ϵ) 232 (4.01), 290 (3.94), 411 (3.98) nm; ^1H and ^{13}C NMR, see Table 1; HR ESI-MS and MS² fragmentation, see Table 2.

3.5. NMR

^1H and ^{13}C NMR spectra were recorded on an Agilent DD2 400 NMR spectrometer at 399.917 and 100.570 MHz, respectively. Chemical shifts are reported relative to TMS (^1H NMR) or solvent peaks (^{13}C , DMSO-*d*₆ 39.5 ppm, MeOH-*d*₄ 49.0 ppm). For samples with low concentrations, ^1H and ^{13}C NMR spectra were recorded on a Bruker Avance Neo 500 NMR spectrometer at 500.234 and 125.797 MHz, respectively, using a 5 mm prodigy probe with TopSpin 4.0.7 spectrometer software. The 2D NMR spectra were recorded on an Agilent VNMR5 600 MHz NMR spectrometer using standard CHEMPACK 8.1 pulse sequences (^1H - ^{13}C gHSQCAD, ^1H - ^1H gCOSY, ^1H - ^1H gTOCSY, and ^1H - ^{13}C gHMBCAD) implemented in Varian VNMRJ 4.2 spectrometer software.

The low-temperature ^{13}C - ^1H long-range correlation HMBC spectrum for structure elucidation of **1** was recorded at 253 K on a Bruker Avance NEO 700 MHz (^1H resonance frequency) instrument equipped with a 5 mm TCI cryoprobe prodigy. Long-range carbon–proton coupling of 8 Hz was used. The time domain matrix of 4k × 256 with 13 ppm (F2) and 80 ppm (F1) spectral width was used. Carrier frequency was set to 5.5 and 135 ppm in the F2 and F1 dimensions, respectively. The number of scans was set to 256 per t1 increment and 2 s of repetition delay was used. The 1,1-ADEQUATE [72] (Bruker pulse sequence: adeq11etgppp) spectrum was recorded on a Bruker Avance III HD 900 MHz (^1H resonance

frequency) instrument equipped with a 5 mm TCI cryoprobe. One-bond carbon–proton and carbon–carbon couplings of 145 and 50 Hz, respectively, were used. The inversion (Crp60, 0.5, 20.1) and refocusing (Crp60, 0.5, 20.1) 180° selective pulses on ^{13}C were set to 500 and 2000 μs , respectively. The time domain matrix of $3\text{k} \times 208$ with 13 ppm (F2) and 147 ppm (F1) spectral width was used. Carrier frequency was set to 6 and 100 ppm in the F2 and F1 dimensions, respectively. The number of scans was set to 256 per t1 increment and 2 s of repetition delay was used. The 1,n-ADEQUATE [48,50,72,73] (Bruker pulse sequence: adeq1netgprdsp) spectrum was recorded on a Bruker Avance NEO 800 MHz (^1H resonance frequency) instrument equipped with a 3 mm TCI cryoprobe. One-bond carbon–proton and carbon–carbon couplings of 145 and 57 Hz (64 Hz), respectively, were used. The desired long-range carbon–proton coupling was set to 9.5 Hz (8 Hz). NMR spectra were processed and analyzed using Topspin 4.1.3 (Bruker, Germany).

3.6. UHPLC-ESI-QqTOF-MS and MS/MS

For mass spectra of pure compounds, the samples (2 μL) were loaded on an EC 150/2 Nucleoshell RP 18 column (C18-phase, ID 2 mm, length 150 mm, particle size 2.7 μm , Macherey Nagel, Düren, Germany) under isocratic conditions (3% eluent B, 1 min) and separated using a linear gradient from 3% to 95% eluent B in 5 min. Separation was performed on an ACQUITY UPLC I-Class UHPLC System (Waters GmbH, Eschborn, Germany) with a flow rate of 0.4 mL/min and 55°C column temperature. Eluents A and B were water and acetonitrile, with 0.1% (*v/v*) formic acid. The column effluent was introduced online into a TripleTOF 6600 quadrupole time-of-flight (QqTOF) mass spectrometer equipped with a DuoSpray ESI/APCI ion source operating in negative ion SWATH (Sequential Windowed Acquisition of All Theoretical Fragment Ion Mass Spectra) mode and controlled by Analyst TF 1.7.1 software (AB Sciex GmbH, Darmstadt, Germany). The TOF scans (MS experiments) were acquired in the *m/z* range of 50 to 1000 (accumulation time 50 ms) with an ion spray voltage of -4.5 kV and 450°C source temperature. Declustering (DP) and collision (CE) potentials were -35 and -10 V , respectively. The product ion spectra (tandem mass spectra, MS/MS) were acquired in the high sensitivity mode (accumulation time 20 ms) in the *m/z* range of 50–350 using unit Q1 resolution with mass resolution above 30,000. Collision potential (CE) was set from -80 to -20 V , whereas collision energy spread (CES) was 15 V. The data were evaluated by Peak View 1.2.0.3 software (AB Sciex GmbH, Darmstadt, Germany).

The crude extract was investigated by applying the MS conditions described in Manurung et al. [8].

3.7. DFT-Calculations

The starting structures representing potential isomers of **1** were built in Maestro 11.4 (Schrödinger Release 2017-4: Maestro; Schrödinger, LLC: New York, NY, USA, 2019.). The conformational search was performed with Macromodel 11.8 (Schrödinger Release 2017-4: Macromodel; Schrödinger, LLC: New York, NY, USA, 2019) using the MMFF forcefield [74] under vacuum and an energy threshold of 5 kcal/mol. Only one dominant conformer was obtained for each structure. All conformers were geometry-optimized at the B3LYP [8–11]/6-31+G(d,p) [75] level of theory with Gaussian09 (Gaussian 09, Revision C.01; Gaussian Inc.: Wallingford, CT, USA, 2010). The energy minimized conformers were used as an input geometry for further DFT calculations. The nuclear shielding constants were calculated at mPW1PW91 [76,77] /6-311+G(d,p) and mPW1PW91/6-311+G(2d,p) levels of theory using GIAO [78] and IEFPCM [79] solvent (methanol) models. The obtained shielding constants were converted into chemical shifts using the scaling factors available on the CHESHIRE (chemical shift repository) [80–83] webpage. DP4+ [84,85] probability was obtained using the experimental and calculated ^1H and ^{13}C chemical shifts.

3.8. ACD-SE Calculations

The ACD/Structure Elucidator (ACD/SE) from ACD/Labs in ACD/Labs version 2018.2.5 (File Version S80S41, Build 108235, 8 April 2019) was used to perform verification of promising structure proposals based on experimental NMR and HRMS data.

3.9. Anti-Bacterial Assay

The compounds were evaluated against the Gram-positive *Bacillus subtilis* 168 (DSM 10), as described by Ware et al. [86]. The tests were performed in 96-well plates based on absorption read-out. Chloramphenicol (100 μ M) was used as a positive control to induce complete inhibition of bacterial growth. The results (mean \pm standard deviation value, $n = 6$) are given in relation to the negative control (bacterial growth in the presence of 1% *v/v* DMSO) as relative values (percent inhibition). Negative values indicate an increase in bacterial growth.

4. Conclusions

In this study, the previously unreported lumnizeralactone (**1**) was isolated and characterized from the true mangrove species *Lumnitzera racemosa*. Elaborate structure elucidation includes ^1H and ^{13}C NMR, 2D NMR (COSY, TOCSY, HSQC, HMBC, 1,1-ADEQUATE, 1,1-ADEQUATE) spectra recorded in different solvents and in special cases under low-temperature conditions, HR-MS, computer-assisted structure elucidation (CASE), DFT calculations, and chemical synthesis. In contrast to expectations, lumnizeralactone (**1**) isolated from the anti-bacterial crude extract did not exhibit significant anti-bacterial activity against *B. subtilis*.

Putative biosynthetic pathways of **1** are suggested, as well as a high probability of the participation of an associated microorganism or its excreted enzymes. Microorganism-based modification or elicitation may also explain the observed differential antibiotic potential of the same species when collected at different sites. Although **1** itself did not show significant anti-bacterial activity, it is present exclusively in anti-bacterial crude extracts. However, the activity of crude extracts can also result from yet unidentified highly bioactive minor components. Considering this, Indonesian mangroves may represent a promising source of potent bioactive compounds that are waiting to be explored further.

Supplementary Materials: The following supporting information can be downloaded at: <https://www.mdpi.com/article/10.3390/md21040242/s1>, Figure S1: TLC after Bornträger reaction, Figure S2: The 1D and 2D NMR spectra of compound **1**, Figure S3: The 1D and 2D NMR spectra of compound **5**, Figure S4: The 1D and 2D NMR spectra of compound **1b**, Figure S5: MS data of compound **1**, Figure S6: MS data of compound **1b**, Figure S7: MS data of compound **5**, Figure S8: Structure Elucidation Report—ACD-SE Calculation, Figure S9: UV spectra of compound **1**, **1b**, and **5**, Figure S10: ^1H NMR spectrum and HPLC chromatogram of the anti-bacterial fraction containing **1** and **3**, Scheme S1: Mechanism of the Bornträger reaction, Scheme S2: Suggested pathway for the biosynthesis of compound **1**, Table S1: ^1H , ^{13}C , and HMBC NMR data of compound **1** with different solvents and field strengths, Table S2: Additional data relating to DFT calculations.

Author Contributions: Conceptualization, L.A.W., A.N.M.-R. and J.M.; methodology, J.K., K.F., A.F., S.P.B.V., C.G., L.A.W. and T.F.; software, J.K. and S.P.B.V.; validation, K.F., A.F., J.K. and S.P.B.V.; formal analysis, J.K., L.M.S. and K.F.; investigation, J.K., J.M. and S.P.B.V.; resources, L.A.W., A.N.M.-R., A.A. and C.G.; data curation, K.F. and S.P.B.V.; writing—original draft, J.K.; writing—review and editing, K.F., J.M., T.F., S.P.B.V., L.M.S., A.F., A.A., A.N.M.-R., C.G. and L.A.W.; visualization, J.K., A.F. and K.F.; supervision, L.A.W., A.N.M.-R., C.G. and K.F.; project administration, L.A.W. and A.N.M.-R.; funding acquisition, L.A.W., A.N.M.-R. and J.M. All authors have read and agreed to the published version of the manuscript.

Funding: Financial support for this study was provided by the project “Indonesian Plant Biodiversity and Human Health—BIOHEALTH” (BMBF grants no. 16GW0120K and 16GW0123) to Ludger Wessjohann and Alexandra Muellner-Riehl. Jonas Kappen and Katrin Franke were funded within the frame of the project ProCognito (to LAW and KF) by EFRE and the state Saxony-Anhalt (ZS/2018/11/95581). Jeprianto Manurung was funded by a PhD grant from the German Academic Exchange Service (DAAD project no. 91653688) hosted by Alexandra Muellner-Riehl. Funding from Max Planck Society to Christian Griesinger is acknowledged.

Institutional Review Board Statement: Not applicable.

Data Availability Statement: Plant material: Plant material is deposited at LIPI, Bogor, Indonesia. Chemical data: All primary data and reference compounds are stored in IPB primary data storage for 10+ years and in the compound depository to the extent available or stable. Pending availability, detailed data can be shared upon request.

Acknowledgments: The authors would like to thank Martina Brode (IPB Halle) for the performance of anti-bacterial bioassays. We are grateful to Pauline Stark, Andrea Porzel, and Gudrun Hahn (IPB Halle) for NMR measurements, as well as to Annegret Laub and Elana Kysil (IPB Halle) for HRMS measurements. We are pleased to thank Jan Schnitzler (Leipzig University/iDiv) for his invaluable assistance in organizing the fieldwork in Indonesia. We extend our gratitude to our partners in Indonesia, including Herbarium Bogoriense (BO) and the National Research and Innovation Agency (BRIN), along with Hetty I.P. Normakristagaluh, Lina Juswara, and Witjaksono (former director of RCB-LIPI) for providing administrative support. We also pay our respects in memoriam to Fajria Novari (Ministry of Environment and Forestry Republic of Indonesia) for assisting with plant material export permits. Furthermore, we extend our appreciation to all the local forestry officers, national parks, and natural resources conservation units. In particular, we thank Bung Petra at Balai Konservasi Sumber Daya Alam (BKSDA) Maluku, Ambon, for their permits and logistic support.

Conflicts of Interest: The authors declare no conflict of interest.

References

- Bandaranayake, W.M. Bioactivities, bioactive compounds and chemical constituents of mangrove plants. *Wetl. Ecol. Manag.* **2002**, *10*, 421–452. [\[CrossRef\]](#)
- Kathiresan, K.; Bingham, B.L. Biology of mangroves and mangrove ecosystems. *Adv. Mar. Biol.* **2001**, *40*, 81–251. [\[CrossRef\]](#)
- Wu, J.; Xiao, Q.; Xu, J.; Li, M.-Y.; Pan, J.-Y.; Yang, M. Natural products from true mangrove flora: Source, chemistry and bioactivities. *Nat. Prod. Rep.* **2008**, *25*, 955–981. [\[CrossRef\]](#)
- Spalding, M.; Kainuma, M.; Collins, L. *World Atlas of Mangroves*; Earthscan: London, UK, 2010; ISBN 9781136530951.
- Wang, L.; Mu, M.; Li, X.; Lin, P.; Wang, W. Differentiation between true mangroves and mangrove associates based on leaf traits and salt contents. *J. Plant Ecol.* **2011**, *4*, 292–301. [\[CrossRef\]](#)
- Manohar, S.M. A review of the botany, phytochemistry and pharmacology of mangrove *Lumnitzera racemosa* Willd. *Phcog. Rev.* **2021**, *15*, 107–116. [\[CrossRef\]](#)
- Patra, J.K.; Thatoi, H.N. Metabolic diversity and bioactivity screening of mangrove plants: A review. *Acta Physiol. Plant* **2011**, *33*, 1051–1061. [\[CrossRef\]](#)
- Manurung, J.; Kappen, J.; Schnitzler, J.; Frolov, A.; Wessjohann, L.A.; Agusta, A.; Muellner-Riehl, A.N.; Franke, K. Analysis of unusual sulfated constituents and anti-infective properties of two Indonesian mangroves, *Lumnitzera littorea* and *Lumnitzera racemosa* (Combretaceae). *Separations* **2021**, *8*, 82. [\[CrossRef\]](#)
- Pattanaik, C.; Reddy, C.S.; Dhal, N.K.; Das, R. Utilisation of mangrove forests in Bhitarkanika Wildlife sanctuary, Orissa. *Indian J. Tradit. Knowl.* **2008**, *7*, 598–603.
- Yvana Glasenapp, I.; Korth, X.; Nguyen, J. Papenbrock. Sustainable use of mangroves as sources of valuable medicinal compounds: Species identification, propagation and secondary metabolite composition. *S. Afr. J. Bot.* **2019**, *121*, 317–328. [\[CrossRef\]](#)
- Neamsuvan, O. A survey of medicinal plants in mangrove and beach forests from Sating Phra Peninsula, Songkhla Province, Thailand. *J. Med. Plants Res.* **2012**, *6*, 2421–2437. [\[CrossRef\]](#)
- Ray, T. Customary use of mangrove tree as a folk medicine among the Sundarban resource collectors. *Int. J. Res. Humanit. Arts Lit.* **2014**, *2*, 43–48.
- Bandaranayake, W.M. Traditional and medicinal uses of mangroves. *Mangr. Salt Mar.* **1998**, *2*, 133–148. [\[CrossRef\]](#)
- Souza, L.D.; Wahidulla, S.; Devi, P. Antibacterial phenolics from the mangrove *Lumnitzera racemosa*. *Indian J. Geo-Mar. Sci.* **2010**, *39*, 294–298.
- Abeyasinghe, P.D. Antibacterial activity of aqueous and ethanol extracts of mangrove species collected from southern Sri Lanka. *Asian J. Pharm. Biol. Res.* **2012**, *2*, 79–83.

16. Abeysinghe, P.D. Antibacterial activity of some medicinal mangroves against antibiotic resistant pathogenic bacteria. *Indian J. Pharm. Sci.* **2010**, *72*, 167–172. [\[CrossRef\]](#)
17. Paul, T.; Ramasubbu, S. The antioxidant, anticancer and anticoagulant activities of *Acanthus ilicifolius* L. roots and *Lumnitzera racemosa* Willd. leaves, from southeast coast of India. *J. App. Pharm. Sci.* **2017**, *7*, 81–87. [\[CrossRef\]](#)
18. Yu, S.-Y.; Wang, S.-W.; Hwang, T.-L.; Wei, B.-L.; Su, C.-J.; Chang, F.-R.; Cheng, Y.-B. Components from the leaves and twigs of mangrove *Lumnitzera racemosa* with anti-angiogenic and anti-inflammatory effects. *Mar. Drugs* **2018**, *16*, 404. [\[CrossRef\]](#)
19. Eswaraiah, G.; Peele, K.A.; Krupanidhi, S.; Indira, M.; Kumar, R.B.; Venkateswarulu, T.C. GC–MS analysis for compound identification in leaf extract of *Lumnitzera racemosa* and evaluation of its in vitro anticancer effect against MCF7 and HeLa cell lines. *J. King. Saud. Univ. Sci.* **2020**, *32*, 780–783. [\[CrossRef\]](#)
20. Nguyen, P.T.; Bui, T.T.L.; Chau, N.D.; Bui, H.T.; Kim, E.J.; Kang, H.K.; Lee, S.H.; Jang, H.D.; Nguyen, T.C.; van Nguyen, T.; et al. In vitro evaluation of the antioxidant and cytotoxic activities of constituents of the mangrove *Lumnitzera racemosa* Willd. *Arch. Pharm. Res.* **2015**, *38*, 446–455. [\[CrossRef\]](#)
21. Ravikumar, S.; Gnanadesigan, M. Hepatoprotective and antioxidant activity of a mangrove plant *Lumnitzera racemosa*. *Asian Pac. J. Trop. Biomed.* **2011**, *1*, 348–352. [\[CrossRef\]](#)
22. Darwish, A.G.G.; Samy, M.N.; Sugimoto, S.; Otsuka, H.; Abdel-Salam, H.; Matsunami, K. Effects of hepatoprotective compounds from the leaves of *Lumnitzera racemosa* on acetaminophen-induced liver damage in vitro. *Chem. Pharm. Bull.* **2016**, *64*, 360–365. [\[CrossRef\]](#)
23. Lin, T.-C.; Hsu, F.-L.; Cheng, J.-T. Antihypertensive activity of corilagin and chebulinic acid, tannins from *Lumnitzera racemosa*. *J. Nat. Prod.* **1993**, *56*, 629–632. [\[CrossRef\]](#)
24. Tiwari, P. Search for antihyperglycemic activity in few marine flora and fauna. *Indian J. Sci. Technol.* **2008**, *1*, 1–5. [\[CrossRef\]](#)
25. Vadlapudi, V.; Naidu, K. Bioefficiency of mangrove plants *Lumintzera racemosa* and *Bruguiera gymnorhiza*. *J. Pharm. Res.* **2009**, *2*, 1591–1592.
26. Bamroongrugs, N. *Bioactive Substances from the Mangrove Resource*; Prince of Songkla University: Hat Yai, Thailand, 1999.
27. Chandrasekaran, M.; Kannathasan, K.; Venkatesalu, V.; Prabhakar, K. Antibacterial activity of some salt marsh halophytes and mangrove plants against methicillin resistant *Staphylococcus aureus*. *World J. Microbiol. Biotechnol.* **2009**, *25*, 155–160. [\[CrossRef\]](#)
28. Anokwuru, C.P.; Chen, W.; van Vuuren, S.; Combrinck, S.; Viljoen, A.M. Bioautography-guided HPTLC–MS as a rapid hyphenated technique for the identification of antimicrobial compounds from selected South African Combretaceae species. *Phytochem. Anal.* **2022**. [\[CrossRef\]](#)
29. Wu, M.-J.; Xu, B.; Guo, Y.-W. Unusual secondary metabolites from the mangrove ecosystems: Structures, bioactivities, chemical, and bio-syntheses. *Mar. Drugs* **2022**, *20*, 535. [\[CrossRef\]](#)
30. Chen, S.; Cai, R.; Liu, Z.; Cui, H.; She, Z. Secondary metabolites from mangrove-associated fungi: Source, chemistry and bioactivities. *Nat. Prod. Rep.* **2022**, *39*, 560–595. [\[CrossRef\]](#)
31. Debbab, A.; Aly, A.H.; Proksch, P. Mangrove derived fungal endophytes—A chemical and biological perception. *Fungal Divers.* **2013**, *61*, 1–27. [\[CrossRef\]](#)
32. Chaepasert, S.; Piapukiew, J.; Whalley, A.J.; Sihanonth, P. Endophytic fungi from mangrove plant species of Thailand: Their antimicrobial and anticancer potentials. *Bot. Mar.* **2010**, *53*, 555–564. [\[CrossRef\]](#)
33. Arnold, A.E. Understanding the diversity of foliar endophytic fungi: Progress, challenges, and frontiers. *Fungal Biol. Rev.* **2007**, *21*, 51–66. [\[CrossRef\]](#)
34. Manurung, J. Evolutionary Ecology and Discovery of New Bioactive Compounds from *Lumnitzera* Mangroves across the Indonesian Archipelago. Ph.D. Thesis, Universität Leipzig, Leipzig, Germany, 2022.
35. Wang, Y.; Shang, X.-Y.; Wang, S.-J.; Mo, S.-Y.; Li, S.; Yang, Y.-C.; Ye, F.; Shi, J.-G.; He, L. Structures, biogenesis, and biological activities of pyrano[4,3-c]isochromen-4-one derivatives from the fungus *Phellinus igniarius*. *J. Nat. Prod.* **2007**, *70*, 296–299. [\[CrossRef\]](#) [\[PubMed\]](#)
36. Schmidt, J. Negative ion electrospray high-resolution tandem mass spectrometry of polyphenols. *J. Mass. Spectrom.* **2016**, *51*, 33–43. [\[CrossRef\]](#) [\[PubMed\]](#)
37. Dulo, B.; Phan, K.; Githaiga, J.; Raes, K.; de Meester, S. Natural quinone dyes: A review on structure, extraction techniques, analysis and application potential. *Waste Biomass Valorization* **2021**, *12*, 6339–6374. [\[CrossRef\]](#)
38. Ma, Q.; Wei, R.; Liu, W.; Sang, Z.; Guo, X. Cytotoxic anthraquinones from the aerial parts of *Acalypha australis*. *Chem. Nat. Compd.* **2017**, *53*, 949–952. [\[CrossRef\]](#)
39. Kuo, Y.-H.; Lin, S.-T. Studies on chromium trioxide-based oxidative coupling reagents and synthesis of lignan-cagayanone. *Chem. Pharm. Bull.* **1993**, *41*, 1507–1512. [\[CrossRef\]](#)
40. Li, N.; Wang, B.; Sun, J.; Wang, X.; Sun, J. Synthesis and hydroxyl radical scavenging activity of 4-aryl-3,4-dihydrocoumarins. *Chem. Nat. Compd.* **2017**, *53*, 860–865. [\[CrossRef\]](#)
41. Al-Majmaie, S.; Nahar, L.; Sharples, G.P.; Wadi, K.; Sarker, S.D. Isolation and antimicrobial activity of rutin and its derivatives from *Ruta chalepensis* (Rutaceae) growing in Iraq. *Rec. Nat. Prod.* **2018**, *13*, 64–70. [\[CrossRef\]](#)
42. Dao, N.T.; Jang, Y.; Kim, M.; Nguyen, H.H.; Pham, D.Q.; Le Dang, Q.; van Nguyen, M.; Yun, B.-S.; Pham, Q.M.; Kim, J.-C.; et al. Chemical constituents and anti-influenza viral activity of the leaves of Vietnamese plant *Elaeocarpus tonkinensis*. *Rec. Nat. Prod.* **2018**, *13*, 71–80. [\[CrossRef\]](#)

43. Tokutomi, H.; Takeda, T.; Hoshino, N.; Akutagawa, T. Molecular structure of the photo-oxidation product of ellagic acid in solution. *ACS Omega* **2018**, *3*, 11179–11183. [\[CrossRef\]](#)
44. Kono, H.; Anai, H.; Hashimoto, H.; Shimizu, Y. ¹³C-detection two-dimensional NMR approaches for cellulose derivatives. *Cellulose* **2015**, *22*, 2927–2942. [\[CrossRef\]](#)
45. Köck, M.; Reif, B.; Fenical, W.; Griesinger, C. Differentiation of HMBC two- and three-bond correlations: A method to simplify the structure determination of natural products. *Tetrahedron Lett.* **1996**, *37*, 363–366. [\[CrossRef\]](#)
46. Köck, M.; Reif, B.; Gerlach, M.; Reggelin, M. Application of the 1,n-ADEQUATE experiment in the assignment of highly substituted aromatic compounds. *Molecules* **1996**, *1*, 41–45. [\[CrossRef\]](#)
47. Martin, G.E. Chapter 5—Using 1,1- and 1,n-ADEQUATE 2D NMR data in structure elucidation protocols. In *Annual Reports on NMR Spectroscopy*; Webb, G.A., Ed.; Academic Press: Cambridge, MA, USA, 2011; pp. 215–291, ISBN 0066-4103.
48. Martin, G.E.; Williamson, R.T.; Dormer, P.G.; Bermel, W. Inversion of ¹J_{CC} correlations in 1,n-ADEQUATE spectra. *Magn. Reson. Chem.* **2012**, *50*, 563–568. [\[CrossRef\]](#)
49. Reif, B.; Köck, M.; Kerssebaum, R.; Schleucher, J.; Griesinger, C. Determination of ¹J, ²J, and ³J carbon-carbon coupling constants at natural abundance. *J. Magn. Reson. Ser. B* **1996**, *112*, 295–301. [\[CrossRef\]](#)
50. Reibarkh, M.; Williamson, R.T.; Martin, G.E.; Bermel, W. Broadband inversion of ¹J_(CC) responses in 1,n-ADEQUATE spectra. *J. Magn. Reson.* **2013**, *236*, 126–133. [\[CrossRef\]](#)
51. Vemulapalli, S.P.B.; Fuentes-Monteverde, J.C.; Karschin, N.; Oji, T.; Griesinger, C.; Wolkenstein, K. Structure and absolute configuration of phenanthro-perylene quinone pigments from the deep-sea crinoid *Hyalocrinus naresianus*. *Mar. Drugs* **2021**, *19*, 445. [\[CrossRef\]](#)
52. Blinov, K.A.; Carlson, D.; Elyashberg, M.E.; Martin, G.E.; Martirosian, E.R.; Molodtsov, S.; Williams, A.J. Computer-assisted structure elucidation of natural products with limited 2D NMR data: Application of the struc.eluc. system. *Magn. Reson. Chem.* **2003**, *41*, 359–372. [\[CrossRef\]](#)
53. Elyashberg, M.; Williams, A. ACD/Structure elucidator: 20 years in the history of development. *Molecules* **2021**, *26*, 6623. [\[CrossRef\]](#)
54. Kummerlöwe, G.; Crone, B.; Kretschmer, M.; Kirsch, S.F.; Luy, B. Residual dipolar couplings as a powerful tool for constitutional analysis: The unexpected formation of tricyclic compounds. *Angew. Chem. Int. Ed.* **2011**, *50*, 2643–2645. [\[CrossRef\]](#)
55. Nicolaou, K.C.; Snyder, S.A. Chasing molecules that were never there: Misassigned natural products and the role of chemical synthesis in modern structure elucidation. *Angew. Chem. Int. Ed.* **2005**, *44*, 1012–1044. [\[CrossRef\]](#) [\[PubMed\]](#)
56. Eschenmoser, A.; Wintner, C.E. Natural product synthesis and vitamin b12. *Science* **1977**, *196*, 1410–1420. [\[CrossRef\]](#) [\[PubMed\]](#)
57. Goossen, L.J.; Manjolinho, F.; Khan, B.A.; Rodríguez, N. Microwave-assisted Cu-catalyzed protodecarboxylation of aromatic carboxylic acids. *J. Org. Chem.* **2009**, *74*, 2620–2623. [\[CrossRef\]](#) [\[PubMed\]](#)
58. Lu, P.; Sanchez, C.; Cornella, J.; Larrosa, I. Silver-catalyzed protodecarboxylation of heteroaromatic carboxylic acids. *Org. Lett.* **2009**, *11*, 5710–5713. [\[CrossRef\]](#) [\[PubMed\]](#)
59. Manurung, J.; Rojas Andrés, B.M.; Barratt, C.D.; Schnitzler, J.; Jönsson, B.F.; Susanti, R.; Durka, W.; Muellner-Riehl, A.N. Deep phylogeographic splits and limited mixing by sea surface currents govern genetic population structure in the mangrove genus *Lumnitzera* (Combretaceae) across the Indonesian archipelago. *J. Syst. Evol.* **2022**, *61*, 299–314. [\[CrossRef\]](#)
60. Aguilar-Zárate, P.; Wong-Paz, J.E.; Rodríguez-Duran, L.V.; Buenrostro-Figueroa, J.; Michel, M.; Saucedo-Castañeda, G.; Favela-Torres, E.; Ascacio-Valdés, J.A.; Contreras-Esquivel, J.C.; Aguilar, C.N. Online monitoring of *Aspergillus niger* GH1 growth in a bioprocess for the production of ellagic acid and ellagitannase by solid-state fermentation. *Bioresour. Technol.* **2018**, *247*, 412–418. [\[CrossRef\]](#)
61. Martínez, A.T.; Ruiz-Dueñas, F.J.; Camarero, S.; Serrano, A.; Linde, D.; Lund, H.; Vind, J.; Tovborg, M.; Herold-Majumdar, O.M.; Hofrichter, M.; et al. Oxidoreductases on their way to industrial biotransformations. *Biotechnol. Adv.* **2017**, *35*, 815–831. [\[CrossRef\]](#)
62. Gasparetti, C.; Nordlund, E.; Jänis, J.; Buchert, J.; Kruus, K. Extracellular tyrosinase from the fungus *Trichoderma reesei* shows product inhibition and different inhibition mechanism from the intracellular tyrosinase from *Agaricus bisporus*. *Biochim. Biophys. Acta* **2012**, *1824*, 598–607. [\[CrossRef\]](#)
63. Wu, Y.; Teng, Y.; Li, Z.; Liao, X.; Luo, Y. Potential role of polycyclic aromatic hydrocarbons (PAHs) oxidation by fungal laccase in the remediation of an aged contaminated soil. *Soil Biol. Biochem.* **2008**, *40*, 789–796. [\[CrossRef\]](#)
64. Shanmugapriya, S.; Manivannan, G.; Selvakumar, G.; Sivakumar, N. Extracellular fungal peroxidases and laccases for waste treatment: Recent improvement. In *Recent Advancement in White Biotechnology through Fungi: Vol. 3: Perspective for Sustainable Environments*, 1st ed.; Yadav, A.N., Singh, S., Mishra, S., Gupta, A., Eds.; Springer International Publishing: Cham, Switzerland, 2019; pp. 153–187, ISBN 978-3-030-25505-3.
65. Strittmatter, E.; Serrer, K.; Liers, C.; Ullrich, R.; Hofrichter, M.; Piontek, K.; Schleicher, E.; Plattner, D.A. The toolbox of *Auricularia auricula-judae* dye-decolorizing peroxidase—Identification of three new potential substrate-interaction sites. *Arch. Biochem. Biophys.* **2015**, *574*, 75–85. [\[CrossRef\]](#)
66. Sáez-Jiménez, V.; Acebes, S.; Guallar, V.; Martínez, A.T.; Ruiz-Dueñas, F.J. Improving the oxidative stability of a high redox potential fungal peroxidase by rational design. *PLoS ONE* **2015**, *10*, e0124750. [\[CrossRef\]](#) [\[PubMed\]](#)
67. Ascacio-Valdés, J.A.; Aguilera-Carbó, A.F.; Buenrostro, J.J.; Prado-Barragán, A.; Rodríguez-Herrera, R.; Aguilar, C.N. The complete biodegradation pathway of ellagitannins by *Aspergillus niger* in solid-state fermentation. *J. Basic Microbiol.* **2016**, *56*, 329–336. [\[CrossRef\]](#) [\[PubMed\]](#)

68. Yan, Y.; Tang, J.; Yuan, Q.; Liu, H.; Huang, J.; Hsiang, T.; Bao, C.; Zheng, L. Ornithine decarboxylase of the fungal pathogen *Colletotrichum higginsianum* plays an important role in regulating global metabolic pathways and virulence. *Environ. Microbiol.* **2022**, *24*, 1093–1116. [[CrossRef](#)] [[PubMed](#)]
69. Kourist, R.; Guterl, J.-K.; Miyamoto, K.; Sieber, V. Enzymatic decarboxylation—An emerging reaction for chemicals production from renewable resources. *ChemCatChem* **2014**, *6*, 689–701. [[CrossRef](#)]
70. Li, M.; Kai, Y.; Qiang, H.; Dongying, J. Biodegradation of gallotannins and ellagitannins. *J. Basic Microbiol.* **2006**, *46*, 68–84. [[CrossRef](#)] [[PubMed](#)]
71. Zhang, W.-K.; Xu, J.-K.; Zhang, X.-Q.; Yao, X.-S.; Ye, W.-C. Chemical constituents with antibacterial activity from *Euphorbia sororia*. *Nat. Prod. Res.* **2008**, *22*, 353–359. [[CrossRef](#)]
72. Reif, B.; Köck, M.; Kerssebaum, R.; Kang, H.; Fenical, W.; Griesinger, C. ADEQUATE, a new set of experiments to determine the constitution of small molecules at natural abundance. *J. Magn. Reson.* **1996**, *118*, 282–285. [[CrossRef](#)]
73. Köck, M.; Kerssebaum, R.; Bermel, W. A broadband ADEQUATE pulse sequence using chirp pulses. *Magn. Reson. Chem.* **2003**, *41*, 65–69. [[CrossRef](#)]
74. Halgren, T.A. Merck molecular force field. I. basis, form, scope, parameterization, and performance of MMFF94. *J. Comput. Chem.* **1996**, *17*, 490–519. [[CrossRef](#)]
75. Hehre, W.J.; Lathan, W.A. Self-consistent molecular orbital methods. XIV. an extended Gaussian-type basis for molecular orbital studies of organic molecules. Inclusion of second row elements. *J. Chem. Phys.* **1972**, *56*, 5255–5257. [[CrossRef](#)]
76. Adamo, C.; Barone, V. Exchange functionals with improved long-range behavior and adiabatic connection methods without adjustable parameters: The mPW and mPW1PW models. *J. Chem. Phys.* **1998**, *108*, 664–675. [[CrossRef](#)]
77. Perdew, J.P.; Chevary, J.A.; Vosko, S.H.; Jackson, K.A.; Pederson, M.R.; Singh, D.J.; Fiolhais, C. Atoms, molecules, solids, and surfaces: Applications of the generalized gradient approximation for exchange and correlation. *Phys. Rev. B Condens. Matter* **1992**, *46*, 6671–6687. [[CrossRef](#)] [[PubMed](#)]
78. Ditchfield, R. Self-consistent perturbation theory of diamagnetism. *Mol. Phys.* **1974**, *27*, 789–807. [[CrossRef](#)]
79. Tomasi, J.; Mennucci, B.; Cammi, R. Quantum mechanical continuum solvation models. *Chem. Rev.* **2005**, *105*, 2999–3093. [[CrossRef](#)] [[PubMed](#)]
80. Lodewyk, M.W.; Siebert, M.R.; Tantillo, D.J. Computational prediction of ^1H and ^{13}C chemical shifts: A useful tool for natural product, mechanistic, and synthetic organic chemistry. *Chem. Rev.* **2012**, *112*, 1839–1862. [[CrossRef](#)]
81. Rablen, P.R.; Pearlman, S.A.; Finkbiner, J. A comparison of density functional methods for the estimation of proton chemical shifts with chemical accuracy. *J. Phys. Chem.* **1999**, *103*, 7357–7363. [[CrossRef](#)]
82. Jain, R.; Bally, T.; Rablen, P.R. Calculating accurate proton chemical shifts of organic molecules with density functional methods and modest basis sets. *J. Org. Chem.* **2009**, *74*, 4017–4023. [[CrossRef](#)]
83. Bally, T.; Rablen, P.R. Quantum-chemical simulation of ^1H NMR spectra. 2. Comparison of DFT-based procedures for computing proton-proton coupling constants in organic molecules. *J. Org. Chem.* **2011**, *76*, 4818–4830. [[CrossRef](#)]
84. Smith, S.G.; Goodman, J.M. Assigning stereochemistry to single diastereoisomers by GIAO NMR calculation: The DP4 probability. *J. Am. Chem. Soc.* **2010**, *132*, 12946–12959. [[CrossRef](#)]
85. Grimblat, N.; Zanardi, M.M.; Sarotti, A.M. Beyond DP4: An improved probability for the stereochemical assignment of isomeric compounds using quantum chemical calculations of NMR shifts. *J. Org. Chem.* **2015**, *80*, 12526–12534. [[CrossRef](#)]
86. Ware, I.; Franke, K.; Hussain, H.; Morgan, I.; Rennert, R.; Wessjohann, L.A. Bioactive phenolic compounds from *Peperomia obtusifolia*. *Molecules* **2022**, *27*, 4363. [[CrossRef](#)] [[PubMed](#)]

Disclaimer/Publisher's Note: The statements, opinions and data contained in all publications are solely those of the individual author(s) and contributor(s) and not of MDPI and/or the editor(s). MDPI and/or the editor(s) disclaim responsibility for any injury to people or property resulting from any ideas, methods, instructions or products referred to in the content.

4 Phytochemical profiling of the Omani medicinal plant *Terminalia dhofarica* (syn. *Anogeissus dhofarica*)

Jonas Kappen¹, Luay Rashan², Katrin Franke¹, and Ludger A. Wessjohann^{1,3}

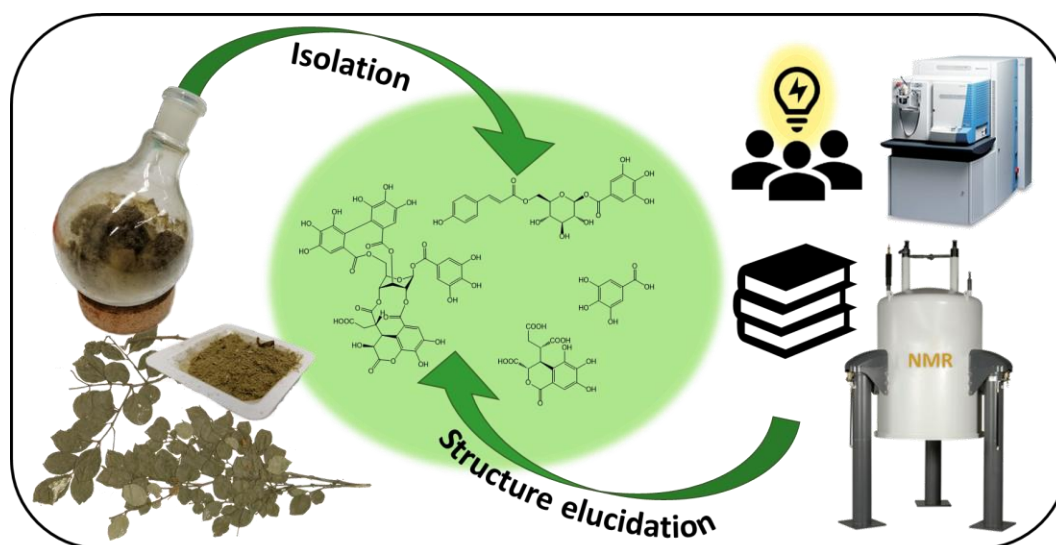
¹ Department of Bioorganic Chemistry, Leibniz Institute of Plant Biochemistry (IPB), 06120 Halle (Saale), Germany

² Biodiversity Unit, Research Center, Dhofar University, Salalah, Oman.

³ Institute of Chemistry, Martin Luther University Halle-Wittenberg, 06120 Halle (Saale), Germany

submitted to *Molecules* (MDPI) in January 2025

Graphical Abstract



Abstract

Several polyphenol-rich *Terminalia* species (Combretaceae) are known to accelerate wound healing. Recently, the Omani medicinal plant *Anogeissus dhofarica* (now *Terminalia dhofarica*) was attributed to the genus *Terminalia* based on phylogenetic studies. Leaves, bark, and extracts of *T. dhofarica* are traditionally used for various medicinal purposes, including wound treatment and personal hygiene. In the present study, the phytochemical profile of leaves from *T. dhofarica* was evaluated by Ultra-High-Performance Liquid Chromatography coupled with Electrospray Ionization High-Resolution Mass Spectrometry (UHPLC-ESI-HRMS), and Nuclear Magnetic Resonance (NMR) spectroscopy. Simple phenolics, polyphenolics (e.g. flavonoids, tannins) and their glucosides were characterized as major metabolite classes. In addition, 20 phenolics were isolated and structurally identified. Fifteen of these compounds were never described before for *T. dhofarica*. For the first time, we provide complete NMR data for 1-*O*-galloyl-6-*O*-*p*-coumaroyl- β -D-glucose (**1**). Biological screening demonstrated a moderate efficacy against Gram-negative bacteria as well as the phytopathogenic fungus *Septoria tritici* and the oomycete *Phytophthora infestans*. In summary, the data expand the knowledge of the phytochemistry of the underexplored species *T. dhofarica* and underscores its potential for therapeutic applications, particularly in the context of traditional medicine.

Keywords

Terminalia dhofarica, *Anogeissus*, Phytochemical profiling, UHPLC-HRMS, NMR, Structure elucidation, antibiotic, antifungal

4.1 Introduction

Terminalia dhofarica (A.J.Scott) Gere & Boatwr. (formerly referred to by the homotypic synonym *Anogeissus dhofarica* A.J.Scott) belongs to the Combretaceae family and is an endemic species of the Dhofar region in Oman and southeastern Yemen, thriving in monsoon ecosystems [1]. Previously integrated in the genus *Anogeissus*, it was transferred with the whole genus *Anogeissus* into the genus *Terminalia* in 2017 [2–4] which led to formal taxonomic name changes.

The former genus *Anogeissus* is primarily distributed across southern Asia, the Arabian Peninsula, and West Africa [5]. Many former *Anogeissus* species have significant ethnomedicinal uses ranging from gastric disorders, skin diseases, and diabetes to wound healing and coughs [6–9]. The bioactivity is primarily attributed to their high content of phenolic compounds such as gallic acid, ellagic acid, and their derivatives, as well as flavonoids like quercetin and rutin [10,11].

Traditionally, leaves, bark, and extracts of *T. dhofarica* are used for various medicinal purposes, including wound treatment and as antiseptic in personal hygiene [8,12]. Previous studies showed that aqueous and alcoholic extracts with a high phenolic content exhibit potent antioxidant activity and display antibacterial and antifungal activities [8,13]. Despite its traditional use and the promising activities, the phytochemical and pharmacological profile of *T. dhofarica* remained underexplored compared to other species of the former genus. However, it is highly probable that it shares many of its bioactive compound classes with other members of the genus. These bioactives include tannins, phenolics, flavonoids, and terpenoids [10]. Recent investigations by Maqsood et al. [14] and Abuarqoub et al. [15] lead to a tentative annotation of 28 compounds, predominantly flavonoids and phenolic acids. These results are in line with the confirmed strong antioxidant and radical scavenging properties. Additionally, the extracts showed potential anticancer, antidiabetic, and anti-inflammatory activities, promote fibroblast migration and enhance wound healing, which confirmed its traditional medicinal uses [14,15].

The current study represents the first comprehensive phytochemical characterization of the species. Methanolic crude extracts from leaves were analyzed by UHPLC-ESI-HRMS and NMR for major metabolites and screened for antibacterial and antifungal activity. The identity of constituents was verified by isolation, characterization and complete structure elucidation based on extensive spectroscopic methods.

4.2 Material and methods

General

Thin layer chromatography (TLC) analyses were performed on silica gel 60 normal phase (SG60), silica gel 60 reversed phase 18 F₂₅₄ (Merck, Darmstadt, Germany) or silica gel 60 reversed phase 2 UV₂₅₄ (Macherey-Nagel, Düren, Germany) using different solvent systems. To visualize the compound spots, long-wavelength UV light (366 nm), short-wavelength UV light (254 nm) and spraying with vanillin-H₂SO₄ reagent, followed by heating or spraying with natural product spray reagent (1 g 2-aminoethyl diphenylborinate/200 mL methanol) were applied.

Low-resolution ESI-MS spectra were performed on a Sciex API-3200 instrument (Applied Biosystems, Concord, Ontario, Canada) combined with a HTC-XT autosampler (CTC Analytics, Zwingen, Switzerland). The UV spectra were recorded on a Jasco V-770 UV-Vis/NIR spectrophotometer (Jasco, Pfungstadt, Germany), using a 10 mm quartz glass cuvette. The specific rotation was recorded on a Jasco P-2000 digital polarimeter (Jasco, Pfungstadt, Germany), using the software Spectra Manager 2 (version

2.14.02). The circular dichroism (CD) spectra were recorded on a Jasco J1500 CD spectrometer (Jasco, Pfungstadt, Germany), using the software Spectra Manager 2 (version 2.15.04).

The semi-preparative HPLC was performed on a Shimadzu prominence system which consists of a SPD-M20A diode array detector, a FRC-10A fraction collector, a CBM-20A communications bus module, a DGU-20A5R degassing unit, a LC-20AT liquid chromatograph, and a SIL-20A HT auto sampler.

^1H and ^{13}C NMR spectra were recorded on an Agilent DD2 400 NMR spectrometer at 399.917 and 100.570 MHz, respectively. Chemical shifts are reported relative to TMS (^1H NMR) or peaks of solvent. For samples with low concentration, 1D ^1H and ^{13}C NMR spectra and 2D spectra (HSQC, HMBC, COSY, TOCSY, NOESY) were recorded on a Bruker Avance Neo 500 NMR spectrometer at 500.234 and 125.797 MHz, respectively, using a 5 mm prodigy probe with the TopSpin 4.0.7 spectrometer software or on an Agilent VNMR5 600 MHz NMR spectrometer equipped with 5 mm inverse detection cryoprobe, using standard CHEMPACK 8.1 pulse sequences implemented in Varian VNMRJ 4.2 spectrometer software.

Plant material

Leaves of *Terminalia dhofarica* (A.J.Scott) Gere & Boatwr. were collected in autumn 2019 and 2020 in Dhofar, Oman. The leaves were shadow-dried at room temperature, pulverized, and stored at room temperature. A voucher (ADA/11/2020) was deposited in the herbarium of the Natural & Medical Sciences Research Center, University of Nizwa, Oman.

Isolation

Dried pulverized leaves (300 g) from *Terminalia dhofarica* were exhaustively extracted assisted by ultrasonication with 80% aq. methanol to give 92 g of dried crude extract after evaporation of the solvent. An aliquot of the crude extract (30.8 g) was successively partitioned by liquid-liquid-extraction between water (700 mL) and *n*-heptane (2 x 250 mL), followed by ethyl acetate (6 x 300 mL). This resulted into three fractions: *n*-heptane (1.6 g), ethyl acetate (4.2 g) and water (20.8 g).

The ethyl acetate fraction was submitted to a RP18 column (l: 34 cm, d: 3.5 cm) and eluted with a mixture of methanol and water (1:1, v/v) which yielded three fractions (A1-A3), based on the TLC profile (RP18, MeOH/H₂O, 1:1, v/v) of which A1 (R_f 0.95 – 0.59) and A2 (R_f 0.59 – 0.38) were further purified. A3 was identified as ellagic acid (**12**, 547.4 mg, R_f = 0.36 in MeOH/H₂O (1:1, v/v) on RP18).

A1 was submitted to a Sephadex G10 column (l: 120 cm, d: 3.5 cm) with a mixture of methanol and water (1:4, v/v), yielding seven fractions (B1 – B7), based on the TLC profile (RP18, MeOH/H₂O, 2:3, v/v), of which B2 (R_f 0.98 – 0.88), B5 (R_f 0.79 – 0.62), and B6 (R_f 0.62 – 0.31) were further purified. B3 (R_f 0.83) was identified as gallic acid (**4**), 153.8 mg, R_f = 0.83 in MeOH/H₂O (2:3, v/v) on RP18.

B2 was purified by preparative reversed phase HPLC (Agilent-Zorbax Eclipse-XDB C18, 5 μm , 9.4 mm x 250 mm) using a water + 0.1 % formic acid (A) and methanol + 0.1 % formic acid (B) gradient system (0–3.0 min, 5% B; 3.0–43.0 min, 5–25% B) and a flow rate of 1.50 mL/min at 25 °C to yield chebulic acid (**7**) (4.6 mg, R_t = 8.80 min), 1-*O*-galloyl-D-glucose (**15**) (2.5 mg, R_t = 12.48 min), protocatechuic acid (**3**) (3.5 mg, R_t = 26.71 min), 12-*O*-methyl chebulic acid (**8**) (8.9 mg, R_t = 28.93 min), 11, 12-*O*-dimethyl chebulic acid (**9**) (4.1 mg, R_t = 38.07 min), and 12, 13-*O*-dimethyl chebulic acid (**10**) (6.5 mg, R_t = 41.40 min).

B5 was submitted to a RP18 column (l: 36 cm, d: 3.5 cm) with a gradient of methanol and water (500 mL, 1:4, v/v; 500 mL, 1:2, v/v; 500 mL, 2:3, v/v), yielding nine fractions (C1 – C9), based on the TLC profile

(RP18, MeOH/H₂O, 1:1, v/v), of which C4 (R_f 0.72), and C7 (R_f 0.70 – 0.54) were further purified.

C4 was submitted to a Sephadex LH20 column (l: 60 cm, d: 2.5 cm) with methanol yielding eight fractions (D1 – D8) of which D3 was identified as chebulagic acid (**18**) (16.5 mg, R_f = 0.57 in MeOH/H₂O (2:3, v/v) on RP18.

C7 was purified by preparative reversed phase HPLC (YMC-Triart C18, 5 μ m, 10 mm x 150 mm) using a water + 0.1 % formic acid (A) and methanol + 0.1 % formic acid (B) gradient system (0–2.5 min, 35% B; 2.5–22.5 min, 35–50% B; 22.5–27.5 min, 50–60% B) and a flow rate of 2.64 mL/min at 25 °C to yield 7''-*O*-methyl flavogallionate (**13**) (2.1 mg, R_t = 11.50 min), and 11-*O*-methyl brevifolincarboxylate (**11**) (1.5 mg, R_t = 13.80 min).

B6 submitted to a RP18 column (l: 36 cm, d: 3.5 cm) and eluted with a 10% step gradient of methanol and water with 0.1 % TFA (10 - 40% MeOH, each 250 mL; 50 – 90 % MeOH, each 200 mL; 100% MeOH, 400 mL) which yielded thirteen fractions (E1-E13), based on the TLC profile (RP18, MeOH/H₂O, 2:3, v/v) of which E8 (R_f 0.63 – 0.25) further purified.

E8 was purified by preparative reversed phase HPLC (Agilent-Zorbax Eclipse-XDB C18, 5 μ m, 9.4 mm x 250 mm) using a water + 0.1 % formic acid (A) and methanol + 0.1 % formic acid (B) gradient system (0–6.0 min, 25% B; 6.0–36.0 min, 25–45% B; 36.0–37.0 min, 45–100%) and a flow rate of 3.3 mL/min at 25 °C to yield phyllanembilin C (**20**) (1.2 mg, R_t = 11.62 min), chebulanin (**17**) (2.4 mg, R_t = 15.92 min), 3,5-di-*O*-galloylshikimic acid (**16**) (1.4 mg, R_t = 18.38 min), and 6'-*O*-methyl-chebulagic acid (**20**) (4.8 mg, R_t = 21.74 min).

A2 was submitted to a Sephadex LH20 column (l: 75 cm, d: 2.5 cm) with methanol, yielding four fractions (F1 – F5), based on the TLC profile (RP18, MeOH/H₂O, 1:1, v/v), of which F1 (R_f 0.62), F2 (R_f 0.55), and F4 (R_f 0.36 – 0.24) were further purified. F3 (R_f 0.53) was identified as 7-*O*-methyl gallic acid (**5**) (15.2 mg, R_f = 0.53 in MeOH/H₂O (1:1, v/v) on RP18.

F1 was purified by preparative reversed phase HPLC (YMC-ODS-A C18, 12 μ m, 10.0 mm x 150 mm) using a water + 0.1 % formic acid (A) and methanol + 0.1 % formic acid (B) gradient system (0–2.5 min, 30% B; 2.5–17.5 min, 30–45% B) and a flow rate of 3.6 mL/min at 25 °C to yield *trans*-*p*-coumaric acid (**6**) (3.3 mg, R_t = 8.41 min).

F2 was purified by preparative reversed phase HPLC (Merck-LiChrospher C18, 5 μ m, 10.0 mm x 250 mm) using a water (A) and acetonitrile (B) gradient system (0–3.5 min, 12% B; 3.5–18.5 min, 12–20% B) and a flow rate of 4.00 mL/min at 25 °C to yield *p*-hydroxybenzaldehyde (**2**) (2.9 mg, R_t = 15.89 min).

F4 was purified by analytical reversed phase HPLC (YMC-ODS-A C18, 12 μ m, 10.0 mm x 150 mm) using a water (A) and methanol (B) gradient system (0–2.5 min, 20% B; 2.5–20.0 min, 20–38% B) and a flow rate of 4.80 mL/min at 25 °C to yield 6-*O*-*trans*-*p*-coumaroyl-D-glucopyranose (**14**) (0.9 mg, R_t = 9.45 min), and 1-*O*-galloyl-6-*O*-*trans*-*p*-coumaroyl-D-glucopyranose (**1**) (0.6 mg, R_t = 19.97 min).

High resolution

The UHPLC-ESI-HRMS spectra were acquired using a TripleTOF (time of flight) 6600-1 mass spectrometer (Sciex, Darmstadt) in positive and negative ion modes. Samples (2 μ L) were loaded on an Waters Acquity UPLC® BEH C18 column (1.7 μ m, 130 Å, 50 × 2.1 mm I.D., Waters GmbH, Eschborn, Germany) under isocratic conditions (3% eluent B, 1 min), and separated using a linear gradient from 3% to 95% eluent B in 5 min. Separation was performed on an ACQUITY UPLC I-Class UHPLC System

(Waters GmbH, Eschborn, Germany) with a flow rate of 0.4 mL/min and 55 °C column temperature. Eluents A and B were water and acetonitrile, with 0.1% formic acid. The mass spectrometer was equipped with an ESI-DuoSpray ion source (spray voltage: 5.5 kV (positive mode), 4.5 kV (negative mode), nebulizer gas: 60 psi, source temperature: 450 °C, drying gas: 70 psi, curtain gas: 55 psi) and was controlled by Analyst 1.7.1 TF software (Sciex, Darmstadt). Data acquisition was performed in MS1-TOF mode in a mass range of m/z 65 to 1250 with an accumulation time of 75 ms. The mass spectrometer was externally calibrated with calibration solutions provided by the manufacturer for positive and negative modes. For MS²-TOF mode the declustering potential was 35 V and the collision potential was 10 V, respectively. The product ion spectra (tandem mass spectra, MS/MS) were acquired in the high sensitivity mode (accumulation time 20 ms) in the m/z range of 50–1000 using unit Q1 resolution with mass resolution above 30,000. Collision potential (CE) was set from –80 to –20 V in negative ion mode. The data were evaluated by Peak View 1.2.0.3 software (AB Sciex GmbH, Darmstadt, Germany).

Biological assays

Antibacterial Assays

The compounds were evaluated against the Gram-negative *Aliivibrio fischeri* (DSM507) and the Gram-positive *Bacillus subtilis* 168 (DSM 10), as described by Kappen et al. [16]. The tests were performed in 96-well plates based on the bioluminescence (*A. fischeri*) or absorption (*B. subtilis*) read-out. Chloramphenicol (100 M) was used as a positive control to induce complete inhibition of bacterial growth. The results (mean \pm standard deviation value, $n = 6$) are given in relation to the negative control (bacterial growth, 1% DMSO without test compound) as relative values (percent inhibition). Negative values indicate an increase in bacterial growth.

Antifungal Assay

The antifungal activity was tested on the phytopathogenic ascomycetes *Botrytis cinerea* Pers. and *Septoria tritici* Desm. and the oomycete *Phytophthora infestans* (Mont.) de Bary in 96-well microtiter plate assays according to protocols from the Fungicide Resistance Action Committee (FRAC) with minor modifications as described by Kappen et al. [16]. Briefly, the isolated compounds were tested at the highest concentration of 500 μ g/mL, while the solvent DMSO in buffer was used as a negative control (max. concentration 2.5%). The commercially used fungicides, epoxiconazole and terbinafine (Sigma-Aldrich, Darmstadt, Germany), served as reference compounds. The pathogen growth was evaluated seven days after inoculation by measurement of the optical density (OD) at L 405 nm with a TecanGENios Pro microplate reader (five measurements per well using multiple reads in 3 x 3 square). Each experiment was carried out in triplicate.

Spectroscopic data

Full data sets for compounds **1-20** are available in the Supporting information and in accordance with available literature [17-37]

4.3 Results and discussion

Dried leaves from *T. dhofarica* were pulverized and exhaustively extracted with 80% methanol to yield a crude extract. On one hand this extract was screened for antibacterial and antifungal activity (fig S4-1–S4-4) to detect bioactivity and to compare with literature reports. On the other hand, it was used to analyze the metabolite profile using UHPLC-ESI-HRMS (fig 4-2, table 4-1). Additionally, an aliquot of the powder was extracted with deuterated methanol and subjected to NMR analysis (fig 4-1).

In our investigation, the methanolic crude extract of leaves exhibited moderate activity against Gram-negative bacteria (*A. fischeri* at a concentration of 500 µg/mL, fig S4-1) but showed no activity against Gram-positive bacteria (*B. subtilis*, data not shown). The literature on this topic is mixed. Maqsood et al. reported no activity against Gram-negative bacteria (*E. hormaechei*) but observed significant inhibition of Gram-positive bacteria (*S. aureus*) in a ZOI assay [14]. Conversely, Marwah et al. reported substantial activity against Gram-positive bacteria (*S. aureus* at 250 µg/mL) and moderate activity against Gram-negative bacteria (*P. aeruginosa* at 500 µg/mL) [8]. Our results do not fully align with available literature reports, potentially due to differences in assay methods, bacterial strains, choice of plant material and extraction conditions (u.i. for artifact formation). Notably, while both previous studies used mixed plant material for extraction, this analysis focused exclusively on leaves.

The NMR screening of the crude leaf extract reveals a profile consistent with the known characteristics of both the species and its genus. Many intense singlet signals appear in the aromatic region of the ¹H spectrum, between 6.2 and 7.5 ppm (fig 4-1 C). The HSQC spectrum associates these signals with a consistent ¹³C shift of approximately 115 ppm (fig 4-1 D). These shifts align remarkably well with protons of gallic acid and its derivatives, such as ellagic acid or follow-up tannin structures. In addition to the expected signals for fatty acids (fig 4-1 A) and free sugars (fig 4-1 B), several distinct signals were identified that, according to literature reports, could be attributed to derivatives with a chebulic acid core (fig 4-1 A–D). Both compound groups, gallic acid derivatives and chebulic acid derivatives overlap for certain compounds, e.g. chebulagic acid (**18**), and are well-known classes within the genus [10] and even reported for the species itself [14].

The presence of gallic acid, chebulic acid and diverse derivatives was further confirmed through UHPLC-ESI-HRMS analysis, which provided a more detailed view of the complexity and diversity of metabolites (table 4-1, fig 4-2). A total of 33 metabolites were preliminary annotated from the total ion chromatogram (TIC) of the crude extract, although in some cases compounds eluted simultaneously and other detected signals remain unidentified.

The majority of all 33 annotations belong to phenolic acids (table 4-1, P1 gallic acid + quinic acid; P3 protocatechuic acid; P11 *p*-coumaric acid), tannins (table 4-1, P2; P3 terflavin B, *O*-galloyl punicalin; P4; P5; P6 brevifolincarboxylate; P7 *O*-galloyl bis-*O*-HHDP-glucose; P8; P9; P10; P12; P13; P14, P16, P17, P18 *O*-methyl ellagic acid, P21, P22), or flavonoids (table 4-1, P7 gallocatechin, P15; P18 galloylvitexin isomer; P19; P20), following the classification of compounds by Singh et al. [10]. Consequently, *T. dhofarica* appears to possess a metabolic profile closely resembling that of its relatives within the genus [10,14,15]. During the isolation process, the crude extract was purified by liquid-liquid partition and different chromatographic techniques. This resulted in the isolation of 20 compounds (fig 4-3). Compound **1**, (1-*O*-galloyl-6-*O*-*p*-coumaroyl-D-glucose) a twice modified glucose molecule with gallic acid at position 1 and *p*-coumaric acid at position 6 was postulated by Mei et al. based on extensive HRMS fragmentation analysis only [17]. Here we provide for the first time complete NMR data for compound **1**. Notably, it was isolated as a mixture of α - and β -D-glucoside. The other compounds were identified by extensive spectroscopic analysis (HRMS, NMR) and comparison with previously reported data from literature. A full spectroscopic data set for compounds **2–20** can be found in the supporting information.

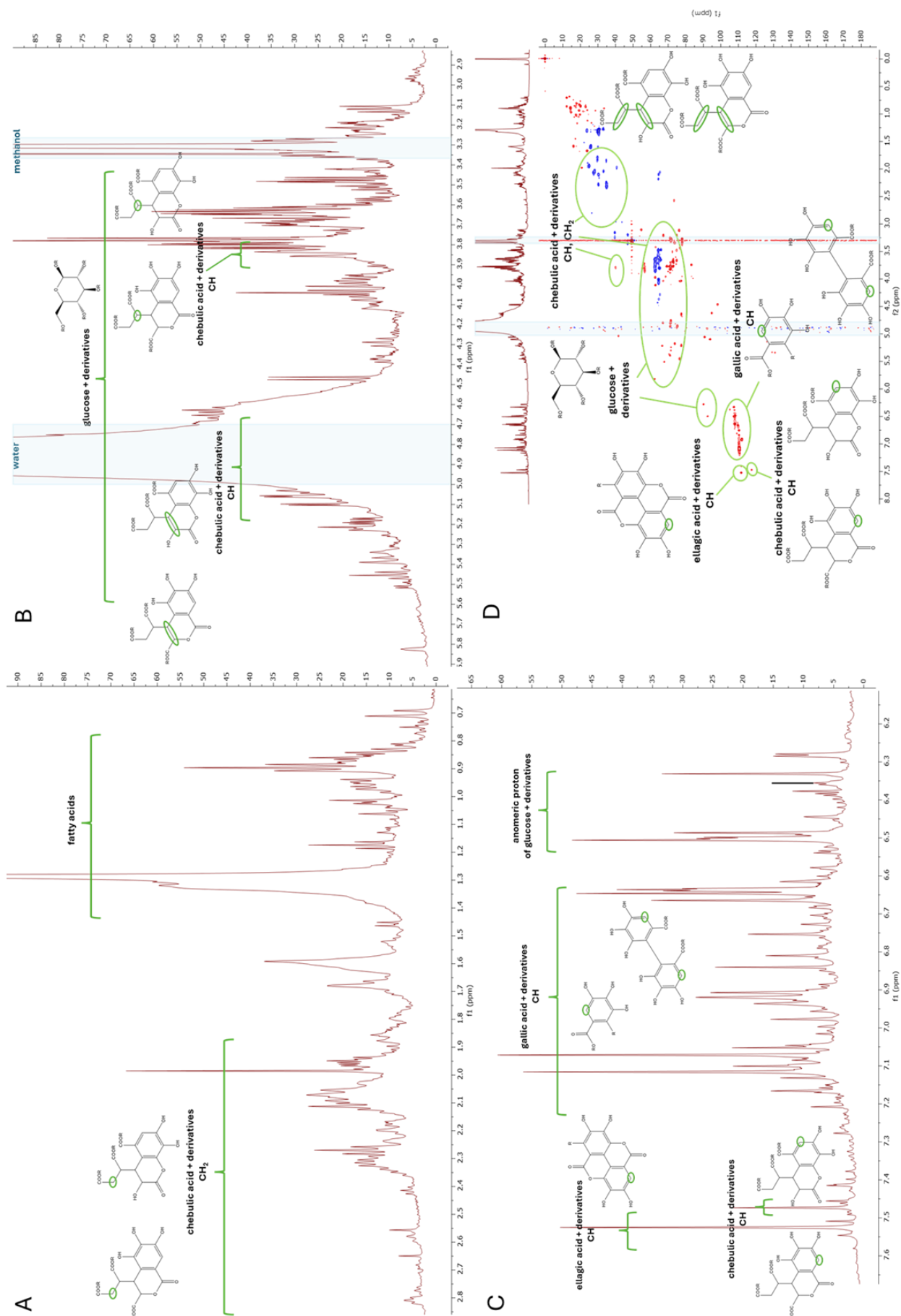


Fig 4-1 NMR screening of crude extract; **A** 0 – 2.9 ppm Chebolic acid and fatty acids; **B** 2.9 – 5.9 ppm Chebolic acid and glucose derivatives; **C** 6.1 – 7.5 ppm Aromatic signals, gallic acid and derivatives; **D** HSQC with annotation of $^1J_{\text{CH}}$ correlations

Table 4-1 Peak list of the UHPLC-ESI-HRMS analysis of the crude extract

Peak	t_R (min)	m/z measured	Error (ppm)	Molecular formula (not ionized)	MS ² product ions, m/z (rel. intensity [%])	Annotation
P1	0.38	169.0151	5.1	C ₇ H ₆ O ₅	169 (28), 125 (100), 81 (6), 79 (22), 69 (6)	[M-H] [−] Gallic acid (4)
		179.0550	−6.2	C ₆ H ₁₂ O ₆	179 (46), 89 (60), 85 (29), 73 (30), 71 (100)	[M-H] [−] Glucose
		191.0562	0.5	C ₇ H ₁₂ O ₆	191 (100), 93 (5), 85 (12)	[M-H] [−] Quinic acid
P2	0.52	355.0310	0.9	C ₁₄ H ₁₂ O ₁₁	355 (31), 337 (100), 293 (6), 249 (29), 205 (50), 193 (40), 187 (8), 179 (22), 163 (26), 149 (18), 135 (5), 121 (3)	[M-H] [−] Chebulic acid (7)
		331.0675	1.3	C ₁₃ H ₁₆ O ₁₀	331 (100), 271 (24), 211 (18), 169 (86), 151 (11), 125 (26), 123 (20), 107 (10)	[M-H] [−] Galloylglucoside e.g. 1- <i>O</i> -Galloyl-β-D-glucose (15)
P3	1.04	153.0191	−1.5	C ₇ H ₆ O ₄	153 (2), 109 (100), 91 (10), 81 (7), 65 (9)	[M-H] [−] Protocatechuic acid (3)
		783.0649	−4.8	C ₃₄ H ₂₂ O ₂₂	783 (100), 631 (3), 481 (4), 451 (16), 301 (53), 275 (14), 257 (3)	[M-H] [−] Terflavin B
		933.0596	−4.7	C ₄₁ H ₂₆ O ₂₆	933 (100), 781 (10), 721 (8), 601 (13), 575 (4), 451 (4), 299 (4)	[M-H] [−] <i>O</i> -Galloyl punicalin e.g. 2- <i>O</i> -Galloyl punicalin
P4	1.58	1083.0570	−2.1	C ₄₈ H ₂₈ O ₃₀	1083 (100), 781 (9), 721 (3), 601 (15), 575 (5), 301 (3) 273 (2)	[M-H] [−] Punicalagin isomer e.g. α-Punicalagin
		541.0243	−3.1	C ₄₈ H ₂₈ O ₃₀	781 (6), 601 (19), 541 (100), 451 (5), 301 (85), 275 (34), 271 (15), 229 (11), 201 (6), 145 (7)	[M-2H] ^{2−} Punicalagin isomer
P5	2.36	1083.0553	−3.7	C ₄₈ H ₂₈ O ₃₀	1083 (100), 781 (10), 721 (2), 601 (18), 575 (5), 301 (2) 273 (2)	[M-H] [−] Punicalagin isomer e.g. β-Punicalagin
		541.0235	−4.6	C ₄₈ H ₂₈ O ₃₀	781 (5), 601 (11), 541 (100), 451 (3), 301 (45), 275 (19), 271 (7), 229 (7), 201 (4), 145 (3)	[M-2H] ^{2−} Punicalagin isomer
P6	2.63	291.0146	−0.1	C ₁₃ H ₈ O ₈	291 (6), 247 (100), 219 (8), 191 (19), 173 (10), 145 (17)	[M-H] [−] Brevifolincarboxylate
		121.0294	−0.9	C ₇ H ₆ O ₂	121 (86), 92 (100), 65 (3)	[M-H] [−] <i>p</i> -Hydroxybenzaldehyde (2)
		1251.0639	n.a.	n.a.	1251 (100), 1207 (75), 1082 (31), 781 (8), 601 (13)	[M-H] [−] unknown
P7	2.82	625.0281	n.a.	n.a.	1083 (7), 781 (6), 625 (6), 603 (100), 603 (30), 541 (80), 531 (11), 301 (81), 275 (32), 273 (17), 229 (12), 123 (11)	[M-2H] ^{2−} unknown
		935.0763	−3.5	C ₄₁ H ₂₆ O ₂₆	935 (100), 633 (9), 301 (5), 275 (17)	[M-H] [−] <i>O</i> -Galloyl bis- <i>O</i> -HHDP-glucose e.g. casuarictin
		305.0693	8.6	C ₁₅ H ₁₄ O ₇	305 (60), 225 (34), 97 (100), 80 (16)	[M-H] [−] Gallocatechin e.g. (+)-Gallocatechin
P8	3.01	325.0920	−2.7	C ₁₅ H ₁₈ O ₈	311 (21), 302 (12), 265 (13), 247 (9), 205 (20), 203 (18), 193 (20), 175 (13), 169 (100), 163 (18), 151 (9), 145 (29), 137 (17), 125 (57), 124 (27), 123 (20), 119 (15), 107 (10), 79 (9)	[M-H] [−] 6- <i>O</i> -trans- <i>p</i> -Coumaroyl-β-D-glucopyranose (14)
		651.0823	−2.46	C ₂₇ H ₂₄ O ₁₉	651 (98), 633 (9), 481 (44), 275 (26), 247 (12), 231 (18), 205 (14), 203 (15), 169 (100), 125 (29)	[M-H] [−] Chebulanin (17)
		469.0039	−2.06	C ₂₁ H ₁₆ O ₁₃	469 (1), 425 (27), 301 (100), 299 (27), 282 (9), 271 (14), 244 (9), 228 (8), 216 (8), 200 (6), 172 (12), 144 (6)	[M-H] [−] Flavogallonnate
P9	3.17	633.0677	−8.90	C ₂₇ H ₂₂ O ₁₈	633 (100), 463 (6), 301 (66), 275 (7)	[M-H] [−] Corillagin

Continuation of Table 4-1 Peak list of the UHPLC-ESI-HRMS analysis of the crude extract

P10	3.31	1235.0712	0.8	C ₅₅ H ₃₂ O ₃₄	1235 (19), 617 (100)	[M-H] ⁻ <i>O</i> -Galloyl punicalagin
		617.0317	0.4	C ₅₅ H ₃₂ O ₃₄	781 (6), 617 (83), 601 (23), 541 (52), 301 (100), 275 (30), 271 (9)	[M-2H] ²⁻ <i>O</i> -Galloyl punicalagin
P11	3.45	163.0401	0.20	C ₉ H ₆ O ₃	163 (3), 119 (100), 117 (8), 93 (62)	[M-H] ⁻ <i>p</i> -Coumaric acid (6)
		600.9896	-0.01	C ₂₈ H ₁₀ O ₁₆	601 (100), 583 (3), 301 (18), 298 (20), 271 (22), 243 (5), 214 (2)	[M-H] ⁻ Terminalin
P12	3.84	433.0397	-3.58	C ₁₉ H ₁₄ O ₁₂	433 (78), 301 (77), 300 (100), 272 (4), 244 (7), 216 (10), 200 (5), 172 (6), 132 (4)	[M-H] ⁻ Ellagic acid glucoside
P13	3.93	953.0899	-0.28	C ₄₁ H ₃₀ O ₂₇	953 (100), 463 (2), 301 (61), 275 (5), 205 (4), 169 (2)	[M-H] ⁻ Chebulagic acid (18)
		476.0410	-0.94	C ₄₁ H ₃₀ O ₂₇	476 (65), 462 (19), 453 (4), 301 (86), 275 (11), 203 (11), 169 (100), 125 (45)	[M-2H] ²⁻ Chebulagic acid (18)
P14	4.02	300.9978	-3.96	C ₁₄ H ₆ O ₈	301 (100), 284 (7), 257 (2), 245 (3), 229 (4), 201 (3), 185 (3), 173 (3), 161 (1), 145 (5)	[M-H] ⁻ Ellagic acid (12)
		603.0021	-5.24	C ₁₄ H ₆ O ₈	301 (100)	[2M-H] ⁻ Ellagic acid (12)
P15	4.20	431.0969	-3.41	C ₂₁ H ₂₀ O ₁₀	431 (48), 341 (25), 323 (6), 311 (100), 283 (54), 269 (6), 161 (6), 117 (8)	[M-H] ⁻ Flavon-C-glucosid e.g. Vitexin (8-C-Glycosyl apigenin)
P16	4.42	955.1002	-5.88	C ₄₁ H ₃₂ O ₂₇	955 (100), 937 (6), 785 (4), 617 (3), 465 (4), 337 (3), 319 (4), 275 (8), 231 (11), 205 (6), 169 (4)	[M-H] ⁻ Chebulinic acid
		477.0466	-5.60	C ₄₁ H ₃₂ O ₂₇	477 (18), 463 (8), 454 (4), 313 (3), 301 (4), 275 (7), 247 (8), 231 (4), 203 (11), 175 (7), 169 (100), 125 (49), 107 (6)	[2M-H] ²⁻ Chebulinic acid
P17	4.53	477.1006	-6.81	C ₂₂ H ₂₂ O ₁₂	477 (100), 313 (6), 265 (26), 235 (7), 211 (5), 205 (7), 169 (37), 163 (6)	[M-H] ⁻ 1- <i>O</i> -Galloyl-6- <i>O</i> - <i>trans-p</i> -coumaroyl-β-D-glucopyranose (1)
P18	4.95	315.0126	-6.48	C ₁₅ H ₈ O ₈	315 (11), 300 (100), 271 (7), 244 (6), 216 (12), 200 (6), 160 (7), 132 (7), 104 (2)	[M-H] ⁻ <i>O</i> -Methyl ellagic acid
		583.1075	-3.14	C ₂₈ H ₂₀ O ₁₄	583 (100), 431 (22), 413 (8), 341 (31), 323 (8), 311 (75), 283 (40), 271 (14), 241 (10), 211 (9), 169 (18), 125 (8)	[M-H] ⁻ Galloylvitexin isomer e.g. 2''- <i>O</i> -Galloylvitexin
P19	5.42	773.3008	-2.34	C ₃₉ H ₃₀ O ₁₆	773 (50), 577 (100), 371 (5), 341 (5), 295 (7), 265 (3), 235 (18), 195 (10), 193 (27), 175 (35), 165 (20), 160 (17), 134 (7)	[M-H] ⁻ unknown
		583.1085	-1.42	C ₂₈ H ₂₂ O ₁₄	583 (84), 431 (37), 341 (55), 311 (100), 323 (17), 283 (53), 271 (27), 211 (14), 169 (23), 125 (9)	[M-H] ⁻ Galloylvitexin isomer e.g. 2''- <i>O</i> -Galloylisovitexin
		547.2170	-2.71	C ₂₈ H ₂₆ O ₁₁	547 (100), 265 (9), 235 (3), 205 (11), 163 (19), 145 (66), 117 (10)	[M-H] ⁻ unknown
P20	5.79	735.1184	-2.57	C ₃₅ H ₂₈ O ₁₈	735 (100), 583 (90), 565 (45), 431 (24), 341 (25), 311 (39), 293 (42), 271 (24), 211 (20), 169 (38), 125 (8)	[M-H] ⁻ Digalloylvitexin isomer e.g. 2'',3''- <i>O</i> -Digalloylvitexin
		545.2010	-3.37	C ₂₈ H ₂₄ O ₁₁	545 (100), 527 (4), 399 (5), 325 (7), 307 (6), 265 (37), 235 (15), 219 (18), 205 (34), 201 (9), 177 (11), 163 (43), 145 (69), 133 (6), 119 (16)	[M-H] ⁻ e.g. cinnamutinosose B
P21	6.24	329.0293	-3.01	C ₁₆ H ₁₀ O ₈	329 (8), 314 (55), 298 (85), 271 (100), 243 (48), 214 (29), 187 (21), 159 (24), 131 (12), 103 (7), 75 (6)	[M-H] ⁻ Di- <i>O</i> -methyl ellagic acid
P22	7.80	343.0443	-4.78	C ₁₇ H ₁₂ O ₈	343 (9), 328 (45), 313 (100), 297 (87), 285 (22), 269 (77), 241 (16), 213 (30), 197 (18), 185 (32), 169 (7), 157 (19), 142 (9), 130 (12)	[M-H] ⁻ Tri- <i>O</i> -methyl ellagic acid
P23	10.17	533.3412	n.a.	n.a.	487 (100)	[M+FA] ⁻ unknown
		487.3361	n.a.	n.a.	487 (100)	[M-H] ⁻ unknown

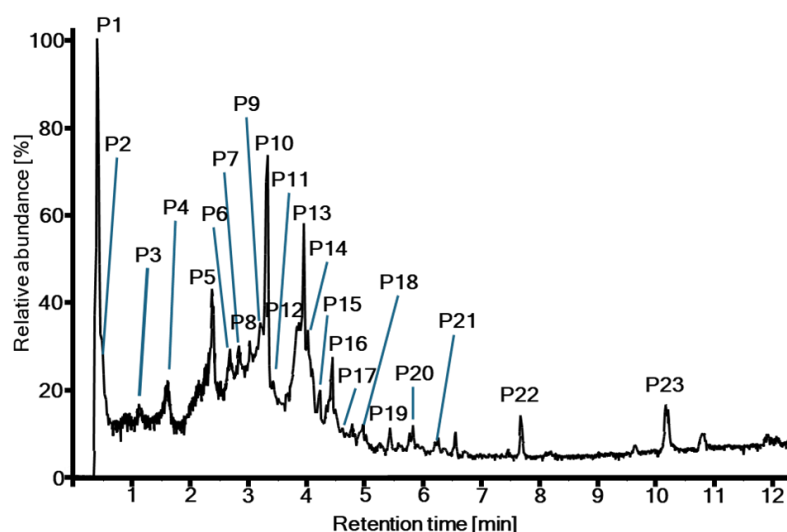


Fig 4-2 UHPLC-ESI-HRMS TIC of the crude extract

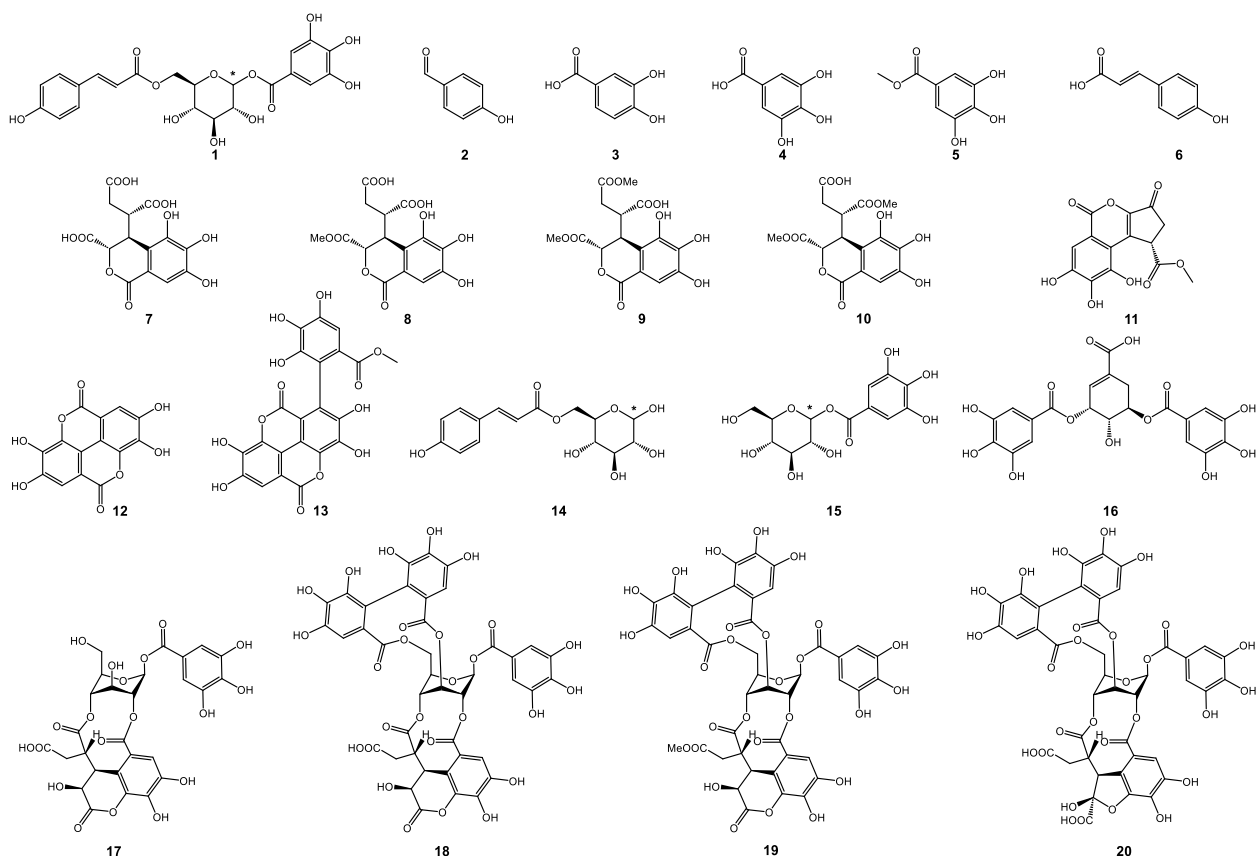


Fig 4-3 Structure of compounds isolated, * both epimers are found

In the study of Abuarqoub et al. [15], seven phenolic acids were identified by retention times of standard substance only. Two of these acids were also found within this study, both in the LC-HRMS screening as well as by isolation approach (gallic acid (**4**), P1; protocatechuic acid (**3**), P3). Noteworthy, Abuarqoub et al. identified *ortho*- and *meta*- but no *para*-coumaric acid which, however, is the only coumaric acid derivative found in this study (**6**, P11). Maqsood et al. [14] annotated 23 compounds by LC-HRMS data from the crude extract. Eight compounds were also found within this study. Remarkably, chebulagic acid

(**18**, P 13), the main compound from this study, was not described by Maqsood et al. although they annotated chebulic acid on one hand and corillagin on the other hand which are the two parts of chebulagic acid. Therefore, the thought accrues that there might be natural product degradation involved. Unfortunately, Maqsood et al. calculated molecular formulas for their annotation based on excessively high error margins [14]. Most of the annotations were done with an error margin of -30 to -50 ppm, but the overall range goes from -299 ppm to $+780$ ppm. This reduces the reliability of these data significantly, since reliable error margins should be lower than ± 10 ppm. However, 15 of 20 isolated compounds within our study were never described before for *T. dhofarica*.

Structure elucidation of compound 1

Compound **1** (fig 4-4) was isolated as a white solid. The molecular formula was identified as $C_{22}H_{22}O_{12}$ by its negative ion at m/z 477.1030 $[M - H]^-$ (calcd. for 477.1038 $C_{22}H_{21}O_{11}^-$) in the ESI-HRMS spectrum. All NMR data as well as 2D correlations are presented in table 4-2. The 1H spectra showed one aromatic singlet at δ 7.13 (2H, s, H-2'+H-6') and two pairs of coupling aromatic protons. The first at δ_H 7.63 and 6.36 (each 1H, *d*, $J = 15.7$ Hz, H-7'' + H-8'') and the second at δ 7.45 and 6.80 (each 2H, *d*, $J = 8.5$ Hz, H-2'' and H-6'' + H-3'' and H-5''). Additionally, a pattern of aliphatic proton signals, in detail two anomeric protons at δ_H 5.66 (1H, *d*, $J = 7.7$ Hz, H-1 β) and 5.66 (1H, *d*, $J = 3.3$ Hz, H-1 α), three multiplet signals at δ_H 3.41-3.46, 3.46-3.52, and 3.65-3.70 as well as a pair of two signals at δ_H 4.31 (1H, *dd*, $J = 5.6, 12.2$ Hz, H-6b) and δ_H 4.50 (1H, *dd*, $J = 2.8, 12.2$ Hz, H-6a) belonging to a CH_2 group suggested the presence of one glucopyranosyl moiety.

This was further supported by strong COSY correlations as well as HSQC correlation of the aliphatic proton signals. The presence of a galloyl group was deduced from HSQC and HMBC correlations of the aromatic proton signal at δ_H 7.13 resulting in the annotation of the ^{13}C signals δ_C 110.5, 120.5, 140.7, 146.6 and 166.9 to this substructure. The pair of aromatic proton signals at δ_H 7.45 and 6.80 strongly suggest a *para* substituted benzene ring. The other pairs at δ 7.63 and 6.36 with the large J of 15.7 Hz indicates a *trans* configured double bond. In combination with the yet to annotate 9 carbons from the molecular formula, this implied the presence of a coumaroyl group. The specific connection pattern of all three moieties was determined by HMBC correlation of the glucose protons H-1 to the galloyl carbon C-7' and of H-6a and H-6b to the coumaroyl carbon C-9'' (table 4-2, fig S4-8). Therefore, the compound is identified as 1-*O*-galloyl-6-*O*-coumaroyl- β -D-glucose. In the glucose moiety α and β configuration appeared in a ratio of 1:1 by comparison of integrals in the 1H spectrum. Structurally, compound **1** is close to fishertannin F (1-*O*-galloyl-6-*O*-feruloyl- β -D-glucose) [38], which possesses an additional methoxy group in the cinnamic acid core. Consequently, the NMR data are mainly in accordance with those reported by Zhang et al. [38].

Remarkably, for compounds **14** and **15**, both anomeric configurations appeared. In the case of **15** both 1H and ^{13}C signals of H-1 overlapped but were still distinguishable in the 1H spectrum due to the different J values. For **14** the two signals for the anomeric proton differ stronger. Compounds **14** (6-*O*-*trans*-*p*-Coumaroyl-D-glucopyranose) and **15** (1-*O*-Galloyl-D-glucose) represent substructures of **1**. This is a well reported phenomenon in tannins [33]. The anomeric protons of the sugar moieties of compounds **17–20** show unusual chemical shifts and small coupling constants (e.g. 6.35, 1H, *d*, $J = 2.8$ Hz, for H-1 in **17**). Usually, β -glucose appears in the energetically favored 4C_1 chair conformation. However, in ellagitannins with bridging 2,4,-*O*-chebuloyl substituents the β -glucose ring is locked into the inverted 1C_4 conformation with all ring protons in equatorial instead of axial positions, resulting in small vicinal couplings (<4 Hz) [36].

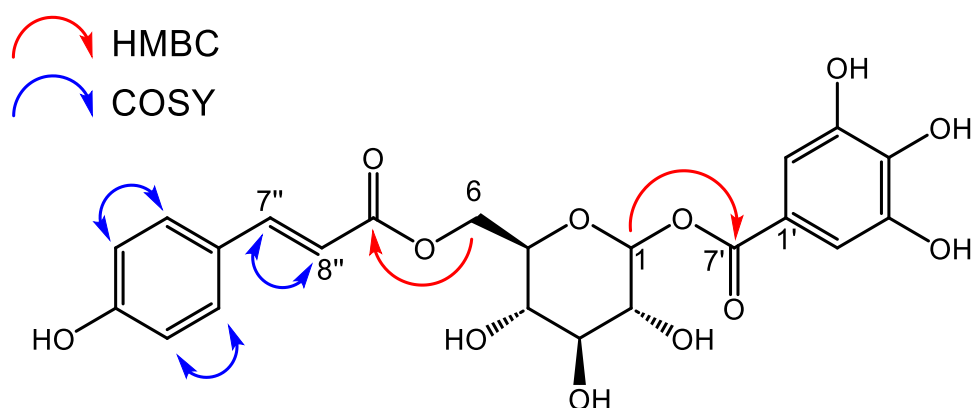


Fig 4-4 Structure of compound **1** with crucial NMR correlations

Table 4-2 NMR data of compound **1**

No.	δ_C	δ_H (multiplicity, J)	HMBC	COSY
Glucose				
1 α	95.9, CH	5.66 (<i>d</i> , 3.3, 0.5H)	3, 4, 7 c	2
1 β		5.66 (<i>d</i> , 7.7, 0.5H)	3, 4, 7 c	2
2	74.1, CH	3.46-3.52 (<i>m</i> , 2H)	1, 3, 4	1, 3
3	78.1, CH	3.46-3.52 (<i>m</i> , 2H)	2, 3, 4	2, 4
4	71.3, CH	3.41-3.46 (<i>m</i> , 1H)	3, 5	3, 5
5	76.3, CH	3.65-3.70 (<i>m</i> , 1H)	1, 3, 4	4, 6a, 6b
6a	64.4, CH ₂	4.50 (<i>dd</i> , $J = 12.2, 2.8$ Hz 1H)	4, 5, 9 $''$	5, 6b
6b	64.4, CH ₂	4.31 (<i>dd</i> , $J = 12.2, 5.6$ Hz, 1H)	4, 5, 9 $''$	5, 6a
Galloyl				
1 c	120.5, C	-	-	-
2 c /6 c	110.5, CH	7.13 (<i>s</i> , 2H)	1 c , 2 c , 3 c , 4 c , 5 c , 6 c , 7 c	-
3 c /5 c	146.6, C	-	-	-
4 c	140.7, C	-	-	-
7 c	166.9, C	-	-	-
Coumaroyl				
1 $''$	127.2, C	-	-	-
2 $''$ /6 $''$	131.2, CH	7.45 (<i>d</i> , $J = 8.5$ Hz, 2H)	2 $''$, 4 $''$, 6 $''$, 7 $''$	3 $''$, 5 $''$
3 $''$ /5 $''$	116.9, CH	6.80 (<i>d</i> , $J = 8.5$ Hz, 2H)	1 $''$, 3 $''$, 4 $''$, 5 $''$	2 $''$, 6 $''$
4 $''$	161.3, C	-	-	-
7 $''$	146.9, CH	7.63 (<i>d</i> , $J = 15.7$ Hz, 1H)	1 $''$, 2 $''$, 6 $''$, 8 $''$, 9 $''$	8 $''$
8 $''$	114.9, CH	6.36 (<i>d</i> , $J = 15.7$ Hz, 1H)	1 $''$, 9 $''$	7 $''$
9 $''$	169.1, C	-	-	-

Evaluation of artifacts

Remarkably, some of the isolated compounds exhibited methylations of carboxyl functional groups (**5**, **8**, **9**, **10**, **11**, **13**, and **19**). However, these compounds were absent in the UHPLC-ESI-HRMS analysis of the crude extract but their unmethylated form was detected such as chebulic acid (**7**) (table 4-1, P2), brevifolincarboxylate (table 4-1, P6), or flavogallonnate (table 4-1, P8). Since methanol was used for extraction of the plant material and as a solvent in multiple purification steps, the mentioned compounds may be artifacts of the isolation process rather than true metabolites of *T. dhofarica*. To investigate this possibility, a small-scale extraction of leaves was performed with methanol vs. ethanol. The analysis of

both total ion chromatograms (TICs) revealed all above-mentioned compounds as probable artifacts. Exemplary, figs 4-5 presents the extracted ion chromatogram (XIC) of the methanolic and ethanolic extracts, filtered for pure chebulagic acid as well as its methylated and ethylated derivatives. The pure compound is present in both extracts, confirming it as a true metabolite. However, the methylated derivative appears only in the methanolic extract, and the ethylated derivative solely in the ethanolic extract, strongly suggesting both are artifacts. This finding is particularly noteworthy, as methylated chebulagic acid was also reported as an artifact in the isolation of *Terminalia chebula* Retz., another species from of the genus [2,39]. In contrast, true methylated metabolites, such as methylated derivatives of ellagic acid (table 1, P18, P21, and P22) were confirmed by UHPLC-ESI-HRMS analysis in both extracts. Thus, to the best of our knowledge, 13 of 20 isolated compounds are likely of plant origin and from these 9 compounds (**1**; **2**; **6**; **14** – **18**; **20**) are described for the first time within this species.

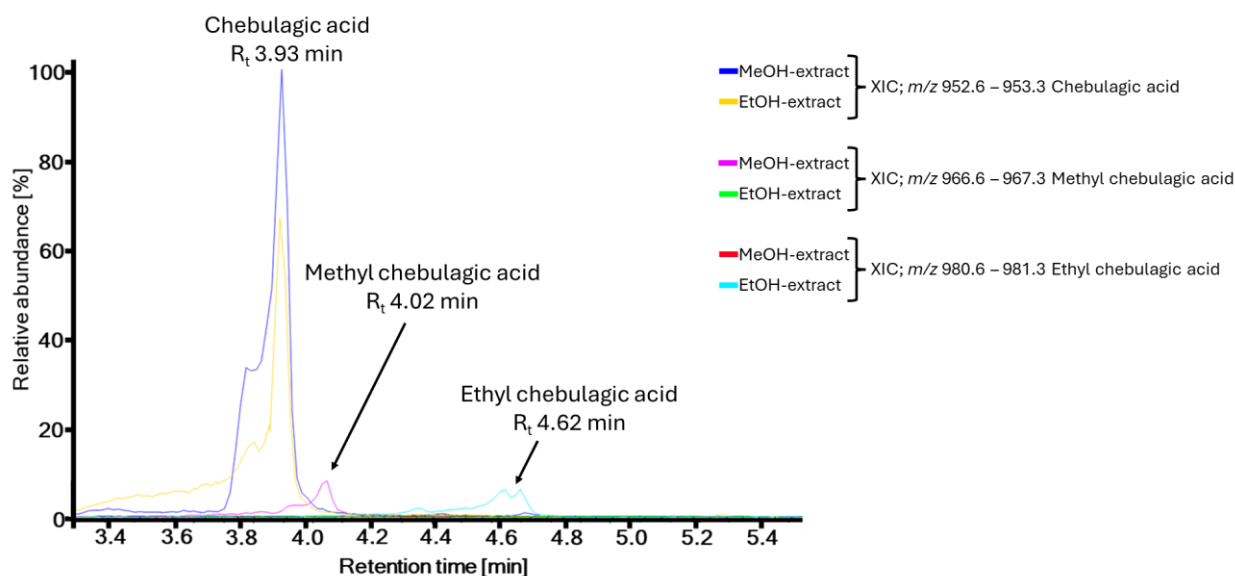


Fig 4-5 Test for artefacts on the example of chebulagic acid and methyl chebulagic acid

Biological activity

Based on the biological effects of the crude extract, all isolated compounds and potential artifacts were screened for biological activity against the Gram-negative bacterium *A. fischeri*, as well as the pathogenic fungi *B. cinerea*, *S. tritici* and *P. infestans*. In contrast to expectations, none of the isolated compounds exhibited inhibitory effects on *A. fischeri*, although, the crude extract displayed moderate activity (fig S4-1). This suggests that the active compound was either not isolated, modified (e.g. by methylation), or that synergistic effects were required, which may have been lost during the separation of synergistic partners. Several compounds demonstrated some level of activity against *S. tritici* and *P. infestans*, although none exhibited outstanding effects at concentrations of 1 μ M (fig S4-2 – S4-4). The most remarkable effect can be reported for the artefact 6'-*O*-methyl-chebulagic acid (**19**), that showed 82% of inhibition against *P. infestans* at a concentration of 10 μ M. The reported antifungal properties of *T. dhofarica* may thus be attributed to the combined effects of various active compounds with nonspecific activity. This is common for mixtures of plant phenolics. It is in alignment with the use of crude mixtures in external (or intestinal) applications, as tanning and gluing effect underlying these compounds effects on microorganism is not systemic.

Conclusion

In conclusion, the Omani medicinal plant *Terminalia dhofarica* was found to be very rich in phenolic acids, tannins, and flavonoids as well as their glucosides as major compound classes. This is consistent with other species in the genus. A total of 20 compounds were isolated, including the first full characterization of compound **1** with a complete set of NMR data to unequivocally determine its structure. However, a critical examination of the data revealed that seven compounds isolated are likely artifacts of the isolation process. Therefore, 13 compounds remain with true plant origin, of which 9 were described for the first time within this species. The evaluation of biological activities of the isolated compounds within this study can corroborate the reported non systemic use of *T. dhofarica* extracts. However, the scope of yet performed studies falls short of adequately identifying all phytochemical compounds relevant for its bioactivity and medicinal applications. Therefore, further studies are needed.

References

- [1] Kürschner, H.; Hein, P.; Kilian, N.; Hubaishan, M.A., The *Hybantho durae-Anogeissetum dhofaricae* ass. nova - phytosociology, structure and ecology of an endemic South Arabian forest community, *Phyto* **2004**, 34, 569–612, doi:10.1127/0340-269X/2004/0034-0569.
- [2] Maurin, O.; Gere, J.; van der Bank, M.; Boatwright, J.S., The inclusion of *Anogeissus*, *Buchenavia* and *Pteleopsis* in *Terminalia* (Combretaceae: Terminaliinae), *Bot. J. Linn.* **2017**, 184, 312–325, doi:10.1093/botlinnean/box029.
- [3] IPNI. *Anogeissus dhofarica*, International Plant Names Index. Available online: <https://www.ipni.org/n/169727-1> (accessed on 8 November 2024).
- [4] IPNI. *Terminalia dhofarica*, International Plant Names Index. Available online: <https://www.ipni.org/n/77164562-1> (accessed on 8 November 2024).
- [5] Scott, A.J., A revision of *Anogeissus* (Combretaceae), *Kew Bulletin* **1979**, 33, 555, doi:10.2307/4109799.
- [6] Jain, A.; Katewa, S.S.; Galav, P.K.; Sharma, P., Medicinal plant diversity of Sitamata wildlife sanctuary, Rajasthan, India. *J. Ethnopharmacol.* **2005**, 102, 143–157, doi:10.1016/j.jep.2005.05.047.
- [7] Meena, K.L.; Yadav, B.L., Studies on ethnomedicinal plants conserved by Garasia tribes of Sirohi district, Rajasthan, India, *Indian J. Nat. Prod. Resour.* **2010**, 1, 500–506.
- [8] Marwah, R.G.; Fatope, M.O.; Mahrooqi, R.A.; Varma, G.B.; Abadi, H.A.; Al-Burtamani, S.K.S., Antioxidant capacity of some edible and wound healing plants in Oman, *Food Chem.* **2007**, 101, 465–470, doi:10.1016/j.foodchem.2006.02.001.
- [9] Manosroi, J.; Moses, Z.Z.; Manosroi, W.; Manosroi, A. Hypoglycemic activity of Thai medicinal plants selected from the Thai/Lanna medicinal recipe database MANOSROI II, *J. Ethnopharmacol.* **2011**, 138, 92–98, doi:10.1016/j.jep.2011.08.049.
- [10] Singh, D.; Baghel, U.S.; Gautam, A.; Baghel, D.S.; Yadav, D.; Malik, J.; Yadav, R., The genus *Anogeissus*: A review on ethnopharmacology, phytochemistry and pharmacology. *J. Ethnopharmacol.* **2016**, 194, 30–56, doi:10.1016/j.jep.2016.08.025.
- [11] Barthélemy, A.; Latifou, L.; Dodehe, Y.; Cyril, A.; Catherine, V.-S., In vitro antiplasmodial and antileishmanial activities of flavonoids from *Anogeissus leiocarpus* (Combretaceae), *Int. J. Pharm. Sci. Rev. Res.* **2011**, 11 (2), 1–6.
- [12] Miller, A.G.; Morris, M., *Plants of Dhofar: The southern region of Oman; traditional, economic and medicinal uses*, First published; The Office of The Adviser for Conservation of The Environment: Oman, **1988**, ISBN 0715708082.
- [13] Al-Noumani, A.J.; Al-Qasbi, M.Z.J.; Al-Shabibi, A.S.A.; Al-Mashani, S.A.I.; Said, S.A., Antimicrobial, antioxidant and cytotoxic activities of *Anogeissus dhofarica* from Oman, *Int. J. Recent Adv. Pharm. Res.* **2013**, 3 (3), 35–38.
- [14] Maqsood, R.; Khan, F.; Ullah, S.; Khan, A.; Al-Jahdhami, H.; Hussain, J.; Weli, M.; Maqsood, D.; Rahman, S.M.; Hussain, A.; Ur Rehman, N.; Al-Harrasi, A., Evaluation of antiproliferative, antimicrobial, antioxidant, antidiabetic and phytochemical analysis of *Anogeissus dhofarica* A. J. Scott, *Antibiotics* **2023**, 12, 354, doi:10.3390/antibiotics12020354.
- [15] Abuarqoub, D.; Aburayyan, W.; Rashan, L.; Dayyih, W.A.; Al-Matubsi, H.Y., Phytochemical analysis and in vitro investigation of wound healing, cytotoxicity, and inflammatory response in potentially active extracts of *Anogeissus dhofarica*, *J. Appl. Pharm. Sci.* **2024**, 14 (10), 152–162, doi:10.7324/JAPS.2024.174429.
- [16] Kappen, J.; Manurung, J.; Fuchs, T.; Vemulapalli, S.P.B.; Schmitz, L.M.; Frolov, A.; Augusta, A.; Muellner-Riehl, A.N.; Griesinger, C.; Franke, K.; Wessjohann, L.A., Challenging structure elucidation of lumnitzeralactone, an ellagic acid derivative from the mangrove *Lumnitzera racemosa*, *Mar. Drugs* **2023**, 21, 242, doi:10.3390/md21040242.
- [17] Mei, Y.; Hu, Y.; Tao, X.; Shang, J.; Qian, M.; Suo, F.; Li, J.; Cao, L.; Wang, Z.; Xiao, W., Chemical profiling of shen-wu-yi-shen tablets using UPLC-Q-TOF-MS/MS and its quality evaluation based on UPLC-DAD combined with multivariate statistical analysis, *J. Chromatogr. Sci.* **2024**, 62, 534–553, doi:10.1093/chromsci/bmae001.
- [18] Kuivila, H.G.; Nahabedian, K.V., Electrophilic displacement reactions. X. General acid catalysis in the protodeboronation of areneboronic acids 1–3, *J. Am. Chem. Soc.* **1961**, 83, 2159–2163, doi:10.1021/ja01470a028.
- [19] Yan, P.; Zeng, R.; Bao, B.; Yang, X.-M.; Zhu, L.; Pan, B.; Niu, S.-L.; Qi, X.-W.; Li, Y.-L.; Ouyang, Q., Red light-induced highly efficient aerobic oxidation of organoboron compounds using spinach as a photocatalyst, *Green Chem.* **2022**, 24, 9263–9268, doi:10.1039/D2GC03055A.
- [20] Meng, Q.; Li, G.; Luo, B.; Wang, L.; Lu, Y.; Liu, W., Screening and isolation of natural antioxidants from *Ziziphora clinopodioides* Lam. with high performance liquid chromatography coupled to a post-column Ce(IV) reduction capacity assay, *RSC Adv.* **2016**, 6, 62378–62384, doi:10.1039/C6RA08588A.
- [21] Zaher, A.M.; Anwar, W.S.; Makboul, M.A.; Abdel-Rahman, I.A.M., Potent anticancer activity of (Z)-3-hexenyl- β -D-glucopyranoside in pancreatic cancer cells, *Naunyn Schmiedeberg's Arch. Pharmacol.* **2024**, 397, 2311–2320, doi:10.1007/s00210-023-02755-4.

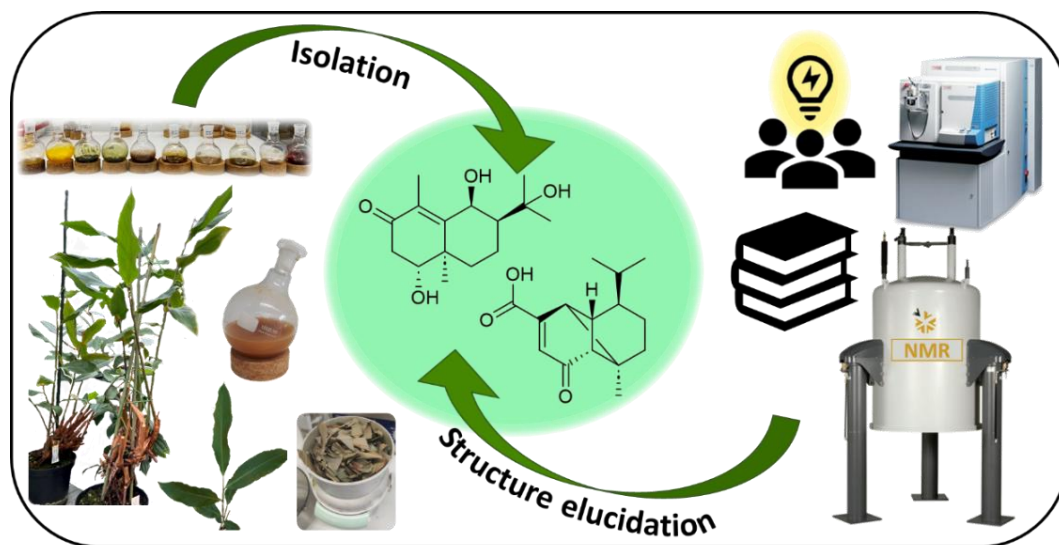
- [22] Xu, K.-Z.; Xiang, S.-L.; Wang, Y.-J.; Wang, B.; Jia, A.-Q., Methyl gallate isolated from partridge tea (*Mallotus oblongifolius* (Miq.) Müll.Arg.) inhibits the biofilms and virulence factors of *Burkholderia thailandensis*, *J. Ethnopharmacol.* **2024**, *320*, 117422, doi:10.1016/j.jep.2023.117422.
- [23] Terfassi, S.; Dauvergne, X.; Cérantola, S.; Lemoine, C.; Bensouici, C.; Fadila, B.; Christian, M.; Marchioni, E.; Benayache, S., First report on phytochemical investigation, antioxidant and antidiabetic activities of *Helianthemum getulum*, *Nat. Prod. Res.* **2022**, *36*, 2806–2813, doi:10.1080/14786419.2021.1928664.
- [24] Liao, C.-R.; Kuo, Y.-H.; Ho, Y.-L.; Wang, C.-Y.; Yang, C.-S.; Lin, C.-W.; Chang, Y.-S., Studies on cytotoxic constituents from the leaves of *Elaeagnus oldhamii* Maxim. in non-small cell lung cancer A549 cells, *Molecules* **2014**, *19*, 9515–9534, doi:10.3390/molecules19079515.
- [25] Lee, H.-S.; Jung, S.-H.; Yun, B.-S.; Lee, K.-W., Isolation of chebulic acid from *Terminalia chebula* Retz. and its antioxidant effect in isolated rat hepatocytes, *Arch. Toxicol.* **2007**, *81*, 211–218, doi:10.1007/s00204-006-0139-4.
- [26] Lee, D.Y.; Kim, H.W.; Yang, H.; Sung, S.H., Hydrolyzable tannins from the fruits of *Terminalia chebula* Retz and their α -glucosidase inhibitory activities, *Phytochemistry* **2017**, *137*, 109–116, doi:10.1016/j.phytochem.2017.02.006.
- [27] Zhao, H.-Y.; Lan, Q.; He, S.; Su, B.-J.; Wang, Y.-Q.; Liao, H.-B.; Wang, H.-S.; Liang, D., Chebulic acid derivatives from *Balakata baccata* and their antineuroinflammatory and antioxidant activities, *Bioorg. Chem.* **2021**, *116*, 105332, doi:10.1016/j.bioorg.2021.105332.
- [28] Chen, F.; Yang, L.; Zhai, L.; Huang, Y.; Chen, F.; Duan, W.; Yang, J., Methyl brevifolincarboxylate, a novel influenza virus PB2 inhibitor from *Canarium album* (Lour.) Raeusch, *Chem. Biol. Drug Des.* **2020**, *96*, 1280–1291, doi:10.1111/cbdd.13740.
- [29] Yang, Z.-N.; Su, B.-J.; Wang, Y.-Q.; Liao, H.-B.; Chen, Z.-F.; Liang, D., Isolation, absolute configuration, and biological activities of chebulic acid and brevifolincarboxylic acid derivatives from *Euphorbia hirta*, *J. Nat. Prod.* **2020**, *83*, 985–995, doi:10.1021/acs.jnatprod.9b00877.
- [30] Navarro, F.; Hamri, S.; Reches, R.; Viñas, M.; Jahani, D.; Ginard, J.; Vilardell, J.; Abián, O.; Pujol, M.D., Convenient synthesis of ellagic acid from methyl gallate and SARS-CoV-2 3CLpro antiviral activity, *Synthesis* **2023**, *55*, 657–662, doi:10.1055/a-1941-1437.
- [31] Srivastava, S.; Mishra, D.; Bisht, R.; Savita, K.; Singh, K.; Rani, P.; Chanda, D.; Dev, K., Psiguanol, a novel α -pyrone derivative from *Psidium guajava* leaves and vasorelaxant activity in rat aorta cells through intracellular cGMP-dependent opening of calcium-activated potassium channels, *Nat. Prod. Res.* **2024**, 1–14, doi:10.1080/14786419.2023.2294477.
- [32] Marzouk, M.S.A.; El-Toumy, S.A.A.; Moharram, F.A.; Shalaby, N.M.M.; Ahmed, A.A.E., Pharmacologically active ellagitannins from *Terminalia myriocarpa*, *Planta Med.* **2002**, *68*, 523–527, doi:10.1055/s-2002-32549.
- [33] Shimomura, H.; Sashida, Y.; Adachi, T., Phenylpropanoid glucose esters from *Prunus buergeriana*, *Phytochemistry* **1988**, *27*, 641–644, doi:10.1016/0031-9422(88)83165-0.
- [34] Ni, J.-C.; Shi, J.-T.; Tan, Q.-W.; Chen, Q.-J., Phenylpropionamides, piperidine, and phenolic derivatives from the fruit of *Ailanthus altissima*, *Molecules* **2017**, *22*, 2107, doi:10.3390/molecules22122107.
- [35] Cheng, M.-J.; Wu, M.-D.; Khamthong, N.; Tseng, M., Polar metabolites from the actinobacterium *Isoptericola chiayiensis* isolated from mangrove soil, *Chem. Nat. Compd.* **2021**, *57*, 1134–1136, doi:10.1007/s10600-021-03569-7.
- [36] Pfundstein, B.; El Desouky, S.K.; Hull, W.E.; Haubner, R.; Erben, G.; Owen, R.W., Polyphenolic compounds in the fruits of Egyptian medicinal plants (*Terminalia bellerica*, *Terminalia chebula* and *Terminalia horrida*): characterization, quantitation and determination of antioxidant capacities, *Phytochemistry* **2010**, *71*, 1132–1148, doi:10.1016/j.phytochem.2010.03.018.
- [37] Zhang, Y.J.; Abe, T.; Tanaka, T.; Yang, C.R.; Kouno, I., Phyllanemblinins A–F, new ellagitannins from *Phyllanthus emblica*, *J. Nat. Prod.* **2001**, *64*, 1527–1532, doi:10.1021/np010370g.
- [38] Zhang, J.; Li, Y.-N.; Guo, L.-B.; He, J.; Liu, P.-H.; Tian, H.-Y.; Zhang, W.-K.; Xu, J.-K., Diverse gallotannins with α -glucosidase and α -amylase inhibitory activity from the roots of *Euphorbia fischeriana* Steud, *Phytochemistry* **2022**, *202*, 113304, doi:10.1016/j.phytochem.2022.113304.
- [39] Lee, D.Y.; Yang, H.; Kim, H.W.; Sung, S.H., New polyhydroxytriterpenoid derivatives from fruits of *Terminalia chebula* Retz. and their α -glucosidase and α -amylase inhibitory activity, *Bioorg. Med. Chem. Lett.* **2017**, *27*, 34–39, doi:10.1016/j.bmcl.2016.11.039.

5 Exploring *Hornstedtia scyphifera*: An extensive multimethod phytochemical investigation reveals the chemical composition and bioactive potential

Jonas Kappen, Andreea David, Klara Pieplow, Annika Wujtschik, Ismail Ware, Dipendu Dhar, Christoph Wagner, Mehdi D. Davari, Katrin Franke, and Ludger A. Wessjohann

Discover Plants 2025, 2, 6; <https://doi.org/10.1007/s44372-024-00085-0>

Graphical abstract



Abstract

Hornstedtia scyphifera (J.Koenig) Steud. represents a lesser-known member of the ginger family (Zingiberaceae) that is used in Malaysia as spice and traditional medicine. The phytochemical investigation of leaves from this species utilizing diverse analytical methods has provided comprehensive insights into its chemical profile for the first time. Headspace gas chromatography-mass spectrometry (HS-GCMS) and GCMS analyses of essential oil and nonpolar extracts verified α -pinene, camphene, *p*-cymene, and camphor as main volatile compounds. Metabolite profiling of the crude extract by ultra-high-performance-liquid chromatography-high resolution mass spectrometry (UHPLC-HRMS) unveiled terpenoids, flavonoids and other phenolics as major compound classes. Isolation and follow-up structure elucidation, involving 1D and 2D NMR, HRMS, UV and CD analysis, yielded two new sesquiterpenoids, (1*R*,5*S*,6*S*,7*R*,10*R*)-mustak-14-oic acid (**1**) and (1*R*,6*S*,7*S*,10*R*)-6-hydroxy-anhuienosol (**2**), along with 24 known compounds (seven terpenoids, seven flavonoids, ten phenolics), 21 of these never reported for *H. scyphifera*. Additionally, the crude extract and fractions from the purification process were screened for antibacterial and antifungal activity. This is supplemented by an extensive literature research for described bioactivities of all isolated compounds. Our results support and explain previously detected antimicrobial, antifungal and neuroprotective effects of *H. scyphifera* extracts and provide evidence for its potential pharmacological importance.

Keywords

Hornstedtia scyphifera; phytochemical investigation; sesquiterpenes; antimicrobial

Discover Plants statement concerning permissions

Open Access This article is licensed under a Creative Commons Attribution 4.0 International License, which permits use, sharing, adaptation, distribution and reproduction in any medium or format, as long as you give appropriate credit to the original author(s) and the source, provide a link to the Creative Commons licence, and indicate if changes were made. The images or other third party material in this article are included in the article's Creative Commons licence, unless indicated otherwise in a credit line to the material. If material is not included in the article's Creative Commons licence and your intended use is not permitted by statutory regulation or exceeds the permitted use, you will need to obtain permission directly from the copyright holder. To view a copy of this licence, visit <http://creativecommons.org/licenses/by/4.0/>.

Discover Plants

Research

Exploring *Hornstedtia scyphifera*: an extensive multimethod phytochemical investigation reveals the chemical composition and bioactive potentialJonas Kappen¹ · Andreea David^{1,2} · Klara Pieplow^{1,3} · Annika Wujtschik^{1,3} · Ismail Ware⁴ · Dipendu Dhar¹ · Christoph Wagner³ · Mehdi D. Davari¹ · Katrin Franke^{1,5,6} · Ludger A. Wessjohann^{1,3,5}

Received: 9 August 2024 / Accepted: 27 December 2024

Published online: 15 January 2025

© The Author(s) 2025 **OPEN**

Abstract

Hornstedtia scyphifera (J.Koenig) Steud. represents a lesser-known member of the ginger family (Zingiberaceae) that is used in Malaysia as spice and traditional medicine. The phytochemical investigation of leaves from this species utilizing diverse analytical methods has provided comprehensive insights into its chemical profile for the first time. Headspace gas chromatography-mass spectrometry (HS-GCMS) and GCMS analyses of essential oil and nonpolar extracts verified α -pinene, camphene, *p*-cymene, and camphor as main volatile compounds. Metabolite profiling of the crude extract by ultra-high-performance-liquid chromatography-high resolution mass spectrometry (UHPLC-HRMS) unveiled terpenoids, flavonoids and other phenolics as major compound classes. Isolation and follow-up structure elucidation, involving 1D and 2D NMR, HRMS, UV and CD analysis, yielded two new sesquiterpenoids, (1*R*,5*S*,6*S*,7*R*,10*R*)-mustak-14-oic acid (**1**) and (1*R*,6*S*,7*S*,10*R*)-6-hydroxy-anhuenosol (**2**), along with 24 known compounds (seven terpenoids, seven flavonoids, ten phenolics), 21 of these never reported for *H. scyphifera*. Additionally, the crude extract and fractions from the purification process were screened for antibacterial and antifungal activity. This is supplemented by an extensive literature research for described bioactivities of all isolated compounds. Our results support and explain previously detected antimicrobial, antifungal and neuroprotective effects of *H. scyphifera* extracts and provide evidence for its potential pharmacological importance.

Keywords *Hornstedtia scyphifera* · Phytochemical investigation · Sesquiterpenes · Antimicrobial

Supplementary Information The online version contains supplementary material available at <https://doi.org/10.1007/s44372-024-00085-0>.

✉ Katrin Franke, kfranke@ipb-halle.de; ✉ Ludger A. Wessjohann, wessjohann@ipb-halle.de | ¹Department of Bioorganic Chemistry, Leibniz Institute of Plant Biochemistry (IPB), 06120 Halle (Saale), Germany. ²Department of Food Science, Faculty of Food Science and Technology, University of Agricultural Sciences and Veterinary Medicine of Cluj-Napoca, 400372 Cluj-Napoca-Napoca, Romania. ³Institute of Chemistry, Martin Luther University Halle-Wittenberg, 06120 Halle (Saale), Germany. ⁴Biotechnology Research Institute, University Malaysia Sabah, Jalan UMS, Kota Kinabalu, 88400 Sabah, Malaysia. ⁵German Centre for Integrative Biodiversity Research (iDiv) Halle-Jena-Leipzig, 04103 Leipzig, Germany. ⁶Institute of Biology/Geobotany and Botanical Garden, Martin Luther University Halle-Wittenberg, 06120 Halle (Saale), Germany.



Discover Plants

(2025) 2:6

| <https://doi.org/10.1007/s44372-024-00085-0>

1 Introduction

The Zingiberaceae family, commonly known as the ginger family, represents the largest family within the Zingiberales order and comprises 53 genera and over 1200 species [1]. The family is subdivided into four major tribes: Alpinieae, Globbeae, Hedychieae, and Zingibereae, distinguished by morphological features only [1]. They grow in tropical regions such as India, Asia, Africa, and Australia [1, 2], characterized as perennial herbaceous species with fleshy-thickened rhizomes [3]. While many species have traditional applications as spices or ornamentals, they are also valued as herbal medicine [2]. The therapeutic properties of numerous members of this family are largely attributed to their abundant bioactive compounds [4, 5], such as terpenes, terpenoids, and flavonoids [6–8]. In the plant, some of these compounds serve to deter herbivores, combat microbial infections, or protect against solar radiation, while others attract pollinators through color or scent [6, 7, 9]. For humans, these secondary metabolites offer various pharmaceutical advantages. So far, extracts and isolates from Zingiberaceae members demonstrated antioxidative [10–12], antimicrobial [11], anti-inflammatory [10, 12] and anticancer [11, 12] properties or even neuroprotective activity [13], indicating considerable potential for application in contemporary medicine.

One of the lesser-known representatives of this highly potent family is *Hornstedtia scyphifera* (J.Koenig) Steud., also known as *Amomum scyphiferum* J.Koenig, *Cardamomum scyphiferum* (J.Koenig) Kuntze, *Greenwaya scyphifer* (J.Koenig) Giseke or *Greenwaya scyphiferus* (J.Koenig) Giseke [14]. The genus *Hornstedtia* comprises about 43 species found in tropical Southeast Asia from the Malay peninsula to the Himalayas [15, 16]. *H. scyphifera* is morphologically characterized by a robust rhizome, positioned just below or at the ground surface and large leaf shoots reaching 2–5 m in height, adorned with green leaves covered at the base by sheaths. The plant bears short inflorescences with a series of scales surrounding the floral bracts. The red flowers open individually for one day and develop smooth, elongated fruits. *H. scyphifera* appears to be the most common species of the genus in Malaysia [15], where it is traditionally used as a spice and for insect repellency [15, 17]. The essential oils from various organs are well researched and predominantly consist of mono- and sesquiterpenes as well as terpenoids, such as camphor and germacrene D, but also borneol and β -selin [17]. However, studies on non-volatile compounds are lacking except for two brief reports describing the isolation of four flavonoids (quercetin, 5-hydroxy-3,7,4'-trimethoxyflavon, kumatakenin, 3,5-dimethylkaempferol), two phytosterols (stigmast-4-en-3-one, 6-hydroxy-stigmast-4-en-3-one) and a fatty acid (dodecanoic acid) from *H. scyphifera* leaves [18, 19]. Extracts of *H. scyphifera* leaves show promising antibacterial and antioxidative activities [18], as well as anti-inflammatory and neuroprotective properties [20]. These effects may be ascribed to a high concentration of sesquiterpenes, which have been linked to antidepressant and neuroprotective properties [13], although other substances may also be involved.

In this study, we conducted a comprehensive phytochemical investigation focusing on both the volatile compounds and the isolation of the non-volatile compounds to fully evaluate the chemical composition and biological activity of *H. scyphifera*.

2 Materials and methods

2.1 General experimental procedures

Thin layer chromatography (TLC) analyses were performed on silica gel 60 normal phase (SG60), silica gel 60 reversed phase 18 F₂₅₄ (Merck, Darmstadt, Germany) or silica gel 60 reversed phase 2 UV₂₅₄ (Macherey–Nagel, Düren, Germany) using different solvent systems. To visualize the compound spots, long-wavelength UV light (366 nm), short-wavelength UV light (254 nm) and spraying with vanillin–H₂SO₄ reagent, followed by heating or spraying with natural product spray reagent (1 g 2-aminoethyl diphenylborinate/200 mL methanol) were applied.

Low-resolution ESI–MS spectra were performed on a Sciex API-3200 instrument (Applied Biosystems, Concord, Ontario, Canada) combined with a HTC-XT autosampler (CTC Analytics, Zwingen, Switzerland). The UV spectra were recorded on a Jasco V-770 UV–Vis/NIR spectrophotometer (Jasco, Pfungstadt, Germany), using a 10 mm quartz glass cuvette. The specific rotation was recorded on a Jasco P-2000 digital polarimeter (Jasco, Pfungstadt, Germany), using the software Spectra Manager 2 (version 2.14.02). The circular dichroism (CD) spectra were recorded on a Jasco J1500 CD spectrometer (Jasco, Pfungstadt, Germany), using the software Spectra Manager 2 (version 2.15.04). The

ultrasound assisted extraction of plant material was performed on a Bandelin Sonorex RK 510 H (9.7 L) (Bandelin electronic GmbH & Co. KG, Berlin, Germany) at 35 kHz for 60 min per cycle.

The semi-preparative HPLC was performed on a Shimadzu prominence system which consists of a SPD-M20A diode array detector, a FRC-10A fraction collector, a CBM-20A communications bus module, a DGU-20A5R degassing unit, a LC-20AT liquid chromatograph, and a SIL-20A HT auto sampler. The following columns were used for separation: column 1 (YMC Pack Pro C18, 5 μ m, 120 Å, 150 \times 4.6 mm I.D., YMC, USA), column 2 (YMC Pack Pro C18, 5 μ m, 120 Å, 150 \times 10.0 mm I.D., YMC, USA) and column 3 (Agilent Eclipse XDB-C18, 5 μ m, 80 Å, 250 \times 9.4 mm I.D., Agilent, USA). Water (A)/methanol (B) (solvent system 1) or water (A)/acetonitrile (B) (solvent system 2) each with 0.1% formic acid were used as mobile phases at a temperature of 25 °C applying different gradients.

^1H and ^{13}C NMR spectra were recorded on an Agilent DD2 400 NMR spectrometer at 399.917 and 100.570 MHz, respectively. Chemical shifts are reported relative to TMS (^1H NMR) or peaks of solvent. For samples with low concentration, 1D ^1H and ^{13}C NMR spectra and 2D spectra (HSQC, HMBC, COSY, TOCSY, NOESY) were recorded on a Bruker Avance Neo 500 NMR spectrometer at 500.234 and 125.797 MHz, respectively, using a 5 mm prodigy probe with the TopSpin 4.0.7 spectrometer software or on an Agilent VNMR5 600 MHz NMR spectrometer equipped with 5 mm inverse detection cryoprobe, using standard CHEMPACK 8.1 pulse sequences implemented in Varian VNMRJ 4.2 spectrometer software.

2.2 Plant material

The plant material of *Hornstedtia scyphifera* (J.Koenig) Steud. was taken from the greenhouse collection of the IPB in Halle (Saale). Dried voucher material is stored at IPB (Identification code DFK214 and DFK221). For the investigations, fresh leaves as well as dried leaves were used. Fresh leaves were washed with water after being harvested and used for extraction immediately. For storage, the leaves were frozen in liquid nitrogen, then kept in a freezer at $-22\text{ }^{\circ}\text{C}$ and finally freeze-dried. The dry material was stored at room temperature until being used for further treatment.

2.3 Extraction and isolation

2.3.1 Isolation from fresh leaves

Fresh leaves (66.40 g) from *H. scyphifera* were ground, followed by an exhaustive ultrasound assisted extraction with methanol (5 \times 500 mL) to give 7.18 g of dried crude extract after evaporation of the solvent. The extract was five times partitioned by liquid–liquid-extraction between water (450 mL) and ethyl acetate (5 \times 500 mL) yielding the ethyl acetate fraction (2.02 g) and the water fraction (2.90 g). The ethyl acetate fraction was submitted to a polyamide SC-6-AC column (l: 21 cm, d: 7 cm) and eluted according to the eluotropic series (*n*-hexane, ethyl acetate, acetone, methanol). The acetone fraction (320.5 mg) was further purified on a RP18 column (l: 10 cm, d: 7 cm) with an increasing methanol gradient (10–100% in water), followed by a preparative RP18 TLC (d: 1 mm, 40% methanol) and final purification by semi-preparative reversed phase HPLC (column 1, solvent system 1, isocratic, 27.5 min, 15% B, flow rate of 1.6 mL/min) to yield compound **22** (*p*-hydroxybenzoic acid, 0.7 mg, R_t = 12.36 min, R_f = 0.67 in MeOH/H₂O (1:1, v/v) on RP18). The methanol fraction of the polyamide column was submitted to a SG60 column (l: 9 cm, d: 5 cm) and eluted with an increasing methanol/chloroform gradient (5–100% MeOH, in 5% steps). Compound **12** (isokaempferid, 6.3 mg, R_f = 0.45 in MeOH/CHCl₃ (1:19, v/v) on SG60) eluted with 5% methanol. The fraction obtained with 10% methanol was further submitted to repetitive column chromatography on RP18 with an isocratic water–methanol-mixture (7:4, v/v) and finally purified by HPLC (column 1, solvent system 1, gradient 0–2.5 min, 30% B; 2.5–12.5 min, 30–50% B, isocratic for 2 min, flow rate of 0.7 mL/min) to yield compound **8** (epicatechin, 0.6 mg, R_t = 11.82 min, R_f = 0.44 in MeOH/H₂O (4:7, v/v) on RP18).

2.3.2 Isolation from dried leaves

Dried pulverized leaves (92.00 g) from *H. scyphifera* were exhaustively extracted assisted by ultrasonication with 80% aq. methanol (6 \times 1 L) to give 18.02 g of dried crude extract after evaporation. The extract was successively partitioned by liquid–liquid-extraction between water and *n*-heptane, followed by ethyl acetate. A water-insoluble residue was later combined with the *n*-heptane fraction due to TLC profiles. This resulted into three fractions: 1) *n*-heptane (3.03 g), 2) ethyl acetate (1.50 g) and 3) water (8.59 g).

The *n*-heptane fraction was submitted to a silica gel 60 column (l: 90 cm, d: 4 cm), eluted with an increasing ethyl acetate/*n*-hexane gradient (0–100% ethyl acetate in 10% steps, each 1.5 L). The fraction eluted with 20% ethyl acetate was

submitted to a preparative RP18 TLC (d: 1 mm, 10% methanol) to yield compounds **14** (5-hydroxy-3,7,4'-trimethoxyflavon, 9.3 mg, R_f =0.78 in *n*-hexane/EtOAc (3:2, v/v) on NP) and **9** (0.9 mg, R_t =9.07 min, R_f =0.51 in MeOH/H₂O (9:1, v/v) on RP18). The fraction eluted with 70% ethyl acetate from the silica 60 column was further purified by preparative HPLC (column 3, solvent system 2, gradient 0–3.0 min, 70% B; 3.0–23.0 min, 70–100% B (isocratic for 6.5 min), flow rate of 1.8 mL/min) to yield compound **3** ((*E*)-14,15,16-trinorlabda-8(17),11-dien-13-oic acid, 0.1 mg, R_t =23.51 min).

The ethyl acetate fraction was submitted to a Sephadex LH20 column (l: 99 cm, d: 2 cm) with an isocratic dichloromethane-methanol-mixture (3:1, v/v) yielding seven fractions (A1–A7) based on the TLC profile (NP, toluol/EtOAc/FA, 10:5:3, v/v), of which A2 (R_f 0.57), A4 (R_f 0.42), A6 (R_f 0.37) and A7 (R_f 0.28) were further purified.

A2 was submitted to a RP18 column (l: 51 cm, d: 3 cm) and eluted with a mixture of methanol and water (7:3, v/v) which yielded six fractions (B1–B6) based on the TLC profile (RP18, MeOH/H₂O, 7:3, v/v), of which B2 (R_f 0.70) and B6 (R_f 0.06) were further purified. B2 was repeatedly submitted to reversed phase HPLC (column 3). The separation with solvent system 1 (gradient 0–3.0 min, 33% B; 3.0–23.0 min, 33–38% B) and a flow rate of 1.0 mL/min yielded compounds **18** (evofolin B, 0.6 mg, R_t =15.39 min), **5** (*cis*-pinononic acid, 0.9 mg, R_t =17.11 min), **21** (syringaldehyde, 1.6 mg, R_t =18.82 min) and **20** (vanillin, 1.2 mg, R_t =19.53 min). In addition, a second gradient system was applied (solvent system 1; gradient 0–3.0 min, 30% B; 3.0–23.0 min, 30–52% B, flow rate of 1.4 mL/min) to yield compound **2** (6-hydroxy-anhuienosol, 2.7 mg, R_t =9.42 min), compound **7** (2-oxo-3-4,5,5-trimethylcyclopentynyl acidic acid, 2.3 mg, R_t =15.42 min) and compound **6** (*cis*-pinonic acid, 2.2 mg, R_t =16.85 min).

B6 was purified by preparative HPLC (column 2, solvent system 1; gradient 0–2.5 min, 80% B; 2.5–17.5 min, 80–100% B; flow rate of 2.64 mL/min) to yield compound **13** (kumatakenin, 2.3 mg, R_t =9.16 min).

A4 was purified by preparative HPLC (column 3, solvent system 1; gradient 0–3.0 min, 35% B; 3.0–23.0 min, 35–100% B, flow rate of 1.8 mL/min) to yield compounds **19** (protocatechualdehyde, 3.6 mg, R_t =11.38 min), **24** (vanillic acid, 3.2 mg, R_t =13.87 min), **25** (protocatechuic acid methylester, 0.1 mg, R_t =16.10 min) and **16/17** (*trans*- and *cis*-ferulic acid, 1.1 mg, R_t =16.70 min).

A6 was submitted to a RP18 column (l: 36 cm, d: 2 cm) and eluted with a methanol–water-mixture (3:7, v/v) which yielded three fractions (C1–C3) based on the TLC profile (RP18, MeOH/H₂O, 3:7, v/v), of which C1 (R_f 0.83) and C2 (R_f 0.80) were further purified by preparative HPLC. C1 was separated on column 3 using solvent system 1 (gradient 0–3.0 min, 8% B; 3.0–20.0 min, 8–32% B, 20.5–28.0 min, 50–70% B) and a flow rate of 1.8 mL/min to yield compound **23** (protocatechuic acid, 2.8 mg, R_t =16.60 min) and compound **26** (5-methoxy salicylic acid, 0.1 mg, R_t =21.95 min). C2 was purified on column 2 using solvent system 1 (gradient 0–2.5 min, 40% B; 2.5–22.5 min, 40–100% B) and a flow rate of 4.4 mL/min to yield compound **1** (mustak-14-oic acid, 0.6 mg, R_t =18.03 min).

A7 was purified by preparative HPLC (column 3, solvent system 1; gradient 0–3.0 min, 35% B; 3.0–23.0 min, 35–100% B, 23.0–30.0 min, 100% B; flow rate of 1.8 mL/min) to yield the compounds **15** (*E*-*p*-coumaric acid, 3.5 mg, R_t =16.60 min), **11** (rutin, 2.3 mg, R_t =17.86 min), **4** (verbenon-10-oic acid, 5.6 mg, R_t =19.23 min) and **10** (quercetin, 2.5 mg, R_t =21.71 min).

2.3.3 Spectral data

(1*R*,5*S*,6*S*,7*R*,10*R*)-Mustak-14-oic acid (**1**): colorless oil; $[\alpha]_D^{20}$ = –69 (c 0.0001, MeOH); UV (MeOH) λ_{\max} (log ϵ) 202 (4.00), 225 (3.71), 277 (3.14); ¹H NMR (500 MHz, Methanol-*d*₄) and ¹³C NMR (obtained from HSQC and HMBC, Methanol-*d*₄) see Table 2; HR-ESI-MS (Orbitrap) *m/z* [M – H][–] 247.1338 (calc for C₁₅H₁₉O₃[–], 247.1329); MS²-Fragmentation (CE = –30 V) *m/z* 221 (8), 203 (100).

(1*R*,6*S*,7*S*,10*R*)-6-Hydroxy-anhuienosol (**2**): yellow oil; $[\alpha]_D^{20}$ = –17 (c 0.0001, MeOH); UV (MeOH) λ_{\max} (log ϵ) 202 (3.87), 238 (3.63); ¹H NMR (500 MHz, Methanol-*d*₄) and ¹³C NMR (obtained from HSQC and HMBC, Methanol-*d*₄) see Table 3; HR-ESI-MS (TOF) *m/z* [M + FA][–] 313.1669 (calc for C₁₆H₂₅O₆[–], 313.1651); MS²-Fragmentation (CE = –20 V) *m/z* 313 (12), 267 (50), 209 (100), 191 (18), 121 (17).

2.4 Computational CD spectral analysis

The absolute configuration of compounds **1–6**, **8**, and **9** was determined by aligning experimental electronic circular dichroism (ECD) spectra with calculated CD spectra obtained by quantum chemical calculation. The initial 3D structures for the molecules, including all possible stereoisomers, were built using Molecular Operating Environment (MOE) 2020 software and the accompanying ChemDraw add-in. All structures and conformational analyses were executed utilizing the Amber10:EHT force field [21]. The energy minimum structures obtained from the force field were subsequently optimized employing the DFT method (B3LYP/def2-TZVP) [22–25] with the ORCA 5.0 program

package [26], incorporating the conductor-like polarizable continuum model (CPCM) solvent field [25] for methanol. For the optimized structures CD spectra were calculated via the ORCA software. The first 25 excited states for each compound and stereoisomers were computed using the TD B3LYP [22–25] with the def2-TZVP basis set [27] and CPCM model for methanol. The SpecDis software (version 1.71) [28] was employed for visualizing and contrasting the calculated spectra with the experimental data. The best similarity factor for the different stereoisomers was calculated and the one with the highest similarity factor was used for comparison at the same shift and sigma factor for a Gaussian band shape.

2.5 MS measurements

2.5.1 High resolution

The UHPLC-ESI-HRMS spectra of compound **2**, **3**, **5–9**, **12**, **14**, **18**, **20–23** and **26** were acquired using a TripleTOF (time of flight) 6600–1 mass spectrometer (Sciex, Darmstadt) in positive and negative ion modes. Samples (2 µL) were loaded on an Waters Acquity UPLC® BEH C18 column (1.7 µm, 130 Å, 50 × 2.1 mm I.D., Waters GmbH, Eschborn, Germany) under isocratic conditions (3% eluent B, 1 min), and separated using a linear gradient from 3 to 95% eluent B in 5 min. Separation was performed on an ACQUITY UPLC I-Class UHPLC System (Waters GmbH, Eschborn, Germany) with a flow rate of 0.4 mL/min and 55 °C column temperature. Eluents A and B were water and acetonitrile, with 0.1% formic acid. The mass spectrometer was equipped with an ESI-DuoSpray ion source (spray voltage: 5.5 kV (positive mode), 4.5 kV (negative mode), nebulizer gas: 60 psi, source temperature: 450 °C, drying gas: 70 psi, curtain gas: 55 psi) and was controlled by Analyst 1.7.1 TF software (Sciex, Darmstadt). Data acquisition was performed in MS1-TOF mode in a mass range of m/z 65 to 1250 with an accumulation time of 75 ms. The mass spectrometer was externally calibrated with calibration solutions provided by the manufacturer for positive and negative modes. For MS²-TOF mode the declustering potential was 35 V and the collision potential was 10 V, respectively. The product ion spectra (tandem mass spectra, MS/MS) were acquired in the high sensitivity mode (accumulation time 20 ms) in the m/z range of 50–1000 using unit Q1 resolution with mass resolution above 30,000. Collision potential (CE) was set from –80 to –20 V in negative ion mode and set from 20 to 80 V in positive ion mode, whereas collision energy spread (CES) was 15 V. The data were evaluated by Peak View 1.2.0.3 software (AB Sciex GmbH, Darmstadt, Germany).

The UHPLC-ESI-HRMS spectra of compounds **1**, **4**, **10**, **11**, **13**, **15–17**, **19**, **24** and **25** were acquired using an Orbitrap Elite mass spectrometer (Thermo Fisher Scientific, Bremen, Germany), coupled with a UHPLC system (Dionex UltiMate 3000, Thermo Scientific) and a photodiode array detector (PDA, Thermo Scientific). The spectra as well as the collision-induced dissociation mass spectra (CID, collision induced dissociation) were recorded in positive and negative ion mode. Samples (3 µL) were loaded on an Waters Acquity UPLC® BEH C18 column (1.7 µm, 130 Å, 50 × 2.1 mm I.D., Waters GmbH, Eschborn, Germany) under isocratic conditions (5% eluent B, 1 min), and separated using a linear gradient from 5 to 95% eluent B in 10 min. Separation was performed on an ACQUITY UPLC I-Class UHPLC System (Waters GmbH, Eschborn, Germany) with a flow rate of 0.4 mL/min and 40 °C column temperature. Eluents A and B were water and acetonitrile, with 0.1% formic acid. Ionization was carried out by electrospray ionization (HESI ion source; spray voltage 4.0 kV in positive ion mode, 3.5 kV in negative ion mode; nebulizing and auxiliary gas: nitrogen; evaporation temperature: 300 °C; capillary temperature: 325 °C, FTMS resolution Full MS: 30,000; MSⁿ: 15,000). The CID mass spectra were recorded automatically using a data-dependent fragmentation mode and a normalized collision energy (NCE) of 35%. The mass spectrometer was externally calibrated with calibration solutions provided by the manufacturer for the negative and positive modes. The spectra were analyzed using Xcalibur 2.2 SP1 software (Thermo Fisher Scientific).

The MSⁿ high-resolution electrospray mass spectra in negative ion mode of kumatakenin (**13**) were acquired using an Orbitrap Elite mass spectrometer (ESI ion source: spray voltage 4.0 kV, capillary temperature 275 °C, nebulizing gas: nitrogen, FTMS resolution 30,000). The sample solution was continuously injected using a syringe pump (flow rate: 5 µL/min). The mass spectrometer was externally calibrated (Pierce® ESI negative ion calibration solution, Product No. 88324, Thermo Fisher Scientific, Rockford, IL, 61,105 USA). The spectra were analyzed using Xcalibur 2.7 SP1 software. The CID-MSⁿ measurements were acquired with relative collision energies: 25% for MS² of m/z 313 in the m/z range of 85–350, 25% for MS³ of m/z 298 in the m/z range of 80–325, 30% for MS⁴ of m/z 283 in the m/z range of 75–300, 35% for MS⁵ of m/z 255 in the m/z range of 75–300.

2.5.2 Headspace GCMS

The headspace GCMS method was adopted from Farhadi et al. [29] with modifications. Ground leaf powder (0.5 g) was submitted into 20 mL headspace vials and then incubated at 100 °C for 30 min with constant shaking in a headspace assembly of CTC GC PAL Injector (Shimadzu Deutschland GmbH, Duisburg, Germany). 500 µL head space of each sample were injected into a ZB-5MS capillary column (30 m × 0.25 mm ID, 0.25 µm film thickness, Phenomenex, Aschaffenburg, Germany) and analyzed by gas chromatography-electron ionization-quadrupole-mass spectrometry (GC-EI-Q-MS) using a GC2010 gas chromatograph coupled online to a quadrupole mass selective detector Shimadzu GCMS QP2010. The temperature program started at 50 °C kept constant for 5 min, then a ramp of 3 °C/min to 140 °C followed by the second ramp of 10 °C/min to 240 °C and finally kept constant for 10 min. MS detection was performed in positive ion mode in m/z range 40–500 Da. Analysis was performed under the control of GCMS Real Time Analysis software (Shimadzu Deutschland GmbH, Duisburg, Germany). The compounds were annotated using the NIST17 library.

2.5.3 GC–MS of essential oil and *n*-hexane extract

To obtain essential oil, dried leaf powder (10 g) of *H. scyphifera* was subjected to hydrodistillation in a Dean Stark Apparatus for 12 h adding 400 mL deionized water into a 1000 mL flask. The pale-yellow essential oil (1.2 mg) was picked using a micro pipette (10 µL, BLAUBRAND, Wertheim, Germany), transferred to a vial and stored in the fridge.

To obtain the *n*-hexane extract, dried leaf powder (8 g) of *H. scyphifera* was subjected to a cellulose thimble and transferred to a Soxhlet extractor. The extractor was filled with 150 mL of *n*-hexane and heated under reflux for 3 h. Afterwards, the solvent was carefully removed using rotary evaporator.

Samples (1 µL) were injected on ZB-5MS capillary column (30 m × 0.25 mm ID, 0.25 µm film thickness, Phenomenex, Aschaffenburg, Germany) and analyzed by gas chromatography-electron ionization-quadrupole-mass spectrometry (GC-EI-Q-MS) using a GC2010 gas chromatograph coupled online to a quadrupole mass selective detector Shimadzu GCMS QP2010. The temperature program was starting at 50 °C kept constant for 5 min, then a ramp 10 °C/min to 120 °C followed by the second ramp 5 °C/min to 300 °C and kept constant for 15 min. MS detection was performed in positive ion mode in m/z range 40–600 Da. The compounds were annotated using the NIST17 library.

2.6 X-Ray analysis

Single crystals of compound **13** (Kumatakenin, C₁₇H₁₄O₆) were obtained by slow evaporation of the solvent from a concentrated methanolic solution in the cold. A suitable crystal was selected and fixed on a STOE IPDS II diffractometer. The crystal was kept at 170 K during data collection. Using Olex2 [30], the structure was solved with the SHELXT [31] structure solution program and refined with the SHELXL [32] refinement package using Least Squares minimization.

2.7 Biological assays

2.7.1 Antibacterial Assays

The compounds were evaluated against the Gram-negative *Aliivibrio fischeri* (DSM507) and the Gram-positive *Bacillus subtilis* 168 (DSM 10), as described by Kappen et al. [33] and Manurung, Kappen et al. [34]. The tests were performed in 96-well plates based on the bioluminescence (*A. fischeri*) or absorption (*B. subtilis*) read-out. Chloramphenicol (100 µM) was used as a positive control to induce complete inhibition of bacterial growth. The results (mean ± standard deviation value, $n = 6$) are given in relation to the negative control (bacterial growth, 1% DMSO without test compound) as relative values (percent inhibition). Negative values indicate an increase in bacterial growth.

2.7.2 Antifungal Assay

The antifungal activity was tested on the phytopathogenic ascomycetes *Botrytis cinerea* Pers. and *Septoria tritici* Desm. and the oomycete *Phytophthora infestans* (Mont.) de Bary in 96-well microtiter plate assays according to protocols from the Fungicide Resistance Action Committee (FRAC) with minor modifications as described by Ware et al. [35, 36]. Briefly, the isolated compounds were tested at the highest concentration of 500 µg/mL, while the solvent DMSO in buffer was used as a negative control (max. concentration 2.5%). The commercially used fungicides, epoxiconazole and terbinafine

(Sigma-Aldrich, Darmstadt, Germany), served as reference compounds. The pathogen growth was evaluated seven days after inoculation by measurement of the optical density (OD) at L 405 nm with a TecanGENios Pro microplate reader (five measurements per well using multiple reads in 3 × 3 square). Each experiment was carried out in triplicate.

3 Results and discussion

3.1 Characterization of crude extracts and volatiles

A first phytochemical investigation of the leaves from *H. scyphifera* involved multiple methodologies. An exhaustive extraction with methanol was performed to yield a crude extract, which was characterized by ultra high-performance liquid chromatography high-resolution mass spectrometry analysis (UHPLC-ESI-HRMS). Additionally, the volatile compounds were screened on one hand by submitting ground plant material to a headspace gas chromatography-mass spectrometry-system (HS-GCMS) (Table S1) and on the other hand by extracting essential oil and a *n*-hexane extract from leaves to compare and verify results with published data (Table S2). Further, the crude extract was submitted to liquid-liquid partitioning and resulting fractions were screened by TLC and for bioactivity in selected assays.

The findings of the HS-GCMS analysis are largely consistent with existing reports on the characterization of the essential oils of *H. scyphifera*. Specifically, the main peaks were identified as α -pinene, camphene, *p*-cymene, and camphor, as reported by Hashim et al. in 2018 [17]. Notably, the presence of butylbenzene (Table S1, H6), constituting 18% of the composition, appears to be previously unreported based on available literature.

Analysis via GC-MS facilitated the tentative annotation of 71 compounds in total, while 49 are abundant in the essential oil (EO) and 24 compounds in the *n*-hexane extract from the leaves. Quantitatively relevant compounds in the EO included *trans*-dihydroagarofuran (14.91%, Table S2, G17), α -caryophyllene (6.77%, Table S2, G36) as well as *cis*-verbenol acetate (5.54%, Table S2, G53) and (*E*)-15,16-dinorlabda-8(17),11-dien-13-one (3.49%, Table S2, G48). The latter was previously isolated from the rhizome of *Globba schomburgii* by Suekaew et al. [37] but here is annotated for the first time in the EO of *H. scyphifera*. In the *n*-hexane fraction, *cis*-verbenone (13.49%, Table S2, G8), camphor (3.95%, Table S2, G4), camphene (4.23%, Table S2, G2), and α -pinene (1.49%, Table S2, G1) were the most abundant compounds. Most compounds identified through headspace analysis were also present in the *n*-hexane extract but were absent in the essential oil (EO). This might be attributed to the high volatility of these compounds, potentially resulting in incomplete condensation during EO distillation.

TLC screening of the crude extract and fractions from liquid-liquid-partitioning showed the highest variety of spots for the *n*-heptane and ethyl acetate fraction, corresponding to individual compounds (Fig. 1, lane 3). This indicated a complex matrix for these extracts suggesting challenging isolation and characterization. The TLC profile of the *n*-heptane fraction as well as the water insoluble residue of the crude extract (Fig. 1, 366 nm, lane 4 and 5) showed both bright yellow spots attributed to compounds **9** and **14** and were therefore combined for further isolation. Both the *n*-heptane and the ethyl

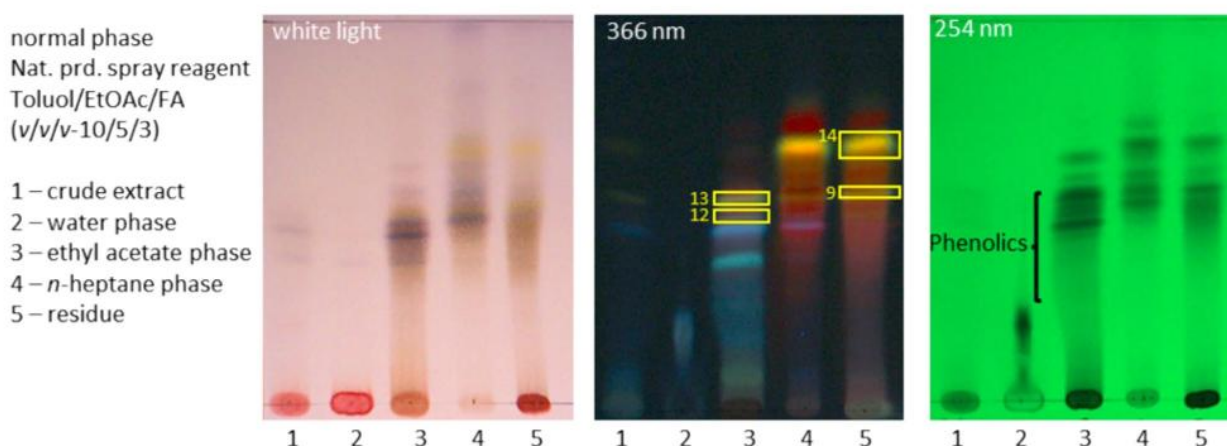


Fig. 1 TLC of crude extract and fractions from liquid-liquid-partitioning of dried leaves after derivatization with natural product reagent. Numbered boxes correspond to isolated compounds

acetate fractions exhibited strong activity against the Gram-negative bacterium *Allivibrio fischeri* (complete inhibition at a concentration of 500 µg/ml) (Fig. S1.1.B) and were therefore considered for further isolation. All fractions inhibited the growth of the phytopathogenic fungus *Botrytis cinerea* (Fig. S1.2.B).

The UHPLC-HRMS analysis allowed for the annotation of 27 individual metabolites from the total ion chromatogram (TIC) of the crude extract (Table 1 and Fig. 2). The most intense signal at R_t 8.2 min (overlapping peaks P22 and P23) was assigned to the previously unknown mustak-14-oic acid (**1**) and the flavonoid kumatakenin (**13**). Further dominating signals could be attributed to ferulic acid derivatives (P9 and P11), the flavonol glycoside rutin (**11**) (P13) and the flavonoid isokaempferide (**12**) (P19). Most signals were assigned to compounds that could also be isolated and identified within the scope of this work. However, not all isolated compounds were detected in the crude extract. This could be due to matrix effects leading to ion suppression of individual substances in the complex crude extract, low solubility in the applied solvent methanol or low substance concentration. Since two thirds of the crude extract mass is allocated to the aqueous fraction, a relatively low concentration of nonpolar and middle polar compounds in the crude extract can be expected. In contrast, the compounds behind other detected peaks were not obtained by isolation, as e.g. P9 and P11 (Table 1 and Fig. 2), which exhibited identical mass and MS^2 spectra and were thus attributed to *cis* and *trans* ferulic acid derivatives. This is supported by the isolation of both *trans*- and *cis*-ferulic acid (**16** + **17**). In conclusion, *H. scyphifera* possesses a multitude of metabolites, the majority of which can be classified into the three groups of (1) terpenes and terpenoids, (2) flavonoids and (3) other phenolics.

3.2 Purification and structure elucidation

The ethyl acetate and the *n*-heptane fraction obtained from successive liquid–liquid partition were further purified by different chromatographic techniques. This resulted in the isolation of 26 compounds (Fig. 3). Beside the two previously undescribed compounds mustak-14-oic acid (**1**) and 6-hydroxy-anhuienosol (**2**), the remaining 24 compounds were identified as (*E*)-14,15,16-trinorlabda-8(17),11-dien-13-oic acid (**3**) [38, 39], (1*S*,5*R*)-verbenon-10-oic acid (**4**) [40, 41], *cis*-pinonic acid (**5**) [42, 43], *cis*-pinonic acid (**6**) [44], 2-oxo-3-4,5,5-trimethylcyclopentynyl acetic acid (**7**) [45, 46], epicatechin (**8**) [47, 48], (2*S*)-sakuranetin (**9**) [49, 50], quercetin (**10**) [51], rutin (**11**) [52, 53], isokaempferid (**12**) [54], kumatakenin (**13**) [19, 55], 5-hydroxy-3,7,4'-trimethoxyflavone (**14**) [19, 56], (*E*)-*p*-coumaric acid (**15**) [57], *trans*-ferulic acid (**16**) [58], *cis*-ferulic acid (**17**) [58], evofolin B (**18**) [59], 3,4-dihydroxybenzaldehyde (**19**) [60], vanillin (**20**) [61, 62], syringaldehyde (**21**) [63], *p*-hydroxybenzoic acid (**22**) [64], protocatechuic acid (**23**) [65], vanillic acid (**24**) [66], protocatechuic acid methyl ester (**25**) [67, 68] and 5-methoxy-salicylic acid (**26**) [69, 70], after comparison with NMR data from literature. Further, spectroscopic data, including NMR and MS for compounds **1** to **26** can be found in the supporting information. The absolute configuration of compounds **1**, **2**, **3**, **4**, **5**, **6**, **8**, and **9** were verified by comparison of experimental and calculated CD spectra (Fig. 4 and 7; Fig. S5–S10; Tables S5, S8–S14). To the best of our knowledge, this is the first report on isolation and identification of compounds **3–9** and **11**, **12**, **15–26** from *H. scyphifera*.

Interestingly, the monoterpene derivatives **5**, **6** and **7** so far were never isolated from a plant source. Compounds **5** and **6** were previously obtained as synthetic oxidation products from α -pinene [42, 44] while **7** was described as degradation product of camphor, induced by plant pathogens [46]. Both potential precursors were abundant in the GC analysis (H4 and H19 in Table S1; G1 and G4 in Table S2). At this point, the biological origin of **5**, **6** and **7** in *H. scyphifera* is unknown. The compounds might be derived from plant biosynthesis or by involvement of associated microorganisms. Similarly, a biosynthetic connection of the isolated (*E*)-14,15,16-trinorlabda-8(17),11-dien-13-oic acid (**3**) and (*E*)-15,16-dinorlabda-8(17),11-dien-13-one (G48, Table S2) detected in GC–MS experiments might be expected due to their structural similarity.

Compound **1** was isolated as a colorless oil in a poor yield of 0.6 mg from 92.0 g of dried material, which may be attributed to its volatile nature and the drying methods employed, e.g. rotatory evaporation and lyophilization. The molecular formula was determined as $C_{15}H_{20}O_3$ from the molecular ion peak at m/z 247.1338 [$M - H$][−] (calcd. for 247.1329), obtained from the HR-ESI–MS spectra. The ¹H NMR spectra (Table 2) displayed a single signal for a proton attached to a conjugated double bond (δ_H 6.26, dd, brt, $J = 1.6$ Hz, H-3), three signals for protons in central positions (δ_H 2.72, brs, H-6; δ_H 2.69 dd, $J = 6.6$, 1.3 Hz, H-1; δ_H 2.66 dd, $J = 6.6$, 0.9 Hz, H-5), followed by two multiplets encompassing six overlapping signals, later resolved by HSQC (δ_H 1.69–1.95, m, H-7, H-8b, H-9a, H-9b; δ_H 1.50–1.66, m, H-8a, H-11). Additionally, three signals annotated to CH₃ groups emerged, with two displaying the same coupling constants, indicating an isopropyl group (δ_H 0.98, s, H-15; δ_H 0.89, d, $J = 6.8$ Hz, H-13; δ_H 0.87, d, $J = 6.8$ Hz, H-12). Due to quantitative limitations, no ¹³C NMR spectra could be acquired. Therefore, ¹³C shifts were obtained from 2D NMR experiments, HSQC and HMBC, which confirmed the presence of all fifteen carbon atoms postulated by HRMS (Table 2). These included a carbonyl group signal (δ_C 209.0, C-2), signals indicative of a double bond (δ_C 124.3 for a CH group, C-3 and δ_C 168.3 for a quaternary carbon, C-4), and a

Table 1 Metabolites annotated in methanolic leaf extract from *H. scyphifera* by reversed phase ultra-high-performance chromatography-tandem mass spectrometry (RP-UHPLC-MS/MS) on Orbitrap

Peak	t_R (min)	m/z measured [M – H] [–]	Error (ppm)	Molecular formula*	MS ² product ions m/z (rel. intensity [%])	Annotation
P1	0.26	341.1086	–1.0	C ₁₂ H ₂₂ O ₁₁	341.1086 (100), 215.0328 (14)	Sucrose
P2	0.63	167.0350	0.2	C ₈ H ₈ O ₄	123.0454 (100)	Vanillic acid (24)
P3	0.72	167.0351	0.8	C ₈ H ₈ O ₄	123.0454 (100)	Protocatechuic acid methyl ester (25)
P4	0.82	153.0194	0.6	C ₇ H ₆ O ₄	109.0297 (100)	3,4-Dihydroxybenzoic acid (23)
P5	1.38	137.0246	1.0	C ₇ H ₆ O ₃	119.0252 (100), 93.0349 (52), 66.0352 (62)	<i>p</i> -Hydroxybenzoic acid (22)
P6	1.51	137.0245	0.7	C ₇ H ₆ O ₃	119.0252 (10), 110.0251 (9), 93.0348 (100), 66.0354 (8)	3,4-Dihydroxybenzaldehyde (19)
P7	2.19	151.041	0.5	C ₈ H ₈ O ₃	–	Vanillin (20)
P8	3.79	577.1339	–1.3	C ₃₀ H ₂₆ O ₁₂	559.1238 (7), 451.103 (34), 425.0874 (100), 407.0767 (42), 289.0716 (19)	Procyanidin (Epicatechin dimer)
P9/	4.03/	399.0928	–1.2	C ₁₇ H ₂₀ O ₁₁	381.0824 (7), 223.0459 (51), 205.0353 (100), 187.0248 (3), 129.0195 (15), 111.0090 (3)	Ferulic acid derivatives, e.g (<i>E</i>) and (<i>Z</i>)-Feruloyl-4- <i>O</i> -methoxyglucaric acid
P11	4.39/	–	–	–	245.0819 (100), 205.0506 (32), 179.0351 (15)	Epicatechine (8)
P10	4.24	289.0716	–0.6	C ₁₅ H ₁₄ O ₆	–	(<i>E</i>)- <i>p</i> -Coumaric acid (15)
P12	4.99	163.0402	0.57	C ₉ H ₈ O ₃	301.035 (100)	Rutin (11)
P13	5.15	609.1453	–1.4	C ₂₇ H ₃₀ O ₁₆	135.0817 (100)	1,5,5 <i>R</i> -Verbenon-10-oic acid (4)
P14	5.38	179.0714	0.1	C ₁₀ H ₁₂ O ₃	125.0973 (100)	unknown
P15	5.69	187.0976	0.1	C ₉ H ₁₆ O ₄	273.0768 (100)	Quercetin (10)
P16	6.24	301.0352	–0.6	C ₁₅ H ₁₀ O ₇	–	2-(2,2,3-Trimethyl-5-oxocyclopent-3-en-1-yl) acetic acid (7)
P17	6.60	181.0870	0.1	C ₁₀ H ₁₄ O ₃	–	2-(3'-Acetyl-2,2'-dimethyl-cyclobutyl) acetic acid (6)
P18	6.67	183.1026	–0.2	C ₁₀ H ₁₅ O ₃	284.0326 (100)	Isokaempferid (12)
P19	6.98	299.0559	–0.9	C ₁₆ H ₁₂ O ₆	371.1498 (100)	Diarylheptanoid derivative, e.g. Tetrahydrocurcumin
P20	7.18	431.1707**	–1.0	C ₂₃ H ₂₈ O ₈	–	6-Hydroxy-anhuinosol (2)
P21	8.00	267.1601	–0.3	C ₁₅ H ₂₄ O ₄	203.1441 (100)	Mustak-14-oic acid (1)
P22	8.22	247.1339	–0.4	C ₁₅ H ₂₀ O ₃	298.0481 (100)	Kumatakenin (13)
P23	8.25	313.0717	–0.3	C ₁₇ H ₁₄ O ₆	259.2067 (100)	Sterol derivative
P24	9.17	287.2015	–0.4	C ₁₉ H ₂₈ O ₂	289.2172 (100), 271.2067 (43)	Diterpenoid, e.g. Agathic acid [71]
P25	9.81	333.2069	–0.8	C ₂₀ H ₃₀ O ₄	–	Diterpenoid glycoside, e.g. Viteoside A [72]
P26	10.63	555.2840	5.3	C ₂₈ H ₄₄ O ₁₁	–	unidentified
P27	10.96	823.4689	–	–	–	–

*Refers to non-ionized compound

**[M + CH₃COO][–]

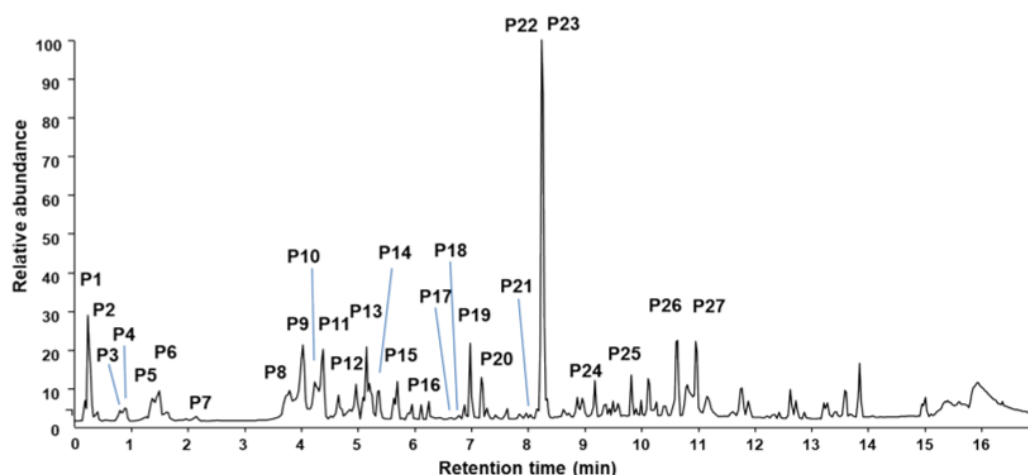


Fig. 2 Total ion chromatogram (TIC), acquired from the methanolic extract obtained from leaves of *H. scyphifera*. Please note that peak numbers are not identical to compound numbers. See Table 1 for assignment

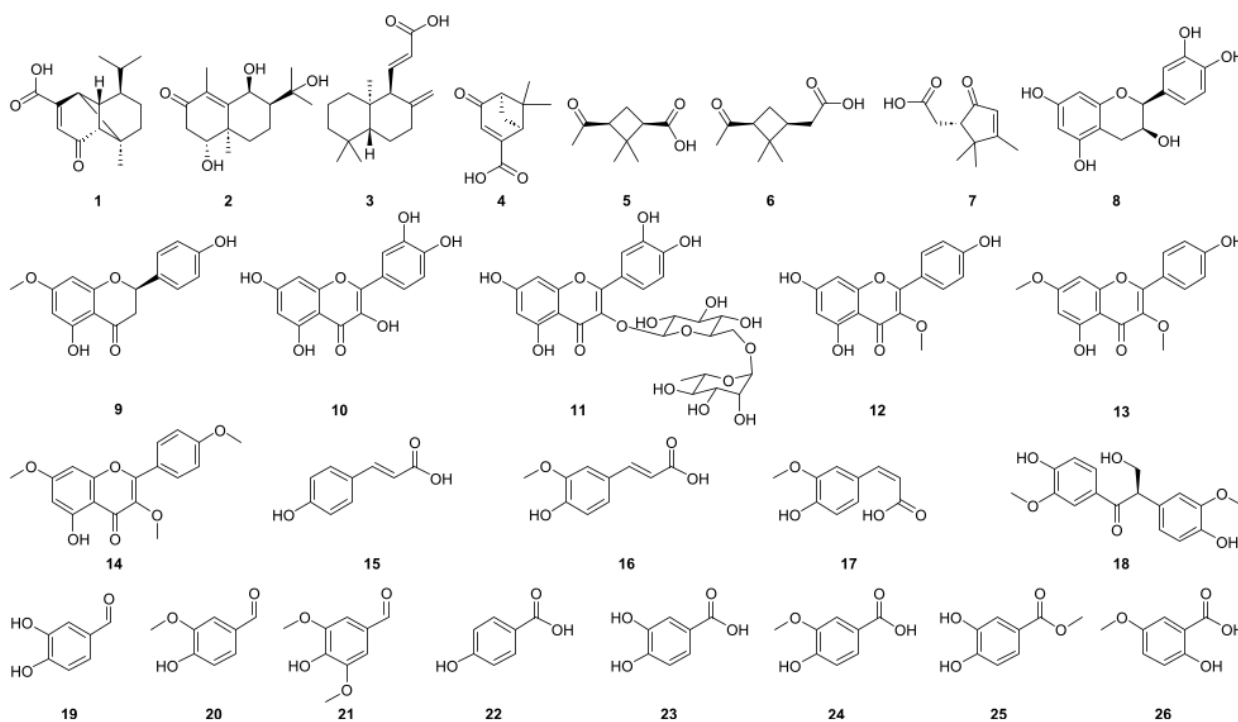


Fig. 3 Structures of all compounds isolated from *H. scyphifera* in this work

carboxylic group signal (δ_C 173.8, C-14). Additional signals observed comprised three CH_3 groups (δ_C 20.8, C-15; δ_C 20.2, C-12 and δ_C 19.9, C-13), two CH_2 groups (δ_C 37.9, C-9 and δ_C 23.1, C-8), five more CH groups (δ_C 58.8, C-6; δ_C 57.0, C-1; δ_C 53.5, C-5; δ_C 46.7, C-7 and δ_C 33.2, C-11), and one more quaternary carbon (δ_C 59.8, C-10). All 1D and 2D NMR spectra are shown in the supporting information (Fig. S2.1–S2.7).

Altogether, the NMR dataset of **1** exhibits a significant resemblance to a cadinane-type sesquiterpene [73] also found in the volatile fraction of *H. scyphifera*. However, the numerous strong HMBC correlations of H-5 and H-6 indicate an intramolecular third ring in accordance with a copaene skeleton [74]. One known copaene, trivially named mustakone, comprises NMR data with high similarity to **1**. This compound has been first isolated from the essential oils of *Cyperus*

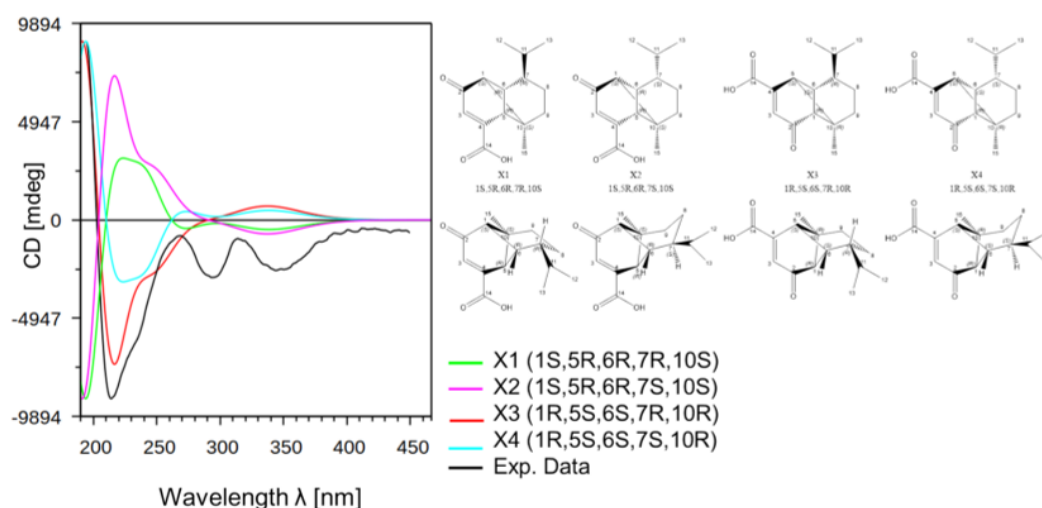


Fig. 4 CD spectrum and calculated spectra of the four stereoisomers X1-X4 of compound **1**

Table 2 NMR data of compound **1** (MeOD, 500 MHz, 25 °C)

No	δ_C^a	δ_H (multiplicity, J)	COSY	NOESY	HMBC
1	57.0, CH	2.69 (dd, 6.6, 1.3 Hz, 1H)	3, 5	8a, 12, 15	2, 3, 5
2	209.0, C				
3	124.3, CH	6.26 (brt, 1.6 Hz, 1H)	1, 5		1, 5, 14
4	168.3, C				
5	53.5, CH	2.66 (dd, 6.6, 0.9 Hz, 1H)	1, 3	7, 9a, 15	1, 3, 4, 6, 7, 9
6	58.8, CH	2.72 (brs, 1H)		7, 11, 12	2, 4, 5, 8, 10, 11, 15
7	46.7, CH	1.77 (m, 1H)	8a, 8b, 11	5, 8a, 13	1, 5, 12
8	23.1, CH ₂	a) 1.61 (m, 1H) b) 1.83 (m, 1H)	7, 8b, 9a, 9b 7, 8a, 9a	1, 8b, 9b, 12 5, 8a, 13	10
9	37.9, CH ₂	a) 1.86 (m, 1H) b) 1.90 (m, 1H)	8a, 8b, 9b 8a, 8b, 9a	5, 8a, 15 1, 8a, 15	5, 10 7
10	59.8, C				
11	33.2, CH	1.55 (m, 1H)	7, 12, 13	6, 8b, 12, 13	12, 13, 8, 7, 6
12	20.2, CH ₃	0.87 (d, 6.8 Hz, 3H)	11	1, 6, 11	13, 11, 7
13	19.9, CH ₃	0.89 (d, 6.8 Hz, 3H)	11	7, 11	7, 11, 12
14	173.8, C				
15	20.8, CH ₃	0.98 (s, 3H)		1, 5, 9a, 9b	1, 5, 9, 10

^a obtained from HSQC and HMBC

rotundus L., an Indian nutgrass variety known as Mustaka in Sanskrit language, by Kapadia et al. in 1963 [75]. To date, it has only been found in five additional species, none of which belong to the Zingiberaceae family [76]. In this study, we could detect mustakone (G27, Table S2) in the *n*-hexane extract by GCMS. The structure of mustakone was primarily determined through chemical modification in combination with IR and ¹H NMR [75], and a strong similarity with verbenone was noted. Full NMR data were later provided by Nyasse et al. [77]. Direct comparison of NMR data from compound **1** and mustakone revealed a missing CH₃ group in **1** (at δ_H 2.02 and δ_C 20.2), as well as an additional significantly shifted carbon signal at 173.8 ppm. The molecular formula of **1** includes two additional oxygen atoms compared to mustakone, implying carboxylation of the methyl group at position 14. This is notable, as a carboxylated derivative of verbenone, (1S,5R)-verbenone-10-oic acid (**4**), was also isolated, bearing the carboxyl function at the same position instead of methylation.

The cyclobutane ring in **1** exhibits increased ring strain due to the carbon–carbon bonds being required to adopt angles close to 90°, rather than the typical 109.5° angle of *sp*³ hybridized carbon in a tetrahedral configuration. This results in a highly rigid structure showing unique H–H couplings. A strong COSY coupling as observed between H-1 and

H-5 ($J=6.6$ Hz) can occur in case of a sterically fixed M or W-shaped arrangement of the coupling nuclei and is typical for $^4J_{HH}$ coupling of *cis* protons situated as bridgehead protons on the opposite side of cyclobutane rings [78, 79]. In contrast, COSY long-range couplings in saturated systems over more than 3 bonds typically have a J value of <1 Hz and are therefore often undetected.

In **1** the signals of both bridgehead protons H-1 (δ_H 2.69, dd, 6.6, 1.3 Hz) and H-5 (δ_H 2.66 dd, $J=6.6$, 0.9 Hz) appear consistent with the data from Nyasse et al. [77] on mustakone as doublet of doublets (dd) due to the long-range coupling to H-3. H-3 appears as a pseudo broad triplet with a J value of 1.6 Hz, resulting from the overlaying effect of the theoretically possible doublet of doublet splitting. In contrast, H-6 appears like in mustakone as a broad singlet which implies in accordance with the Karplus curve an approximate angle of 90° between H-6 and all three neighboring protons H-1, H-5 and H-7. While this may pose a challenge for structure elucidation, it provides key information for the relative configuration of these compounds. Mustakone, like **1**, features 5 stereocenters, which theoretically leads to 32 possible stereo isomers. However, due to the intramolecular cyclobutane ring, the associated steric constraints, and the multiplicity of H-6, only 4 possible stereo isomers remain after geometrical optimization (Fig. 4, X1–X4). A Minimize Energy MM2 calculation in Chem3D to optimize the spatial structure of the stereo isomers, followed by angle determination and calculation of theoretical coupling constants, did not lead to the exclusion of any of the possible stereoisomers (Table S3).

For further determination of the relative stereochemistry, NOESY data were employed (Table 2, Fig. 5). Generally, NOESY coupling is possible for protons at distances less than 4 \AA apart. Distances between selected protons and crucial NOESY couplings of compound **1** are shown in Fig. 5. Respective values of all four stereoisomers of **1** are summarized in Table S4. The observed strong NOESY correlation between H-1 and the isopropyl methyl group H_3-12 (distance of 2.6 \AA , Table S4) can be only explained by the relative configuration of the enantiomers X2 (possessing 1*S*,5*R*,6*R*,7*S*,10*S*-configuration) or X3 (possessing the 1*R*,5*S*,6*S*,7*R*,10*R*-configuration). To determine the absolute configuration, the CD spectrum of **1** was recorded and compared with calculated CD spectra of the possible enantiomers (Fig. 4), which verified X3 unequivocally as the correct structure. Thus, the new compound **1** has the absolute 1*R*,5*S*,6*S*,7*R*,10*R*-configuration and was given the trivial name mustak-14-oic acid. The absolute stereochemistry of **1** is in agreement with that of (–)-mustakone, as described by Kapadia et al. [80].

Compound **2** was isolated as yellow oil in a yield of 2.7 mg. The molecular formula was determined as $C_{15}H_{24}O_4$ from the formic acid adduct of the molecular ion peak at m/z 313.1669 $[M + FA]^-$ (calcd. for $C_{16}H_{26}O_6$, 313.1651), obtained from the HR-ESI-MS spectra. The analysis of 1D and 2D NMR spectra (Fig. S2.1–S2.7.) implied that the basic structure of compound **2** is sesquiterpene-like and especially close to the structure of anhuienosol ($C_{15}H_{24}O_3$) by comparison with literature data [81–83] (Table 3, Table S8). However, the CH_2 group present in anhuienosol at position 6 (δ_C 28.6, δ_H 2.91 (brd, $J=13.7$ Hz) + 1.94 (1H, br, $J=13.7$ Hz)) (Table S8) [83] in **2** is replaced by an oxygenated CH group (δ_C 68.05, δ_H 5.26 (d, $J=2.7$ Hz, 1H) implying a hydroxylation at this position. With four stereocenters present in this molecule, theoretically, there could exist 16 possible stereoisomers. None of these can be eliminated based on geometric limitations. Nevertheless, targeted exclusion of isomers through NOESY correlations is attainable. The protons of the methyl group at position 14 (H_3-14) exhibit NOESY correlations to only one hydrogen of each CH_2 group at positions 2, 8, and 9, indicating the same spatial alignment of the respective protons 2a, 8a and 9a. Thus, the absence of NOESY correlation between H_3-14 and H-1 necessitates an orientation in the opposite direction. This is further supported by NOESY correlations between H-1 and H-9b. Therefore, only either 1*R*,10*R* or 1*S*,10*S* configuration is possible. With two additional unspecified stereocenters at positions 6 and 7, eight potential structures remain (Y1–Y8, Fig. S4, Table S6). Following geometric optimizations and MM2 minimize energy calculations, 3D structures of all stereoisomers were created to measure the distances of protons and to compare with observed NOESY correlations. The H_3-15 methyl group appears relatively

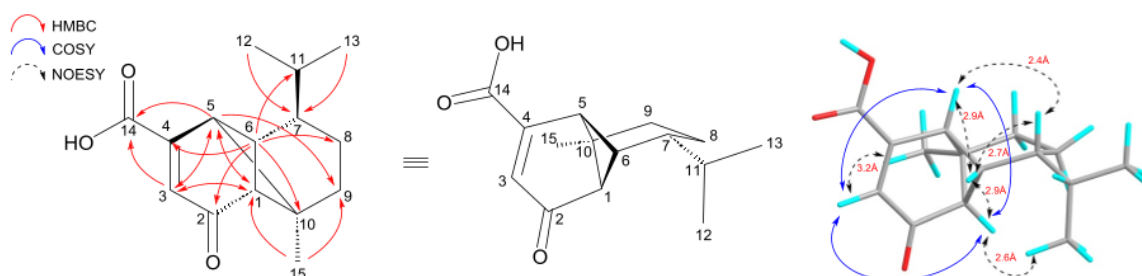


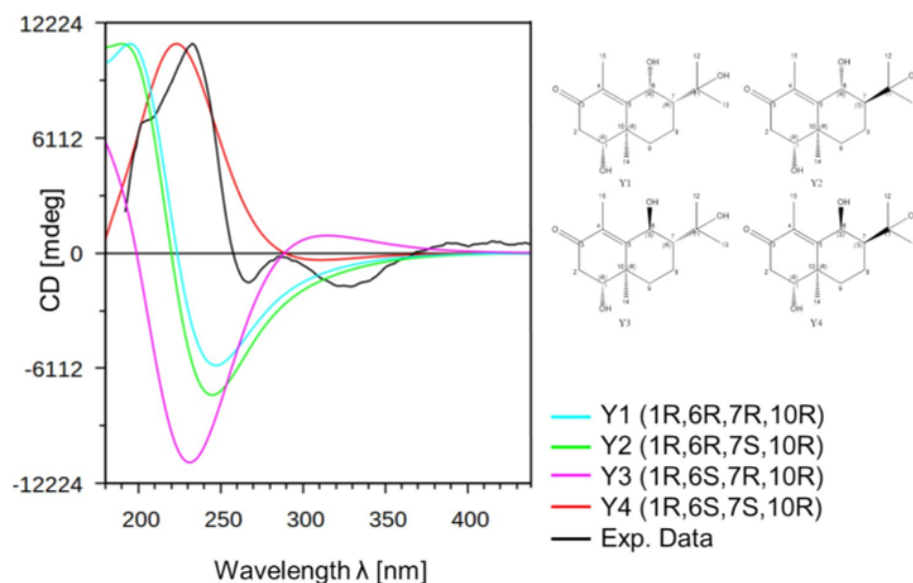
Fig. 5 2D NMR correlations for X3/compound **1**

Table 3 NMR data of compound **2** (MeOD, 500 MHz, 25 °C)

No	δ_C^a	δ_H (multiplicity, J)	COSY	NOESY	HMBC ^b
1	75.2, CH	3.66 (dd, 5.1, 13.1 Hz, 1H)	2a, 2b	2a, 2b, 9b	2, 9, 10, 14
2	43.0, CH ₂	a) 2.60 (dd, 13.1, 16.7 Hz, 1H) b) 2.52 (dd, 5.1, 16.7 Hz, 1H)	1, 2b 1, 2a	1, 2b, 14 1, 2a	1, 3, 10 1, 3, 4, 10
3	201.1, C				
4	132.1, C				
5	161.8, C				
6	68.0, CH	5.26 (d, 2.7 Hz, 1H)	7	7, 13, 15	4, 5, 7, 8, 10, 11
7	50.7, CH	1.30 (m, 1H)	6, 8a, 8b	6	8, 9, 13
8	16.6, CH ₂	a) 2.02 (m, 1H) b) 1.70 (m, 1H)	7, 8b, 9b 8a	8b, 14 8a, 9a, 12	6, 7, 9 6, 7, 9, 10, 11
9	38.3, CH ₂	a) 2.15 (m, 1H) b) 1.25 (m, 1H)	9b 8a, 9a	9b 1, 9a	5, 7, 8, 10, 14 8, 110, 14
10	41.5, C				
11	73.8, C				
12	27.9, CH ₃	1.27 (s, 3H)		8b, 13	7, 11, 13
13	28.2, CH ₃	1.38 (s, 3H)		6, 7, 12	7, 11, 12
14	17.7, CH ₃	1.31 (s, 3H)		2a, 8a, 9a	1, 5, 9, 10
15	9.9, CH ₃	1.85 (s, 3H)		6	3, 4, 5, 10

^a obtained from HSQC and HMBC, ^b600 MHz, 160 scans

isolated and only displays NOESY correlation with H-6. Notably, the orientation of H-6 is irrelevant in this context, as the distance to H₃–15 is less than 3 Å in all stereoisomers (2.0–2.4 Å, Table S6). In addition, H-6 shows NOESY correlations with H-7 (2.3–3.0 Å in all stereoisomers, Table S6) and H₃–13 (2.1–2.3 Å in all stereoisomers, Table S6), but none with any of the ring-bound protons H-1, H-8a/b or H-9a/b. Therefore, an equatorial rather than an axial position for H-6 is suspected. A comparison of distances between H-6 and all ring-bound protons for all stereoisomers revealed that only the enantiomers Y4/Y8 have consistently distances of > 4 Å and the expected equatorial position for H-6 and thus possess the correct relative configuration (Table S6). The elucidation of the absolute stereochemistry was done by comparison of experimental CD spectra with the calculated CD spectra of the possible stereoisomers (Fig. 6), which verified Y4 with the absolute 1*R*,6*S*,7*S*,10*R* configuration unequivocally as correct structure for the here isolated compound **2**, trivially named 6-hydroxy-anhuienosol (Fig. 7).

Fig. 6 CD spectra + calculated spectra of stereoisomers Y1–Y4 of compound **2**

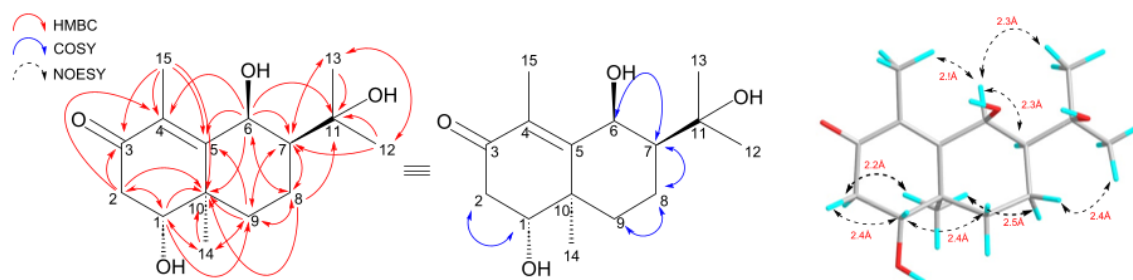


Fig. 7 2D NMR correlations for Y4/compound **2**

Beside terpenoids and simple phenolics, flavonoids constitute a major compound class of *H. scyphifera* with kumatakenin (**13**) as main representative. In addition to structure identification by NMR data, (SI, Spectroscopic data of isolated compounds, No. 13), we describe here for the first time the structure of kumatakenin by X-ray crystallography. The X-ray analysis was performed on a crystal with the size of $0.295 \times 0.029 \times 0.015$ mm (Fig. S11). It is a monoclinic crystal that shows a $P2_1/c$ space group. From the data it was possible to obtain all atom bonding which results in verification of the molecular structure (Fig. 8). Nevertheless, due to the small dimension of the crystal, only a weak dataset could be achieved, which is visible among others in the Goof of 0.863 (Table S15).

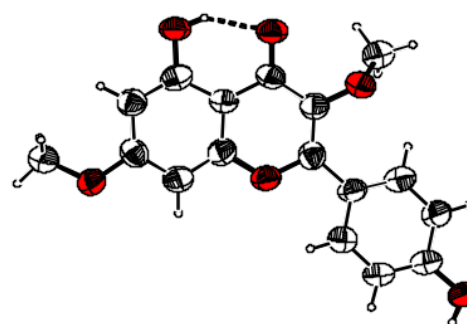
Exemplarily, we performed an extensive MS^n analysis of kumatakenin and present a fragmentation pathway (Fig. 9) in accordance with well researched fragmentation mechanisms of flavonoids [84–88]. From HRMS the molecular formula of $C_{17}H_{14}O_6$ was known. The follow-up MS^n experiments, performed in four steps from MS^2 to MS^5 , showed the subsequent losses of methyl radicals followed by characteristic CO and CO_2 elimination (Fig. 9).

3.3 Considerations on biological activity

Most of the compounds isolated from *H. scyphifera* leaves are widely distributed in plants and known for decades. Therefore, their biological effects were already exhaustively evaluated in previous studies. In addition, limitations in the yield of new compounds did not allow the submission to bioassays. Thus, we performed a literature review and focused on known sources and reported bioactivities for all 24 known compounds and on structurally related compounds for the two new isolates **1** and **2** (Table 4).

The Zingiberaceae family is known for various biological activities like e.g. anti-inflammatory and neuroprotective properties. Inflammatory and neurological diseases commonly arise in the presence of proinflammatory and proliferation-inducing cytokines, as well as through an escalation in the proliferation rate of immune system cells, or as a result of high levels of free radicals being released [20]. Cytokines are small proteins that act as messengers between cells, that are involved in the inflammatory response. In Zingiberaceae the pungent constituents like gingerols and shogaols, form one characteristic compound classes of this family, and are considered to be responsible for many pharmaceutical effects [89, 90]. These flavor components are phenolic ketones and structurally related to diarylheptanoids, like curcumin. Their anti-inflammatory effect arises from the inhibition of the synthesis of prostaglandins [91] as well as the inhibition of enzymes that produce NO radicals [92]. They also inhibit the synthesis and secretion of proinflammatory cytokines [90, 93, 94] such as interleukin-2 (IL-2). The extracts obtained from leaves of *H. scyphifera* were reported to

Fig. 8 Structure of kumatakenin (**13**), obtained from X-Ray



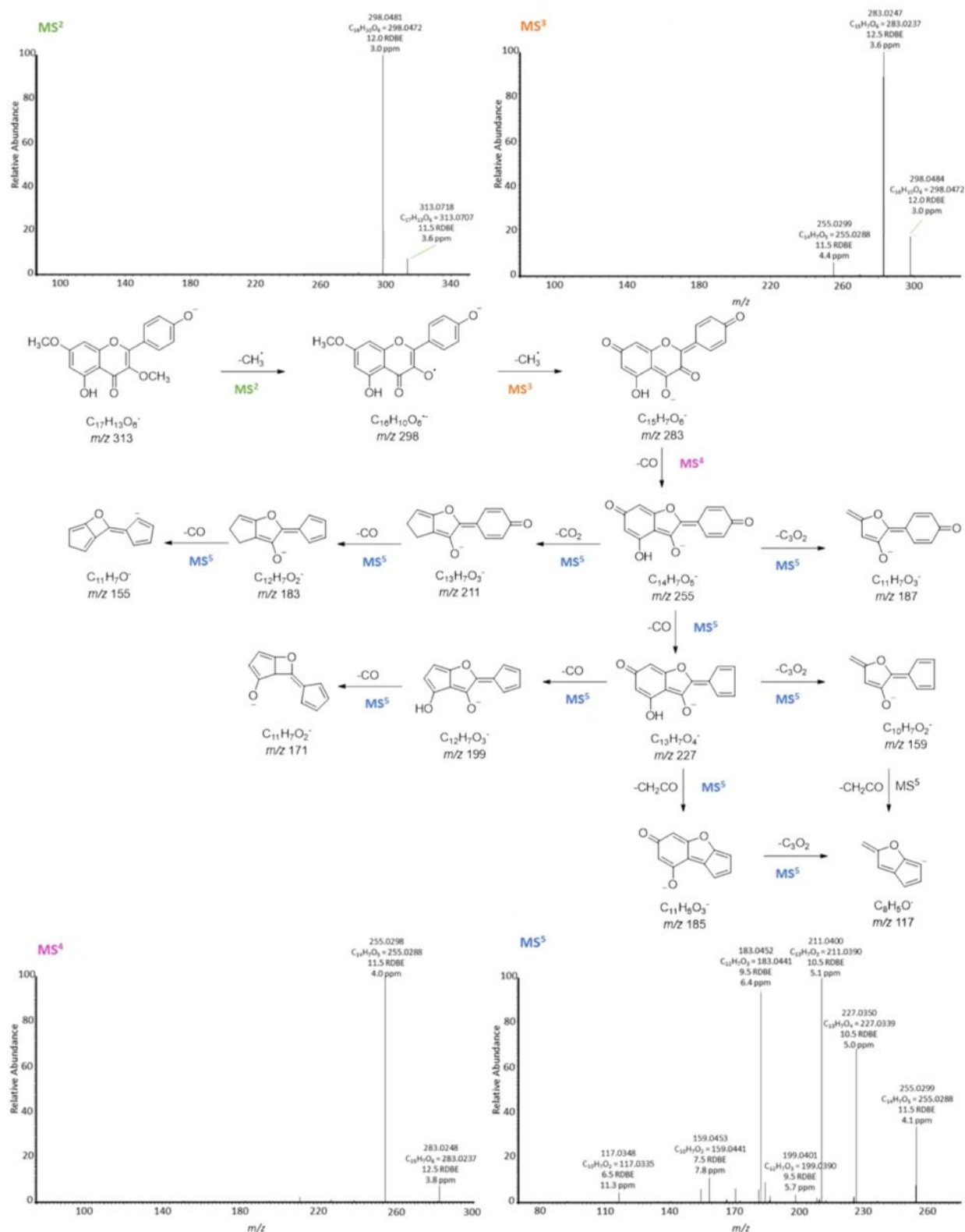


Fig. 9 Spectra and fragmentation pathway of the MS^n analysis of kumatakenin (13) in negative ion mode

Table 4 Reported sources and biological properties of compounds isolated from the crude extracts of *H. scyphifera* leaves

No	Name (Chemical Formula)	Compound class	Also known from: Family (Species)	Bioactivity described
3	(E)-14,15,16-Trinorlabda-8(17),11-dien-13-oic acid (C ₁₇ H ₂₆ O ₂)	Labdane-type diterpene	Zingiberaceae (<i>Curcuma amada</i> [123], <i>Alpinia pahangensis</i> [124])	Antibacterial [124]
4	Verbenon-10-oic acid (C ₁₀ H ₁₂ O ₃)	Monoterpene	Lamiaceae (<i>Hyssopus cuspidatus</i> [40])	Antimicrobial [40], antifungal [40]
5	cis-Pinonic acid (C ₉ H ₁₄ O ₃)	Ketoacid	Synthesis product of Verbenon [42]	-
6	cis-Pinonic acid (C ₁₀ H ₁₆ O ₃)	Ketoacid	Synthesis product Verbenon [44]	-
7	2-(2,2,3-Trimethyl-5-oxocyclopent-3-en-1-yl) acetic acid (C ₁₀ H ₁₄ O ₃)	Ketoacid	Degradation product of Camphor [46]	-
8	Epicatechin (C ₁₅ H ₁₄ O ₆)	Flavonoid/Flavanol	Rosaceae (apple pomace [125])	Anticancer [126], antiinflammatory [126], antioxidant [105, 125, 127], neuroprotective [128, 129]
9	Sakuranetin (C ₁₆ H ₁₄ O ₅)	Flavonoid/Flavanon	Rubiaceae (<i>Gardenia ternifolia</i> [130]) Heliotropiceae (<i>Heliotropium glutinosum</i> [131]) Asteraceae (<i>Ageratina havanensis</i> [132], <i>Baccharis retusa</i> [109])	Antioxidant [130, 131], antiviral [132], antimicrobial [109]
10	Quercetin (C ₁₅ H ₁₀ O ₇)	Flavonoid/Flavonol	Amaryllidaceae (onions (<i>Allium</i>) [104, 133]) Rutaceae (<i>Citrus aurantifolia</i> [104, 134]) Apiaceae (<i>Petroselinum crispum</i> [104, 135]) Oleaceae (olives (<i>Ole</i>) [104, 136]) Hypericaceae (<i>Hypericum perforatum</i> [104, 137]) Ginkgoaceae (<i>Ginkgo biloba</i> [104, 138]) Zingiberaceae (<i>Hornstedtia scyphifera</i> [18], <i>Zingiber officinale</i> [95])	Antibacterial [104, 139], antiinflammatory [104, 140] neuroprotective [141, 142], anticancer [95, 104, 141], antioxidant [95, 104, 134, 135]
11	Rutin (C ₂₇ H ₃₀ O ₁₆)	Flavonoid/Flavonol glycoside	Rutaceae (<i>Citrus aurantifolia</i> [134]) Oleaceae (olives (<i>Ole</i>) [136]) Fabaceae (<i>Sophora japonica</i> [143]) Polygonaceae (<i>Fagopyrum esculentum</i> [144]) Rutaceae (<i>Ruta graveolens</i> [145]) Strelitziaceae (<i>Strelitzia reginae</i> [146, 147]) Marantaceae (<i>Maranta leuconeura</i> [146, 147]) Solanaceae (tobacco leaves (<i>Nicotiana</i> [146, 147])	Antidiabetic [143], neuroprotective [142], hepatoprotective [148], anticancer [146], antiinflammatory [147, 149], antioxidant [134, 147, 150]
12	Isokaempferide (C ₁₆ H ₁₂ O ₆)	Flavonoid/Flavonol	Zingiberaceae (<i>Hornstedtia reticulata</i> [19], Fabaceae (<i>Amburana cearensis</i> [151]) Lamiaceae (<i>Dracocephalum subcapitatum</i> [152], <i>D. kotschy</i> [153]) Zingiberaceae (<i>Alpinia galanga</i> [96]) Asteraceae (<i>Centaurea jacea</i> [154]) Fabaceae (<i>Amburana cearensis</i> [155])	Antiproliferative [151], antitumor [154], anti-inflammatory [155], antioxidant [153]
13	Kumatakenin (C ₁₇ H ₁₄ O ₆)	Flavonoid/Flavonol	Zingiberaceae (<i>Hornstedtia scyphifera</i> [19]) Lamiaceae (<i>Ballota glandulosissima</i> [110]) Boraginaceae (<i>Alkanna orientalis</i> [156]) Myrtaceae (<i>Syzygium aromaticum</i> [157]) Scrophulariaceae (<i>Buddleja albiflora</i> [158])	Antimicrobial [110], antifungal [110], antiviral [156], anticancer [157], insecticidal [158]

Table 4 (continued)

No	Name (Chemical Formula)	Compound class	Also known from: Family (Species)	Bioactivity described
14	5-Hydroxy-3,7,4'-trimethoxyflavon ($C_{18}H_{16}O_6$)	Flavonoid/Flavonol	Zingiberaceae (<i>H. scyphifera</i> [19], <i>Kaempferia parviflora</i> [98]) Tamaricaceae (<i>Tamarix gallica</i> [159]) Lamiaceae (<i>Ballota inaequidens</i> [110])	Antimicrobial [110], antifungal [110], antioxidant [159]
15	(E) <i>p</i> -Coumaric acid ($C_9H_8O_3$)	Phenolic acid	Poaceae (barley [160]) Polygonaceae (buckwheat [161]) Rubiaceae (<i>Oldenlandia diffusa</i> [162])	Antioxidant [161], antimicrobial [111], anti-inflammatory [162], anticancer [163], antibacterial [164]
16	<i>trans</i> -Ferulic acid ($C_{10}H_{10}O_4$)	Phenolic acid	Poaceae (<i>Zea mays</i> hybrid maize [165])	Anti-inflammatory [166], antioxidant [112], antimicrobial [112]
17	<i>cis</i> -Ferulic acid ($C_{10}H_{10}O_4$)	Phenolic acid	Pinaceae (white spruce [167]) Poaceae (<i>Triticum aestivum</i> [168])	
18	Evofofin B ($C_{17}H_{18}O_6$)	Phenolic	Malvaceae (<i>Sida acuta</i> [113], <i>Sida rhombifolia</i> [169]) Fabaceae (<i>Caesalpinia bondu</i> [170])	Antibacterial [113], antioxidant [169], cytotoxic [170]
19	Protocatechualdehyde ($C_7H_6O_3$)	Phenolic aldehyde	Musaceae (green cavendish banana [121]) Rosaceae (Japanese apricot, <i>Prunus mume</i> [171]) Hymenophyllaceae (<i>Trichomanes chinense</i> fern [114]) Rhodamelaceae (<i>Polysiphonia morrowii</i> [172])	Fungistatic [121], antioxidant [114], antiallergic [172]
20	Vanillin ($C_8H_8O_3$)	Phenolic aldehyde	Orchidaceae (<i>Vanilla planifolia</i> [173], <i>V. tahitensis</i> [174])	Anticancer [175], antioxidant [176], anti-inflammatory [177], antibacterial [178], neuroprotective [179]
21	Syringaldehyde ($C_9H_{10}O_4$)	Phenolic aldehyde	Asteraceae (<i>Mikania laevigata</i> [180], <i>M. glomerata</i> [180])	Antioxidant [181], antimicrobial [182], antifungal [182], anticancer [183]
22	<i>p</i> -Hydroxybenzoic acid ($C_7H_6O_3$)	Phenolic acid	Apiaceae (<i>Daucus carota</i> [184]) Cucurbitaceae (cucumber, <i>Cucumis sativus</i> [185]) Arecaceae (<i>Phoenix dactylifera</i> [186])	Antimicrobial [187, 188], anti-inflammatory [189], antioxidant [188]
23	Protocatechuic acid ($C_7H_6O_4$)	Phenolic acid	Zingiberaceae (<i>Roscoe purpurea</i> [99], <i>Alpinia zerumbet</i> [190]) Aquifoliaceae (<i>Ilex chinensis</i> [191])	Anti-inflammatory [190, 192, 193], antinociceptive [190], antipyretic [190], antioxidant [191], analgesic [193]
24	Vanillic acid ($C_8H_8O_4$)	Phenolic acid	Lamiaceae (<i>Origanum vulgare</i> [194])	Antioxidant [194, 195], antinociceptive [196], nephroprotective [197], antidiabetic [198]
25	Protocatechuic acid methyl ester ($C_8H_8O_4$)	Phenolic ester	Amaranthaceae (<i>Chenopodium murale</i> [195])	Pulmonary protective [199]
26	5-Methoxy salicylic acid ($C_8H_8O_4$)	Phenolic acid	Zingiberaceae (<i>Amomum xanthioides</i> [100]) Phyllanthaceae (<i>Antidesma bunius</i> [200])	

inhibit the release of cytokine IL-2 from activated T-cells, reduce the proliferation rate of these T-cells and also minimize the release of nitric oxide radicals (NO) from activated microglial cells [20]. However, in our study of *H. scyphifera* we did not find any of the characteristic pungent compounds. Thus, the observed effects should result from other compound classes. We detected in *H. scyphifera* seven components known to occur in various species from the ginger family such as (*E*)-14,15,16-trinorlabda-8(17),11-dien-13-oic acid (**3**) from *Zingiber ottensii* [39], quercetin (**10**) from *Zingiber officinale* [95], isokaempferide (**12**) from *Alpinia galanga* [96] or *H. reticulata* [19], kumatakenin (**13**) from *Curcuma aromatica* [97] or *H. scyphifera* [19], 5-hydroxy-3,7,4'-trimethoxyflavone (**14**) from *Kaempferia parviflora* [98] or *H. scyphifera* [19], protocathechuic acid (**23**) from *Roscoea purpurea* [99], and protocathechuic acid methyl ester (**25**) from *Amomum xanthioides* [100]. These compounds reflect all three major compound groups identified in this study for *H. scyphifera*, namely terpenoids (**3**), flavonoids (**10**, **12**, **13** and **14**) and other phenolics (**23** and **25**). All three groups are known for anti-inflammatory effects [101]. Flavonoids such as epicatechin, sakuranetin, and quercetin are known to actively inhibit the release of cytokines like IL1 β , and consequently passively suppress the IL1 β -induced expression of NO radicals [102–104]. They are also able to trap radicals actively by donating phenolic hydrogen [105]. The same ability of free radical scavenging is reported for many phenolic compounds including isolates from *H. scyphifera*, namely ferulic acid (**16**, **17**), vanillin (**20**), vanillic acid (**24**), *p*-coumaric acid (**15**) and protocathechuic acid (**23**) [106]. Recently, El Omari et al. [107] showed, that sesquiterpene lactones are able to reduce specifically the IL-2 secretion, like Zipp, Ullrich et al. [20] reported earlier for *H. scyphifera* extracts. The same effects might be attributed to the newly found sesquiterpene lactone mustak-14-oic acid (**1**). In conclusion, the presence of flavonoids, phenols and terpenoids in combination could explain the reported anti-inflammatory and neuroprotective activities of *H. scyphifera* extract [20].

There is also a number of reports concerning the antifungal and antimicrobial activity of *H. scyphifera* isolates which aligns with the results of the growth-inhibition assays against the Gram-negative bacterium *A. fischeri* (Fig. S1.1.B) and the fungus *Botrytis cinerea* (Fig. S1.2.B) in the present study and with reports from literature [18, 20]. These bioactivities probably arise mainly from flavonoids and phenolics. Antimicrobial compounds are **4** [40], **8** [101], **9** [108, 109], **10** [18, 104], **13** [110], **14** [94, 110], **15** [111], **16** [112], **18** [113], **19** [114], **21** [115, 116], **22** [117], and **23** [118], and antifungal compounds are **9** [119], **13** [110], **14** [120], **19** [121], **20** [121], **21** [115, 116, 122]. However, terpenoids are often relevant for antifungal activity, like verbenon-10-oic acid (**4**) [40] and mustakone [77], a compound structurally closely related to sesquiterpenoid **1**. Applications of 20 μ g in standardized disc assays resulted in the inhibition of *Candida albicans* [40] and *Penicillium crustosum* [77].

Further potential effects *H. scyphifera* might exhibit based on the discovered constituents can be taken from the literature review (Table 4). Based on this, the species appears to be a promising study subject for more intensive investigations to unravel its full pharmaceutical potential. In summary, among the 26 isolated compounds, the predominant biological activities found so far cover antimicrobial and antifungal as well as anti-inflammatory and neuroprotective potentials, the latter effect often linked to the anti-inflammatory action. However, the high number of different active compounds suggests, that effects of the extract also might result from the combined powers of several active constituents, rather than being exerted by a single component with high specificity.

4 Conclusion

In conclusion, the phytochemical investigation of *H. scyphifera* leaves using multiple analytical methods has provided valuable insights into its chemical composition. Through GCMS analysis of headspace and of the essential oil, the presence of common aroma components such as α -pinene, camphene, *p*-cymene, and camphor were confirmed, along with the identification of a previously unreported compound, butylbenzene. Further analysis via UHPLC-HRMS allowed for the annotation of additional metabolites, identifying flavonoids, terpenoids and phenolics as the major compound classes of *H. scyphifera*. Purification of the crude extract led to the isolation of the two new sesquiterpenoids mustak-14-oic acid (**1**) and 6-hydroxy-anhuienosol (**2**) along with 24 known compounds. Structural elucidation of these compounds was achieved through a combination of extensive spectroscopic techniques, including 1D and 2D NMR and HRMS as well as comparison with literature data. Furthermore, the determination of stereochemistry was facilitated by NOESY correlations and CD spectroscopy. As an example of the flavonoid class, a four step MSⁿ analysis of kumatakenin (**13**) was performed and based on known fragmentation mechanisms, a full annotated fragmentation pathway could be established. This is also the first time that the keto acids **5**, **6** and **7** were isolated from plant origin. While the possibility that they originate from plant-associated bacteria or fungi cannot be ruled out, the quantities observed strongly suggest a plant origin.

Bioassays revealed antimicrobial and antifungal activities in fractions enriched with nonpolar isolated compounds. Intensive literature research of all isolated compounds showed that many of them are known for mild activities in such assays. For *H. scyphifera* activity, this implies an additive, maybe synergistic, combination of several constituents rather than one individual highly active compound with high selectivity being responsible. Along with the antimicrobial activity mentioned, there are further beneficial effects known for the isolated compounds, namely anti-inflammatory and neuroprotective activities which support observed effects of *H. scyphifera* extracts described in the literature. Overall, the comprehensive phytochemical investigation of *H. scyphifera* leaves has contributed to a deeper understanding of their chemical composition and increased the molecular basis for understanding its observed biological activities, laying the foundation for further studies on pharmacological and therapeutic applications.

Acknowledgements The authors would like to thank M. Brode (IPB Halle) for the performance of antibacterial and antifungal bioassays. We are grateful to P. Stark, A. Porzel, and G. Hahn (IPB Halle) for NMR, CD, UV and specific rotation measurements, as well as to A. Laub, J. Schmidt, A. Soboleva, M. Hempel, and E. Kysil (IPB Halle) for HRMS measurements. We thank the colleagues/groups of Prof. F. Zipp (Magdeburg, now Mainz), Prof. O. Ullrich (Magdeburg, now Zürich) and Prof. J. Heilmann (Regensburg) for discussions on *H. scyphifera* effects prior to the project.

Author contributions J.K. performed the main phytochemical investigations, data analysis and visualization and wrote the main manuscript. A.D. performed studies on volatiles and literature searches on biological activities of known compounds leading to Tables S2 and 4, respectively. K.P., A.W. and I.W. contributed to the isolation and structure elucidation of constituents. D.D. and M.D. performed computational CD spectral analysis and prepared Figs. 6, S5, S6, S7 and Tables S3–S6; S9–S14. C.W. performed X-Ray crystallography of kumatakenin connected to Figs. 8, S11 and Table S15. K.F. was involved in data curation and validation and supervised the work. L.A.W. designed the study, acquired funding, provided resources and supervision. All authors reviewed and edited the manuscript.

Funding Financial support for this study was provided by the project “Indonesian Plant Biodiversity and Human Health – BIOHEALTH” (BMBF grants no. 16GW0120K) to L.A. Wessjohann. J. Kappen and K. Franke were also funded within the frame of the project ProCognito by EFRE and the state Saxony-Anhalt (ZS/2018/11/95581). I. Ware was funded by the German Academic Exchange Service (DAAD grant number 57299294, ST34). We also thank the MOE Fellowship program of the Deutsche Bundesstiftung Umwelt (DBU) for the support of A. David.

Data availability Data are included in the article and the supplementary material. The raw data supporting the conclusions of this article will be made available by the corresponding authors on request. The plant material is deposited at IPB, Germany. All primary data and reference compounds are stored at the IPB primary data storage for 10+ years, and in the compound depository to the extent available or stable.

Code availability Not applicable.

Declarations

Ethics approval and consent to participate Not applicable.

Consent for publication Not applicable.

Competing interests The authors declare no competing interests.

Open Access This article is licensed under a Creative Commons Attribution 4.0 International License, which permits use, sharing, adaptation, distribution and reproduction in any medium or format, as long as you give appropriate credit to the original author(s) and the source, provide a link to the Creative Commons licence, and indicate if changes were made. The images or other third party material in this article are included in the article's Creative Commons licence, unless indicated otherwise in a credit line to the material. If material is not included in the article's Creative Commons licence and your intended use is not permitted by statutory regulation or exceeds the permitted use, you will need to obtain permission directly from the copyright holder. To view a copy of this licence, visit <http://creativecommons.org/licenses/by/4.0/>.

References

1. Kress WJ, Prince LM, Williams KJ. The phylogeny and a new classification of the gingers (Zingiberaceae): evidence from molecular data. *Am J Bot.* 2002. <https://doi.org/10.3732/ajb.89.10.1682>.
2. Pancharoen O, Prawat U, Tuntiwachwuttikul P. Phytochemistry of the Zingiberaceae. In: Rahman Au, editor. *Studies in natural products chemistry bioactive natural products (Part D)*. Cambridge: Elsevier; 2000.
3. Wu D, Larsen K. Zingiberaceae. In: Wu Z, Peter HR, editors. *Flora of China*. Beijing: Science-Press Missouri Botanical Garden Press.; 2000.
4. Braga MC, Vieira ECS, Oliveira TF. *Curcuma longa* L. leaves: characterization (bioactive and antinutritional compounds) for use in human food in Brazil. *Food Chem.* 2018. <https://doi.org/10.1016/j.foodchem.2018.05.096>.
5. Alolga RN, Wang F, Zhang X, Li J, Tran LP, Yin X. Bioactive compounds from the Zingiberaceae family with known antioxidant activities for possible therapeutic uses. *Antioxidants*. 2022. <https://doi.org/10.3390/antiox11071281>.
6. Wink M. Plant breeding: Importance of plant secondary metabolites for protection against pathogens and herbivores. *Theor Appl Genet.* 1988. <https://doi.org/10.1007/BF00303957>.

7. Wink M. Modes of action of herbal medicines and plant secondary metabolites. *Medicines*. 2015. <https://doi.org/10.3390/medicines2030251>.
8. Pagare S, Bhatia M, Tripathi N, Bansal YK. Secondary metabolites of plants and their role: overview. *Curr Trends Biotechnol Pharm*. 2015;9(3):293–304.
9. Lake JA, Field KJ, Davey MP, Beerling DJ, Lomax BH. Metabolomic and physiological responses reveal multi-phasic acclimation of *Arabidopsis thaliana* to chronic UV radiation. *Plant Cell Environ*. 2009. <https://doi.org/10.1111/j.1365-3040.2009.02005.x>.
10. Souissi M, Azelmat J, Chaieb K, Grenier D. Antibacterial and anti-inflammatory activities of cardamom (*Elettaria cardamomum*) extracts: potential therapeutic benefits for periodontal infections. *Anaerobe*. 2020. <https://doi.org/10.1016/j.anaerobe.2019.102089>.
11. Dahham SS, Tabana YM, Iqbal MA, Ahamed MBK, Ezzat MO, Majid ASA, Majid AMSA. The anticancer, antioxidant and antimicrobial properties of the sesquiterpene β -caryophyllene from the essential oil of *Aquilaria crassna*. *Molecules*. 2015. <https://doi.org/10.3390/molecules200711808>.
12. Menon VP, Sudheer AR. Antioxidant and anti-inflammatory properties of curcumin. *Adv Exp Med Biol*. 2007. https://doi.org/10.1007/978-0-387-46401-5_3.
13. Ge W, Li H, Zhao Y, Cai E, Zhu H, Gao Y, Liu S, Yang H, Zhang L. Study on antidepressant activity of sesquiterpenoids from ginseng root. *J Funct Foods*. 2017. <https://doi.org/10.1016/j.jff.2017.03.057>.
14. Govaerts R. *The World Checklist of Vascular Plants (WCVP)*. The Royal Botanic Gardens. Kew. 2022. <https://www.gbif.org/dataset/5e8ba9ca-1cac-4ddb-88c8-c14c098ad104#citation>. Accessed 27 May 2024.
15. Holttum RE. The Zingiberaceae of the Malay Peninsula. The Gardens bulletin. Singapore. 1950.
16. Newman M, Lhuillier A, Poulsen AD. *Checklist of the Zingiberaceae of Malesia*. Nat Herbar Nederland Uni Leiden. Leiden. 2004.
17. Hashim SE, Sirat HM. Chemical composition, antioxidant, antimicrobial, and α -glucosidase activities of essential oils of *Hornstedtia scyphifera* (Zingiberaceae). *Nat Prod Commun*. 2018. <https://doi.org/10.1177/1934578X1801300228>.
18. John UI, Hauwa AU, Ojochenemi Y, Isaac UK. Isolation and characterization of chemical constituents, cytotoxicity antibacterial and antioxidant activity of the isolates, crude extract from *Hornstedtia scyphifera* var leaf. *GSC Biol Pharm Sci*. 2020. <https://doi.org/10.30574/gscbps.2020.10.2.0027>.
19. Hashim SE, Sirat HM, Yen KH, Ismail IS, Matsuki SN. Antioxidant and α -glucosidase inhibitory constituents from *Hornstedtia* species of Malaysia. *Nat Prod Commun*. 2015. <https://doi.org/10.1177/1934578X1501000919>.
20. Zipp F, Ullrich O. Extracts from the plant *Hornstedtia scyphifera* and immunosuppressive effects. EP2163253A1. 2008.
21. Suekaew N, Na Pombajra S, Kulsing C, Doungchawee J, Khotavivattana T. Bioassay-guided fractionation, chemical compositions and antibacterial activity of extracts from rhizomes of *Globba schomburgkii* Hook f. *Chem Biodivers*. 2020. <https://doi.org/10.1002/cbdv.202000173>.
22. Songsri S, Nuntawong N. Cytotoxic labdane diterpenes from *Hedychium ellipticum* Buch Ham ex Sm. *Molecules*. 2016. <https://doi.org/10.3390/molecules21060749>.
23. Akiyama K, Kikuzaki H, Aoki T, Okuda A, Lajis NH, Nakatani N. Terpenoids and a diarylheptanoid from *Zingiber ottensii*. *J Nat Prod*. 2006. <https://doi.org/10.1021/np0603119>.
24. Aihaiti K, Li J, Xu N, Tang D, Aisa HA. Monoterpenoid derivatives from *Hyssopus cuspidatus* Boriss and their bioactivities. *Fitoterapia*. 2023. <https://doi.org/10.1016/j.fitote.2023.105432>.
25. Zhang JF, Zhong WC, Li YC, Song YQ, Xia GY, Tian GH, Ge GB, Lin S. Bioactivity-guided discovery of human carboxylesterase inhibitors from the roots of *Paeonia lactiflora*. *J Nat Prod*. 2020. <https://doi.org/10.1021/acs.jnatprod.0c00464>.
26. Passaro LC, Webster FX. Synthesis of the female sex pheromone of the citrus mealybug. *Planococcus citri* J Agric Food Chem. 2004. <https://doi.org/10.1021/ja01529a060>.
27. Kukovinets OS, Zvereva TI, Kasradze VG, Galin FZ, Frolova LL, Kuchin AV, Spirikhin LV, Abdullin MI. Novel synthesis of *Planococcus citri* pheromone. *Chem Nat Compd*. 2006. <https://doi.org/10.1007/s10600-006-0082-x>.
28. Bellcross A, Bé AG, Geiger FM, Thomson RJ. Molecular chirality and cloud activation potentials of dimeric α -pinene oxidation products. *J Am Chem Soc*. 2021. <https://doi.org/10.1021/jacs.1c07509>.
29. Leisch H, Shi R, Grosse S, Morley K, Bergeron H, Cygler M, Iwaki H, Hasegawa Y, Lau PCK. Cloning, Baeyer-Villiger biooxidations, and structures of the camphor pathway 2-oxo- $\Delta(3)-4,5,5$ -trimethylcyclopentenylacetyl-coenzyme a monooxygenase of *Pseudomonas putida* ATCC 17453. *Appl Environ Microbiol*. 2012. <https://doi.org/10.1128/AEM.07694-11>.
30. Bradshaw WH, Conrad HE, Corey EJ, Gunsalus IC, Lednicer D. Microbiological degradation of (+)-camphor. *J Am Chem Soc*. 1959. <https://doi.org/10.1021/ja01529a060>.
31. Dugar S, Mahajan D, Giannousis PP, Singh V, Kapoor KK. A novel process for synthesis of polyphenols. EP2668176B1. 2012.
32. Shen CC, Chang YS, Hott LK. Nuclear magnetic resonance studies of 5,7-dihydroxyflavonoids. *Phytochemistry*. 1993. [https://doi.org/10.1016/0031-9422\(93\)85370-7](https://doi.org/10.1016/0031-9422(93)85370-7).
33. Piao S, Qi Y, Jin M, Diao S, Zhou W, Sun J, Jin X, Li G. Two new quinones and six additional metabolites with potential anti-inflammatory activities from the roots of *Juglans mandshurica*. *Nat Prod Res*. 2022. <https://doi.org/10.1080/14786419.2020.1862831>.
34. Lee YJ, Cui J, Lee J, Han AR, Lee EB, Jang HH, Seo EK. Cytotoxic compounds from *Juglans sinensis* Dode display anti-proliferative activity by inducing apoptosis in human cancer cells. *Molecules*. 2016. <https://doi.org/10.3390/molecules21010120>.
35. Lou Y, Xu T, Cao H, Zhao Q, Zhang P, Shu P. Natural antioxidants, tyrosinase and acetylcholinesterase inhibitors from *Cercis glabra* leaves. *Molecules*. 2022. <https://doi.org/10.3390/molecules27248667>.
36. Oliveira DM, Siqueira EP, Nunes YR, Cota BB. Flavonoids from leaves of *Mauritia flexuosa*. *Rev Bras Farmacogn*. 2013. <https://doi.org/10.1590/S0102-695X2013005000061>.
37. Fernandes FHA, Da Silva SS, Bekbolatova E, Boylan F, Salgado HRN. Pharmacological, toxicological and phytochemical analysis of *Spondias dulcis* parkinson. *Nat Prod Res*. 2024. <https://doi.org/10.1080/14786419.2023.2210254>.
38. Costa AG, Yoshida NC, Garcez WS, Perdomo RT, Matos MC, Garcez FR. Metabolomics approach expands the classification of propolis samples from midwest Brazil. *J Nat Prod*. 2020. <https://doi.org/10.1021/acs.jnatprod.9b00783>.

39. Dao T, Nguyen T, Nguyen V, Tran T, Tran N, Nguyen C, Nguyen HH, Sichaem J, Tran CL, Duong TH. Flavones from *Combretum quadrangulare* growing in Vietnam and their α -glucosidase inhibitory activity. *Molecules*. 2021. <https://doi.org/10.3390/molecules26092531>.
40. Lu K, Chu J, Wang H, Fu X, Quan D, Ding H, Yao Q, Yu P. Regioselective iodination of flavonoids by N-iodosuccinimide under neutral conditions. *Tetrahedron Lett*. 2013. <https://doi.org/10.1016/j.tetlet.2013.09.051>.
41. Ma T, Sun Y, Wang L, Wang J, Wu B, Yan T, Jia Y. An investigation of the anti-depressive properties of phenylpropanoids and flavonoids in *Hemerocallis citrina* Baroni. *Molecules*. 2022. <https://doi.org/10.3390/molecules27185809>.
42. Salum ML, Robles CJ, Erra-Balsells R. Photoisomerization of ionic liquid ammonium cinnamates: One-pot synthesis-isolation of Z-cinnamic acids. *Org Lett*. 2010. <https://doi.org/10.1021/ol1019508>.
43. Liu XY, Guo Q, Zhang YS, Tu PF, Zhang QY. Enantiomeric phenylpropanoids from *Uncaria rhynchophylla*. *Chem Nat Compd*. 2022. <https://doi.org/10.1007/s10600-022-03860-1>.
44. Jiang X, Chi J, Feng Q, Wu H, Wang Z, Dai L. Isolation and identification of antioxidant constituents from the flowers of *Salvia miltiorrhiza*. *Nat Prod Res*. 2023. <https://doi.org/10.1080/14786419.2023.2198710>.
45. Mahnashi MH, Alyami BA, Alqahtani YS, Alqarni AO, Jan MS, Hussain F, Zafar R, Rashid U, Abbas M, Tariq M, Sadiq A. Antioxidant molecules isolated from edible prostrate knotweed: Rational derivatization to produce more potent molecules. *Oxidative Med Cell Longev*. 2022. <https://doi.org/10.1155/2022/3127480>.
46. Chung C, Hsia S, Lee M, Chen H, Cheng F, Chan L, Kuo Y, Lin Y, Chiang W. Gastroprotective activities of adlay (*Coix lachryma-jobi* L var *ma-yuen* Stapf) on the growth of the stomach cancer AGS cell line and indomethacin-induced gastric ulcers. *J Agric Food Chem*. 2011. <https://doi.org/10.1021/jf2009556>.
47. Chen Y, Hou J, Huang L, Khan A, Xing F, Zhang X, Han D, Yan S, Cao G, Jiao QY, Liu D, Zhu X, Hu Q, Lou H. Chemical constituents of *Viscum coloratum* (Kom) Nakai and their cytotoxic activities. *Nat Prod Res*. 2022. <https://doi.org/10.1080/14786419.2020.1837816>.
48. Jung YW, Lee JA, Lee JE, Cha H, Choi YH, Jeong W, Choi CW, Oh JS, Ahn EK, Hong SS. Anti-adipogenic activity of secondary metabolites isolated from *Silax sieboldii* Miq on 3T3-L1 adipocytes. *Int J Mol Sci*. 2023. <https://doi.org/10.3390/ijms24108866>.
49. Meng Q, Li G, Luo B, Wang L, Lu Y, Liu W. Screening and isolation of natural antioxidants from *Ziziphora clinopodioides* Lam with high performance liquid chromatography coupled to a post-column Ce(IV) reduction capacity assay. *RSC Adv*. 2016. <https://doi.org/10.1039/C6RA08588A>.
50. Jeong GH, Kim TH. New anti-glycative lignans from the defatted seeds of *Sesamum indicum*. *Molecules*. 2023. <https://doi.org/10.3390/molecules28052255>.
51. Hong SS, Choi CW, Choi YH, Oh JS. Coixlachryside A: a new lignan glycoside from the roots of *Coix lachryma-jobi* L var *ma-yuen* Stapf. *Phytochem Lett*. 2016. <https://doi.org/10.1016/j.phytol.2016.07.004>.
52. Castro-Vazquez D, Sánchez-Carranza JN, Alvarez L, Juárez-Mercado KE, Sánchez-Cruz N, Medina-Franco JL, Antunez-Mojica M, González-Maya L. Methyl benzoate and cinnamate analogs as modulators of DNA methylation in hepatocellular carcinoma. *Chem Biol Drug Des*. 2022. <https://doi.org/10.1111/cbdd.14061>.
53. Sangsopha W, Kanokmedhakul K, Lekphrom R, Kanokmedhakul S. Chemical constituents and biological activities from branches of *Colubrina asiatica*. *Nat Prod Res*. 2018. <https://doi.org/10.1080/14786419.2017.1320787>.
54. Wang Y, Gevorgyan V. General method for the synthesis of salicylic acids from phenols through palladium-catalyzed silanol-directed C-H carboxylation. *Angew Chem Int Ed Engl*. 2015. <https://doi.org/10.1002/anie.201410375>.
55. He L, Hou J, Gan M, Shi J, Chantapromma S, Fun HK, Williams ID, Sung HHY. Cadinane sesquiterpenes from the leaves of *Eupatorium adenophorum*. *J Nat Prod*. 2008. <https://doi.org/10.1021/np800242w>.
56. Menon LN, Shameer PS, Sarma J, Rameshkumar KB. Profiles of volatile chemicals from the leaves of six *Garcinia* species from North East India. *Nat Prod Res*. 2021. <https://doi.org/10.1080/14786419.2019.1667349>.
57. Kapadia VH, Nagasampagi BA, Naik VG, Dev S. Structure of mustakone and copaene. *Tetrahedron Lett*. 1963. [https://doi.org/10.1016/S0040-4039\(01\)90945-1](https://doi.org/10.1016/S0040-4039(01)90945-1).
58. Lian MY, Zhang YJ, Dong SH, Huang XX, Bai M, Song SJ. Terpenoids from *Litsea lancilimba* Merr and their chemotaxonomic significant. *Biochem Syst Ecol*. 2022. <https://doi.org/10.1016/j.bse.2022.104456>.
59. Nyasse B, Ghogomu RBL, Sondengam T, Martin MT, Bodo B. Mandassidione and other sesquiterpenic ketones from *Cyperus articulatus*. *Phytochemistry*. 1988. [https://doi.org/10.1016/0031-9422\(88\)80055-4](https://doi.org/10.1016/0031-9422(88)80055-4).
60. Friebolin H. Ein- und zweidimensionale NMR-Spektroskopie. 5th ed. Weinheim: Wiley-VCH; 2013.
61. Abraham RJ, Cooper MA, Salmon JR, Whittaker D. The NMR spectra and conformations of cyclic compounds V: proton couplings and chemical shifts in bridged cyclobutanes. *Org Magn Reson*. 1972. <https://doi.org/10.1002/mrc.1270040409>.
62. Kapadia VH, Nagasampagi BA, Naik VG, Dev S. Studies in sesquiterpenes - XXII. *Tetrahedron Lett*. 1965. [https://doi.org/10.1016/S0040-4020\(01\)82231-6](https://doi.org/10.1016/S0040-4020(01)82231-6).
63. Kawaguchi Y, Ochi T, Takaishi Y, Kawazoe K, Lee KH. New sesquiterpenes from *Capsicum annum*. *J Nat Prod*. 2004. <https://doi.org/10.1021/np0305472>.
64. Nie LX, Dong J, Huang LY, Qian XY, Lian CJ, Kang S, Dai Z, Ma SC. Microscopic mass spectrometry imaging reveals the distribution of phytochemicals in the dried root of *Isatis tinctoria*. *Front pharmacol*. 2021. <https://doi.org/10.3389/fphar.2021.685575>.
65. Suresh G, Poornima B, Babu KS, Yadav PA, Rao MSA, Siva B, Prasad KR, Nayak VL, Ramakrishna S. Cytotoxic sesquiterpenes from *Hedychium spicatum*: Isolation, structure elucidation and structure-activity relationship studies. *Fitoterapia*. 2013. <https://doi.org/10.1016/j.fitote.2013.02.004>.
66. Cuyckens F, Claeys M. Mass spectrometry in the structural analysis of flavonoids. *J Mass Spectrom*. 2004. <https://doi.org/10.1002/jms.585>.
67. Fabre N, Rustan I, Hoffmann E, Quetin-Leclercq J. Determination of flavone, flavonol, and flavanone aglycones by negative ion liquid chromatography electrospray ion trap mass spectrometry. *J Am Soc Mass Spectrom*. 2001. [https://doi.org/10.1016/S1044-0305\(01\)00226-4](https://doi.org/10.1016/S1044-0305(01)00226-4).
68. Frański R, Gierczyk B, Kozik T, Popenda Ł, Beszterda M. Signals of diagnostic ions in the product ion spectra of M⁺ - H⁺ ions of methoxylated flavonoids. *Rapid Commun Mass Spectrom*. 2019. <https://doi.org/10.1002/rcm.8316>.

69. Justesen U. Collision-induced fragmentation of deprotonated methoxylated flavonoids, obtained by electrospray ionization mass spectrometry. *J Mass Spectrom.* 2001. <https://doi.org/10.1002/jms.118>.
70. Schmidt J. Negative ion electrospray high-resolution tandem mass spectrometry of polyphenols. *J Mass Spectrom.* 2016. <https://doi.org/10.1002/jms.3712>.
71. Ashraf K, Sultan S, Shah SAA. Phytochemistry, phytochemical, pharmacological and molecular study of *Zingiber officinale roscoe*: a review. *Int J Pharm Pharm Sci.* 2017. <https://doi.org/10.22159/ijpps.2017v9i11.19613>.
72. Ali BH, Blunden G, Tanira MO, Nemmar A. Some phytochemical, pharmacological and toxicological properties of ginger (*Zingiber officinale Roscoe*): a review of recent research. *Food Chem Toxicol.* 2008. <https://doi.org/10.1016/j.fct.2007.09.085>.
73. Kiuchi F, Iwakami S, Shibuya M, Hanaoka F, Sankawa U. Inhibition of prostaglandin and leukotriene biosynthesis by gingerols and diarylheptanoids. *Chem Pharm Bull.* 1992. <https://doi.org/10.1248/cpb.40.387>.
74. Aktan F, Henness S, van Tran H, Duke CC, Roufogalis BD, Ammit AJ. Gingerol metabolite and a synthetic analogue capsarol inhibit macrophage NF-kappaB-mediated iNOS gene expression and enzyme activity. *Planta Med.* 2006. <https://doi.org/10.1055/s-2006-931588>.
75. Grzanna R, Lindmark L, Frondoza CG. Ginger-and herbal medicinal product with broad anti-inflammatory actions. *J Med Food.* 2005. <https://doi.org/10.1089/jmf.2005.8.125>.
76. Grzanna R, Phan P, Polotsky A, Lindmark L, Frondoza CG. Ginger extract inhibits beta-amyloid peptide-induced cytokine and chemokine expression in cultured THP-1 monocytes. *J Altern Complement Med.* 2004. <https://doi.org/10.1089/acm.2004.10.1009>.
77. Ahmed N, Karobari MI, Yousaf A, Mohamed RN, Arshad S, Basheer SN, Peeran SW, Noorani TY, Assiry AA, Alharbi AS, Yean CY. The antimicrobial efficacy against selective oral microbes, antioxidant activity and preliminary phytochemical screening of *Zingiber officinale*. *Infect Drug Resist.* 2022. <https://doi.org/10.2147/IDR.S364175>.
78. Tungmunthum D, Tanaka N, Uehara A, Iwashina T. Flavonoids profile, taxonomic data, history of cosmetic uses, anti-oxidant and anti-aging potential of *Alpinia galanga* (L) Willd. *Cosmetics.* 2020. <https://doi.org/10.3390/cosmetics7040089>.
79. Sharma V, Singh V. Phytochemical characterization of *Curcuma aromatica* (rhizome). *Eur Chem Bull.* 2023. <https://doi.org/10.48047/ecb/2023.12.si4.584>.
80. Thao NP, Luyen BTT, Lee SH, Jang HD, Kim YH. Anti-osteoporotic and antioxidant activities by rhizomes of *Kaempferia parviflora* Wall ex Baker. *Nat Prod Sci.* 2016. <https://doi.org/10.20307/nps.2016.22.1.13>.
81. Srivastava S, Misra A, Kumar D, Srivastava A, Sood A, Rawat A. Reversed-phase high-performance liquid chromatography-ultraviolet photodiode array detector validated simultaneous quantification of six bioactive phenolic acids in *Roscoe purpurea* tubers and their *in vitro* cytotoxic potential against various cell lines. *Pharmacogn Mag.* 2015. <https://doi.org/10.4103/0973-1296.168944>.
82. Jung WC, Kim KH, Il Kyun L, Choi SU, Lee KR. Phytochemical constituents of *Amomum xanthioides*. *Nat Prod Sci.* 2009;15(1):44–9.
83. Prakash M, Basavaraj BV, Chidambara KN. Biological functions of epicatechin: plant cell to human cell health. *J Funct Foods.* 2019. <https://doi.org/10.1016/j.jff.2018.10.021>.
84. Kim MJ, Ryu GR, Kang JH, Sim SS, Min DS, Rhie DJ, Yoon SH, Hahn SJ, Jeong IK, Hong KJ, Kim MS, Jo YH. Inhibitory effects of epicatechin on interleukin-1beta-induced inducible nitric oxide synthase expression in RINm5F cells and rat pancreatic islets by down-regulation of NF-kappaB activation. *Biochem Pharmacol.* 2004. <https://doi.org/10.1016/j.bcp.2004.06.031>.
85. Taguchi L, Pinheiro NM, Olivo CR, Choqueta-Toledo A, Grecco SS, Lopes FDTQS, Caperuto LC, Martins MA, Tiberio IFLC, Lago JHG, Prado CM. A flavanone from *Baccharis retusa* (Asteraceae) prevents elastase-induced emphysema in mice by regulating NF-kB, oxidative stress and metalloproteinases. *Respir Res.* 2015. <https://doi.org/10.1186/s12931-015-0233-3>.
86. Rajesh RU, Dhanaraj S. A critical review on quercetin bioflavonoid and its derivatives: Scope, synthesis, and biological applications with future prospects. *Arab J Chem.* 2023. <https://doi.org/10.1016/j.arabjc.2023.104881>.
87. Mendoza-Wilson AM, Glossman-Mitnik D. Theoretical study of the molecular properties and chemical reactivity of (+)-catechin and (–)-epicatechin related to their antioxidant ability. *J Mol Struct.* 2006. <https://doi.org/10.1016/j.theochem.2006.01.001>.
88. Mathew S, Abraham TE, Zakaria ZA. Reactivity of phenolic compounds towards free radicals under *in vitro* conditions. *J Food Sci Technol.* 2015. <https://doi.org/10.1007/s13197-014-1704-0>.
89. El Omari N, El Menyiy N, Zengin G, Goh BH, Gallo M, Montesano D, Naviglio D, Bouyahya A. Anticancer and anti-inflammatory effects of tomentosin: cellular and molecular mechanisms. *Separations.* 2021. <https://doi.org/10.3390/separations8110207>.
90. Valdes E, Gonzalez C, Diaz K, Vasquez-Martinez Y, Mascayano C, Torrent C, Cabezas F, Mejias S, Montoya M, Cortez-San MM, Munoz MA, Joseph-Nathan P, Osorio M, Taborga L. Biological properties and absolute configuration of flavanones from *Calceolaria thyrsiflora* Graham. *Front pharmacol.* 2020. <https://doi.org/10.3389/fphar.2020.01125>.
91. Dos Grecco S, Dorigueto AC, Landre IM, Soares MG, Martho K, Lima R, Pascon RC, Vallim MA, Capello TM, Romoff P, Sartorelli P, Lago JH. Structural crystalline characterization of sakuranetin—an antimicrobial flavanone from twigs of *Baccharis retusa* (Asteraceae). *Molecules.* 2014. <https://doi.org/10.3390/molecules19067528>.
92. Çitoğlu GS, Sever B, Antus S, Baitz-Gács E, Altanlar N. Antifungal flavonoids from *Ballota glandulosissima*. *Pharm Biol.* 2008. <https://doi.org/10.1080/13880200308951339>.
93. Boz H. *p*-Coumaric acid in cereals: presence, antioxidant and antimicrobial effects. *Int J Food Sci Tech.* 2015. <https://doi.org/10.1111/ijfs.12898>.
94. Rezaeirosan A, Saedi M, Morteza-Semnani K, Akbari J, Hedayatizadeh-Omran A, Goli H, Nokhodchi A. Vesicular formation of *trans*-ferulic acid: an efficient approach to improve the radical scavenging and antimicrobial properties. *J Pharm Innov.* 2021. <https://doi.org/10.1007/s12247-021-09543-8>.
95. Oluleye IO, Folahan FF, Nabuikie CP, Ahmed MM. Antibacterial activity and phytochemical screening of leaf extracts of *Sida acuta* from North-Central Nigeria. *Res Square.* 2022. <https://doi.org/10.21203/rs.3.rs-1206214/v1>.
96. Syafni N, Putra DP, Arbain D. 3,4-Dihydroxybenzoic acid and 3,4-dihydroxybenzaldehyde from the fern *Trichomanes chinense* L isolation, antimicrobial and antioxidant properties. *Indones J Chem.* 2012. <https://doi.org/10.2146/ijc.21342>.
97. Thakur K, Kalia S, Kaith BS, Pathania D, Kumar A. Surface functionalization of coconut fibers by enzymatic biografting of syringaldehyde for the development of biocomposites. *RSC Adv.* 2015. <https://doi.org/10.1039/C5RA14891J>.
98. Youssef ASA, Hemdan MM, Azab ME, Emara SA, Elsayed GA, Kamel RM. Syringaldehyde as a scaffold for the synthesis of some biologically potent heterocycles. *J Heterocycl Chem.* 2020. <https://doi.org/10.1002/jhet.3850>.

99. Chaudhary J, Jain A, Manuja R, Sachdeva S. A comprehensive review on biological activities of *p*-hydroxy benzoic acid and its derivatives. *Int J Pharm Sci Rev Res*. 2013;22(2):210.
100. Semaming Y, Pannengpetch P, Chattipakorn SC, Chattipakorn N. Pharmacological properties of protocatechuic acid and its potential roles as complementary medicine. *Evid Based Complement Alternat Med*. 2015. <https://doi.org/10.1155/2015/593902>.
101. Omosa LK, Amugune B, Ndunda B, Milugo TK, Heydenreich M, Yenesew A, Midiwo JO. Antimicrobial flavonoids and diterpenoids from *Dodonaea angustifolia*. *S Afr J Bot*. 2014. <https://doi.org/10.1016/j.sajb.2013.11.012>.
102. Çitoğlu GS, Sever B, Antus S, Baitz-Gács E, Altanlar N. Antifungal diterpenoids and flavonoids from *Ballota inaequidens*. *Pharm Biol*. 2005. <https://doi.org/10.1080/13880200490902626>.
103. Mulvena D, Webb EC, Zerner B. 3,4-Dihydroxybenzaldehyde, a fungistatic substance from green *Cavendish bananas*. *Phytochemistry*. 1969. [https://doi.org/10.1016/S0031-9422\(00\)85436-9](https://doi.org/10.1016/S0031-9422(00)85436-9).
104. Kalyani AG, Jamunarani R, Pushparaj FJM. Oxidation of salicylaldehyde by alkaline hexacyanoferrate (III)-A kinetic and mechanistic study. *Int J Chemtech Res*. 2015;7:251–8.
105. Labute P, Williams C. Application of Hückel theory to pharmacophore discovery. *CICSJ Bull*. 2015. <https://doi.org/10.11546/cicsj.33.33>.
106. Becke AD. Density-functional thermochemistry I the effect of the exchange-only gradient correction. *J Chem Phys*. 1992. <https://doi.org/10.1063/1.462066>.
107. Becke AD. Density-functional thermochemistry III the role of exact exchange. *J Chem Phys*. 1993. <https://doi.org/10.1063/1.464913>.
108. Lee C, Yang W, Parr RG. Development of the Colle-Salvetti correlation-energy formula into a functional of the electron density. *Phys Rev B Condens*. 1988. <https://doi.org/10.1103/physrevb.37.785>.
109. Vosko SH, Wilk L, Nusair M. Accurate spin-dependent electron liquid correlation energies for local spin density calculations: a critical analysis. *Can J Phys*. 1980. <https://doi.org/10.1139/p80-159>.
110. Neese F. Software update: the ORCA program system, version 4.0 (2018)
111. Weigend F, Ahlrichs R. Balanced basis sets of split valence, triple zeta valence and quadruple zeta valence quality for H to Rn: design and assessment of accuracy. *Phys Chem Chem Phys*. 2005. <https://doi.org/10.1039/B508541A>.
112. Bruhn T, Schaumlöffel A, Hemberger Y, Pescitelli G, SpecDis version 1.71 (Berlin, Germany, 2017)
113. Farhadi F, Iranshahi M, Taghizadeh SF, Asili J. Volatile sulfur compounds: The possible metabolite pattern to identify the sources and types of asafetida by headspace GC/MS analysis. *Ind Crops Prod*. 2020. <https://doi.org/10.1016/j.indcrop.2020.112827>.
114. Dolomanov OV, Bourhis LJ, Gildea RJ, Howard JAK, Puschmann H. OLEX2: A complete structure solution, refinement and analysis program. *J Appl Crystallogr*. 2009. <https://doi.org/10.1107/S0021889808042726>.
115. Sheldrick GM. SHELXT—integrated space-group and crystal-structure determination. *Acta Crystallogr A*. 2015. <https://doi.org/10.1107/S2053273314026370>.
116. Sheldrick GM. Crystal structure refinement with SHELXL. *Acta Crystallogr C*. 2015. <https://doi.org/10.1107/S2053229614024218>.
117. Kappen J, Manurung J, Fuchs T, Vemulapalli SPB, Schmitz LM, Frolov A, Agusta A, Muellner-Riehl AN, Griesinger C, Franke K, Wessjohann LA. Challenging structure elucidation of lumnizeralactone, an ellagic acid derivative from the mangrove *Lumnitzera racemosa*. *Mar Drugs*. 2023. <https://doi.org/10.3390/md21040242>.
118. Manurung J, Kappen J, Schnitzler J, Frolov A, Wessjohann LA, Agusta A, Muellner-Riehl AN, Franke K. Analysis of unusual sulfated constituents and anti-infective properties of two Indonesian mangroves, *Lumnitzera littorea* and *Lumnitzera racemosa* (Combretaceae). *Separations*. 2021. <https://doi.org/10.3390/separations8060082>.
119. Ware I, Franke K, Dube M, El Ali EH, Wessjohann LA. Characterization and bioactive potential of secondary metabolites Isolated from *Piper sarmentosum* Roxb. *Int J Mol Sci*. 2023. <https://doi.org/10.3390/ijms24021328>.
120. Ware I, Franke K, Hussain H, Morgan I, Rennert R, Wessjohann LA. Bioactive phenolic compounds from *Peperomia obtusifolia*. *Molecules*. 2022. <https://doi.org/10.3390/molecules27144363>.
121. Gardner DR, Panter KE, James LF. Pine needle abortion in cattle: metabolism of isocupressic acid. *J Agric Food Chem*. 1999. <https://doi.org/10.1021/jf981322d>.
122. Win NN, Ito T, Ngwe H, Win YY, Prema Okamoto Y, Tanaka M, Asakawa Y, Abe I, Morita H. Labdane diterpenoids from *Curcuma amada* rhizomes collected in Myanmar and their antiproliferative activities. *Fitoterapia*. 2017. <https://doi.org/10.1016/j.fitote.2017.08.006>.
123. Yasodha S, Halijah I, Audra S, Palian SAA, Nurur R, Awang K. A new bis-labdanic diterpene from the rhizomes of *Alpinia pahangensis*. *Planta Med*. 2013. <https://doi.org/10.1055/s-0033-1351075>.
124. Lu Y, Foo LY. Antioxidant and radical scavenging activities of polyphenols from apple pomace. *Food Chem*. 2000. [https://doi.org/10.1016/S0308-8146\(99\)00167-3](https://doi.org/10.1016/S0308-8146(99)00167-3).
125. Shay J, Elbaz HA, Lee I, Zielske SP, Malek MH, Huttemann M. Molecular mechanisms and therapeutic effects of (-)-epicatechin and other polyphenols in cancer, inflammation, diabetes, and neurodegeneration. *Oxid Med Cell Longev*. 2015. <https://doi.org/10.1155/2015/181260>.
126. Zhang R, Wang J, Xia R, Li D, Wang F. Antioxidant processes involving epicatechin decreased symptoms of pine wilt disease. *Front Plant Sci*. 2022. <https://doi.org/10.3389/fpls.2022.1015970>.
127. Shah ZA, Li RC, Ahmad AS, Kensler TW, Yamamoto M, Biswal S, Dore S. The flavanol (-)-epicatechin prevents stroke damage through the Nrf2/HO1 pathway. *J Cereb Blood Flow Metab*. 2010. <https://doi.org/10.1038/jcbfm.2010.53>.
128. van Praag H, Lucero MJ, Yeo GW, Stecker K, Heivand N, Zhao C, Yip E, Afanador M, Schroeter H, Hammerstone J, Gage FH. Plant-derived flavanol (-)-epicatechin enhances angiogenesis and retention of spatial memory in mice. *J Neurosci*. 2007. <https://doi.org/10.1523/JNEUROSCI.0914-07.2007>.
129. Awas E, Omosa LK. Antioxidant activities of flavonoid aglycones from Kenyan *Gardenia ternifolia* Schum and Thonn. *Int J Pharma Bio Sci*. 2016. <https://doi.org/10.9790/3008-110304136141>.
130. Modak B, Rojas M, Torres R, Rodilla J, Luebert F. Antioxidant activity of a new aromatic geranyl derivative of the resinous exudates from *Heliotropium glutinosum* Phil. *Molecules*. 2007. <https://doi.org/10.3390/12051057>.
131. Del Barrio G, Spengler I, García T, Roque A, Álvarez Á, Calderón JS, Parra F. Antiviral activity of *Ageratina havanensis* and major chemical compounds from the most active fraction. *Rev Bras Farmacogn*. 2011. <https://doi.org/10.1590/s0102-695x2011005000159>.

132. Moon JH, Nakata R, Oshima S, Inakuma T, Terao J. Accumulation of quercetin conjugates in blood plasma after the short-term ingestion of onion by women. *Am J Physiol Regul Integr Comp Physiol*. 2000. <https://doi.org/10.1152/ajpregu.2000.279.2.R461>.
133. Brito A, Ramirez JE, Areche C, Sepúlveda B, Simirgiotis MJ. HPLC-UV-MS profiles of phenolic compounds and antioxidant activity of fruits from three citrus species consumed in Northern Chile. *Molecules*. 2014. <https://doi.org/10.3390/molecules191117400>.
134. Hadidi M, Keshavarz SA, Mohammad SM, Mahboob SA, Rashidi MR. Effects of parsley (*Petroselinum crispum*) and its flavonol constituents, kaempferol and quercetin, on serum uric acid levels, biomarkers of oxidative stress and liver xanthine oxidoreductase activity in oxonate-induced hyperuricemic rats. *Iran J Pharm Res*. 2011;10:811.
135. Bagalagel AA, El-Hawary SS, Alaaeldin R, Elmaidomy AH, Altemani FH, Waggas DS, Algehainy NA, Saeedi NH, Alsenani F, Mokhtar FA, Elrehany MA, Al-Sanea MM, Abdelmohsen UR. The protective and therapeutic anti-alzheimer potential of *Olea europaea* L cv picual: An in silico and in vivo study. *Metabolites*. 2022. <https://doi.org/10.3390/metabo12121178>.
136. Milutinović M, Miladinović M, Gašić U, Dimitrijević-Branković S, Rajilić-Stojanović M. Recovery of bioactive molecules from *Hypericum perforatum* L dust using microwave-assisted extraction. *Biomass Conv Bioref*. 2024. <https://doi.org/10.1007/s13399-022-02717-5>.
137. Hu D, Wang HJ, Yu LH, Guan ZR, Jiang YP, Hu JH, Yan YX, Zhou ZH, Lou JS. The role of *Ginkgo Folium* on antitumor: bioactive constituents and the potential mechanism. *J Ethnopharmacol*. 2024. <https://doi.org/10.1016/j.jep.2023.117202>.
138. Salehi B, Machin L, Monzote L, Sharifi-Rad J, Ezzat SM, Salem MA, Merghany RM, El Mahdy NM, Kilic CS, Sytar O, Sharifi-Rad M, Sharopov F, Martins N, Martorell M, Cho WC. Therapeutic potential of quercetin: new insights and perspectives for human health. *ACS Omega*. 2020. <https://doi.org/10.1021/acsomega.0c01818>.
139. Li Y, Yao J, Han C, Yang J, Chaudhry MT, Wang S, Liu H, Yin Y. Quercetin, inflammation and immunity. *Nutrients*. 2016. <https://doi.org/10.3390/nu8030167>.
140. Dajas F. Life or death: neuroprotective and anticancer effects of quercetin. *J Ethnopharmacol*. 2012. <https://doi.org/10.1016/j.jep.2012.07.005>.
141. Pu F, Mishima K, Irie K, Motohashi K, Tanaka Y, Orito K, Egawa T, Kitamura Y, Egashira N, Iwasaki K, Fujiwara M. Neuroprotective effects of quercetin and rutin on spatial memory impairment in an 8-arm radial maze task and neuronal death induced by repeated cerebral ischemia in rats. *J Pharmacol Sci*. 2007. <https://doi.org/10.1254/jphs.fp0070247>.
142. Ghorbani A. Mechanisms of antidiabetic effects of flavonoid rutin. *Biomed Pharmacother*. 2017. <https://doi.org/10.1016/j.biopha.2017.10.001>.
143. Kreft S, Knapp M, Kreft I. Extraction of rutin from buckwheat (*Fagopyrum esculentum* Moench) seeds and determination by capillary electrophoresis. *J Agric Food Chem*. 1999. <https://doi.org/10.1021/jf990186p>.
144. Shahrajabian MH. A candidate for health promotion, disease prevention and treatment, common rue (*Ruta graveolens* L.), an important medicinal plant in traditional medicine. *Curr Rev Clin Exp Pharmacol*. 2022. <https://doi.org/10.2174/2772432817666220510143902>.
145. Satari A, Ghasemi S, Habtemariam S, Asgharian S, Lorigooini Z. Rutin: A flavonoid as an effective sensitizer for anticancer therapy; insights into multifaceted mechanisms and applicability for combination therapy. *Evid Based Complement Alternat Med*. 2021. <https://doi.org/10.1155/2021/9913179>.
146. Chua LS. A review on plant-based rutin extraction methods and its pharmacological activities. *J Ethnopharmacol*. 2013. <https://doi.org/10.1016/j.jep.2013.10.036>.
147. Janbaz KH, Saeed SA, Gilani AH. Protective effect of rutin on paracetamol- and CCl₄-induced hepatotoxicity in rodents. *Fitoterapia*. 2002. [https://doi.org/10.1016/S0367-326X\(02\)00217-4](https://doi.org/10.1016/S0367-326X(02)00217-4).
148. Selloum L, Bouriche H, Tigrine C, Boudoukha C. Anti-inflammatory effect of rutin on rat paw oedema, and on neutrophils chemotaxis and degranulation. *Exp Toxicol Pathol*. 2003. <https://doi.org/10.1078/0940-2993-00260>.
149. Yang J, Guo J, Yuan J. In vitro antioxidant properties of rutin. *Food Sci Technol*. 2008. <https://doi.org/10.1016/j.lwt.2007.06.010>.
150. Costa-Lotufo LV, Jimenez PC, Wilke DV, Leal LKAM, Cunha GMA, Silveira ER, Canuto KM, Viana GSB, Moraes MEA, Moraes MO, Pessoa C. Antiproliferative effects of several compounds isolated from *Amburana cearensis* A. C Smith J Biosci. 2003. <https://doi.org/10.1515/znc-2003-9-1014>.
151. Saeidnia S, Gohari AR, Ito M, Kiuchi F, Honda G. Bioactive constituents from *Dracocephalum subcapitatum* (O Kuntze) Lipsky. *J Biosci*. 2005. <https://doi.org/10.1515/znc-2005-1-204>.
152. Fattahi M, Nazeri V, Torras-Claveria L, Sefidkon F, Cusido RM, Zamani Z, Palazon J. Identification and quantification of leaf surface flavonoids in wild-growing populations of *Dracocephalum kotschyi* by LC-DAD-ESI-MS. *Food Chem*. 2013. <https://doi.org/10.1016/j.foodchem.2013.03.019>.
153. Forgo P, Zupko I, Molnar J, Vasas A, Dombi G, Hohmann J. Bioactivity-guided isolation of antiproliferative compounds from *Centaurea jacea* L. *Fitoterapia*. 2012. <https://doi.org/10.1016/j.fitote.2012.04.006>.
154. Leal LK, Canuto KM, Da Silva Costa KC, Nobre-Junior HV, Vasconcelos SM, Silveira ER, Ferreira MV, Fontenele JB, Andrade GM, de Barros Viana GS. Effects of amburosides A and isokaempferide, polyphenols from *Amburana cearensis*, on rodent inflammatory processes and myeloperoxidase activity in human neutrophils. *Basic Clin Pharmacol Toxicol*. 2008. <https://doi.org/10.1111/j.1742-7843.2008.00329.x>.
155. El Sohly HN, El Ferali FS, Joshi AS, Walker LA. Antiviral flavonoids from *Alkanna orientalis*. *Planta Med*. 1997. <https://doi.org/10.1055/s-2006-957713>.
156. Woo JH, Ahn JH, Jang DS, Lee KT, Choi JH. Effect of kumatakenin isolated from cloves on the apoptosis of cancer cells and the alternative activation of tumor-associated macrophages. *J Agric Food Chem*. 2017. <https://doi.org/10.1021/acs.jafc.7b01543>.
157. Zhang XY, Shen J, Zhou Y, Wei ZP, Gao JM. Insecticidal constituents from *Buddleja albiliflora* Hemsl. *Nat Prod Res*. 2016. <https://doi.org/10.1080/14786419.2016.1247080>.
158. Lefahal M, Zaabat N, Djarri L, Benahmed M, Medjroubi K, Laouer H, Akkal S. Evaluation of the antioxidant activity of extracts and flavonoids obtained from *Bunium alpinum* Waldst & Kit (Apiaceae) and *Tamarix gallica* L (Tamaricaceae). *Curr Issues Pharm Med Sci*. 2017. <https://doi.org/10.1515/cipms-2017-0001>.
159. Ndolo VU, Beta T. Comparative studies on composition and distribution of phenolic acids in cereal grain botanical fractions. *Cereal Chem*. 2014. <https://doi.org/10.1094/CCHEM-10-13-0225-R>.
160. Gorinstein S, Lojek A, Číž M, Pawelzik E, Delgado-Licon E, Medina OJ, Moreno M, Salas IA, Goshev I. Comparison of composition and antioxidant capacity of some cereals and pseudocereals. *Int J Food Sci Tech*. 2008. <https://doi.org/10.1111/j.1365-2621.2007.01498.x>.

161. Zhu H, Liang QH, Xiong XG, Wang Y, Zhang ZH, Sun MJ, Lu X, Wu D. Anti-inflammatory effects of *p*-coumaric acid, a natural compound of *Oldenlandia diffusa*, on arthritis model rats. *Evid Based Complement Alternat Med*. 2018. <https://doi.org/10.1155/2018/5198594>.
162. Tehami W, Nani A, Khan NA, Hichami A. New insights into the anticancer effects of *p*-coumaric acid: focus on colorectal cancer. *Dose Response*. 2023. <https://doi.org/10.1177/15593258221150704>.
163. Lou Z, Wang H, Rao S, Sun J, Ma C, Li J. *p*-Coumaric acid kills bacteria through dual damage mechanisms. *Food Control*. 2011. <https://doi.org/10.1016/j.foodcont.2011.11.022>.
164. Zavala-Lopez M, Flint-Garcia S, Garcia-Lara S. Compositional variation in trans-ferulic, *p*-coumaric, and diferulic acids levels among kernels of modern and traditional maize (*Zea mays* L.) hybrids. *Front Nutr*. 2020. <https://doi.org/10.3389/fnut.2020.600747>.
165. Rezaeirosan A, Saeedi M, Morteza-Semnani K, Akbari J, Gahsemi M, Nokhodchi A. Development of *trans*-ferulic acid niosome: an optimization and an *in-vivo* study. *J Drug Deliv Sci Technol*. 2020. <https://doi.org/10.1016/j.jddst.2020.101854>.
166. Agarwal UP, Atalla RH. Formation and identification of *cis/trans* ferulic acid in photoyellowed white spruce mechanical pulp. *J Wood Chem Technol*. 1990. <https://doi.org/10.1080/02773819008050235>.
167. Wu H, Haig T, Pratley J, Lemerle D, An M. Allelochemicals in wheat (*Triticum aestivum* L.): Variation of phenolic acids in root tissues. *J Agric Food Chem*. 2000. <https://doi.org/10.1021/jf0006473>.
168. Laili ER, Aminah NS, Kristanti AN, Wardana AP, Rafi M, Rohman A, Insanu M, Tun KNW. Comparative study of *Sida rhombifolia* from two different locations. *Rasayan J Chem*. 2022. <https://doi.org/10.31788/rjc.2022.1516588>.
169. Thu Hau NT, Thi HL. Chemical constituents of *Caesalpinia bonduc*. *J Sci Nat Sci Technol*. 2022. <https://doi.org/10.25073/2588-1140/vnunst.5500>.
170. Kono R, Nomura S, Okuno Y, Nakamura M, Maeno A, Kagiya T, Tokuda A, Inada K, Matsuno A, Utsunomiya T, Utsunomiya H. 3,4-Dihydroxybenzaldehyde derived from *Prunus mume* seed inhibits oxidative stress and enhances estradiol secretion in human ovarian granulosa tumor cells. *Acta Histochem Cytochem*. 2014. <https://doi.org/10.1267/ahc.14003>.
171. Kim EA, Han EJ, Kim J, Fernando IPS, Oh JY, Kim KN, Ahn G, Heo SJ. Anti-allergic effect of 3,4-dihydroxybenzaldehyde isolated from *Polysiphonia morrowii* in IgE/BSA-stimulated mast cells and a passive cutaneous anaphylaxis mouse model. *Mar Drugs*. 2022. <https://doi.org/10.3390/md20020133>.
172. Arya SS, Rookes JE, Cahill DM, Lenka SK. Vanillin: a review on the therapeutic prospects of a popular flavouring molecule. *Adv Tradit Med*. 2021. <https://doi.org/10.1007/s13596-020-00531-w>.
173. Sinha AK, Sharma UK, Sharma N. A comprehensive review on vanilla flavor: extraction, isolation and quantification of vanillin and others constituents. *Int J Food Sci Nutr*. 2008. <https://doi.org/10.1080/09687630701539350>.
174. Ma W, Zhang Q, Li X, Ma Y, Liu Y, Hu S, Zhou Z, Zhang R, Du K, Syed A, Yao X, Chen P. IPM712, a vanillin derivative as potential antitumor agents, displays better antitumor activity in colorectal cancers cell lines. *Eur J Pharm Sci*. 2020. <https://doi.org/10.1016/j.ejps.2020.105464>.
175. Taguchi L, Sawano T, Yazama F. Antioxidant properties of ethyl vanillin in vitro and in vivo. *Biosci Biotechnol Biochem*. 2011. <https://doi.org/10.1271/bbb.110524>.
176. Guo W, Liu B, Hu G, Kan X, Li Y, Gong Q, Xu D, Ma H, Cao Y, Huang B, Fu S, Liu J. Vanillin protects the blood-milk barrier and inhibits the inflammatory response in LPS-induced mastitis in mice. *Toxicol Appl Pharmacol*. 2019. <https://doi.org/10.1016/j.taap.2018.12.022>.
177. Wu Q, Cai H, Yuan T, Li S, Gan X, Song B. Novel vanillin derivatives containing a 1,3,4-thiadiazole moiety as potential antibacterial agents. *Bioorg Med Chem Lett*. 2020. <https://doi.org/10.1016/j.bmcl.2020.127113>.
178. Salau VF, Erukainure OL, Ibeji CU, Olasehinde TA, Koorbanally NA, Islam MS. Vanillin and vanillic acid modulate antioxidant defense system via amelioration of metabolic complications linked to Fe²⁺-induced brain tissues damage. *Metab Brain Dis*. 2020. <https://doi.org/10.1007/s11011-020-00545-y>.
179. Gasparetto JC, de Francisco TM, Campos FR, Pontarolo R. Development and validation of two methods based on high-performance liquid chromatography-tandem mass spectrometry for determining 1,2-benzopyrone, dihydrocoumarin, *o*-coumaric acid, syringaldehyde and kaurenoic acid in guaco extracts and pharmaceutical preparations. *J Sep Sci*. 2011. <https://doi.org/10.1002/jssc.201000792>.
180. Belkheiri N, Bouguerne B, Bedos-Belval F, Duran H, Bernis C, Salvayre R, Nègre-Salvayre A, Baltas M. Synthesis and antioxidant activity evaluation of a syringic hydrazones family. *Eur J Med Chem*. 2010. <https://doi.org/10.1016/j.ejmech.2010.03.031>.
181. Chelogoi PK, Mulholland DA, Coombes PH, Randrianarivelojosa M. An azole, an amide and a limonoid from *Vepris uguenensis* (Rutaceae). *Phytochemistry*. 2008. <https://doi.org/10.1016/j.phytochem.2007.12.013>.
182. González-Sarrias A, Li L, Seeram NP. Anticancer effects of maple syrup phenolics and extracts on proliferation, apoptosis, and cell cycle arrest of human colon cells. *J Funct Foods*. 2012. <https://doi.org/10.1016/j.jff.2011.10.004>.
183. Sircar D, Mitra A. Accumulation of *p*-hydroxybenzoic acid in hairy roots of *Daucus carota* 2: Confirming biosynthetic steps through feeding of inhibitors and precursors. *J Plant Physiol*. 2009. <https://doi.org/10.1016/j.jplph.2009.02.006>.
184. Huang C, Xu L, Jin-Jing S, Zhang Z, Fu M, Teng H, Yi K. Allelochemical *p*-hydroxybenzoic acid inhibits root growth via regulating ROS accumulation in cucumber (*Cucumis sativus* L.). *J Integr Agric*. 2019. [https://doi.org/10.1016/s2095-3119\(19\)62781-4](https://doi.org/10.1016/s2095-3119(19)62781-4).
185. Latreche K, Rahmania F. High extracellular accumulation of *p*-hydroxybenzoic acid, *p*-hydroxycinnamic acid and *p*-hydroxybenzaldehyde in leaves of *Phoenix dactylifera* L. affected by the brittle leaf disease. *Physiol Mol Plant Pathol*. 2011. <https://doi.org/10.1016/j.pmpp.2011.08.001>.
186. Cho JY, Moon JH, Seong KY, Park KH. Antimicrobial activity of 4-hydroxybenzoic acid and *trans* 4-hydroxycinnamic acid isolated and identified from rice hull. *Biosci Biotechnol Biochem*. 1998. <https://doi.org/10.1271/bbb.62.2273>.
187. Merkl R, Hrádková I, Filip V, Šmídkal J. Antimicrobial and antioxidant properties of phenolic acids alkyl esters. *Czech J Food Sci*. 2010. <https://doi.org/10.17221/132/2010-CJFS>.
188. Luecha P, Umehara K, Miyase T, Noguchi H. Antiestrogenic constituents of the Thai medicinal plants *Capparis flavicans* and *Vitex glabrata*. *J Nat Prod*. 2009. <https://doi.org/10.1021/np9006298>.
189. Ghareeb MA, Sobeh M, Rezaq S, El-Shazly AM, Mahmoud MF, Wink M. HPLC-ESI-MS/MS profiling of polyphenolics of a leaf extract from *Alpinia zerumbet* (Zingiberaceae) and its anti-inflammatory, anti-nociceptive, and antipyretic activities in vivo. *Molecules*. 2018. <https://doi.org/10.3390/molecules23123238>.

190. Li X, Wang X, Chen D, Chen S. Antioxidant activity and mechanism of protocatechuic acid in vitro. *Funct Foods Health Dis*. 2011. <https://doi.org/10.31989/ffhd.v1i7.127>.
191. Yu YS, Hsu CL, Yen GC anti-inflammatory effects of the roots of *Alpinia pricei* Hayata and its phenolic compounds. *J Agric Food Chem*. 2009. <https://doi.org/10.1021/jf901327g>.
192. Lende AB, Kshirsagar AD, Deshpande AD, Muley MM, Patil RR, Bafna PA, Naik SR. Anti-inflammatory and analgesic activity of protocatechuic acid in rats and mice. *Inflammopharmacology*. 2011. <https://doi.org/10.1007/s10787-011-0086-4>.
193. Chou TH, Ding HY, Hung WJ, Liang CH. Antioxidative characteristics and inhibition of alpha-melanocyte-stimulating hormone-stimulated melanogenesis of vanillin and vanillic acid from *Origanum vulgare*. *Exp Dermatol*. 2010. <https://doi.org/10.1111/j.1600-0625.2010.01091.x>.
194. Ghareib HRA, Abdelhamed MS, Ibrahim OH. Antioxidative effects of the acetone fraction and vanillic acid from *Chenopodium murale* on tomato plants. *Weed Biol Manage*. 2010. <https://doi.org/10.1111/j.1445-6664.2010.00368.x>.
195. Yrbas ML, Morucci F, Alonso R, Gorzalczy S. Pharmacological mechanism underlying the antinociceptive activity of vanillic acid. *Pharmacol Biochem Behav*. 2015. <https://doi.org/10.1016/j.pbb.2015.02.016>.
196. Sindhu G, Nishanthi E, Sharmila R. Nephroprotective effect of vanillic acid against cisplatin induced nephrotoxicity in wistar rats: a biochemical and molecular study. *Environ Toxicol Pharmacol*. 2015. <https://doi.org/10.1016/j.etap.2014.12.008>.
197. Chang WC, Wu JS, Chen CW, Kuo PL, Chien HM, Wang YT, Shen SC. Protective effect of vanillic acid against hyperinsulinemia, hyperglycemia and hyperlipidemia via alleviating hepatic insulin resistance and inflammation in high-fat diet (HFD)-fed rats. *Nutrients*. 2015. <https://doi.org/10.3390/nu7125514>.
198. Ameeramja J, Kanagaraj VV, Perumal E. Protocatechuic acid methyl ester modulates fluoride induced pulmonary toxicity in rats. *Food Chem Toxicol*. 2018. <https://doi.org/10.1016/j.fct.2018.05.031>.
199. Yellianty Y, Kartasasmita RE, Surantaatmadja SI, Rukayadi Y. Identification of chemical constituents from fruit of *Antidesma bunius* by GC-MS and HPLC-DAD-ESI-MS. *Food Sci Technol*. 2022. <https://doi.org/10.1590/fst.61320>.
200. Ono M, Ito Y, Nohara T. A labdane diterpene glycoside from fruit of *Vitex rotundifolia*. *Phytochemistry*. 1998. [https://doi.org/10.1016/S0031-9422\(97\)00863-7](https://doi.org/10.1016/S0031-9422(97)00863-7).

Publisher's Note Springer Nature remains neutral with regard to jurisdictional claims in published maps and institutional affiliations.

6 Discussion and conclusion

Since ancient times, plants have been used as treatment for many kinds of disease including infections. Following generations used this traditional knowledge to determine folk wisdom with reliable scientific methods and reproducible studies, with success! Humankind developed from natural products antibiotics, vaccines, and painkillers, just to mention a few. In our days, due to increasing resistance against these first hour antibiotics, the discovery of new effective bioactive compounds is urgently needed. This can be achieved by various ways like targeted or untargeted metabolomic approaches, synthetic libraries, derivatization of known bioactive backbones or by explorative investigation of yet underresearched medicinal plants. The aim of this thesis was the phytochemical characterization of three promising but understudied plants, including the screening of crude extracts for bioactivity, the evaluation of the major compound classes as well as the structure elucidation of isolated compounds, primarily with LC-HRMS and intensive NMR analysis. Since all chosen plants were used in traditional medicine, they were expected to exhibit (bioactive) compounds, some of which might be new to the scientific community.

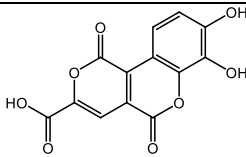
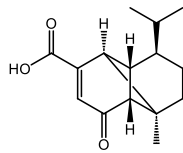
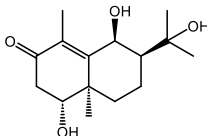
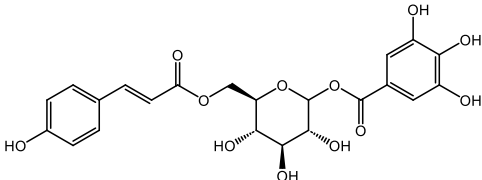
One approach for investigation would be the classical bioactivity-guided isolation. This method involves continuous bioactivity monitoring of extracts and fractions after every isolation step. However, it is both costly and highly time-consuming [1] and requires substantial amounts of extracts and fractions that are then lost for further isolation. Furthermore, the isolation process is significantly delayed by constant interruptions and the necessity to wait for bioassay results. To bypass these limitations, in my investigation the method was modified to initially screen the crude extracts or the first fractions after early separation steps and proceed with a complete isolation process afterward. Once the isolation was completed, the purified compounds were subsequently tested. However, it turned out that although there was no constant time-consuming screening and no partly loss of organic material, the amounts of isolated compounds were still quite low and sometimes insufficient for the planned screening of pure compounds. Nevertheless, the modified strategy proved promising, as it resulted in a maximum number of compounds isolated and characterized while comprehensive reports on the phytochemical composition of the species investigated were largely absent in available literature. Thus, the aim was to isolate all compounds in order to comprehensively describe the phytochemical profiles of the investigated plants and to maximize the probability of identifying potentially bioactive compounds. However, the used modified method bares a typical bias, which is well-documented in the literature [2,3]. By isolating every possible compound, it is impossible to exclude the reisolation of already known compounds. This bias may be considered by some as a waste of time and resources. But with the mentioned goal to investigate and describe the phytochemical profile in a most accurate way, reisolation was neither unexpected nor unwanted. Additionally, also known compounds can show yet unknown properties e.g. as anti-infectives, when they are reisolated and further investigated. Across all three species studied, a total of 53 compounds were isolated. Noteworthy, three compounds were new to science (tab 6-1) and 38 compounds were described for the first time in the investigated species to the best of our knowledge. Among the remaining 50 previously known compounds three substances were isolated in two different species. The isolated compounds can be classified into simple phenolics (tab 6-2), more complex polyphenolics (tab 6-3 and 6-4), terpenoids and keto acids (tab 6-5). This high number of known compounds in combination with low amounts of the individual constituents prevented the performance of bioassays on all isolates, due to insufficient quantities. Instead, for such compounds, an extensive literature review on their bioactivities was conducted (ch. 5). In general, there are various potential reasons for the low yield of isolated substances. On the one hand, the initial

concentration in the crude extract might have been low, or the chosen extraction conditions may not have been optimal for the respective compound classes.

However, at first glance, this seems unlikely for most compounds in this study, as relevant signals were observed during LC-HRMS screening through MS and UV/Vis detection, which correlate with concentration. In chapter 5, the preliminary ^1H NMR screening of the *H. scyphifera* extract indicated the presence of certain quantities of target compounds. Moreover, the extraction conditions were selected based on both literature references and in-house laboratory expertise. On closer inspection, however, it turns out that there were many structurally similar compounds with overlapping retention times and similar NMR signal shifts presence. It turned out that the concentration of any single compound eventually was lower than initially presumed.

Another explanation are the complex matrices of these plant extracts. The secondary metabolites targeted for isolation may exist in free form and as bound to highly polymerized matrix molecules such as proteins, polysaccharides, or high molecular weight polyphenols. As a result, not all forms of these compounds behave uniformly during the isolation process. For instance, peak broadening or binding to stationary phases could occur during chromatographic purification, potentially leading to significant losses during processing. Another crucial factor is the stability of natural products. Their stability can be significantly influenced by light exposure, temperature fluctuations, pH, or the presence of oxidizing agents such as atmospheric oxygen. Under certain conditions, some compounds may even undergo self-polymerization, resulting in effects like those caused by binding to matrix associated polymers. This phenomenon is particularly likely for phenolic compounds, that were one of the major compound classes, investigated within this study. Despite the aforementioned challenges in the isolation process, in the frame of this thesis, three novel compounds were successfully isolated and fully characterized.

Table 6-1 New compounds isolated.

chapter-comp.no.	name (class)	structure	plant
3-1	lumnitzeralacton (polyphenol)		<i>L. racemosa</i>
5-1	mustak-14-oic acid (sesquiterpenoid)		<i>H. scyphifera</i>
5-2	6-hydroxy-anhuienosol (sesquiterpenoid)		<i>H. scyphifera</i>
4-1	1-O-galloyl-6-O-trans-p-coumaroyl-D-glucopyranose (polyphenol)		<i>T. dhofarica</i>

The first is the ellagic acid derivative, lumnizeralactone (**3-1**, tab 6-1), derived from the mangrove species *Lumnitzera racemosa*. The other two are terpenoids: mustak-14-oic acid (**5-1**, tab 6-1) and 6-hydroxy-anhuienosol (**5-2**, tab 6-1), both isolated from the Zingiberaceae species *Hornstedtia scyphifera*. Additionally noteworthy is the first-time isolation of 1-*O*-galloyl-6-*O*-*trans*-*p*-coumaroyl-D-glucopyranose from *Terminalia dhofarica* (**4-1**, tab 6-1), which enabled the acquisition of reliable NMR data for this compound. However, this compound had recently been described through intensive HRMS investigations in parallel to this work [4]. Despite the expectations, especially for lumnizeralactone (**3-1**), none of these compounds exhibited significant antimicrobial activity. Nevertheless, considering that most secondary metabolites serve a specific purpose for the producing organism under evolutionary pressure, it is highly likely that the actual function of these newly discovered compounds has not yet been identified. Since the screening of crude extracts yielded promising results (*L. racemosa* crude extract at 500 µg/mL was active against Gram-positive *B. subtilis*; *T. dhofarica* crude extract at 500 µg/mL was active against Gram-negative *A. fischeri* and at 100 µg/mL against the fungus *P. infestans*; *H. scyphifera* crude extract at 100 µg/mL was active against the fungus *B. cinerea*, and the ethyl acetate fraction at 500 µg/mL was active against Gram-negative *A. fischeri*, inhibition of >80% is considered as active), the question arises as to the source of this activity. This is especially intriguing given that no new bioactive compounds were isolated and characterized.

On one hand, it is possible that highly bioactive compounds were produced by the plants but remain undiscovered, as they were not isolated during this study. This cannot be ruled out, as a complete classical bioactivity-guided isolation process has not been carried out. Consequently, fractions with potentially strong activity may not have been subjected to further isolation. However, this scenario appears unlikely, as all quantitatively significant fractions were processed to the stage of isolating pure substances. Fractions that were not further processed had on the one hand a low mass (approx. < 20 mg) and, on the other hand, showed a complex mixture of multiple compounds in LC-HRMS or ¹H-NMR screening. This complexity made the successful isolation of one or more individual substances unlikely. Another possible explanation for the observed activity in crude extracts is the additive or even synergistic interaction of certain compounds. A synergistic compound may only exhibit a strong bioactive effect when its complementary partners are present. After successful isolation, this synergy is disrupted, leading to a loss of activity in subsequent bioassays. This explanation appears particularly plausible for lumnizeralactone (**3-1**), which showed no activity in individual bioassays but represents the prominent differential compound in antibacterial crude extracts of various mangrove plants analyzed (ch. 2 and 3). After observing and to prevent the loss of synergistic effects, a synergy-guided isolation approach, as described by Junio et al. [5] or a reversed metabolomics analysis [6], would be the method of choice for another attempt. This method, just like the bioactivity-guided isolation, evaluates both the activity and metabolic profile of each fraction using LC-HRMS analysis. By tracking activity loss, this approach provides potential clues about compounds, based on their *m/z* values, that might be crucial for the observed activity. However, this method is even more labor-intensive and time-consuming than conventional bioactivity-guided isolation and still not infallible. For instance, crucial compounds could remain undetected due to ion suppression or poor ionization efficiency, leaving their synergistic roles unresolved despite noticeable activity declines. Nevertheless, it might be worth investing the required efforts of this method to finally identify the synergistic acting partners from *L. racemosa*. Another strategy to investigate synergistic interactions involves specific reconstitution experiments, in which isolated compounds suspected of synergy are recombined. This approach requires sufficient quantities of pure substances. In the case of lumnizeralactone (**3-1**), such an experiment was conducted. A late-stage fraction demonstrated good

activity against *B. subtilis*, and both MS and NMR analyses revealed that it primarily contained lumnizeralactone (**3-1**) and trimethyl ellagic acid (**2-16**, tab 6-3). When these two compounds were tested in combination, however, their activity did not exceed that of trimethyl ellagic acid alone. Therefore, no synergistic effect could be confirmed (data not shown). A third possibility is the nonspecific additive effect of numerous weakly bioactive compounds, which together exhibit a significant effect in the crude extract. This could potentially explain the activity observed in the extracts of the investigated Combretaceae species *L. racemosa* and *T. dhofarica*. Both species demonstrated a wide range of galloyl derivatives (chap 2 and 4, tab 6-2, 6-3, and 6-4) that are characteristic constituents of this plant family. As discussed in the chapters, these compound class shows plenty of unspecific bioactivities due to their tannin-like properties and antioxidative character. In *L. racemosa*, sulfated trimethyl ellagic acid (**2-16**, tab 6-3) was identified as the major compound. Conversely, in *T. dhofarica*, the gallotannin chebulagic acid (**4-18**, tab 6-4), extensively modified with galloyl groups, was predominantly identified. Both compounds are derivatives of gallic acid (GA) (**4-4**, tab 6-2). Ellagic acid (EA) (**2-6** and **4-12**, tab 6-3) represents a dilactone of a dimeric gallic acid derivative. GA and EA are ubiquitous in the plant kingdom and function as secondary metabolites with antioxidant properties, as well as defensive agents against microbial pathogens such as bacteria and fungi. Furthermore, by forming tannin structures, plants render themselves less appealing as a food source for herbivores due to tannins' strong bitterness and ability to hinder gastrointestinal digestion [7]. Pharmacologically, EA exhibits a broad spectrum of activities, including anticancer, anti-inflammatory, wound-healing, hepatoprotective, and neuroprotective effects [8]. Similarly, GA has been extensively studied and is recognized for its antioxidative, antimicrobial, anticancer, antiaging, and antiviral properties [9]. The higher molecular gallo- and ellagitannins are believed to exhibit comparable activity, partly due to the release of GA or EA upon application. As members of the hydrolysable tannin subgroup, these compounds display tannin-specific characteristics, such as nonspecific receptor or enzyme binding through protein precipitation [10]. Interestingly, studies have also revealed inhibitory actions beyond nonspecific effects. For instance, EA and its derivatives act as potent aldose reductase inhibitors, contributing to the management of diabetic complications [11]. Ellagitannins have been shown to inhibit tyrosinase by inducing conformational changes in the enzyme, which can mitigate pigmentation disorders and potentially prevent neurodegenerative conditions such as Parkinson's disease [12]. Other compounds, including punicalagin (P4, tab 4-1), chebulinic acid (P16, tab 4-1), and corilagin (P9, tab 4-1), annotated in the crude extract of *T. dhofarica*, inhibit acetylcholinesterase, resulting in neuroprotective anti-Alzheimer's disease effects [13]. In conclusion, the extensive diversity of tannin structures derived from GA and EA makes them highly plausible candidates for the reported medicinal applications of investigated plants. However, their efficacy is likely due to combined effects rather than the activity of individual, highly potent compounds.

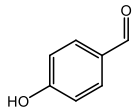
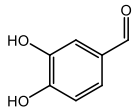
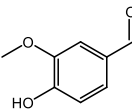
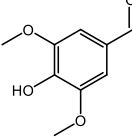
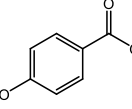
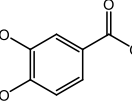
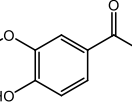
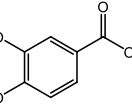
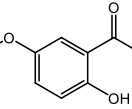
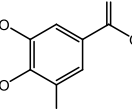
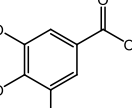
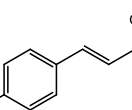
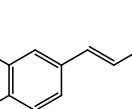
A notable finding during the investigation of the mangrove *L. racemosa* was its remarkably high proportion of sulfated compounds (**2-2**; **2-3**; **2-15**, tab 6-2 and 6-3). Although sulfated phenolics are known, they are rare natural products in plants and had not previously been reported for the Combretaceae family. Mangroves grow in a tidal environment that exposes soil with increased sulfate levels, partly due to sulfate-reducing microbial communities [14]. This abundance of sulfate likely contributes to an elevated uptake as well as an increased biosynthesis of sulfated compounds in mangrove species. The specific biological role of sulfated secondary phenolics in plants remains uncertain. However, sulfate groups enhance water solubility and ion strength within tissues. Additionally, sulfated structures driven from natural products are recognized as effective antifouling agents with minimal environmental toxicity [15]. This suggests a possible analogous ecological role for these compounds in mangrove roots.

Surprisingly, no family-typical pungent compounds were detected in the Zingiberaceae species *Hornstedtia scyphifera*. Instead, terpenoids, phenolics, and particularly flavonoids were identified as the dominant compound classes, with the flavonoid kumatakenin (**5-13**, tab 6-3) emerging as the major isolated compound. Its identity was confirmed through HRMS, NMR, and X-ray crystallography, revealing a previously undescribed crystal structure. Furthermore, MSⁿ analysis elucidated the complete fragmentation pattern using known published fragmentation reactions. Reported medicinal effects of *H. scyphifera*, such as anti-inflammatory and neuroprotective activities [16], are likely linked to its antioxidant flavonoid content, since effects are already well described for members of this group including the isolated compounds epicatechin (**5-8**, tab 6-3), quercetin (**5-10**, tab 6-3), and rutin (**5-11**, tab 6-3). Quercetin is also a crucial compound in senolytics [17].

Another topic evolved in this thesis connects to structure elucidation. Challenges arise in this field from many directions but proton deficiency as well as proton oversupply became the most relevant ones. Structure elucidation, despite significant progress in automation, remains a time-intensive and complex process, particularly for novel compounds. A major challenge is the lack of non-exchangeable protons within a molecule. NMR spectroscopy remains the most powerful tool for this purpose, with experiments like HSQC and HMBC being central after the fundamental ¹H and ¹³C experiments. These rely on *J*_{CH} correlations across 1-4 bonds. Protons act as kind of “spotlights,” revealing clues about their close molecular surroundings. Fewer protons result in fewer clues, complicating structure determination. Advanced techniques like 1,1-ADEQUATE, 1,n-ADEQUATE, and computational methods (CASE, DFT calculations) are powerful tools in such cases, as demonstrated by the successful elucidation of the highly proton-deficient lumnizeralacton (**3-1**) in chapter 3. Especially the combination of the 1,1-ADEQUATE data in the CASE calculations were crucial to confirm the structure by this method. On the other hand, excessive numbers of chemically similar protons lead to signal overlap, resulting in the loss of information and indistinguishable multiplets. COSY spectra are usually valuable for tracing ³*J*_{HH}-connections but become ineffective in such scenarios, especially with additional intramolecular linkages causing even more complex correlation patterns, like in the case of the terpenoid mustaka-14-oic (**5-1**, table 6-1) acid in chapter 5. Another difficulty was the unexpected multiplicity of H-6 in mustaka-14-oic acid, a pseudo singlet, although showing strong COSY correlations. Nevertheless, by using NOESY, and TOCSY experiments, as well as 3D calculation of the molecule, to clarify spatial distances and angles between H-6 and its neighboring protons, it was possible to reveal the reason for the signal appearance. The pseudo singlet is arising from minimal coupling constants due to approximate 90° angles to all three neighbors which is in accordance with the Karplus-curve and only possible due to the strong tension caused by the intramolecular cyclobutane ring.

In conclusion, this thesis has substantially contributed to the phytochemical knowledge of three understudied medicinal plants by isolating 53 metabolites and identifying their major compound classes. It also underscores the untapped potential of traditional medicinal plants as sources for novel bioactive compounds and as target for future pharmacological investigations. The successfully performed characterization and structure elucidation of three novel compounds with hard to solve structures by combining established techniques with modern computer-assisted methods contributes to natural products research and might help to speed-up future research on similar topics. By performing reliable fundamental research in the field on natural product chemistry and addressing the limitations of the methods used, future research can hopefully move closer to discover novel therapeutic agents and unlock the full potential of plant-derived compounds.

Table 6-2 isolated simple phenolics from *L. racemosa* (chap 2), *T. dhofarica* (chap. 4), and *H. scyphifera* (chap 5)

chap.- comp.no.	name (class)	structure
4-2	<i>p</i> -hydroxybenzaldehyde (phenolic aldehyde)	
5-19	protocatechualdehyde (phenolic aldehyde)	
5-20	vanillin (phenolic aldehyde)	
5-21	syringaldehyde (phenolic aldehyde)	
5-22	<i>p</i> -hydroxybenzoic acid (phenolic acid)	
4-3 and 5-23	protocatechuic acid (phenolic acid)	
5-24	vanillic acid (phenolic acid)	
5-25	protocatechuic acid methylester (phenolic ester)	
5-26	5- <i>O</i> -methyl salicylic acid (phenolic acid)	
4-4	gallic acid (phenolic acid)	
4-5	7- <i>O</i> -methyl gallate (phenolic ester)	
4-6 and 5-15	<i>trans-p</i> -coumaric acid (phenolic acid)	
5-16	<i>trans</i> -ferulic acid (phenolic acid)	

Continuation of Table 6-2

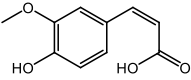
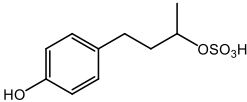
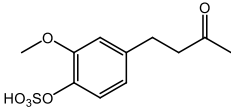
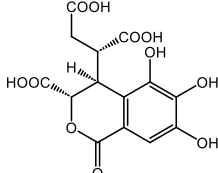
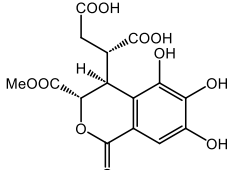
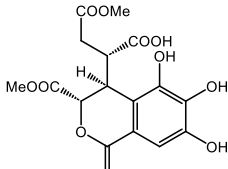
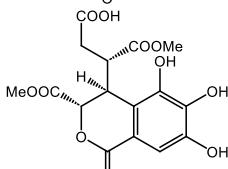
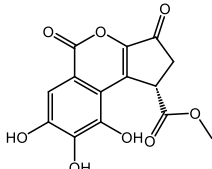
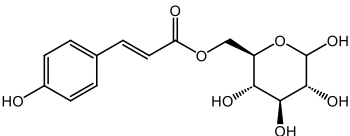
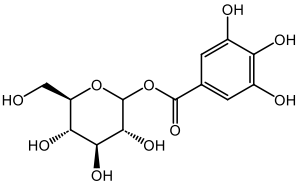
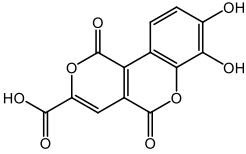
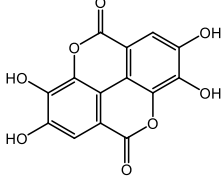
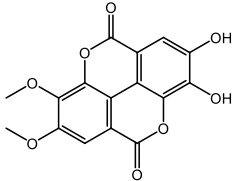
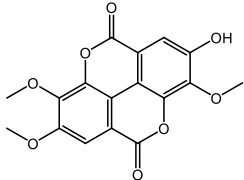
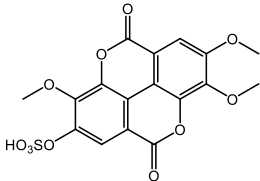
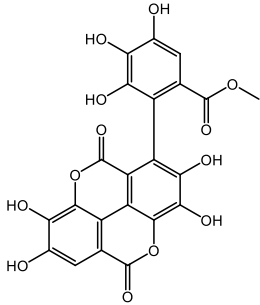
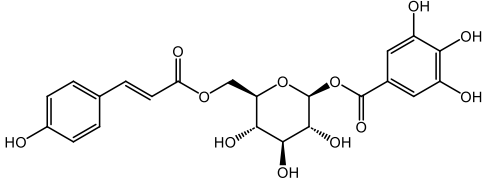
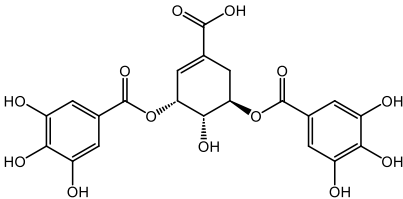
chap.- comp.no.	name (class)	structure
5-17	<i>cis</i> -ferulic acid (phenolic acid)	
2-2	4-(4-hydroxyphenyl) butan-2-ol sulfate (sulfated phenolic)	
2-3	4-(4-sulfoxy-3-methoxyphenyl)-butan-2-one (sulfated phenolic)	
4-7	chebolic acid (phenolic acid)	
4-8	12-O-methyl chebolic acid (phenolic ester)	
4-9	11, 12-O-dimethyl chebolic acid (phenolic ester)	
4-10	12, 13-O-dimethyl chebolic acid (phenolic ester)	
4-11	11-O-methyl brevifolincarboxylate (phenolic ester)	
4-14	6-O- <i>trans</i> - <i>p</i> -coumaroyl-D-glucopyranose (phenolic glucoside)	
4-15	1-O-galloyl-D-glucopyranose (phenolic glucoside)	

Table 6-3 isolated polyphenols from *L. racemosa* (chap 2 + 3), *T. dhofarica* (chap 4), and *H. scyphifera* (chap 5)

chap.- comp.no.	name (class)	structure
3-1	lumnizeralacton (polyphenol)	
2-6 and 4-12	ellagic acid (polyphenol)	
2-13	3,4- <i>O</i> -dimethyl ellagic acid (ellagitannin)	
2-16	3,3',4'- <i>O</i> -trimethyl ellagic acid (ellagitannin)	
2-15	3,3',4'- <i>O</i> -trimethyl ellagic acid-4-sulfate (sulfated ellagitannin)	
4-13	7''- <i>O</i> -methyl flavogallonnate (ellagitannin)	
4-1	1- <i>O</i> -galloyl-6- <i>O</i> - <i>trans-p</i> -coumaroyl- β -D- glucopyranose	
4-16	3,5- <i>O</i> -digalloyl shikimic acid (polyphenol)	

Continuation of Table 6-3

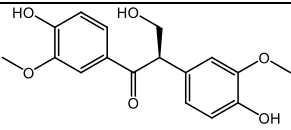
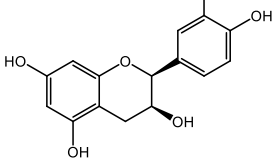
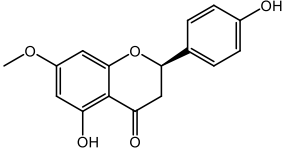
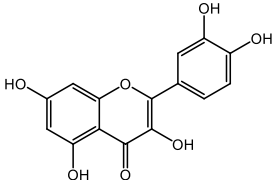
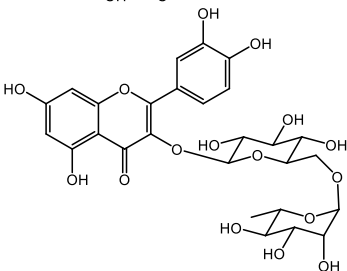
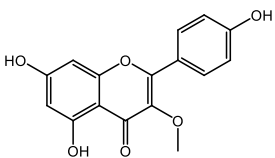
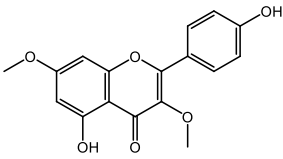
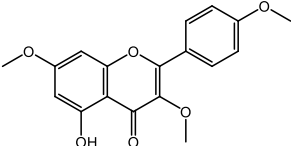
chap.- comp.no.	name (class)	structure
5-18	evofolin B (polyphenol)	
5-8	epicatechin (flavanol)	
5-9	sakuranetin (flavanon)	
5-10	quercetin (flavanol)	
5-11	rutin (flavanol glycoside)	
5-12	isokaempferide (flavanol)	
5-13	kumatakenin (flavanol)	
5-14	5-hydroxy-3,7,4'-trimethoxyflavon (flavanol)	

Table 6-4 isolated gallotannins from *T. dhofarica* (chap 4)

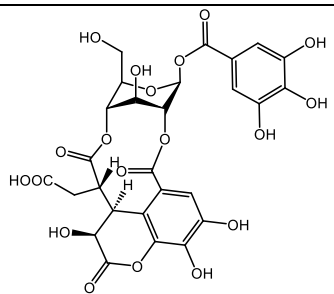
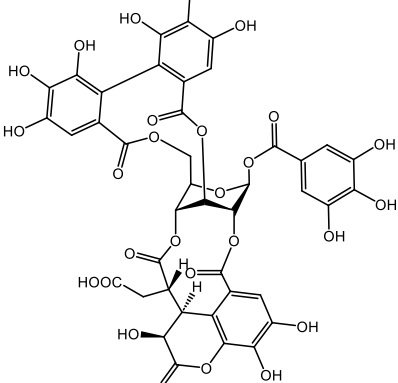
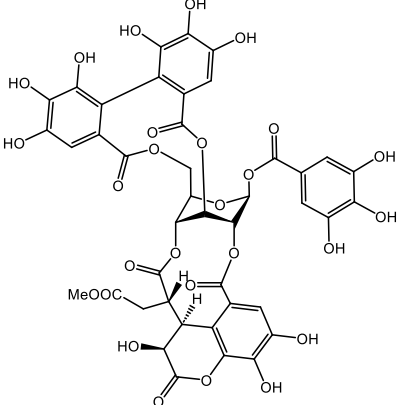
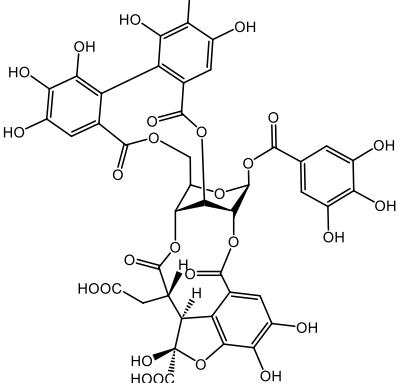
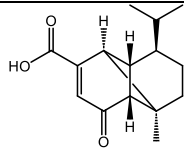
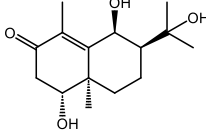
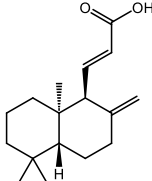
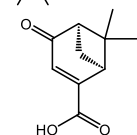
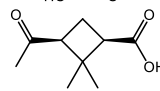
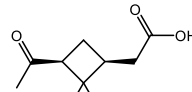
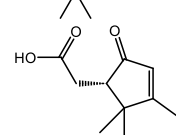
chap.- comp.no.	name (class)	structure
4-17	chebulanin (gallotannin)	
4-18	chebulagic acid (gallotannin)	
4-19	6'-O-methyl-chebulagic acid (gallotannin)	
4-20	phyllanembilinin C (gallotannin)	

Table 6-5 isolated terpenoids and keto acids from *H. scyphifera* (chap 5)

chap.- comp.no.	name (class)	structure
5-1	mustak-14-oic acid (sesquiterpenoid)	
5-2	6-hydroxy-anhuienosol (sesquiterpenoid)	
5-3	14,15,16-trinorlabda- 8(17),11-dien-13-oic acid (diterpenoid)	
5-4	verbenon-10-oic acid (monoterpenoid)	
5-5	cis-pinononic acid (keto acid)	
5-6	cis-pinonic acid (keto acid)	
5-7	2-(2,2,3-trimethyl-5-oxocyclopent- 3-en-1-yl) acetic acid (keto acid)	

References

- [1] Baumgartner, R.R.; Steinmann, D.; Heiss, E.H.; Atanasov, A.G.; Ganzera, M.; Stuppner, H.; Dirsch, V.M., Bioactivity-guided isolation of 1,2,3,4,6-penta-*O*-galloyl- β -glucopyranose from *Paeonia lactiflora* roots as a PTP1B inhibitor, *J. Nat. Prod.* **2010**, *73*, 1578–1581, doi:10.1021/np100258e.
- [2] Atanasov, A.G.; Waltenberger, B.; Pferschy-Wenzig, E.-M.; Linder, T.; Wawrosch, C.; Uhrin, P.; Temml, V.; Wang, L.; Schwaiger, S.; Heiss, E.H.; et al., Discovery and resupply of pharmacologically active plant-derived natural products: A review, *Biotechnol. Adv.* **2015**, *33*, 1582–1614, doi:10.1016/j.biotechadv.2015.08.001.
- [3] Vogl, S.; Atanasov, A.G.; Binder, M.; Bulusu, M.; Zehl, M.; Fakhrudin, N.; Heiss, E.H.; Picker, P.; Wawrosch, C.; Saukel, J.; et al., The herbal drug *Melampyrum pratense* L. (Koch): Isolation and identification of its bioactive compounds targeting mediators of inflammation, *Evid. Based Complement. Alternat. Med.* **2013**, *2013*, 395316, doi:10.1155/2013/395316.
- [4] Mei, Y.; Hu, Y.; Tao, X.; Shang, J.; Qian, M.; Suo, F.; Li, J.; Cao, L.; Wang, Z.; Xiao, W., Chemical profiling of shen-zu-yi-shen tablets using UPLC-Q-TOF-MS/MS and its quality evaluation based on UPLC-DAD combined with multivariate statistical analysis, *J. Chromatogr. Sci.* **2024**, *62*, 534–553, doi:10.1093/chromsci/bmae001.
- [5] Junio, H.A.; Sy-Cordero, A.A.; Ettetfagh, K.A.; Burns, J.T.; Micko, K.T.; Graf, T.N.; Richter, S.J.; Cannon, R.E.; Oberlies, N.H.; Cech, N.B., Synergy-directed fractionation of botanical medicines: A case study with goldenseal (*Hydrastis canadensis*), *J. Nat. Prod.* **2011**, *74*, 1621–1629, doi:10.1021/np200336g.
- [6] Degenhardt, A.; Wittlake, R.; Seilwind, S.; Liebig, M.; Runge, C.; Hilmer, J.-M.; Krammer, G.; Gohr, A.; Wessjohann, L., Quantification of important flavor compounds in beef stocks and correlation to sensory results by “reverse metabolomics” (Ferreira, V. & Lopez, R., eds.). 15-19, (2014) ISBN: 9780124017245, doi: 10.1016/B978-0-12-398549-1.00003-9
- [7] Hadidi, M.; Liñán-Atero, R.; Tarahi, M.; Christodoulou, M.C.; Aghababaei, F., The potential health benefits of gallic acid: Therapeutic and food applications, *Antioxidants* **2024**, *13*, doi:10.3390/antiox13081001.
- [8] Sharifi-Rad, J.; Quispe, C.; Castillo, C.M.S.; Caroca, R.; Lazo-Vélez, M.A.; Antonyak, H.; Polishchuk, A.; Lysiuk, R.; Oliinyk, P.; Masi, L. de; et al., Ellagic acid: A review on its natural sources, chemical stability, and therapeutic potential, *Oxid. Med. Cell. Longev.* **2022**, *2022*, 3848084, doi:10.1155/2022/3848084
- [9] Şabik, A.E.; Sevindik, M.; Mohammed, F.S.; Uysal, I.; Bal, C., Gallic acid: Derivatives and biosynthesis, pharmacological and therapeutic effect, biological activity, *Bulletin UASVM Food Science and Technology* **2024**, *81*, 18–27, doi:10.15835/buasvmcn-fst:2023.0017.
- [10] Zhu, M.; Phillipson, J.D.; Greengrass, P.M.; Bowery, N.E.; Cai, Y., Plant polyphenols: Biologically active compounds or non-selective binders to protein?, *Phytochemistry* **1997**, *44*, 441–447, doi:10.1016/s0031-9422(96)00598-5.
- [11] Terashima, S.; Shimizu, M.; Nakayama, H.; Ishikura, M.; Ueda, Y.; Imai, K.; Suzui, A.; Morita, N., Studies on aldose reductase inhibitors from medicinal plant of "sinfito," *Potentilla candicans*, and further synthesis of their related compounds, *Chem. Pharm. Bull.* **1990**, *38*, 2733–2736, doi:10.1248/cpb.38.2733.
- [12] Chai, W.; Wei, W.; Hu, X.; Bai, Q.; Guo, Y.; Zhang, M.; Li, S.; Pan, Q., Inhibitory effect and molecular mechanism on tyrosinase and browning of fresh-cut apple by longan shell tannins, *Int. J. Biol. Macromol.* **2024**, *274*, 133326, doi:10.1016/j.ijbiomac.2024.133326.
- [13] Li, Y.-J.; Liang, C.-C.; Jin, L.; Chen, J., Inhibition mechanisms of four ellagitannins from *Terminalia chebula* fruits on acetylcholinesterase by inhibition kinetics, spectroscopy and molecular docking analyses, *Spectrochim. Acta A Mol. Biomol. Spectrosc.* **2023**, *302*, 123115, doi:10.1016/j.saa.2023.123115.
- [14] Balk, M.; Keuskamp, J.A.; Laanbroek, H.J., Potential for sulfate reduction in mangrove forest soils: Comparison between two dominant species of the Americas, *Front. Microbiol.* **2016**, *7*, 1855, doi:10.3389/fmicb.2016.01855.
- [15] Almeida, J.R.; Correia-da-Silva, M.; Sousa, E.; Antunes, J.; Pinto, M.; Vasconcelos, V.; Cunha, I., Antifouling potential of nature-inspired sulfated compounds, *Sci. Rep.* **2017**, *7*, 42424, doi:10.1038/srep42424.
- [16] Zipp, F.; Ullrich, O., Extracts from the plant *Hornstedtia scyphifera* and immunosuppressive effects, EP2163253A1, **2008**.
- [17] Arndt, H.; Bachurski, M.; Yuanxiang, P.; Franke, K.; Wessjohann, L. A.; Kreutz, M. R.; Grochowska, K. M., A screen of plant-based natural products revealed that quercetin prevents amyloid- β uptake in astrocytes as well as resulting astrogliosis and synaptic dysfunction, *Mol. Neurobiol.* (2024). **2024**, doi: 10.1007/s12035-024-04509-6

7 Appendix

7.1 Supporting Information of chapter 2

Supporting Information

Analysis of Unusual Sulfated Constituents and Anti-infective Properties of Two Indonesian Mangroves, *Lumnitzera littorea* and *Lumnitzera racemosa* (Combretaceae)

Jeprianto Manurung^{1,2,3,a}, Jonas Kappen^{3,a}, Jan Schnitzler^{1,2}, Andrej Frolov^{3,4}, Ludger A. Wessjohann^{2,3}, Andria Agusta⁵, Alexandra N. Muellner-Riehl^{1,2,*} and Katrin Franke^{3,*}

¹ Department of Molecular Evolution and Plant Systematics & Herbarium (LZ), Institute of Biology, Leipzig University, Germany; jeprianto_m@apps.ipb.ac.id (J.M.); j.schnitzler06@alumni.imperial.ac.uk (J.S.); muellner-riehl@uni-leipzig.de (A.N.M.-R.)

² German Centre for Integrative Biodiversity Research (iDiv) Halle-Jena-Leipzig, Leipzig, Germany

³ Department of Bioorganic Chemistry, Leibniz Institute of Plant Biochemistry (IPB), Halle (Saale), Germany; katrin.franke@ipb-halle.de (K.F.); andrej.frolov@ipb-halle.de (A.F.); jkappen@ipb-halle.de (J.K.); ludger.wessjohann@ipb-halle.de (L.A.W.)

⁴ Department of Biochemistry, St. Petersburg State University, St. Petersburg, Russia

⁵ Research Center for Chemistry, Indonesian Institute of Sciences (LIPI), Bogor, Indonesia; andr002@lipi.go.id (A.A.)

* Correspondence: muellner-riehl@uni-leipzig.de (phylogeny); katrin.franke@ipb-halle.de (chemistry); Tel.: +49-341-97-38581 (A.N.M.-R.); +49-345-5582-1380 (K.F.)

^a J.M and J.K. contributed equally to this work.

Content	Page
Fig. S1: MS/MS spectra of compounds 1-21	2
Fig. S2: PDA chromatograms of root extracts from <i>L. littorea</i> (LL1-LL12) and <i>L. racemosa</i> (LR1-LR19)	14
Tab. S1: Peak areas (TIC) of main compounds detected in root extracts of <i>L. littorea</i> and <i>L. racemosa</i>	15
Fig. S3: Anthelmintic activity of root extracts from <i>L. littorea</i> (LL1-12) and <i>L. racemosa</i> (LR1-19)	16
Fig. S4: Cytotoxic activity of root extracts from <i>L. littorea</i> (LL3, LL11) and <i>L. racemosa</i> (LR5, LR15)	17
Tab. S2: 2D NMR data of compound 2	18
Fig. S5: NMR and MS spectra of compound 2	19
Tab. S3: 2D NMR data of compound 3	22
Fig. S6: NMR and MS spectra of compound 3	23
Fig. S7: NMR and MS spectra of compound 6	26
Tab. S4: 2D NMR data of compound 13	28
Fig. S8: NMR and MS spectra of compound 13	29
Tab. S5: 2D NMR data of compound 15	32
Fig. S9: NMR and MS spectra of compound 15	33
Tab. S6: 2D NMR data of compound 16	37
Fig. S10: NMR and MS spectra of compound 16	38

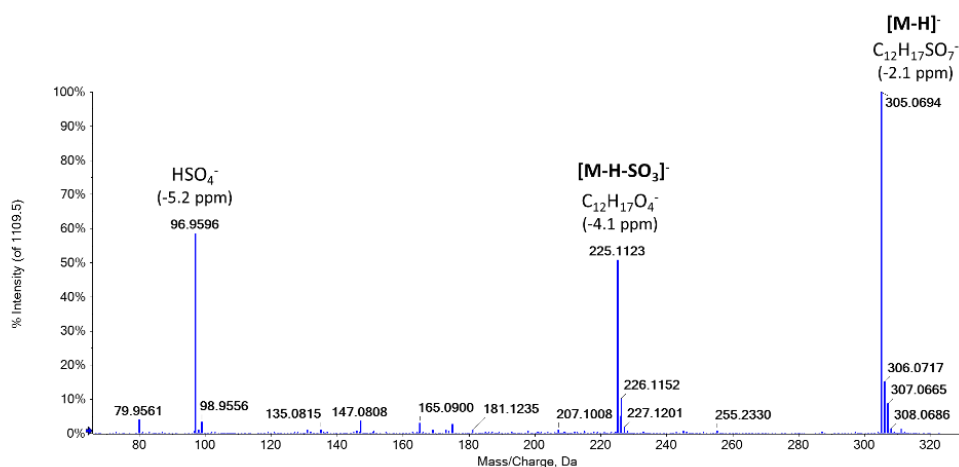


Figure S1-1. Tandem mass spectrum of m/z 305.0996 at t_R 3.5 min of compound **1**, annotated in methanolic root extract of *Lumnitzera littorea*. The spectrum was acquired with a QqTOF mass spectrometer operated in the negative SWATH mode (m/z window 289.0–315.0).

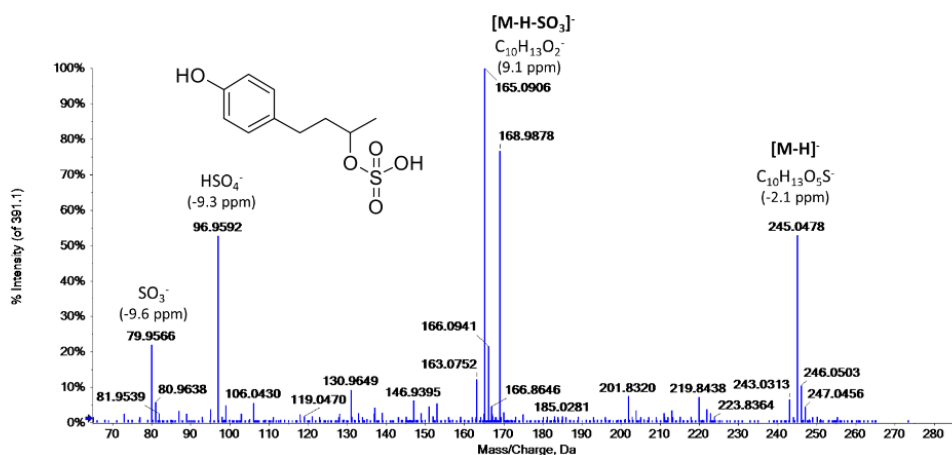


Figure S1-2. Tandem mass spectrum of m/z 245.0488 at t_R 3.8 min of compound **2**, annotated in methanolic root extracts of *Lumnitzera littorea* and *L. racemosa*. The spectrum was acquired with a QqTOF mass spectrometer operated in the negative SWATH mode (m/z window 239.0–265.0).

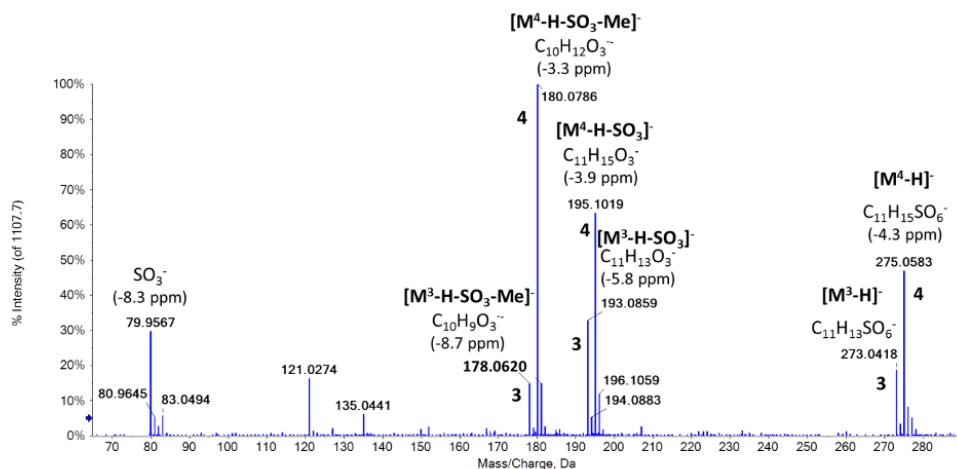


Figure S1-3. Tandem mass spectrum of m/z 273.0436 and 275.0591 at t_R 3.9 min of overlapping compounds **3** and **4**, respectively, annotated in methanolic root extracts of *Lumnitzera littorea* and *L. racemosa*. The spectrum was acquired with a QqTOF mass spectrometer operated in the negative SWATH mode (m/z window 264.0–290.0).

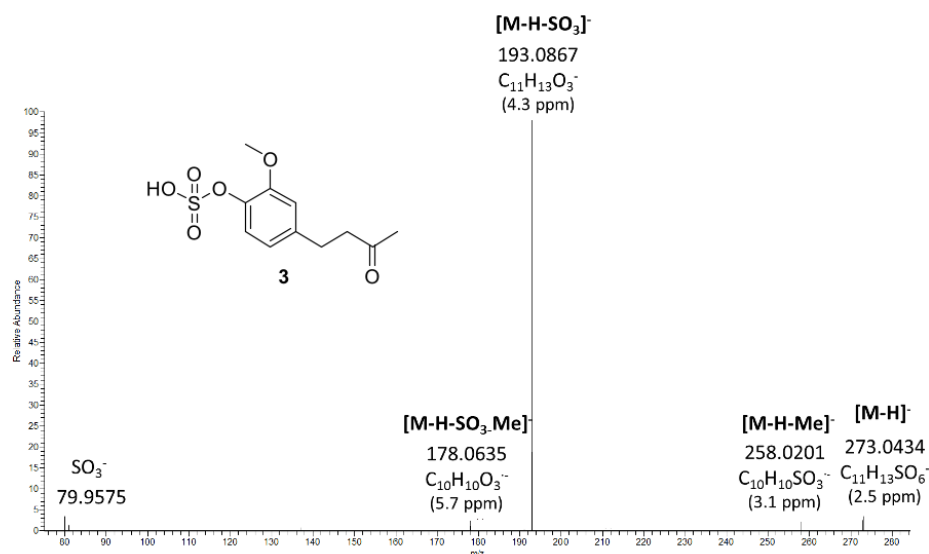


Figure S1-4. Tandem mass spectrum of m/z 273.0436 at t_R 3.9 min of compound **3**, annotated in methanolic root extracts of *Lumnitzera littorea* and *L. racemosa*. The spectrum was acquired with LIT-Orbitrap-MS in negative ion mode with CID activation (30% relative collision energy).

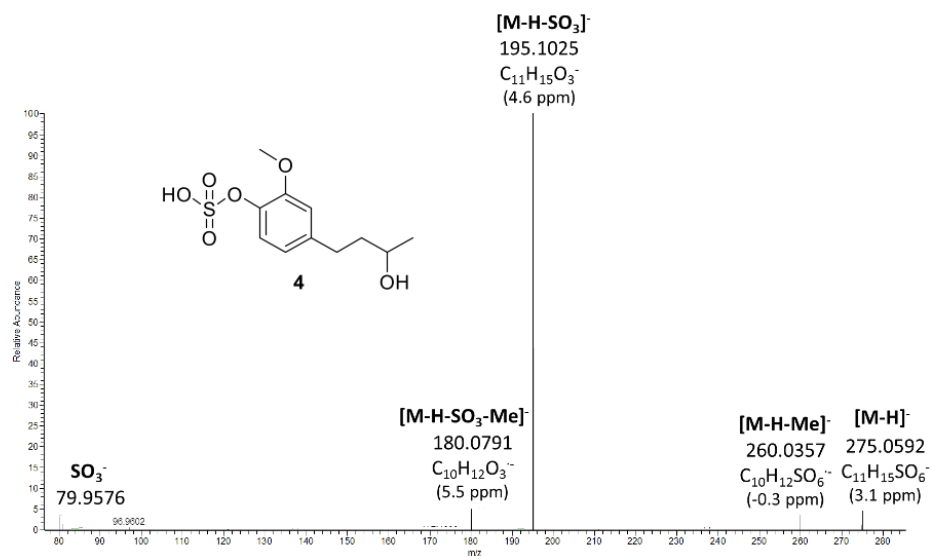


Figure S1-5. Tandem mass spectrum of m/z 275.0591 at t_R 3.9 min of compound **4**, annotated in methanolic root extracts of *Lumnitzera littorea* and *L. racemosa*. The spectrum was acquired with LIT-Orbitrap-MS in negative ion mode with CID activation (30% relative collision energy).

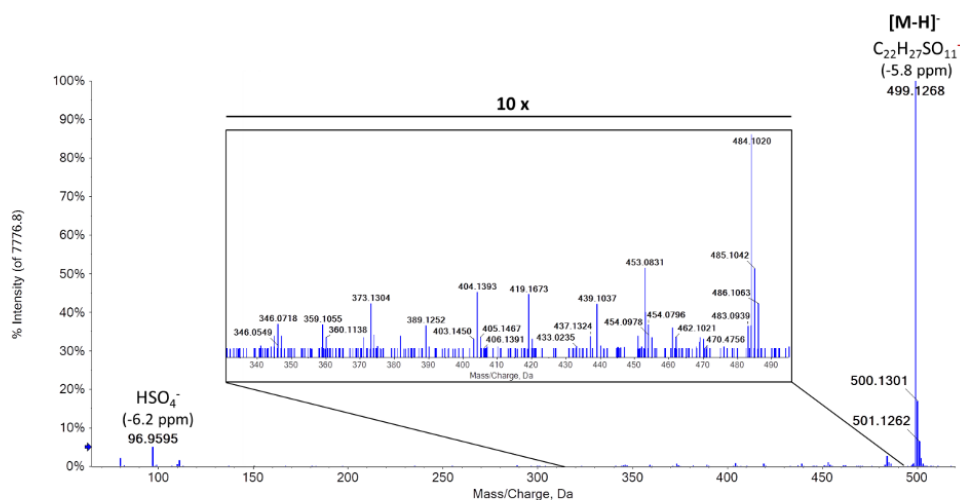


Figure S1-6. Tandem mass spectrum of m/z 499.1267 at t_R 4.4 min of compound **5**, annotated in methanolic root extracts of *Lumnitzera littorea*. The spectrum was acquired with a QqTOF mass spectrometer operated in the negative SWATH mode (m/z window 489.0–515.0).

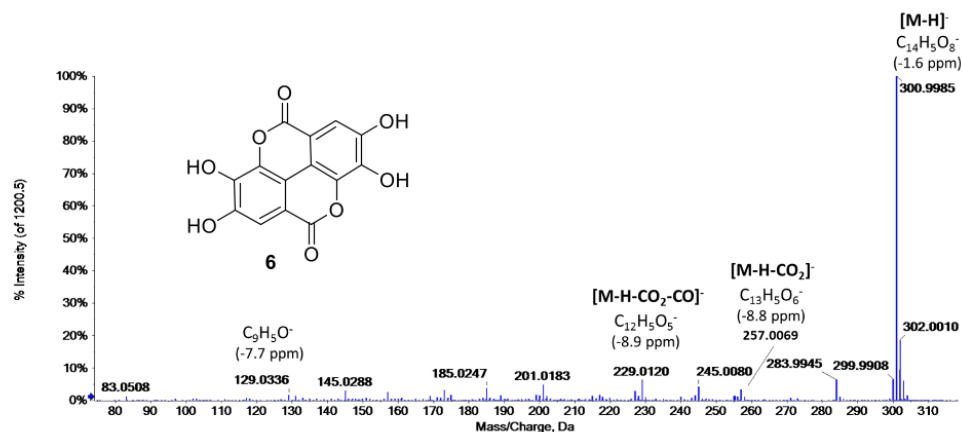


Figure S1-7. Tandem mass spectrum of m/z 300.9989 at t_R 4.4 min of compound **6**, annotated in methanolic root extracts of *Lumnitzera littorea*. The spectrum was acquired with a QqTOF mass spectrometer operated in the negative SWATH mode (m/z window 289.0–315.0).

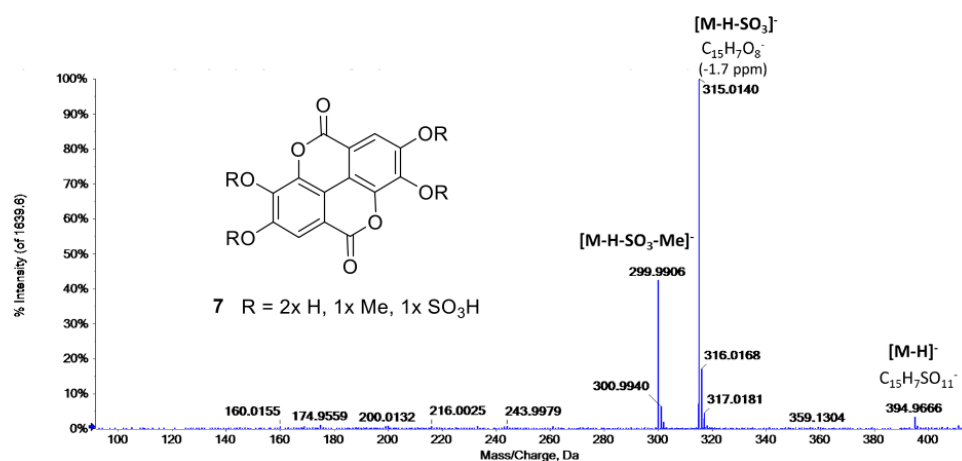


Figure S1-8. Tandem mass spectrum of m/z 394.9707 at t_R 5.3 min of compound **7**, annotated in methanolic root extracts of *Lumnitzera racemosa*. The spectrum was acquired with a QqTOF mass spectrometer operated in the negative SWATH mode (m/z window 389.0–415.0).

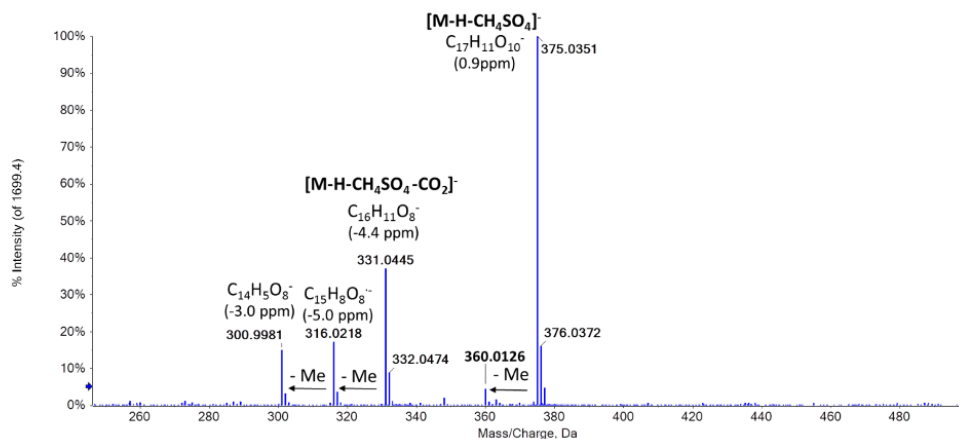


Figure S1-9. Tandem mass spectrum of m/z 487.0179 at t_R 5.5 min of compound **8**, annotated in the methanolic root extract of *Lumnitzera racemosa*. The spectrum was acquired with a QqTOF mass spectrometer operated in the negative SWATH mode (m/z window 464.0–490.0).

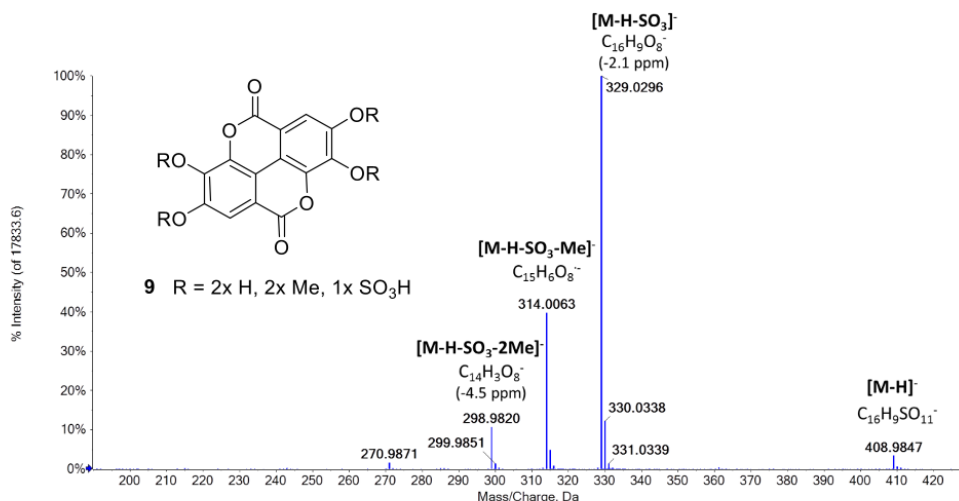


Figure S1-10. Tandem mass spectrum of m/z 408.9898 at t_R 5.7 min of compound **9**, annotated in methanolic root extracts of *Lumnitzera littorea* and *L. racemosa*. The spectrum was acquired with a QqTOF mass spectrometer operated in the negative SWATH mode (m/z window 389.0–415.0).

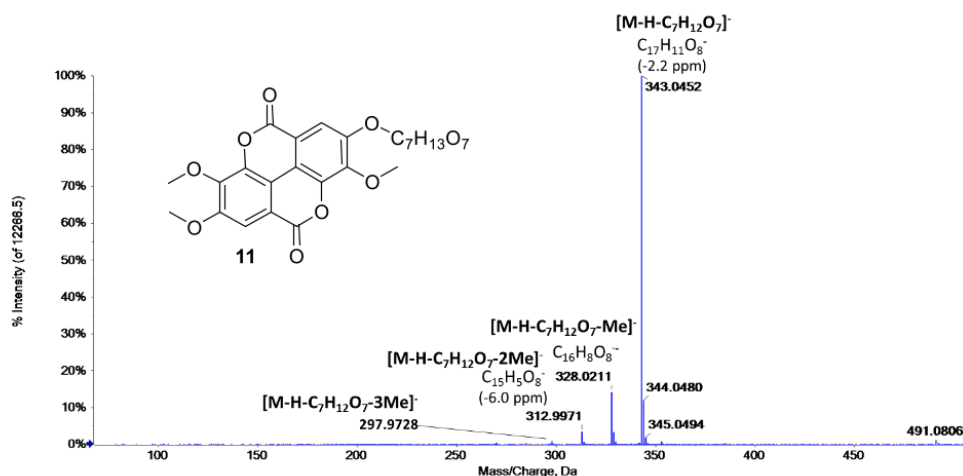


Figure S1-11. Tandem mass spectrum of m/z 551.1027 at t_R 6.0 min of compound **10**, annotated in methanolic root extracts of *Lumnitzera racemosa*. The spectrum was acquired with a QqTOF mass spectrometer operated in the negative SWATH mode (m/z window 539.0–565.0).

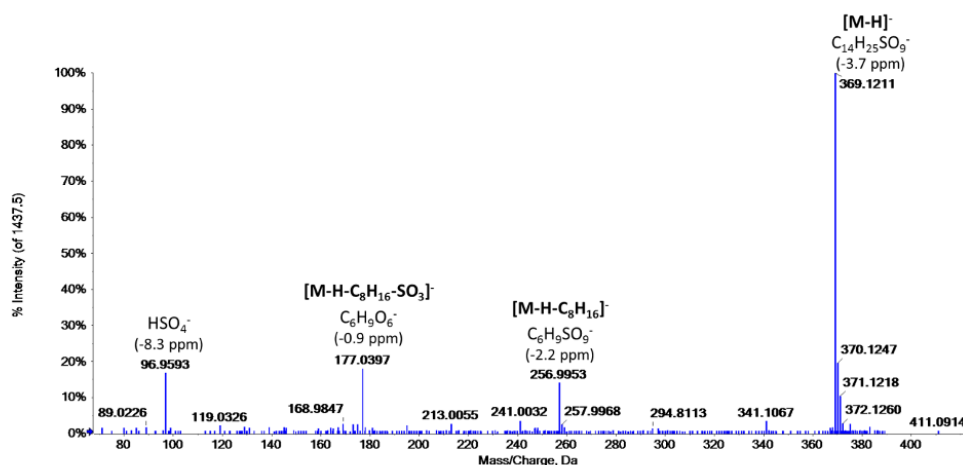


Figure S1-12. Tandem mass spectrum of m/z 369.1225 at t_R 6.1 min of compound **11**, annotated in methanolic root extracts of *Lumnitzera littorea*. The spectrum was acquired with a QqTOF mass spectrometer operated in the negative SWATH mode (m/z window 364.0–390.0).

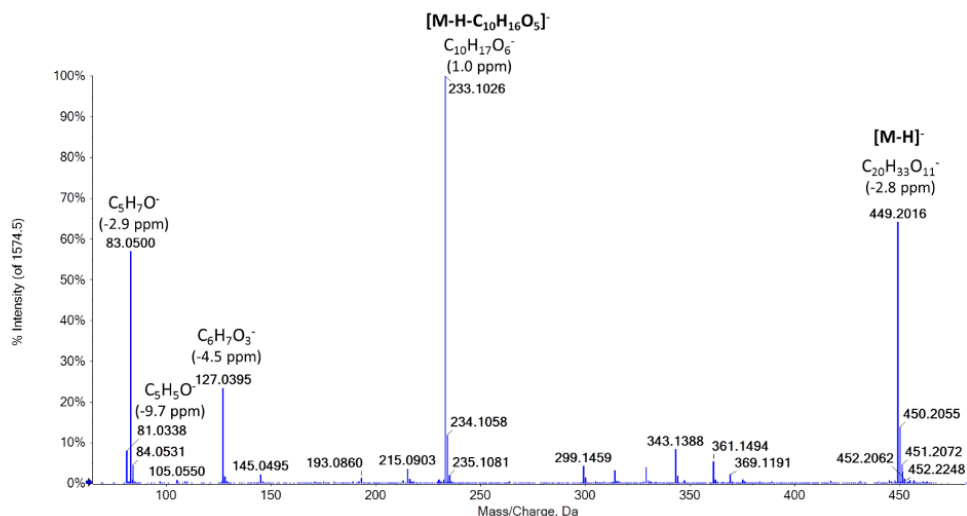


Figure S1-13. Tandem mass spectrum of m/z 449.2027 at t_R 6.3 min of compound **12**, annotated in methanolic root extracts of *Lumnitzera littorea* and *L. racemosa*. The spectrum was acquired with a QqTOF mass spectrometer operated in the negative SWATH mode (m/z window 439.0–465.0).

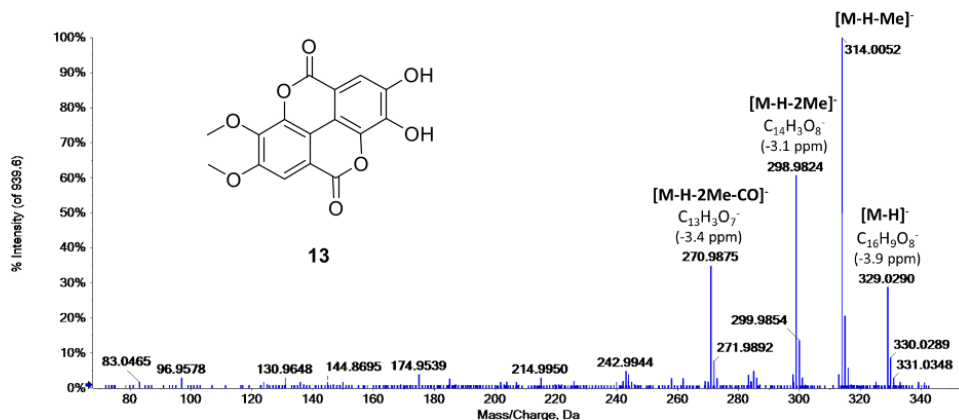


Figure S1-14. Tandem mass spectrum of m/z 329.0301 at t_R 6.4 min of compound **13**, annotated in methanolic root extracts of *Lumnitzera littorea* and *L. racemosa*. The spectrum was acquired with a QqTOF mass spectrometer operated in the negative SWATH mode (m/z window 314.0–340.0).

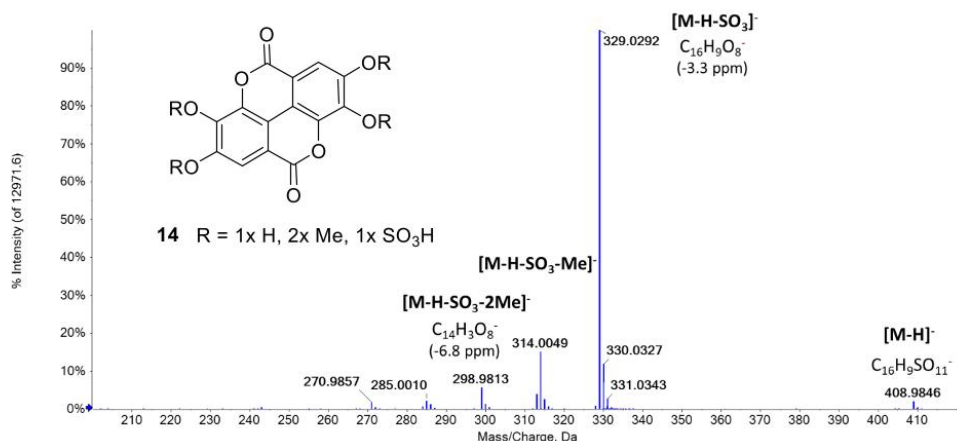


Figure S1-15. Tandem mass spectrum of m/z 408.9867 at t_R 6.5 min of compound **14**, annotated in methanolic root extracts of *Lumnitzera racemosa*. The spectrum was acquired with a QqTOF mass spectrometer operated in the negative SWATH mode (m/z window 389.0–415.0).

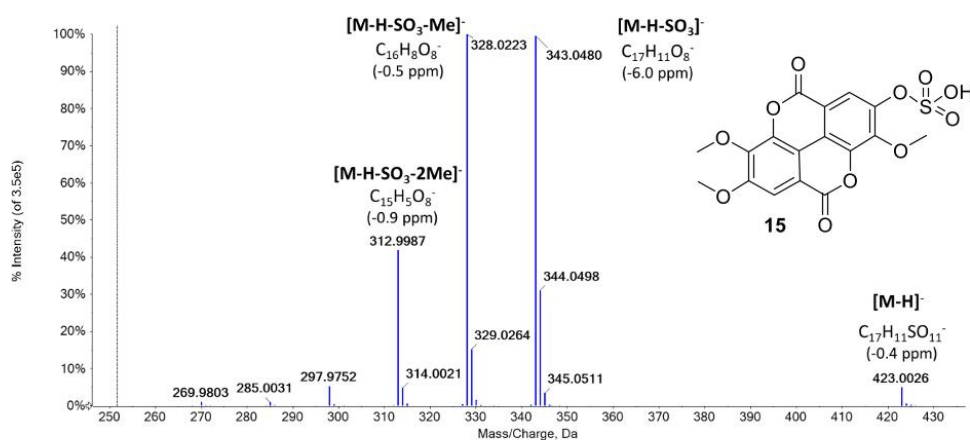


Figure S1-16. Tandem mass spectrum of m/z 423.0035 at t_R 6.9 min of compound **15**, annotated in methanolic root extracts of *Lumnitzera littorea* and *L. racemosa*. The spectrum was acquired with a QqTOF mass spectrometer operated in the negative SWATH mode (m/z window 414.0–440.0).

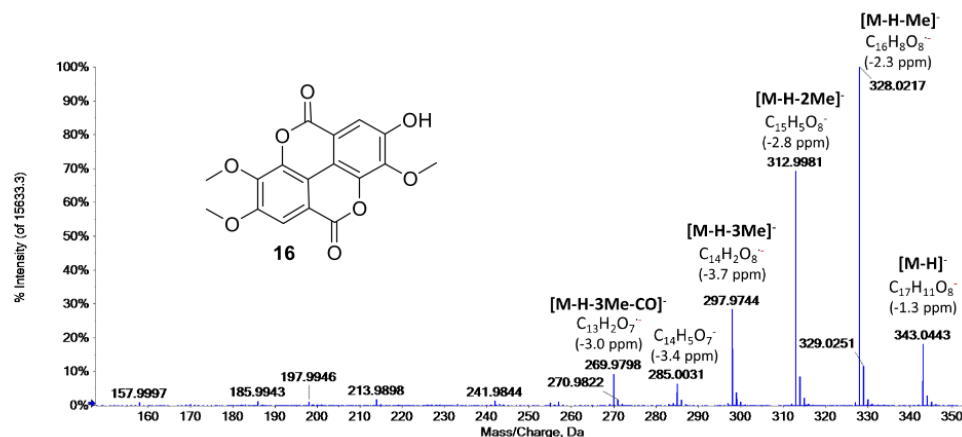


Figure S1-17. Tandem mass spectrum of m/z 343.0455 at t_R 7.7 min of compound **16**, annotated in methanolic root extracts of *Lumnitzera littorea* and *L. racemosa*. The spectrum was acquired with a QqTOF mass spectrometer operated in the negative SWATH mode (m/z window 339.0–365.0).

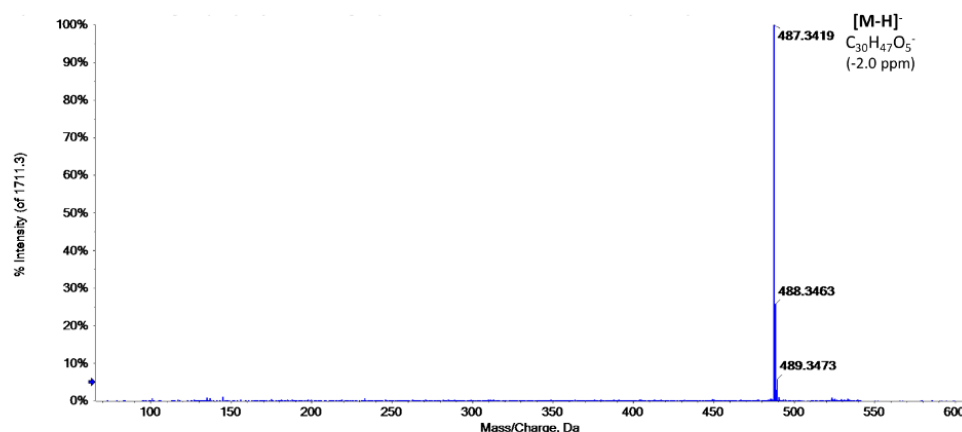


Figure S1-18. Tandem mass spectrum of m/z 533.3480 at t_R 9.8 min of the formiate adduct of compound **17**, annotated in methanolic root extracts of *Lumnitzera littorea* and *L. racemosa*. The spectrum was acquired with a QqTOF mass spectrometer operated in the negative SWATH mode (m/z window 514.0–540.0).

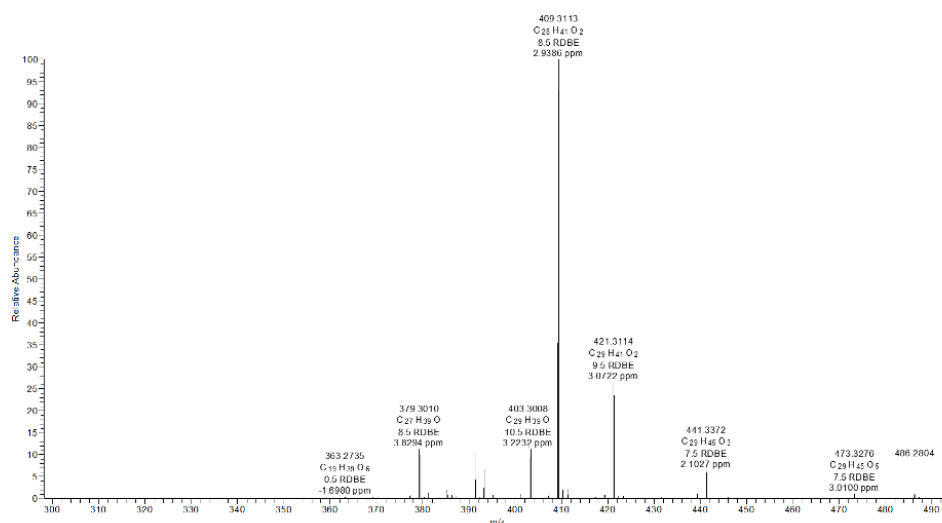


Figure S1-19. Tandem mass spectrum of m/z 487.3425 at t_R 9.8 min of compound **17**, annotated in methanolic root extracts of *Lumnitzera littorea* and *L. racemosa*. The spectrum was acquired with LIT-Orbitrap-MS in negative ion mode with CID activation (35% relative collision energy).

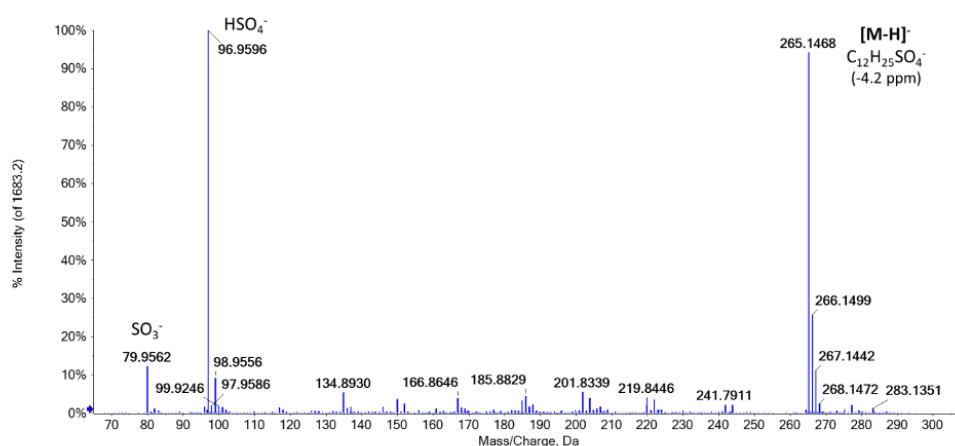


Figure S1-20. Tandem mass spectrum of m/z 265.1476 at t_R 12.2 min of compound **18**, annotated in methanolic root extracts of *Lumnitzera littorea* and *L. racemosa*. The spectrum was acquired with a QqTOF mass spectrometer operated in the negative SWATH mode (m/z window 264.0–290.0).

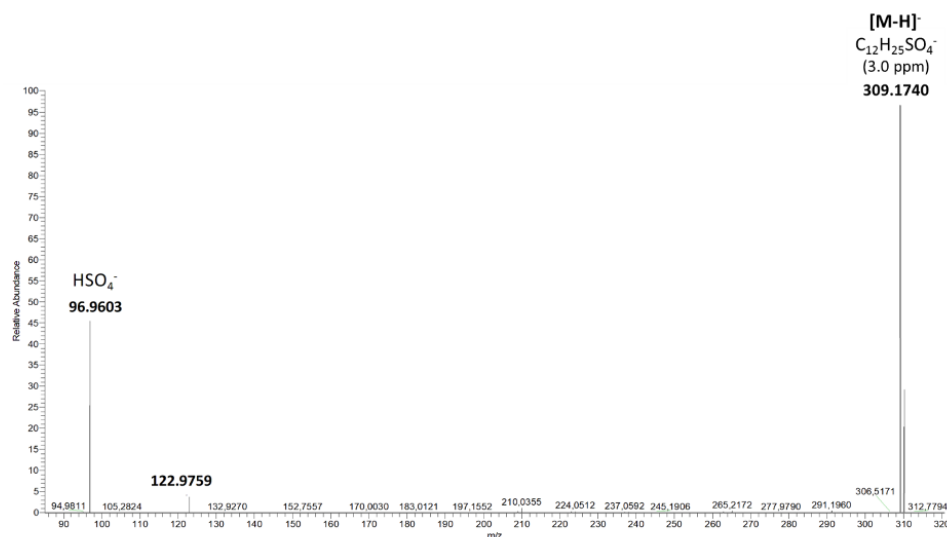


Figure S1-21. Tandem mass spectrum of m/z 309.1733 at t_R 13.4 min of compound **19**, annotated in methanolic root extracts of *L. littorea* and *L. racemosa*. The spectrum was acquired with LIT-Orbitrap-MS in negative ion mode with CID activation (35% relative collision energy).

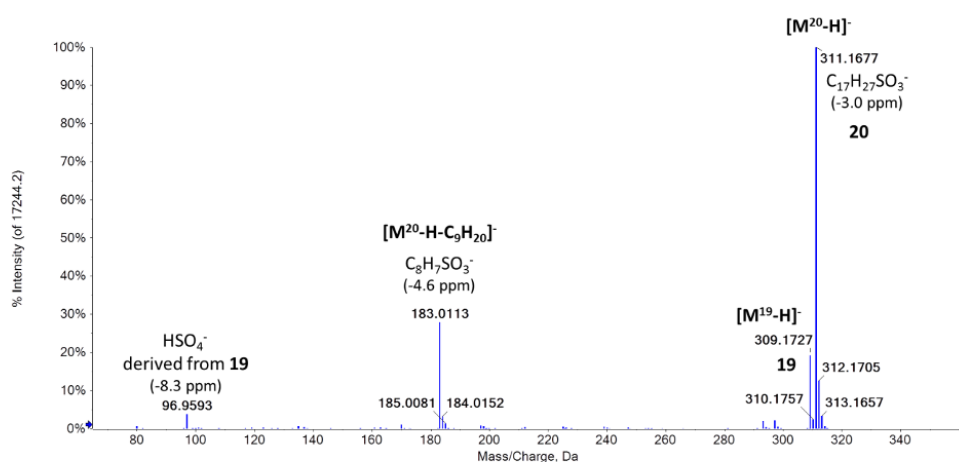


Figure S1-22. Tandem mass spectrum of m/z 309.1733 and 311.1685 at t_R 13.4 min of compounds **19** and **20**, respectively, annotated in methanolic root extracts of *Lumnitzera littorea* and *L. racemosa*. The spectrum was acquired with a QqTOF mass spectrometer operated in the negative SWATH mode (m/z window 289.0–315.0).

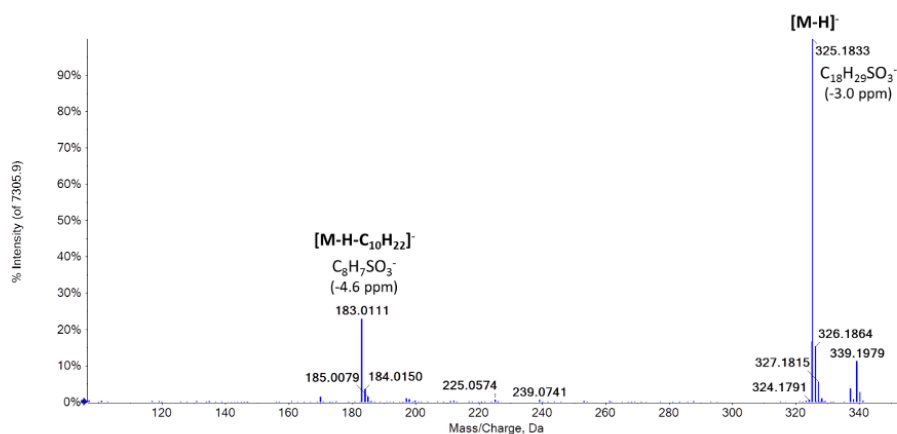


Figure S1-23. Tandem mass spectrum of m/z 325.1833 at t_R 14.6 min of compound **21**, annotated in methanolic root extracts of *Lumnitzera littorea* and *L. racemosa*. The spectrum was acquired with a QqTOF mass spectrometer operated in the negative SWATH mode (m/z window 314.0–340.0).

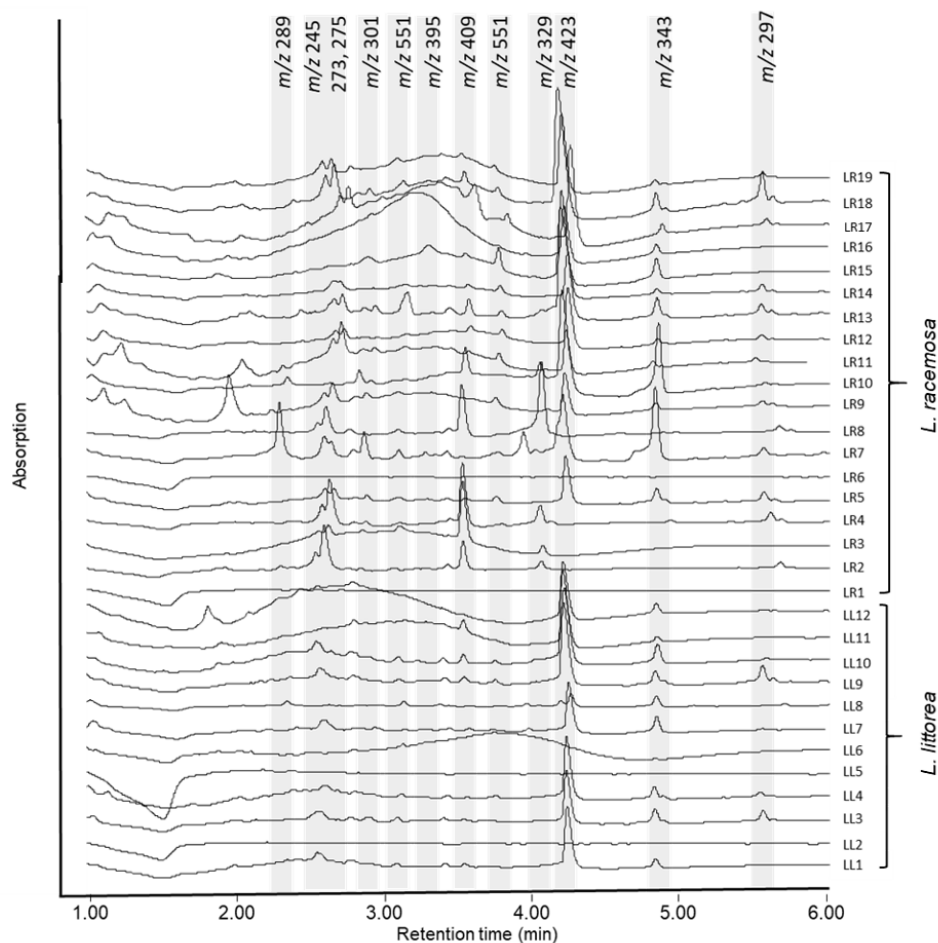


Figure S2. PDA chromatogram (200-400 nm) of root extracts from *Lumnitzera littorea* (LL1-LL12) and *L. racemosa* (LR1-LR19) obtained by an ACQUITY UHPLC-ESI-Q-MS* system.

***UHPLC-ESI-Q-MS**

Eluents A and B are water and acetonitrile, respectively, both containing 0.1% (v/v) formic acid. Samples (2 μ L) were loaded on an Acquity UPLC Reversed-Phase Ethylene Bridged Hybrid (BEH) column (C18-phase, ID 1 mm, length 50 mm, particle size 1.7 μ m, Waters GmbH, Eschborn, Germany) under isocratic conditions (95% eluent A, 5% B, 2 min), and separated using a linear gradient from 5 to 90% eluent B in 9 min. Separation was performed on an ACQUITY UPLC I-Class UHPLC System (Waters GmbH, Eschborn, Germany) with a flow rate of 0.4 mL/min and 40 °C column temperature. The column effluents were introduced on-line into a photodiode array detector (Waters PDA e λ , 200 – 400 nm, sampling rate 10 Hz, 4.8 nm) and further in a Waters QDa quadrupole mass spectrometer, operated in a mass detector/negative ion mode. MS data were acquired in a negative scan mode with a target sampling rate of 8 points/second. Cone voltage was set to -15 V, capillary voltage to -0.8 kV.

Tab. S1. Peak areas (presented as counts per second) of main compounds integrated in total ion chromatograms (TIC) acquired for root extracts of *Lumnitzera littorea* (LL1-LL12) and *L. racemosa* (LR1-LR19) by UHPLC-ESI-Q-MS.

Compound	2	4	3	6	7	9	10	13	15	16
rt (min)	2,5	2,55	2,6	2,8	3,25	3,5	3,7	4,0	4,2	4,8
m/z	245	275	273	301	395	409	551	329	423	343
LL1	16305					6238			110995	16608
LL2	no results									
LL3	13630			1513		122511			114942	22498
LL4	24579					4649			88144	22967
LL5	no results									
LL6	no results									
LL7				6535		5462			106017	36740
LL8	3789					1057		2670	40123	37841
LL9	21145					9796			151009	23011
LL10	25221		4150			16614			198140	40378
LL11		3748		2550	12559	28413	2299		151567	13810
LL12	6384					3478			149719	26341
LR1	no results									
LR2			78929	4551		56839		18648	-	-
LR3	2505	1491		5236	3122	122511		19629	-	-
LR4			79472	7763		138091		40885	-	-
LR5		15620	14988	10647	2798	6100	15731	1745	109580	33141
LR6	no results									
LR7		81480		51234		1907		51480	169288	159443
LR8			53366			129533		192405	-	-
LR9	2960		36775	12512			19070		104486	18387
LR10		5159		7683	2742	62649	4764	38071	268823	176536
LR11			51202	8262		5296	19239		89767	trace
LR12		12224	14599	2868	3528	13273	15569		135585	13301
LR13			24944			34692	14871	5170	321378	43682
LR14		73803				8577	15843		103275	12378
LR15		12486			37950	13877	58091		253222	64018
LR16				6150		3113	5317		151301	30436
LR17		9662	29179	6747	8754	52981	22757		193709	18905
LR18	15725		58754	12312	8944	27402	17967		340237	42964
LR19		22624	22765			8366	8810		224365	9920

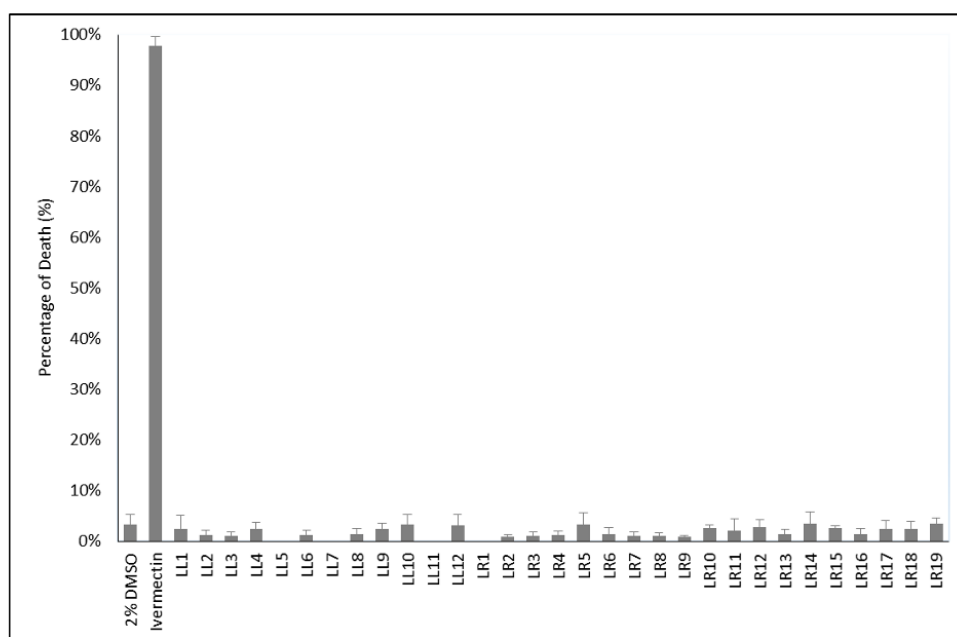


Figure S3. Anthelmintic activity of root extracts from *Lumnitzera littorea* (LL1-LL12) and *L. racemosa* (LR1-LR19) at the concentration of 500 µg/ml against *Caenorhabditis elegans*. The solvent DMSO (2% v/v) and the standard anthelmintic drug ivermectin (10 µg/mL, 100% dead worms after 30 min incubation) were used as negative and positive controls, respectively. Results are given as percentage of dead worms.

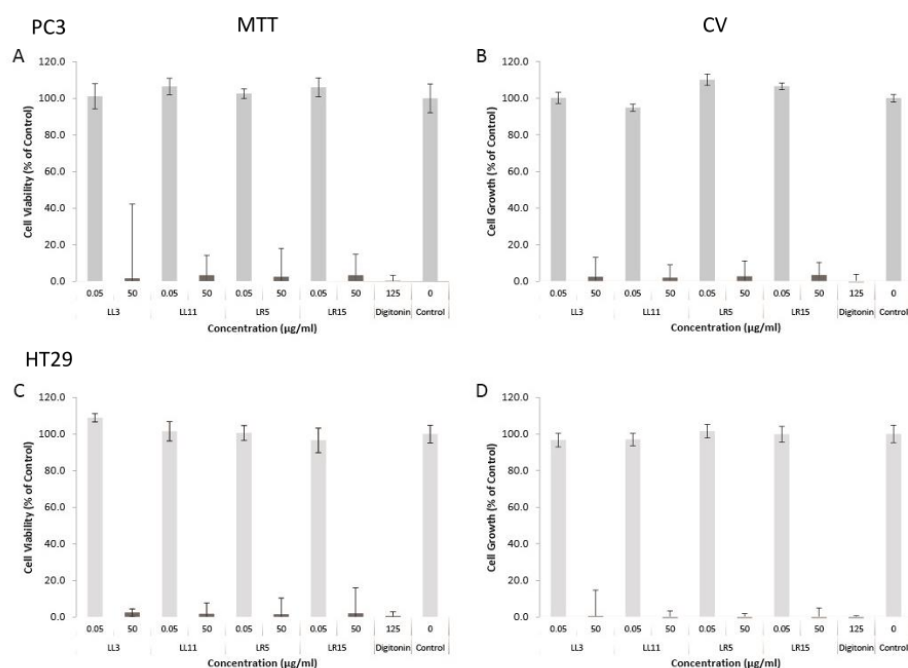
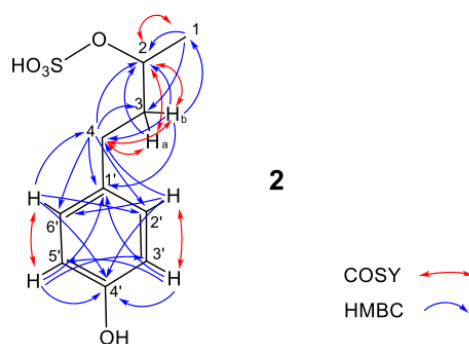


Figure S4. Cytotoxic activity of root extracts from *Lumnitzera littorea* (LL3, LL11) and *L. racemosa* (LR5, LR15) against the human prostate cancer cell line PC3 (A and B) and the colon adenocarcinoma cell line HT29 (C and D) determined by MTT (A, C) and CV assays (B, D). Digitonin (125 µg/mL) was used as positive control. The results are given as percentage of control values without treatment (= 100%).

Table S2. NMR spectroscopic data (400 MHz, methanol-d₄) for 4-(4-hydroxyphenyl)-2-butanol 2-*O*-sulfate (**2**).

position	δ_c^a , type	δ_H (J in Hz)	COSY	HMBC
1	21.2, CH ₃	1.33, d (6.3)	2	2, 3
2	76.8, CH	4.46, m	1, 3a,b	
3	40.5, CH ₂	1.89 (3a), m	2, 4	2
		1.75 (3b), m		1, 2, 4, 1'
4	31.8, CH ₂	2.55-2.70, m	3a,b	2, 3, 1', 2', 6'
1'	134.6 ^b , C			
2'	130.3, CH	7.03, d-like (8.4)	3'	4, 4', 6'
3'	116.1, CH	6.67, d-like (8.4)	2	1', 4', 5'
4'	156.4 ^b , C			
5'	116.1, CH	6.67, d-like (8.4)	6'	1', 3', 4'
6'	130.3, CH	7.03, d-like (8.4)	5'	4, 2', 4'

^a derived from HSQC or ^b HMBC

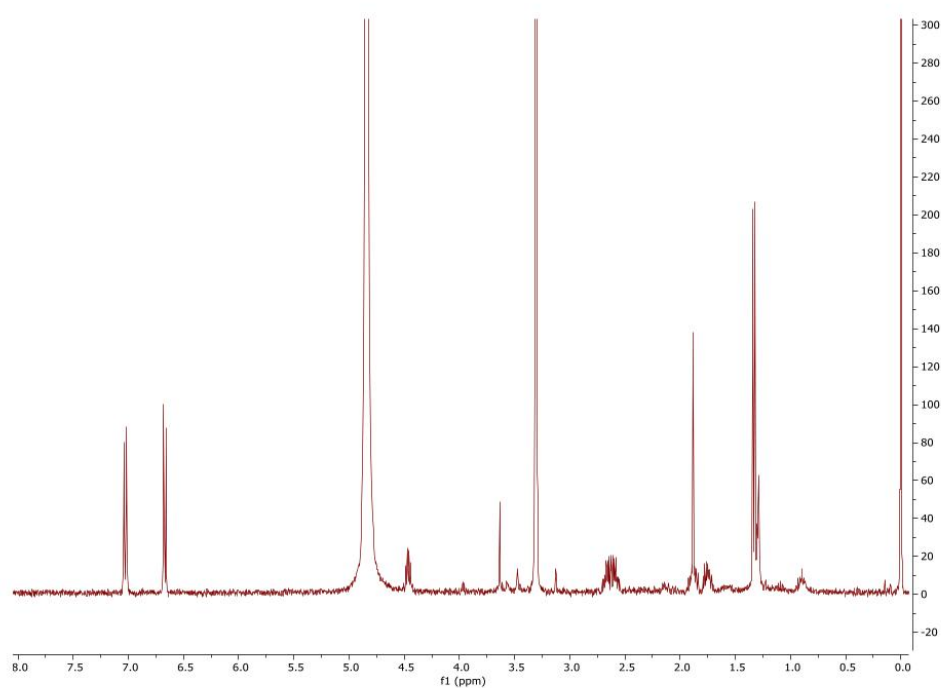


Figure S5-1. ^1H NMR spectrum of 4-(4-hydroxyphenyl)-2-butanol 2-*O*-sulfate (**2**).

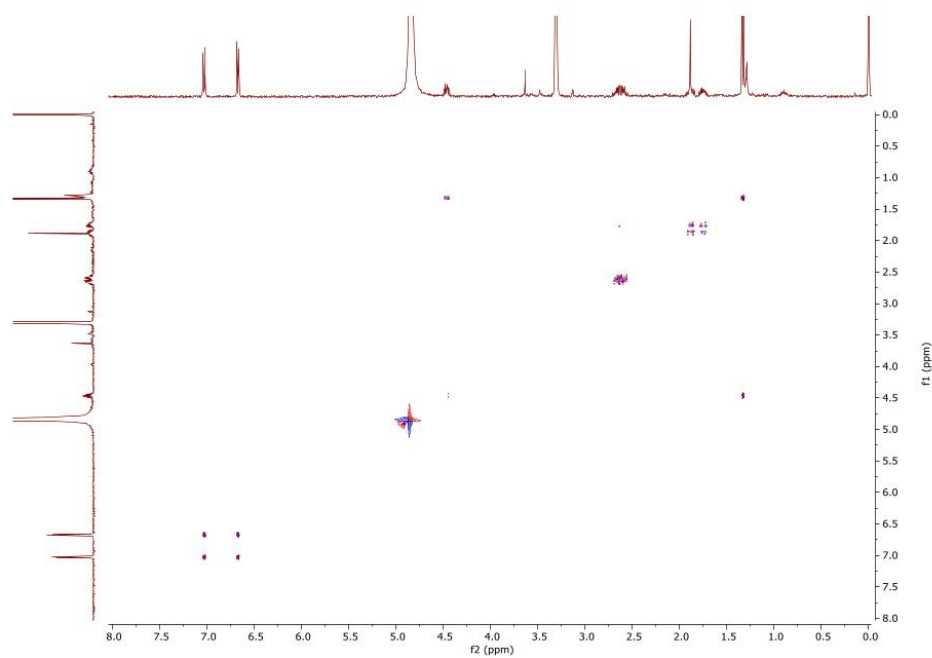


Figure S5-2. COSY spectrum of 4-(4-hydroxyphenyl)-2-butanol 2-*O*-sulfate (**2**).

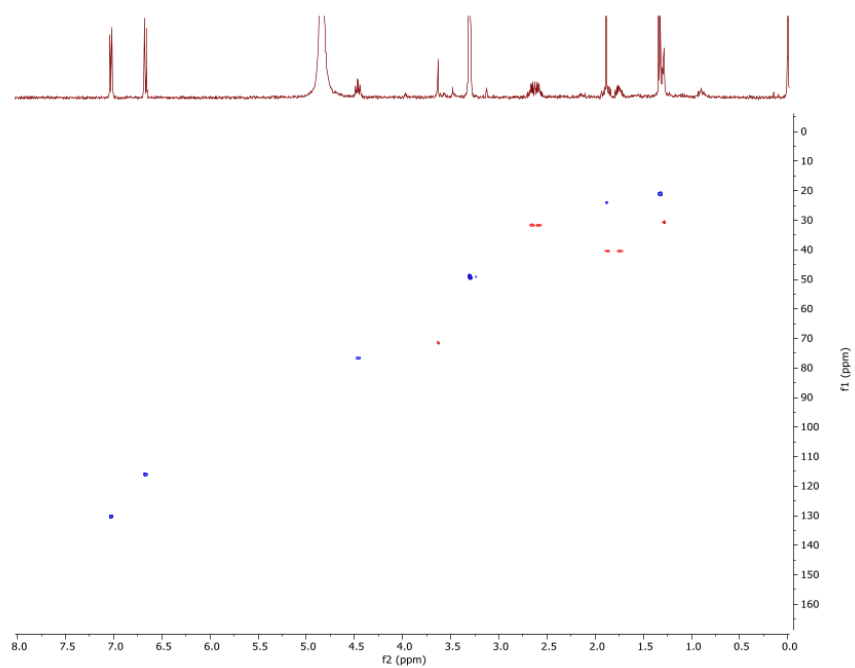


Figure S5-3. HSQC spectrum of 4-(4-hydroxyphenyl)-2-butanol 2-*O*-sulfate (**2**).

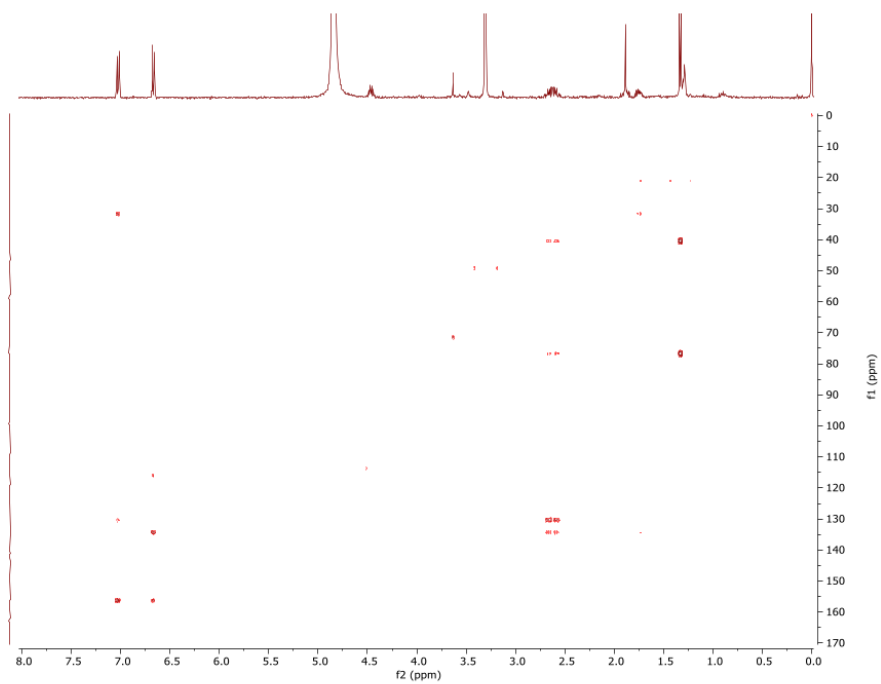


Figure S5-4. HMBC spectrum of 4-(4-hydroxyphenyl)-2-butanol 2-*O*-sulfate (**2**).

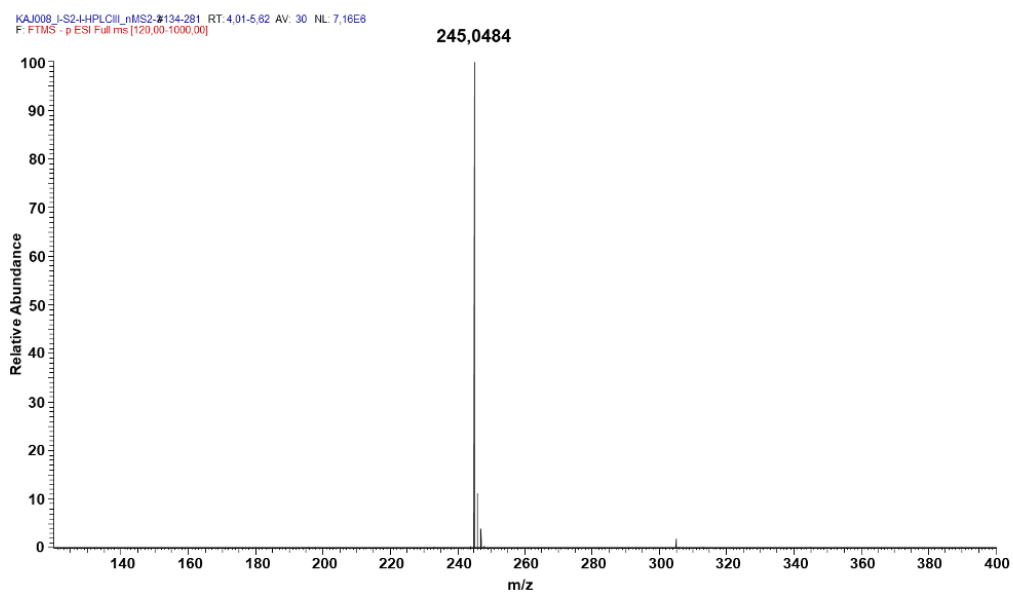


Figure S5-5. Full HRMS spectrum of 4-(4-hydroxyphenyl)-2-butanol 2-*O*-sulfate (**2**) acquired with LIT-Orbitrap-MS in negative ion mode.

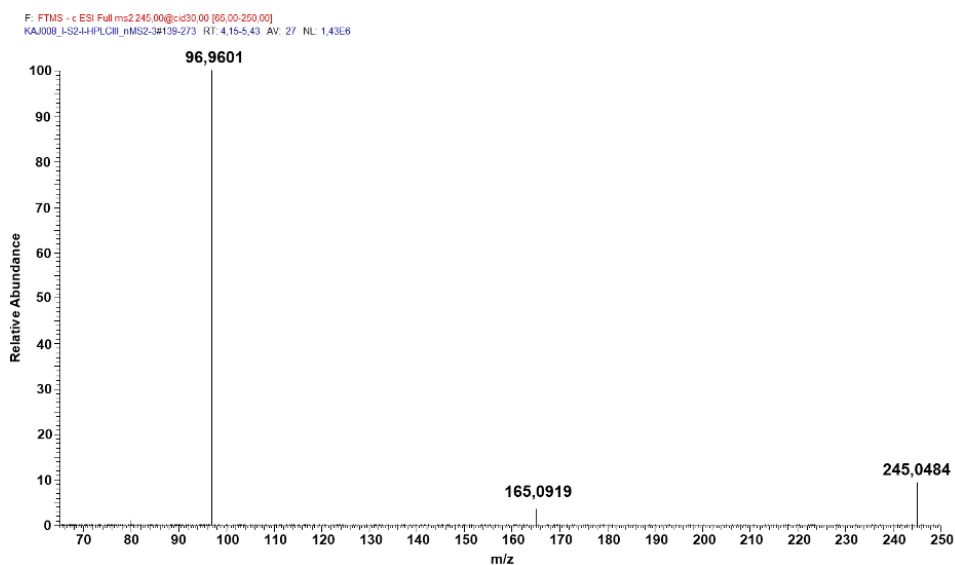
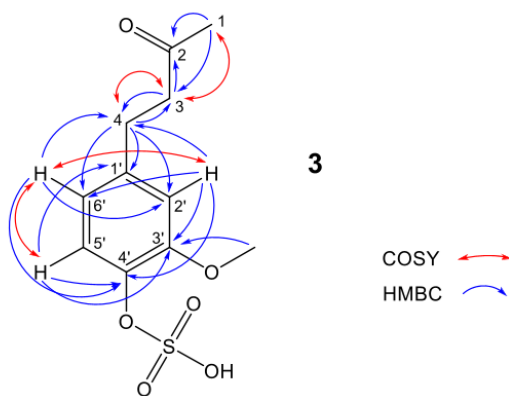


Figure S5-6. MS2 spectrum of 4-(4-hydroxyphenyl)-2-butanol 2-*O*-sulfate (**2**) acquired with LIT-Orbitrap-MS in negative ion mode with CID activation (30% relative collision energy).

Table S3. NMR spectroscopic data (400 MHz, methanol-d₄) for 4-(4-sulfoxy-3-methoxyphenyl)-butan-2-one (**3**).

position	δ_c , type	δ_H (J in Hz)	COSY	HMBC
1	30.06, CH ₃	2.11, s	3	2, 3
2	211.47, C=O			
3	46.30, CH ₂	2.76, s	1, 4	2, 4
4	30.55, CH ₂	2.76, s	3	3, 1', 2', 6'
1'	134.02, C			
2'	113.14, CH	6.77, d (2.0)	6'	4, 3', 4', 6'
3'	148.96, C	-		
4'	145.85, C	-		
5'	116.20, CH	6.68, d (8.0)	6'	1', 3', 4',
6'	121.70, CH	6.61, dd (8.0, 2.0)	2', 5'	4, 2', 4'
3'-OMe	56.39, CH ₃	3.82, s		3'



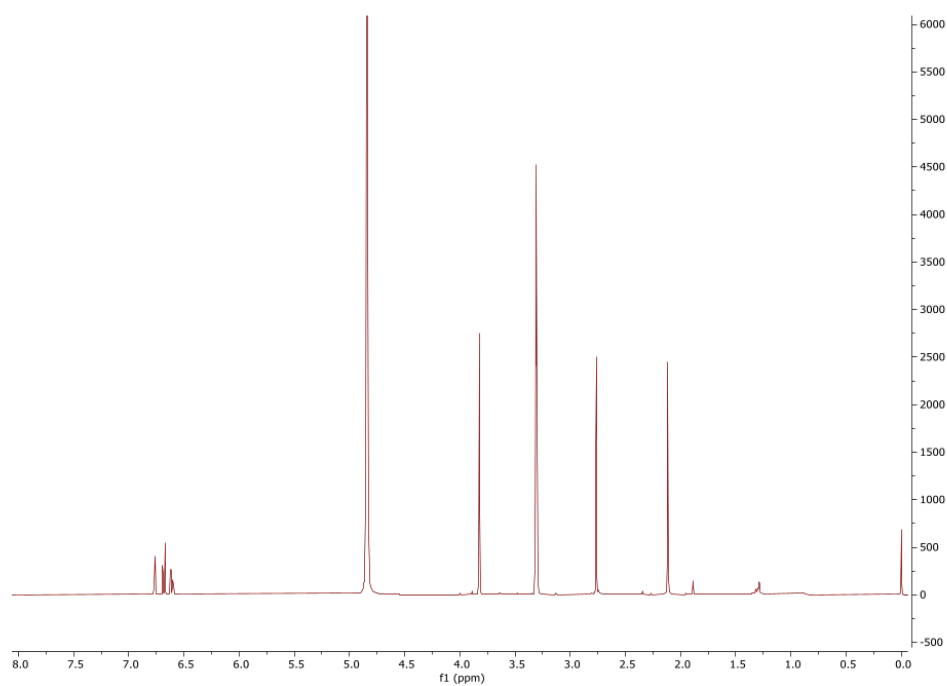


Figure S6-1. ^1H NMR spectrum of 4-(4-sulfoxy-3-methoxyphenyl)-butan-2-one (**3**).

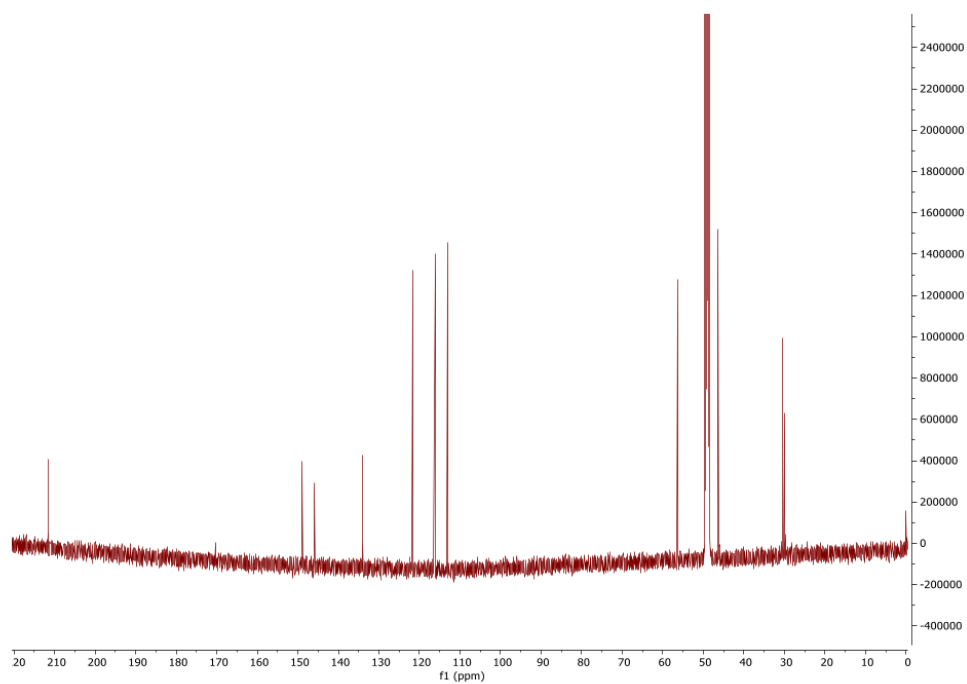


Figure S6-2. ^{13}C NMR spectrum of 4-(4-sulfoxy-3-methoxyphenyl)-butan-2-one (**3**).

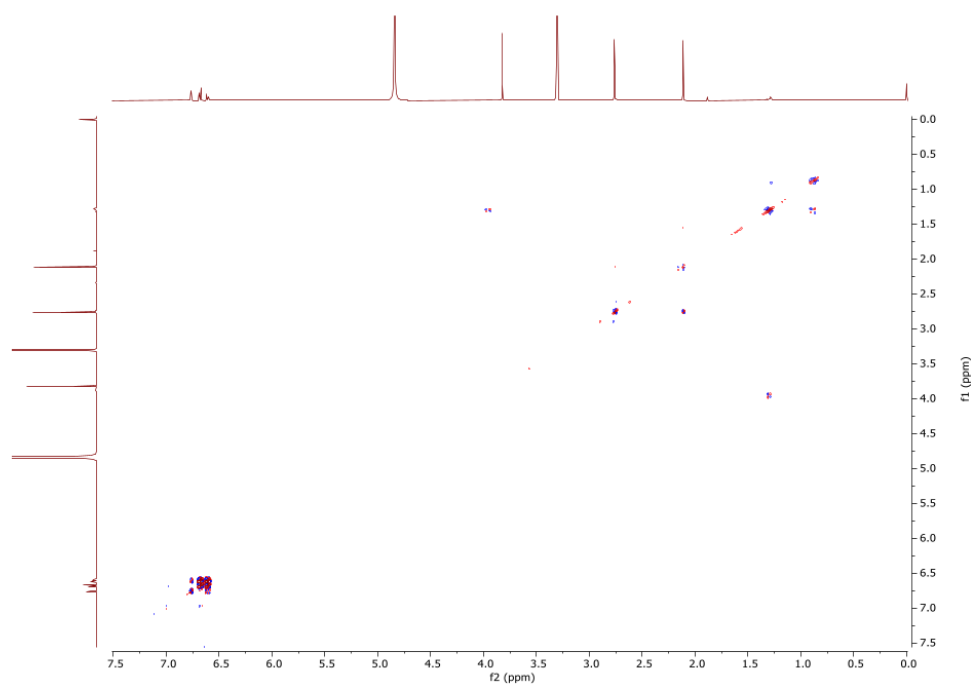


Figure S6-3. COSY spectrum of 4-(4-sulfoxy-3-methoxyphenyl)-butan-2-one (**3**).

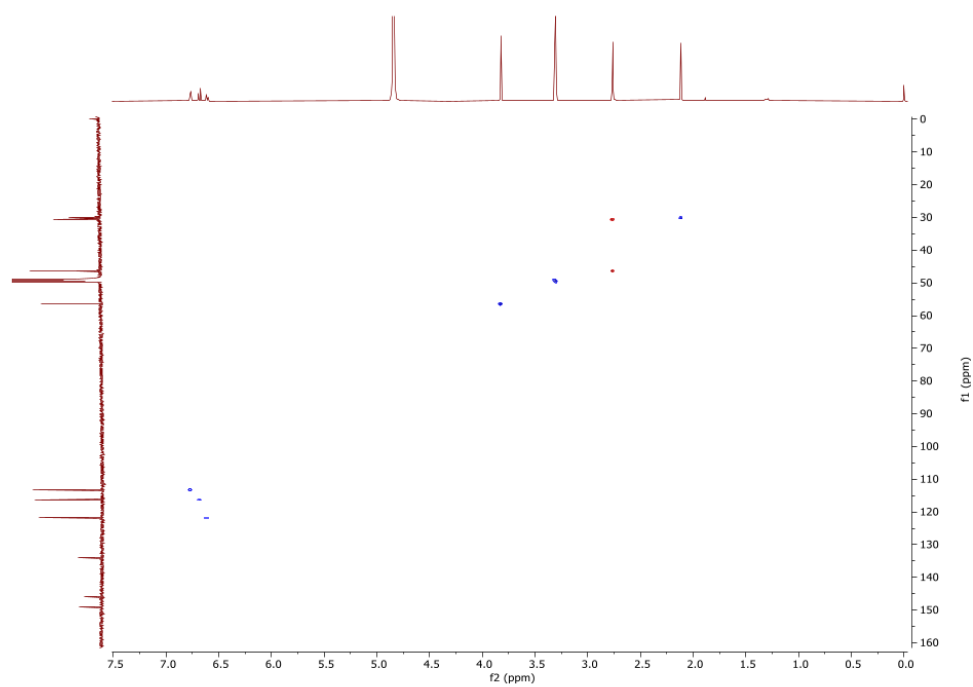


Figure S6-4. HSQC spectrum of 4-(4-sulfoxy-3-methoxyphenyl)-butan-2-one (**3**).

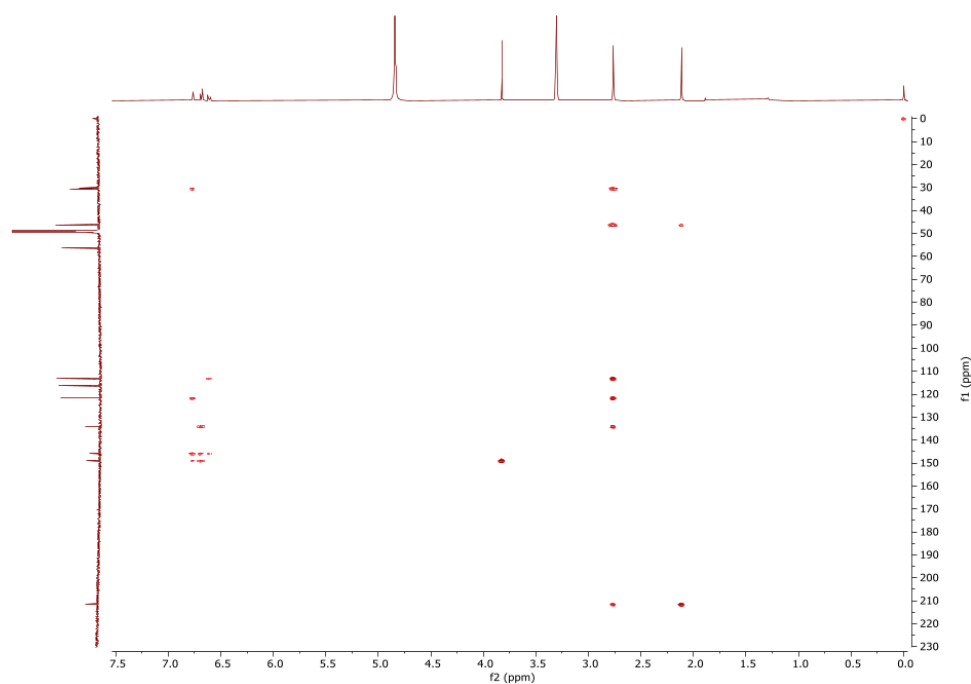


Figure S6-5. HMBC spectrum of 4-(4-sulfoxy-3-methoxyphenyl)-butan-2-one (**3**).

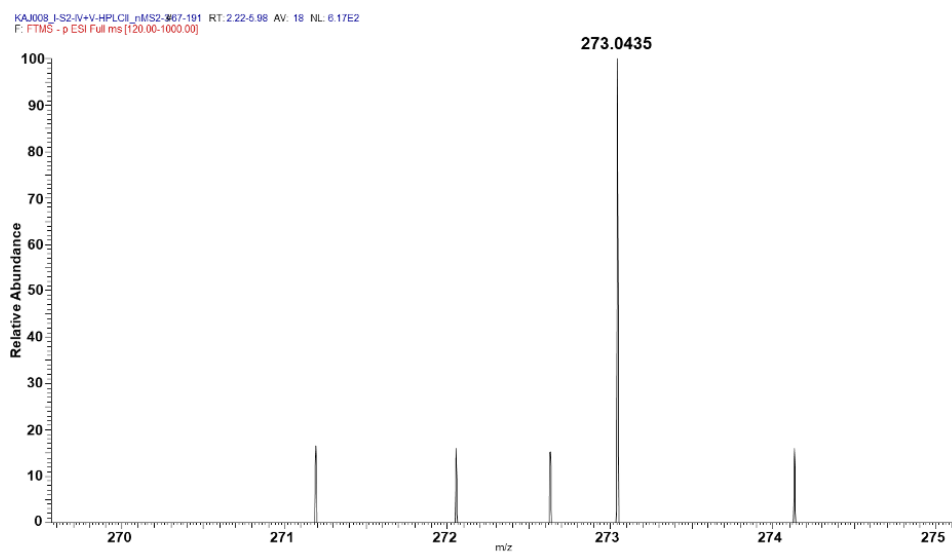


Figure S6-6. Full HRMS spectrum of 4-(4-sulfoxy-3-methoxyphenyl)-butan-2-one (**3**) acquired with LIT-Orbitrap-MS in negative ion mode.

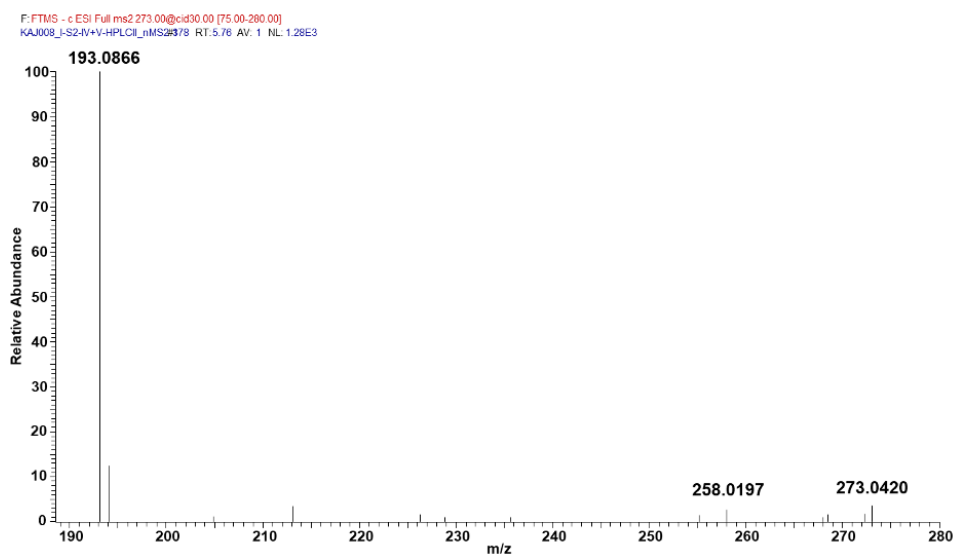


Figure S6-7. MS2 spectrum of 4-(4-sulfoxy-3-methoxyphenyl)-butan-2-one (**3**) acquired with LIT-Orbitrap-MS in negative ion mode with CID activation (30% relative collision energy).

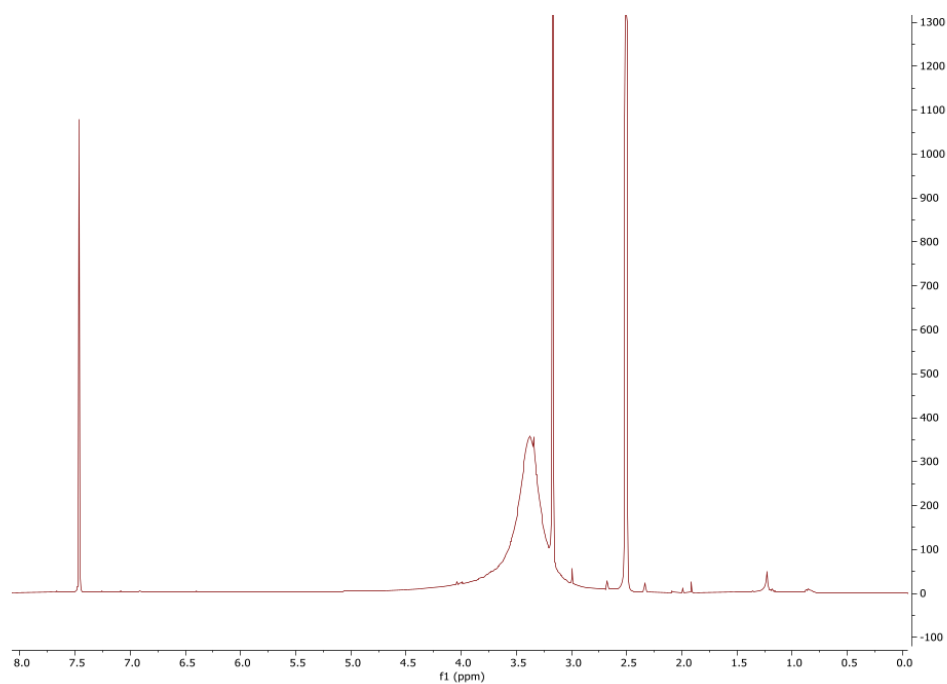


Figure S7-1. ¹H NMR spectrum (DMSO-d₆) of ellagic acid (**6**).

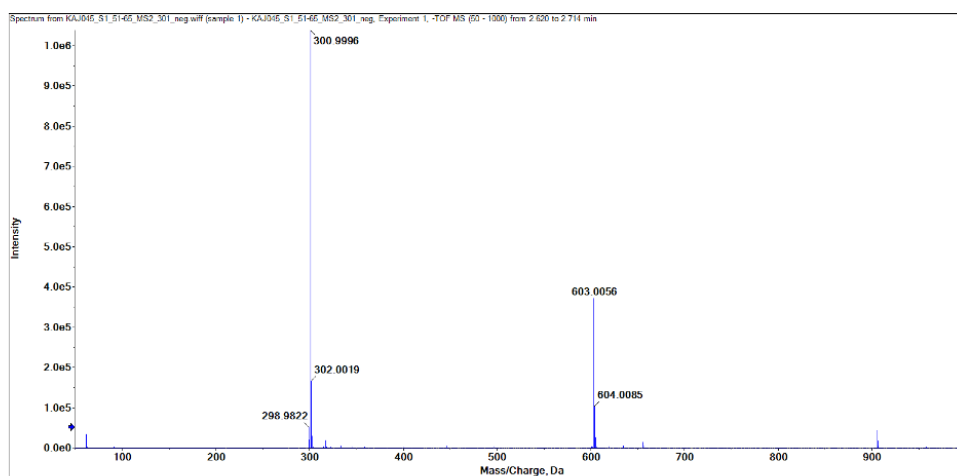


Figure S7-2. HRMS spectrum of ellagic acid (**6**) acquired with a QqTOF mass spectrometer in negative ion mode.

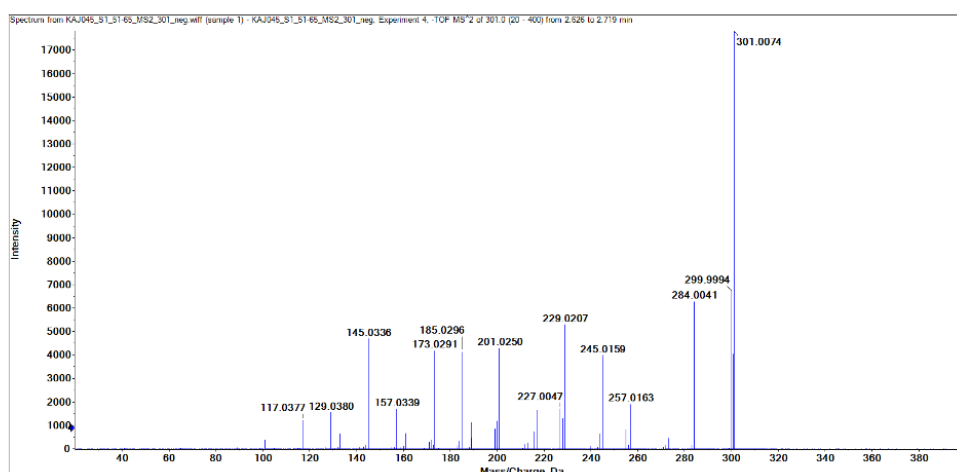
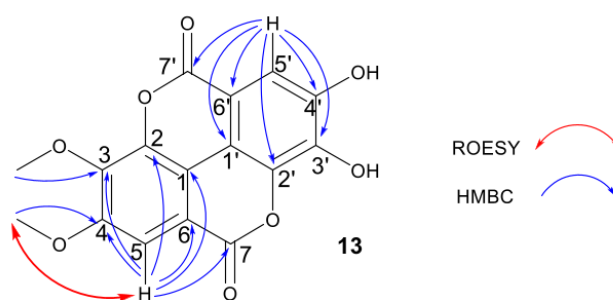


Figure S7-3. MS2 spectrum of ellagic acid (**6**) acquired with a QqTOF mass spectrometer in negative ion mode.

Table S4. NMR spectroscopic data (600 MHz, DMSO-d₆) for 3,4-di-*O*-methylellagic acid (**13**).

position	δ_{H} (J in Hz)	δ_{C} *, type	HMBC	ROESY
1		115.00, C		
2		141.79, C		
3		140.04, C		
4		152.73, C		
5	7.53, s	105.83, CH	1, 2, 3, 4, 6, 7	4-OMe
6		112.95, C		
7		160.22, C		
1'		114.97, C		
2'		134.51, C		
3'		151.92, C		
4'		156.46, C		
5'	7.09, s	104.63, CH	1', 2', 3', 4', 6', 7'	
6'		113.09, C	5'	
7'		159.15, C	5'	
3-OMe	3.99, s	60.83, CH ₃	3	
4-OMe	3.97, s	56.32, CH ₃	4, 5	5



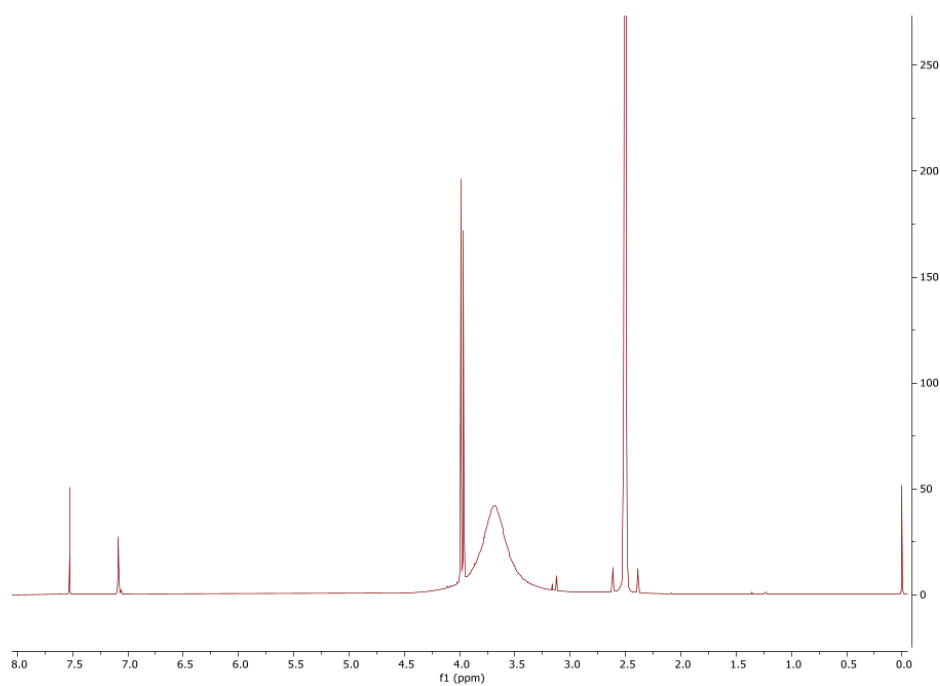


Figure S8-1. ^1H NMR spectrum (DMSO- d_6) of 3,4-di-*O*-methylellagic acid (**13**).

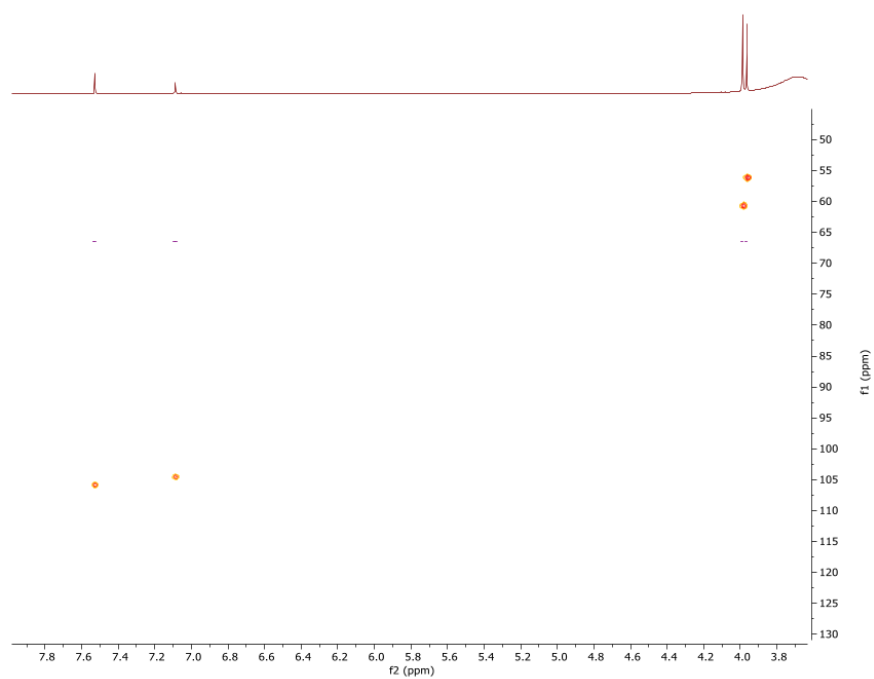


Figure S8-2. HSQC spectrum (DMSO- d_6) of 3,4-di-*O*-methylellagic acid (**13**).

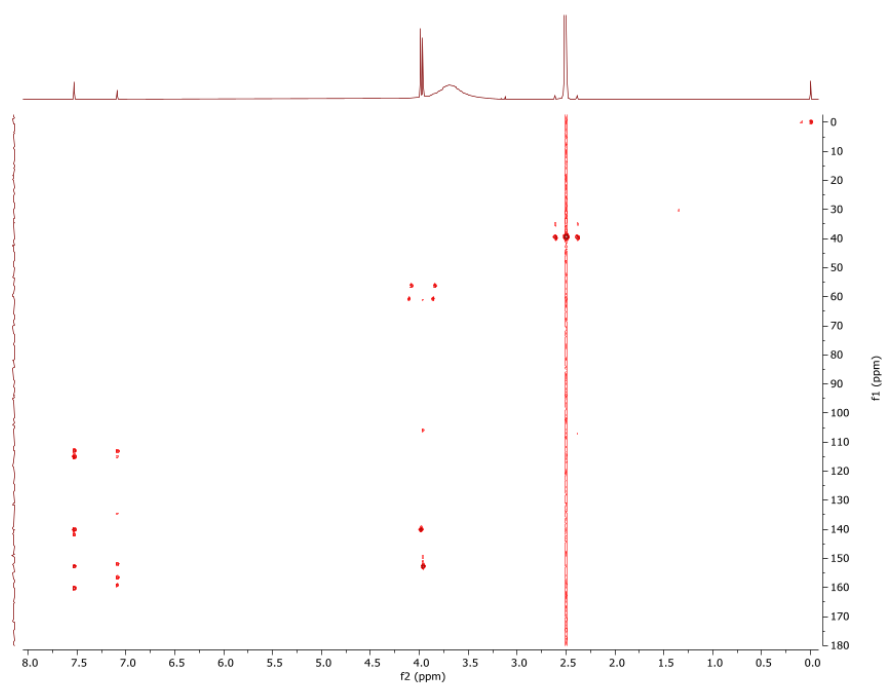


Figure S8-3. HMBC spectrum (DMSO-d₆) of 3,4-di-*O*-methylellagic acid (**13**).

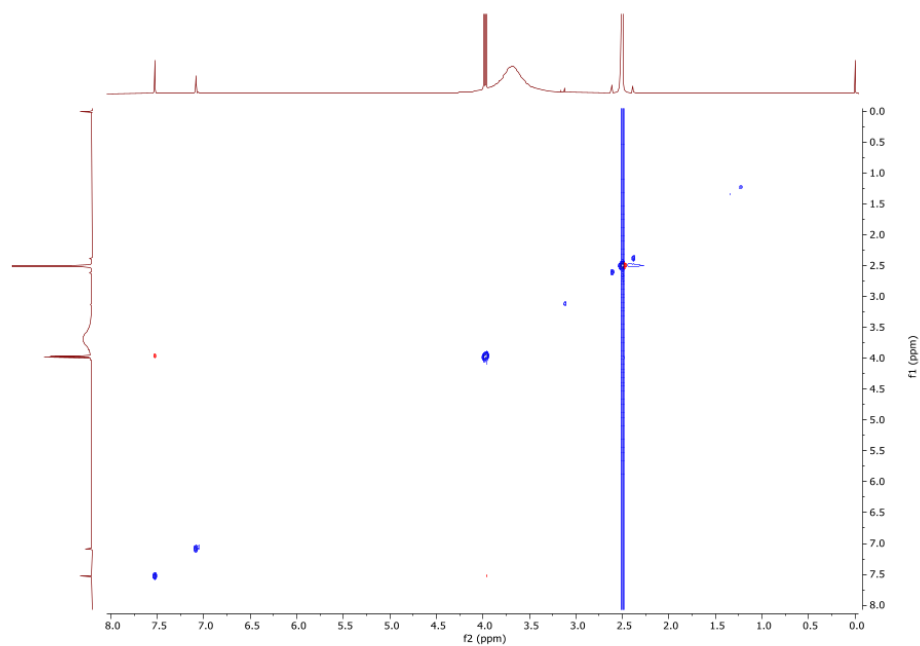


Figure S8-4. ROESY spectrum (DMSO-d₆) of 3,4-di-*O*-methylellagic acid (**13**).

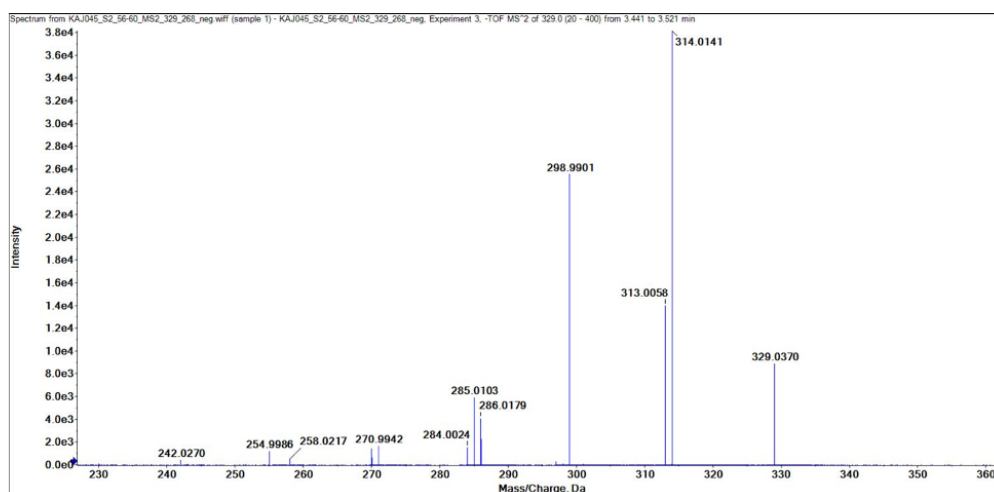
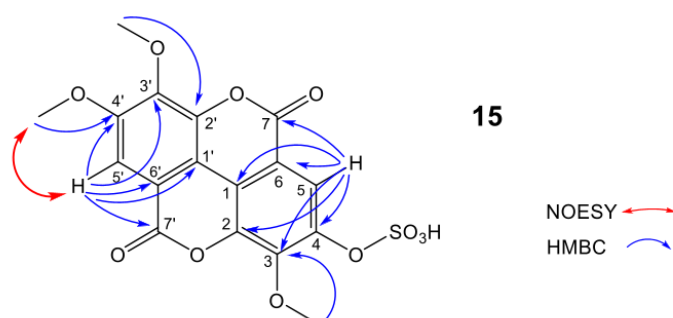


Figure S8-5. MS² spectrum of 3,4-di-*O*-methylelagic acid (**13**) acquired with a QqTOF mass spectrometer in negative ion mode.

Table S5. NMR spectroscopic data (400 MHz, DMSO-*d*6) for 3,3',4'-tri-*O*-methylellagic acid 4-sulfate (**15**).

position	δ_c , type	δ_H	NOESY	HMBC
1	112.96, C			
2	140.86, C			
3	143.32, C			
4	147.64, C			
5	117.61, CH	8.24, s		1, 2, 3, 4, 6, 7
6	111.52, C			
7	158.31, C=O			
1'	114.13, C			
2'	140.89, C			
3'	141.34, C			
4'	154.37, C			
5'	107.50, CH	7.66, s	4'-OMe	1', 2', 3', 4', 6', 7'
6'	112.83, C			
7'	158.46, C=O			
3'-OMe	61.32, CH ₃	4.06, s		2'
4'-OMe	56.75, CH ₃	4.02, s	5'	4'
3-OMe	61.47, CH ₃	4.12, s		3



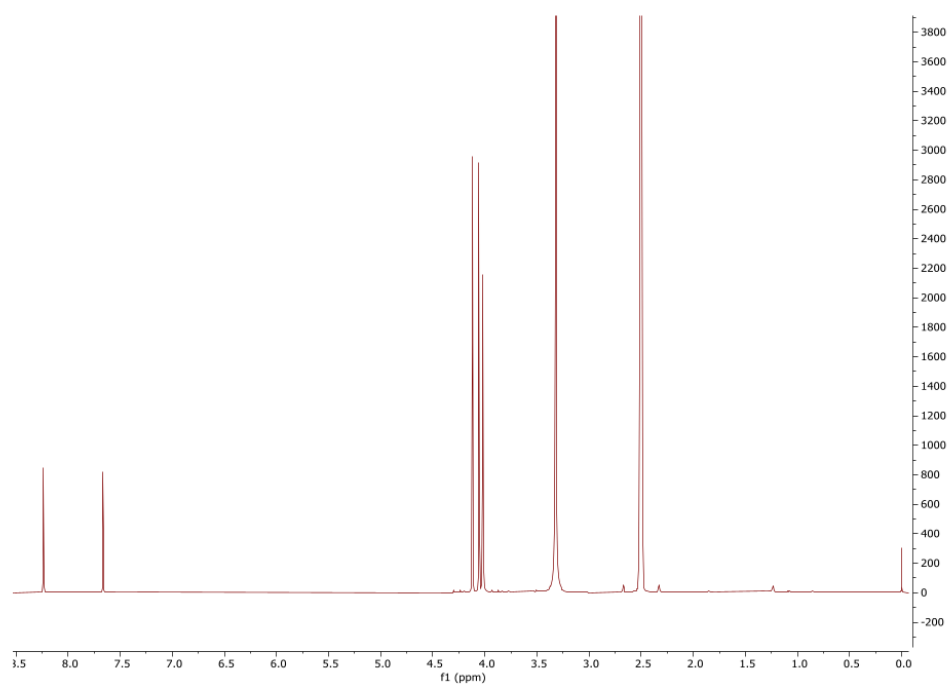


Figure S9-1. ^1H NMR spectrum of 3,3',4'-tri-*O*-methylellagic acid 4-sulfate (**15**).

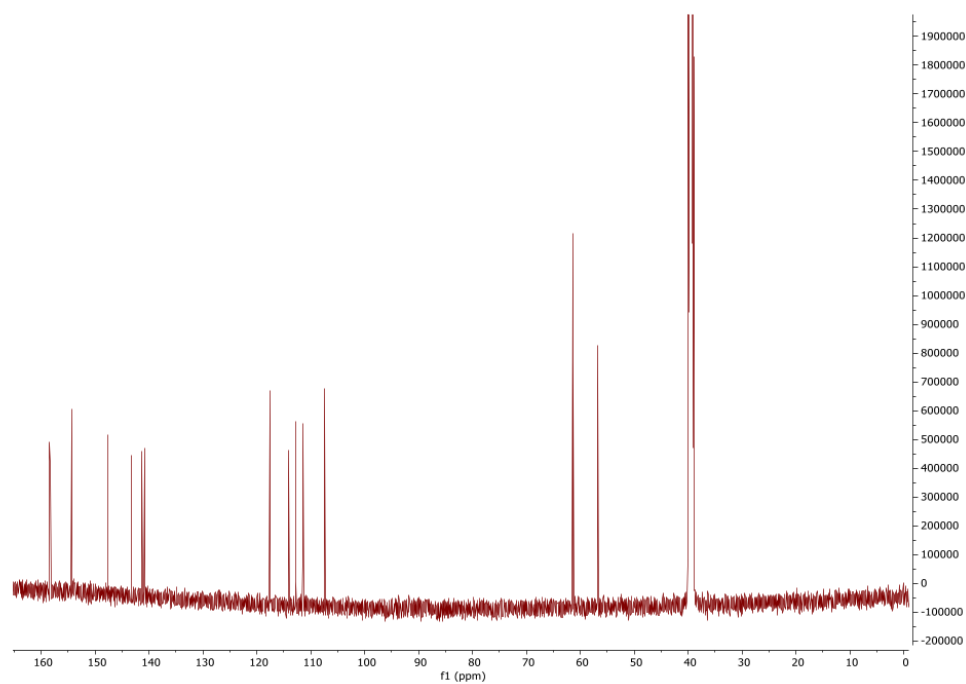


Figure S9-2. ^{13}C NMR spectrum of 3,3',4'-tri-*O*-methylellagic acid 4-sulfate (**15**).

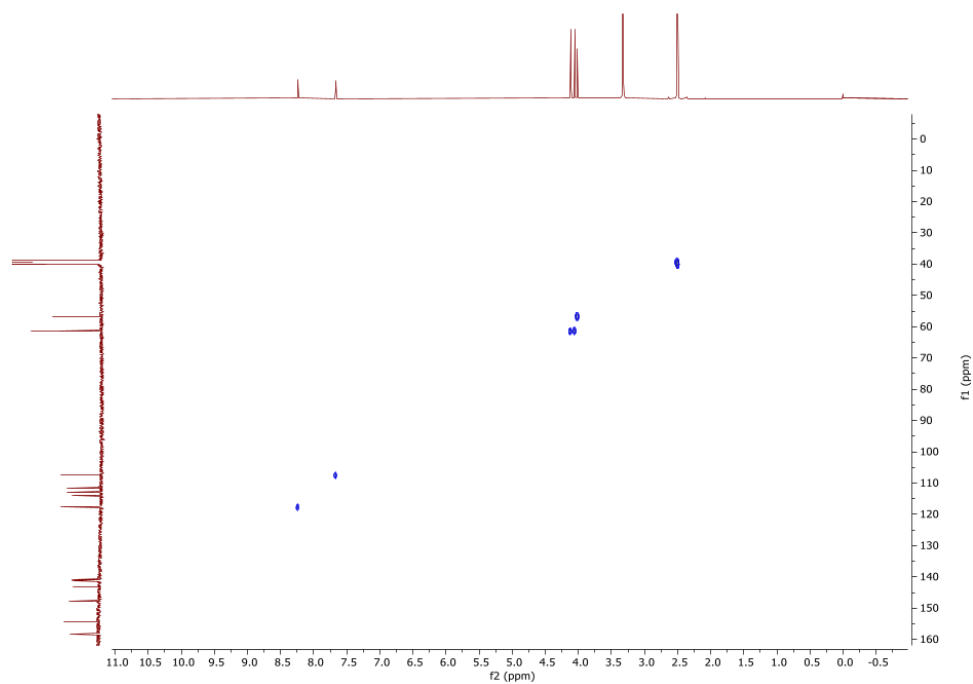


Figure S9-3. HSQC spectrum of 3,3',4'-tri-*O*-methylellagic acid 4-sulfate (**15**).

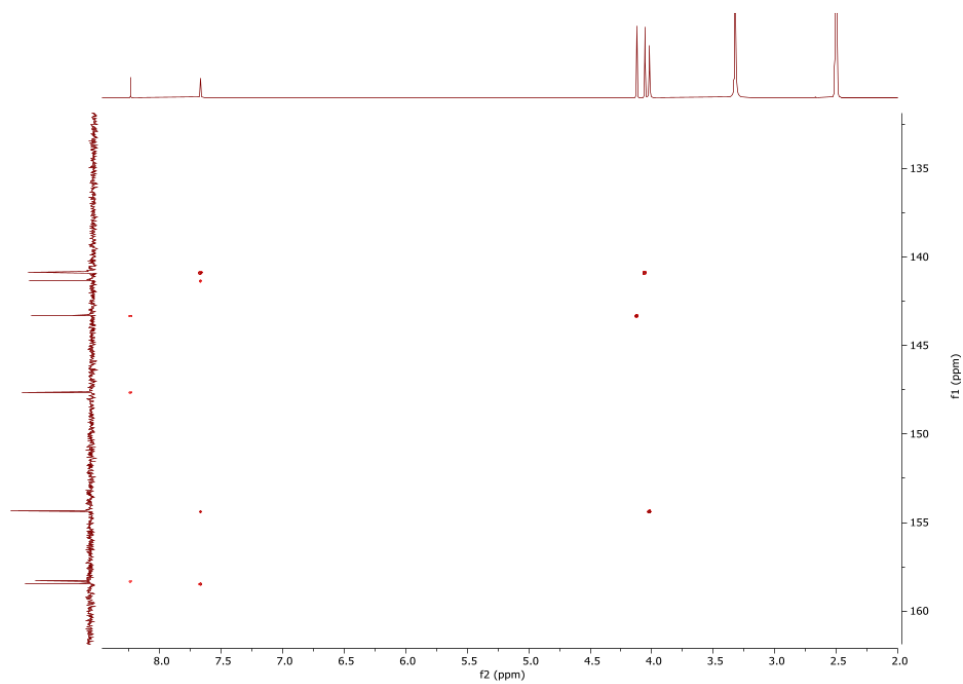


Figure S9-4. HMBC spectrum of 3,3',4'-tri-*O*-methylellagic acid 4-sulfate (**15**).

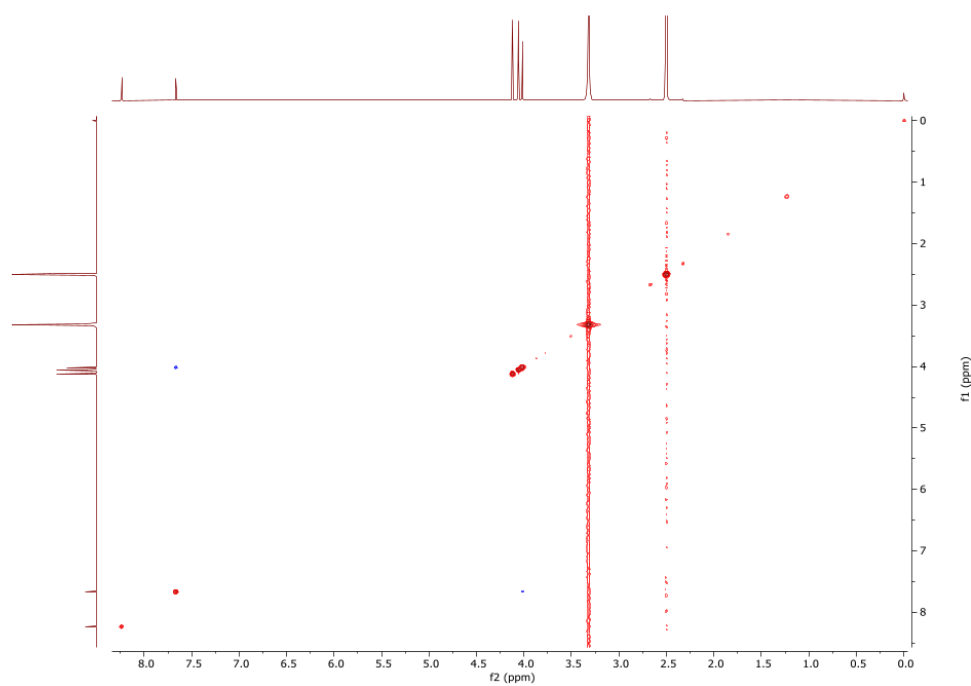


Figure S9-5. NOESY spectrum of 3,3',4'-tri-*O*-methylellagic acid 4-sulfate (**15**).

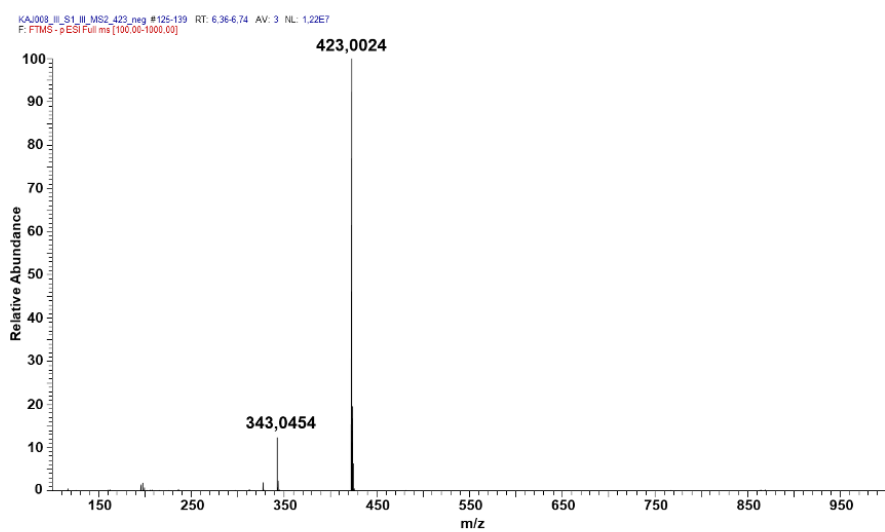


Figure S9-6. Full HRMS spectrum of 3,3',4'-tri-*O*-methylellagic acid 4-sulfate (**15**) acquired with LIT-Orbitrap-MS in negative ion mode.

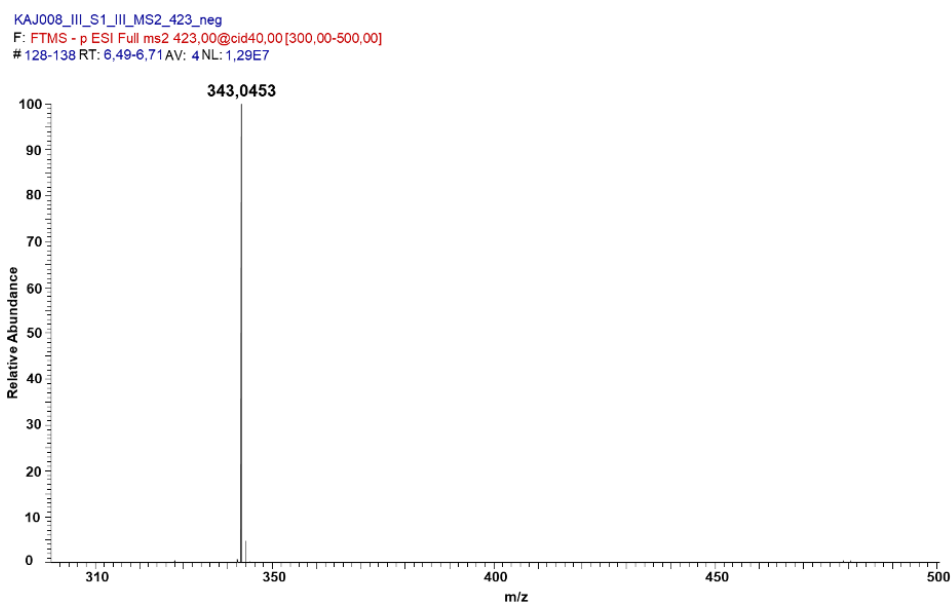
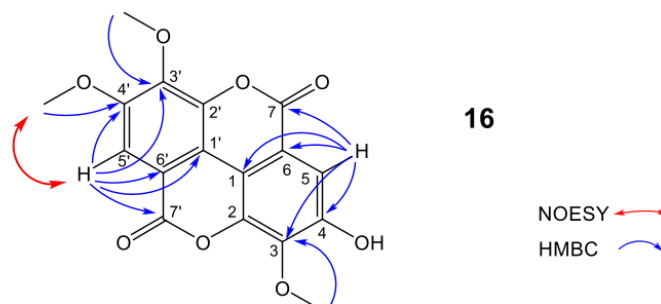


Figure S9-7. MS2 spectrum of 3,3',4'-tri-*O*-methylelagic acid 4-sulfate (**15**) acquired with LIT-Orbitrap-MS in negative ion mode with CID activation (40% relative collision energy).

Table S6. NMR spectroscopic data (400 MHz, DMSO-*d*₆) for 3,3',4'-trimethylellagic acid (**16**).

position	δ_c	δ_H (J in Hz)	NOESY	HMBC
1	110.80, C			
2	140.67, C			
3	140.18, C			
4	152.96, C			
5	111.67, CH	7.52, s		1, 3, 4, 6, 7
6	112.39, C			
7	158.24, C=O			
1'	111.74, C			
2'	141.37, C			
3'	140.85, C			
4'	153.62, C			
5'	107.33, CH	7.61, s	4'-OMe	1', 3', 4', 6', 7'
6'	113.33, C			
7'	158.44, C=O			
3'-OMe	61.19, CH ₃	4.04, s		3'
4'-OMe	56.60, CH ₃	4.00, s	5'	4'
3-OMe	60.83, CH ₃	4.06, s		3



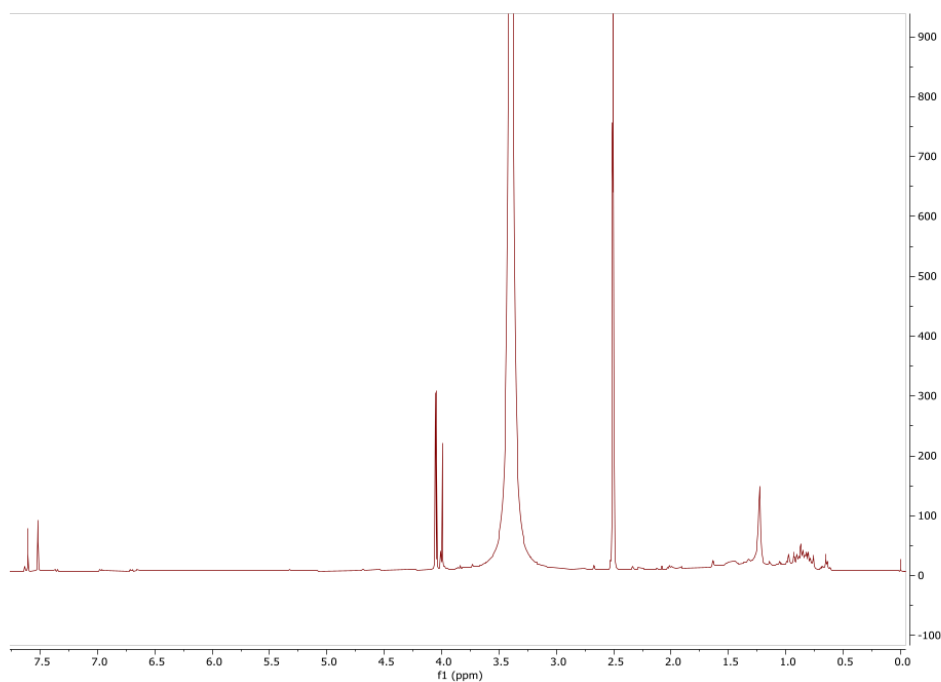


Figure S10-1. ^1H NMR spectrum of 3,3',4'-tri-*O*-methylellagic acid (**16**).

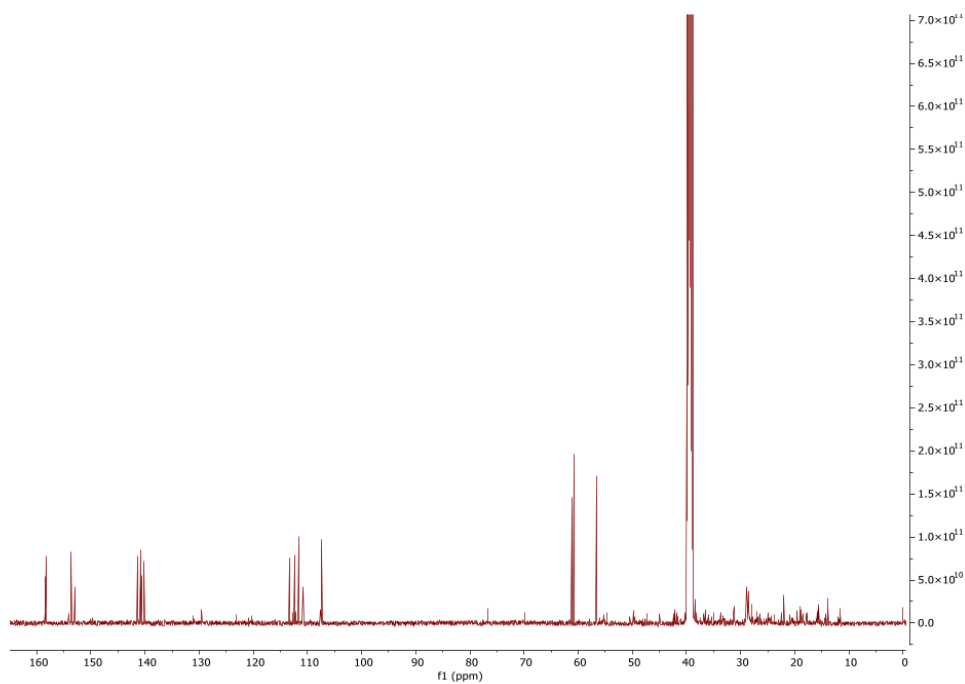


Figure S10-2. ^{13}C NMR spectrum of 3,3',4'-tri-*O*-methylellagic acid (**16**).

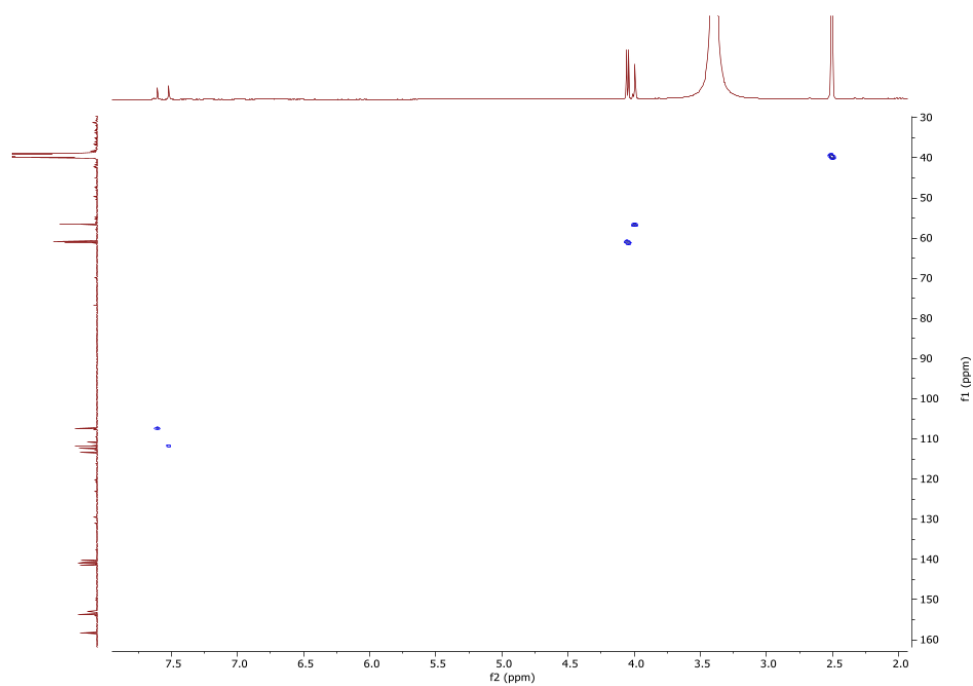


Figure S10-3. HSQC spectrum of 3,3',4'-tri-*O*-methylellagic acid (**16**).

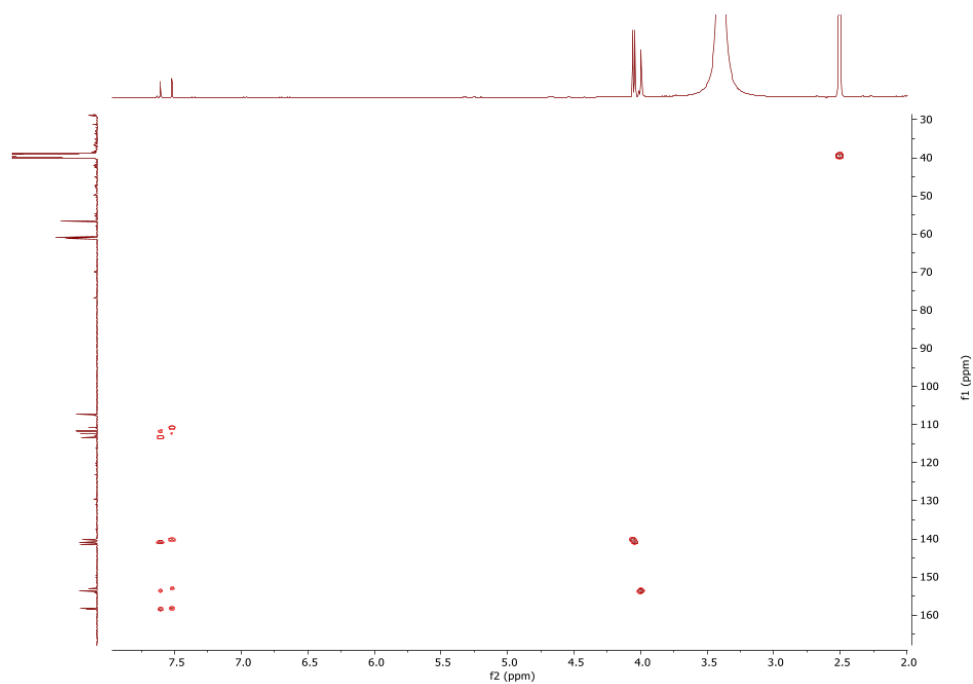


Figure S10-4. HMBC spectrum of 3,3',4'-tri-*O*-methylellagic acid (**16**).

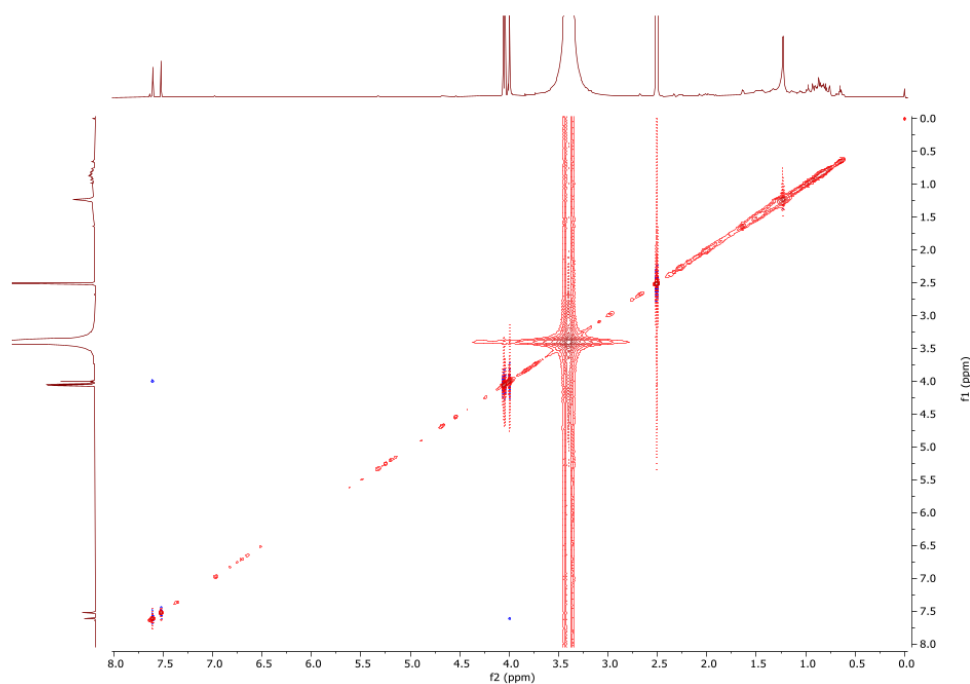


Figure S10-5. NOESY spectrum of 3,3',4'-tri-*O*-methylellagic acid (**16**).

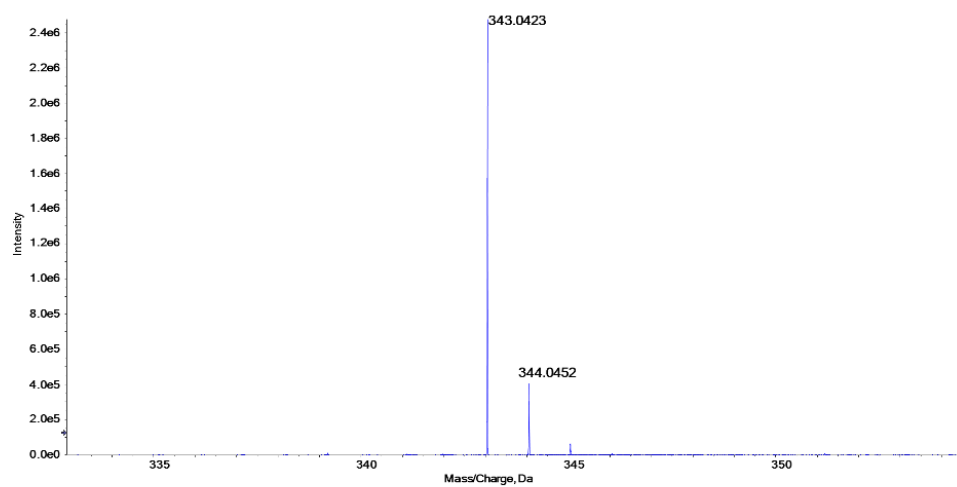


Figure S10-6. Negative HR-MS spectrum of 3,3',4'-tri-*O*-methylellagic acid (**16**) acquired with a QqTOF mass spectrometer.

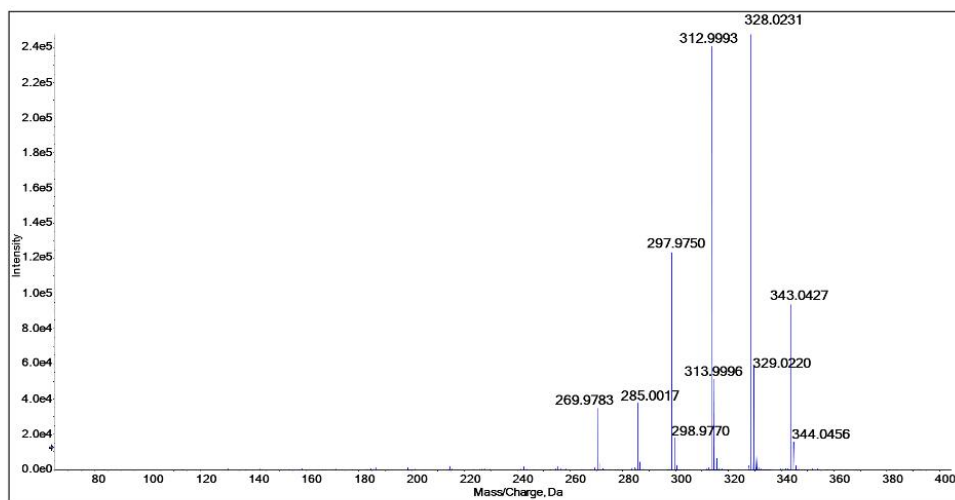


Figure S10-7. MS2 spectrum of 3,3',4'-tri-*O*-methylellagic acid (**16**) acquired with a QqTOF mass spectrometer in negative mode.

7.2 Supporting information of chapter 3

Supporting Information

Challenging structure elucidation of lumnitzerolactone, an ellagic acid derivative from the mangrove *Lumnitzera racemosa*

Jonas Kappen¹, Jeprianto Manurung^{1,2,3}, Tristan Fuchs¹, S. Phani B. Vemulapalli^{4,5}, Lea M. Schmitz¹, Andrej Frolov¹, Andria Agusta⁶, Alexandra N. Muellner-Riehl^{2,3}, Christian Griesinger^{4*}, Katrin Franke^{1,3,7*} and Ludger A. Wessjohann^{1,3*}

¹ Department of Bioorganic Chemistry, Leibniz Institute of Plant Biochemistry (IPB), 06120 Halle (Saale), Germany; jkappen@ipb-halle.de (J.K.); tfuchs@ipb-halle.de (T.F.); lschmitz@ipb-halle.de (L.M.S.); andrej.frolov@ipb-halle.de (A.F.); wessjohann@ipb-halle.de (L.A.W.); kfranke@ipb-halle.de (K.F.)

² Department of Molecular Evolution and Plant Systematics & Herbarium (LZ), Institute of Biology, Leipzig University, 04103 Leipzig, Germany; jeprianto_m@apps.ipb.ac.id (J.M.); muellner-riehl@uni-leipzig.de (A.N.M.R.)

³ German Centre for Integrative Biodiversity Research (iDiv) Halle-Jena-Leipzig, 04103 Leipzig, Germany

⁴ Department of NMR-Based Structural Biology, Max Planck Institute for Multidisciplinary Sciences, Am Fassberg 11, 37077 Göttingen, Germany; save@mpinat.mpg.de (S.P.B.V.); cigr@mpinat.mpg.de (C.G.)

⁵ Research Group for Marine Geochemistry, Institute for Chemistry and Biology of the Marine Environment (ICBM), Carl von Ossietzky Universität Oldenburg, Carl-von-Ossietzky-Str. 9-11, 26129 Oldenburg, Germany

⁶ Research Center for Pharmaceutical Ingredients and Traditional Medicine, National Research and Innovation Agency (BRIN), Jl. M.H. Thamrin No. 8, Jakarta 10340, Indonesia; andr005@brin.go.id (A.A.)

⁷ Institute of Biology/Geobotany and Botanical Garden, Martin Luther University Halle-Wittenberg, Halle, Germany

* Correspondence: cigr@mpinat.mpg.de, Tel: +49 551 201-2201 (C.G.); kfranke@ipb-halle.de, Tel: +49-345-5582-1380 (K.F.); wessjohann@ipb-halle.de, Tel: +49-345-5582-1301 (L.A.W.)

Content	page
Figure S1: TLC after the Bornträger-reaction	3
Scheme S1: Putative mechanism of the Bornträger reaction	3
Figure S2-1–S2-13: 1D and 2D NMR spectra of compound 1	4
Table S1-1–S1-3: ^1H , ^{13}C and HMBC data of compound 1 in different solvents and field strengths	11
Figure S3-1–S3-4: 1D and 2D NMR spectra of compound 5	12
Figure S4-1–S4-5: 1D and 2D NMR spectra of compound 1b	14
Figure S5-1–S5-2: MS data of compound 1	16
Figure S6-1–S6-2: MS data of compound 1b	17
Figure S7-1–S7-2: MS data of compound 5	18
Table S2-1–S2-2: Additional data DFT-Calculations	20
Figure S8-1–S8-3: Structure elucidation report - ACD-SE-Calculation	24
Scheme S2-1: Suggested pathway for the biosynthesis of compound 1	27
Figure S9-1–S9-2: UV spectra of compound 1 , 1b and 5	28
Figure S10-1–S10-2: ^1H NMR spectrum and HPLC chromatogram of the fraction containing 1 and 3	29

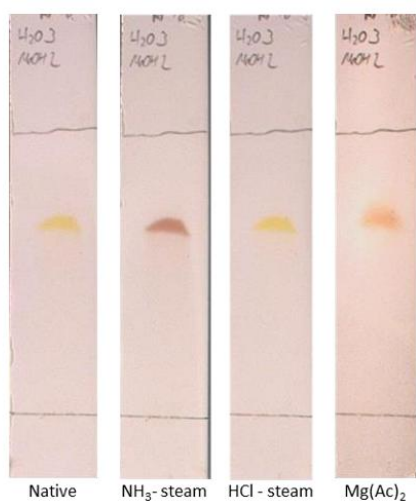
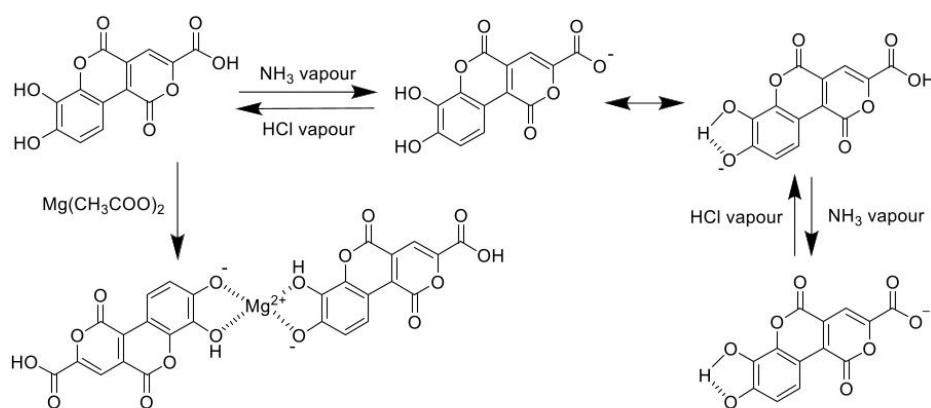
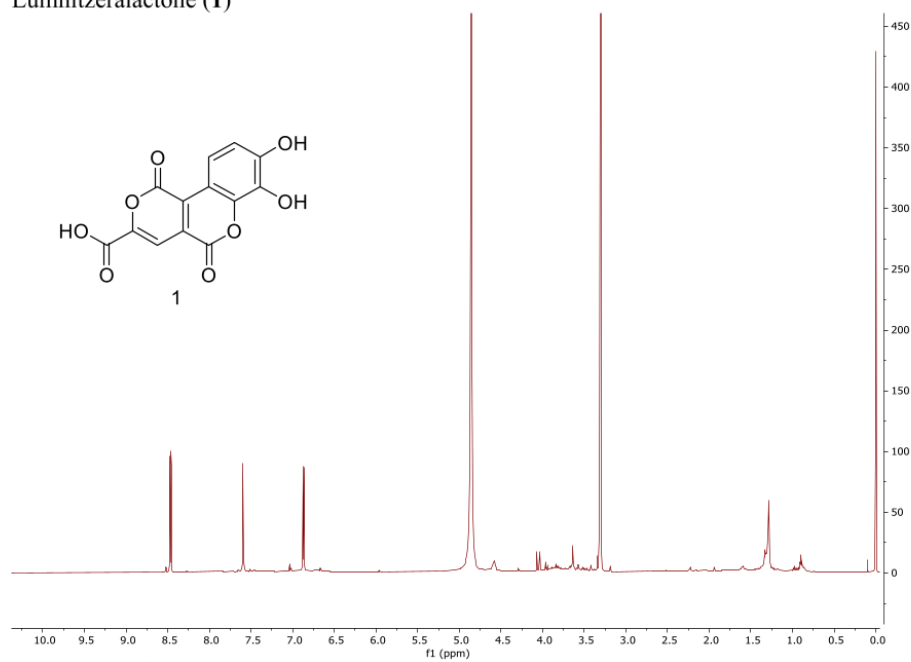
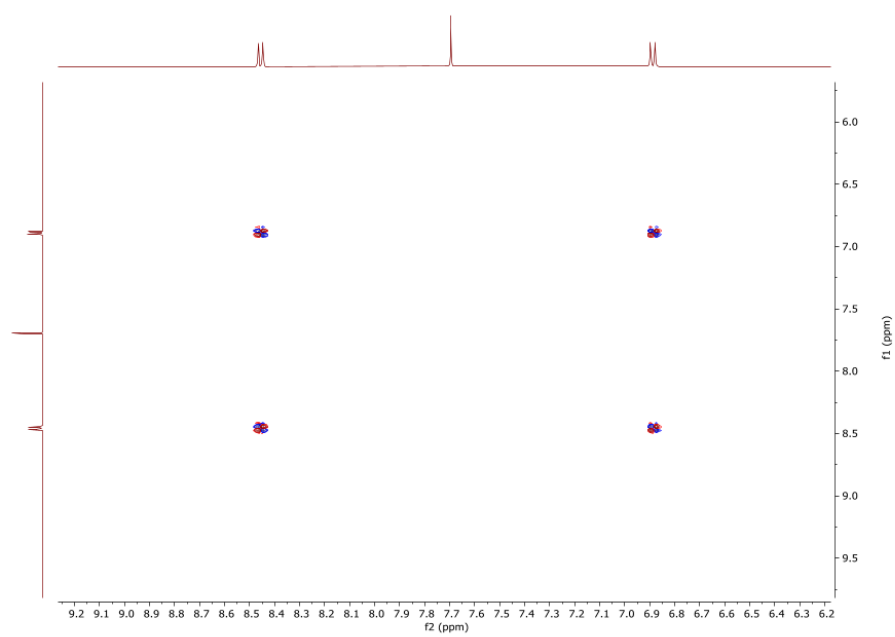


Figure S1. TLC of lumnizeralactone (**1**) after the Bornträger reaction; stationary phase: RP18, solvent system: H₂O:MeOH, 3:2 v/v.



Scheme S1. Putative mechanism of the Bornträger reaction for lumnizeralactone (**1**)

Lumnitzeralactone (**1**)**Figure S2-1.** ¹H NMR spectrum of compound **1** in MeOH-*d*₄, 600 MHz**Figure S2-2.** COSY spectrum of compound **1** in MeOH-*d*₄, 500 MHz

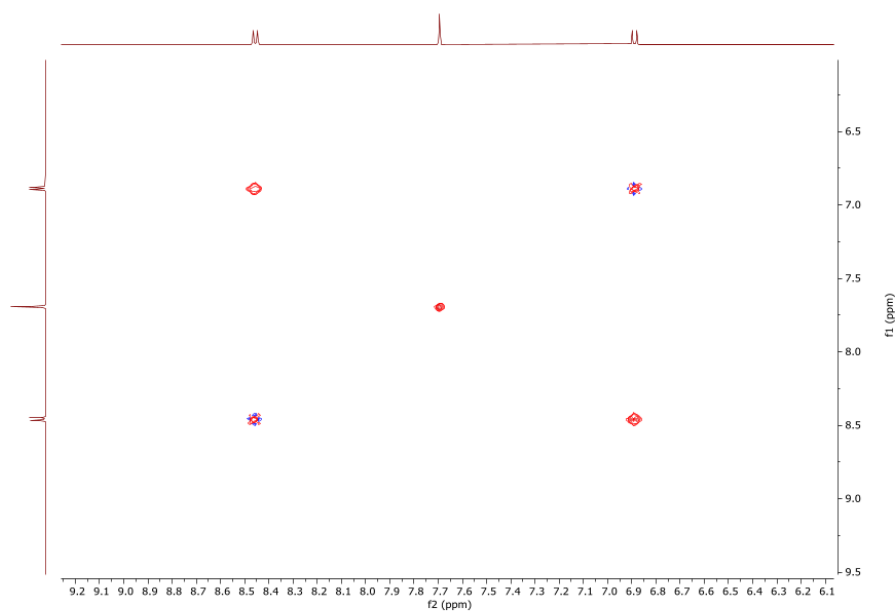


Figure S2-3. TOCSY spectrum of compound **1** in MeOH-*d*₄, 500 MHz

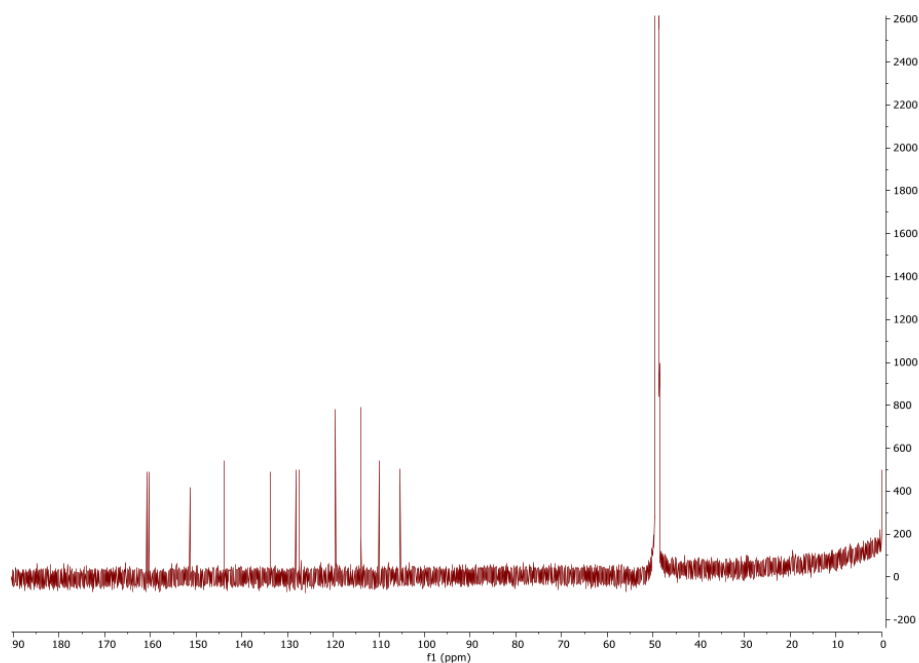


Figure S2-4. ¹³C-NMR spectrum of compound **1** in MeOH-*d*₄, 150 MHz

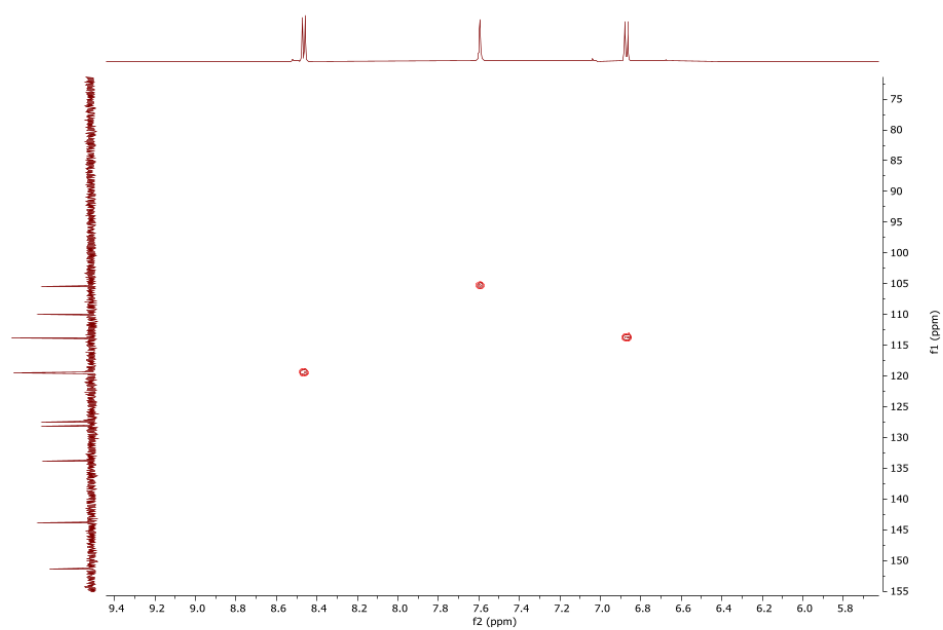


Figure S2-5. HSQC spectrum of compound **1** in MeOH-*d*₄, 600/150 MHz

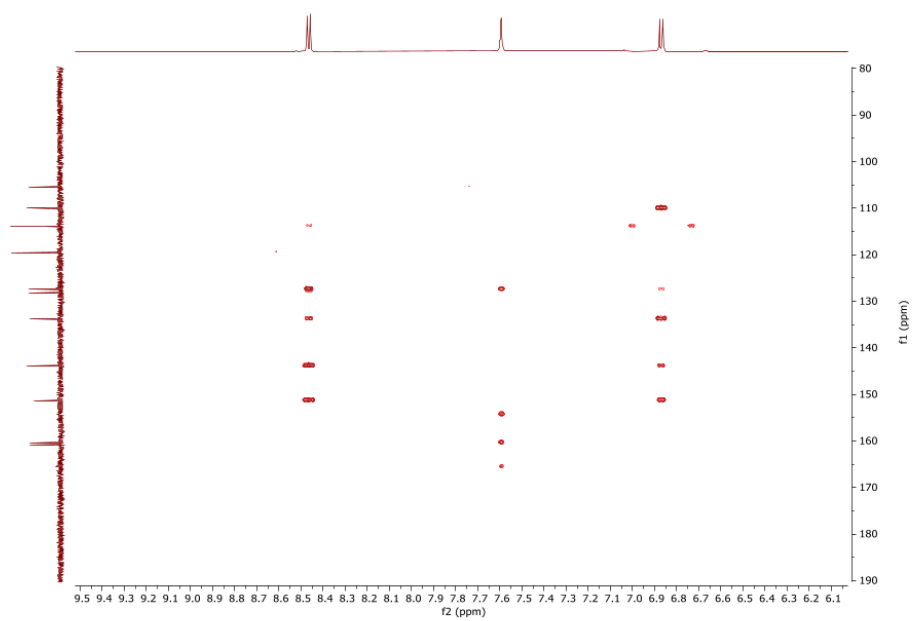


Figure S2-6. HMBC spectrum of compound **1** in MeOH-*d*₄, 600/150 MHz

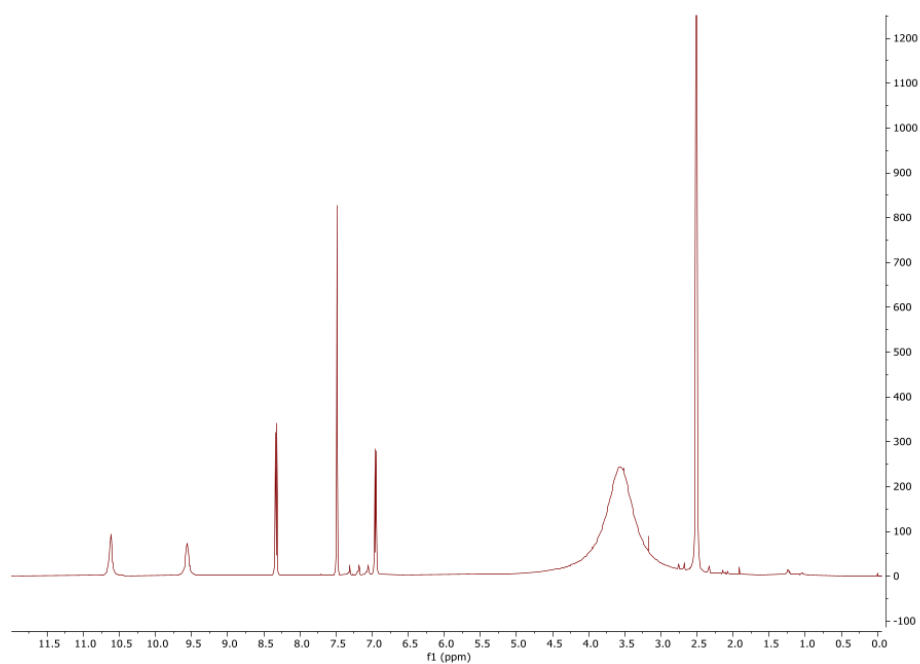


Figure S2-7. ^1H NMR spectrum of compound **1** in DMSO- d_6 , 400 MHz

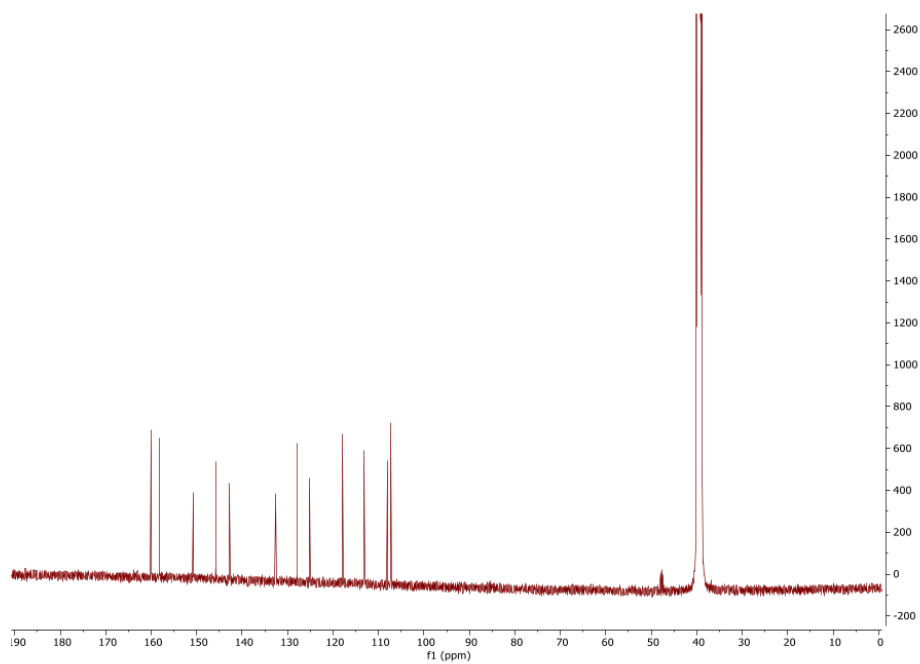


Figure S2-8. ^{13}C NMR spectrum of compound **1** in DMSO- d_6 , 100 MHz

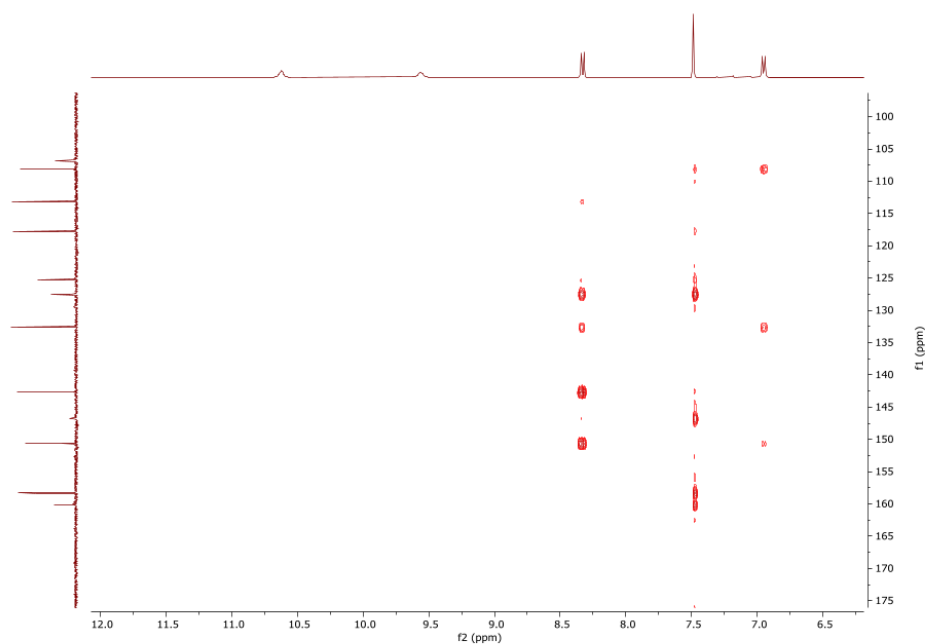


Figure S2-9. HMBC spectrum of compound **1** in DMSO-*d*₆, 600/150 MHz

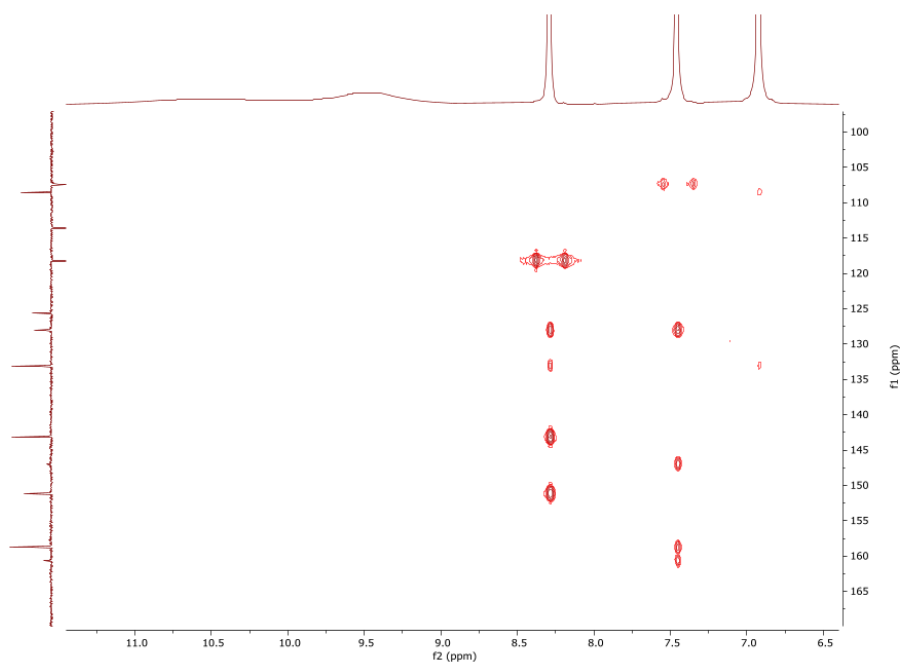


Figure S2-10. HMBC spectrum of compound **1** in DMSO-*d*₆, 900/226 MHz

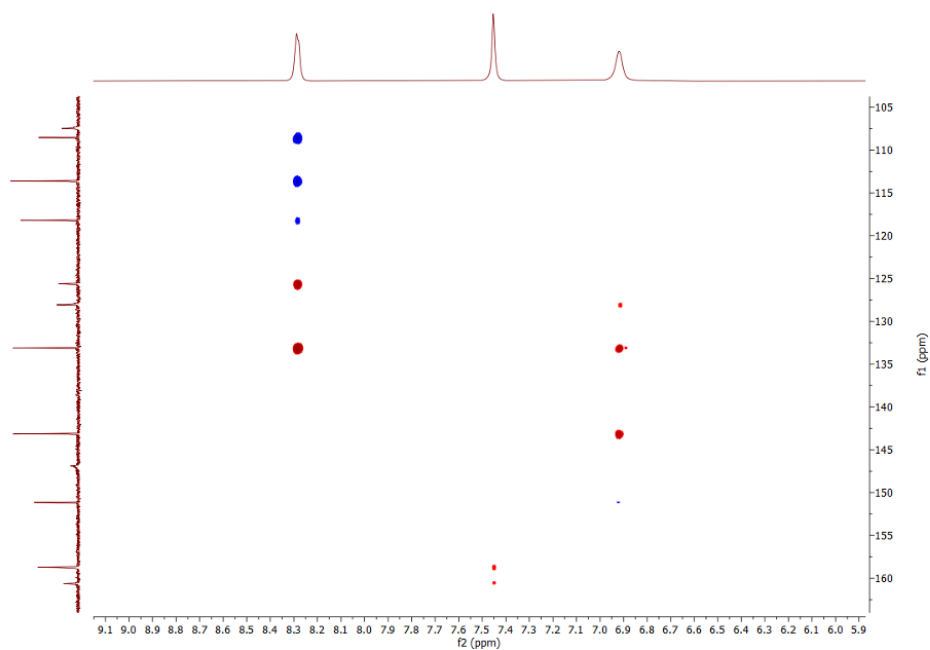


Figure S2-11. 1,n-ADEQUATE spectrum of compound **1** in DMSO-*d*₆, 800/200 MHz

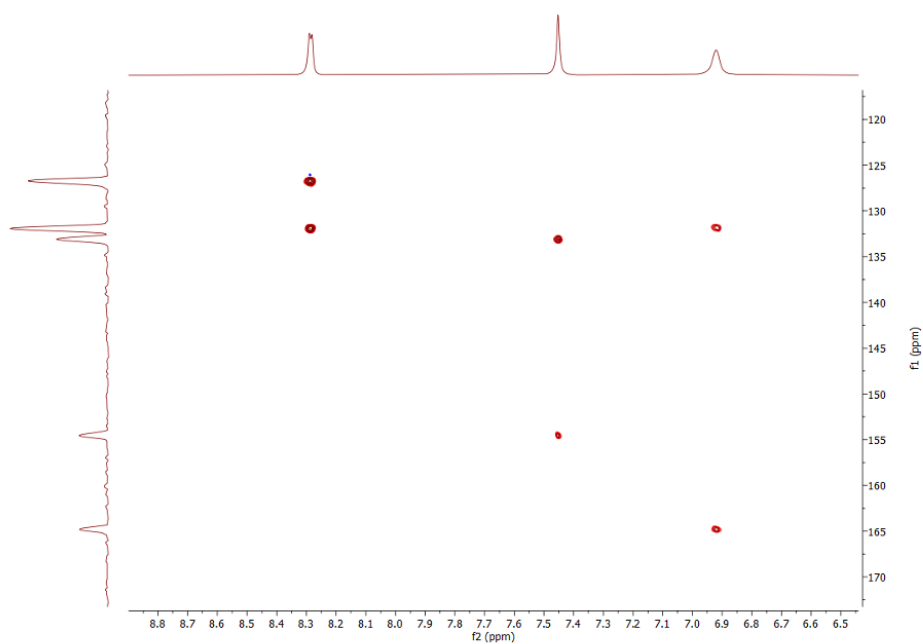


Figure S2-12. 1,1-ADEQUATE spectrum of compound **1** in DMSO-*d*₆, 900/226 MHz

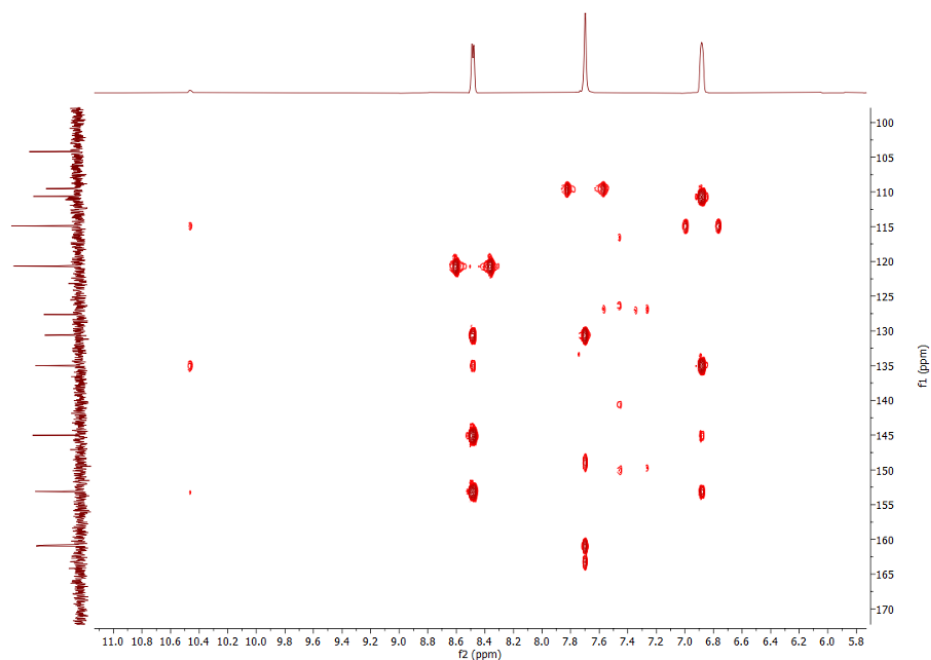


Figure S2-13. HMBC spectrum of compound **1** in MeOH-*d*₃, 700/176 MHz, 253 K

Table S1-1. ¹H NMR data of compound **1** acquired in different solvents and under varying field strengths

No.	type	$\delta_{\text{H}}^{\text{a}}$ MeOH- <i>d</i> 4 600 MHz	δ_{H} MeOH- <i>d</i> 4 400 MHz	δ_{H} DMSO- <i>d</i> 6 400 MHz	δ_{H} DMSO- <i>d</i> 6 800 MHz ^c	δ_{H} DMSO- <i>d</i> 6 900 MHz ^c	δ_{H} DMSO- <i>d</i> 6 600 MHz ^c	$\delta_{\text{H}}^{\text{b}}$ MeOH- <i>d</i> 3 800 MHz ^c	$\delta_{\text{H}}^{\text{b}}$ MeOH- <i>d</i> 3 700 MHz ^c
4	CH	7.59, s	7.69, s	7.49, s	7.45, s	7.45, s	7.52, s	7.70, s	7.70, s
9	CH	6.87, d (9.0)	6.88, d (9.0)	6.95, d (9.0)	6.92, br d (6.8)	6.92, br d (7.8)	6.99, br d (8.3)	6.89, d (9.0)	6.88, d (9.0)
10	CH	8.46, d (9.0)	8.45, d (9.0)	8.33, d (9.0)	8.28, d (6.8)	8.28, d (7.8)	8.35, d (8.3)	8.48, d (9.0)	8.48, d (9.0)
7	COH			9.56, s	9.52, s	9.53, s	9.60, s	9.74, s	9.90, s
8	COH			10.62, s	10.60, s	10.65, s	10.70, s	10.30, s	10.46, s

^a compound obtained under non-acidic conditions^b low temperature**Table S1-2.** ¹³C NMR data of compound **1** acquired in different solvents and under varying field strengths

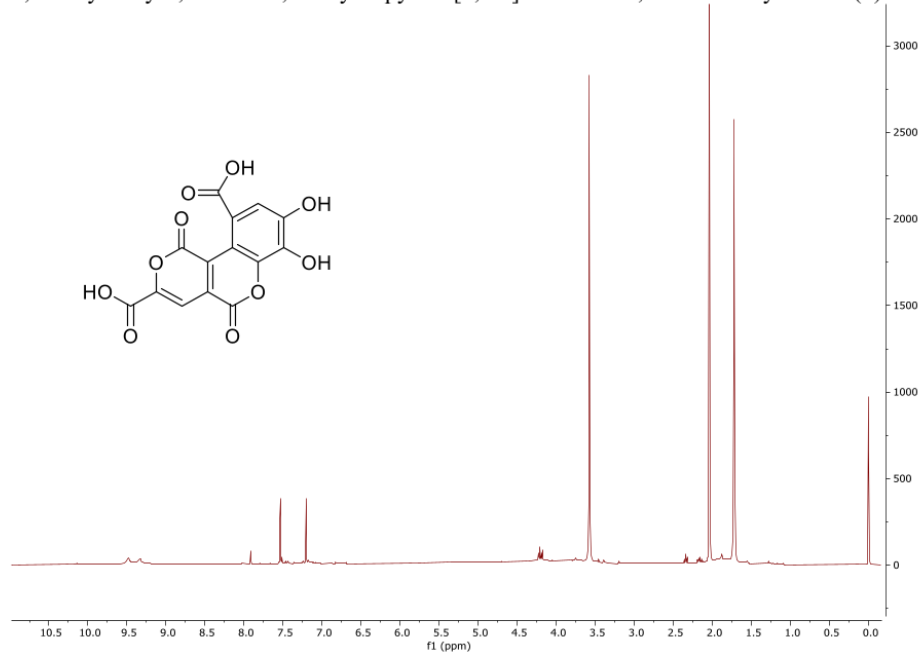
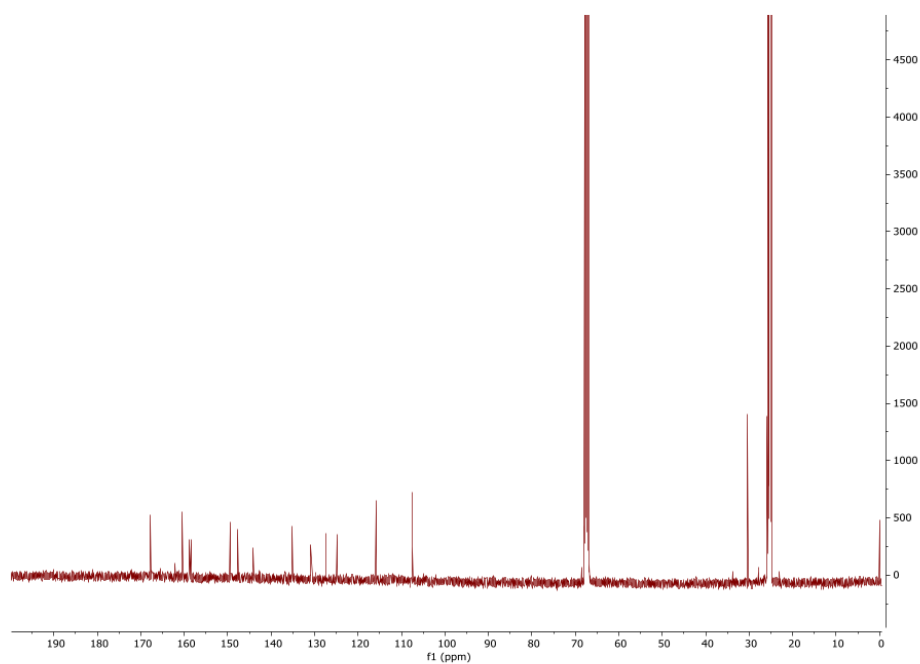
No.	type	$\delta_{\text{C}}^{\text{a}}$ MeOH- <i>d</i> 4 151 MHz	δ_{C} MeOH- <i>d</i> 4 126 MHz	δ_{C} DMSO- <i>d</i> 6 101 MHz	δ_{C} DMSO- <i>d</i> 6 201 MHz ^c	δ_{C} DMSO- <i>d</i> 6 151 MHz ^c	δ_{C} DMSO- <i>d</i> 6 226 MHz ^c	$\delta_{\text{C}}^{\text{b}}$ MeOH- <i>d</i> 3 176 MHz
1	C=O	160.3	159.7	158.2	158.7	158.7	158.7	158.5
3	C	154.4 ^c	147.4	145.8	146.9	146.9	147.9	144.7
4	CH	105.3	108.9	107.3	107.4	107.4	107.4	107.17
4a	C	128.1	126.5	125.1	125.6	125.6	125.7	125.2
5	C=O	160.8	159.9	158.3	158.7	158.7	158.7	158.6
6a	C	143.8	144.3	142.8	143.1	143.0	143.1	142.6
7	C	133.7	133.9	132.7	133.1	133.1	133.0	132.6
8	C	151.3	152.2	150.8	151.2	151.1	151.1	150.8
9	CH	113.8	114.1	113.2	113.6	113.6	113.6	112.6
10	CH	119.5	120.0	117.9	118.2	118.3	118.2	118.4
10a	C	110.0	109.7	108.1	108.5	108.5	108.5	108.3
10b	C	127.4	129.9	127.9	128.0	128.1	128.1	128.2
11	C=O	165.6 ^c	161.8	160.0	160.7	160.5	160.6	161.8

^a compound obtained under non-acidic conditions^b low temperature^c derived from HMBC**Table S1-3.** HMBC data of compound **1** acquired in different solvents and under varying field strengths

No.	CD ₃ OD- <i>d</i> 4 ^a (600, 151 MHz)	DMSO- <i>d</i> 6 (600, 151 MHz)	CD ₃ OD- <i>d</i> 4 ^a (500, 126 MHz)	DMSO- <i>d</i> 6 (600, 151 MHz)	CD ₃ OH- <i>d</i> 3 ^b (701, 176 MHz)	CD ₃ OH- <i>d</i> 3 ^b (800, 201 MHz)	DMSO- <i>d</i> 6 (900, 226 MHz)
4	3, 5, 10a, 10b, 11	3, 4a, 5, 10a, 10b, 11	3, 5, 10b, 11	3, 5, 10b, 11	3, 5, 10b, 11	5, 10b, 11	3, 5, 10b, 11
9		6a, 7, 8, 10a	6a, 7, 8, 10a	-	6a, 7, 8, 10a	6a, 7, 8, 10, 10a, 10b	7, 10a
10		4a, 6a, 7, 8, 9, 10b	6a, 7, 8, 10b	6a, 7, 8, 10b	6a, 7, 8, 10b	1, 4a, 6a, 7, 8, 9, 10b	6a, 7, 8, 10b
7-OH					-		
8-OH					7, 8, 9		

blue = weak signal

^a compound obtained under non-acidic conditions^b low temperature

7,8-Dihydroxy-1,5-dioxo-1,5-dihydropyrano[4,3-c]chromene-3,10-dicarboxylic acid (**5**)**Figure S3-1.** ¹H spectrum of compound **5** in THF-*d*₈, 400 MHz**Figure S3-2.** ¹³C spectrum of compound **5** in THF-*d*₈, 100 MHz

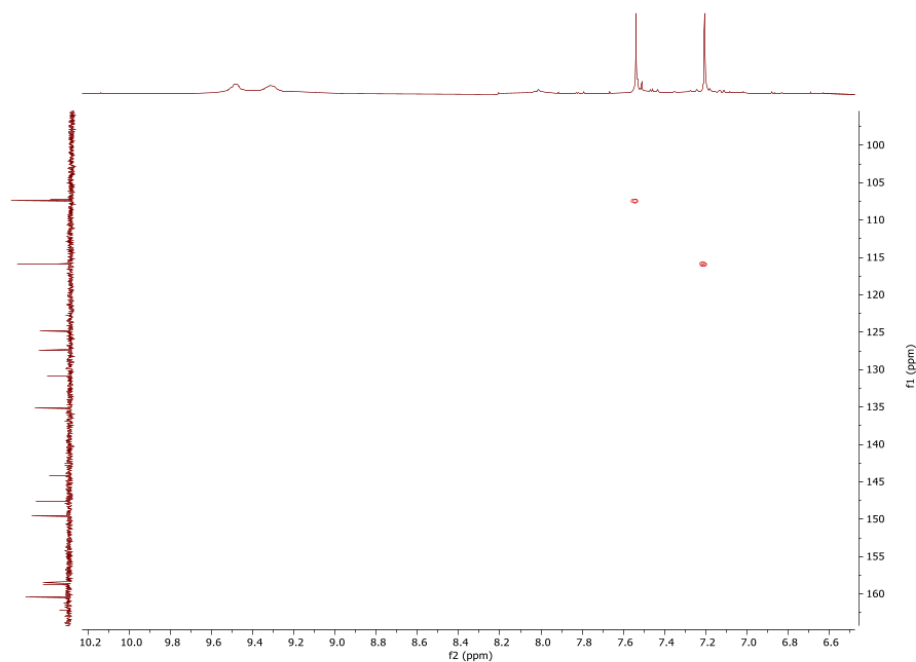


Figure S3-3. HSQC spectrum of compound **5** in THF-*d*₈, 400/100 MHz

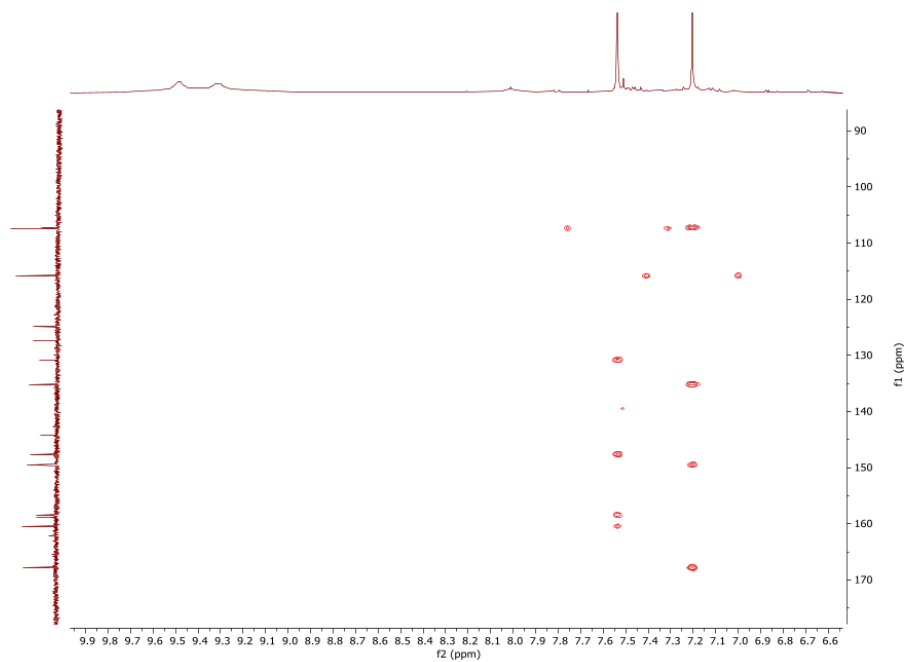


Figure S3-4. HMBC spectrum of compound **5** in THF-*d*₈, 400/100 MHz

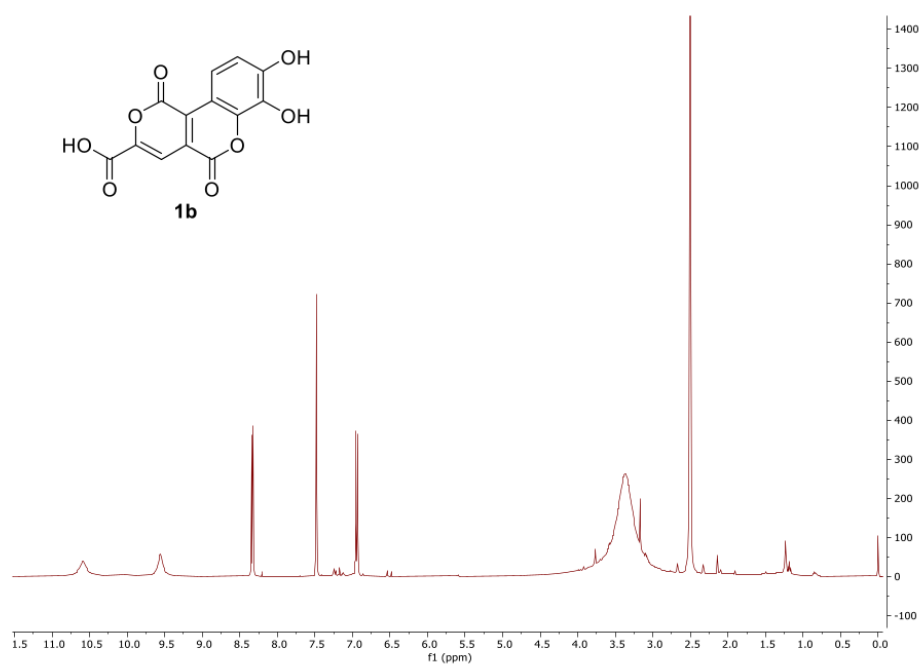


Figure S4-1. ¹H spectrum of compound **1b** in DMSO-*d*₆, 400MHz

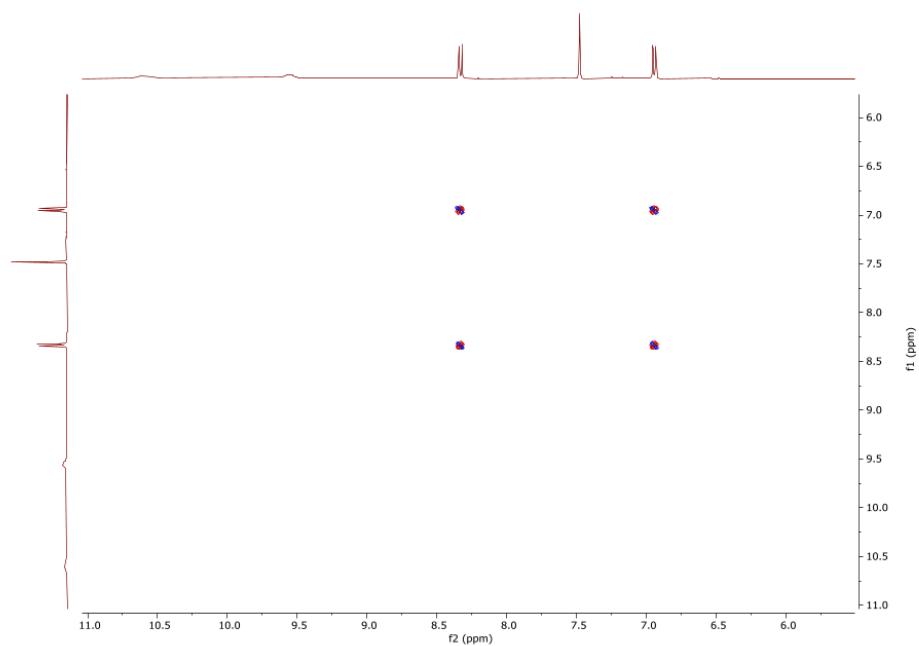


Figure S4-2. COSY spectrum of compound **1b** in DMSO-*d*₆, 400MHz

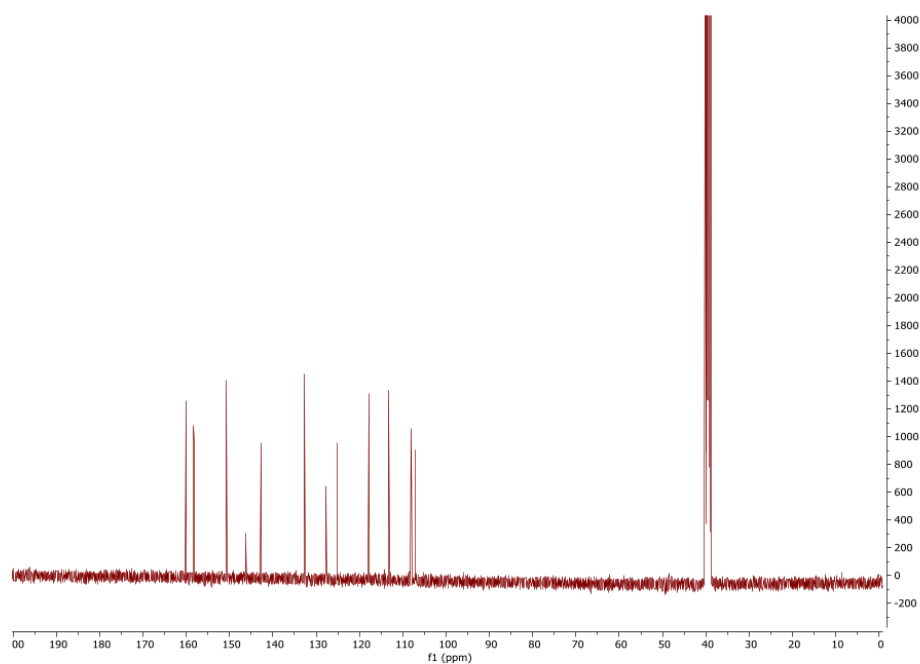


Figure S4-3. ^{13}C spectrum of compound **1b** in $\text{DMSO-}d_6$, 100MHz

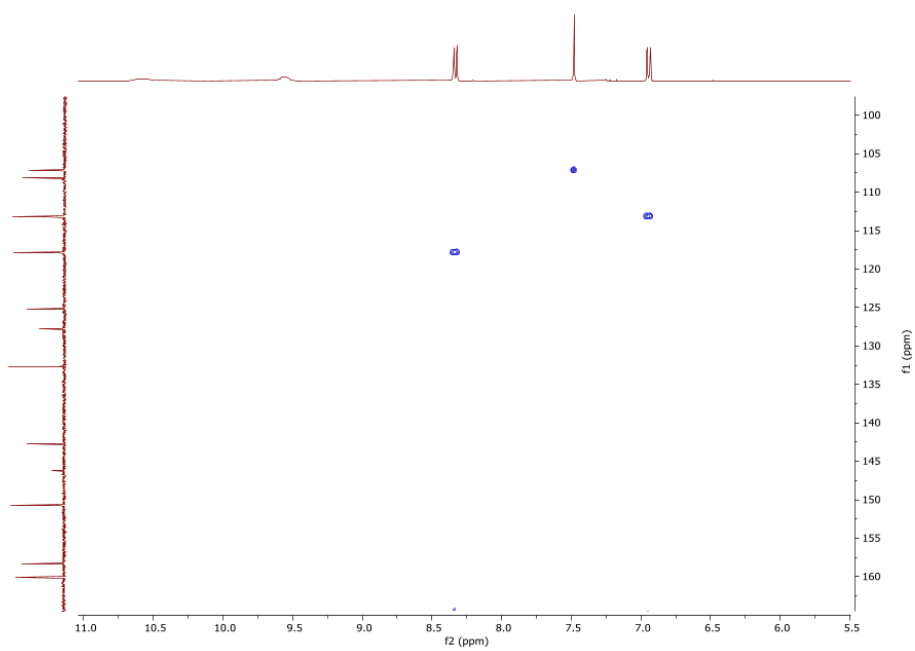


Figure S4-4. HSQC spectrum of compound **1b** in $\text{DMSO-}d_6$, 400/100MHz

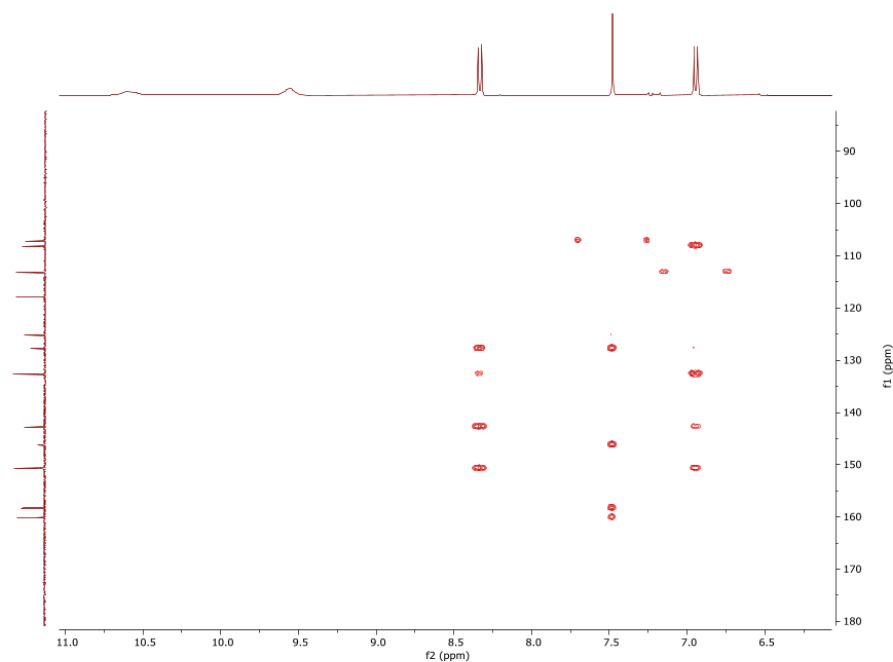


Figure S4-5. HMBC spectrum of compound **1b** in DMSO-*d*₆, 400/100MHz

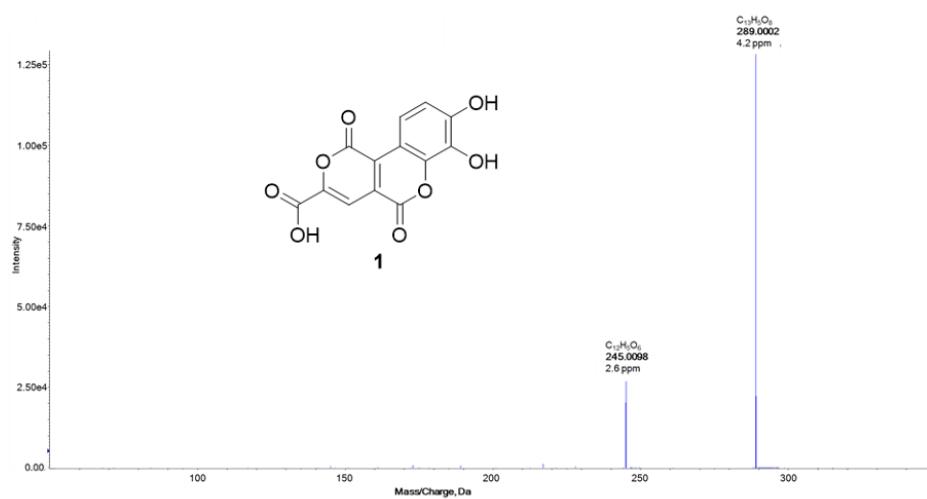


Figure S5-1. High resolution mass spectra (HRMS) acquired with quadrupole-time-of-flight-tandem instrument (QqTOF-MS) of compound **1**.

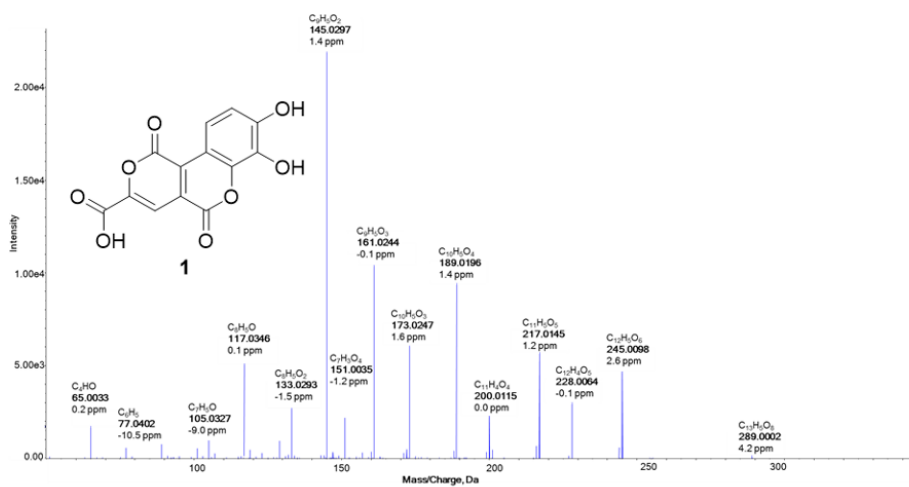


Figure S5-2. MS² of compound **1** acquired with quadrupole-time-of-flight-tandem instrument (QqTOF-MS/MS).

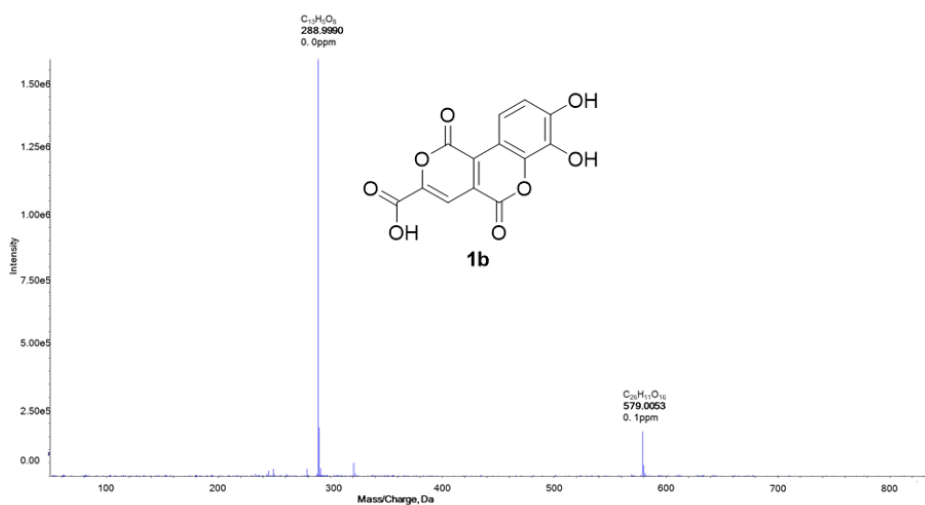


Figure S6-1. High resolution mass spectra (HRMS) acquired with quadrupole-time-of-flight-tandem instrument (QqTOF-MS) of synthetic compound **1b**

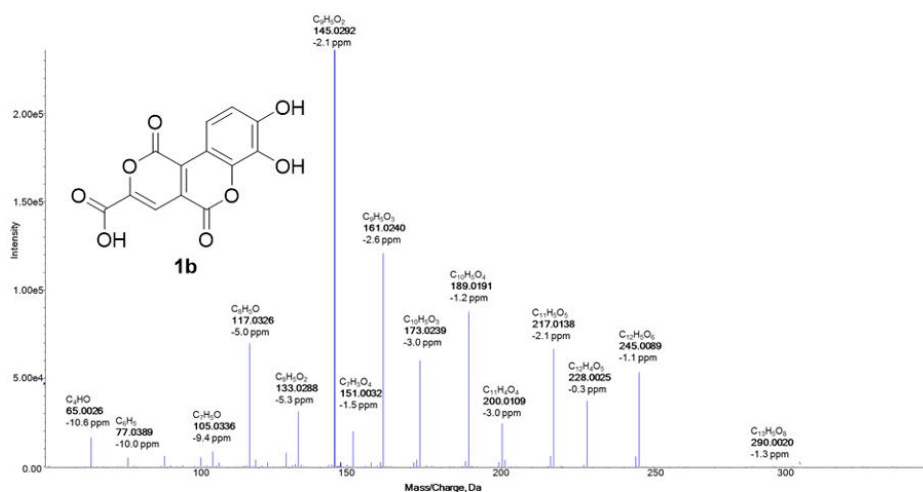


Figure S6-2. MS² of synthetic compound **1b** acquired with quadrupole-time-of-flight-tandem instrument (QqTOF-MS/MS)

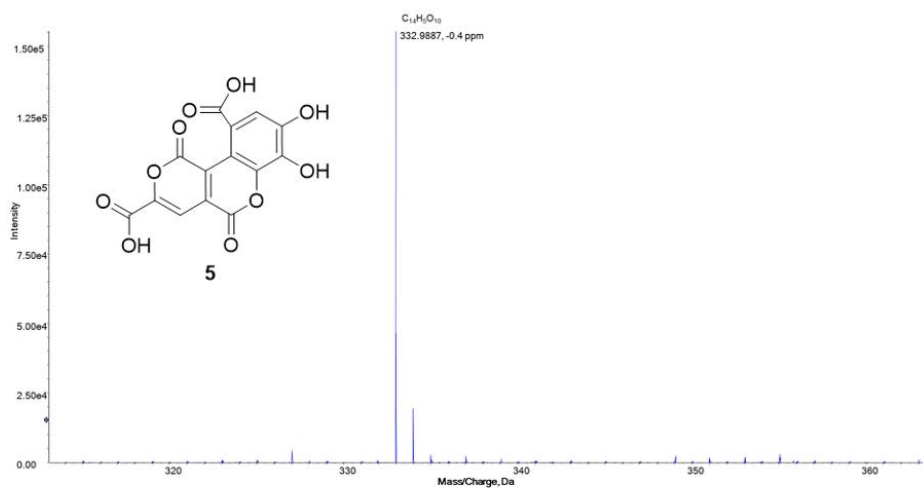


Figure S7-1. High resolution mass spectra (HRMS) acquired with quadrupole-time-of-flight-tandem instrument (QqTOF-MS) of synthetic compound **5**

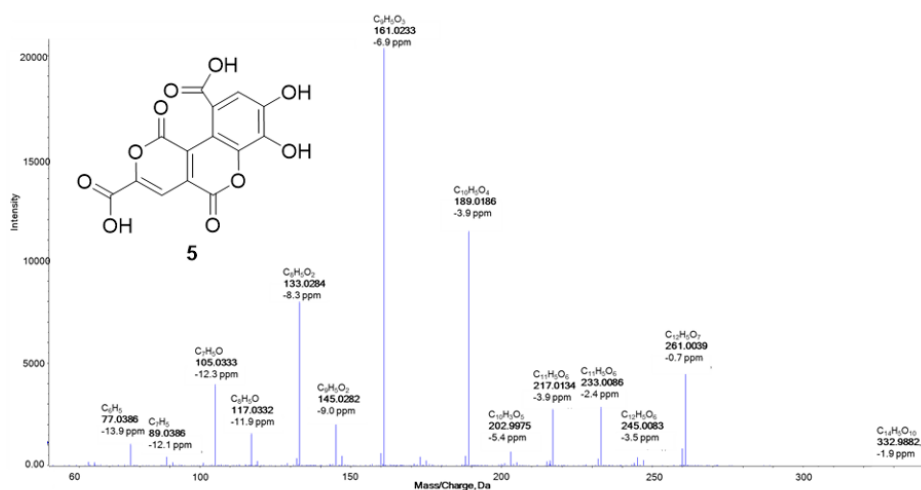
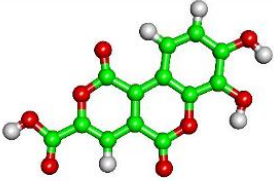
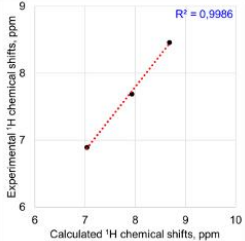
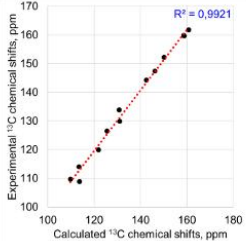
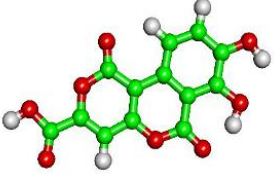
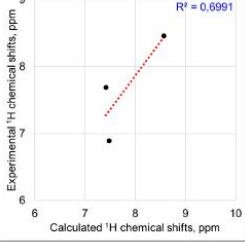
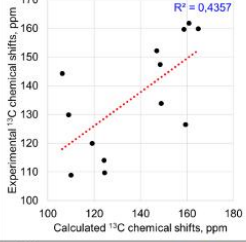

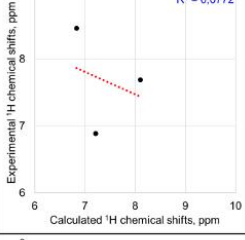
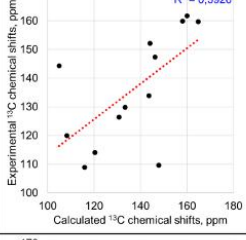

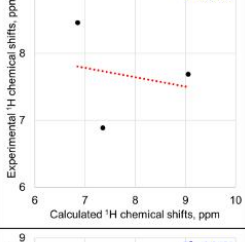
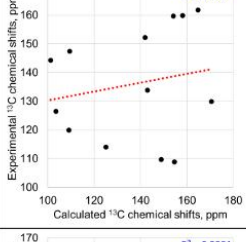

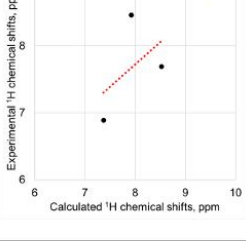
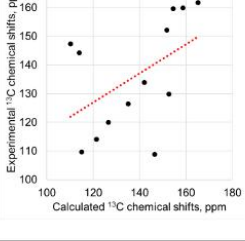


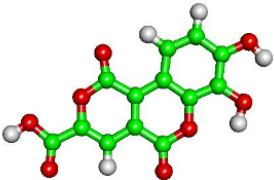
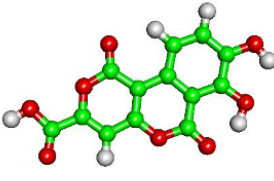
Figure S7-2. MS² of synthetic compound **5** acquired with quadrupole-time-of-flight-tandem instrument (QqTOF-MS/MS)

Table S2-1. DFT calculations: comparison between experimental and calculated chemical shifts*

Molecular structure and calculated J -coupling	$\delta(^1\text{H})$, ppm	$\delta(^{13}\text{C})$, ppm
 Lumnizalactone (I), $^3J_{\text{HH}} = 8.1$ Hz		
 Isomer (II), $^3J_{\text{HH}} = 7.7$ Hz		
 Isomer (III), $^3J_{\text{HH}} = 7.5$ Hz		
 Isomer (IV), $^3J_{\text{HH}} = 7.7$ Hz		
 Isomer (V), $^3J_{\text{HH}} = 7.4$ Hz		

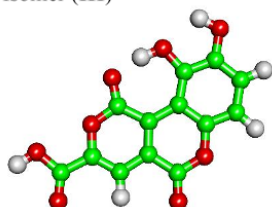
* Geometry optimization: # opt b3lyp/6-31+g(d,p) geom=connectivity;
 NMR: # nmr=(giao,spinspin) mpw1pw91/6-311+g(2d,p) scrf=(iefpcm,solvent=methanol) geom=connectivity

Table S2-2. Cartesian coordinates of structures A-E used in DFT calculations

Structure	Cartesian Coordinates			
Lumnitzeralactone (I)	Element	X	Y	Z
	C	-1.94132100	0.54152900	0.00026300
	C	-3.33084100	0.50949900	-0.00030500
	C	-3.98314000	-0.72941700	-0.00082200
	C	-3.22924500	-1.91141900	-0.00050000
	C	-1.84330900	-1.86882800	0.00018300
	C	-1.15460200	-0.63107300	0.00053400
	C	0.27884300	-0.44001400	0.00075300
	C	0.81984100	0.83835500	0.00065600
	C	-0.04131300	2.03720300	0.00080200
	O	-1.40116600	1.80630300	0.00049700
	C	1.21064600	-1.59411500	0.00133900
	O	2.56367800	-1.29172600	-0.00003900
	C	3.05078900	-0.02352500	-0.00016200
	C	2.23161200	1.05309500	0.00033500
	O	-5.33558800	-0.79300300	-0.00152400
	O	-4.10945400	1.63388700	-0.00089900
	O	0.34751100	3.18120500	0.00127700
	O	0.90621200	-2.76447900	0.00248000
	C	4.53371200	0.09503900	-0.00100800
	O	5.10957000	1.16480800	-0.00101700
	O	5.15801700	-1.09716300	-0.00189500
	H	-3.75590200	-2.85933000	-0.00075300
	H	-1.27151300	-2.78523200	0.00050300
	H	2.64049200	2.05464800	0.00035300
	H	-5.69923700	0.10672600	-0.00152600
	H	-3.54784100	2.42413900	0.00043200
	H	6.11372000	-0.91758000	-0.00246000
	Element	X	Y	Z
	C	-1.86489300	0.51052000	0.00016300
	C	-3.26876200	0.39705300	0.00012100
	C	-3.86340200	-0.87719600	0.00002900
	C	-3.05494400	-2.01153900	0.00006300
	C	-1.66225800	-1.91267800	0.00003800
	C	-1.03947400	-0.65605600	0.00007800
	C	0.39892900	-0.43641100	-0.00002300
	C	0.88959500	0.85337000	-0.00016900
	C	1.36759100	-1.53803600	-0.00014000
	O	2.72307600	-1.17418000	-0.00017500
	C	3.14446900	0.10719700	-0.00033200
	C	2.28020800	1.15064100	-0.00032400
	O	-5.21409500	-1.00004200	-0.00000600
	O	-4.11371000	1.45165500	0.00001300
	O	1.12821500	-2.72306400	-0.00013900
	C	4.62198300	0.30780700	-0.00048900
	O	5.13414900	1.40930600	0.00015100
	O	5.30901100	-0.84686500	0.00063400
	H	-3.53482400	-2.98491000	0.00004000
	H	-1.05658700	-2.80735700	0.00002700
	H	2.63989800	2.17086300	-0.00043100

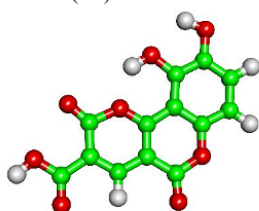
H	-5.60848500	-0.11287900	-0.00022200
H	-3.56998600	2.27649100	-0.00042200
H	6.25435500	-0.61850900	0.00122200
C	-1.29358800	1.84276300	0.00026200
O	-1.92801500	2.89048300	0.00010400
O	0.07923300	1.94916900	-0.00006600

Isomer (III)



Element	X	Y	Z
C	1.93955700	1.36213900	0.01368000
C	3.28940800	1.66851600	0.01450300
C	4.22531900	0.63676100	0.00148800
C	3.79249200	-0.68168300	-0.01446000
C	2.41870100	-1.00490500	-0.01467300
C	1.42850800	0.02759200	0.00363000
C	-0.03188100	-0.09655300	0.00694600
C	-0.82525800	1.04795600	-0.00096100
C	-0.23734700	2.40570800	0.00213600
O	1.11508300	2.46861100	0.02124600
C	-0.76220400	-1.38448200	0.03411400
O	-2.12483300	-1.35064800	0.01567500
C	-2.85915100	-0.20687200	-0.00420700
C	-2.25005900	0.99768700	-0.00911900
O	-0.88686300	3.42825400	-0.00531600
O	-0.28038000	-2.51085200	0.07763400
C	-4.33477200	-0.38833000	-0.01670000
O	-5.10840300	0.54663200	-0.03395200
O	-4.70488900	-1.68159700	-0.00695800
H	-2.82670100	1.91308400	-0.02024400
H	-5.67722000	-1.70203700	-0.01635600
O	4.70775400	-1.68750200	-0.03206100
O	2.20852500	-2.33576600	-0.04319900
H	1.23416700	-2.55134400	0.00735000
H	4.22387600	-2.53015100	-0.03832600
H	5.29013900	0.84222400	0.00131000
H	3.58791300	2.70995900	0.02346300

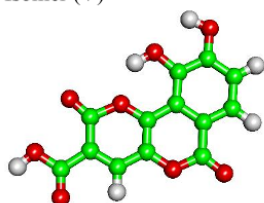
Isomer (IV)



Element	X	Y	Z
C	-2.10813900	1.32765400	-0.00003200
C	-3.48682900	1.48435800	-0.00042300
C	-4.30032400	0.34949400	-0.00054600
C	-3.75196900	-0.93391800	-0.00016000
C	-2.36106200	-1.09914700	0.00002100
C	-1.51677100	0.03884800	0.00009000
C	-0.08668000	0.00095600	0.00016600
C	0.68010100	1.15115000	0.00057400
C	0.03830200	2.46991500	0.00062800
O	-1.34589100	2.46896700	0.00042000
C	2.72158200	-0.19851800	0.00037400
C	2.09082600	1.02296700	0.00034200
O	0.61538800	3.53112100	-0.00070200
C	4.21304300	-0.19512300	-0.00034000

O	4.87016800	0.82947300	0.00055400
O	4.77017500	-1.42001500	-0.00213000
H	2.69882300	1.92268100	0.00011500
H	5.73360000	-1.28612900	-0.00247900
O	-4.57721600	-2.01634100	-0.00029700
O	-1.92812600	-2.38737900	0.00003200
H	-0.95610000	-2.43155200	0.00025100
H	-4.03859300	-2.82305900	0.00016500
H	-5.38092000	0.44600000	-0.00141800
H	-3.90899900	2.48221800	-0.00007300
C	1.94597400	-1.42796400	0.00127500
O	2.26644200	-2.58162600	0.00105700
O	0.50204300	-1.20597100	0.00002000

Isomer (V)



Element	X	Y	Z
C	-2.09352600	1.19109600	-0.00033300
C	-3.48950100	1.23289000	-0.00010700
C	-4.22842400	0.05252800	-0.00005900
C	-3.57970600	-1.18466700	0.00001000
C	-2.17347400	-1.25306800	-0.00009500
C	-1.42107900	-0.06509900	-0.00031000
C	0.01358000	-0.02061800	-0.00017400
C	0.69415000	1.16887500	-0.00009900
C	2.81962200	-0.01396300	-0.00008900
C	2.10331000	1.16205500	-0.00012600
C	4.30565600	0.10757900	-0.00016600
O	4.87794700	1.18318000	0.00109700
O	4.95987800	-1.06680100	-0.00182000
H	2.64411500	2.10373000	-0.00014600
H	5.90933200	-0.85536500	-0.00177500
O	-4.31070200	-2.32243800	0.00008900
O	-1.66228200	-2.51458900	-0.00032400
H	-0.68893900	-2.49805200	-0.00018200
H	-3.70955100	-3.08526900	0.00034000
H	-5.31296800	0.06769200	-0.00042600
H	-3.98181500	2.19840900	0.00025800
C	2.13657900	-1.30061400	0.00029700
O	2.55983100	-2.42462800	0.00191500
O	0.69824800	-1.18880800	-0.00004200
C	-1.34604800	2.46083900	-0.00027900
O	-1.83221100	3.56614100	0.00066800
O	0.04591400	2.37317500	-0.00019600

Structure Elucidation Report for "SE_Lumlac_aftercalculation" (Page 1)

Structure Elucidation Report for "SE_Lumlac_aftercalculation"

Initial Data

Composition Restrictions:
 Molecular Weight = 0.000-1000.000
 Double Bonds Equivalent = 0.00-100.00
 Allowed Composition = C(0-100) H(0-100) O(0-20) N(0-10)
 Molecular Formula = C₁₃H₆O₈

Spectral Data:
 standard ¹H (user) - 5 peaks
 merged ¹H - 4 peaks
 standard ¹³C (user) - 13 peaks
 merged ¹³C - 13 peaks
 COSY ¹H-¹H (user) - 2 peaks
 HSQC ¹³C-¹H (user) - 3 peaks
 HMBC ¹³C-¹H (user) - 20 peaks
 1,n-ADEQUATE(inverted) ¹³C-¹H (user) - 7 peaks
 1,1-ADEQUATE ¹³C-¹H (user) - 6 peaks

Result of Automatic Elucidation

No molecule(s) have been found by NMR spectra in 0 database(s).
 0 stereoisomer(s) have been excluded from the search result.
 No molecule(s) have been found by NMR spectra in 0 database(s).
 0 stereoisomer(s) have been excluded from the search result.
 1 Molecular Connectivity Diagram (MCD) has been created from 1 MF
 Current Molecular Connectivity Diagram (MCD) passed all tests
 No updates performed.
 31061041 molecule(s) have been generated by Correlation Spectroscopy Based Generator and 44 molecule(s) have been stored.
 Generation time: 18 h 10 m 27 s (Check: 0 s, Generation: 18 h 10 m 27 s 325 ms)
 No (from No) connectivities have been extended during generation
 ACD/CNMR Spectrum (Neural Net) has been calculated for 44 of 44 structure(s) from Generated Molecules
 44 of 44 structure(s) have been stored in Generated Molecules after removing duplicates
 ACD/HNMR Spectrum (Neural Net) has been calculated for 44 of 44 structure(s) from Generated Molecules
 44 molecules have been found for the current spectrum query.

Most Probable Structure

Following structure has been placed to the first position after spectra calculation

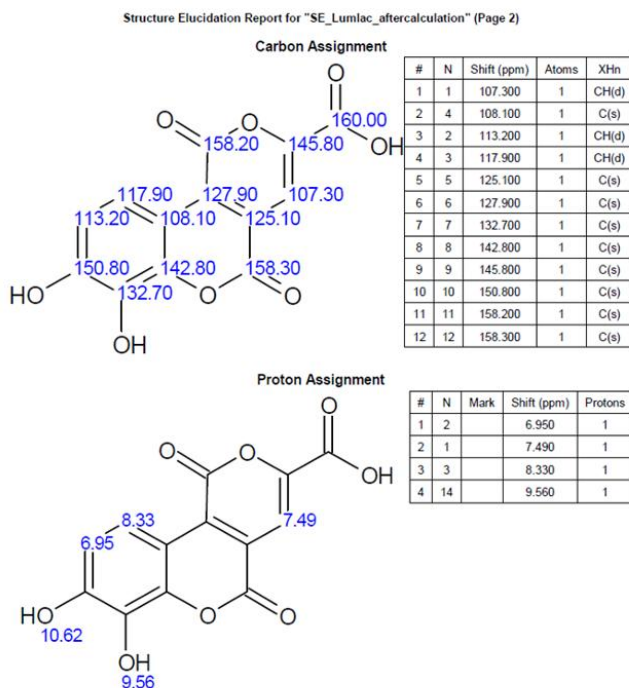


Figure S8-1. Part of ACD-SE report

28/Jan/2022 16:15:58 SE_Lumiac_aftercalculation.gnr - Generated Molecules Page: 1(2)

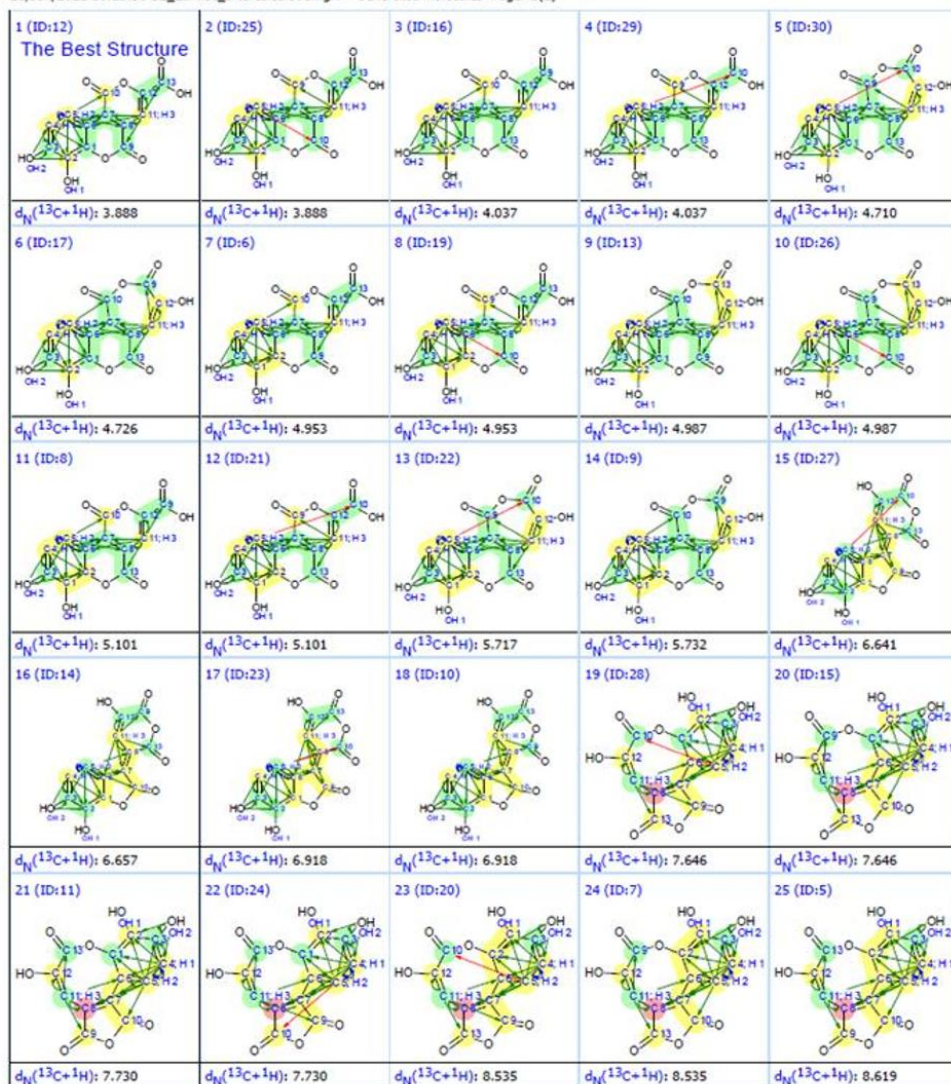


Figure S8-2. Overview of structures generated by ACD-SE

28/Jan/2022 16:16:00 SE_Lumiac_aftercalculation.gnr - Generated Molecules Page: 2(2)

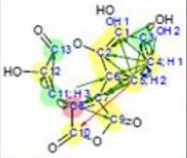
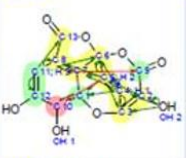
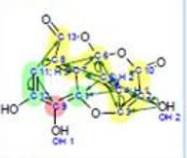
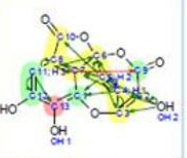
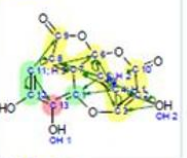
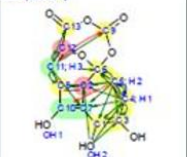
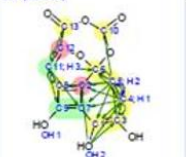
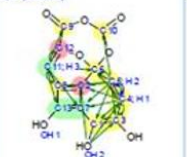
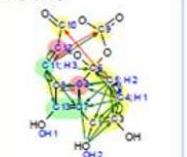
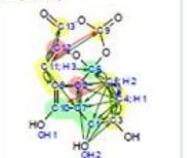
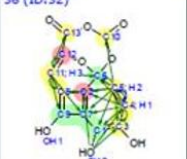
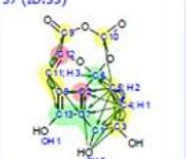
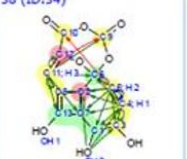

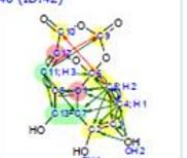
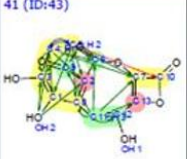
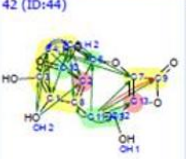
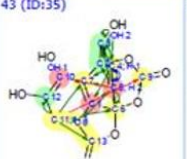
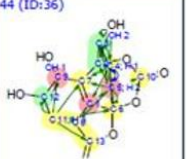
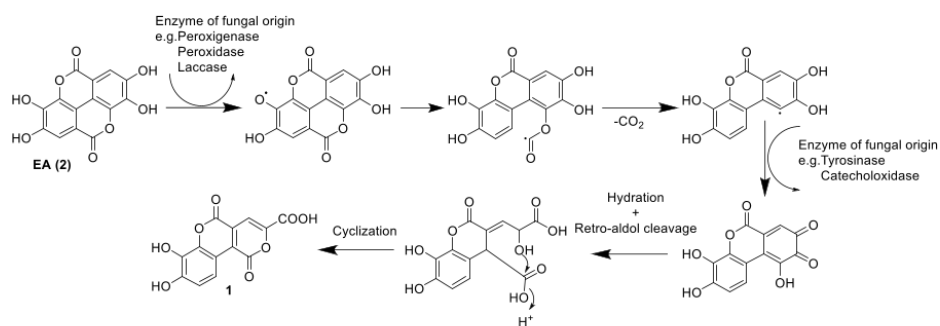
26 (ID:18) 	27 (ID:3) 	28 (ID:4) 	29 (ID:1) 	30 (ID:2) 
$d_N(^{13}\text{C}+^1\text{H}): 8.619$	$d_N(^{13}\text{C}+^1\text{H}): 12.437$	$d_N(^{13}\text{C}+^1\text{H}): 12.452$	$d_N(^{13}\text{C}+^1\text{H}): 12.714$	$d_N(^{13}\text{C}+^1\text{H}): 12.714$
31 (ID:37) 	32 (ID:38) 	33 (ID:39) 	34 (ID:40) 	35 (ID:31) 
$d_N(^{13}\text{C}+^1\text{H}): 13.851$	$d_N(^{13}\text{C}+^1\text{H}): 13.851$	$d_N(^{13}\text{C}+^1\text{H}): 13.851$	$d_N(^{13}\text{C}+^1\text{H}): 13.851$	$d_N(^{13}\text{C}+^1\text{H}): 13.942$
36 (ID:32) 	37 (ID:33) 	38 (ID:34) 	39 (ID:41) 	40 (ID:42) 
$d_N(^{13}\text{C}+^1\text{H}): 13.942$	$d_N(^{13}\text{C}+^1\text{H}): 13.942$	$d_N(^{13}\text{C}+^1\text{H}): 13.942$	$d_N(^{13}\text{C}+^1\text{H}): 14.843$	$d_N(^{13}\text{C}+^1\text{H}): 14.843$
41 (ID:43) 	42 (ID:44) 	43 (ID:35) 	44 (ID:36) 	
$d_N(^{13}\text{C}+^1\text{H}): 16.713$	$d_N(^{13}\text{C}+^1\text{H}): 16.713$	$d_N(^{13}\text{C}+^1\text{H}): 18.033$	$d_N(^{13}\text{C}+^1\text{H}): 18.033$	

Figure S8-2, continued. Overview of structures generated by ACD-SE



Scheme S2-1. A suggested pathway for the biosynthesis of lumnizeralactone (**1**), including a radical induced decarboxylation step (dark pathway)

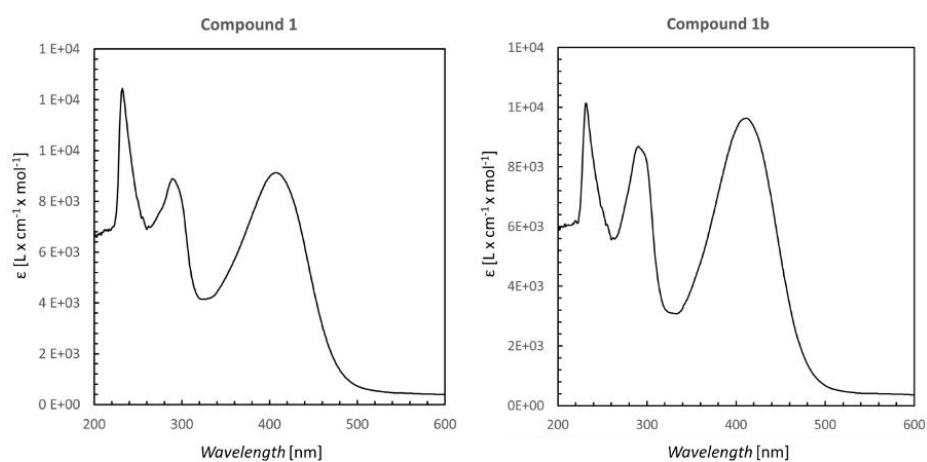


Figure S9-1. UV spectra of isolated compound **1** and synthetic **1b**

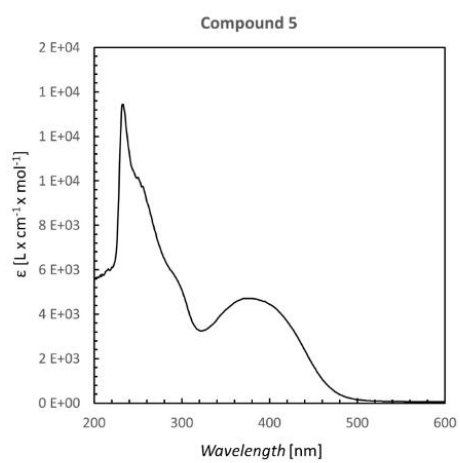


Figure S9-2. UV spectrum of compound **5**

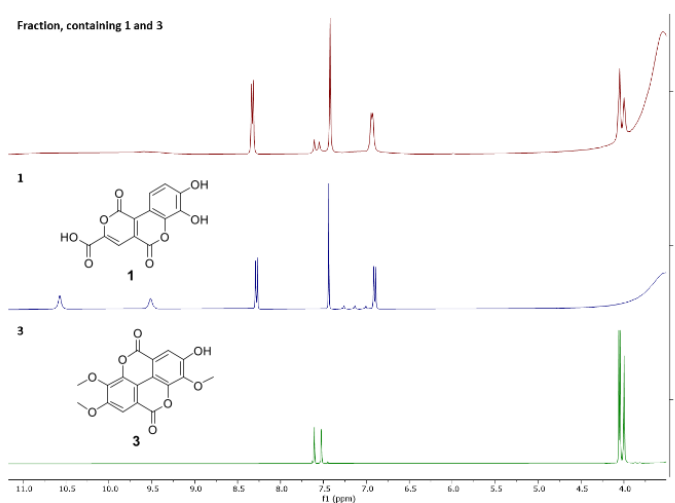


Figure S10-1. ^1H NMR spectrum of the antibacterial fraction containing **1** and **3** compared to the isolated compounds **1** and **3** in $\text{DMSO-}d_6$, 400 MHz.

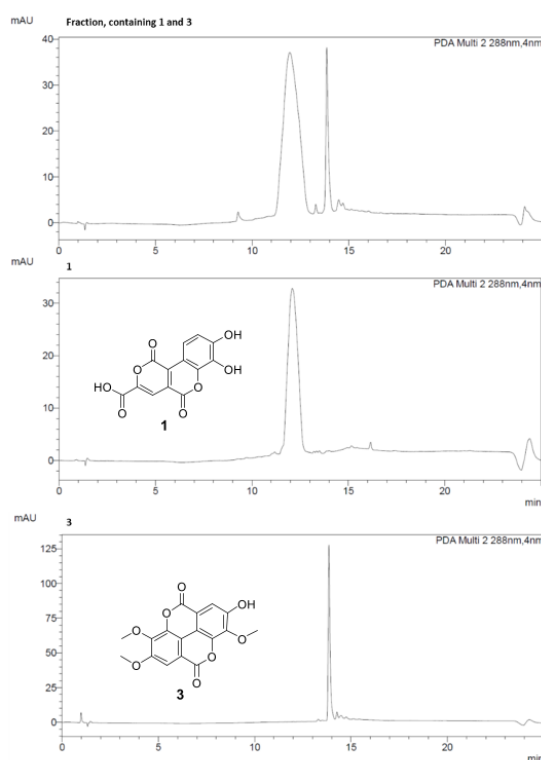






Figure S10-2. HPLC chromatogram of the antibacterial fraction containing **1** and **3** compared to the isolated compounds **1** and **3** (YMC-Triart C18; water (A)/methanol (B) gradient: 0-5, 5% B; 2-12 min, 5-100% B; 12-20 min, 100% B isocratic, flow rate of 1.5 mL/min).

7.3 Supporting information of chapter 4

Supporting Information

Phytochemical profiling of the Omani medicinal plant

Terminalia dhofarica (syn. *Anogeissus dhofarica*)

Jonas Kappen¹, Luay Rashan², Katrin Franke^{1*}, Ludger A. Wessjohann^{1,3*}

¹ Department of Bioorganic Chemistry, Leibniz Institute of Plant Biochemistry (IPB), 06120 Halle (Saale), Germany

² Biodiversity Unit, Research Center, Dhofar University, Salalah, Oman.

³ Institute of Chemistry, Martin Luther University Halle-Wittenberg, 06120 Halle (Saale), Germany

* Correspondence: Katrin Franke, kfranke@ipb-halle.de, Tel: +49-345-5582-1313 (K.F.)
Ludger Wessjohann, wessjohann@ipb-halle.de, Tel: +49-345-5582-1301 (L.A.W.)

Content	page
Fig. S1 – S4. Screening for antibacterial and antifungal biological activities	2
Fig. S5 – S9. 1D and 2D NMR spectra of compound 1	4
Full spectroscopic data set of compounds 1-20	7

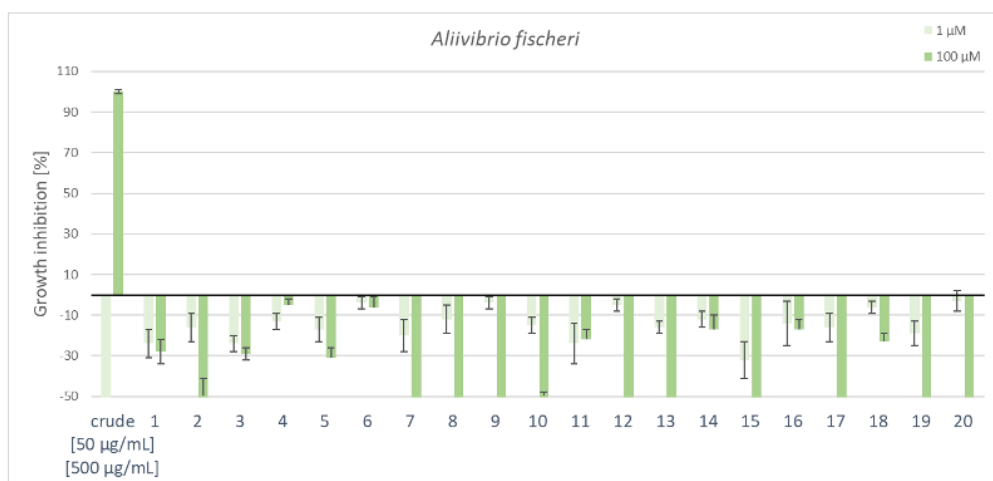


Figure S1 Antibacterial assays of crude methanolic extract of *T. dhofarica* and constituents and artifacts (1-20) against Gram negative *A. fischeri*

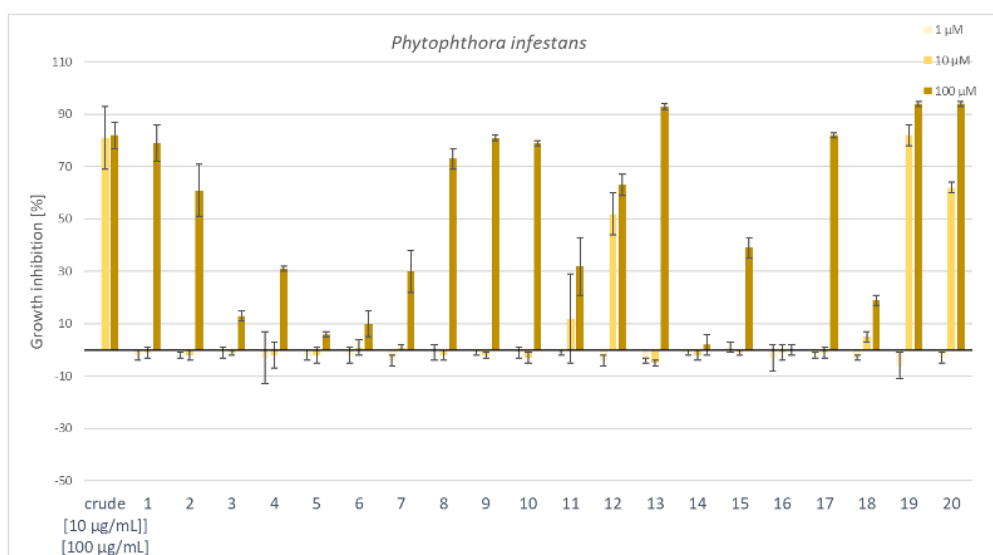


Figure S2 Antifungal assays of crude methanolic extract of *T. dhofarica* and constituents and artifacts (1-20) against *P. infestans*

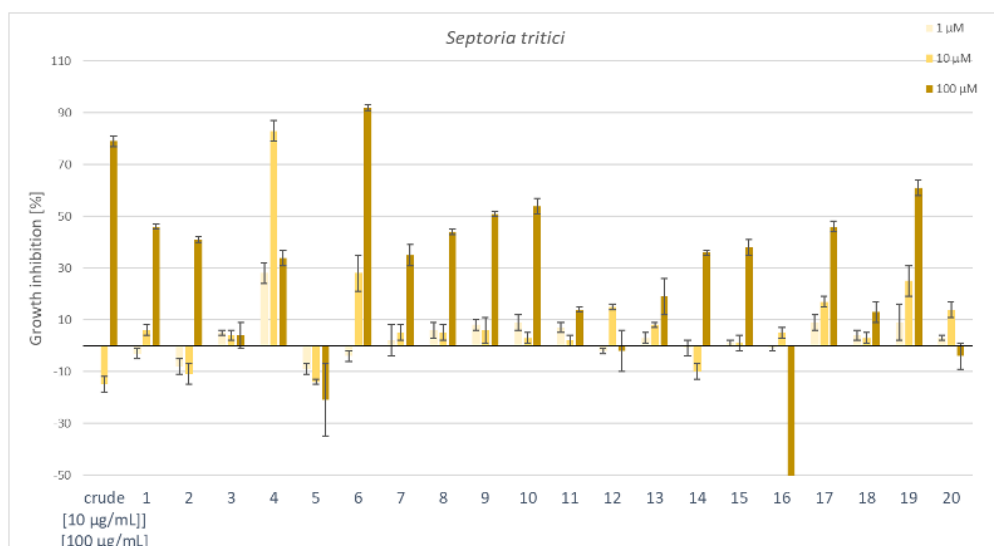


Figure S3 Antifungal assays of crude methanolic extract of *T. dhofarica* and constituents and artifacts (1-20) against *S. tritici*

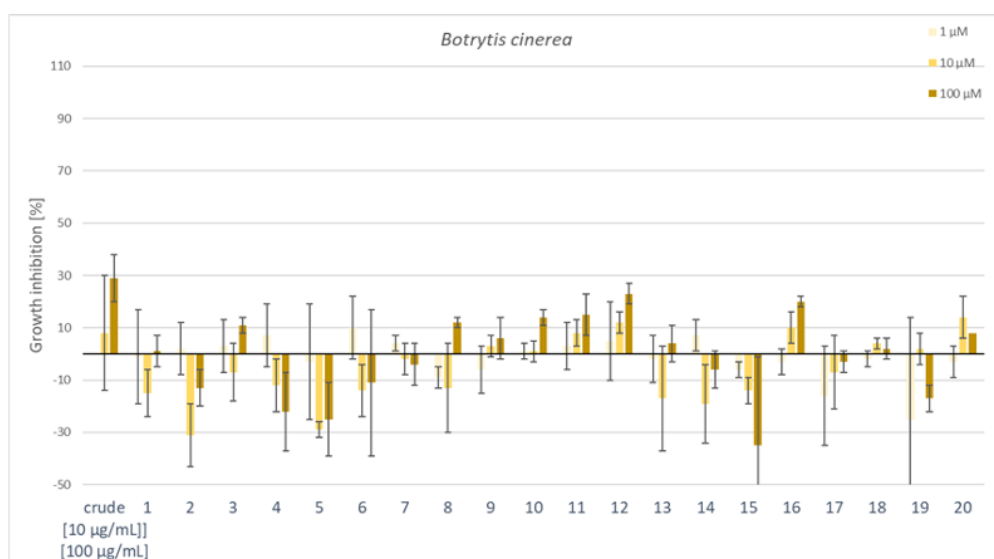


Figure S4 Antifungal assays of crude methanolic extract of *T. dhofarica* and constituents and artifacts (1-20) against *B. cinerea*

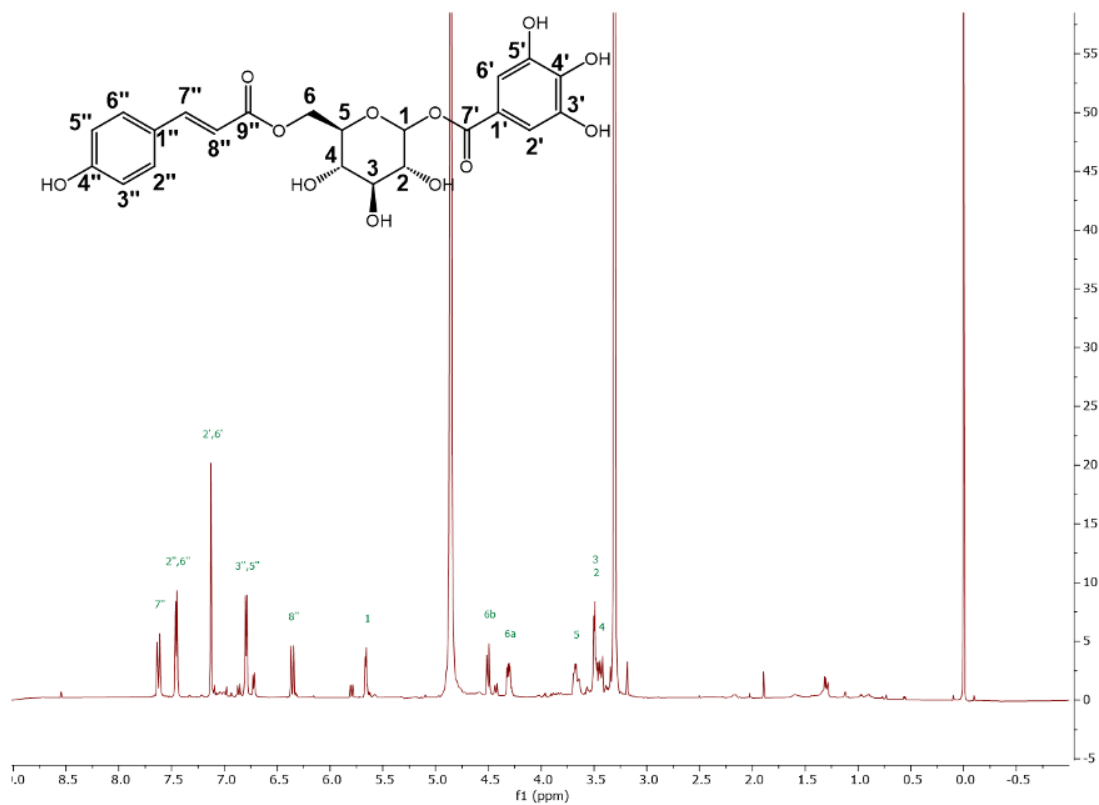


Figure S5 ^1H spectrum of compound **1**, MeOD, 25°C, 600 MHz, 40 scans

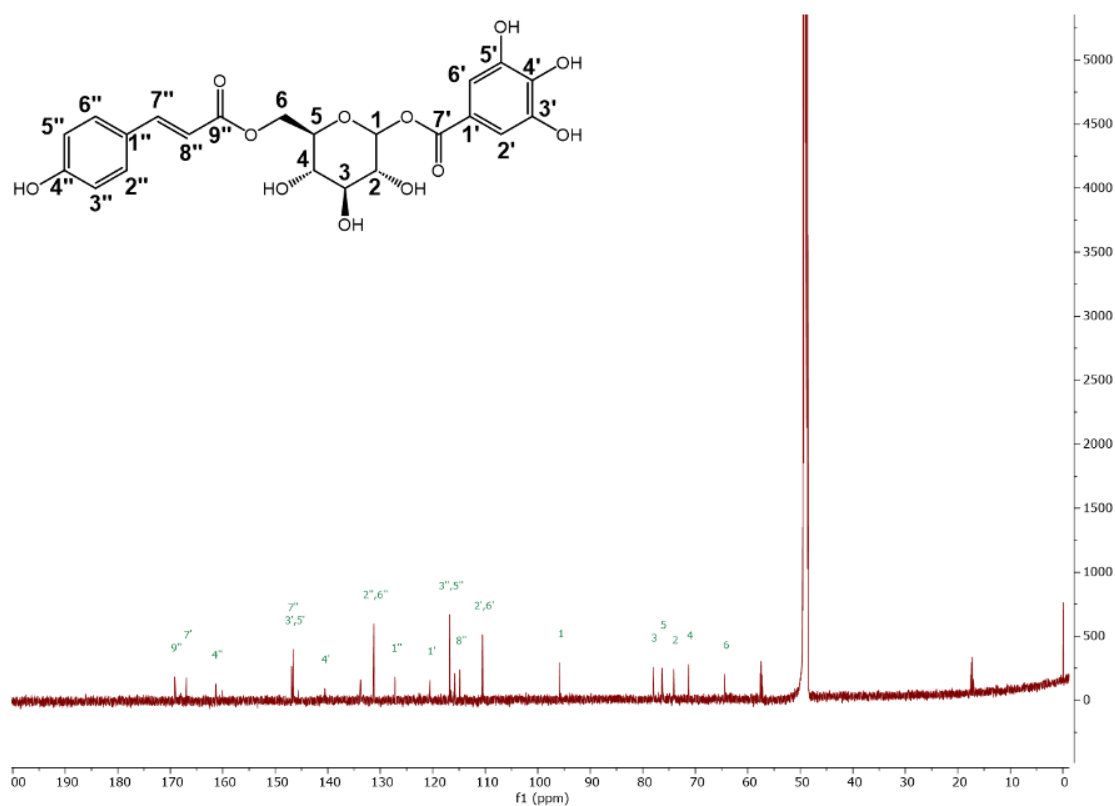


Figure S6 ^{13}C spectrum of compound **1**, MeOD, 25°C, 150 MHz, 25,000 scans

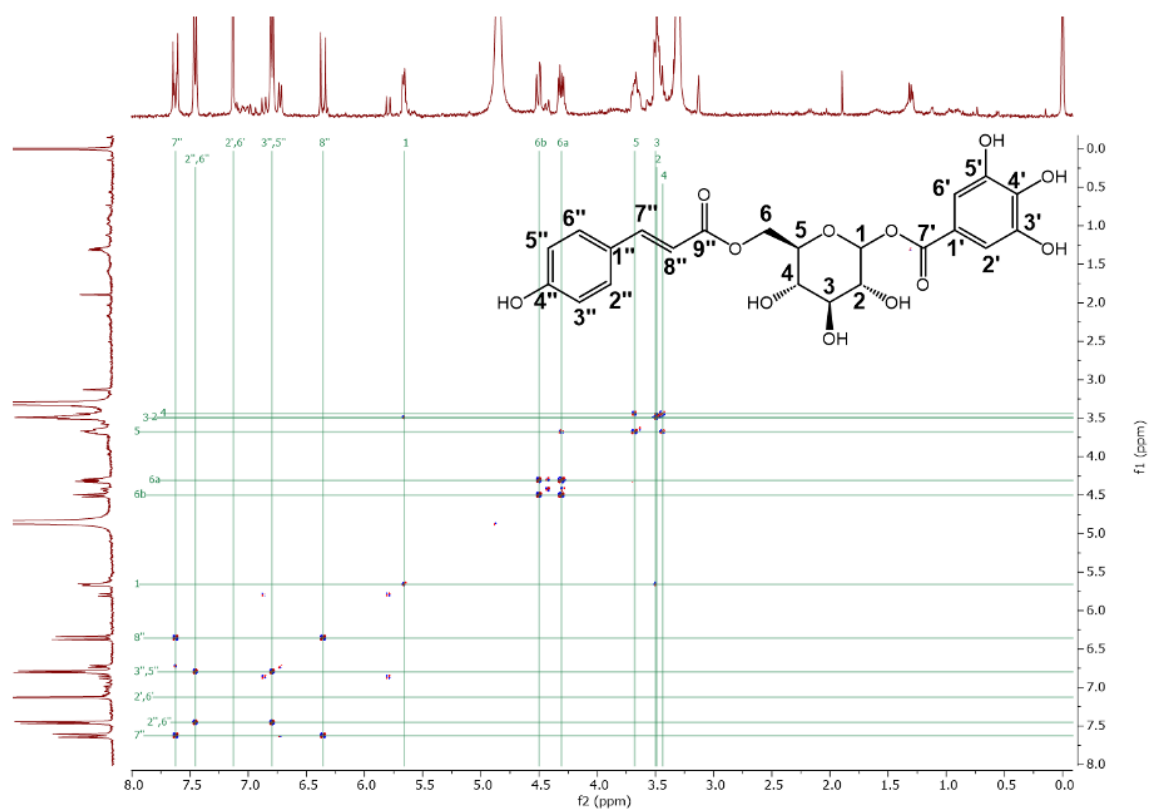


Figure S7 COSY spectrum of compound **1**, MeOD, 25°C, 600 MHz/600 MHz, 25 scans

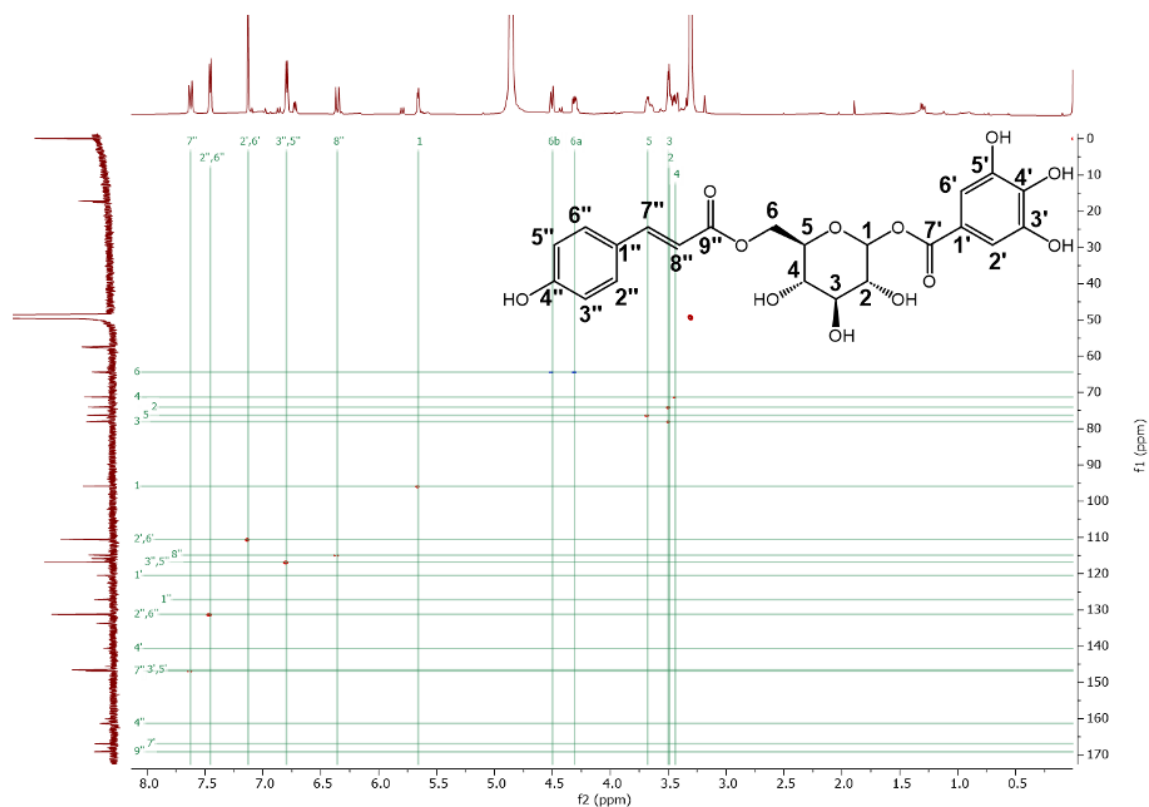


Figure S8 HSQC spectrum of compound **1**, MeOD, 25°C, 600 MHz/150 MHz, 32 scans

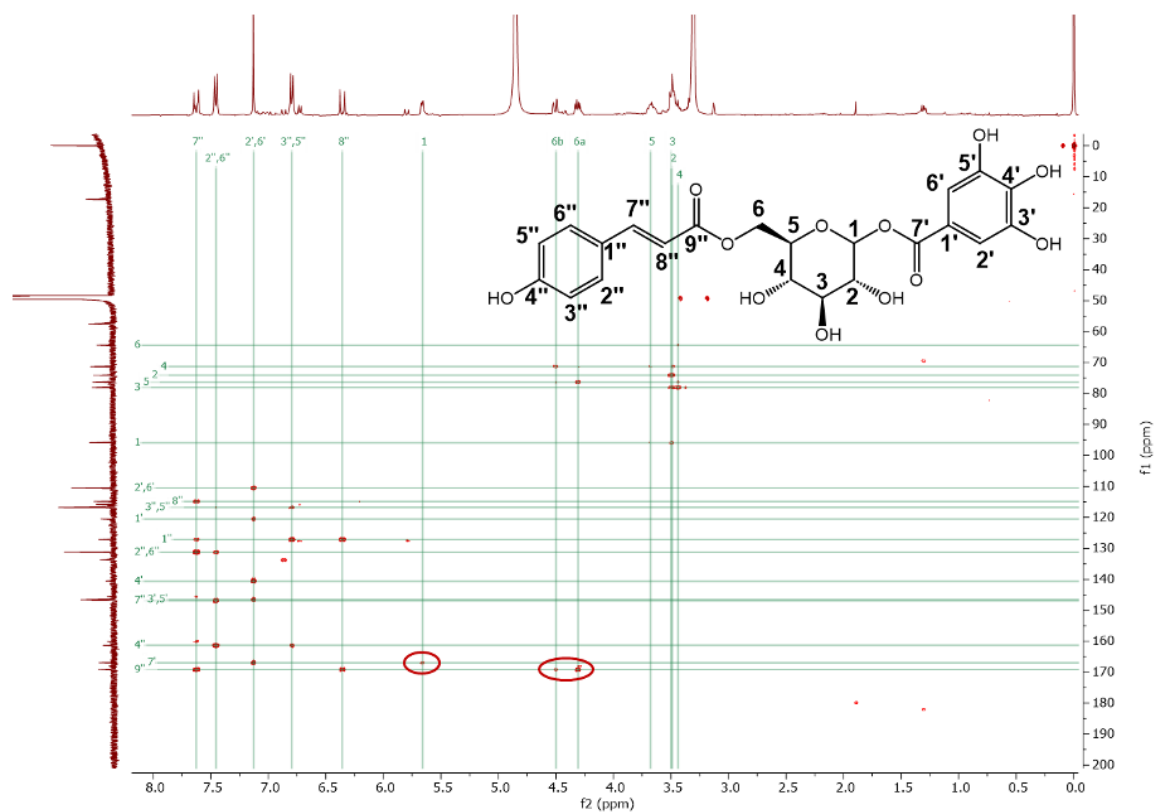


Figure S9 HMBC spectrum of compound **1**, MeOD, 25°C, 600 MHz/150 MHz, 80 scans, two red rings mark the crucial correlations for the connection pattern of H-1 and H6a+ H-6b

Full spectroscopic data set of compounds 1-20

1-*O*-Galloyl-6-*O*-*trans*-*p*-coumaroyl -D-glucopyranose (**1**): white solid; ^1H NMR (600 MHz, Methanol- d_4) δ 7.63 (1H, *d*, J = 15.7 Hz, H-7''), 7.45 (2H, *d*, J = 8.5, H-2'' + H-6''), 7.13 (2H, *s*, H-2' + H-6'), 6.80 (2H, *d*, J = 8.5 Hz, H-3'' + H-5''), 6.36 (1H, *d*, J = 15.7 Hz, H-8''), 5.66 (1H, *d*, J = 7.7, H-1 β), 5.66 (1H, *d*, J = 3.3, H-1 β), 4.50 (1H, *d*, J = 12.0 Hz, H-6a), 4.31 (1H, *dd*, J = 12.0, 5.6 Hz, H-6b), 3.68 (1H, *m*, H-5), 3.51-3.40 (3H, *m*, H-2 + H-3 + H-4); ^{13}C NMR (150 MHz, Methanol- d_4) δ 169.1 (C, C-9''), 166.9 (C, C-7'), 161.3 (C, C-4''), 146.9 (CH, C-7''), 146.6 (2C, C-3' + C-5'), 140.7 (C, C-4'), 131.2 (2CH, C-2'' + C-6''), 127.2 (C, C-1''), 120.5 (C, C-1'), 116.8 (2CH, C-3'' + C-5''), 114.9 (CH, C-8''), 110.5 (2CH, C-2' + C-6'), 95.9 (CH, C-1), 78.1 (CH, C-3), 76.3 (CH, C-5), 74.1 (CH, C-2), 71.3 (CH, C-4), 64.4 (CH₂, C-6); HR-ESI-MS (TOF) m/z [M-H]⁻ 477.1030 (calc for C₂₂H₂₂O₁₂⁻, 477.1033); MS²-fragmentation (CE = -40 V) m/z 477 (5), 313 (5), 265 (45), 235 (10), 211 (13), 205 (48), 177 (7), 169 (100), 163 (53), 161 (16), 151 (20), 145 (21), 125 (32), 123 (27), 119 (17). MS-data correspond to literature [17].

p-Hydroxybenzaldehyde (**2**): pale yellow solid; ^1H NMR (500 MHz, DMSO- d_6) δ 9.79 (1H, *s*, H-7), 7.76 (2H, *d*, J = 8.3 Hz, H-2 + H-6), 6.93 (2H, *d*, J = 8.3 Hz, H-3 + H-5); ^{13}C NMR (obtained from HSQC and HMBC, DMSO- d_6) δ 190.6 (CH, C-7), 163.4 (C, C-4), 132.1 (2CH, C-2 + C-6), 128.4 (C, C-1), 115.9 (2CH, C-3 + C-5); HR-ESI-MS (TOF) m/z [M-H]⁻ 121.0287 (calc for C₇H₅O₂⁻, 121.0290); MS²-fragmentation (CE = -20 V) m/z 121 (86), 92 (100), 65 (3). Data correspond to literature [18, 19].

Protocatechuic acid (**3**): white amorphous powder; ^1H NMR (600 MHz, DMSO- d_6) δ 12.13 (1H, *brds*, 7-COOH), 9.34 (2H, *brds*, 3-OH + 4-OH), 7.33 (1H, *d*, J = 2.1 Hz, H-2), 7.28 (1H, *dd*, J = 8.2, 2.1 Hz, H-6), 6.78 (1H, *d*, J = 8.2 Hz, H-5); ^{13}C NMR (obtained from HSQC and HMBC, DMSO- d_6) δ 167.4 (C, C-7), 149.8 (C, C-4), 144.6 (C, C-3), 121.7 (C, C-6), 121.4 (CH, C-1), 116.4 (CH, C-2), 115.0 (CH, C-5); HR-ESI-MS (TOF) m/z [M-H]⁻ 153.0193 (calc for C₇H₅O₄⁻, 153.0188); MS²-fragmentation (CE = -30 V) m/z 153 (3), 109 (100), 108 (56), 91 (10), 81 (8), 65 (9). Data correspond to literature [20].

Gallic acid (**4**): white solid; ^1H NMR (400 MHz, DMSO- d_6) δ 6.86 (2H, *s*, H-2 + H-6); ^{13}C NMR (100 MHz, DMSO- d_6) δ 170.3 (C, C-7), 145.5 (2C, C-3 + C-5), 137.0 (C, C-4), 125.8 (C, C-1), 108.9 (2CH, C-2 + C-6); HR-ESI-MS (TOF) m/z [M-H]⁻ 169.0152 (calc for C₇H₅O₅⁻, 169.0137); MS²-fragmentation (CE = -50 V) m/z 125 (50), 124 (77), 107 (7), 97 (10), 81 (11), 79 (100), 69 (39), 67 (30), 53 (12), 51 (98), 45 (7), 43 (9), 41 (39). Data correspond to literature [21].

7-*O*-Methyl gallate (**5**): white amorphous solid; ^1H NMR (400 MHz, Methanol- d_4) δ 7.03 (2H, *s*, H-2 + H-6), 3.81 (3H, *s*, 7-OMe); ^{13}C NMR (obtained from HSQC and HMBC, Methanol- d_4) δ 169.2 (C, C-7), 146.7 (2C, C-3 + C-5), 140.1 (C, C-4), 121.0 (C, C-1), 110.1 (2CH, C-2 + C-6), 52.2 (CH₃, 7-OMe); HR-ESI-MS (TOF) m/z [M-H]⁻ 183.0296 (calc for C₈H₇O₅⁻, 183.0293); MS²-fragmentation (CE = -20 V) m/z 183 (100), 168 (13), 124 (88). Data correspond to literature [22,23].

trans-*p*-Coumaric acid (**6**): white solid; ^1H NMR (500 MHz, Methanol- d_4) δ 7.59 (1H, *d*, J = 15.9 Hz, H-7), 7.45 (2H, *d*, J = 8.6 Hz, H-2 + H-6), 6.80 (2H, *d*, J = 8.6 Hz, H-3 + H-5), 6.28 (1H, *d*, J = 15.9 Hz, H-8); ^{13}C NMR (126 MHz, Methanol- d_4) δ 171.1 (CH, C-9), 161.1 (C, C-4), 146.5 (CH, C-7), 131.1 (2CH, C-2 + C-6), 127.3 (C, C-1), 116.8 (2CH, C-3 + C-5), 115.8 (C, C-8); HR-ESI-MS (TOF) m/z [M-H]⁻ 163.0393 (calc for C₉H₇O₃⁻, 163.0395); MS²-fragmentation (CE = -45 V) m/z 119 (100), 117 (12), 93 (35), 91 (4), 65 (3). Data correspond to literature [24].

Chebolic acid (**7**): yellow solid; ^1H NMR (400 MHz, Methanol- d_4) δ 7.04 (1H, *s*, H-8), 5.23 (1H, *s*, H-3), 3.86 (1H, *d*, $J = 8.6$ Hz, H-4), 3.11 (1H, *td*, $J = 9.4, 4.4$ Hz, H-9), 2.87 (1H, *dd*, $J = 17.1, 10.4$ Hz, H-10a), 2.35 (1H, *dd*, $J = 17.1, 4.4$ Hz, H-10b); ^{13}C NMR (100 MHz, Methanol- d_4) δ 176.9 (C, C-13), 175.5 (C, C-11), 172.6 (C, C-12), 166.8 (C, C-1), 146.7 (C, C-7), 144.0 (C, C-5), 140.6 (C, C-6), 118.1 (C, C-4a), 116.3 (C, C-8a), 109.3 (CH, C-8), 79.0 (CH, C-3), 45.5 (CH, C-9), 37.4 (CH, C-4), 35.2 (CH₂, C-10). HR-ESI-MS (TOF) m/z $[\text{M}-\text{H}]^-$ 355.0302 (calc for C₁₄H₁₂O₁₁⁻, 355.0301); MS²-fragmentation (CE = -45 V) m/z 355 (30), 337 (100), 249 (28), 205 (43), 193 (37), 187 (5), 179 (12), 163 (22), 161 (14), 149 (10), 135 (5). Data correspond to literature [25].

12-*O*-Methyl chebolic acid (**8**): yellow solid; ^1H NMR (600 MHz, Methanol- d_4) δ 7.04 (1H, *s*, H-8), 5.34 (1H, *s*, H-3), 3.84 (1H, *d*, $J = 9.1$ Hz, H-4), 3.62 (3H, *s*, H-12OMe), 3.12 (1H, *td*, $J = 9.6, 4.4$ Hz, H-9), 2.87 (1H, *dd*, $J = 17.1, 10.4$ Hz, H-10a), 2.35 (1H, *dd*, $J = 17.1, 4.4$ Hz, H-10b); ^{13}C NMR (150 MHz, Methanol- d_4) δ 176.7 (C, C-13), 175.3 (C, C-11), 171.3 (C, C-12), 166.3 (C, C-1), 146.8 (C, C-7), 144.0 (C, C-5), 140.7 (C, C-6), 117.7 (C, C-4a), 115.9 (C, C-8a), 109.3 (CH, C-8), 78.7 (CH, C-3), 53.3 (CH₃, 12-OMe), 45.2 (CH, C-9), 37.2 (CH, C-4), 35.1 (CH₂, C-10); HR-ESI-MS (TOF) m/z $[\text{M}-\text{H}]^-$ 369.0554 (calc for C₁₅H₁₃O₁₁⁻, 369.0458); MS²-fragmentation (CE = -45 V) m/z 369 (3), 351 (83), 307 (12), 251 (49), 231 (100), 219 (7), 207 (25), 205 (18), 203 (83), 192 (11), 187 (16), 177 (19), 175 (29), 163 (11), 159 (15), 147 (13), 135 (10). Data correspond to literature [26].

11,12-*O*-Dimethyl chebolic acid (**9**): yellow solid; ^1H NMR (600 MHz, Methanol- d_4) δ 7.03 (1H, *s*, H-8), 5.34 (1H, *s*, H-3), 3.88 (1H, *d*, $J = 9.1$ Hz, H-4), 3.62 (3H, *s*, 12-OMe), 3.51 (3H, *s*, 11-OMe), 3.17 (1H, *td*, $J = 9.1, 5.6$ Hz, H-9), 2.81 (1H, *dd*, $J = 17.1, 8.8$ Hz, H-10a), 2.46 (1H, *dd*, $J = 17.1, 5.6$ Hz, H-10b); ^{13}C NMR (150 MHz, Methanol- d_4) δ 176.6 (C, C-13), 173.8 (C, C-11), 171.3 (C, C-12), 166.3 (C, C-1), 146.9 (C, C-7), 144.1 (C, C-5), 140.8 (C, C-6), 117.5 (C, C-4a), 116.2 (C, C-8a), 109.3 (CH, C-8), 78.9 (CH, C-3), 53.3 (CH₃, 12-OMe), 52.2 (CH₃, 11-OMe), 45.1 (CH, C-9), 37.1 (CH, C-4), 35.1 (CH₂, C-10); HR-ESI-MS (TOF) m/z $[\text{M}-\text{H}]^-$ 383.0613 (calc for C₁₆H₁₅O₁₁⁻, 383.0614); MS²-fragmentation (CE = -45 V) m/z 351 (100), 307 (6), 251 (29), 231 (63), 207 (12), 203 (48), 187 (7), 177 (9), 175 (12), 159 (6). Data correspond to literature [26,27].

12,13-*O*-Dimethyl chebolic acid (**10**): yellow solid; ^1H NMR (600 MHz, Methanol- d_4) δ 7.03 (1H, *s*, H-8), 5.27 (1H, *d*, $J = 1.1$ Hz, H-3), 3.88 (1H, *d*, $J = 7.2, 1.1$ Hz, H-4), 3.67 (3H, *s*, 13-OMe), 3.63 (3H, *s*, 12-OMe), 3.17 (1H, *td*, $J = 9.1, 5.6$ Hz, H-9), 2.81 (1H, *dd*, $J = 17.1, 8.8$ Hz, H-10a), 2.46 (1H, *dd*, $J = 17.1, 5.6$ Hz, H-10b); ^{13}C NMR (150 MHz, Methanol- d_4) δ 175.22 (C, C-13), 175.18 (C, C-11), 171.3 (C, C-12), 166.2 (C, C-1), 146.9 (C, C-7), 143.9 (C, C-5), 140.9 (C, C-6), 117.6 (C, C-4a), 116.1 (C, C-8a), 109.1 (CH, C-8), 78.9 (CH, C-3), 53.4 (CH₃, 12-OMe), 52.8 (CH₃, 13-OMe), 45.3 (CH, C-9), 37.4 (CH, C-4), 35.0 (CH₂, C-10); HR-ESI-MS (TOF) m/z $[\text{M}-\text{H}]^-$ 383.0610 (calc for C₁₆H₁₅O₁₁⁻, 383.0614); MS²-fragmentation (CE = -45 V) m/z 351 (90), 307 (7), 263 (5), 251 (46), 231 (100), 207 (20), 203 (80), 192 (8), 187 (12), 177 (20), 175 (22), 163 (8), 159 (10), 147 (9). Data correspond to literature [26,27].

11-*O*-Methyl brevifolincarboxylate (**11**): white amorphous solid; ^1H NMR (500 MHz, Methanol- d_4) δ 7.35 (1H, *s*, H-7), 4.55 (1H, *dd*, $J = 7.7, 2.2$ Hz, H-8), 3.73 (3H, *s*, 11-OMe), 3.01 (1H, *dd*, $J = 18.9, 7.7$ Hz, H-9a), 2.51 (1H, *dd*, $J = 18.9, 2.2$ Hz, H-9b); ^{13}C NMR (obtained from HSQC and HMBC, Methanol- d_4) δ 195.1 (C, C-10), 175.1 (C, C-11), 162.6 (C, C-1), 151.3 (C, C-5), 147.4 (C, C-2), 144.9 (C, C-4), 142.6 (C, C-6), 141.0 (C, C-3), 116.1 (C, C-3a), 114.0 (C, C-7a), 109.2 (CH, C-7), 52.8 (CH₃,

11-OMe), 42.1 (CH, C-8), 38.4 (CH₂, C-9); HR-ESI-MS (TOF) m/z [M-H]⁻ 305.0325 (calc for C₁₄H₉O₈⁻, 305.0297); MS²-fragmentation (CE = -40 V) m/z 273 (12), 245 (53), 229 (5), 217 (100), 201 (9), 189 (23), 173 (9), 161 (16), 145 (13), 133 (10), 117 (5), 105 (2). Data correspond to literature [28,29].

Ellagic acid (**12**): yellow solid; ¹H NMR (500 MHz, DMSO-*d*₆) δ 7.31 (2H, *s*, H-5 + H-5'); ¹³C NMR (obtained from HSQC and HMBC, DMSO-*d*₆) δ 159.5 (2C, C-7 + C-7'), 148.6 (2C, C-4 + C-4'), 140.7 (2C, C-3 + C-3'), 113.0 (2C, C-6 + C-6'), 112.5 (2C, C-1 + C-1'), 108.1 (2CH, C-5 + C-5'); HR-ESI-MS (TOF) m/z [M-H]⁻ 300.9978 (calc for C₁₄H₅O₈, 300.9984). Data correspond to literature [30,31].

7''-O-Methyl flavogallionate (**13**): yellow amorphous solid; ¹H NMR (400 MHz, Methanol-*d*₄) δ 7.54 (1H, *s*, H-5), 7.22 (1H, *s*, H-6''), 3.50 (3H, *s*, 7''-OMe); ¹³C NMR (obtained from HSQC and HMBC, Methanol-*d*₄) δ 169.1 (C, C-7''), 161.9 (C, C-7), 149.4 (C, C-4), 145.4 (C, C-5''), 140.8 (C, C-3), 114.5 (C, C-1), 111.8 (CH, C-5), 111.4 (CH, C-6''), 52.2 (CH₃, 7''-OMe); HR-ESI-MS (TOF) m/z [M-H]⁻ 483.0197 (calc for C₂₂H₁₁O₁₃⁻, 483.0200); MS²-fragmentation (CE = -40 V) m/z 483 (2), 451 (100), 432 (15), 422 (6), 407 (8), 395 (8), 379 (7), 367 (7), 351 (5), 335 (3), 323 (3), 299 (3). Data correspond to literature [32].

6-*O*-*trans*-*p*-Coumaroyl-D-glucopyranose (**14**): white amorphous solid; ¹H NMR (600 MHz, Methanol-*d*₄) δ 7.63 (1H, *d*, *J* = 15.8 Hz, H-7'), 7.45 (2H, *d*, *J* = 8.3 Hz, H-2' + H-6'), 6.80 (2H, *d*, *J* = 8.3 Hz, H-3' + H-5'), 6.33 (1H, *d*, *J* = 15.8 Hz, H-8'), 5.10 (1H, *d*, *J* = 3.9 Hz, H-1α), 4.50 (H, *d*, *J* = 8.1 Hz, H-1β), 4.46 (1H, *m*, H-6a), 4.30 (1H, *dd*, *J* = 12.0, 5.9 Hz, H-6b), 3.54 (1H, *m*, H-5), 3.40 – 3.31 (3H, *m*, H-2 + H-3 + H-4); ¹³C NMR (obtained from HSQC and HMBC, Methanol-*d*₄) δ 169.1 (C, C-9'), 161.1 (C, C-4'), 146.8 (CH, C-7'), 131.2 (2CH, C-2' + C-6'), 127.3 (C, C-1), 116.9 (2CH, C-3', C-5'), 114.9 (CH, C-8), 98.4 (CH, C-1β), 94.1 (CH, C-1α), 77.9 (CH, C-3), 75.4 (CH, C-5), 73.8 (CH, C-2), 71.9 (CH, C-4), 64.8 (CH₂, C-6); HR-ESI-MS (TOF) m/z [M-H]⁻ 325.0936 (calc for C₁₅H₁₇O₈⁻, 325.0923); MS²-fragmentation (CE = -20 V) m/z 325 (28), 307 (5), 265 (16), 217 (6), 204 (20), 187 (100), 163 (48), 161 (7), 145 (100), 119 (10), 113 (10), 89 (4). Data correspond to literature [33].

1-*O*-Galloyl-D-glucose (**15**): white solid; ¹H NMR (400 MHz, Methanol-*d*₄) δ 7.13 (2H, *s*, H-2' + H-6'), 5.65 (1H, *d*, *J* = 8.0 Hz, H-1β), 5.65 (1H, *d*, *J* = 3.1 Hz, H-1α), 3.85 (1H, *dd*, *J* = 12.1, 1.8 Hz, H-6a), 3.70 (1H, *dd*, *J* = 12.1, 4.5 Hz, H-6b), 3.49 – 3.43 (2H, *overlaid m*, H-2 + H-5), 3.42 – 3.37 (2H, *overlaid m*, H-3 + H-4); ¹³C NMR (obtained from HSQC and HMBC, Methanol-*d*₄) δ 166.6 (C, C-7'), 145.9 (2C, C-3' + C-5'), 139.8 (C, C-4'), 120.2 (C, C-1'), 109.8 (2CH, C-2' + C-6'), 95.6 (CH, C-1), 78.4 (CH, C-3), 77.7 (CH, C-5), 73.7 (CH, C-2), 70.5 (CH, C-4), 61.9 (CH₂, C-6); HR-ESI-MS (TOF) m/z [M-H]⁻ 331.0640 (calc for C₁₃H₁₅O₁₀⁻, 331.0665); MS²-fragmentation (CE = -50 V) m/z 331 (100), 271 (10), 211 (16), 169 (58), 151 (15), 125 (17), 123 (21). Data correspond to literature [34].

3,5-Di-*O*-galloylshikimic acid (**16**): whitish solid; ¹H NMR (600 MHz, Methanol-*d*₄) δ 7.13 (2H, *s*, H-2' + H-6'), 7.08 (2H, *s*, H-2'' + H-6''), 6.73 (1H, *pst*, *J* = 1.8 Hz, H-2), 5.76 (1H, *tt*, *J* = 3.7, 1.8 Hz, H-3), 5.42 (1H, *dt*, *J* = 7.4, 5.1 Hz, H-5), 4.23 (1H, *dd*, *J* = 7.4, 4.0 Hz, H-4), 2.98 (1H, *ddt*, *J* = 18.6, 5.1, 2.0 Hz, H-6a), 2.48 (1H, *ddt*, *J* = 18.6, 5.1, 1.7 Hz, H-6b); ¹³C NMR (obtained from HSQC and HMBC, Methanol-*d*₄) δ 167.5 (C, C-7'), 167.4 (C, C-7''), 146.3 (2C, C-3'' + C-5''), 146.2 (2C, C-2' + C-5'), 139.7 (C, C-4'), 139.6 (C, C-4''), 135.2 (C, C-1), 131.6 (CH, C-2), 121.2 (C, C-1'), 121.0 (C, C-1''), 110.2 (2CH, C-2' + C-6'), 110.1 (2CH, C-2'' + C-6''), 71.6 (CH, C-5), 70.8 (CH, C-3), 68.1 (CH, C-3), 29.6 (CH₂, C-6); HR-ESI-MS (TOF) m/z [M-H]⁻ 477.0647 (calc for C₂₁H₁₇O₁₃⁻, 477.0675); MS²-

fragmentation (CE = -45 V) m/z 477 (100), 307 (12), 289 (39), 263 (23), 169 (81), 137 (45), 125 (48), 124 (17), 93 (20). Data correspond to literature [35].

Chebularin (**17**): brown amorphous solid; ^1H NMR (600 MHz, Methanol- d_4) δ 7.45 (1H, *s*, H-2''), 7.13 (2H, *s*, H-2''' + H-6'''), 6.35 (1H, *d*, J = 2.8 Hz, H-1), 5.20 (1H, *dt*, J = 2.8, 1.8 Hz, H-2), 5.09 (1H, *dd*, J = 7.1, 1.5 Hz, H-3'), 4.80 (2H, *brs*, H-3 + H-4), 4.77 (1H, *d*, J = 7.1 Hz, H-2'), 4.31 (1H, *t*, J = 6.5 Hz, H-5), 4.06 (1H, *dd*, J = 11.2, 6.6 Hz, H-6a), 4.00 (1H, *dd*, J = 11.2, 6.5 Hz, H-6b), 3.81 (1H, *ddd*, J = 12.0, 3.3, 1.5 Hz, H-4'), 2.17 (1H, *dd*, J = 17.0, 3.3 Hz, H-5'a), 2.11 (1H, *dd*, J = 17.0, 12.0 Hz, H-5'b); ^{13}C NMR (obtained from HSQC and HMBC, Methanol- d_4) δ 175.1 (C, C-6'), 174.7 (C, C-7'), 170.8 (C, C-1'), 166.8 (C-7''), 166.4 (C, C-7'''), 147.4 (C, C-3''), 146.8 (2C, C-3''' + C-5'''), 141.5 (C, C-5''), 140.3 (C, C-4'''), 140.2 (C, C-4''), 120.7 (C, C-1'''), 119.5 (C, C-1''), 117.6 (CH, C-2''), 116.1 (C-6''), 110.4 (2CH, C-2''' + C-6'''), 93.2 (CH, C-1), 79.9 (CH, C-5), 74.3 (CH, C-2), 72.3 (CH, C-4), 67.3 (CH, C-2'), 63.8 (CH₂, C-6), 62.1 (CH, C-3), 41.8 (CH, C-3'), 40.2 (CH, C-4'), 31.0 (CH₂, C-5'); HR-ESI-MS (TOF) m/z [M-H]⁻ 651.0837 (calc for C₂₇H₂₃O₁₉⁻, 651.0834); MS²-fragmentation (CE = -45 V) m/z 651 (58), 633 (12), 481 (28), 463 (9), 453 (10), 437 (10), 49 (10), 381 (12), 331 (9), 319 (11), 293 (11), 275 (23), 247 (12), 231 (24), 205 (17), 203 (16), 193 (11), 175 (9), 169 (100), 125 (24). Data correspond to literature [36].

Chebularic acid (**18**): brown amorphous solid; ^1H NMR (500 MHz, Methanol- d_4) δ 7.48 (1H, *s*, H-2''), 7.07 (2H, *s*, H-2''' + H-6'''), 6.84 (1H, *s*, 3,6-HHDP-H-5), 6.63 (1H, *s*, 3,6-HHDP-H-5'), 6.50 (1H, *psd t*, J = 1.2 Hz, H-1), 5.82 (1H, *td*, J = 0.9, 2.3 Hz, H-3), 5.39 (1H, *brs*, H-2), 5.22 (1H, *psd d*, J = 3.2 Hz, H-4), 5.04 (1H, *dd*, J = 7.1, 1.4 Hz, H-3'), 4.90 (1H, *overlaid m*, H-6b), 4.83 (1H, *overlaid m*, H-5), 4.80 (1H, *d*, J = 7.1 Hz, H-2'), 4.37 (1H, *dd*, J = 10.4, 7.8 Hz, H-6a), 3.79 (1H, *dd*, J = 11.8, 3.7 Hz, H-4'), 2.19 (1H, *dd*, J = 17.0, 3.7 Hz, H-5'b), 2.11 (1H, *dd*, J = 17.0, 11.8 Hz, H-5'a); ^{13}C NMR (126 MHz, Methanol- d_4) δ 175.1 (C, C-6'), 174.4 (C, C-7'), 170.8 (C, C-1'), 170.1 (C, 3,6-HHDP-C-7'), 167.5 (C, 3,6-HHDP-C-7), 166.4 (C-7''), 166.3 (C, C-7'''), 147.4 (C, C-3''), 146.5 (2C, C-3''' + C-5'''), 146.1 (C, 3,6-HHDP-C-4'), 145.6 (C, 3,6-HHDP-C-4), 145.5 (C, 3,6-HHDP-C-2), 145.3 (C, 3,6-HHDP-C-2'), 141.4 (C, C-5''), 140.8 (C, C-4'''), 140.4 (C, C-4''), 138.7 (C, 3,6-HHDP-C-3), 137.6 (C, 3,6-HHDP-C-3'), 125.6 (C, 3,6-HHDP-C-6'), 124.5 (C, 3,6-HHDP-C-6), 120.1 (C, C-1'''), 119.0 (C, C-1''), 117.6 (1CH + 1C, C-2'' + 3,6-HHDP-C-1), 116.2 (C, C-3,6-HHDP-C-1'), 116.0 (C-6''), 110.9 (2CH, C-2''' + C-6'''), 110.4 (CH, 3,6-HHDP-C-5), 108.2 (CH, 3,6-HHDP-C-5'), 92.5 (CH, C-1), 74.3 (CH, C-5), 71.1 (CH, C-2), 67.0 (C, C-2'), 66.8 (CH, C-4), 64.7 (CH₂, C-6), 62.4 (CH, C-3), 41.7 (CH, C-3'), 40.0 (CH, C-4'), 30.6 (CH₂, C-5'); HR-ESI-MS (TOF) m/z [M-H]⁻ 953.0830 (calc for C₄₁H₂₉O₂₇⁻, 953.0896); MS²-fragmentation (CE = -50 V) m/z 953 (41), 935 (4), 783 (2), 633 (5), 615 (3), 481 (6), 463 (5), 337 (10), 319 (8), 301 (100), 275 (16), 249 (3), 231 (3), 205 (8), 169 (4). Data correspond to literature [36].

6'-O-Methyl-chebularic acid (**19**): brown amorphous solid; ^1H NMR (400 MHz, Methanol- d_4) δ 7.47 (1H, *s*, H-2''), 7.07 (2H, *s*, H-2''' + H-6'''), 6.84 (1H, *s*, 3,6-HHDP-H-5), 6.64 (1H, *s*, 3,6-HHDP-H-5'), 6.50 (1H, *brs*, H-1), 5.76 (1H, *td*, J = 0.9, 2.4 Hz, H-3), 5.39 (1H, *brs*, H-2), 5.23 (1H, *psd d*, J = 3.5 Hz, H-4), 5.06 (1H, *dd*, J = 7.2, 1.2 Hz, H-3'), 4.93 (1H, *d*, J = 10.7 Hz, H-6b), 4.83 (1H, *overlaid m*, H-5), 4.81 (1H, *d*, J = 7.2 Hz, H-2'), 4.37 (1H, *dd*, J = 10.7, 7.8 Hz, H-6a), 3.83 (1H, *ddd*, J = 11.6, 3.7, 1.2 Hz, H-4'), 3.58 (3H, *s*, H-6'OMe), 2.20 (1H, *dd*, J = 16.7, 3.9 Hz, H-5'b), 2.12 (1H, *dd*, J = 17.0, 11.6 Hz, H-5'a); ^{13}C NMR (100 MHz, Methanol- d_4) δ 174.3 (C, C-7'), 173.6 (C, C-7'), 170.6 (C, C-1'), 170.1 (C, 3,6-HHDP-C-7'), 167.5 (C, 3,6-HHDP-C-7), 166.3 (C-7''), 166.2 (C, C-7'''), 147.5 (C, C-

3''), 146.5 (2C, C-3''' + C-5'''), 146.2 (C, 3,6-HHDP-C-4'), 145.6 (C, 3,6-HHDP-C-4), 145.5 (C, 3,6-HHDP-C-2), 145.4 (C, 3,6-HHDP-C-2'), 141.4 (C, C-5''), 140.9 (C, C-4'''), 140.4 (C, C-4''), 138.7 (C, 3,6-HHDP-C-3), 137.6 (C, 3,6-HHDP-C-3'), 125.6 (C, 3,6-HHDP-C-6'), 124.5 (C, 3,6-HHDP-C-6), 120.1 (C, C-1'''), 119.0 (C, C-1''), 117.6 (1CH + 1C, C-2'' + 3,6-HHDP-C-1), 116.2 (C, C-3,6-HHDP-C-1'), 115.8 (C-6''), 110.9 (2CH, C-2''' + C-6'''), 110.5 (CH, 3,6-HHDP-C-5), 108.2 (CH, 3,6-HHDP-C-5'), 92.4 (CH, C-1), 74.1 (CH, C-5), 71.0 (CH, C-2), 67.0 (C, C-2'), 66.8 (CH, C-4), 64.7 (CH₂, C-6), 62.4 (CH, C-3), 52.5 (CH₃, C-6'OMe), 41.8 (CH, C-3'), 39.9 (CH, C-4'), 30.5 (CH₂, C-5'); HR-ESI-MS (TOF) m/z [M-H]⁻ 967.1026 (calc for C₄₂H₃₁O₂₇⁻, 953.1053); MS²-fragmentation (CE = -45 V) m/z 967 (100), 923 (18), 797 (5), 301 (62), 275 (10), 237 (7), 205 (8), 169 (5). Data correspond to literature [26].

Phyllanembilinin C (**20**): yellow solid; ¹H NMR (600 MHz, Methanol-*d*₄) δ 7.05 (2H, *s*, H-2''' + H-6'''), 7.01 (1H, *s*, H-2''), 6.81 (1H, *s*, 3,6-HHDP-H-5), 6.63 (1H, *s*, 3,6-HHDP-H-5'), 6.49 (1H, *s*, H-1), 5.93 (1H, *m*, H-3), 5.26 (1H, *brs*, H-2), 5.17 (1H, *d*, *J* = 3.5 Hz, H-4), 4.94 (1H, *q*, *J* = 10.6 Hz, H-6b), 4.80 (1H, *overlaid m*, H-5), 4.72 (1H, *d*, *J* = 2.2 Hz, H-3'), 4.34 (1H, *dd*, *J* = 10.6, 8.2 Hz, H-6a), 3.70 (1H, *dt*, *J* = 11.7, 2.2 Hz, H-4'), 2.67 (1H, *dd*, *J* = 17.4, 2.1 Hz, H-5'b), 1.93 (1H, *dd*, *J* = 17.4, 11.7 Hz, H-5'a); ¹³C NMR (obtained from HSQC and HMBC, Methanol-*d*₄) δ 176.4 (C, C-6'), 174.9 (C, C-7'), 174.8 (C, C-1'), 170.2 (C, 3,6-HHDP-C-7'), 167.7 (C, 3,6-HHDP-C-7), 166.5 (C, C-7''), 166.2 (C, C-7'''), 148.0 (C, C-5''), 147.8 (C, C-3''), 146.6 (2C, C-3''' + C-5'''), 146.3 + 146.0 (2C, 3,6-HHDP-C-2' + 3,6-HHDP-C-4'), 145.8 + 145.5 (2C, 3,6-HHDP-C-2 + 3,6-HHDP-C-4), 140.7 (C, C-4'''), 138.6 (C, 3,6-HHDP-C-3), 137.6 (C, 3,6-HHDP-C-3'), 136.1 (C, C-4''), 125.6 (C, 3,6-HHDP-C-6'), 124.7 (C, 3,6-HHDP-C-6), 122.2 (C, C-1''), 120.4 (C, C-1'''), 117.6 (C, 3,6-HHDP-C-1), 117.4 (C, C-6''), 116.4 (C, 3,6-HHDP-C-1'), 112.2 (CH, C-2''), 111.0 (2CH, C-2''' + C-6'''), 110.0 (CH, 3,6-HHDP-C-5), 108.2 (CH, 3,6-HHDP-C-5'), 93.0 (CH, C-1), 74.1 (CH, C-5), 70.1 (CH, C-2), 66.9 (CH, C-4), 64.9 (CH₂, C-6), 62.1 (CH, C-3), 50.1 (CH, C-3'), 42.6 (CH, C-4'), 31.6 (CH₂, C-5'); HR-ESI-MS (TOF) m/z [M-H]⁻ 969.0831 (calc for C₄₁H₂₉O₂₈⁻, 969.0845); MS²-fragmentation (CE = -45 V) m/z 969 (100), 925 (4), 711 (2), 633 (2), 463 (3), 301 (45), 275 (4), 247 (17), 203 (6), 175 (2). Data correspond to literature [37].

7.4 Supporting information of chapter 5

Supporting Information

Exploring *Hornstedtia scyphifera*: An extensive multimethod phytochemical investigation reveals the chemical composition and bioactive potential

Jonas Kappen^{a, b}, Andreea David^{a, b}, Klara Pieplow^{a, c}, Annika Wujtschik^{a, c}, Ismail Ware^d, Dipendu Dhar^a, Christoph Wagner^c, Mehdi D. Davari^a, Katrin Franke^{a, c, f*}, Ludger A. Wessjohann^{a, c, f*}

^a Department of Bioorganic Chemistry, Leibniz Institute of Plant Biochemistry (IPB), 06120 Halle (Saale), Germany

^b Department of Food Science, Faculty of Food Science and Technology, University of Agricultural Sciences and Veterinary Medicine of Cluj-Napoca, 400372 Cluj-Napoca, Romania

^c Institute of Chemistry, Martin Luther University Halle-Wittenberg, 06120 Halle (Saale), Germany

^d Biotechnology Research Institute, University Malaysia Sabah, Jalan UMS, Kota Kinabalu 88400, Sabah, Malaysia

^e German Centre for Integrative Biodiversity Research (iDiv) Halle-Jena-Leipzig, 04103 Leipzig, Germany

^f Institute of Biology/Geobotany and Botanical Garden, Martin Luther University Halle-Wittenberg, 06120 Halle (Saale), Germany

* Correspondence: Katrin Franke, kfranke@ipb-halle.de, Tel: +49-345-5582-1313 (K.F.)
Ludger Wessjohann, wessjohann@ipb-halle.de, Tel: +49-345-5582-1301 (L.A.W.)

Content	page
Tab. S1. HS-GCMS analysis of leaves	1
Tab. S2. GCMS analysis of essential oil and <i>n</i> -hexane-extract	2
Fig. S1. Screening for antibacterial and antifungal biological activities	4
Fig. S2. 1D and 2D NMR spectra of compound 1	5
Tab. S3. Dihedral angles between H-6 and its neighbouring protons in compound 1	8
Tab. S4. Crucial NOESY correlations and proton distances of compound 1	8
Tab. S5. CD calculations of compound 1	8
Fig. S3. 1D and 2D NMR spectra of compound 2	9
Fig. S4. Stereoisomers Y1-Y8 of compound 2	12
Tab. S6. MM2 calculations, crucial NOESY correlations and proton distances of compound 2	12
Tab. S7. CD calculations of compound 2	12
Tab. S8. Comparison of NMR data of compound 2 and anhuienosol	13
Fig. S5. CD spectrum and calculated spectra of stereoisomers of compound 3	14
Tab. S9. CD calculations of compound 3	14
Fig. S6. CD spectrum and calculated spectra of stereoisomers of compound 4	15

Tab. S10. CD calculations of compound 4	15
Fig. S7. CD spectrum and calculated spectra of stereoisomers of compound 5	16
Tab. S11. CD calculations of compound 5	16
Fig. S8. CD spectrum and calculated spectra of stereoisomers of compound 6	17
Tab. S12. CD calculations of compound 6	17
Fig. S9. CD spectrum and calculated spectra of stereoisomers of compound 8	18
Tab. S13. CD calculations of compound 8	18
Fig. S10. CD spectrum and calculated spectra of stereoisomers of compound 9	19
Tab. S14. CD calculations of compound 9	19
Spectroscopic data of isolated compounds 1-26	20
Fig. S11. Crystal of kumatakenin	24
Tab. S15. Crystal data and structure refinement for kumatakenin	24

Table S1. HS-GCMS analysis of compounds annotated from leaves of *H. scyphifera*

No	R _t (min)	Fragments (m/z)	Molecular formula	MW (g/mol)	Compound proposal	Similarity (NIST 17)	Area (%)
H1	6.60	41, 79, 93	C ₁₁ H ₁₆	148	exo-Tetracyclo[5.3.1.0(2,6),0(8,10)]undecane	87	0.28
H2	8.31	41, 77, 91, 93	C ₁₀ H ₁₆	136	Tricyclene	97	1.81
H3	8.52	53, 77, 93, 121	C ₁₀ H ₁₆	136	α -Thujene	96	0.80
H4	8.82	67, 93, 121	C ₁₀ H ₁₆	136	α -Pinene	97	45.32
H5	9.53	91, 119	C ₁₀ H ₁₆	136	Camphene	97	33.04
H6	9.72	43, 77, 93	C ₁₀ H ₁₄	134	Butylbenzene (1-Phenylbutane)	96	18.05
H7	10.66	41, 93, 121	C ₁₀ H ₁₆	136	Sabinene	95	0.34
H8	10.84	41, 77, 91, 191	C ₁₀ H ₁₆	136	β -Pinene	97	5.52
H9	11.49	41, 91	C ₁₀ H ₁₄	134	Cycloheptane	90	1.30
H10	12.24	65, 91, 119, 134	C ₁₀ H ₁₄	134	<i>p</i> -Mentha-1,5,8-triene	91	1.71
H11	13.20	43, 77, 93, 121, 136	C ₁₀ H ₁₄	134	<i>p</i> -Cymene	96	10.64
H12	14.94	43, 77, 79, 93, 137	C ₁₀ H ₁₆	136	γ -Terpinene	94	0.39
H13	15.57	65, 117, 132	C ₁₀ H ₁₈ O ₂	170	2-Hydroxy- α ,4-trimethyl-1-hydroxymethyl-3-cyclohexene	83	0.82
H14	16.54	41, 81, 93, 110	C ₁₀ H ₁₂	132	<i>p</i> -Cymenene	87	0.88
H15	17.87	67, 93, 108	C ₁₀ H ₁₈ O	154	Isothujol	84	0.45
H16	18.31	55, 67, 83, 95, 109	C ₁₀ H ₁₆ O	152	α -Campholenal	93	0.74
H17	18.78	55, 92, 119	C ₉ H ₁₄ O	138	(+)-Nopinone	96	0.61
H18	18.94	55, 69, 81, 95, 108	C ₁₀ H ₁₆ O	152	[1S-(1 α ,3 α ,5 α)]-6,6-dimethyl-2-methylene-bicyclo[3.1.1]heptan-3-ol	95	2.91
H19	19.20	53, 81, 108, 135	C ₁₀ H ₁₆ O	152	Camphor	97	10.33
H20	19.99	43, 65, 91, 135	C ₁₀ H ₁₄ O	150	Pinocarvone	93	2.15
H21	21.33	41, 79, 91, 107	C ₁₀ H ₁₄ O	150	<i>p</i> -Cymen-8-ol	94	0.72
H22	21.61	88, 91, 107, 135, 150	C ₁₀ H ₁₄ O	150	(1 <i>R</i>)-(-)-Myrtanal	97	1.85
H23	22.18	93, 105, 119, 161	C ₁₀ H ₁₄ O	150	Levoverbenone	96	8.18
H24	29.98	41, 79, 93	C ₁₅ H ₂₄	204	Copaene	95	0.73

Table S2. GCMS analysis of essential oil (EO) and *n*-hexane extracts of *H. scyphifera*

No	R _t (min)	Similarity (NIST17)	Compound proposal	MW (g/mol)	Molecular formula	Area%	
						EO	<i>n</i> -Hexane
G1	7.87	96	α -Pinene	136	C ₁₀ H ₁₆		1.49
G2	8.28	96	Camphene	136	C ₁₀ H ₁₆		4.23
G3	12.24	93	<i>L-trans</i> -Pinocarveol	152	C ₁₀ H ₁₆ O		1.56
G4	12.33	96	Camphor	152	C ₁₀ H ₁₆ O		3.95
G5	12.63	90	α -Pinocarvone	150	C ₁₀ H ₁₄ O		0.94
G 6	12.79	97	endo-Borneol	154	C ₁₀ H ₁₈ O		2.86
G 7	13.25	92	Myrtenal	150	C ₁₀ H ₁₄ O		0.79
G 8	13.44	97	<i>cis</i> -Verbenone	150	C ₁₀ H ₁₄ O		13.49
G 9	14.89	95	2-Camphanol acetate	196	C ₁₂ H ₂₀ O ₂	0.37	4.55
G10	19.16	86	β -Guaiene	204	C ₁₅ H ₂₄	0.11	
G11	19.24	97	β -Selinene	204	C ₁₅ H ₂₄	0.29	
G12	19.61	93	Dihydro- β -agarofuran	222	C ₁₅ H ₂₆ O	1.53	
G13	19.96	81	Aromadendrane-4,10-diol	238	C ₁₅ H ₂₆ O ₂	1.44	
G14	20.18	87	α -Dehydro-ar-himachalene	200	C ₁₅ H ₂₀	0.46	
G15	20.34	90	α -Calacorene	200	C ₁₅ H ₂₀	0.21	
G16	20.47	90	Elemol	222	C ₁₅ H ₂₆ O	0.46	
G17	20.81	91	<i>trans</i> -Dihydroagarofuran	222	C ₁₅ H ₂₆ O	14.91	1.47
G18	21.24	90	β -Caryophyllene epoxide	220	C ₁₅ H ₂₄ O	0.25	
G19	21.74	92	Ledol	222	C ₁₅ H ₂₆ O	0.38	
G20	21.84	85	Humulene epoxide	220	C ₁₅ H ₂₄ O	0.32	
G21	22.20	86	Di-epi-1,10-cubenol	222	C ₁₅ H ₂₆ O	0.30	
G22	22.29	96	γ -Eudesmol	222	C ₁₅ H ₂₆ O	1.24	
G23	22.53	82	α -epi-Muurolol	222	C ₁₅ H ₂₆ O	0.38	
G24	22.79	94	β -Eudesmol	222	C ₁₅ H ₂₆ O	2.28	
G25	23.00	87	Guai-1(10)-en-11-ol	222	C ₁₅ H ₂₆ O	0.85	
G26	23.16	96	Cadalene	198	C ₁₅ H ₁₈	3.26	
G27	23.21	80	Mustakone	218	C ₁₅ H ₂₂ O		2.49
G28	24.69	79	(7a-Isopropenyl-4,5-dimethyloctahydroinden-4-yl)-methanol	222	C ₁₅ H ₂₆ O	0.44	
G29	25.58	84	<i>cis</i> -Chrysanthemol acetate	194	C ₁₂ H ₁₈ O ₂	0.59	
G30	25.70	83	Iso-3-thujyl acetate	196	C ₁₂ H ₂₀ O ₂	2.78	
G31	25.85	92	Ambrial	234	C ₁₆ H ₂₆ O	2.90	
G32	26.01	82	1-Methyl-1-(4-methyl-3-cyclohexenyl)ethylphenyl-carbamate	273	C ₁₇ H ₂₃ NO ₂	7.05	
G33	26.30	81	3(7)-Carene, 4-hydroxy-methyl-, exo-	166	C ₁₁ H ₁₈ O	4.95	
G34	26.48	94	7,11,15-Trimethyl-3-methylenehexadecene	278	C ₂₀ H ₃₈		3.34
G35	26.56	94	2-Pentadecanone, 6,10,14-trimethyl-	268	C ₁₈ H ₃₆ O	4.15	
G36	26.80	81	α -Caryophyllene	204	C ₁₅ H ₂₄	6.77	
G37	26.90	96	Phthalic acid	278	C ₁₆ H ₂₂ O ₄	0.54	
G38	26.97	82	Neophytadiene	278	C ₂₀ H ₃₈		0.87
G39	27.07	78	β -Santalol	220	C ₁₅ H ₂₄ O	0.14	
G40	27.26	85	(1 <i>S</i> ,4 <i>R</i>)- <i>p</i> -Mentha-2,8-diene, 1-hydroperoxide	168	C ₁₀ H ₁₆ O ₂	0.90	
G41	27.39	80	α -Farnesene	204	C ₁₅ H ₂₄	2.4	
G42	27.62	84	Humulene monoxide	220	C ₁₅ H ₂₄ O	4.1	
G43	28.35	81	Δ - Guaiene	204	C ₁₅ H ₂₄	0.78	
G44	28.64	97	Isophytol	296	C ₂₀ H ₄₀ O	1.16	
G45	28.80	83	Phthalic acid	356	C ₂₂ H ₂₈ O ₄	1.22	
G46	28.97	92	Ascorbic acid 2,6-dihexadecanoate	652	C ₃₈ H ₆₈ O ₈	2.05	
G47	29.27	81	γ -Bicyclohomofarnesal	234	C ₁₆ H ₂₆ O	0.22	
G48	29.39	85	(<i>E</i>)-15,16-Dinorlabda-8(17),11-dien-13-one	260	C ₁₈ H ₂₈ O	3.49	
G49	29.52	84	Carvyl acetate	194	C ₁₂ H ₁₈ O ₂	0.62	
G50	29.97	83	Cyclopentanecarboxylic acid, 3-isopropylidene-, bornyl ester	290	C ₁₉ H ₃₀ O ₂	1.92	

G51	30.22	80	Eremophila-1,11-dien-9-one, 8- α -hydroxy-	234	C ₁₅ H ₂₂ O ₂	1.4	
G52	30.55	80	(3 <i>S</i> ,6 <i>R</i>)-3-Hydroperoxy-3-methyl-6-(prop-1-en-2-yl)cyclohexene	168	C ₁₀ H ₁₆ O ₂	0.31	
G53	30.70	81	<i>cis</i> -Verbenolacetate	194	C ₁₂ H ₁₈ O ₂	5.54	
G54	30.97	80	Bicyclo[2.2.2]oct-2-ene, 1,2,3,6-tetramethyl-	168	C ₁₀ H ₁₆ O ₂	0.88	
G55	31.25	81	Acorenone B	220	C ₁₅ H ₂₄ O	2.28	
G56	31.62	83	2-Hexyl-decanol	242	C ₁₆ H ₃₄ O	1.17	
G57	31.79	97	Phytol	296	C ₂₀ H ₄₀ O	5.91	
G58	32.39	86	Copalol	290	C ₂₀ H ₃₄ O	1.97	
G59	32.74	80	1,2-Ethanediol, 1,2-dimyrtenyl-	302	C ₂₀ H ₃₀ O ₂	1.55	
G60	35.84	94	4,8,12,16-Tetramethyl-heptadecan-4-olide	324	C ₂₁ H ₄₀ O ₂	0.76	
G61	36.04	84	(<i>E</i>)-Labda-8(17),12-diene-15,16-dial	302	C ₂₀ H ₃₀ O ₂		0.62
G62	38.77	97	Di- <i>n</i> -2-propylpentyl-phthalate	390	C ₂₄ H ₃₈ O ₄		5.97
G63	43.30	86	α -Tocospiro B	462	C ₂₉ H ₅₀ O ₄		1.74
G64	43.60	87	α -Tocospiro A	462	C ₂₉ H ₅₀ O ₄		2.74
G65	44.16	96	Hexatriacontane	506	C ₃₆ H ₇₄		9.65
G66	45.50	90	<i>n</i> -Dotriacontane	450	C ₃₂ H ₆₆		1.56
G67	46.35	81	3 β -Cholesta-4,6-dien-3-ol	384	C ₂₇ H ₄₄ O		1.66
G68	46.79	96	Dotriacontane	450	C ₃₂ H ₆₆		5.14
G69	48.75	81	Stigmasterol	412	C ₂₉ H ₄₈ O		3.98
G70	49.26	79	α -Cortolone	366	C ₂₁ H ₃₄ O ₅		3.28
G71	49.58	95	(3 β ,24 <i>S</i>)-Stigmast-5-en-3-ol	414	C ₂₉ H ₅₀ O		21.63

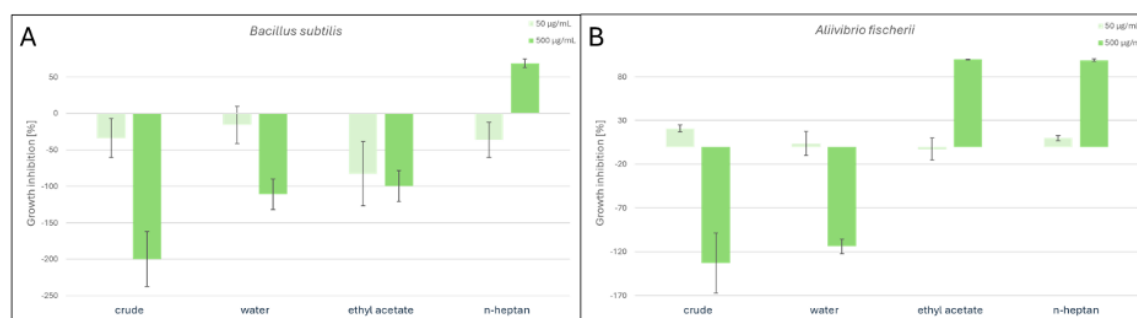


Figure S1.1. Antimicrobial activities of the crude extract and the fractions from the liquid-liquid partition; **A** against Gram-positive *B. subtilis*; **B** against Gram-negative *A. fischeri*

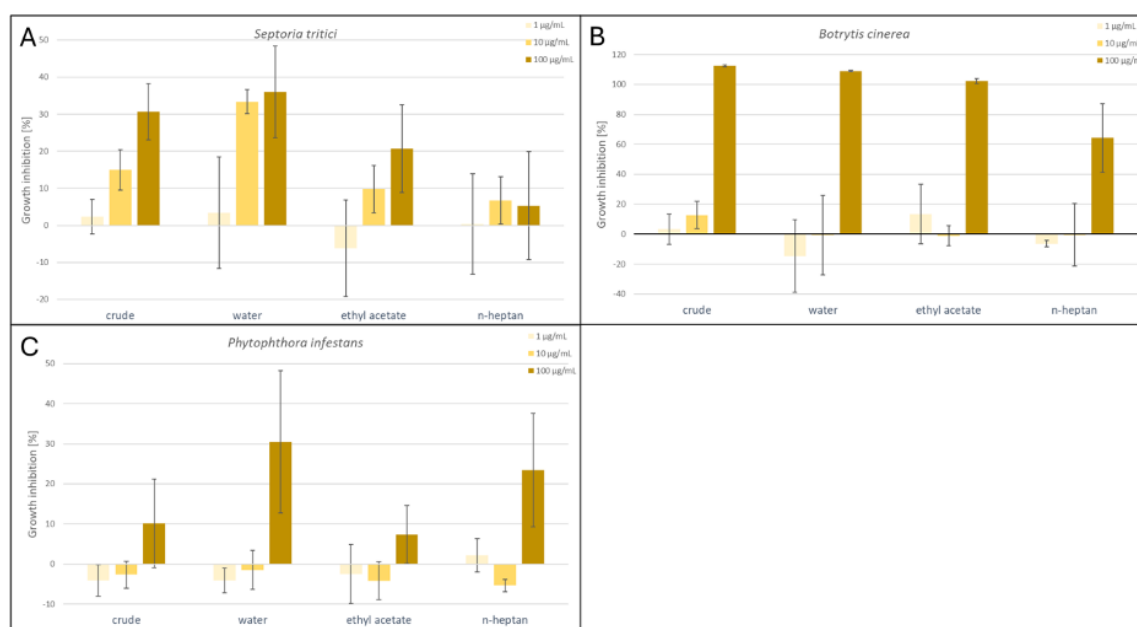


Figure S1.2. Antifungal activities of the crude extract and the fractions from the liquid-liquid partition; **A** against *Septoria tritici*, **B** against *Botrytis cinerea*, **C** against *Phytophthora infestans*

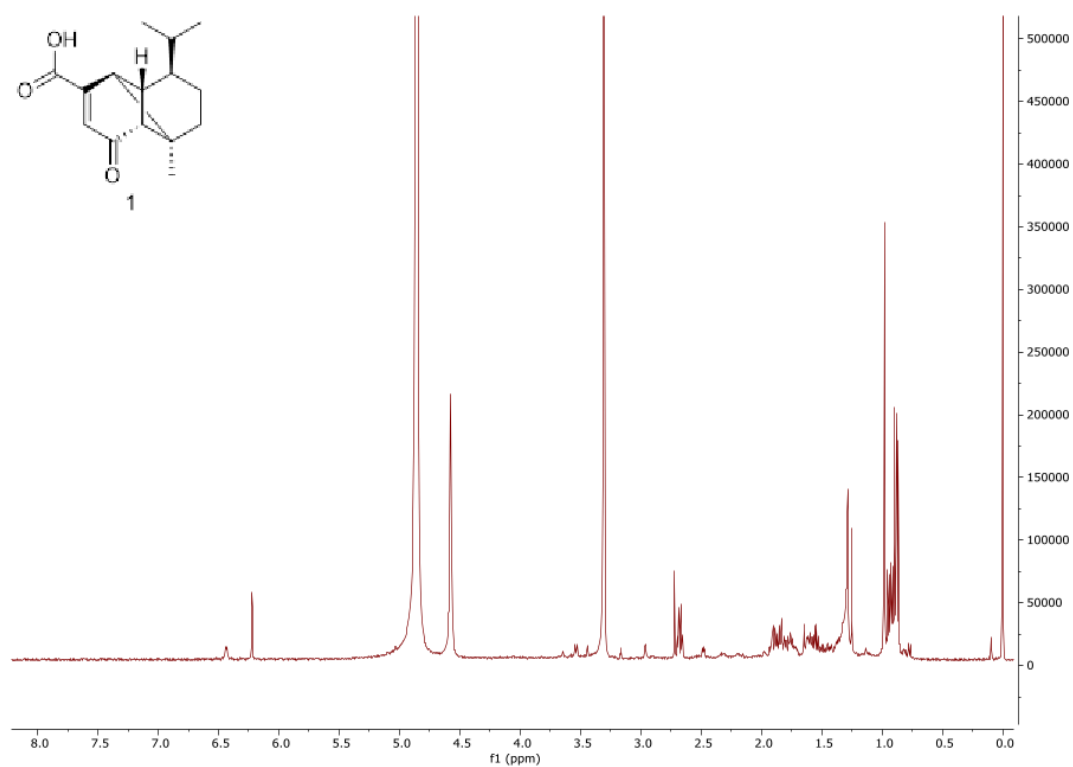


Figure S2.1. ¹H NMR spectrum of compound 1

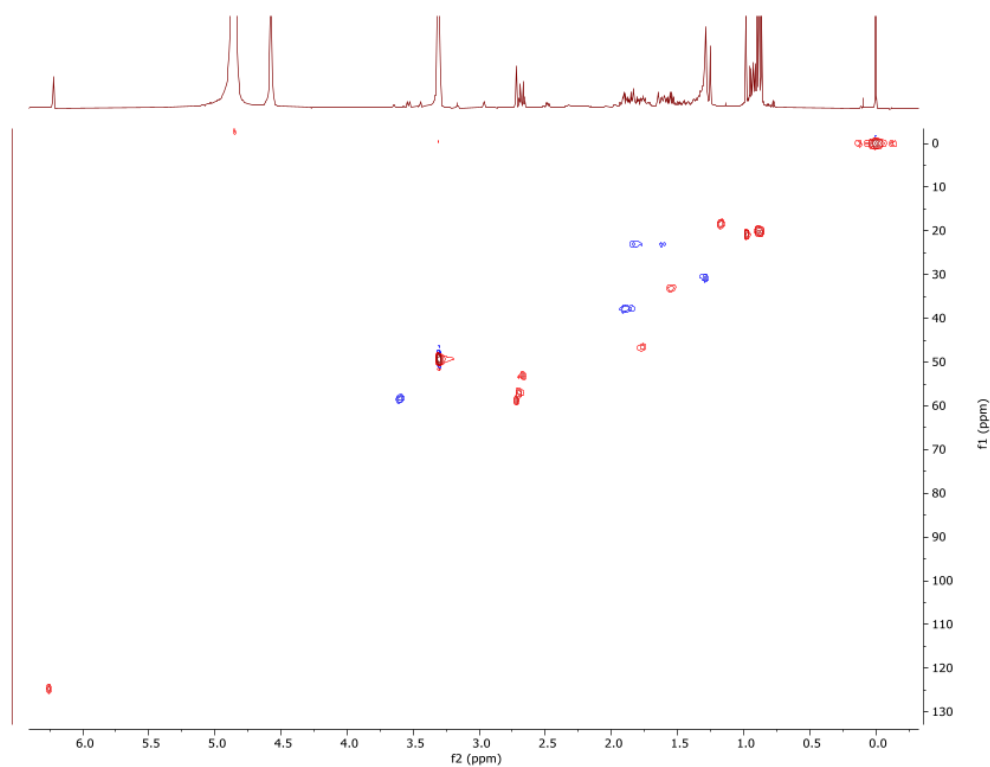


Figure S2.2. HSQC spectrum of compound 1

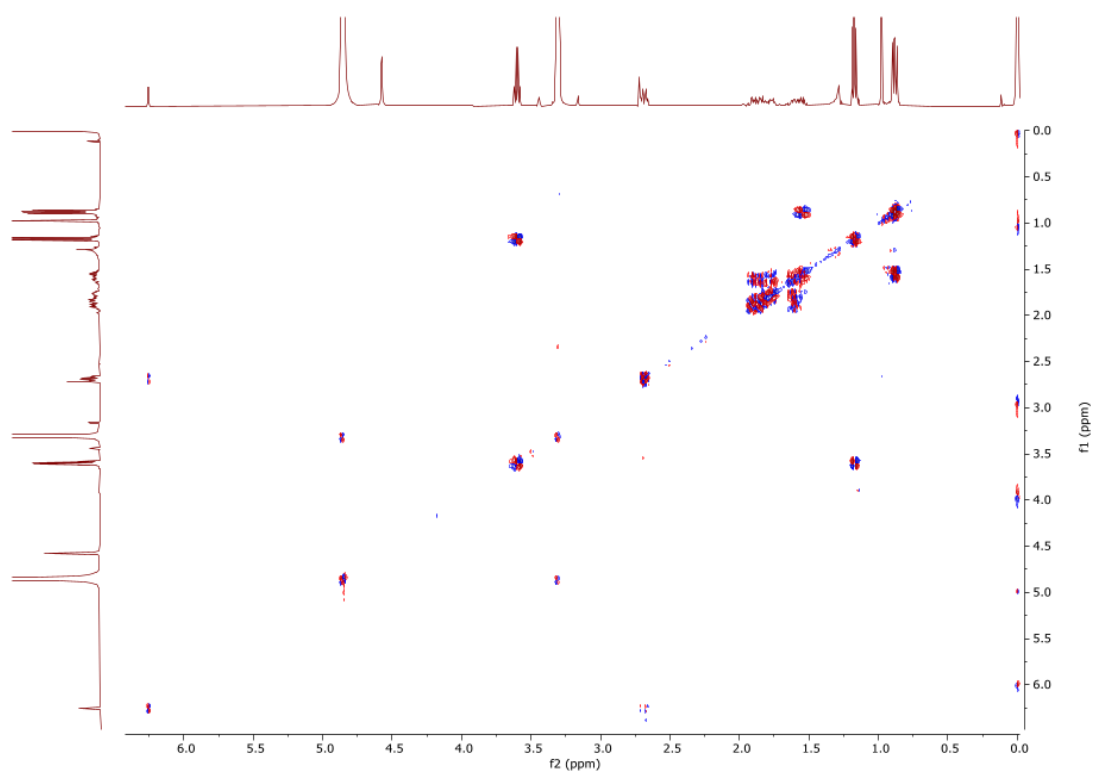


Figure S2.3. COSY spectrum of compound **1**

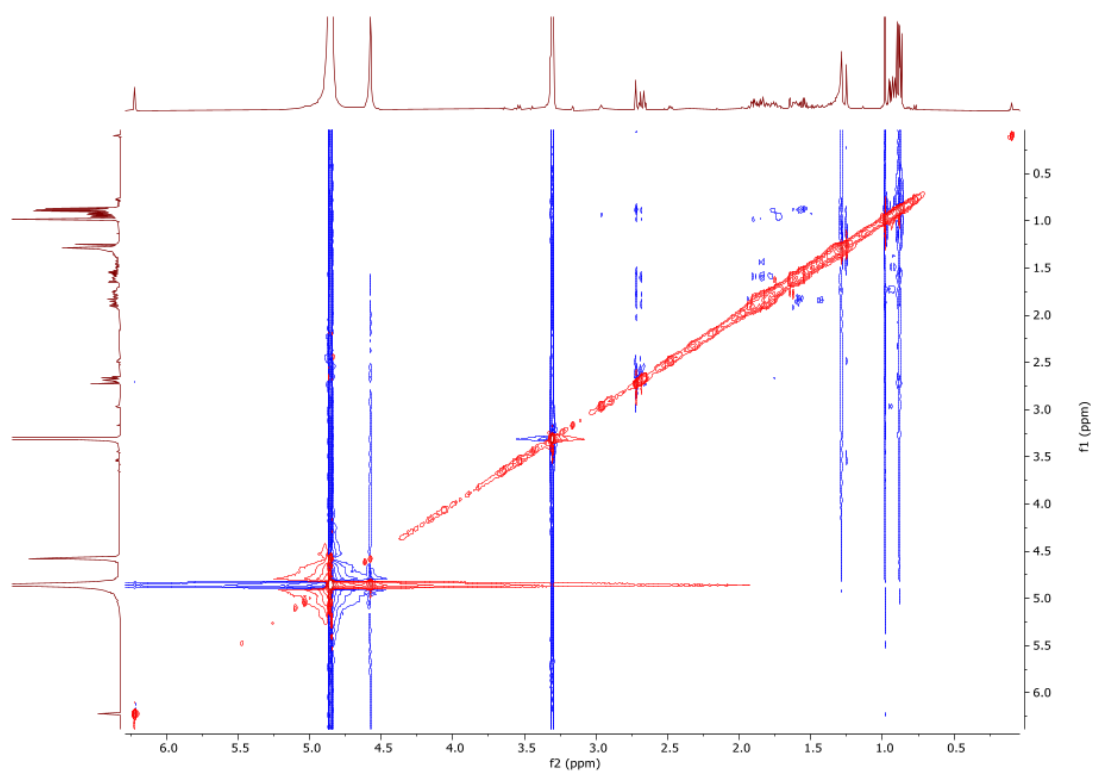


Figure S2.4. NOESY spectrum of compound **1**

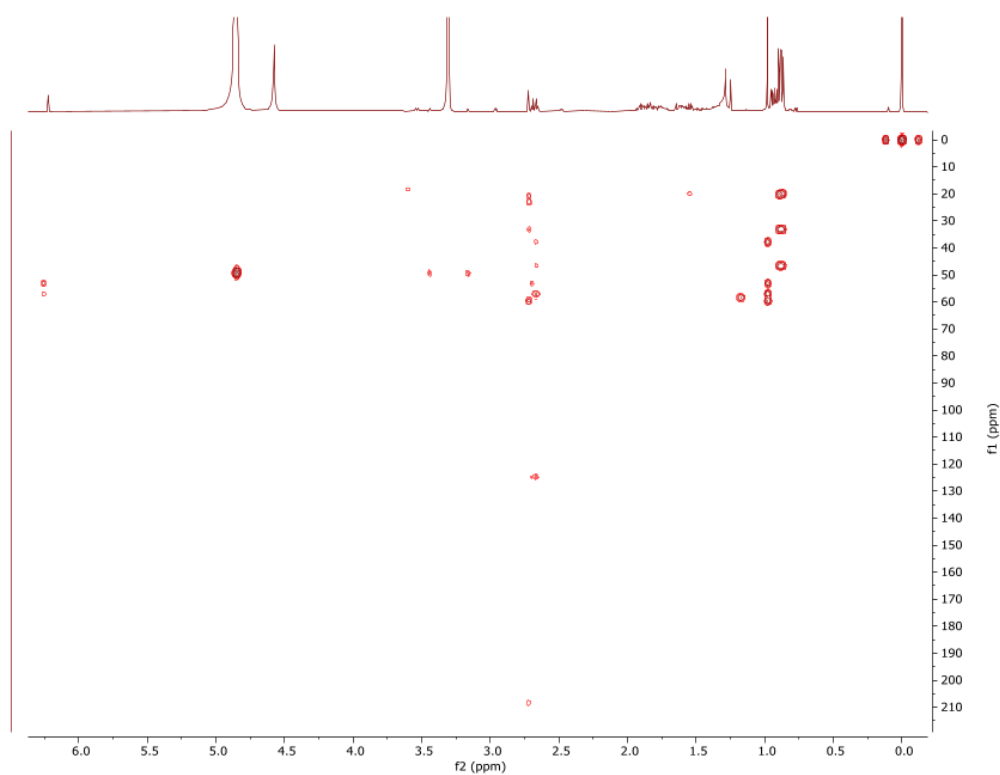


Figure S2.5. HMBC spectrum of compound **1**, 500 MHz, 128 scans

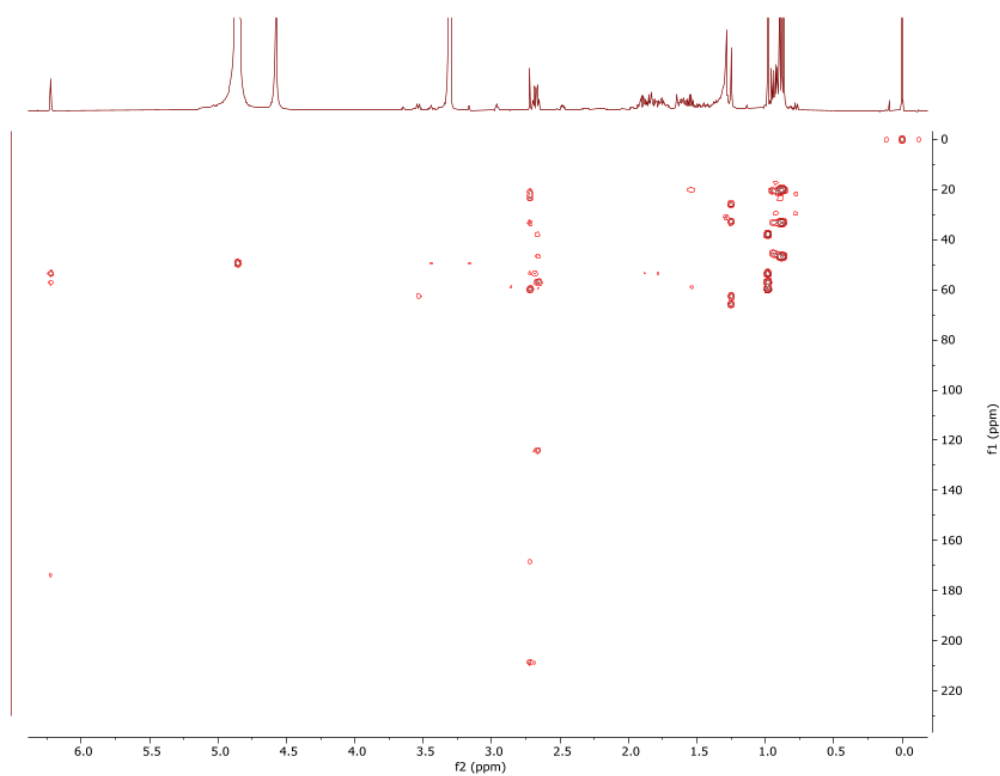


Figure S2.6. HMBC spectrum of compound **1**, 500 MHz, 160 scans

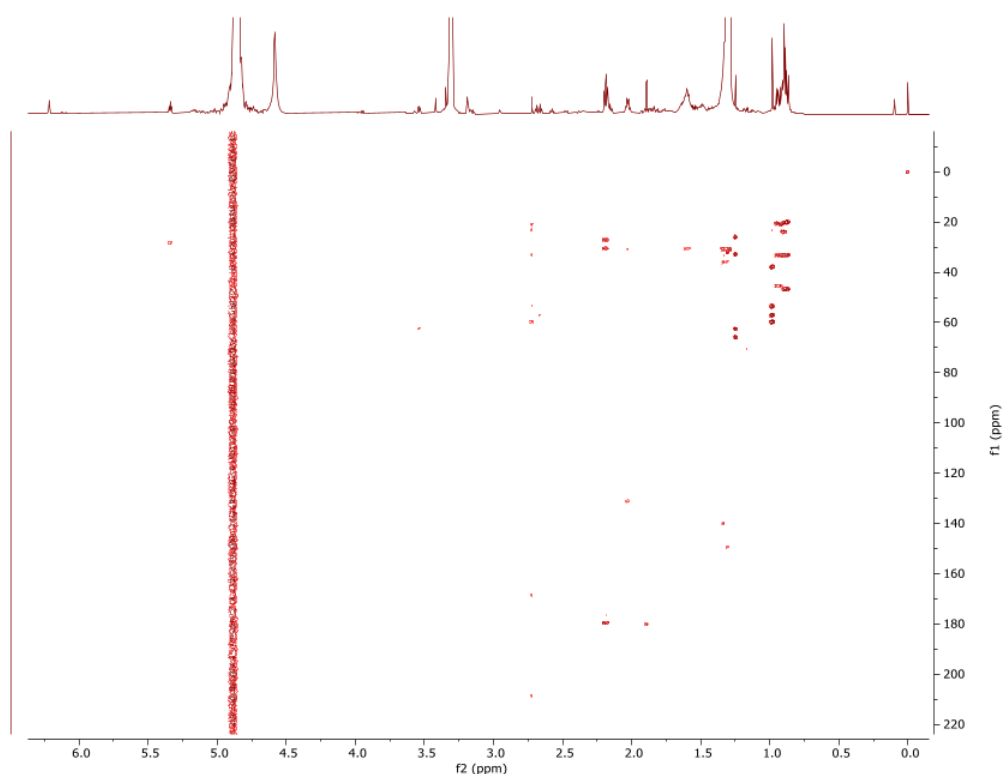


Figure S2.7. HMBC spectrum of compound **1**, 600 MHz, 160 scans

Table S3. Dihedral angles between H-6 and its neighbouring protons in stereoisomers of compound **1**

Dihedral angle	X1	X2	X3	X4
H1↔H6	94.1°	97.1°	−97.1°	−94.1°
Calc. J_{3HH}	0.92 Hz	1.06 Hz	1.06 Hz	0.92 Hz
H5↔H6	−97.6°	−94.5°	94.5°	97.6°
Calc. J_{3HH}	1.09 Hz	0.93 Hz	0.93 Hz	1.09 Hz
H7↔H6	−81.1°	80.8°	−80.8°	81.1
Calc. J_{3HH}	0.89 Hz	0.90 Hz	0.90 Hz	0.89 Hz

Angles obtained from Chem3D after MM2 calculation (minimize energy), J_{3HH} calculations obtained from <http://www.stenutz.eu/conf/haasnoot.php> (15.11.2024, 10:35 am)

Table S4. Crucial NOESY correlation and distances in stereoisomers of compound **1**

	X1 [Å]	X2 [Å]	X3 [Å]	X4 [Å]
H1↔H7	2.4	3.9	3.9	2.4
H1↔H12	4.9	2.6	2.6	4.9
H5↔H7	3.9	2.4	2.4	3.9
H5↔H9a	3.1	2.5	2.5	3.1
H6↔H11	2.5	2.5	2.5	2.5
H6↔H12	2.5	2.5	2.5	2.5

Table S5. CD calculations of compound **1**

Name	Configuration	Similarity Factor (S)	Sigma (eV)	Shift (nm)
X1	1 <i>S</i> ,5 <i>R</i> ,6 <i>R</i> ,7 <i>R</i> ,10 <i>S</i>	0.1522	0.29	−51
X2	1 <i>S</i> ,5 <i>R</i> ,6 <i>R</i> ,7 <i>S</i> ,10 <i>S</i>	0.7827	0.29	−51
X3	1 <i>R</i> ,5 <i>S</i> ,6 <i>S</i> ,7 <i>R</i> ,10 <i>R</i>	0.8798	0.29	−51
X4	1 <i>R</i> ,5 <i>S</i> ,6 <i>S</i> ,7 <i>S</i> ,10 <i>R</i>	0.1418	0.29	−51

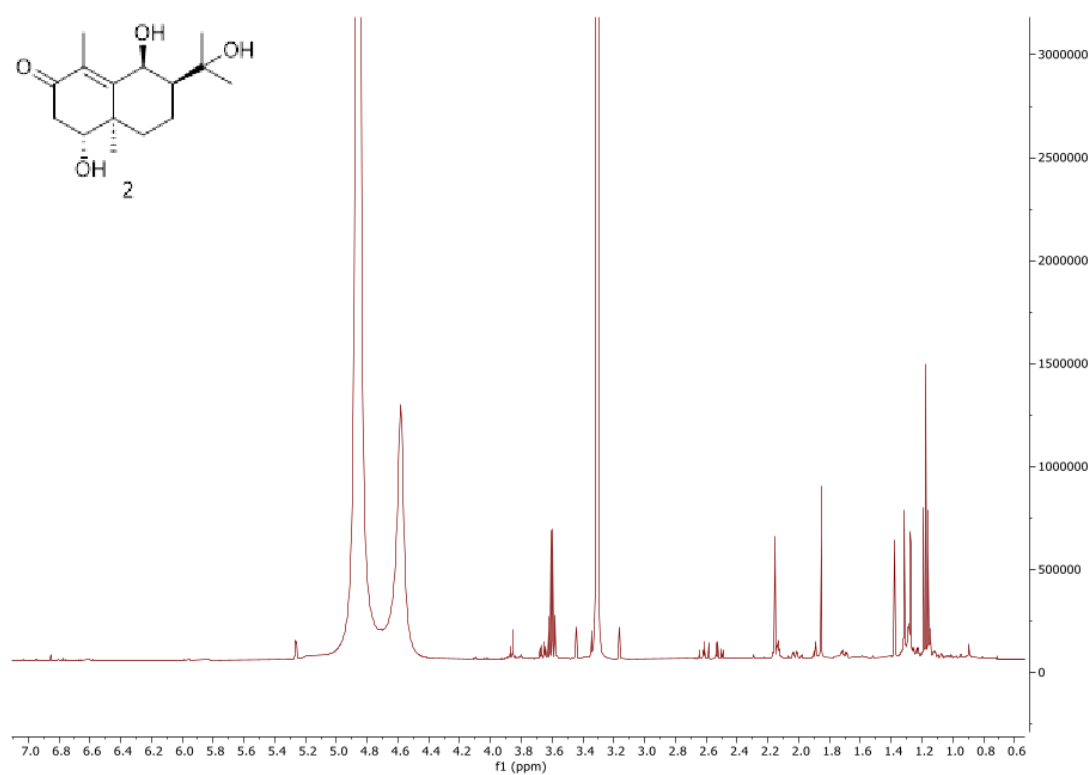


Figure S3.1. ^1H NMR spectrum of compound **2**

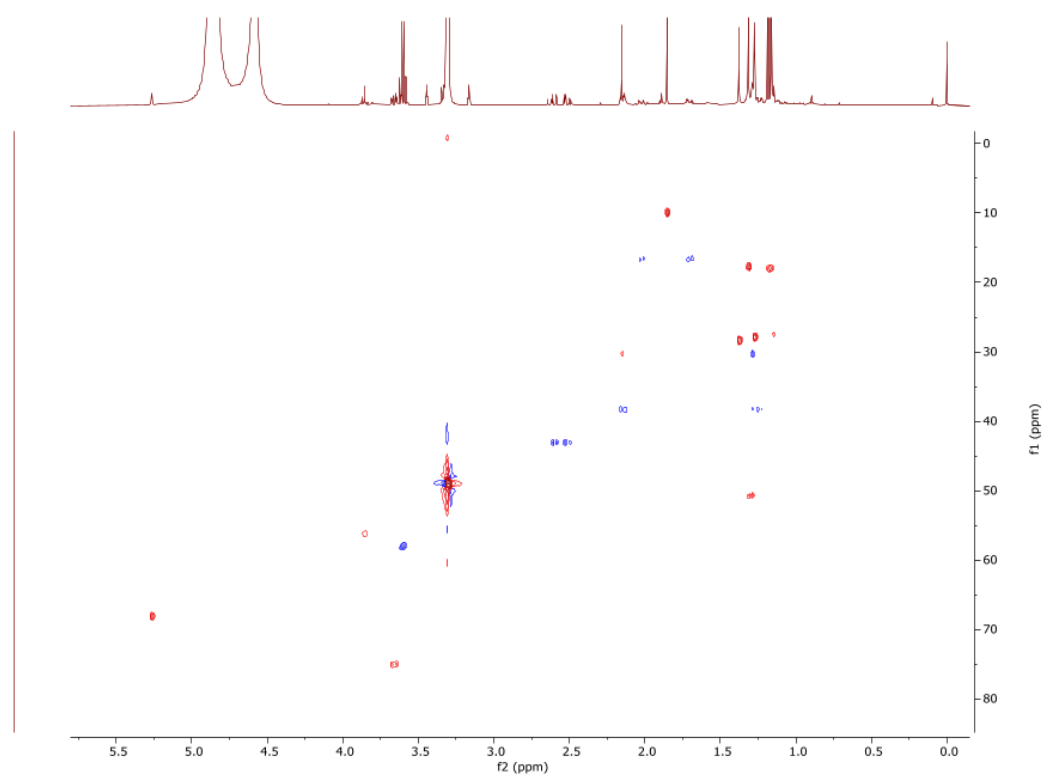


Figure S3.2. HSQC spectrum of compound **2**

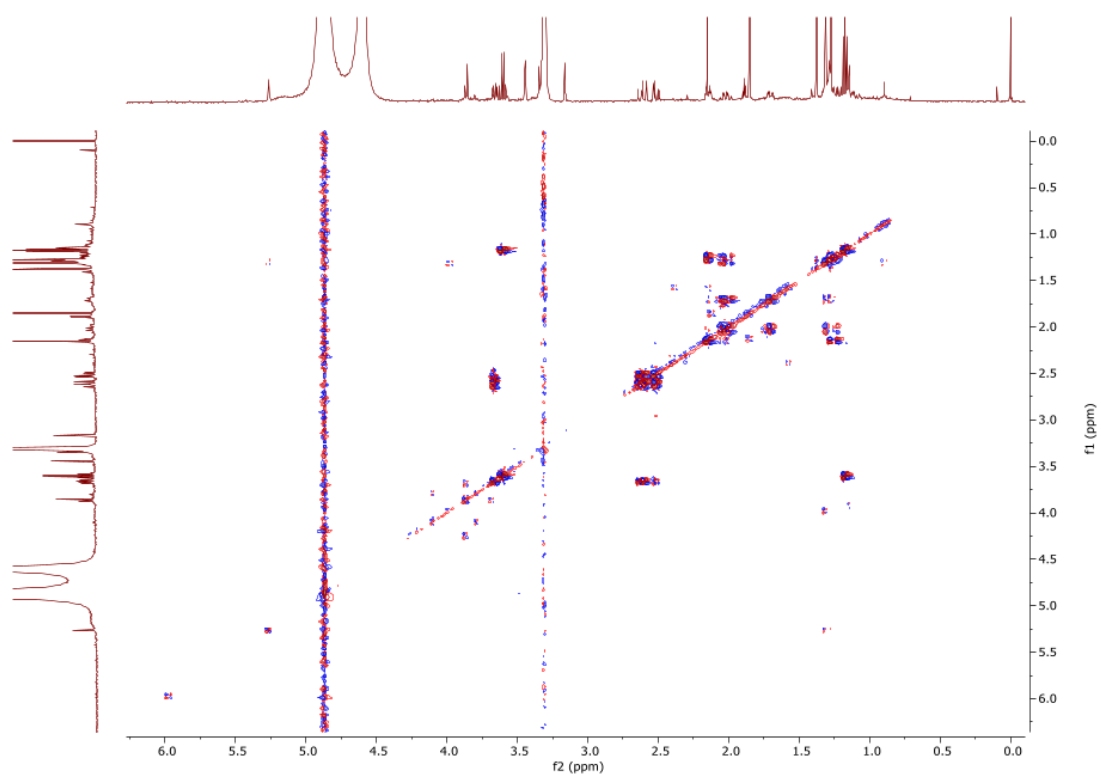


Figure S3.3. COSY spectrum of compound **2**

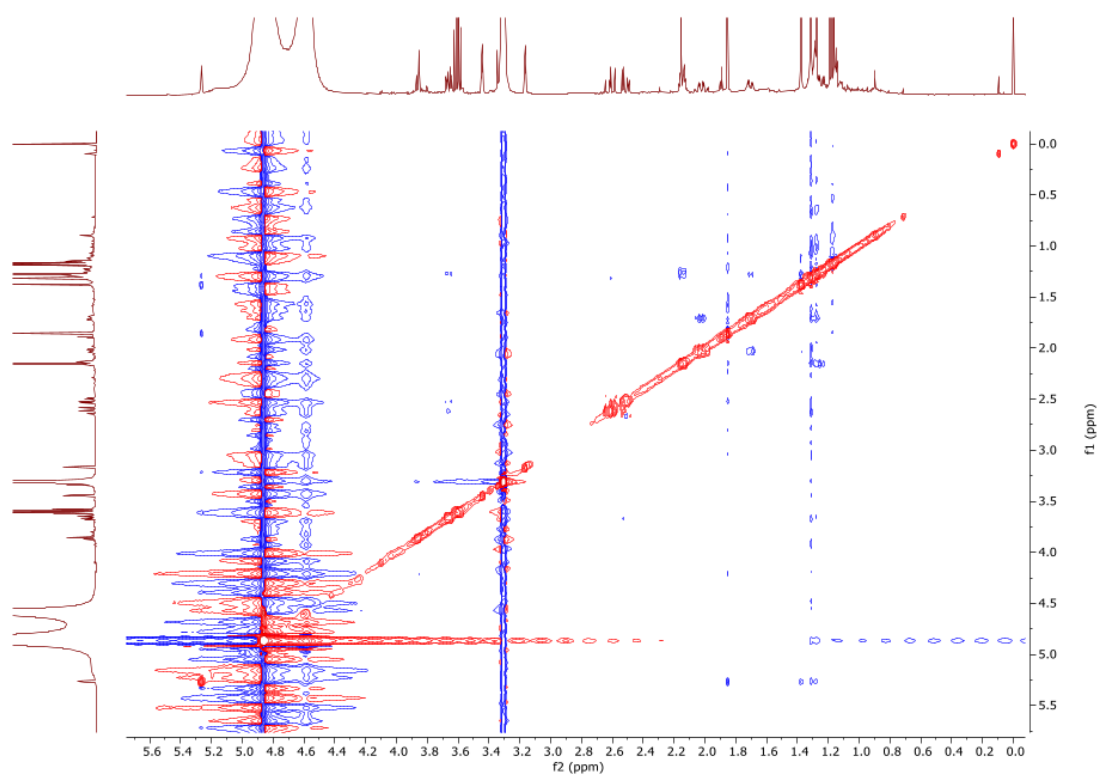


Figure S3.4. NOESY spectrum of compound **2**

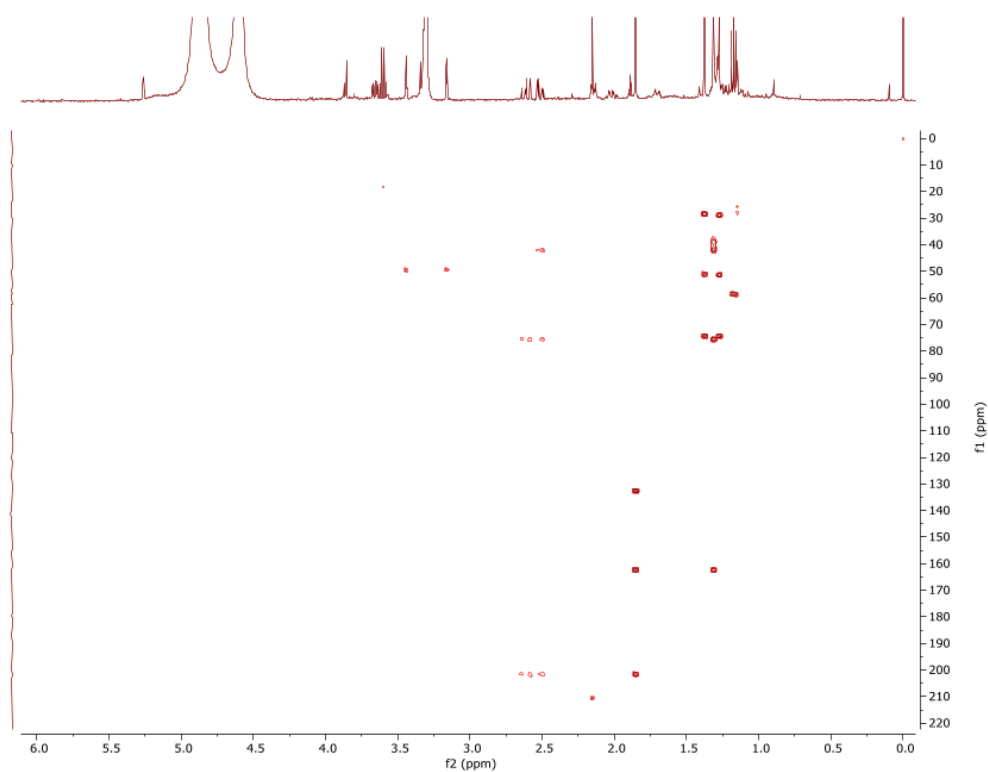


Figure S3.5. HMBC spectrum of compound **2**, 500 MHz, 128 scans

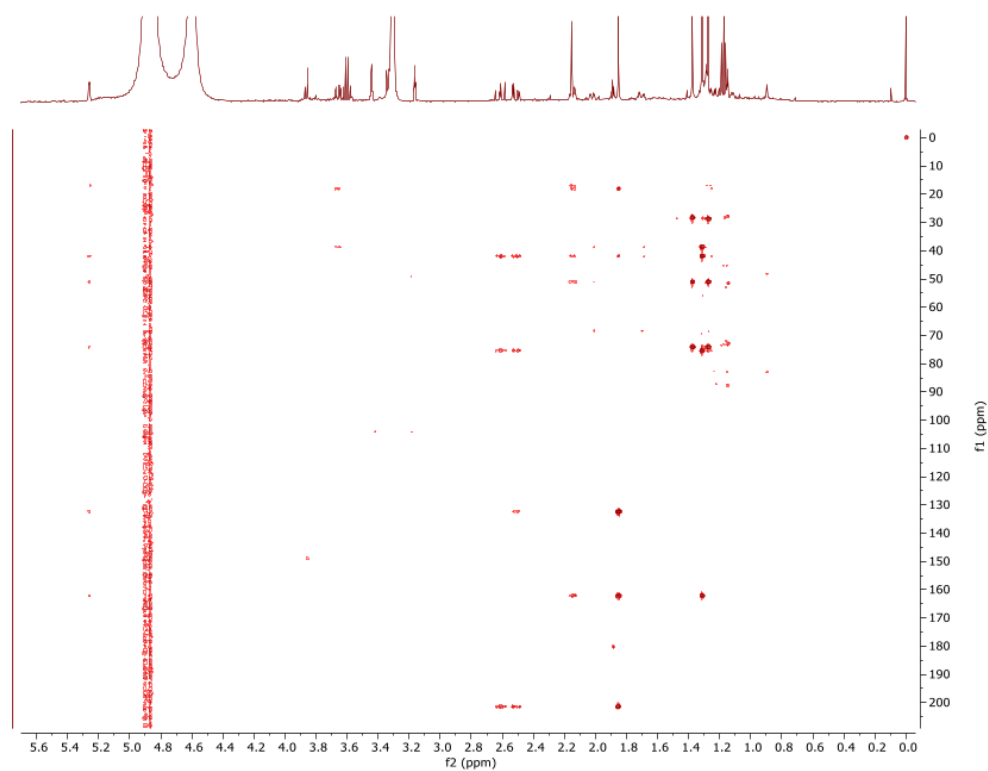


Figure S3.6. HMBC spectrum of compound **2**, 600 MHz, 160 scans

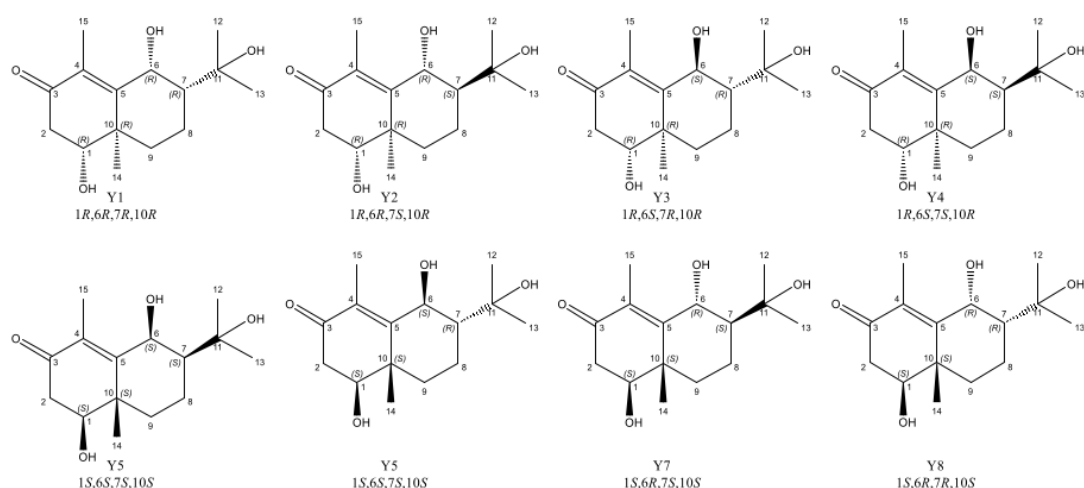


Figure S4. Eight possible stereoisomers (Y1-Y8) for compound **2**

Table S6. MM2 calculation and crucial NOESY correlation and distances of stereoisomers Y1-Y8 of compound **2**

Name	Configuration	MM2 calculation [kcal/mol]	H-1↔H-14 [Å]	H-1↔H-7 [Å]	H-1↔H-9b [Å]	H-6↔H-13 [Å]	H-6↔H-7 [Å]
Y1/Y5	1 <i>R</i> ,6 <i>R</i> ,7 <i>R</i> ,10 <i>R</i> / 1 <i>S</i> ,6 <i>S</i> ,7 <i>S</i> ,10 <i>S</i>	20.4782	3.8	4.0	2.3	2.3	2.3
Y2/Y6	1 <i>R</i> ,6 <i>R</i> ,7 <i>S</i> ,10 <i>R</i> / 1 <i>S</i> ,6 <i>S</i> ,7 <i>R</i> ,10 <i>S</i>	23.9610	3.8	5.3	2.3	2.1	2.5
Y3/Y7	1 <i>R</i> ,6 <i>S</i> ,7 <i>R</i> ,10 <i>R</i> / 1 <i>S</i> ,6 <i>R</i> ,7 <i>R</i> ,10 <i>S</i>	25.2799	3.9	4.0	2.4	2.3	3.0
Y4/Y8	1 <i>R</i> ,6 <i>S</i> ,7 <i>S</i> ,10 <i>R</i> / 1 <i>S</i> ,6 <i>R</i> ,7 <i>R</i> ,10 <i>S</i>	22.6833	3.8	5.1	2.4	2.3	2.3
		H-6↔H-15 [Å]	H-6↔H-1 [Å]	H-6↔H-8a [Å]	H-6↔H-8b [Å]	H-6↔H-9a [Å]	H-6↔H-9b [Å]
Y1/Y5		2.0	4.4	3.9	4.3	4.9	3.9
Y2/Y6		2.2	4.6	3.7	4.3	5.0	4.3
Y3/Y7		2.4	4.8	2.9	4.0	4.6	4.1
Y4/Y8		2.1	4.8	4.2	4.1	4.9	4.0

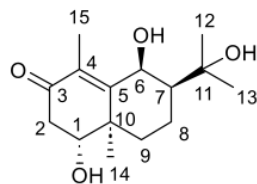
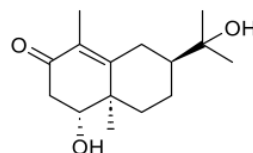
Table S7. CD calculations of compound **2**

Name	Configuration	Similarity Factor (S)	Sigma (eV)	Shift (nm)
Y1	1R,6R,7R,10R	0.4570	0.57	-41
Y2	1R,6R,7S,10R	0.4186	0.57	-41
Y3	1R,6S,7R,10R	0.0559	0.57	-41
Y4	1R,6S,7S,10R	0.9556	0.57	-41

Table S8. Comparison of NMR data of **2** with literature data of anhuienosol

Compound 2			Anhuienosol	(Suresh et al. 2013 ⁶⁶)
No.	¹³ C* MeOD	¹ H MeOD	¹³ C CDCl ₃	¹ H CDCl ₃
1	75.2, CH	3.66 (dd, <i>J</i> = 5.1, 13.1 Hz, 1H)	74.6	3.75 (dd, <i>J</i> = 12.7, 5.8 Hz, 1H)
2	43.0, CH ₂	a) 2.60 (dd, <i>J</i> = 16.7, 13.1 Hz, 1H) b) 2.52 (dd, <i>J</i> = 16.7, 5.1 Hz, 1H)	42.5	a) 2.57 (each dd, <i>J</i> = 15.6, 5.8 Hz) b) 2.51
3	201.1, C		196.6	
4	132.1, C		129.8	
5	161.8, C		161.5	
6	68.0, CH	5.26 (d, <i>J</i> = 2.7 Hz, 1H)	28.6	a) 2.91 (brd, <i>J</i> = 13.7 Hz) b) 1.94 (brd, <i>J</i> = 13.7 Hz, 1H)
7	50.7, CH	1.30 (m, 1H)	48.8	1.38–1.42 (m, 1H)
8	16.6, CH ₂	a) 2.02 (m, 1H) b) 1.70 (m, 1H)	22.4	1.76–1.83 & 1.41–1.46 (m, 2H)
9	38.3, CH ₂	a) 2.15 (m, 1H) b) 1.25 (m, 1H)	37.9	a) 2.14–2.20 (m, 1H) b) 1.28–1.32 (m, 1H)
10	41.5, C		41.3	
11	73.8, C		72.4	
12	27.9, CH ₃	1.27 (s, 3H)	26.8	1.23 (3H, s)
13	28.2, CH ₃	1.38 (s, 3H)	27.8	1.25 (3H, s)
14	17.7, CH ₃	1.31 (s, 3H)	16.3	1.16 (3H, s)
15	9.9, CH ₃	1.85 (s, 3H)	11.1	1.77 (3H, s)

*obtained from HSQC and HMBC

Compound **2**

Anhuienosol

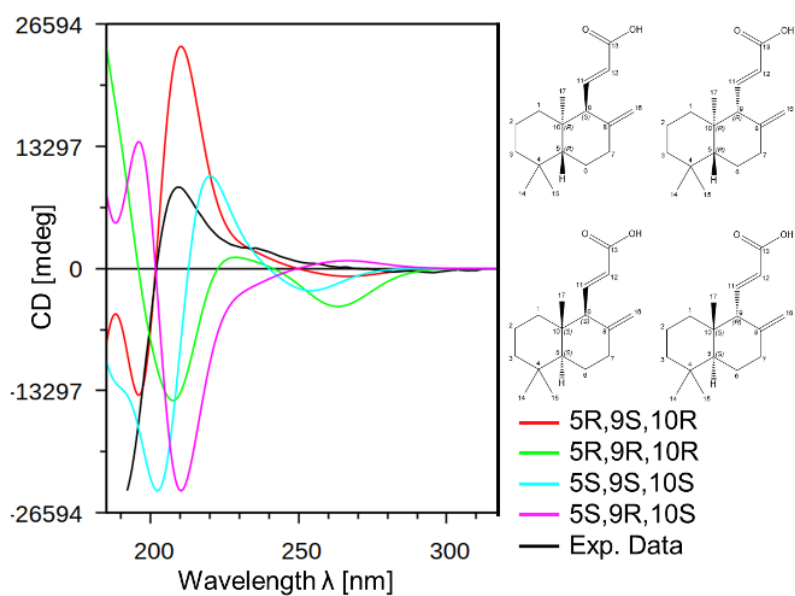


Figure S5. CD calculations of compound **3**

Table S9. CD calculations of compound **3**

Name	Similarity Factor (S)	Sigma (eV)	Shift (nm)
5R,9S,10R	0.9649	0.24	-19
5R,9R,10R	0.2578	0.24	-19
5S,9S,10S	0.5077	0.24	-19
5S,9R,10S	0.0074	0.24	-19

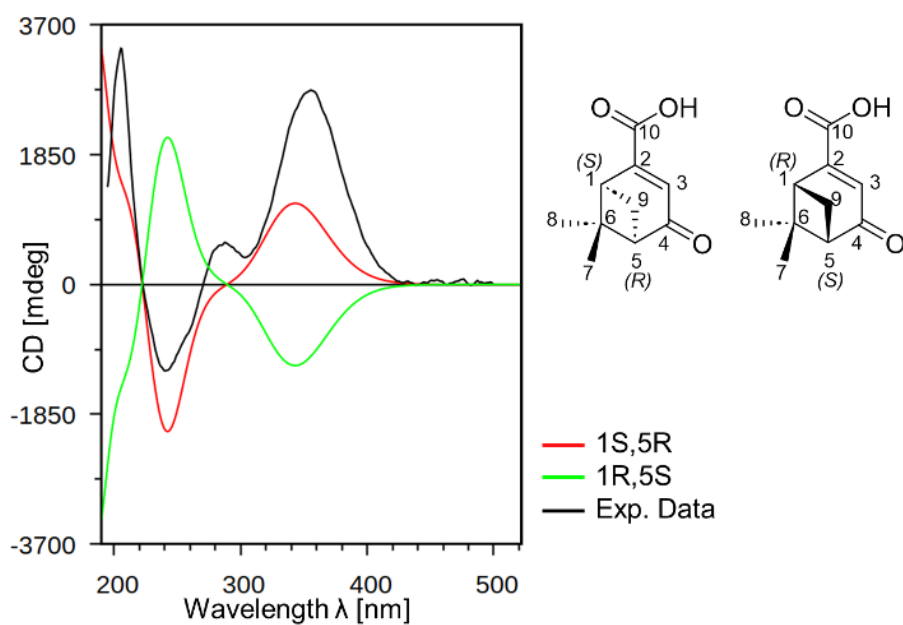


Figure S6. CD calculations of compound **4**

Table S10. CD calculations of compound **4**

Name	Similarity Factor (S)	Sigma (eV)	Shift (nm)
2R,5S	0.0028	-41	0.3
2S,5R	0.9683	-41	0.3

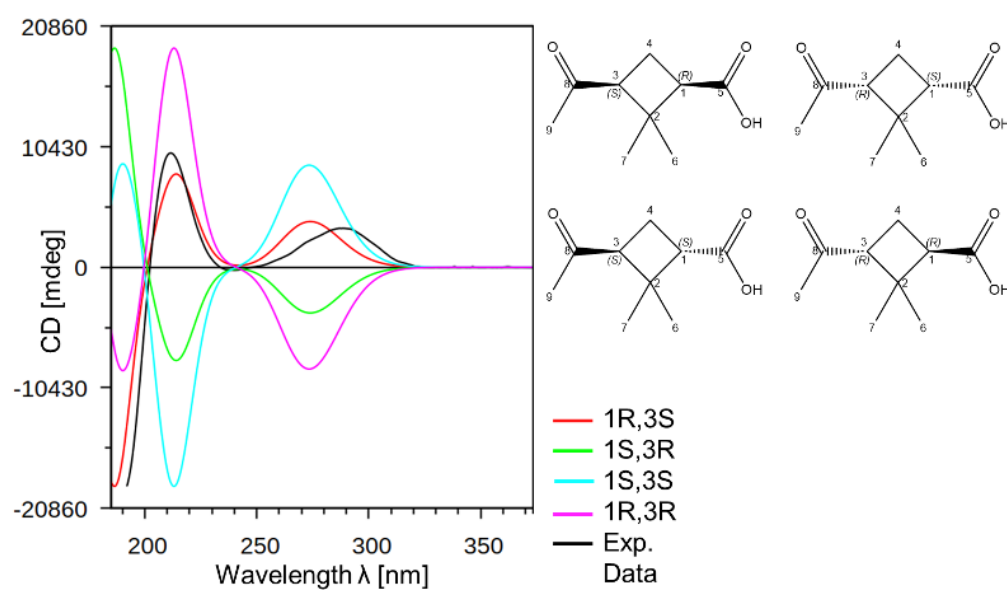


Figure S7. CD calculations of compound **5**

Table S11. CD calculations of compound **5**

Name	Similarity Factor (S)	Sigma (eV)	Shift (nm)
1S,3S	0.2658	-7	0.29
1R,3S	0.9400	-7	0.29
1S,3R	0.0036	-7	0.29
1R,3R	0.6696	-7	0.29

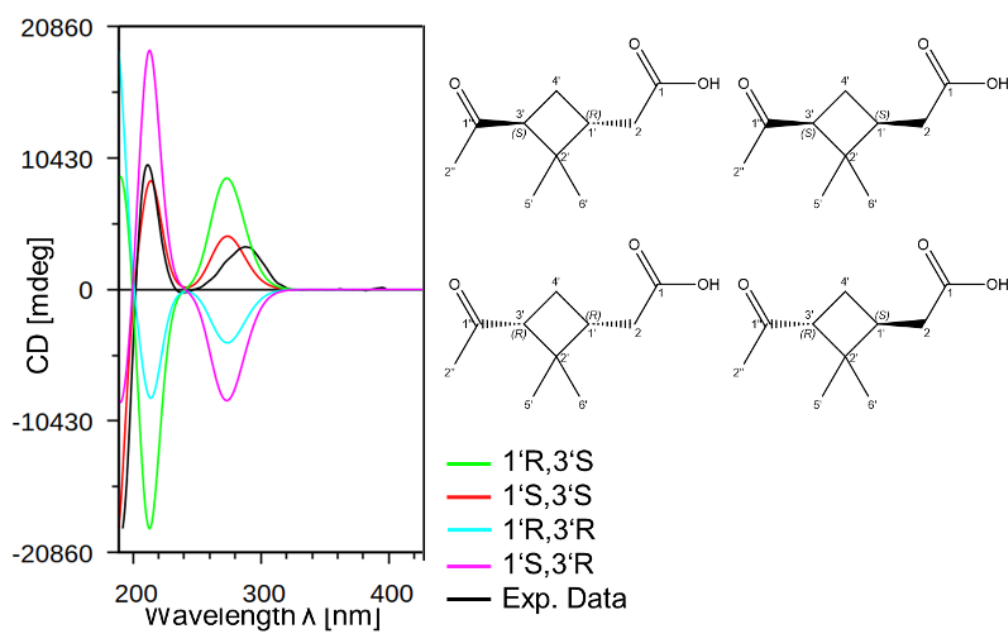


Figure S8. CD calculations of compound **6**

Table S12. CD calculations of compound **6**

Name	Similarity Factor (S)	Sigma (eV)	Shift (nm)
1'R,3'S	0.2658	0.29	-7
1'S,3'S	0.9400	0.29	-7
1'R,3'R	0.0036	0.29	-7
1'S,3'R	0.6596	0.29	-7

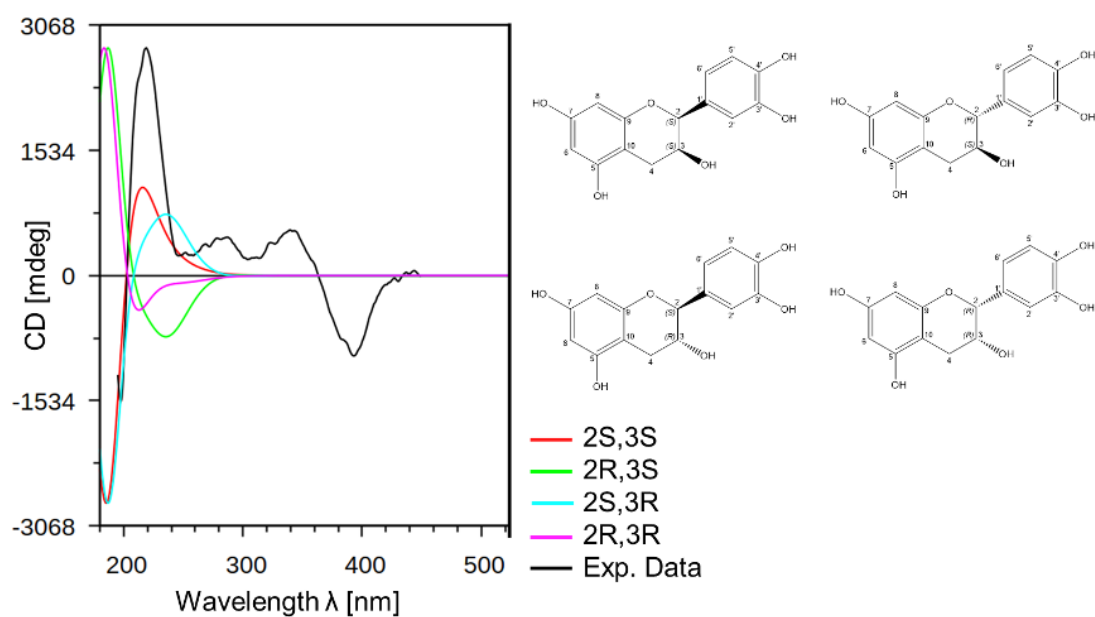


Figure S9. CD calculations of compound 8

Table S13. CD calculations of compound 8

Name	Similarity Factor (S)	Sigma (eV)	Shift (nm)
2S,3S	0.8690	0.52	-7
2R,3S	0.0276	0.52	-7
2S,3R	0.6037	0.52	-7
2R,3R	0.0002	0.52	-7

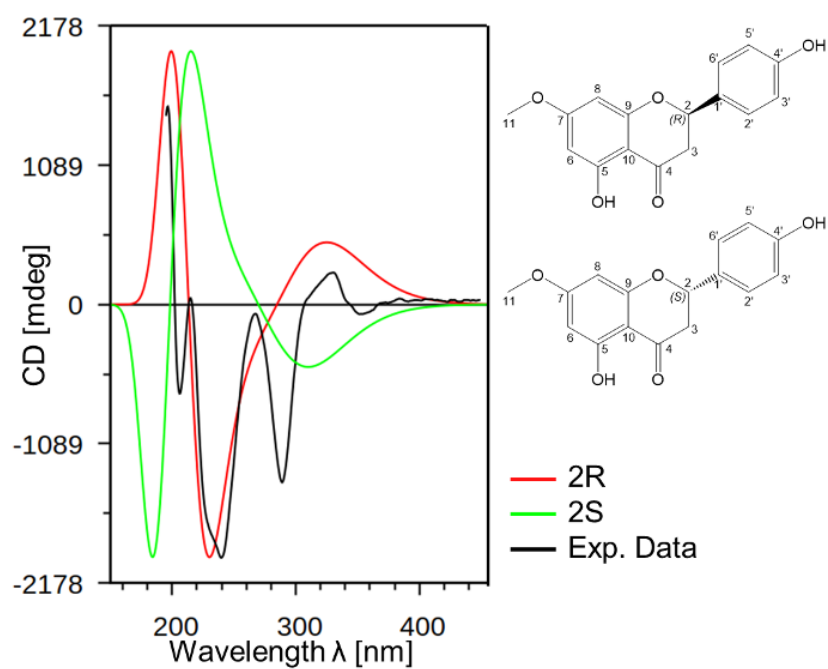


Figure S10. CD calculations of compound **9**

Table S14. CD calculations of compound **9**

Name	Similarity Factor (S)	Sigma (eV)	Shift (nm)
2S	0.3015	15	0.6
2R	0.7797	15	0.6

Spectroscopic data of isolated compounds 1-26

(1*R*,5*S*,6*S*,7*R*,10*R*)-Mustak-14-oic acid (**1**): colorless oil; $[\alpha]_D^{20} = -69$ (c 0.00001, MeOH); UV (MeOH) λ_{\max} (log ϵ) 202 (4.00), 225 (3.71), 277 (3.14); ^1H NMR (500 MHz, Methanol- d_4) δ 6.26 (1H, brt, $J = 1.6$ Hz, H-3), 2.72 (1H, brs, H-6), 2.69 (1H, dd, $J = 6.6, 1.3$ Hz, H-1), 2.66 (1H, dd, $J = 6.6, 0.9$ Hz, H-5), 1.90 (1H, m, H-9b), 1.86 (1H, m, H-9a), 1.83 (1H, m, H-8b), 1.77 (1H, m, H-7), 1.61 (1H, m, H-8a), 1.55 (1H, m, H-11), 0.98 (3H, s, H-15), 0.89 (3H, d, $J = 6.8$ Hz, H-13), 0.87 (3H, d, $J = 6.8$ Hz, H-12); ^{13}C NMR (obtained from HSQC and HMBC, Methanol- d_4) δ 209.0 (C, C-2), 173.8 (C, C-14), 168.3 (C, C-4), 124.3 (CH, C-3), 59.8 (C, C-10), 58.8 (CH, C-6), 57.0 (CH, C-5), 53.5 (CH, C-1), 46.7 (CH, C-7), 37.9 (CH₂, C-9), 33.2 (CH, C-11), 23.1 (CH₂, C-8), 20.8 (CH₃, C-15), 20.2 (CH₃, C-12), 19.9 (CH₃, C-13); HR-ESI-MS (Orbitrap) m/z $[\text{M}-\text{H}]^-$ 247.1338 (calc for $\text{C}_{15}\text{H}_{20}\text{O}_3^-$, 247.1329); MS²-Fragmentation (CE = -30 V) m/z 221 (8), 203 (100).

(1*R*,6*S*,7*S*,10*R*)-6-Hydroxy-anhuienosol (**2**): yellow oil; $[\alpha]_D^{20} = -17$ (c 0.0001, MeOH); UV (MeOH) λ_{\max} (log ϵ) 202 (3.87), 238 (3.63); ^1H NMR (500 MHz, Methanol- d_4) δ 5.26 (1H, d, $J = 2.7$ Hz, H-6), 3.66 (1H, dd, $J = 13.1, 5.1$ Hz, H-1), 2.60 (1H, dd, $J = 16.7, 13.1$ Hz, H-2a), 2.52 (1H, dd, $J = 16.7, 5.1$ Hz, H-2b), 2.15 (1H, m, H-9a), 2.02 (1H, m, H-8a), 1.85 (3H, s, H-15), 1.70 (1H, m, H-8b), 1.38 (3H, s, H-13), 1.31 (3H, s, H-14), 1.30 (1H, m, overlaid, H-7), 1.27 (3H, s, H-12), 1.25 (1H, m, H-9b); ^{13}C NMR (obtained from HSQC and HMBC, Methanol- d_4) δ 201.11 (C, C-3), 161.85 (C, C-5), 132.13 (C, C-4), 75.18 (CH, C-1), 73.82 (C, C-11), 68.05 (CH, C-6), 50.7 (CH, C-7), 43.04 (CH₂, C-2), 41.50 (C, C-10), 38.34 (CH₂, C-9), 28.2 (CH₃, C-13), 27.89 (CH₃, C-12), 17.74 (CH₃, C-14), 16.62 (CH₂, C-8), 9.92 (CH₃, C-15); HR-ESI-MS (TOF) m/z $[\text{M}+\text{FA}]^+$ 313.1669 (calc for $\text{C}_{16}\text{H}_{26}\text{O}_6^+$, 313.1651); MS²-Fragmentation (CE = -20 V) m/z 313 (12), 267 (50), 209 (100), 191 (18), 121 (17).

(5*R*,9*S*,10*R*)-(*E*)-14,15,16-Trinorlabda-8(17),11-dien-13-oic acid (**3**): white solid; $[\alpha]_D^{20} = -23$ (c 0.0001, MeOH); UV (MeOH) λ_{\max} (log ϵ) 202 (3.93), 222 (3.51); ^1H NMR (600 MHz, Methanol- d_4) δ 6.83 (1H, dd, $J = 15.5, 10.3$ Hz, H-11), 5.79 (1H, d, $J = 15.5$ Hz, H-12), 4.75 (1H, d, $J = 2.0$ Hz, H-16a), 4.48 (1H, d, $J = 2.0$ Hz, H-16b), 2.47 (1H, d, $J = 10.3$ Hz, H-9), 2.47 – 2.41 (1H, m, H-7a), 2.11 (1H, td, $J = 13.3, 5.3$ Hz, H-7b), 1.79 – 1.66 (1H, m, H-6a), 1.64 – 1.52 (1H, m, H-2a), 1.47 – 1.38 (4H, m, H-1a + H-2b + H-3a + H-6b), 1.23 (1H, td, $J = 13.6, 12.9, 4.0$ Hz, H-3b), 1.16 (1H, dd, $J = 12.6, 2.7$ Hz, H-5), 1.06 (1H, td, $J = 14.4, 13.6, 4.1$ Hz, H-1a), 0.90 (3H, s, H-14), 0.89 (3H, s, H-17), 0.86 (3H, s, H-15); ^{13}C NMR (obtained from HSQC and HMBC, Methanol- d_4) δ 173.2 (C, C-13), 150.2 (C, C-8), 145.2 (CH, C-11), 128.9 (CH, C-12), 109.0 (CH₂, C-16), 61.8 (CH, C-9), 56.2 (CH, C-5), 43.3 (CH₂, C-3), 41.9 (CH₂, C-1), 40.4 (C, C-10), 37.9 (CH₂, C-7), 34.1 (CH₃, C-14), 34.5 (C, C-4), 24.6 (CH₂, C-6), 22.6 (CH₃, C-15), 20.1 (CH₂, C-2), 15.6 (CH₃, C-17); HR-ESI-MS (TOF) m/z $[\text{M}+\text{H}]^+$ 263.2008 (calc for $\text{C}_{17}\text{H}_{27}\text{O}_2^+$, 263.2006); MS²-Fragmentation (CE = 40 V) m/z 263 (57), 245 (42), 227 (15), 217 (100), 207 (12), 193 (15), 177 (73), 175 (12), 163 (12), 161 (32), 149 (12), 147 (24), 137 (23), 135 (18), 133 (11), 123 (23), 121 (30), 119 (9), 109 (29), 107 (20), 95 (24), 81 (11), 69 (5). Data correspond to literature. [22, 23]

(1*S*,5*R*)-Verbenon-10-oic acid (**4**): white solid; $[\alpha]_D^{20} = +55$ (c 0.0027, MeOH); UV (MeOH) λ_{\max} (log ϵ) 203 (2.63), 256 (2.34); ^1H NMR (500 MHz, Methanol- d_4) δ 6.51 (1H, s, H-3), 3.08 (1H, dd, $J = 5.9, 1.6$ Hz, H-1), 2.98 (1H, td, $J = 9.6, 5.9$ Hz, H-9a), 2.70 (1H, td, $J = 5.9, 1.6$ Hz, H-5), 2.08 (1H, d, $J = 9.6$ Hz, H-9b), 1.58 (3H, s, H-7), 0.97 (3H, s, H-8). ^{13}C NMR (126 MHz, Methanol- d_4) δ 206.0 (C, C-4), 168.6 (C, C-10), 159.4 (C, C-2), 129.1 (CH, C-3), 59.9 (CH, C-5), 55.7 (C, C-6), 45.2 (CH, C-1), 41.9 (CH₂, C-9), 26.8 (CH₃, C-7), 22.3 (CH₃, C-8); HR-ESI-MS (Orbitrap) m/z $[\text{M}-\text{H}]^-$ 179.0718 (calc for $\text{C}_{10}\text{H}_{11}\text{O}_3^-$, 179.0703); MS²-Fragmentation (CE = -35 V) m/z 135 (100). Data correspond to literature. [24, 25]

(1*R*,3*S*)-*cis*-Pinononic acid (**5**): colorless oil; $[\alpha]_D^{20} = -5$ (c 0.0001, MeOH); UV (MeOH) λ_{\max} (log ϵ) 202 (2.91), 277 (1.72); ^1H NMR (500 MHz, Methanol- d_4) δ 2.95 (1H, dd, $J = 10.0, 7.7$ Hz, H-3'), 2.38 (1H, m, H-1'), 2.22 (1H, m, H-2b), 2.11 (1H, m, H-2a), 2.02 (3H, s, H-2''), 1.85 – 1.95 (2H, m, H-4'), 1.31 (3H, s, H-5'), 0.85 (3H, s, H-6'); ^{13}C NMR (obtained from HSQC and HMBC, Methanol- d_4) δ 210.8 (C, C-1'), 180.0 (C, C-1), 55.0 (CH, C-3'), 44.3 (C, C-2'), 39.8 (CH, C-1'), 38.3 (CH₂, C-2), 30.1 (CH₃, C-5'), 29.7 (CH₃, C-2''), 24.1 (CH₂, C-4'), 17.1 (CH₃, C-6'); HR-ESI-MS (TOF) m/z $[\text{M}-\text{H}]^-$ 169.0866 (calc for $\text{C}_9\text{H}_{13}\text{O}_3^-$, 169.0870). Data correspond to literature. [26, 27]

(1'S,3'S)-*cis*-Pinonic acid (**6**): pale yellow oil; $[\alpha]_D^{20} = +5$ (c 0.0001, MeOH); ^1H NMR (500 MHz, Methanol- d_4) δ 2.95 (1H, dd, $J = 10.0, 7.7$ Hz, H-3'), 2.38 (1H, m, H-1'), 2.22 (1H, m, H-2b), 2.11 (1H, m, H-2a), 2.02 (3H, s, H-2''), 1.85 - 1.95 (2H, m, H-4'), 1.31 (3H, s, H-5'), 0.85 (3H, s, H-6'); ^{13}C NMR (obtained from HSQC and HMBC, Methanol- d_4) δ 210.8 (C, C-1'), 180.0 (C, C-1), 55.0 (CH, C-3'), 44.3 (C, C-2'), 39.8 (CH, C-1'), 38.3 (CH₂, C-2), 30.1 (CH₃, C-5'), 29.7 (CH₃, C-2''), 24.1 (CH₂, C-4'), 17.1 (CH₃, C-6'); HR-ESI-MS (TOF) m/z $[\text{M}-\text{H}]^-$ 183.1029 (calc for C₁₀H₁₅O₃⁻, 183.10247). Data correspond to literature. [28]

(S)-2-oxo-3-4,5,5-Trimethylcyclopentynyl acidic acid (**7**): yellow solid; $[\alpha]_D^{20} = -6$ (c 0.0002, MeOH); ^1H NMR (500 MHz, Methanol- d_4) δ 5.82 (1H, d, $J = 1.3$ Hz, H-4), 2.73 (1H, dd, $J = 10.0, 4.7$ Hz, H-1), 2.64 (1H, dd, $J = 16.1, 4.7$ Hz, H-2'b), 2.23 (1H, dd, $J = 16.1, 10.0$ Hz, H-2'a), 2.08 (3H, d, $J = 1.3$ Hz, H-8), 1.28 (3H, s, H-7), 1.10 (3H, s, H-6); ^{13}C NMR (obtained from HSQC and HMBC, Methanol- d_4) δ 211.6 (C, C-5), 188.9 (C, C-3), 179.8 (C, C-1'), 127.8 (CH, C-4), 56.9 (CH, C-9), 47.6 (C, C-2), 34.3 (CH₂, C-2'), 26.5 (CH₃, C-7), 23.4 (CH₃, C-6), 14.3 (CH₃, C-8); HR-ESI-MS (TOF) m/z $[\text{M}-\text{H}]^-$ 181.0874 (calc for C₁₀H₁₃O₃⁻, 181.0865). Data correspond to literature. [29, 30]

(2S,3S)-Epicatechin (**8**): colourless solid; ^1H NMR (400 MHz, DMSO- d_6) δ 9.09 (s, 1H, 5-OH), 8.88 (s, 1H, 7-OH), 8.79 (s, 1H, 4'-OH), 8.71 (s, 1H, 3'-OH), 6.88 (d, $J = 1.6$ Hz, 1H, H-2'), 6.66 (d, $J = 8.0$ Hz, 1H, H-5'), 6.64 (dd, $J = 8.0, 1.6$ Hz, 1H, H-6'), 5.89 (d, $J = 2.4$ Hz, 1H, H-6), 5.71 (d, $J = 2.4$ Hz, 1H, H-8), 4.73 (s, 1H), 4.65 (d, $J = 4.7$ Hz, 1H, 3-OH), 4.00 (m, 1H, H-3), 2.67 (dd, $J = 16.0, 4.2$ Hz, 1H, H-4a), 2.47 (dd, $J = 4.2$ Hz, 1H, H-4b); ^{13}C NMR (150 MHz, DMSO- d_6) δ 77.9 (CH, C-2), 64.8 (CH, C-3), 28.1 (CH₂, C-4), 156.4 (C, C-5), 94.9 (CH, C-6), 156.1 (C, C-7), 94.0 (CH, C-8), 155.7 (C, C-9), 98.4 (C, C-10), 130.5 (C, C-1'), 114.8 (CH, C-2'), 144.3 (C, C-3'), 144.3 (C, C-4'), 114.6 (CH, C-5'), 117.8 (CH, C-6'); HR-ESI-MS (TOF) m/z $[\text{M}-\text{H}]^-$ 289.0721 (calc for C₁₅H₁₃O₆⁻, 289.0712); MS²-Fragmentation (CE = -30 V) m/z 289 (39), 245 (77), 221 (65), 205 (52), 203 (93), 187 (24), 179 (22), 161 (21), 151 (52), 149 (26), 137 (34), 125 (71), 123 (67), 121 (19), 109 (100), 97 (22). Data correspond to literature. [31, 32]

(2R)-Sakuranetin (**9**): light yellow amorphous solid; $[\alpha]_D^{24} = -14$ (c 0.0007, MeOH); ^1H NMR (500 MHz, Methanol- d_4) δ 7.31 (2H, d, $J = 8.5$ Hz, H-2' + H-6'), 6.81 (2H, d, $J = 8.5$ Hz, H-3' + H-5'), 6.06 (1H, d, $J = 2.3$ Hz, H-8), 6.04 (1H, d, $J = 2.3$ Hz, H-6), 5.38 (1H, dd, $J = 13.0, 2.9$ Hz, H-2), 3.81 (3H, s, H-7OMe), 3.16 (1H, m, H-3a), 2.74 (1H, m, H-3b); ^{13}C NMR (obtained from HSQC and HMBC, Methanol- d_4) δ 198.1 (C, C-4), 169.6 (C, C-7), 159.4 (C, C-4'), 130.9 (C, C-1'), 129.2 (2CH, C-2' + C-6'), 116.4 (2CH, C-3' + C-5'), 95.8 (CH, C-6), 95.0 (CH, C-8), 80.7 (CH, C-2), 56.4 (CH₃, C-7-OMe), 44.3 (CH₂, C-3); HR-ESI-MS (TOF) m/z $[\text{M}-\text{H}]^-$ 285.0779 (calc for C₁₆H₁₃O₅⁻, 285.0763); MS²-Fragmentation (CE = -35 V) m/z 285 (84), 165 (68), 119 (100), 93 (3). Data correspond to literature. [33, 34]

Quercetin (**10**): yellow solid; ^1H NMR (500 MHz, Methanol- d_4) δ 7.73 (1H, d, $J = 2.2$ Hz, H-2'), 7.63 (1H, dd, $J = 8.5, 2.2$ Hz, H-6'), 6.88 (1H, d, $J = 8.5$ Hz, H-5'), 6.39 (1H, d, $J = 2.1$ Hz, H-8), 6.18 (1H, d, $J = 2.1$ Hz, H-6); ^{13}C NMR (obtained from HSQC, Methanol- d_4) δ 122.0 (CH, C-6'), 116.5 (CH, C-5'), 116.3 (CH, C-2'), 99.5 (CH, C-6), 94.7 (CH, C-8); HR-ESI-MS (Orbitrap) m/z $[\text{M}-\text{H}]^-$ 301.0370 (calc for C₁₅H₉O₇⁻, 301.0354); MS²-Fragmentation (CE = -35 V) m/z 273 (12), 179 (100), 151 (77). Data correspond to literature. [35]

Rutin (**11**): yellow amorphous powder; ^1H -NMR (500 MHz, Methanol- d_4) δ : 7.66 (1H, d, $J = 2.2$ Hz, H-2'), 7.63 (1H, dd, $J = 8.4, 2.2$ Hz, H-6'), 6.88 (1H, d, $J = 8.4$ Hz, H-5'), 6.41 (1H, d, $J = 2.1$ Hz, H-8), 6.22 (1H, d, $J = 2.1$ Hz, H-6), 5.11 (1H, d, $J = 7.7$ Hz, H-1''), 4.52 (1H, d, $J = 1.7$ Hz, H-1'''), 3.80 (1H, dt, $J = 10.9, 1.3$ Hz, H-6''b), 3.62 (1H, dd, $J = 3.4, 1.7$ Hz, H-2'''), 3.53 (1H, dd, $J = 9.5, 3.4$ Hz, H-3'''), 3.26-3.47 (4H, m, H-2'', H-3'', H-4'', H-5''), 3.44 (1H, m, H-5'''), 3.38 (1H, m, H-6''a), 3.26 (1H, m, H-4'''), 1.12 (3H, d, $J = 6.2$ Hz, C-6'''); ^{13}C NMR (obtained from HSQC, Methanol- d_4) δ 123.7 (CH, C-6'), 117.8 (CH, C-2'), 116.2 (CH, C-5'), 104.9 (CH, C-1''), 102.5 (CH, C-1'''), 100.2 (CH, C-6), 94.9 (CH, C-8), 78.3 (CH, C-5''), 77.4 (CH, C-3''), 75.8 (CH, C-2''), 74.0 (CH, C-4'''), 72.4 (CH, C-3'''), 72.2 (CH, C-2'''), 71.6 (CH, C-4''), 69.8 (CH, C-5'''), 68.9 (CH₂, C-6''), 18.0 (CH₃, C-6'''); HR-ESI-MS (Orbitrap) m/z $[\text{M}-\text{H}]^-$ 609.1469 (calc for C₂₇H₂₉O₁₆⁻, 609.1450); MS²-Fragmentation (CE = -35 V) m/z 343 (9), 301 (100), 271 (7). Data correspond to literature. [36, 37]

Isokaempferid (**12**): yellow amorphous solid; ^1H NMR (600 MHz, Methanol- d_4) δ 7.99 (2H, d, J = 8.8 Hz, H-2' + H-6'), 6.93 (2H, d, J = 8.8 Hz, H-3' + H-5'), 6.41 (1H, d, J = 2.1 Hz, H-8), 6.20 (1H, d, J = 2.1 Hz, H-6), 3.78 (3H, s, H-3OMe); ^{13}C NMR (obtained from HSQC and HMBC, Methanol- d_4) δ 180.0 (C, C-4), 165.9 (C, C-7), 163.1 (C, C-5), 161.7 (C, C-4'), 158.4 (C, C-9), 158.1 (C, C-2), 139.5 (C, C-3), 131.4 (CH, C-2' + C-6'), 122.5 (C, C-1'), 116.6 (CH, C-3' + C-5'), 105.9 (C, C-10), 99.8 (CH, C-6), 94.8 (CH, C-8), 60.6 (CH₃, C-3OMe); HR-ESI-MS (TOF) m/z $[\text{M}-\text{H}]^-$ 299.0568 (calc for $\text{C}_{16}\text{H}_{11}\text{O}_6^-$, 299.0556); MS²-Fragmentation (CE = -35 V) m/z 284 (45), 255 (100), 227 (58), 183 (1). Data correspond to literature. [38]

Kumatakenin (**13**): yellow solid, ^1H NMR (500 MHz, Methanol- d_4) δ 7.98 (2H, d, J = 8.5 Hz, H-2' + H-6'), 6.89 (2H, d, J = 8.5 Hz, H-3' + H-5'), 6.58 (1H, d, J = 2.2 Hz, H-8), 6.30 (1H, d, J = 2.2 Hz, H-6), 3.85 (3H, s, H-7OMe), 3.75 (3H, s, H-3OMe); ^{13}C NMR (obtained from HSQC and HMBC, Methanol- d_4) δ 166.5 (C, C-7), 162.1 (C, C-5), 161.2 (C, C-4'), 157.9 (C, C-2), 157.5 (C, C-9), 138.8 (C, C-3), 130.7 (2CH, C-2' + C-6'), 121.5 (C, C-1'), 115.9 (2CH, C-3' + C-5'), 106.1 (C, C-10), 98.1 (CH, C-6), 92.3 (CH, C-8), 59.7 (CH₃, C-3OMe), 55.7 (CH₃, C-7OMe); HR-ESI-MS (Orbitrap) m/z $[\text{M}-\text{H}]^-$ 313.0717 (calc for $\text{C}_{17}\text{H}_{13}\text{O}_6^-$, 313.0718); MSⁿ-Fragmentation: MS¹: 313.0717 ($\text{C}_{17}\text{H}_{13}\text{O}_6^-$); MS²: 298.0480 ($\text{C}_{16}\text{H}_{10}\text{O}_6^-$); MS³: 283.0247 ($\text{C}_{15}\text{H}_7\text{O}_6^-$); MS⁴: 255.0298 ($\text{C}_{14}\text{H}_7\text{O}_5^-$); MS⁵: 227.0350 ($\text{C}_{13}\text{H}_7\text{O}_4^-$, 69), 211.0401 ($\text{C}_{13}\text{H}_7\text{O}_3^-$, 96), 183.0453 ($\text{C}_{12}\text{H}_7\text{O}_2^-$, 100), 171.0453 ($\text{C}_{11}\text{H}_7\text{O}_2^-$, 7), 159.0453 ($\text{C}_{10}\text{H}_7\text{O}_2^-$, 11), 117.0348 ($\text{C}_8\text{H}_5\text{O}^-$, 5). Data correspond to literature. [39]

5-Hydroxy-3,7,4'-trimethoxyflavon (**14**): yellow amorphous solid; ^1H NMR (500 MHz, Methanol- d_4) δ 8.10 (2H, d, J = 9.1 Hz, H-2' + H-6'), 7.09 (2H, d, J = 9.1 Hz, H-3' + H-5'), 6.63 (1H, d, J = 2.2 Hz, H-8), 6.35 (1H, d, J = 2.2 Hz, H-6), 3.89 (6H, s, H-7OMe + H-4'OMe), 3.80 (3H, s, H-3OMe). ^{13}C NMR (126 MHz, Methanol- d_4) δ 180.2 (C, C-4'), 167.4 (C, C-7), 162.9 (C, C-5), 158.4 (C, C-9), 158.0 (C, C-2), 140.0 (C, C-3), 131.4 (2CH, C-2' + C-6'), 123.8 (C, C-1'), 115.2 (2CH, C-3' + C-5'), 106.8 (C, C-10), 99.1 (CH, C-6), 93.2 (CH, C-8), 60.6 (CH₃, C-3-OMe), 56.5 (CH₃, C-7-OMe), 56.0 (CH₃, C-4'-OMe); HR-ESI-MS (TOF) m/z $[\text{M}+\text{H}]^+$ 329.1041 (calc for $\text{C}_{18}\text{H}_{17}\text{O}_6^+$, 329.1025); MS²-Fragmentation (CE = 30 V) m/z 329 (100), 314 (60), 313 (10), 299 (10), 271 (12), 243 (9), 135 (2). Data correspond to literature. [40]

(*E*)-*p*-Coumaric acid (**15**): yellow oil, ^1H NMR (500 MHz, Methanol- d_4) δ 7.59 (1H d, J = 15.9 Hz, H-7), 7.45 (2H, d, J = 8.6 Hz, H-2 + H-6), 6.80 (2H, d, J = 8.6 Hz, H-3 + H-5), 6.28 (1H, d, J = 15.9 Hz, H-8); ^{13}C NMR (obtained from HSQC and HMBC, Methanol- d_4) δ 171.0 (C, C-9), 161.0 (C, C-4), 146.5 (CH, C-7), 130.9 (2CH, C-2 + C-6), 127.0 (C, C-1), 116.6 (2CH, C-3 + C-5), 115.5 (CH, C-8); HR-ESI-MS (Orbitrap) m/z $[\text{M}-\text{H}]^-$ 163.0405 (calc for $\text{C}_9\text{H}_7\text{O}_3^-$, 163.0390); MS²-Fragmentation (CE = -40 V) m/z 119 (100). Data correspond to literature. [41]

Trans- and *cis*-Ferulic acid (**16+17**): yellowish amorphous powder, HR-ESI-MS (Orbitrap) m/z $[\text{M}-\text{H}]^-$ 193.0512 (calc for $\text{C}_{10}\text{H}_9\text{O}_4^-$, 193.0506)

trans-Ferulic acid (**10**): ^1H NMR (500 MHz, Methanol- d_4) δ 7.57 (1H, d, J = 15.8 Hz, H-7), 7.17 (1H, d, J = 2.5 Hz, H-2), 7.05 (1H, dd, J = 8.2, 2.5 Hz, H-6), 6.80 (1H, d, J = 8.2 Hz, H-5), 6.31 (1H, d, J = 15.8 Hz, H-8), 3.89 (3H, s, H-3OMe); ^{13}C NMR (126 MHz, Methanol- d_4) δ 171.5 (C, C-9), 150.4 (C, C-4), 149.4 (C, C-3), 146.4 (CH, C-7), 127.9 (C, C-1), 123.9 (CH, C-6), 116.6 (CH, C-8), 116.5 (CH, C-5), 111.6 (CH, C-2), 56.4 (CH₃, C-3OMe). Data correspond to literature. [42]

cis-Ferulic acid (**11**): ^1H NMR (500 MHz, Methanol- d_4) δ 7.65 (1H, d, J = 2.0 Hz, H-2), 7.05 (1H, dd, J = 2.0; 8.2 Hz, H-6), 6.74 (1H, d, J = 8.2 Hz, H-5), 6.67 (1H, d, J = 12.8 Hz, H-7), 5.80 (1H, d, J = 12.8 Hz, H-8), 3.85 (3H, s, H-3OMe); ^{13}C NMR (126 MHz, Methanol- d_4) δ 170.0 (C, C-9), 148.8 (C, C-4), 148.4 (C, C-3), 141.2 (CH, C-7), 128.7 (C, C-1), 125.8 (CH, C-6), 119.4 (CH, C-8), 115.6 (CH, C-5), 114.5 (CH, C-2), 56.3 (CH₃, C-3OMe). Data correspond to literature. [42]

(8*R*)-Evofofin B (**18**): yellowish oil; $[\alpha]_D^{23}$ -6 (c 0.0001, MeOH); ^1H NMR (400 MHz, Methanol- d_4) δ 7.60 (1H, dd, J = 8.4, 2.0 Hz, H-6), 7.55 (1H, d, J = 1.5 Hz, H-2), 6.89 (1H, d, J = 1.8 Hz, H-2'), 6.78 (1H, d, J = 8.4 Hz, H-5), 6.75 (1H, dd, J = 8.2, 1.8 Hz, H-6'), 6.72 (1H, d, J = 8.2 Hz, H-5'), 4.74 (1H, m (overlapped, H-8), 4.24 (1H, dd, J = 10.6, 8.8 Hz, H-9b), 3.86 (3H, s, H-3'OMe), 3.82 (3H, s, H-3OMe), 3.71 (1H, dd, J = 10.8, 5.3 Hz, H-9a); ^{13}C NMR (obtained from HSQC and HMBC, Methanol- d_4) δ 199.7 (C, C-7), 153.5 (C, C-4), 149.5 (C, C-3'), 149.3 (C, C-3), 147.2 (C, C-4'), 130.7 (C, C-1), 130.0 (C, C-1'), 125.4 (CH, C-6), 122.4 (CH, C-6'), 116.8 (CH, C-5'), 116.0 (CH, C-5), 113.0 (CH, C-2'), 112.7 (CH, C-2), 65.6 (CH, C-9),

56.5 (CH₃, C-3OMe), 56.4 (CH₃, C-3'OMe), 56.3 (CH, C-8); HR-ESI-MS (TOF) m/z [M-H]⁻ 317.1032 (calc for C₁₇H₁₉O₆⁻, 317.1025). Data correspond to literature. [43]

Protocatechualdehyde (**19**): white amorphous powder, ¹H NMR (400 MHz, Methanol-*d*₄) δ 9.69 (1H, s, H-7), 7.30 (1H, dd, overlapped, J = 1.9 Hz, H-6), 7.29 (1H, d, overlapped, H-2), 6.91 (1H, d, J = 7.9 Hz, H-5); ¹³C NMR (101 MHz, Methanol-*d*₄) δ 193.1 (CH, C-7), 153.8 (C, C-4), 147.2 (C, C-3), 130.8 (C, C-1), 126.4 (CH, C-6), 116.2 (CH, C-5), 115.4 (CH, C-2). HR-ESI-MS (Orbitrap) m/z [M-H]⁻ 137.0247 (calc for C₇H₅O₃⁻, 137.0244); MS²-Fragmentation (CE = -35 V) m/z 137 (100), 109 (9), Data correspond to literature. [44]

Vanillin (**20**): white solid, ¹H NMR (500 MHz, Methanol-*d*₄) δ 9.66 (1H, s, H-7), 7.38 - 7.41 (1H, m, H-6), 7.39 (1H, s, H-2), 6.86 (1H, d, J = 8.6 Hz, H-5), 3.89 (3H, s, H-3-OMe); ¹³C NMR (obtained from HSQC and HMBC, Methanol-*d*₄) δ 192.0 (CH, C-7), 150.9 (C, C-3), 150.1 (C, C-4), 128.8 (CH, C-6), 127.7 (C, C-1), 116.9 (CH, C-5), 110.5 (CH, C-2), 56.1 (CH₃, C-3OMe); HR-ESI-MS (TOF) m/z [M-H]⁻ 151.0401 (calc for C₈H₇O₃⁻, 151.0401). Data correspond to literature. [45, 46]

Syringaldehyde (**21**): white powder; ¹H NMR (400 MHz, Methanol-*d*₄) δ 9.70 (1H, s, H-1), 7.21 (2H, s, H-2 + H-6), 3.90 (6H, s, H-3OMe + H-5OMe); ¹³C NMR (obtained from HSQC and HMBC, Methanol-*d*₄) δ 192.5 (CH, C-7), 149.7 (2C, C-2 + C-5), 145.1 (C, C-4), 128.0 (C, C-1), 108.4 (2CH, C-2 + C-6), 56.8 (2CH₃, C-3-OMe + C-5-OMe); HR-ESI-MS (TOF) m/z [M-H]⁻ 181.0538 (calc for C₉H₉O₄⁻, 181.0506). Data correspond to literature. [47]

p-Hydroxybenzoic acid (**22**): brown solid; ¹H NMR (500 MHz, Methanol-*d*₄) δ 7.85 (2H, d, J = 8.7 Hz, H-2 + H-6), 6.78 (2H, d, J = 8.7 Hz, H-3+H-5); ¹³C NMR (obtained from HSQC and HMBC, Methanol-*d*₄) δ 172.0 (C, C-7), 162.7 (C, C-4), 132.8 (CH, C-2+C-6), 125.0 (C, C-1), 115.8 (CH, C-3+C-5); HR-ESI-MS (TOF) m/z [M-H]⁻ 137.0254 (calc for C₇H₅O₃⁻, 137.0239); MS²-Fragmentation (CE = -40 V) m/z 93 (100), 83 (1), 75 (3), 65 (18). Data correspond to literature. [48]

Protocatechuic acid (**23**): white amorphous powder, ¹H NMR (500 MHz, DMSO-*d*₆) δ 9.64 (2H, bs, H-3OH + H-4OH), 7.32 (1H, d, J = 2.1 Hz, H-2), 7.27 (1H, dd, J = 8.2, 2.1 Hz, H-6), 6.76 (1H, d, J = 8.2 Hz, H-5); ¹³C NMR (obtained from HSQC and HMBC, DMSO-*d*₆) δ 167.8 (C, C-7), 149.9 (C, C-4), 144.7 (C, C-3), 122.5 (C, C-1), 121.8 (CH, C-6), 117.0 (CH, C-2), 115.3 (CH, C-5); HR-ESI-MS (TOF) m/z [M-H]⁻ 153.0193 (calc for C₇H₅O₄⁻, 153.0188). Data correspond to literature. [49]

Vanillic acid (**24**): yellowish amorphous powder, ¹H NMR (400 MHz, Methanol-*d*₄) δ 7.56 (1H, d, J = 1.8 Hz, H-2), 7.55 (1H, dd, J = 8.7 Hz, 1.8 Hz, H-6), 6.83 (1H, d, J = 8.7 Hz, H-5), 3.89 (3H, s, H-3OMe); ¹³C NMR (101 MHz, Methanol-*d*₄) δ 170.2 (C, C-7), 152.6 (C, C-4), 148.7 (C, C-3), 125.2 (CH, C-6), 123.3 (C, C-1), 115.8 (CH, C-5), 113.8 (CH, C-2), 56.4 (CH₃, C-3OMe); HR-ESI-MS (Orbitrap) m/z [M-H]⁻ 167.0355 (calc for C₈H₇O₄⁻, 167.0339). Data correspond to literature. [50]

Protocatechuic acid methyl ester (**25**): white amorphous powder, ¹H NMR (500 MHz, Methanol-*d*₄) δ 7.42 (1H, d, J = 2.0 Hz, H-2), 7.41 (1H, dd, J = 8.7, 2.0 Hz, H-6), 6.80 (1H, d, J = 8.7 Hz, H-5), 3.83 (3H, s, H-7OMe); ¹³C NMR (obtained from HSQC and HMBC, Methanol-*d*₄) δ 168.7 (C, C-7), 151.5 (C, C-4), 146.0 (C, C-3), 123.3 (CH, C-6), 122.3 (C, C-1), 117.0 (CH, C-2), 115.4 (CH, C-5), 51.7 (CH₃, C-7OMe); HR-ESI-MS (Orbitrap) m/z [M-H]⁻ 167.0354 (calc for C₈H₇O₄⁻, 167.0350). Data correspond to literature. [51, 52]

5-Methoxy salicylic acid (**26**): white amorphous powder, ¹H NMR (400 MHz, DMSO-*d*₆) δ 7.41 (1H, d, J = 1.9 Hz, H-6), 7.27 (1H, dd, J = 8.1, 1.9 Hz, H-4), 6.60 (1H, d, J = 8.1 Hz, H-3), 3.73 (3H, s, H-5OMe); ¹³C NMR (obtained from HSQC and HMBC, DMSO-*d*₆) δ 146.0 (C, C-5), 122.0 (CH, C-4), 113.8 (CH, C-3), 113.0 (CH, C-6), 55.2 (CH₃, C-5OMe); HR-ESI-MS (TOF) m/z [M-H]⁻ 167.0348 (calc for C₈H₇O₄⁻, 167.0344). Data correspond to literature. [53, 54]

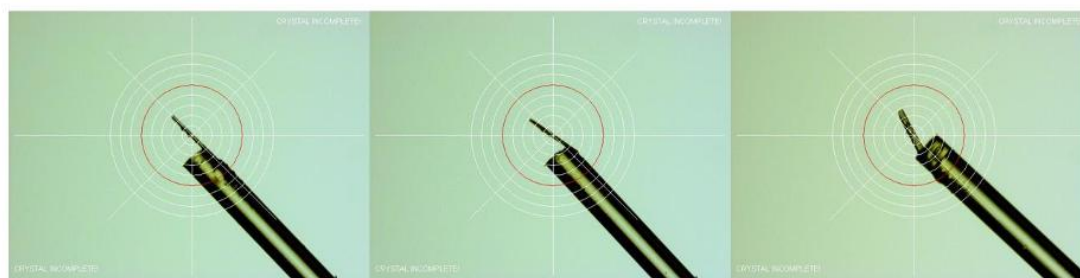


Figure S11. Crystal of Kumatakenin (13)

Table S15. Crystal data and structure refinement for Kumatakenin (ipds6326)

	Kumatakenin (13)
Empirical formula	C ₁₇ H ₁₄ O ₆
Formula weight	314.28
Temperature/K	170
Crystal system	monoclinic
Space group	P2 ₁ /c
a/Å	17.899(2)
b/Å	3.9339(3)
c/Å	19.465(3)
α/°	90
β/°	95.665(11)
γ/°	90
Volume/Å ³	1363.9(3)
Z	4
ρ _{calc} /g/cm ³	1.530
μ/mm ⁻¹	0.117
F(000)	656.0
Crystal size/mm ³	0.295 × 0.029 × 0.015
Radiation	Mo Kα (λ = 0.71073)
2θ range for data collection/°	4.574 to 49.994
Index ranges	−21 ≤ h ≤ 21, −4 ≤ k ≤ 3, −22 ≤ l ≤ 22
Reflections collected	5958
Independent reflections	2328 [R _{int} = 0.1600, R _{sigma} = 0.1766]
Data/restraints/parameters	2328/0/213
Goodness-of-fit on F ²	0.869
Final R indexes [I ≥ 2σ (I)]	R ₁ = 0.0649, wR ₂ = 0.1358
Final R indexes [all data]	R ₁ = 0.2094, wR ₂ = 0.1997
Largest diff. peak/hole / e Å ⁻³	0.23/−0.22

Declaration on author contributions

The present cumulative dissertation is based on the following peer-reviewed scientific publications and an unpublished chapter:

Chapter 2: Analysis of Unusual Sulfated Constituents and Anti-infective Properties of Two Indonesian Mangroves, *Lumnitzera littorea* and *Lumnitzera racemosa* (Combretaceae)

Journal: *Separations* 2021, 8, 82

DOI: <https://doi.org/10.3390/separations8060082>

Authors: Manurung, J.*; **Kappen, J.***; Schnitzler, J.; Frolov, A.; Wessjohann, L.A.; Agusta, A.; Muellner-Riehl, A.N.; Franke, K.

***shared first authorship**

J.K. performed the extraction, isolation, structure elucidation including interpretation of HRMS and NMR data, visualisation and writing of the connected parts in the original manuscript draft as well as revision and editing of the manuscript. The original draft was further written by J.M., K.F. and A.N.M.R. The conceptualization was done by J.M., A.N.M.-R. and L.A.W.. J.M. and A.A. provided the plant material. J.M. was involved in laboratory work, the data analysis and interpretation of results. J.S. performed the genomic analysis. A.F. was involved in the evaluation of MS data. L.A.W., A.N.M.R. and K.F. supervised the project, and revised the manuscript. All authors provided fruitful discussions and performed reviewing und editing.

Chapter 3: Challenging Structure Elucidation of Lumnitzerallactone, an Ellagic Acid Derivative from the Mangrove *Lumnitzera racemosa*

Journal: *Marine Drugs* 2023, 21, 242

DOI: <https://doi.org/10.3390/md21040242>

Authors: **Kappen, J.**; Manurung, J.; Fuchs, T.; Vemulapalli, S.P.B.; Schmitz, L.M.; Frolov, A.; Agusta, A.; Muellner-Riehl, A.N.; Griesinger, C.; Franke, K.; Wessjohann, L.A.

J.K. performed the extraction, isolation, structure elucidation including interpretation of HRMS, MS² and NMR data, first synthesis step, and CASE calculations of lumnitzerallactone as well as writing the original manuscript draft. J.M. and A.A. provided the plant material. T.F. supported the planning of the synthesis and performed the second synthesis step. S.P.B.V. performed the NMR analysis in Göttingen and the DFT calculations. A.F. supported the MS data interpretation. L.M.S., S.P.B.V., C.G. and K.F. contributed by fruitful intensive discussion to the determination of the absolute structure of lumnitzerallactone. L.A.W., A.N.M.-R., and K.F. supervised the project, and revised the manuscript. All authors provided reviewing und editing.

Chapter 4 Phytochemical profiling of the Omani medicinal plant *Terminalia dhofarica* (syn. *Anogeissus dhofarica*)

Authors: **Kappen, J.**; Dhar, D.; Rshan, L.; Franke, K.; Wessjohann, L.A.

Status: submitted to *Molecules* (MDPI)

J.K. performed the extraction, isolation, structure elucidation including interpretation of HRMS, MS², MSⁿ, ECD and NMR data of all isolated compounds as well as writing the original manuscript draft. L.R. provided the plant material. D.D. performed the CD calculations. L.A.W. and K.F. planned, coordinated and supervised the project, as well as revised the manuscript. All authors provided reviewing und editing.

Chapter 5 Exploring *Hornstedtia scyphifera*: An extensive multimethod phytochemical investigation reveals the chemical composition and bioactive potential

Journal: *Discover Plants* 2025, 2, 6

DOI: <https://doi.org/10.1007/s44372-024-00085-0>

Authors: **Kappen, J.**; David, A.; Pieplow, K.; Wujtschik, A.; Ware, I.; Dhar, D.; Wagner, C.; Davari, M.; Franke, K.; Wessjohann, L.A.

J.K. developed the methods, planned and performed the isolation and structure elucidation of secondary metabolites including interpretation of HRMS, MS², ECD and NMR data as well as writing the original manuscript draft. L.A.W. and J.K. supervised the work of K.P. and A.W. as diploma students on this project. K.P. and A.W. contributed to extraction, isolation, and structure elucidation of secondary metabolites. A.D. performed the essential oil extraction, related GC-MS analysis and literature research especially about bioactivities as well as contributed to the original manuscript draft on connected parts. I.W. contributed by scientific advise and preliminary experiments. D.D. and M.D. performed the ECD calculations. C.W. performed X-ray measurements. L.A.W. and K.F. planned, coordinated and supervised the project, as well as revised the manuscript. All authors provided reviewing und editing.

Curriculum vitae

Personal details

Name Jonas Kappen
 Date and place of birth
 Nationality German

Formal education

05/20 – present Scientific Assistant (PhD candidate) at the Leibniz Institute of Plant Biochemistry (IPB), Department of Bioorganic Chemistry, Halle (Saale)
 Title: “Phytochemical Investigation and Bioactivity Screening of promising Medicinal plants of the families Combretaceae and Zingiberaceae”
 Supervisor: Prof. Dr. Ludger A. Wessjohann
 Mentor: Dr. Katrin Franke

05/19 – 04/20 Vocational training as a state-certified food chemist at the State Office for Consumer Protection Saxony-Anhalt (LAV), Halle (Saale)
 Degree: State-certified food chemist
 Grade: 2.1

10/13 – 05/19 Study of Food Chemistry at the Martin-Luther University Halle-Wittenberg, Halle (Saale)
 Degree: Diplom food chemist (Dipl.-LMChem.)
 Grade: 1.3
 Title: “Posttranslationale Proteinmodifikationen im Alterungsprozess “
 Supervisor: Prof. Dr. Marcus Glomb
 Mentor: Dr. Tim Baldensperger

08/17 – 10/17 IAESTE – Internship at Chemical Institute of the Universidade Federal de Vicosia (Brasil)
 Topic: Analysis of volatile components from brewery products

05/16 – 08/16 ERASMUS⁺ - Internship at Department of Chemistry of the University of Environmental and Lifescience in Wrocław (Poland)

2003 – 2012 Private secondary school Gymnasium der Ursulinen Calvarienberg, Bad Neuenahr-Ahrweiler
 Degree: Abitur, General qualification for University entrance
 Grade: 2.2

Work experience:

05/2020 – present Scientific Assistant, Leibniz Institute of Plant Biochemistry, Department of Bioorganic Chemistry, Halle (Saale)

Publications

Publications in peer-reviewed journals

Kappen, J.; David, A.; Pieplow, K.; Wujtschik, A.; Ware, I.; Dhar, D.; Wagner, C.; Davari, M.; Franke, K.; Wessjohann, L.A., Exploring *Hornstedtia scyphifera*: An extensive multimethod phytochemical investigation reveals the chemical composition and bioactive potential. *Discover Plants* **2025**, 2, 6, doi: 10.1007/s44372-024-00085-0.

Kappen, J.; Manurung, J.; Fuchs, T.; Vemulapalli, S.P.B.; Schmitz, L.M.; Frolov, A.; Agusta, A.; Muellner-Riehl, A.N.; Griesinger, C.; Franke, K.; Wessjohann, L.A., Challenging structure elucidation of lumnizeralactone, an ellagic acid derivative from the mangrove *Lumnitzera racemosa*. *Marine Drugs* **2023**, 21, 242, doi: 10.3390/md21040242.

Manurung, J.*; **Kappen, J.***; Schnitzler, J.; Frolov, A.; Wessjohann, L.A.; Agusta, A.; Muellner-Riehl, A.N.; Franke, K., Analysis of Unusual Sulfated Constituents and Anti-infective Properties of Two Indonesian Mangroves, *Lumnitzera littorea* and *Lumnitzera racemosa* (Combretaceae), *Separations* **2021**, 8, 82, doi: 10.3390/separations8060082

***shared first authorship**

Baldensperger, T.; Eggen, M.; **Kappen, J.**; Winterhalter, P.R.; Pfirrmann, T.; Glomb, M.A., Comprehensive analysis of posttranslational protein modifications in aging of subcellular compartments. *Scientific Reports* **2020**, 10, 7596, doi: 10.1038/s41598-020-64265-0

Publications in submission process

Kappen, J.; Dhar, D.; Rashan, L.; Franke, K.; Wessjohann, L.A., Profiling and Bioactivity of Polyphenols from the Omani medicinal plant *Terminalia dhofarica*, in submission process in *Molecules* **2025**

Oral presentations

Kappen, J.; Fuchs, T.; Vemulapalli, S.P.B.; Schmitz, L.M.; Frolov, A.; Manurung, J.; Agusta, A.; Muellner-Riehl, A.N.; Griesinger, C.; Franke, K.; Wessjohann, L.A., Chasing molecules - a structure elucidation journey, Phytochemical Society of Europe conference (PSE), Brno (Czech Republic), 21th - 24th May 2024.

Kappen, J.; Fuchs, T.; Vemulapalli, S.P.B.; Schmitz, L.M.; Frolov, A.; Manurung, J.; Agusta, A.; Muellner-Riehl, A.N.; Griesinger, C.; Franke, K.; Wessjohann, L.A., Chasing molecules - a structure elucidation journey, 60th Natural Products Meeting, Würzburg (Germany), 06th October 2023.

Kappen, J.; Fuchs, T.; Vemulapalli, S.P.B.; Schmitz, L.M.; Frolov, A.; Manurung, J.; Agusta, A.; Muellner-Riehl, A.N.; Griesinger, C.; Franke, K.; Wessjohann, L.A., Chasing molecules - a structure elucidation journey, Plant science students conference (PSSC), Gatersleben (Germany), 04th July 2023. doi: 10.5281/ZENODO.8155194

Poster presentations

Kappen, J.; Fuchs, T.; Vemulapalli, S.P.B.; Schmitz, L.M.; Frolov, A.; Manurung, J.; Agusta, A.; Muellner-Riehl, A.N.; Griesinger, C.; Franke, K.; Wessjohann, L.A., Chasing molecules - interdisciplinary approaches in modern structure elucidation, Phytochemical Society of Europe conference (PSE), Brno (Czech Republic), 21th - 24th May 2024.

Publications

Kappen, J.; Fuchs, T.; Vemulapalli, S.P.B.; Schmitz, L.M.; Frolov, A.; Manurung, J.; Agusta, A.; Muellner-Riehl, A.N.; Griesinger, C.; Franke, K.; Wessjohann, L.A., Chasing molecules - interdisciplinary approaches in modern structure elucidation, Leucorea - IPB internal retreat, Wittenberg (Germany), 4th - 5th April 2024.

Kappen, J.; Manurung, J.; Bachurski, M.; Frolov, A.; Muellner-Riehl, A.N.; Kreutz, M.; Wessjohann, L.A., Franke, K., Beyond ellagic acid - Unusual sulfated mangrove constituents with potential health benefits, Final Symposium - Research Association Autonomie im Alter, Magdeburg (Germany), 30th June 2022.

Kappen, J.; Manurung, J.; Bachurski, M.; Frolov, A.; Muellner-Riehl, A.N.; Kreutz, M.; Wessjohann, L.A., Franke, K., Beyond ellagic acid - Unusual sulfated mangrove constituents with potential health benefits, Young Scientists Workshop - Research Association Autonomie im Alter, Magdeburg (Germany), 29th June 2022.

Kappen, J.; Manurung, J.; Bachurski, M.; Frolov, A.; Muellner-Riehl, A.N.; Kreutz, M.; Wessjohann, L.A., Franke, K., Beyond ellagic acid - Unusual sulfated mangrove constituents with potential health benefits, Plant science students conference (PSSC), online, 14th – 17th June 2022.

Kappen, J.; Manurung, J.; Bachurski, M.; Frolov, A.; Muellner-Riehl, A.N.; Kreutz, M.; Wessjohann, L.A., Franke, K., Beyond ellagic acid - Unusual sulfated mangrove constituents with potential health benefits, Leibniz Conference on Bioactive Compounds, Hamburg (Germany), 5th – 6th May 2022.

Awards

Best poster presentation award,
at Leucorea - IPB internal retreat, Wittenberg (Germany), 4th - 5th April 2024

Best oral presentation award,
at Plant science students conference (PSSC), Gatersleben (Germany), 04th July 2023

Eidesstattliche Erklärung

Ich erkläre an Eides statt, dass ich die vorliegende Dissertation zur Erlangung der Doktorwürde, unter der Betreuung von Herrn Prof. Dr. Ludger A. Wessjohann und Frau Dr. Katrin Franke, selbstständig verfasst und angefertigt habe.

Andere als die angegebenen Quellen und Hilfsmittel wurden von mir nicht benutzt. Alle angeführten Zitate wurden kenntlich gemacht. Des Weiteren versichere ich, dass ich diese Arbeit an keiner anderen Institution eingereicht habe.

Halle (Saale), den

Jonas Kappen